BLENDING N- AND O-DONOR LIGANDS ON A M(II) (M = Ni, Cu) OR Fe(III) CENTRE AS A ROUTE TO PARAMAGNETIC ASSEMBLIES

Thesis submitted for the degree of

Doctor of Philosophy

at the University of Leicester

by

Rajinder Kaur Chaggar MChem Hons. (Leicester)

Department of Chemistry

University of Leicester

August 2005

ProQuest LLC
789 East Eisenhower Parkway
P.O. Box 1346
Ann Arbor, MI 48106-1346

STATEMENT OF ORIGINALITY

The accompanying thesis submitted for the degree of Ph.D. entitled *Blending N- and O-Donor Ligands on a M(II) (M = Ni, Cu) or Fe(III) Centre as a Route to Paramagnetic Assemblies*, is based on work conducted by the author in the Department of Chemistry at the University of Leicester mainly during the period between October 2001 and August 2005. All the work recorded in this thesis is original unless otherwise acknowledged in the text or by references. None of the work has been submitted for another degree in this or any other University.

Signed ..... Date 10/3/06

RAJINDER KAUR CHAGGAR

BLENDING N- AND O-DONOR LIGANDS ON A M(II) (M = Ni, Cu) OR Fe(III) CENTRE AS A ROUTE TO PARAMAGNETIC ASSEMBLIES

ABSTRACT

The thesis describes the synthesis, characterisation and magnetic properties of some novel well-defined paramagnetic polymetallic arrays based on the 3*d* metal ions Fe(III), Ni(II) and Cu(II).

Chapter 1 begins with an overview of modern applications of paramagnetic assemblies and then examines synthetic strategies that can be employed for their preparation before identifying the aims and objectives set for the thesis.

In **Chapter 2**, the reactivity of a ligand blend consisting of a combination of two different bifunctional 2-pyridine alcohols [drawn from 2-{$(CH_2)_nOH$}-6-X-C_5H_3N] (X = H or halide; n = 0 – 3) towards $M(OAc)_2.xH_2O$ (M = Ni, Cu) in the presence of triethylamine is systematically examined. A range of mixed-ligand-containing clusters, including $\{M_2\}$, $\{M_4\}$ (M = Ni or Cu) and polymeric $\{Cu_n\}$ species, are described; an EPR study on an open-cubane $\{Cu_4\}$ species indicates the presence of two spin states.

In **Chapter 3**, neutral and charged $\{M_2\}$, $\{M_3\}$ and $\{M_4\}$ (M = Ni or Cu) species are accessible on treatment of $M(OAc)_2.xH_2O$ with a ligand blend consisting of benzilic acid and [2-{$(CH_2)_nOH$}-6-X-C_5H_3N] (X = H, or halide; n = 0 – 3). A study of the role of the base employed (NEt_3 *vs.* NaOMe) on product type has also been investigated. The presence of very weak magnetic exchange interactions is a feature of the open di-cuboidal dianion $\{Ni_4\}^{2-}$ prepared.

In **Chapter 4**, isophthalic acid and [2-{$(CH_2)_nOH$}-6-X-C_5H_3N] (X = H or halide; n = 1 – 3) are used as components of the ligand blend in combination with $M(OAc)_2.xH_2O$ affording polynuclear mixed-ligand $\{M_2\}$ and $\{M_n\}$ (M = Ni, Cu) complexes. In contrast, the combination of isophthalic acid and an aryl-substituted formamidine leads to the neutral spheroidal $\{Cu_{24}\}$ clusters (nanoballs) and in one case to a 1-D $\{Cu_n\}$ polymer; strong antiferromagnetic behaviour is a feature of the nanoball.

In **Chapters 5** and **6**, a selection of discrete polynuclear iron complexes [*e.g.*, $\{Fe_2\}$, $\{Fe_4\}$, $\{Fe_6\}$, $\{Fe_8\}$, $\{Fe_{10}\}$ and $\{Fe_{11}\}$] containing mixed-ligand sets have been prepared. Specifically, **Chapter 5** focuses on an oxo/L (L = carboxylate, 2-pyridine alkoxide, phen) ligand blend with particular attention paid to the electronic and steric attributes of L, while **Chapter 6** is concerned with the more air sensitive imido group $[N(R)^{2-}$ (R = aryl, 2-picolyl)] in combination with L (L = carboxylate, amide, formamidinate). Notably, the iron-oxo $\{Fe_{10}\}$ system shows the hallmarks of a Single-Molecule Magnet.

In **Chapter 7**, full details of the experimental procedures along with spectroscopic, analytical and X-ray data (*ca.* 50 structures) are reported.

Acknowledgements

God, thank you for giving me the inspiration, perseverance and for everything I have achieved. I need to thank my mother and father for supporting me in every possible way they could throughout the years and my brother Ranjit and sister Dawinder for being my constant companions, also my nephew Gurdev for uplifting my spirits. I need to mention my late uncle Mr. H. S. Soor who was a great intellect and my late neighbour Mrs. L. Manger for inspiring and motivating me to do well in my studies. My research supervisor Dr. G. A. Solan has to be thanked for his belief in my success, his constant advice, support, guidance and for giving me the opportunity to carry out research. Thanks to Dr. E. Raven for constructive advice as my Ph.D. committee member and the technical and support staff at the University of Leicester including; Dr J. Fawcett for his expansive contribution towards X-ray crystallography, Kuldip Singh for general advice, Dr G. Eaton for supplying numerous mass spectra and Dr G. Griffith for the provision of NMR data. Many thanks to Professor A. Harrison (Edinburgh University) for his generous efforts, despite his busy schedule for the provision of variable temperature magnetic data, invaluable analysis and advice and Dr. J. Wolowska/Dr. E. J. McInnes (Manchester University, EPSRC EPR service) for providing me with helpful EPR data, analysis and advice. Thanks to Dr. Clive Metcalfe and Yohan Champouret for reading the final draft of Chapter 2 in this thesis. Finally, I will thank *all* past and present friends/laboratory colleagues at the University of Leicester for their companionship, humour and enthusiasm. Success can only be achieved with additional support from encouraging role-models, teachers, family and friends.

With heartfelt thanks to everyone who supported me

Rajinder

Glossary of Complexes

Chapter 2

$[Ni(chp)_2(hmpH)_2]$	**1a**
$[Ni(chp)_2(hepH)_2]$	**1b**
$[Ni(chp)_2(hppH)_2]$	**1c**
$[Ni(hmpH)_2(CH_3CO_2)_2]$	**2a**
$[Ni(hepH)_2(CH_3CO_2)_2]$	**2b**
$[Cu(chp)(hmp)]_n$	**3**
$[Cu(chp)(mehmp)]_n$	**3'**
$[Cu(chp)(hep)]_2$	**4a**
$[Cu(bhp)(hep)]_2$	**4b**
$[Cu(chp)(hpp)]_2$	**5a**
$[Cu(bhp)(hpp)]_2 \cdot 2MeOH$	**5b**
$[Cu(hmp)(CH_3CO_2)]_4 \cdot 2H_2O$	**6**
$[Cu(hmpH)_2(CH_3CO_2)_2]$	**7**
$[Cu(hep)(CH_3CO_2)]_2$	**8**

Chapter 3

$[Ni_4(chp)_4(bnzH)_4(MeO)_2(H_2O)_2][NEt_3H]_2 \cdot 2MeCN$	**9a/**
$[Ni_4(chp)_4(bnzH)_4(MeO)_2(MeOH)_2][NEt_3H]_2 \cdot 2MeCN$	**9b**
$[Ni_4(bhp)_4(bnzH)_4(MeO)_2(H_2O)_2][NEt_3H]_2 \cdot 2MeCN$	**10a/**
$[Ni_4(bhp)_4(bnzH)_4(MeO)_2(MeOH)_2][NEt_3H]_2 \cdot 2MeCN$	**10b**
$[Ni_4(hmp)_4(bnzH)_4(MeOH)_2]$	**11a**
$[Ni_4(hmp)_4(Ph_2C\{H\}CO_2)_4(MeOH)_2]$	**11b**
$[Ni(hmpH)_2(bnzH)_2]$	**12a**
$[Ni(hmpH)_2(Ph_2C\{H\}CO_2)_2]$	**12b**
trans-$[Ni(hepH)_2(bnzH)_2]$	**13a**
trans-$[Ni(hepH)_2(Ph_2C\{H\}CO_2)_2]$	**13b**
cis-$[Ni(hmpH)_2(bnzH)_2]$	**14a**
cis-$[Ni(hepH)_2(Ph_2C\{H\}CO_2)_2]$	**14b**
$[Ni(hppH)_2(bnzH)_2]$	**15**
$[Cu_3(chp)_4(bnz)(bnzH)][NEt_3H] \cdot 4MeOH$	**16a**
$[Cu_3(hp)_4(bnz)(bnzH)][NEt_3H]$	**16b**
$[Cu(hmpH)_2(bnzH)_2]$	**17a**
$[Cu(mehmpH)_2(bnzH)_2]$	**17a'**
$[Cu(hmpH)_2(Ph_2C\{H\}CO_2)_2]$	**17b**
$[Cu(hep)(bnzH)]_2$	**18a**
$[Cu(hep)(Ph_2C\{H\}CO_2)]_2$	**18b**
$[Cu(hppH)(bnz)]_2$	**19**
$[Cu(hpp)(Ph_2C\{H\}CO_2)]_2$	**20**
$[Cu(bnzH)_3][NEt_3H]$	**21**
$[CuNa_2(bnz)_2(MeOH)_4(MeCN)_2]_n$	**22**

Chapter 4

$[Ni(hmpH)_2(m\text{-BDC})]_2 \cdot 1.5MeCN$	**23a**
$[Ni(mehmpH)_2(m\text{-BDC})]_2$	**23a'**
$[Ni(hepH)_2(m\text{-BDC})]_2 \cdot CH_2Cl_2$	**23b**
$\{[Ni(hepH)_2(m\text{-BDC})] \cdot MeOH\}_n$	**24**
$[Ni(hppH)_2(m\text{-BDC})]_n$	**25**
$\{[Cu(hmpH)_2(m\text{-BDC})] \cdot CH_2Cl_2\}_n$	**26**
$[Cu(mehmpH)_2(m\text{-BDC})]_n$	**26'**
$[Cu(hmpH)_2(m\text{-BDC})]$	**27**
$[Cu(hepH)_2(m\text{-BDC})]_n$	**28**
$[Cu(hppH)_2(m\text{-BDC})]_n$	**29**
$[Cu(phen)_2(m\text{-BDC})] \cdot 6H_2O \cdot CH_2Cl_2$	**30**
$[Cu_{24}(m\text{-BDC})_{24}(HDmesF)_{12}(H_2O)_{12}] \cdot 2MeCN \cdot 12H_2O$	**31a**
$[Cu_{24}(m\text{-BDC})_{24}(HDo\text{-tolF})_{12}(H_2O)_{12}]$	**31b**
$[Cu_{24}(m\text{-BDC})_{24}(HD2,6\text{-xylF})_{12}(H_2O)_{12}]$	**31c**
$[Cu(HD2,6\text{-xylF})_2(m\text{-BDC})]_n$	**32**

Chapter 5

$[Fe_{10}Na_2(O)_6(OH)_4(C_6H_5CH_2CO_2)_{10}(chp)_6(H_2O)_2(MeCN)_2] \cdot 9MeCN$	**33**
$[Fe_{11}(O)_6(OH)_6(p\text{-}\{CH_3\}\text{-}C_6H_4CO_2)_{15}] \cdot 15MeCN$	**34**
$[Fe_8(O)_4(OH)_2(hmp)_4(Ph_2C\{H\}CO_2)_{10}(MeOH)] \cdot 2MeCN \cdot MeOH$	**35**
$[Fe_6(O)_2(OH)_2(hep)_2(Ph_2C\{H\}CO_2)_{10}] \cdot 12MeCN$	**36**
$[Fe_6(O)_2(hmp)_8Cl_4](Cl)_2 \cdot 4H_2O$	**37**
$[Fe_4(O)_2(phen)_2(Ph_2C\{H\}CO_2)_6(Cl)_2] \cdot 2MeCN$	**38a**
$[Fe_4(O)_2(phen)_2(PhCH_2CO_2)_6(Cl)_2] \cdot 2MeCN$	**38b**
$[Fe_4(O)_2(phen)_2(CH_3CH_2CO_2)_6(Cl)_2]$	**38c**

Chapter 6

$[Fe_2(NMes)(CH_3C\{O\}NMes)_2Cl_2] \cdot 2MeCN$	**39**

Contents

Abbreviations

FAB	Fast Atom Bombardment
ESI	Electrospray Ionisation
MALDI	Matrix-Assisted Laser Desorption Ionisation
Da.	Daltons
UV	Ultra Violet
NMR	Nuclear Magnetic Resonance
EPR	Electron Paramagnetic Resonance
HFEPR	High Frequency EPR
SQUID	Superconducting Quantum Interference Device
Hhp	2-hydroxypridinol
Hchp	6-chloro-2-pyridinol
Hbhp	6-bromo-2-pyridinol
hmpH	2-(α-hydroxymethyl)pyridine
mehmpH	α-methyl-2-pyridinemethanol
hepH	2-(β-hydroxyethyl)pyridine
hppH	2-(γ-hydroxypropyl)pyridine
$bnzH_2$	benzilic Acid
***m*-$BDCH_2$**	*m*-benzenedicarboxylic acid
phen	1,10-*N,N*-phenanthroline
$pyCO_2H$	pyridinecarboxylic acid
Mes	2,4,6-trimethylphenyl
HDmesF	*N,N'*-bis(2,4,6-trimethylphenyl)formamidine
HD2,6-xylF	*N,N'*-bis(2,6-dimethylphenyl)formamidine
HD*o*-tolF	*N,N'*-bis(2-methylphenyl)formamidine
ITR	Imido Transfer Reagent
$ampH_2$	2-(aminomethylpyridine)/2-picolylamine
$ampLi_2$	2-[(dilithium)aminomethyl]pyridine
$amp(SiMe_3)_2$	2-[bis(trimethylsilyl)aminomethyl]pyridine
DMF	dimethylformamide
DME	dimethoxyethane
THF	tetrahydrofuran
SBU	Secondary Building Unit
MOF	Metal Organic Framework
ZFS	Zero-Field Splitting
SMM	Single-Molecule Magnet
SCM	Single-Chain Magnet
POM	polyoxometallate
EO	End-on
N/A	Not Applicable

bpea	*N,N'*-bis(2-pyridyl)ethylamine
btaH	benzotriazole
dpk	dipyridylketone
dpma	*N,N*-di(pyrrol-α-methyl)-*N*-ethylamine
Dtox	$[ON=\{Me\}CCH_2SCH_2\text{-}CH_2SCH_2C\{Me\}=NO]^{2-}$
enzbipy	[*N,N*-bis(pyridin-2-yl)benzylidene]ethane-1,2-diamine
Hbpca	bis(2-pyridylcarbonyl)amine
H_4cit	citric acid
Hdbm	dibenzoylmethane
H_2edea	*N*-ethyldiethanol
Hdpm	dipivaloylmethane
$H_3etheidi$	$N(CH_2CO_2H)_2(CH\{Et\}CH_2OH)$
hfac	hexafluoroacetylacetone
H_3heidi	$N(CH_2CO_2H)_2(CH_2CH_2OH)$
$H_3metheidi$	$N(CH_2CO_2H)_2(CH\{Me\}CH_2OH)$
H_3ntp	$N(CH_2CH_2COOH)_3$
$H_2{}^cpent\text{-}ida$	*N*-cyclopentyliminodiacetate
HSalea	*N*-{2-hydroxybenzyl}-2-amino-1-ethanol
Hsae	$C_6H_4(2\text{-}OH)C=N(CH_2)_2OH$
H_3thme	1,1,1-tris(hydroxymethyl)ethane
H_6talen	2,4,6-tris(1-(2-salicylaldimino-methylpropylimino)-ethyl)-1,3,5-trihydroxybenzene
Meimid	*N*-methylimidazole
Me_2oxpn	*N,N'*-bis(3-amino-2,2'-dimethylpropyl)oxamido
pm	pyrimidine
py	pyridine
pao	pyridine-2-aldoximate
Salen	*N,N'*-ethane-1,2-diylbis(salicyaldiminato)
salox	salicylaldoximato dianion
salpa	*N*-(2-hydroxybenzyl)-3-amino-1-propanol
saltmen	*N,N'*-(1,1,2,2-tetramethylethylene)bis(salicylideneiminate)
tacn	1,4,7-triazacyclononane
TCNE	tetracyanoethylene
TCNQ	7,7,8,8-tetracyano-*p*-quinodimethane
$teaH_3$	triethanolamine
tmen	*N,N,N',N'*-tetramethylethylenediamine
Tp	tris(pyrazolyl)hydroborate
TTF	tetrathiafulvene
$XDKH_2$	*m*-xylylenediamine
esd	Error of standard deviation

Chapter 1

1.0 Introduction

The recognition that large assemblies of paramagnetic transition metal ions can have technological applications, *e.g.*, in advanced pharmaceutical products, industrial coatings and fast computing processes, has witnessed a considerable growth of reports in this type of chemistry.[1a] The exponential demands for these applications has impacted and surged upon the development of functional materials with interesting physical or bioinorganic activity.[1b,2]

As chemists, the controlled synthetic screening of combinations of transition metal ions and ligands allow us to synthesise molecules with potentially interesting structural and physical properties that may be useful for one or more of the above applications. In this chapter, some of the research currently being carried out within this field, which can be broadly described as facets of coordination chemistry, is reviewed (section 1.1). In addition, the areas selected for further development (section 1.2) and the aims and objectives of this work are described (section 1.3).

1.1 Overview of Novel Paramagnetic Molecules

There are many types of paramagnetic assemblies that can be described as either extended polymeric networks or well-defined discrete metallic frameworks and frequently these types of molecules have common features. Selected types of complexes currently being studied and developed are described in the following sections (1.1.1 – 1.1.7). Inevitably, several of the following sections impinge on one another but are regarded as separate enough to warrant individual discussion.

1.1.1 Nanomolecules

The self-assembly of molecular building blocks for the construction of diamagnetic or paramagnetic nanomolecular structures is termed the *bottom-up synthetic approach* and

employs, the use of techniques such as natural self assembly,[2a] nanoreactors,[2b] crystal engineering of supramolecular species,[3] hierarchical self assembly by polymerisation of nanoparticles,[4] nanocasting of porous hollow inorganic structures[5] and monodispersion.[6,7] Recently, the *Soft Chemistry Approach* was identified as a controlled synthetic pathway for the preparation of nanomolecules using methods of self assembly influenced by structure directing agents, controlled polymerisation processes or directed assembly of nanoscale *building blocks*.[8]

The potential physical or biological applications of nanomolecular materials have in common one or more of the following; porosity,[9,10] phase separation, catalysis (Figure 1),[2b,2c,11] ionic effects, optical effects,[12] electronic effects,[13,14] conductivity, switching, luminescence, nuclear rearrangement,[15] MRI applications,[16] viral mimickry,[2b,17] drug delivery,[18] cell targeting,[19] bacterial capture, DNA manipulation[20] and muscle fabrication.[21]

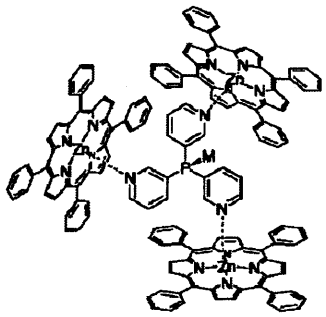

Figure 1 Encapsulation of nanoscale transition metal catalysts [M = $PdCl_2$, Rh(acac)(CO)] using zinc tetrakis(*meso*-phenyl)porphyrin.[2b,2c]

1.1.2 Single-Molecule Magnetism

Since the 1990's, the discovery of a class of molecules termed *Single-Molecule Magnets* (SMMs) has been the subject of significant attention. These SMMs have been shown to exhibit slow-relaxation of magnetisation and are being developed for prospective high-density memory storage devices.[22-29] *Single-Chain Magnets* (SCMs) have also been recently discovered.[28d,28s,29h-29l,82]

The two basic requirements of SMMs include a large spin state (S) and an easy axis of magnetisation measured as parameter D. The latter is directly related to the presence of uniaxial anisotropy. The two parameters of D and S combine to provide an overall high energy (U_{eff}) for spin reorientation due to slow-relaxation of magnetisation (Equation 1).

$$U_{eff} = |D|S^2$$

Equation 1 Relationship of barrier to magnetisation relaxation (U_{eff}) easy axis of magnetisation (D) and spin state of molecule (S).

In general, a series of magnetic measurements based on the detection of slow-magnetisation relaxation along with U_{eff}, D and S, have to be performed in order to identify an SMM. Firstly, DC variable temperature susceptibility/$\chi_M T$ against T measurements can be employed to account for the basic magnetic behaviour of the molecule. Secondly, AC variable temperature susceptibility/$\chi_M''T$ against T measurements are used to locate an out-of-phase signal possessing a peak plateau. The peak plateau is indicative of slow-relaxation of magnetisation thus, derivation of U_{eff} is possible by use of the Arrhenius equation (Equation 2). Thirdly, reduced magnetisation ($N\mu_\beta$) against several field/temperature (H/T) measurements, indicate the presence of D if the isofield measurements are non-superimposed. At this point these measurements may be modelled to obtain values for both D and S. Finally, magnetic moment ($N\mu_\beta$) against field (H) measurements exhibit low temperature hysteresis due to slow-relaxation magnetisation. In addition, HFEPR measurements are often taken to support and/or evaluate these parameters.

$$\tau = \tau_0 e^{\frac{U_{eff}}{kT}}$$

Equation 2 Arrhenius equation for derivation of U_{eff} (Equation 1), Boltzmann constant (k), temperature (T) and relaxation time (τ).

The largest known SMM is based on eighty-four manganese ions [$\{Mn_{84}\}$] and has a diameter of 4.3 nm[25a] while the $\{Mn_{12}\}$ family of cluster complexes are the most extensively studied to date (Figure 2).[26,91] As a drawback, all SMMs known so far exhibit

magnetic relaxation behaviour at impractical cryogenic temperatures. SMMs based on iron, nickel and copper ions are summarised in Table 1.

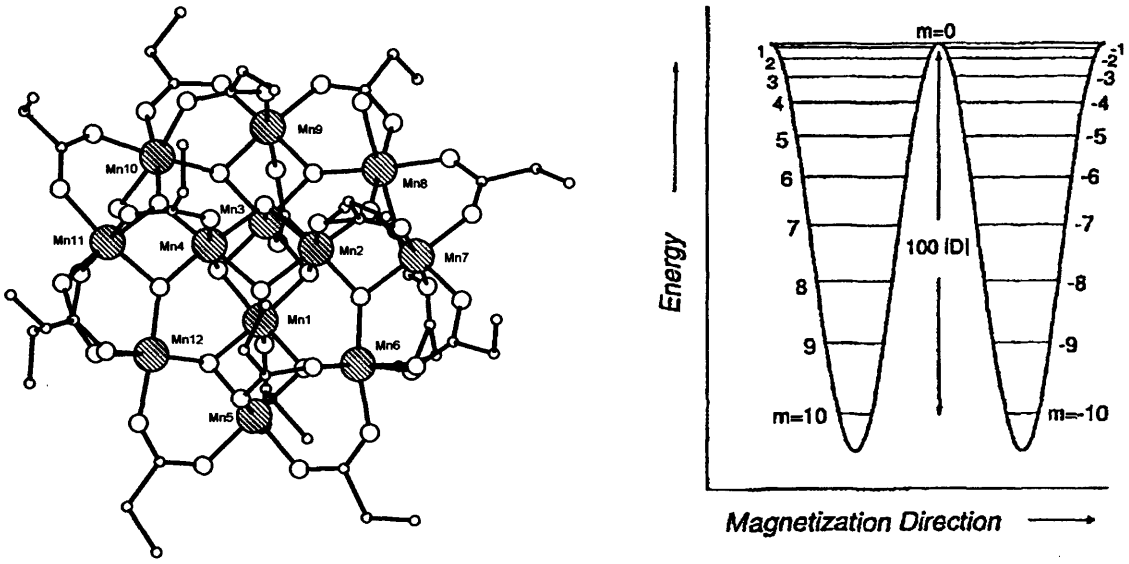

Figure 2 Molecular structure of $[Mn_{12}O_{12}(O_2CEt)_{16}(H_2O)_4]$ (left) with axial symmetry (easy-axis anisotropy) and $S = 10$. The effective energy barrier of $100|D|$ between the $M_s = \pm 10$ states is derived from Equation 1, this is depicted by a double-well potential energy plot (right).[26]

1.1.3 Models for Metalloenzymes

Transition metal ion assemblies are also being investigated as models for biologically important molecules. For example, iron-based clusters have been used to model the active sites in metalloenzymes/proteins for dioxygen activation such as methane monooxygenase (MMO),[30] the oxygen transport protein hemerythrin,[31] the enzyme nitrogenase (Figure 3)[32] and, over the last decade, the iron-storage protein, ferritin.[34] Recently, several manganese-based clusters have been used as models to probe the function of catalase.[33]

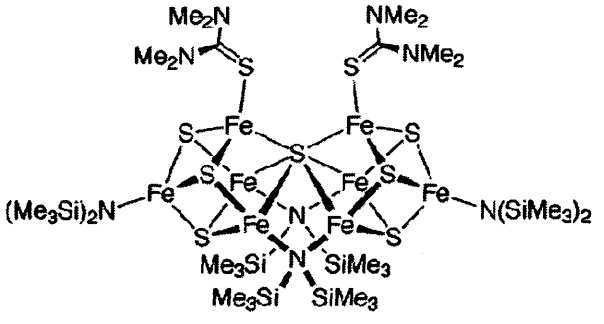

Figure 3 A nitrogen-anion-ligated structural relative of the nitrogenase clusters $[Fe_8S_7(N(SiMe_3)_2)_4(S{=}C(NMe_2)_2)_2]$.[32]

Table 1 SMMs featuring Fe, Ni and Cu ions

Complex	SCM*	S	$-D$ / K	U_{eff} / K	References
$[Fe_{19}O_6(OH)_{14}(heidi)_{10}(H_2O)_{12}]\cdot[Fe_{17}O_4(OH)_{16}(heidi)_8(H_2O)_{12}](NO_3)_4$	No	33/2	–	–	24a,24b
$[Fe_{19}O_6(OH)_{14}(metheidi)_{10}(H_2O)_{12}](NO_3)$	No	33/2	0.02	15.7	24c
$[Fe_{19}O_6(OH)_{14}(etheidi)_{10}(H_2O)_{12}](NO_3)$	No	–	0.03	–	24c
$[Fe_{10}Na_2O_6(OH)_4(chp)_6(PhCO_2)_{10}(H_2O)_2(Me_2CO)_2]$	No	11	–	5.3	24d,24e
$[Fe_9(N_3)_2(MeCO_2)_8\{(2\text{-py})_2CO_2\}_4]$	No	14	–	41	24f
$\{[Fe_8O_2(OH)_{12}(C_6H_{15}N_3)_6]Br_7(H_2O)\}Br$	No	10	0.27	24.5	24g,24h
$[Fe_4(OMe)_6(dpm)_6]$	No	5	0.14	3.5	24i,24j
$[Fe_4(sae)_4(MeOH)_4]$	No	8	0.44	28	24k, 24l
$[Fe_4(5\text{-Br-sae})_4(MeOH)_4]$	No	8	0.46	30	24k,24l
$[Fe_4(3,5\text{-}Cl_2\text{-sae})_4(MeOH)_4]$	No	8	0.47	26	24k,24l
$[Fe_4(thme)_2(dpm)_6]$	No	5	0.31	16.0	24m
$[Fe_2F_9](NEt_4)_3$	No	5	0.22	2.4	24n,24o
$[Fe(ClO_4)_2\{Fe(bpca)_2\}]ClO_4$[a]	Yes	2.5	14.9	27	24p
$[Mn_2(5\text{-MeOsalen})_2Fe(CN)_6][NEt_4]$	Yes	9/2	0.94	14	29l
$[Fe_8Cu_6(Tp)_8(H_2O)_6(CN)_{24}]$	No	7	0.11	5.42	29c
$[(Tp)_2Fe_2(CN)_6Cu(MeOH)\cdot 2MeOH]_n$	Yes	–	–	112.3	29m
$[Ni_{21}(cit)_{12}(OH)_{10}(H_2O)_{10}][Na_2(NMe_4)_{14}]$	No	3	0.32	2.9	23a
$[Ni_{12}(chp)_{12}(MeCO_2)_{12}(H_2O)_6(THF)_6]$	No	12	0.07	9.6	23b,23c,23d
$[Ni_4(C_5H_{11}O_3)_4(MeCN)_4](NO_3)_4$	No	4	0.30	–	23e
$[Ni_4(hmp)_4(Cl)_4(MeOH)_4]$	No	4	0.33	–	23f,23g
$[Ni_4(hmp)_4(N_3)_4(MeOH)_4]$	No	4	0.07	–	23f
$[Ni_4(hmp)_4(Cl)_4(EtOH)_4]$	No	4	0.87	–	23g
$[Ni_4(hmp)_4(Cl)_4(t\text{-BuEtOH})_4]$	No	4	0.88	–	23g
$[Ni_4(hmp)_4(3,3\text{-dimethyl-1-butanol})_4Cl_4]$	No	4	0.48	–	23h
$[Ni_{0.09}Zn_{3.91}(hmp)_4(3,3\text{-dimethyl-1-butanol})_4Cl_4]$	No	3	3.57	0.83	23h
$[Mn_2Ni_2(salpa)_2Cl_2]$	No	6	0.49	25.02	29h
$[Mn_2(5\text{-Br-salen})_2(H_2O)_2Fe(CN)_6][K]$	No	9/2	0.90	17.38	29k
$[Mn_2(saltmen)_2Ni(pao)_2(bipyridyl)_2][ClO_4]_2$	Yes	2	0.16	–	29n
$[Mn_2(5\text{-Cl-saltmen})_2Ni(pao)_2(bipyridyl)_2][ClO_4]_2$	Yes	2	0.14	–	29n
$[Mn_2(5\text{-Br-saltmen})_2Ni(pao)_2(bipyridyl)_2][ClO_4]_2$	Yes	2	0.16	–	29n
$[Mn_2(5\text{-MeO-saltmen})_2Ni(pao)_2(bipyridyl)_2][ClO_4]_2$	Yes	2	0.13	–	29n
$[Mn_2(saltmen)_2Ni(pao)_2(4\text{-py}CO_2)_2][ClO_4]_2$	Yes	3	~ 0.55-3.64	68.0	29o
$[Mn_2(saltmen)_2Ni(pao)_2(4\text{-Bu}^t\text{py})_2][ClO_4]_2$	Yes	3	~ 0.55-3.64	68.3	29o
$[Mn_2(saltmen)_2Ni(pao)_2(N\text{-Meimid})_2][ClO_4]_2$	Yes	3	~ 0.55-3.64	70.9	29o
$[Mn_2(saltmen)_2Ni(pao)_2(py)_2][BF_4]_2$	Yes	3	~ 0.55-3.64	67.6	29o
$[Mn_2(saltmen)_2Ni(pao)_2(py)_2][PF_6]_2$	Yes	3	~ 0.55-3.64	67.8	29o
$[Mn_2(saltmen)_2Ni(pao)_2(py)_2][ReO_4]_2$	Yes	3	~ 0.55-3.64	72.6	29o
$[Mn_2(saltmen)_2Ni(pao)_2(py)_2][ClO_4]_2$	Yes	3	1.73	72	29o,29p
$[(LCu)_2Ln(NO_3)]$[b]	Yes	–	–	28.5	29q
$[Cu(Me_2oxpn)Ni(NO_2)(tmen)](ClO_4)$	–	–	–	–	29r
$[CuL'Tb(hfac)_2]_2$[c]	No	–	–	21	29s

*SCM = Single-Chain Magnet. [a]The spin carriers [Fe(III)/Fe(II)] possess hard-axis/easy-plane anisotropy (Positive D) and an overall net easy axis anisotropy along the alternating chain. [b]H_3L = 2-(Hydroxy-*N*-{2-[(2-hydroxyethyl)amino]ethyl}benzamide). [c]H_3L' = 1-(2-hydroxybenzamido)-2-(2-hydroxy-3-methoxy-benzylidenediamino)ethane.

1.1.4 High Nuclearity Iron-based Complexes

As discussed in section 1.1.3, iron clusters have been largely investigated for the understanding of biological minerals and proteins.[78-80] As a spin-off of these studies the unusual magnetic properties displayed by discrete iron-based paramagnetic clusters has come to the fore.[35,36] As a consequence, research in this area has developed at a considerable rate leading to libraries of high nuclearity iron systems ($\geq \{Fe_{12}\}$). These include a dendrimeric $\{Fe_{24}\}$ nanocluster at ~ 3 nm[39a] and a variety of discrete cluster-based ferric complexes (Table 2). There has also been much research directed towards the development of polymeric networks or nano-scale molecules based on ferrocene units in order to exploit the electronic and redox properties exhibited by the resultant complexes.[37].

Table 2 ($\geq \{Fe_{12}\}$ clusters

Complex	Ref.
$[Fe_{19}O_6(OH)_{14}(heidi)_{10}(H_2O)_{12}]\cdot[Fe_{17}O_4(OH)_{16}(heidi)_8(H_2O)_{12}](NO_3)_4$	24a,24b
$[Fe(OH)(XDK)Fe_2(OMe)_4(MeCO_2)_2]_6$ (Figure 4)	39b
$[Fe_{17}O_{15}(OH)_6(chp)_{12}(phen)_8(OMe)_3]$	39c
$[Fe_{16}MO_{10}(OH)_{10}(PhCO_2)_{20}]$ (M = Mn or Co)	39d
$[Fe_{16}(EtO)_4(PhCO_2)_{16}(Hthme)_{12}](NO_3)_4$	39e
$[Fe(I)(SSiBu^t)]_{14}$	39f
$[Fe_{14}O_6(bta)_6(OMe)_{18}Cl_6]$	39g,39h
$[Fe_{13}O_{14}F_{24}(OMe)_{12}]^{5-}$	39i
$[Fe(OMe)_2(dbm)]_{12}$	39j
$[Fe_2(OMe)_2(proline)]_{12}[ClO_4]_{12}$	39k
$[Fe(Cl)(SSiBu^t)]_{12}$	39f
$[Fe(OMe)_2(bnzH)]_{12}$	39l
$[Fe_{12}O_4(O_2CMe)_8(thme)_2(NH_2\{CH_2\}_2O)_2(L)_6]$	39m

L = 2-{C(Me)=N(CH$_2$)$_2$}-C$_6$H$_4$OH.

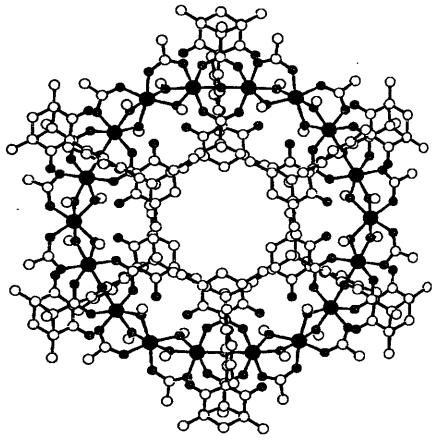

Figure 4 Molecular structure of [Fe-(OH)(XDK)Fe$_2$(OMe)$_4$(MeCO$_2$)$_2$]$_6$.[39b]

1.1.5 Polyoxometallates

Polyoxometallates (POMs)[48a] are electronically versatile inorganic metallo-oxygen-based supramolecular complexes (section 1.1.6) that can be diamagnetic or paramagnetic in nature. This class of molecules have been explored for several potential applications such as in catalysis, medicine, materials science,[48b] building block-based crystal engineering,[49] and Kagomé lattices that exhibit magnetic hysteresis.[50]

A specific type of POMs include the extensively studied polyoxomolybdate 'molybdenum blue' supramolecular nanoclusters $\{Mo_n\}$ (n = 368 – 80). These are built-up from molybdenum-oxide *building blocks* and often result in the formation of elaborate torus shaped or keplerate-based clusters with diameters ranging from ~ 2 – 4 nm. A number of these polyoxomolybdates have large cavities and can incorporate other transition metal ions into their framework (Figure 5).[40] The potential applications of these species are as materials for hydrogenation/dehydrogenation catalysts, superconductors, electrochromic devices and 'smart' windows.[40g]

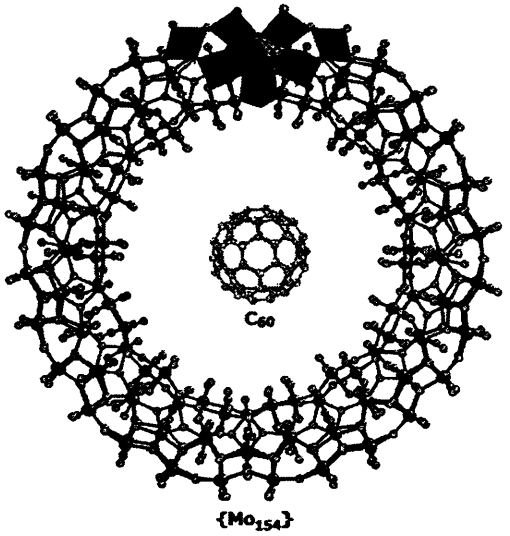

Figure 5 Molecular structure of $[Mo^{VI}_{126}Mo^{V}_{28}O_{462}H_{14}(H_2O)_{70}]^{14-}$ (~ 3.5 nm diameter) with C_{60} incorporated in the cavity for size comparison ($\{Mo_8\}$ building block is highlighted).[40e]

1.1.6 Supramolecular Complexes

The field of supramolecular chemistry is expanding rapidly and current research themes have been focussed on the synthesis of large molecules approaching nanoscale regimes. As with nanomolecules (section 1.1.1), these complexes can be diamagnetic or paramagnetic. Ordered supramolecular complexes termed Metal organic frameworks (MOFs) built-up from rigid component Secondary Building Units (SBUs) have been of considerable interest over the past two decades (Figure 6).[42d,42g] These MOFs are being engineered as supramolecular coordination materials that possess physical properties including non-linear

G

optical (NLO) activity, conductivity, molecular adsorption, catalysis, porosity, thermal stability, magnetic spin-transition[42] and photochemistry.[41]

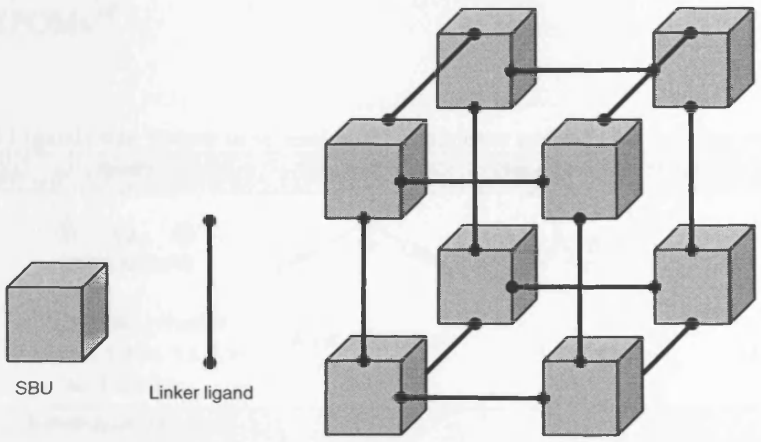

Figure 6 Diagrammatic representation of a hypothetical cubic net-based MOF (portion) built-up from metallo-organic SBUs and organic linker ligands. An SBU is *'a component of a structure common to several frameworks which can rationalize and predict structures'*.[42b]

Metallo-supramolecular complexes predominantly involve the use of multidentate ligands. For example, terpyridine ligands,[43] rigid tris-chelating ligands, ditopic linker ligands (*e.g.*, di-carboxylates),[42c,42d] *m*-benzodihydroxamate,[45] oxalate,[46] formate,[69] porphyrin[47] and pyridazine[51] have been studied as essential components of supramolecular assemblies with potentially useful physical properties. In summary, the field of supramolecular chemistry is vast and often overlaps with other types of novel complexes.

1.1.7 'Speciality' Paramagnetic Complexes

In this section, complexes assembled by the use of well-defined/pre-disposed ligands are described. Firstly, there has been much interest in the azido ligand which often mediates ferromagnetic interactions when coordinated to transition metal ions in the 1,1 end-on (EO) bridging mode (Table 3).[52] A large number of cyano- or hexacyanoferrate-containing complexes have been investigated for their magnetic behaviour as analogues of Prussian blue (Table 3).[53-56] In addition, ligands isoelectronic with azides and cyanides such as, dicyanamides $[N(CN)_2]^-$, have resulted in the synthesis of complexes with novel magnetic properties (Table 3).[57] Other novel functional materials include metal tetrathiafulvene

(TTF)-based magnetic conductors (Table 3),[58] radical-based molecular magnets,[59] radical-based nanowires and lanthanide complexes,[60] lanthanide-based magnetic materials[61] and lanthanide-based POMs.[62]

Table 3 Ligands that feature in several novel complexes and selected bonding modes

Cyano	Azido	Dicyanamido	Hexafluoroacetonate	Alkynyl
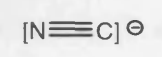	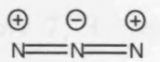	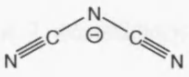		
μ-C, 1,2-μ, μ-C;η^2,	η^1, 1,3-μ EE, 1,1-μ EO, 1,1,3-μ, 1,1,1-μ_3, 1,1,1,1-μ_4, 1,1,3,3-μ_4	1,3,5-μ, 1,5-μ, μ_3, μ_4, 1,1-μ, 1,3-μ	1,3-μ chelate	μ-C, μ_3, μ_4, μ_5, μ-C;η^2
Nitronyl Nitroxide	**2-Anilino-4,6-di-*tert*-butylphenol**	**TCNE**	**TCNQ**	**TTF**
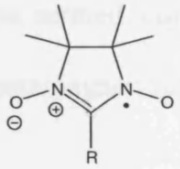	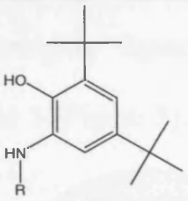	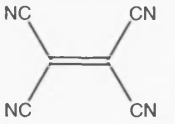	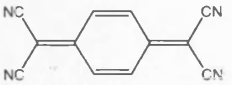	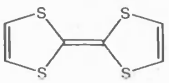
Radical-based	Various radical-based complexes on deprotonation	Radical and anionic salt-based complexes	Radical and anionic salt-based complexes	π-Interaction and cationic salt-based complexes

EE End-End, EO End-on

During the 1970's, nitronyl nitroxide-based ligands were established as spin probes, and have since been used to synthesise complexes with interesting magnetic properties (Table 3).[63] Complexes containing the hexafluoroacetylacetonate (hfac) ligand have also been explored for their interesting magnetic properties.[64] Also, hfac has been used in combination with alkynyl ligands affording complexes with non-linear optical (NLO), conductive, and luminescent properties (Table 3).[65] Molecular-based magnets featuring 7,7,8,8-tetracyano-*p*-quinodimethane (TCNQ) or tetracyanoethylene (TCNE) ligands are well established (Table 3)[66] and magnetic molecules based on phenolate radicals such as *o*-semibenzoquinonato are being investigated for their redox and non-innocent magnetic properties (Table 3).[67] In addition, a variety of spin crossover complexes are being developed by utilising a diverse range of ligands.[68a-p]

1.2 Influencing Cluster Assembly by Ligand Control

The use of a single type of multifunctional ligand or a combination of ligands (*viz.* ligand blend) to aid in the assembly of 3*d* metal ions to give discrete paramagnetic clusters has been the subject of a large number of publications. In general, the design strategy in this approach is based on an inorganic core (1 in Figure 7) surrounded by a hydrophobic periphery (2 in Figure 7). Component 1 constitutes the metallic framework in which an assembly of metal ions is tethered together by the corresponding donor atoms of the ligands while 2 is composed of the organic moieties of the ligands. It is also possible to have a situation where the donor atoms within the core are not connected with 2; these will be termed *core bridging* ligands. The overall combination of 1 and 2 affords the paramagnetic cluster 3 (Figure 7).

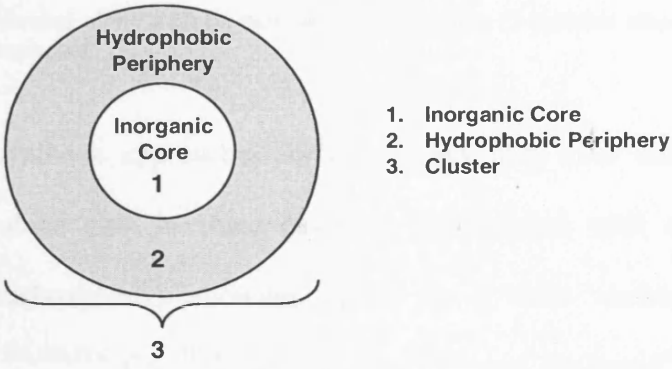

Figure 7 Schematic approach to paramagnetic clusters (3).

In this work, we aim to develop this design strategy by targeting assemblies of soft metal ions with a hydrophobic periphery based on a combination of a range of *N*- and/or *O*-donor ligands that have the capacity to undergo covalent and non-covalent interactions; the inorganic core is composed of Fe(III), Ni(II) or Cu(II) ions and the corresponding donor atoms. The following sections identify the selection of *N*- and/or *O*-based ligands to be employed and outline their track record in cluster synthesis to date. The synthetic strategies for these approaches will be elaborated upon in section 1.3.

1.2.1 2-Pyridinols and 2-Pyridine Alcohols

2-Pyridinols and 2-pyridine alcohols (collectively to be called 2-pyridine alcohols) and their deprotonated derivatives (2-pyridine alkoxides) of generic formula 2-{$(CH_2)_nOH$}-6-X-C_5H_3N and 2-{$(CH_2)_nO$}-6-X-C_5H_3N [X = H, hydrocarbyl, halide; n = 0, 1, 2], respectively (Figure 8) have been widely used in the synthesis of discrete paramagnetic clusters. This can be largely attributed to the diversity of bonding modes exhibited by this bifunctional ligand frame (see Chapter 2).

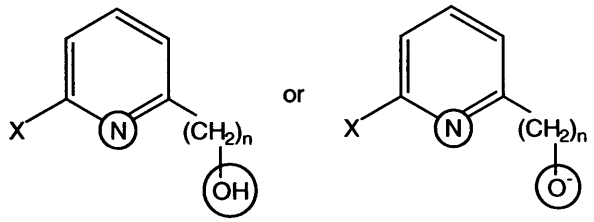

2-{$(CH_2)_nOH$}-6-X-C_5H_3N
[X = H, hydrocarbyl, halide; n = 0, 1, 2]

Figure 8 2-Pyridine alcohol along with its monoanionic derivative (2-pyridine alkoxide); the two potential binding domains are encircled.

Generally, synthetic approaches for cluster assembly have utilised the 2-pyridine alcohol/alkoxide alone and, in some cases, in combination with a co-ligand (mostly monofunctional carboxylates) allowing access to a wide variety of paramagnetic polynuclear Mn-,[27a,27b,71x] Co-,[71h-n] Ni-,[71a-g] Cu-[71o-w] and Fe-based[92a-d] complexes; the structural type being dictated by the precise 2-pyridine alcohol/alkoxide employed.[70] Furthermore, there are several examples of polynuclear SMMs containing 2-pyridine alkoxide ligands including $\{Fe_{10}\}$,[24d,24e] $\{Ni_{21}\}$ (Figure 9),[23b-d] $\{Ni_4\}$ complexes (Table 1)[23f-h] and the manganese-based SMMs; $[Mn_{21}O_{14}(OH)_2(O_2CMe)_{16}(hmp)_8(pic)_2(py)(H_2O)](ClO_4)_4$,[25g] $[Mn_{18}O_{14}(O_2CMe)_{18}(hep)_4(hepH)_2(H_2O)_2](ClO_4)_2$,[25i,25j] $[Mn_{12}O_8(O_2CPh)_8(hmp)_6Cl_4]$,[27a-b] $[Mn_4(hmp)_6(H_2O)_2Br_2]Br_2\cdot 4H_2O$, $[Mn_4(mehmp)_6(H_2O)_2Cl_4]\cdot 4H_2O$,[28s] $[Mn_4(hmp)_6(CH_3CN)_2(H_2O)_4](ClO_4)_4\cdot 2CH_3CN$[28t] and $\{[Mn_4(hmp)_6(H_2O)_2Cl_2](ClO_4)_2\}_n$.[28v]

Given the distinct structural types achievable by using a single type of 2-pyridine alcohol/alkoxide, an investigation into combining two different types of 2-pyridine alcohols/alkoxides offers considerable potential for generating unique structural motifs. Hence, Chapter 2 targets this approach with emphasis placed on the systematic variation of 2-pyridine alcohol/alkoxide methylene chain length (Figure 8, n = 0, 1, 2 or 3).

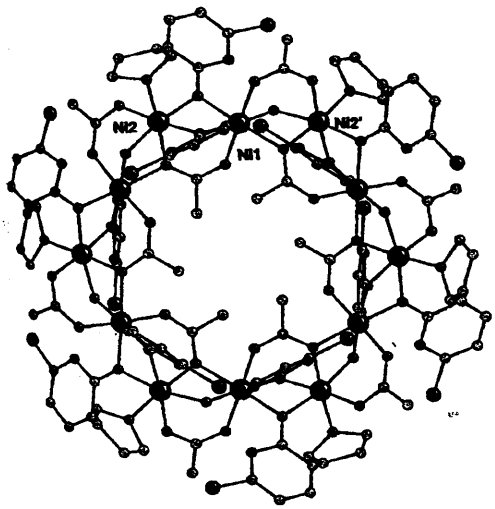

Figure 9 Molecular structure of $[Ni_{12}(chp)_{12}(CH_3CO_2)_{12}(H_2O)_6(THF)_6]$.[23b-d]

1.2.2 Benzilic Acid ($bnzH_2$)

Benzilic acid (diphenylglycolic acid, $bnzH_2$) and its deprotonated forms ($bnzH^-/bnz^{2-}$) (Figure 10), have been widely utilised for several medicinal purposes, physical applications and investigations into biological and enzymatic activity.[72a-c] With regard to its coordination behaviour in small molecules most attention has been placed on metal ions such as V(IV)/V(V),[72b-c] Zn(II),[73h-i] Ln(III),[72d-f] Ti(IV)[72g] and Al(III)[72d] whereby the doubly deprotonated form dominates the coordination chemistry.

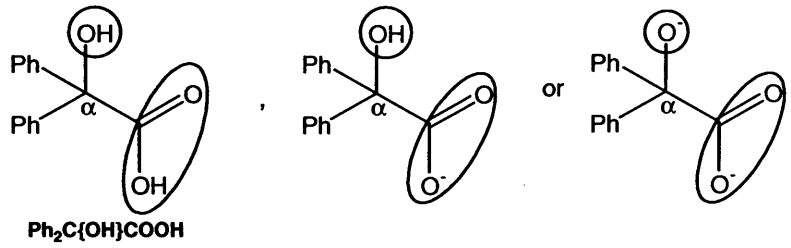

Figure 10 Benzilic acid; the two potential binding domains are encircled.

However, there are only a few examples of benzilate-based monometallic complexes containing electron rich metals such as Ni(II), Co(II) or Cu(II)[73b-i] and more significantly there are just two reports on benzilate-based polymetallic assemblies containing high spin transition metal ions including $[Fe(OMe)_2(bnzH)]_{12}$ (Chapter 3),[391] $[(Me_3tacn)_2Fe_2(O)_2(salox)_2(bnzH)_3Fe_2](ClO_4)$, $[(Me_3tacn)_2Mn_2(O)_2(salox)_2(bnzH)_3Mn_2](ClO_4)$ (Figure 11) and $[(Me_3tacn)_2Fe_2(O)_2(salox)_2(bnzH)_3Mn_2](ClO_4)$.[73a] Nevertheless, it is clear from the work reported to date that benzilate has the capacity to act as a versatile bifunctional ligand for cluster assembly (see potential binding domains in Figure 10). Therefore, in Chapter 3 the use of benzilic acid alone and incorporated into a blend (with a 2-pyridine alcohol) is investigated as a means of accessing paramagnetic clusters.

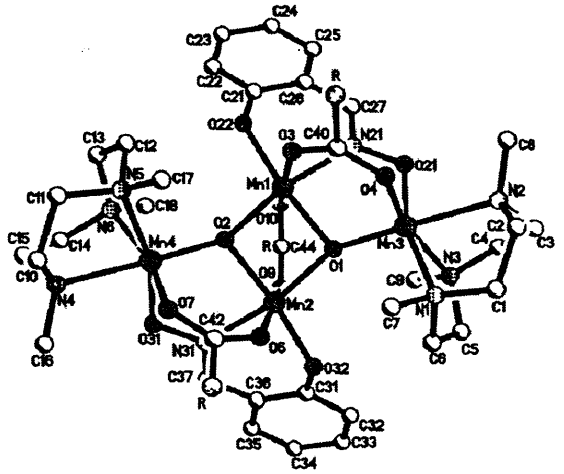

Figure 11 Molecular structure of cationic $[(Me_3tacn)_2Mn_2(O)_2(salox)_2(bnzH)_3Mn_2]^+$.[73a]

1.2.3 Isopthalic Acid (*m*-$BDCH_2$)

Isopthalic acid (*m*-$BDCH_2$) and its deprotonatable (*m*-$BDCH^-$/*m*-BDC^{2-}) forms (Figure 12), have featured in many MOF-based supramolecular complexes (section 1.1.6) *e.g.*, polymeric coordination networks.[42,74,75] Most paramagnetic network-based *m*-BDC-containing complexes involve lanthanides,[74a] Co,[74f,74n] Ni[74n] and Cu ions.[74a-d,74f,74i-j,74o-q,-75a-b,75d] and often involve the use of ligand blends as part of their synthesis [*e.g.*, with solvent molecules,[74n,75d] carboxylates,[74o,75a] bipyridyl,[74q] phenanthroline,[74a,74d,74m,74o

pyridine,[75b,74j,74n] quinoline,[74f] imidazole,[74b-c] 1,4,7-triazacyclononane (tacn),[74p] and bis-/tris-(pyrazoyl)methane[74r]].

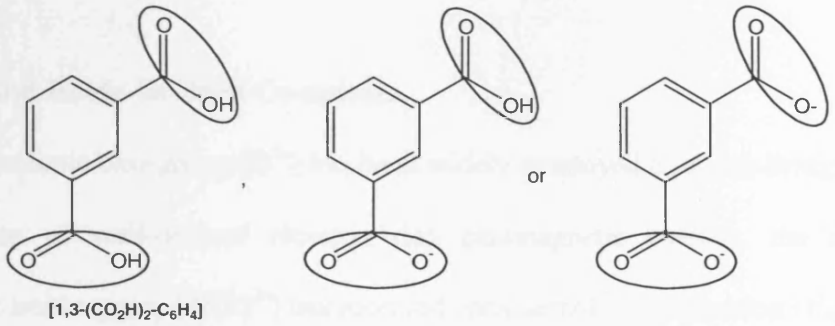

Figure 12 Isopthalic acid; the two potential binding domains are encircled.

However, discrete paramagnetic assemblies featuring isopthalate alone or in combination with another ligand set are scarcer despite the capacity of the ligand to enforce its two donor sites to be disposed at 120° to one another. One notable example is the use of isopthalate in combination with dimethylformamide, methanol, water, pyridine or *p*-methoxypyridine ligands which allow access to discrete bis-copper *m*-BDC (SBU) paddle wheel-based assemblies (Figure 13).[76]

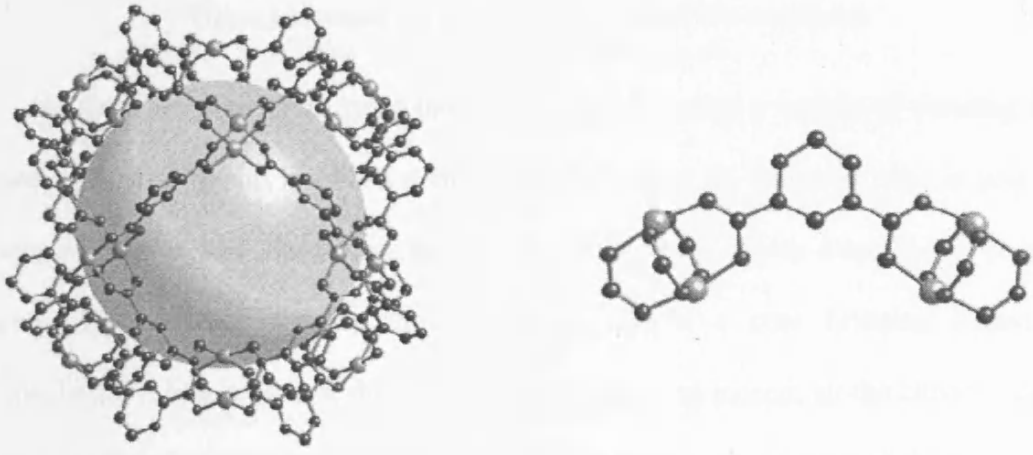

(a) (b)

Figure 13 (a) $[Cu_{24}(m\text{-BDC})_{24}]$ [MOP-1], (b) based on twelve $Cu_2(CO_2)_4$ SBU paddle wheel units .[76a]

Therefore, in Chapter 4 the use of isopthalic acid in combination with a bifunctional ligand that has a track record for the synthesis of discrete clusters was viewed as a means of inhibiting network formation. As a consequence, combinations of isopthalic acid and 2-

pyridine alcohols (section 1.2.1) and a variety of neutral *N,N'*-ligands (section 1.2.5) are systematically evaluated as ligand blends for cluster synthesis.

1.2.4 Oxo- and Imido-Bridged Complexes

While the dianionic oxo-group [O^{2-}] has been widely employed as a core bridging ligand in the formation of well-defined electron rich paramagnetic clusters, the isolobal and isoelectronic imido-group [$N(R)^{2-}$] has received considerably less attention (Figure 14).[81-90] For example, there are numerous examples of first-row transition metal ion-containing clusters with oxo-core bridging ligands [*e.g.*, within SMMs (section 1.1.2), metal oxides commonly found in nature (sections 1.1.3 and 1.1.4) and supramolecular polyoxometallates (section 1.1.5)], while reports of clusters containing the imido-group are limited to a handful of publications and none containing detailed magnetic studies.[81-90]

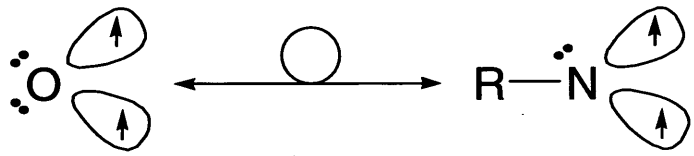

Figure 14 Isolobal and isoelectronic oxo- and imido-substituents.

Nevertheless, the capacity of the imido-group to adopt a variety of bonding modes related to the oxo-group has been demonstrated (Chapter 6). However, due in part to the presence of the imido-substituent, the number of bonding modes displayed is restricted. Moreover, the ability for the imido-group to act as a core bridging ligand (*i.e.*, encapsulated) is less probable, due to steric hinderance and indeed, all the clusters reported to date contain the imido-substituents occupying a peripheral position of the cluster (2 in Figure 7 and Figure 15).

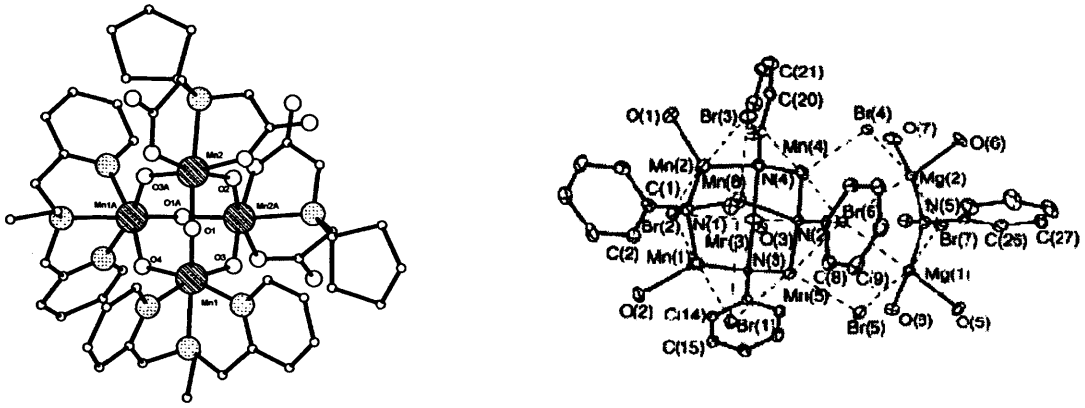

(a) $[Mn_4(\mu_2\text{-}O)_6(bpea)_2(^cpent\text{-}ida)_2]$[93] (b) $\{Mn_6(\mu_3\text{-}NPh)_4Br_3(THF)_4\}\{Mg_2(\mu\text{-}NHPh)_4(\mu\text{-}Br)_3Br_2(THF)_4\}$[90a]

Figure 15 Molecular structures of adamantyl framework-based (a) oxo- $\{[Mn(IV)_4(\mu_2\text{-}O)_6]^{4+}$ core$\}$ [H-atoms omitted][93]and (b) imido- [ORTEP plot 30% probability thermal ellipsoids, H and non N(R) C atoms omitted] $\{[Mn(II)_6(\mu_3\text{-}NPh)_4]^{4+}$ core$\}$ [90a] complexes.

To show the potential of the imido-bridge to mediate magnetism in a similar fashion to an oxo-bridge Murray and Warren *et al.* have carried out a comparative study on related [(Salen)Fe-(μ-X)-Fe(Salen)] [Salen = *N,N'*-ethane-1,2-diylbis(salicyaldiminato)][82a] and $[Me_2NN]Co\text{-}(\mu\text{-}X)_2\text{-}Co[NNMe_2]$ [$NNMe_2$ = *N,N*-bis(2,6-xylyl) substituted β-diketiminato ligand], respectively.[83c] Whether oxo- or imido-bridged, there is little variation in the overall antiferromagnetic behaviour for a particular combination of metals (Table 4) and indeed, the structural parameters for both types of complexes are similar. Interestingly, there is also an example of a binuclear cobalt mixed oxo-/imido- complex (Table 4, last entry) which displays characteristics that are similar to the doubly bridged oxo- or imido-containing di-cobalt complexes.[83c]

In Chapter 5 and 6, complexes containing the oxo- and imido-group, respectively, in combination with a range of bifunctional ligands that have a track record for the formation of discrete clusters are targeted. To a large extent, we have focused on attempts at making complexes containing oxo/carboxylate or imido/carboxylate combinations and in turn examining the sterics and electronics of both the imido-substituent and the carboxylate. In addition, in Chapter 5, we have broadened the range of oxo/L combinations.

Table 4 Metal-oxo, -imido and -oxo/-imido complex comparisons[82a,82c]

Structure	M-X (Å)	M-(μ-X)-M (°)	J (cm^{-1})	μ_{eff} / BM (T_N / K)
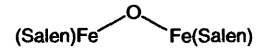	1.78	144.6	– 89	1.8[79]
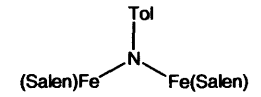	1.87	129.6	– 103	2.7[a]
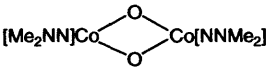	1.79	98.8	–	3.9[a]/4.0[b] (50)[a]
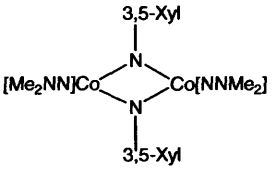	1.98	101.1	–	8.4[a]/8.8[c] (25)[a]
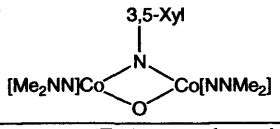	1.78[d] 1.82	100.4[d] 97.6	–	4.6[a]

[a]Néel temperature (T_N)/μ_{eff} was determined from solid-state VT SQUID plots. Magnetic moment (Evan's method) taken in solution state ~ 300 K: [b]toluene-d_8, [c]benzene-d_6. Spin only value expected for 2 × S = 2 [high-spin d^6 {Co(III)}] is 6.93 BM and 2 × S = 5/2 [high-spin d^6 {Fe(III)}] is 8.4 BM (g = 2.00). [d]Oxo-part of complex.

1.2.5 Neutral *N,N'*-Donor Ligands

In the previous sections, potential anionic ligands have been targeted as components for mixed-ligand-containing clusters. As an extension to these studies, the use of a range of neutral *N,N'*-ligands has been identified for their role as potential coordination site fillers rather than as bridging ligands. In particular, aryl-substituted formamidine (HDLF) ligands and the well-studied phen ligand have been targeted for their applications for this function (Figure 16).

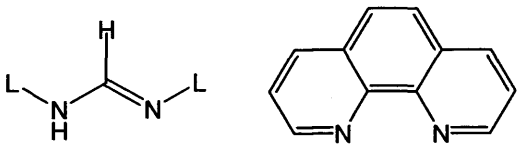

Figure 16 Neutral *N,N'*-ligands to be employed.

While some reports of phen as a coordination site-filler have featured for the assembly of paramagnetic clusters (Figure 17), neutral HDLF unlike its deprotonated derivative[77] has not, to the knowledge of the author, received any attention for this role. Furthermore, the amenability of the HDLF ligand manifold to be readily functionalised offers considerable opportunities to examine the role of steric and electronic properties of

the coordination site-filler on cluster assembly. As a consequence, Chapters 4 and 5 are concerned with the selected use of these ligand frames as components of the ligand blend.

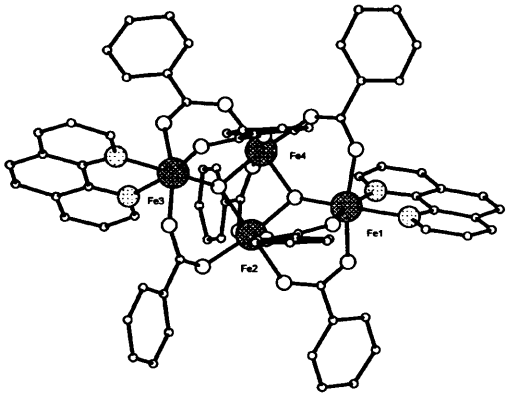

Figure 17 Molecular structure of cationic $[Fe_4O_2(phen)_2(OAc)_7]^+$.[94]

1.3 Aims and Objectives

The previous sections (1.2.1 – 1.2.5) have identified the target *N*- and/or *O*-donor ligands to be employed for the synthesis of paramagnetic complexes in this work. In this section, the synthetic strategies and characterisation methods employed in the forthcoming chapters are outlined. The general synthetic strategy to be employed in the first three parts of this work (Chapters 2, 3 and 4) involves an acid-base equilibrium, whereby a ligand blend composed of ligands with similar pK_a values act as the acid and the metal acetate as the base in the formation of the paramagnetic assembly (Scheme 1). Part of the driving force in this type of synthetic pathway is displacement of acetic acid. An additional base is used to drive the reaction towards completion and can also participate by forming a salt of the complex or by incorporating itself within the complex. Table 5 illustrates the combinations of LH^1 and LH^2 and the high-spin metal ions to be incorporated in Chapters 2, 3 and 4. As a sub-section to each of these chapters the use of a neutral *N,N'*-ligand (L^3) in place of LH^2 is also examined.

$$M(OAc)_2.xH_2O + \underbrace{LH^1 + LH^2}_{\text{LIGAND BLEND}} \underset{\text{mixed solvent system}}{\overset{\text{base}}{\rightleftharpoons}} [M_n] + AcOH$$

Scheme 1 Synthetic strategy for Chapters 2, 3 and 4.

Table 5 Ligand blends to be examined in Chapters 2, 3 and 4

Chapter	Metal ions	LH^1	LH^2	L^3
2	Ni(II),Cu(II)	2-pyridine alcohols	2-pyridine alcohols	–
3	Ni(II), Cu(II)	benzilic acid	2-pyridine alcohols	–
4	Ni(II), Cu(II)	isopthalic acid	2-pyridine alcohols	–
4	Cu(II)	isopthalic acid	–	1,10-*N,N*-phenanthroline
4	Cu(II)	isopthalic acid	–	*N,N'*-arylformamidines

The second general synthetic strategy to be employed in the final parts of this work (Chapters 5 and 6) is directed towards the preparation of mixed ligand Fe(III)-based oxo- and imido-complexes, respectively. The methodology involves a metathesis reaction pathway in which the ligand blend consists of a combination of s-block salts [$M'L^1$ and/or $M'L^2$] which are treated with a $[X_mML]_n$ species (X = halide, L = O, NR). The major driving force of this synthetic pathway is salt elimination (Scheme 2). Table 6 illustrates the combinations of $M'L^1$ and $M'L^2$ to be employed in Chapters 5 and 6. As a sub-section to Chapter 5 the use of a neutral *N,N'*-ligand (L^3) in place of $M'L^2$ is also examined.

$$[X_mML]_n + \underbrace{M'L^1 + M'L^2}_{\text{LIGAND BLEND}} \rightleftharpoons^{\text{solvent(s)}} [M_n] + M'X$$

Scheme 2 Synthetic strategy for Chapters 5 and 6.

Table 6 Ligand blends examined in Chapters 5 and 6

Chapter	L	$M'L^1$	$M'L^2$	L^3
5	O	sodium carboxylates	sodium 2-pyridine alkoxides	–
5	O	sodium carboxylates	–	1,10-*N,N*-phenanthroline
6	NR	sodium/lithium carboxylates	–	–
6	NR	sodium/lithium amides	–	–
6	NR	sodium/lithium amidinates	–	–

As can be seen from above, the work targets Fe(III), Ni(II) or Cu(II) complexes. Compared to the well magnetically studied Mn complexes, these metal ions have not received as much attention even though they possess interesting magnetic attributes including high-spin [Fe(III), S = 5/2], zero-field splitting [Ni(II)] and a variety of coordination geometries [Cu(II)]. To complement the synthetic aspects of the work (Chapter 7) considerable emphasis is placed on examining the magnetochemical and EPR properties of the resultant paramagnetic species, where possible, the solution state properties of a number of the complexes are examined by paramagnetic ^1H NMR studies.

1.4 References

1. (*a*) D. Mulhall, in *Our Molecular Future: how nanotechnology, robotics, genetics, and artificial intelligence will transform our world*, Prometheus Books, New York, USA, 2002., Chapter 2, *Molecular Building Blocks, Molecular Chemistry*, p. 41; (b) *ibid.*, Part 1, *The Molecular Age*, pp. 25 – 139.
2. (*a*) S. Mann, *Chem. Commun.*, 2004, 1; (*b*) D. M. Vriezema, M. Comellas-Aragonès, J. A. A. W. Elemans, J. J. L. M. Cornelissen, A. E. Rowan and J. M. Rowland, *Chem. Rev.*, 2005, **105**, 1445; (*c*) V. F. Slagt, J. N. H. Reek, P. C. J. Karner and P. W. N. M. van Leeuwen, *Angew. Chem. Int. Ed., Engl.*, 2001, **40**, 4271.
3. D. Braga, *Chem. Commun.*, 2003, 2751.
4. O. Ikkala and G. Brinke, *Chem. Commun.*, 2004, 2131.
5. S. Polarz and M. Antonietti, *Chem. Commun.*, 2002, 2593.
6. T. Haeyon, *Chem. Commun.*, 2003, 927.
7. E. M. Barea, V. Fornés, A. Corma, P. Bourges, E. Guillon and V. F. Puntes, *Chem. Commun.*, 2004, 1974.
8. (*a*) Z. Wang, B. Zhang, T. Otsuka, K. Inoue, H. Kobayashi and M. Kurmoo, *Dalton Trans.*, 2004, 2209; (*b*) H. Eckert and M. Ward, *Chem. Mater.*, 2001, **13**, 3059.
9. *See references within* M. Scmittel, H. Ammon, V. Kalsani, A. Wiegrefe and C. Michel, *Chem. Commun.*, 2002, 2566.
10. C.-Y. Su, A. M. Goforth, M. D. Smith, P. J. Pellechia and H.-C. zur Loye, *J. Am. Chem. Soc.*, 2004, **126**, 3576.
11. J. Grunes, J. Zhu and G. A. Zomorjai, *Chem. Commun.*, 2003, 2257.
12. G. Ozin, *Chem. Commun.*, 2003, 2639.
13. D. M. Guldi and M. Prato, *Chem. Commun.*, 2004, 2517.
14. *See entire issue of Dalton Trans.*, 2004, 2979 – 3152.
15. V. Balzini, A. Credi and M. Venturi, *Chem. Eur. J.*, 2002, **8**, 5525.
16. S. J. Bryne, S. A. Corr, Y. K. Gun'ko, J. M. Kelly, D. F. Broughman and S. Ghosh, *Chem. Commun.*, 2004, 2560.
17. J. L. Atwood, L. J. Barbour, S. J. Delgarno, M. J. Hardie, C. L. Raston and H. R. Webb, *J. Am. Chem. Soc.*, 2004, **126**, 13170.
18. H. Gu, P.-L. Ho, K. W. Tsang, C.-W. Yu and B. Zhu, *Chem. Commun.*, 2003, 1966.
19. D. Pan, J. L. Turner and K. L. Wooley, *Chem. Commun.*, 2003, 2400.
20. K. Matsuura, T. Yamashita, Y. Igaami and N. Kimizuka, *Chem. Commun.*, 2003, 376.
21. M. C. Jimenez-Molero, C. Dietrich-Buchecker and J.-P. Sauvage, *Chem. Commun.*, 2003, 1613.
22. R. Sessoli and D. Gatteschi, *Angew. Chem. Int. Ed., Engl.*, 2003, **42**, 268.
23. *Various SMMs* (*a*) S. T. Ochsenbein, M. Murrie, E. Rusanov, H. Stœckli-Evans, C. Sekine and H.-U. Güdel, *Inorg. Chem.*, 2002, **41**, 5133; (*b*) A. J. Blake, C. M. Grant, S. Parsons, J. M. Rawson and R. E. P. Winpenny, *J. Chem. Soc., Chem. Commun.*, 1994, 2363; (*c*) C. Caddiou, M. Murrie, C. Paulsen, V. Villar, W. Wernsdorfer and R. E. P. Winpenny, *Chem. Commun.*, 2001, 2666; (*d*) H. Andres, R. Basler, A. J. Blake, C. Cadiou, G. Chaboussant, C. M. Grant, H.-U. Güdel, M. Murrie, S. Parsons, C. Paulsen, F. Semadini, V. Villar, W. Wernsdorfer and R. E. P. Winpenny, *Chem. Eur. J.*, 2002, **8**, 4867; (*e*) M. Moragues-Cánovas, M. Helliwell, L. Ricard, E. Rivière, W. Wernsdorfer, E. Brechin and T. Mallah, *E. J. Inorg. Chem.*, 2004, 2219; (*f*) A. Escuer, M. Font-Bardía, S. B. Kumar, X. Solans and R. Vicente, *Polyhedron*, 1999, **18**, 909; (*g*) E.-C. Yang, W. Wernsdorfer, S. Hill, R. S. Edwards, M. Nakano, S. Meccagnano, L. N. Zakharov, A. L. Rheingold, G. Christou and D. N. Hendrickson, *Polyhedron*, 2003, **22**, 1727; (*h*) E.-C. Yang, C. Kirman, J. Lawrence, L. N. Zakharov, A. L. Rheingold, S. Hill and D. N. Hendrickson, *Inorg. Chem.*, 2005, **44**, 3827; (*i*) Y. Song, P, Zhang, X.-M. Ren, X.-F. Shen, Y.-Z. Li and X.-Z. You, *J. Am. Chem. Soc.*, 2005, **127**, 3708; (*j*) M. Murrie, S. J. Teat, H. Stœckli-Evans and H.-U. Güdel, *Angew. Chem. Int. Ed., Engl.*, 2003, **42**, 4653; (*k*) S. L. Castro, Z. Sun, C. M. Grant, J. C.

Bollinger, D. N. Hendrickson and G. Christou, *J. Am. Chem. Soc.*, 1998, **120**, 2365; (*l*) S. Kurusawa, G. Zhou, H. Morikawa and N. Koga, *J. Am. Chem. Soc.*, 2003, **125**, 13676; (*m*) S. Kanegawa, S. Karasawa, M. Nakano and N. Koga, *Chem. Commun.*, 2004, 1750; (*n*) N. Ishikawa, M. Sugita, N. Tanaka, T. Ishikawa, S.-y. Koshihara and Y. Kaizu, *Inorg. Chem.*, 2004, **43**, 5498; (*o*) N. Ishikawa, M. Sugita and W. Wernsdorfer, *J. Am. Chem. Soc.*, 2005, **127**, 3650.

24. *Fe-based SMMs* (*a*) A. K. Powell, S. L. Heath, D. Gatteschi, L. Pardi, R. Sessoli, G. Spina, F. D. Giallo and F. Pieralli, *J. Am. Chem. Soc.*, 1995, **117**, 2491; (*b*) W. Scmitt, M. Murugesu, J. C. Goodwin, J. P. Hill, A. Mandel, R. Balla, C. E. Anson, S. L. Heath and A. K. Powell, *Polyhedron*, 2001, **20**, 1687; (*c*) J. C. Goodwin, R. Sessoli, D. Gatteschi, W. Wernsdorfer, A. K. Powell and S. L. Heath, *J. Chem. Soc., Dalton Trans.*, 2000, 1835; (*d*) C. Benelli, S. Parsons, G. A. Solan and R. E. P. Winpenny, *Angew. Chem. Int. Ed., Engl.*, 1996, **35**, 1825; (*e*) C. Benelli, J. Cano, Y. Journaux, R. Sessoli, G. A. Solan and R. E. P. Winpenny, Inorg. Chem., 2001, 40, 188; (*f*) A. K. Boudalis, B. Donnadieu, V. Nastopoulos, J. M. Clemente-Juan, A. Mari, Y. Sanakis, J.-P. Tuchagues and S. P. Perlepes, *Angew. Chem. Int. Ed., Engl.*, 2004, **43**, 2266; (*g*) K. Wieghardt, K. Pohl, I. Jibil and G. Huttner, *Angew. Chem. Int. Ed., Engl.*, 1984, **23**, 77; (*h*) C. Sangregorio, T. Ohm, C. Paulsen, R. Sessoli and D. Gatteschi, *Phys. Rev. Lett.*, 1997, **78**, 4645; (*i*) A. L. Barra, A. Caneschi, A. Cornia, F. F. de Biani, D. Gatteschi, C. Sangregorio, R. Sessoli and L. Sorace, *J. Am. Chem. Soc.*, 1999, **121**, 5302; (*j*) A. Bouwen, A. Caneschi, D. Gatteschi, E. Goovaerts, D. Schoemaker, L. Sorace and M. Stefan, *J. Phys. Chem., Sect. B*, 2001, **105**, 2658; (*k*) H. Oshio, N. Hoshino, T. Ito and M. Nakano, *J. Am. Chem. Soc.*, 2004, **126**, 8805; (*l*) H. Oshio, N. Hoshino and T. Ito, *J. Am. Chem. Soc.*, 2000, **122**, 12602; (*m*) A. Caneschi, A. C. Fabretti, P. Garrisi, C. Mortalò, D. Bonacchi, D. Gatteschi, R. Sessoli, L. Sorace, W. Wernsdorfer and A.-L. Barra, *Angew. Chem. Int. Ed., Engl.*, 2004, 43, 1136; (*n*) R. Schenker, M. N. Leuenberger, G. Chaboussant, H.-U. Güdel and D. Loss, *Chem. Phys. Lett.*, 2002, **358**, 413; (*o*) R. Schenker, H. Weihe and H.-U. Güdel, *Inorg. Chem.*, 2001, **40**, 4319; (*p*) T. Kajiwara, M. Nakano, Y. Kaneko, S. Takaishi, T. Ito, M. Yamashita, A. Igashira-Kamiyama, H. Nojiri, Y. Ono and N. Kojima, *J. Am. Chem. Soc.*, 2005, **127**, 10150.

25. *SMMs > {Mn_{12}}* (*a*) A. J. Tasiopoulos, A. Vinslava, W. Wernsdorfer, K. A. Abboud and G. Christou, *Angew. Chem. Int. Ed., Engl.*, 2004, **43**, 2117; (*b*) M. Soler, E. Rumberger, K. Folting, D. N. Hendrickson and G. Christou, *Polyhedron*, 2001, **20**, 1365; (*c*) M. Soler, W. Wernsdorfer, K. Folting, M. Pink and G. Christou, *J. Am. Chem. Soc.*, 2004, **126**, 2156; (*d*) C. Dendrinou-Samara, M. Alexiou, C. M. Zaleski, J. W. Kampf, M. L. Kirk, D. P. Kessissoglou and V. S. Pecoraro, *Angew. Chem. Int. Ed., Engl.*, 2003, **42**, 3736; (*e*) M. Murugesu, M. Habrych, W. Werndorfer, K. A. Abboud and G. Christou, *J. Am. Chem. Soc.*, 2004, **126**, 4766; (*f*) M. Murugesu, J. Raftery, W. Wernsdorfer, G. Christou and E. K. Brechin, *Inorg. Chem.*, 2004, **43**, 4203; (*g*) E. C. Sañudo, W. Wernsdorfer, K. A. Abboud and G. Christou, *Inorg. Chem.*, 2004, **43**, 4137; (*h*) J. T. Brockman, J. C. Huffman and G. Christou, *Angew. Chem. Int. Ed., Engl.*, 2002, **41**, 2506; (*i*) E. K. Brechin, C. Boskovic, W. Wernsdorfer, J. Yoo, A. Yamaguchi, E. C. Sañudo, T. R. Concolino, A. L. Rheingold, H. Ishimoto, D. N. Hendrickson and G. Christou, *J. Am. Chem. Soc.*, 2002, **124**, 9710; (*j*) E. K. Brechin, E. C. Sañudo, W. Wernsdorfer, C. Boskovic, J. Yoo, D. N. Hendrickson, A. Yamaguchi, H. Ishimoto, T. E. Concolino, A. L. Rheingold and G. Christou, *Inorg. Chem.*, 2005, **44**, 502; (*k*) D. J. Price, S. R. Batten, B. Moubaraki and K. S. Murray, *Chem. Commun.*, 2002, 762; (*l*) P. King, W. Wernsdorfer, K. A. Abboud and G. Christou, *Inorg. Chem.*, 2004, **43**, 7315.

26. *SMMs {Mn_{12}}* (*a*) R. Sessoli, H.-L. Tsai, A. R. Schake, S. Wang, J. B. Vincent, K. Folting, D. Gatteschi, G. Christou and D. N. Hendrickson, *J. Am. Chem. Soc.*, 1993, **115**, 1804; (*b*) A. Caneschi, D. Gatteschi, R. Sessoli, A. L. Barra, L.C. Brunel and M. Guillot, *J. Am. Chem. Soc.*, 1993, **113**, 5873; (*c*) A. L. Barra, A. Caneschi, A. Caneschi and R. Sessoli, *J. Am. Chem. Soc.*, 1995, **117**, 8855; (*d*) R. Sessoli, D. Gatteschi, A. Caneschi and M. A. Novak, *Nature*, 1993, **365**, 141; (*e*) A. R. Schake, H.-L. Tsai, N. de Vries, R. J. Webb, K. Folting, D. N. Hendrickson and G. Christou, *J. Chem. Soc., Chem. Commun.*, 1992, 181; (*f*) D. Ruiz-Molina, P. Gerbier, E. Rumberger, D. A. Amabilino, I. A. Guzei, K. Folting, J. C. Huffman, A. Rheingold, G. Christou, J. Veciana and D. N. Hendrickson, *J. Mater. Chem.*, 2002, **12**,

1152; (*g*) M. Soler, W. Wernsdorfer, Z. Sun, J. C. Huffman, D. N. Hendrickson and G. Christou, *Chem. Commun.*, 2003, 2672; (*h*) C. Boskovic, M. Pink, J. C. Huffman, D. N. Hendrickson and G. Christou, *J. Am. Chem. Soc.*, 2001, **123**, 9914; (*i*) P. Artus, C. Boskovic, J. Yoo, W. E. Streib, L.-C. Brunel, D. N. Hendrickson and G. Christou, *Inorg. Chem.*, 2001, **40**, 4199; (*j*) T. Koroda-Sowa, M. Lam, A. L. Rheingold, C. Frommen, W. M. Reiff, M. Nakano, J. Yoo, A. L. Maniero, L.-C. Brunel, G. Christou and D. N. Hendrickson, *Inorg. Chem.*, 2001, **40**, 6469; (*k*) M. Soler, P. Artus, K. Folting, J. C. Huffman, D. N. Hendrickson and G. Christou, *Inorg. Chem.*, 2001, **40**, 4902; (*l*) S. M. J. Aubin, Z. Sun, H. J. Eppley, E. M. Rumberger, I. A. Guzei, K. Folting, P. K. Gantzel, A. L. Rheingold, G. Christou and D. N. Hendrickson, *Inorg. Chem.*, 2001, **40**, 2127; (*m*) A. Cornia, A. C. Fabretti, M. Pacchioni, L. Zobbi, D. Bonacchi, A. Caneschi, D. Gatteschi, R. Biagi, U. D. Pennino, V. D. Renzi, L. Gurevich and H. S. J. Van der Zant, *Angew. Chem. Int. Ed., Engl.*, 2003, **42**, 1645; (*n*) S. M. J. Aubin, Z. Sun, L. Pardi, J. Krzystek, K. Folting, L.-C. Brunel, A. L. Rheingold, G. Christou and D. N. Hendrickson, *Inorg. Chem.*, 1999, **38**, 5329; (*o*) H. J. Eppley, H.-L. Tsai, N. de Vries, K. Folting, G. Christou and D. N. Hendrickson, *J. Am. Chem. Soc.*, 1995, **117**, 301; (*p*) E. Coronado, M. Feliz, A. Forment-Aliaga, C. J. Gómez-García, R. Llusar and F. M. Romero, *Inorg. Chem.*, 2001, **40**, 6084; (*q*) A. Forment-Aliaga, E. Coronado, M. Feliz, A. Gaita-Ariño, R. Llusar and F. M. Romero, *Inorg. Chem.*, 2003, **42**, 8019; (*r*) E. Coronado, A. Forment-Aliaga, A. Gaita-Ariño, C. Giménez-Saiz, F. M. Romero and W. Wernsdorfer, *Angew. Chem. Int. Ed., Engl.*, 2004, **43**, 6152; (*s*) Y. Miyazaki, A. Bhattacharjee, M. Nakano, K. Saito, S. M. J. Aubin, H. J. Eppley, G. Christou, D. N. Hendrickson and M. Sorai, *Inorg. Chem.*, 2001, **40**, 6632; (*t*) E. J. L. McInnes, E. Pidcock, V. S. Oganesyan, M. R. Cheesman, A. K. Powell and A. J. Thompson, *J. Am. Chem. Soc.*, 2002, **124**, 9219; (*u*) M. Soler, W. Wernsdorfer, K. A. Abboud, J. C. Huffman, E. R. Davidson, D. N. Hendrickson and G. Christou, *J. Am. Chem. Soc.*, 2003, **125**, 3576; (*v*) A. J. Tasiopoulos, W. Wernsdorfer, K. A. Abboud and G. Christou, , *Angew. Chem. Int. Ed., Engl.*, 2004, **43**, 6338; (*w*) H. Zhao, C. P. Berlinguette, J. Basca, A. V. Prosvirin, J. K. Bera, S. E. Tichy, E. J. Schelter and K. R. Dunbar, *Inorg. Chem.*, 2004, **43**, 1359; (*x*) G.-Q. Bian, T. Kuroda-Sowa, H. Konaka, M. Hatano, M. Maekawa, M. Munakata, H. Miyasaka and M. Yamashita, *Inorg. Chem.*, 2004, **43**, 4790; (*y*) N. E. Chakov, W. Wernsdorfer, K. A. Abboud, D. N. Hendrickson and G. Christou, *Dalton Trans.*, 2004, 2243.

27. *Other SMMs {Mn_{12}}* (*a*) C. Boskovic, E. K. Brechin, W. E. Streib, K. Folting, D. N. Hendrickson and G. Christou, *Chem. Commun.*, 2001, 467; (*b*) C. Boskovic, E. K. Brechin, W. E. Streib, K. Folting, J. C. Bollinger, D. N. Hendrickson and G. Christou, *J. Am. Chem. Soc.*, 2002, **124**, 3725; (*c*) G. Rajaraman, M. Murugesu, E. C. Sañudo, M. Soler, W. Wernsdorfer, M. Helliwell, C. Muryn, J. Raftery, S. J. Teat, G. Christou and E. K. Brechin, *J. Am. Chem. Soc.*, 2004, **126**, 15445; (*d*) E. M. Rumberger, S. J. Shah, C. C. Beedle, L. N. Zakharov, A. L. Rheingold and D. N. Hendrickson, *Inorg. Chem.*, 2005, **44**, 2742.

28. *SMMs < {Mn_{12}}* (*a*) E. K. Brechin, M. Soler, J. Davidson, D. N. Hendrickson, S. Parsons and G. Christou, *Chem. Commun.*, 2002, 2252; (*b*) C. Boskovic, W. Wernsdorfer, K. Folting, J. C. Huffman, D. N. Hendrickson and G. Christou, *Inorg. Chem.*, 2002, **41**, 5107; (*c*) S. Piligkos, G. Rajaraman, M. Soler, N. Kirchner, J. van Slageren, R. Bircher, S. Parsons, H.-U. Güdel, J. Kortus, W. Wernsdorfer, G. Christou and E. K. Brechin, *J. Am. Chem. Soc.*, 2005, **127**, 5572. (*d*) M. Soler, G. Christou, M. Helliwell, S. J. Teat and W. Wernsdorfer, *Chem. Commun.*, 2003, 1276; (*e*) N. E. Chakov, W. Wernsdorfer, K. A. Abboud and G. Christou, *Inorg. Chem.*, 2004, **43**, 5919; (*f*) S. Koizumi, M. Nihei, M. Nakano and H. Oshio, *Inorg. Chem.*, 2005, **44**, 1208; (*g*) C. J. Milios, C. P. Raptopoulou, A. Terzis, F. Lloret, R. Vicente, S. P. Perlepes and A. Escuer, *Angew. Chem. Int. Ed., Engl.*, 2004, **43**, 210; (*h*) A. V. Palii, S. M. Ostrovsky, S. I. Klokishner, B. S. Tsukerblat, C. P. Berlinguette, K. R. Dunbar and J. R. Galán-Mascarós, *J. Am. Chem. Soc*, 2004, **126**, 16860; (*i*) C. P. Berliguette, D. Vaughn, C. Cañada-Vilalta, J. R. Galán-Mascarós and K. R. Dunbar, *Angew. Chem. Int. Ed., Engl.*, 2003, **42**, 1523; (*j*) S. M. J. Aubin, N. R. Dilley, L. Pardi, J. Krzystek, M. W. Wemple, L.-C. Brunel, M. B. Maple, G. Christou and D. N. Hendrickson, *J. Am. Chem. Soc.*, 1998, **120**, 4991; (*k*) H. Andres, R. Basler, H.-U. Güdel, G. Aromí, G. Christou, H. Büttner and B. Rufflé, *J. Am. Chem. Soc.*, 2000, **122**, 12469; (*l*) S. Wang, H.-L. Tsai, E. Libby, K. Folting, W. E. Streib,

D. N. Hendrickson and G. Christou, *Inorg. Chem.*, 1996, **35**, 7578; (*m*) S. M. J. Aubin, M. W. Wemple, D. M. Adams, H.-L. Tsai, G. Christou and D. N. Hendrickson, *J. Am. Chem. Soc.*, 1996, **118**, 7746; (*n*) G. Aromí, S. Bhaduri, P. Artús, K. Folting and G. Christou, *Inorg. Chem.*, 2002, **41**, 805; (*o*) J. Yoo, E. K. Brechin, A. Yamaguchi, M. Nakano, J. C. Huffman, A. L. Maniero, L.-C. Brunel, K. Awaga, H. Ishimoto, G. Christou and D. N. Hendrickson, *Inorg. Chem.*, 2000, **39**, 3615; (*p*) B. Albela, M. S. E. Fallah, J. Ribas, K. Folting, G. Christou and D. N. Hendrickson, *Inorg. Chem.*, 2001, **40**, 1037; (*q*) C. Boskovic, R. Bircher, P. L. W. Treganna-Piggott, H.-U. Güdel, C. Paulsen, W. Wernsdorfer, A.-L. Barra, E. Khatsko, A. Neels and H. Stœckli-Evans, *J. Am. Chem. Soc.*, 2003, **125**, 14046; (*r*) N. Aliaga-Alcalde, R. S. Edwards, S. O. Hill, W. Wernsdorfer, K. Folting and G. Christou, *J. Am. Chem. Soc.*, 2004, **126**, 12503; (*s*) J. Yoo, A. Yamaguchi, M. Nakano, J. Krzystek, W. E. Streib, L.-C. Brunel, H. Ishimoto, G. Christou and D. N. Hendrickson, *Inorg. Chem.*, 2001, **40**, 4604; (*t*) L. Lecren, Y.-G. Li, W. Wernsdorfer, O. Roubeau, H. Miyasaka and R. Clérac, *Inorg. Chem. Commun.*, 2005, **8**, 626; (*u*) L. M. Wittick, K. S. Murray, B. Moubaraki, S. R. Batten, L. Spiccia and K. J. Berry, *Dalton Trans.*, 2004, 1003; (*v*) J. Yoo, W. Wernsdorfer, E.-C. Yang, M. Nakano, A. Rheingold and D. N. Hendrickson, *Inorg. Chem.*, 2005, **44**, 3377; (*w*) N. Shaikh, A. Panja, S. Goswami, P. Banerjee, P. Vojtíšek, Y.-Z. Zhang, G. Su and S. Gao, *Inorg. Chem.*, 2004, **43**, 849; (*x*) R. T. W. Scott, S. Parsons, M. Murugesu, W. Wernsdorfer, G. Christou and E. K. Brechin, *Chem. Commun.*, 2005, 2083, (*y*) H. Miyasaka, R. Clérac, W. Wernsdorfer, L. Lecren, C. Bonhomme, K. Sugiura and M. Yamashita, *Angew. Chem. Int. Ed., Engl.*, 2004, **43**, 2801.

29. *SMMs mixed metal* (*a*) Y. Song, P. Zhang, X.-M. Ren, X.-F. Shen, Y.-Z. Li and X.-Z. You, *J. Am. Chem. Soc.*, 2005, **127**, 3708; (*b*) N. Ishikawa, M. Sugita and W. Wernsdorfer, *J. Am. Chem. Soc.*, 2005, **127**, 3650; (*c*) S. Wang, J.-L. Zuo, H.-C. Zhou, H.-J. Choi, Y. Ke, J. R. Long and X.-Z. You, *Angew. Chem. Int. Ed., Engl.*, 2004, **43**, 5940; (*d*) A. Mishra, W. Wernsdorfer, K. A. Abboud and G. Christou, *J. Am. Chem. Soc.*, 2004, **126**, 15648; (*e*) C. M. Zaleski, E. C. Depperman, J. W. Kampf, M. L. Kirk and V. L. Pecoraro, *Angew. Chem. Int. Ed., Engl.*, 2004, **43**, 3912; (*f*) A. J. Tasiopoulos, W. Wernsdorfer, B. Moulton, M. J. Zawarotko and G. Christou, *J. Am. Chem. Soc.*, 2003, **125**, 15274; (*g*) E. J. Schelter, A. V. Prosvirin and K. R. Dunbar, *J. Am. Chem. Soc.*, 2004, **126**, 15004; (*h*) H. Oshio, M. Nihei, S. Koizumi, T. Shiga, H. Nojiri, M. Nakano, N. Shirikawa and M. Akatsu, *J. Am. Chem. Soc.*, 2005, **127**, 4568; (*i*) A. Mishra, W. Wernsdorfer, S. Parsons, G. Christou and E. K. Brechin, *Chem. Commun.*, 2005, 2086; (*j*) T. Yamase, E. Ishikawa, K. Fukaya, H. Nojiri, T. Tamaguchi and T. Atake, *Inorg. Chem.*, 2004, **43**, 8150; (*k*) H. J. Choi, J. J. Sokol and J. R. Long, *Inorg. Chem.*, 2004, **43**, 1606; (*l*) M. Ferbinteanu, H. Miyasaka, W. Wernsdorfer, K. Nakata, K. Sigiura, M. Yamashita, C. Coulon and R. Clérac, *J. Am. Chem. Soc.*, 2005, **127**, 3090; (*m*) S. Wang, J.-L. Zuo, S. Gao, Y. Song, H.-C. Zhou, Y.-Z. Zhang and X.-Z. You, *J. Am. Chem. Soc.*, 2004, **126**, 8900; (*n*) H. Miyasaka, T. Nezu, K. Sugimoto, K. Sugiura, M. Yamashita and R. Clérac, *Inorg. Chem.*, 2004, **43**, 5486; (*o*) H. Miyasaka, R. Clérac, K. Muzushima, K. Sugiura, M. Yamashita, W. Wernsdorfer, and C. Coulon, *Inorg. Chem.*, 2003, **42**, 8203; (*p*) R. Clérac, H. Miyasaka, M. Yamashita and C. Coulon, *J. Am. Chem. Soc.*, 2002, **124**, 12837; (*q*) J.-P. Costes, J. M. Clemente-Juan, F. Dahan and J. Milon, *Inorg. Chem.*, 2004, **43**, 8200; (*r*) J. Tercero, C. Diaz, J. Ribas, J. Mahía and M. Maestro, *Chem. Commun.*, 2002, 364; (*s*) S. Osa, T. Kido, N. Matsumoto, N. Re, A. Pochaba and J. Mrozinski, *J. Am. Chem. Soc.*, 2004, **126**, 420; (*t*) J. K. Sokol, A. G. Hee and J. R. Long, *J. Am. Chem. Soc.*, 2002, **124**, 7656.

30. (*a*) W. B. Tolman and L. Que, Jr., *J. Chem. Soc., Dalton Trans.*, 2002, 653; (*b*) D. Lee and S. J. Lippard, *Inorg. Chem.*, 2002, **41**, 827; (*c*) S. Yoo and S. J. Lippard, *J. Am. Chem. Soc.*, 2004, **126**, 2666; (*c*) S. V. Kryatov, S. Taktak, I. V. Korendovych, E. V. Rybak-Akimova, J. Kaizer, S. Torelli, X. Shan, S. Mandal, V. L. MacMurdo, M. Mairata, I. Payeras and L. Que, Jr., *Inorg. Chem.*, 2005, **44**, 65.

31. J. Mukherjee, V. Balamurugan, R. Gupta and R. Mukherjee, *Dalton Trans.*, 2003, 3686.

32. S. C. Lee and R. H. Holm, *Chem. Rev.*, 2004, **104**, 1135.

33. A. J. Wu, J. E. Penner-Hahn and V. L. Pecararo, *Chem. Rev.*, 2004, **104**, 903.

34. (*a*) K. L. Taft, G. C. Papeafthymiou and S. J. Lippard, *Science*, 1993, **259**, 1302; (*b*) S. Gider, D. D. Awschalom, T. Douglas, S. Man and M. Chaparala, *Science*, 1995, **268**, 77; (*c*) S. A. Malone, A. Lewin, M. A. Kilic, D. A. Svistunenko, C. E. Cooper, M. T. Wilson, N. E. Le Brun, S. Spiro and G. R. Moore, *J. Am. Chem. Soc.*, 2004, **126**, 496; (*d*) R. Naikjima, M. Tsuruta, M. Higuchi and K. Yamamoto, *J. Am. Chem. Soc.*, 2004, **126**, 1630.

35. (*a*) D. Gatteschi, A. Caneschi, R. Sessoli and A. Cornia, *Chem. Soc. Rev.*, 1996, 101; (*b*) J.-P. Jolivet, C. Chanéac and E. Tronc, *Chem. Commun.*, 2004, 481.

36. (*a*) F. X. Redl, C. T. Black, G. C. Papafthymiou, R. S. Sandstrom, M. Yin, C. B. Murray and S. P. O'Brien, *J. Am. Chem. Soc.*, 2004, **126**, 14538; (*b*) J. Cheon, N.-J. Kang, S.-M. Lee, J.-H. Lee, J.-H. Yoon and S. J. Oh, *J. Am. Chem. Soc.*, 2004, **126**, 1950; (*c*) C. Xu, K. Xu, H. Gu, R. Zheng, H. Liu, X. Zhang, Z. Guo and B. Xu, *J. Am. Chem. Soc.*, 2004, **126**, 9938; (*d*) X. Gao, K. M. K. Yu, K. Y. Tam and S. C. Tsang, *Chem. Commun.*, 2003, 2998; (*e*) J.-P. Lellouche, N. Perlman, A. Joseph, S. Govindaraji, L. Buzhansky, A. Yakir and I. Bruce, *Chem. Commun.*, 2004, 560; (*f*) W. W. Yu, J. C. Faulkner, C. T. Yavuz and V. L. Covin, *Chem. Commun.*, 2004, 2306; (*g*) J. Geng, D. A. Jefferson and B. F.G. Johnson, *Chem. Commun.*, 2004, 2442.

37. (*a*) D. Braga, M. Polito, M. Bracaccini, D. D'Addario, E. Tagliavini, L. Sturba and F. Grepioni, Organometallics, 2003, **22**, 2142; (*b*) H. Hou, Y. Fan and Y. Qiao, *Inorg. Chem.*, 2004, **43**, 4767; (*c*) R. Horikoshi, C. Nambu and T. Mochida, *New J. Chem.*, 2004, **28**, 26; (*d*) G. Li, H. Hou, L. Li, X. Meng, Y. Fan and Y. Zhu, *Inorg. Chem.*, 2003, **42**, 428; (*e*) *Bisnitronyl nitroxide radical ferrocene-manganese copolymer* C. Sporer, K. Wurst, D. B. Amabilino, D. Ruiz-Milina, H. Kopacka, P. Jaitner and J. Veciana, *Chem. Commun.*, 2002, 2342; (*f*) D. Braga, M. Curzi, L. Maini, M. Polito and F. Grepioni, *Dalton Trans.*, 2004, 2432.

38. M. Kondo, R. Shinigawa, M. Miyazawa, M. K. Kabir, Y. Irie, T. Horiba, T. Naito, K. Maeda, S. Utsuno and F. Uchida, *Dalton Trans.*, 2003, 515.

39. (*a*) J. Geng, H. LI, W. T. S. Huck and B. F. G. Johnson, *Chem. Commun.*, 2004, 2122; (*b*) S. P. Watton, P. Fuhrmann, L. E. Pence, A. Caneschi, A. Cornia, G. L. Abbati and S. J. Lippard, *Angew. Chem. Int. Ed., Engl.*, 1997, **36**, 2774; (*c*) S. Parsons, G. A. Solan and R. E. P. Winpenny, *J. Chem. Soc., Dalton Trans.*, 1995, 1987; (*d*) W. Micklitz and S. J. Lippard, *J. Am. Chem. Soc.*, 1989, **111**, 6856; (*e*) R. Carrasco, J. Cano, T. Mallah, L. F. Jones, D. Collison and E. K. Brechin, *Inorg. Chem.*, 2004, **43**, 5410; (*f*) O. L. Sydora, P. T. Wolczanski and E. B. Lobkovsky, *Angew. Chem. Int. Ed., Engl.*, 2003, **42**, 2685; (*g*) D. M. Low, L. F. Jones, A. Bell, E. K. Brechin, T. Mallah, E. Rivière, S. J. Teat and E. J. L. McInnes, *Angew. Chem. Int. Ed., Engl.*, 2003, **42**, 3781; (*h*) G. Rajaraman, J. Cano, E. K. Brechin and E. J. L. McInnes, *Chem. Commun.*, 2004, 1476; (*i*) A. Bino, M. Ardon, D. Lee, B. Spingler and S. J. Lippard, *J. Am. Chem. Soc.*, 2002, **124**, 4578; (*j*) A. Caneschi, A. Cornia, A. C. Fabretti and D. Gatteschi, *Angew. Chem. Int. Ed., Engl.*, 1999, **38**, 1295; (*k*) A.-A. H. Abu-Nawwas, J. Cano, P. Christian, T. Mallah, G. Rajaraman, S. J. Teat, R. E. P. Winpenny and Y. Yukuwa, *Chem. Commun.*, 2004, 314; (*l*) C. P. Raptopoulou, V. Tangoulis and E. Devlin, *Angew. Chem. Int. Ed., Engl.*, 2002, **41**, 2386; (*m*) C. Boskovic, H.-U. Güdel, G. Labat, A. Neels, W. Wernsdorfer, B. Moubaraki and K. S. Murray, *Inorg. Chem.*, 2005, **44**, 3181.

40. *See references therein* (*a*) A. Müller, *Chem. Commun.*, 2003, 803; (*b*) A. Müller and C. Serain, *Acc. Chem. Res.*, 2000, **33**, 2; (*c*) A. Müller, M. Koop, H. Bögge, M. Schmidtman and C. Beugholt, *Chem. Commun.*, 1998, 1501; (*d*) A. Müller, E. Krickmeyer, J. Meyer, H. Bögge, F. Peters, W. Plass, E. Diemann, S. Dillanger, F. Nonnenbruch, M. Randerath and C. Menke, *Angew. Int. Ed., Engl.*, 1995, **34**, 2122; (*e*) A. Müller, P. Kögerler and C. Kuhlmann, Chem. Commun., 1999, 1347; (*f*) A. Müller, S. Roy, M. Schmidtmann and H. Bögge, *Chem. Commun.*, 2002, 2000; (*g*) A. Müller, E. Krickmeyer, J. Meyer, H. Bögge, M. Schmidtmann, C. Beugholt, S. K. Das and F. Peters, *Chem. Eur. J.*, 1999, **5**, 1496; (*h*) A. Müller, E. Krickmeyer, J. Meyer, H. Bögge, M. Schmidtmann, F. Peters, C. Menke and J. Meyer, *Angew. Int. Ed., Engl.*, 1997, **36**, 484; (*i*) L. Cronin, E. Krickmeyer, M. Schmidtmann, H. Bögge, P. Kögerler, T. T. K. Luong and A. Müller, *Angew. Int. Ed., Engl.*, 2002, **41**, 2805; (*j*) A. Müller, E. Krickmeyer, H.

Bögge, M. Schmidtmann and F. Peters, *Angew. Int. Ed., Engl.*, 1998, **37**, 3360; (*k*) A. Müller, Y. Zhou, L. Zhang, H. Bögge, M. Schmidtmann, M. Dressel and J. van Slageren, *Chem. Commun.*, 2004, 2038; (*l*) A. Müller, B. Botar, H. Bögge, P. Kögerler and A. Berkle, *Chem. Commun.*, 2002, 2944; (*m*) A. Müller, L. Toma, H. Bögge, M. Schmidtmann and P. Kögerler, *Chem. Commun.*, 2003, 2000.

41. N. J. Turro, *Chem. Commun.*, 2002, 2279.

42. (*a*) C. Janiak, *Dalton Trans.*, 2003, 2781; (*b*) D. Bradshaw, J. B. Claridge, E. J. Cussen, T. J. Prior and M. J. Rosseinsky, *Acc. Chem. Res.*, 2005, **38**, 273; (*c*) N. L. Rosi, J. Kim, M. Eddaoudi, B. Chen, M. O'Keeffe and O. M. Yaghi, *J. Am. Chem. Soc.*, 2005, **127**, 1504; (*d*) N. W. Ockwig, O. Delgado-Friedrichs, M. O'Keeffe and O. M. Yaghi, *Acc. Chem. Res.*, 2005, **38**, 176; (*e*) G. Férey, C. Mellot-Draznieks, C. Serre and F. Millange, *Acc. Chem. Res.*, 2005, **38**, 217; (*f*) A. C. Sudik, A. P. Côté and O. M. Yaghi, *Inorg. Chem.*, 2005, **44**, 2998; (*g*) O. M. Yaghi, M. O'Keeffe, N. W. Ockwig, H. K Chae and M. Eddaoudi, *Nature*, 2003, **423**, 705; (*h*) M. Eddaoudi, D. B. Moler, H. Li, B. Chen, T. M. Reineke, M. O'Keeffe and O. M. Yaghi, *Acc. Chem. Res.*, 2001, **34**, 319; (*i*) J. Kim, B. Chen, T. M. Reineke, H. Li, M. Eddaoudi, D. B. Moler, M. O'Keeffe and O. M. Yaghi, *J. Am. Chem. Soc.*, 2001, **123**, 8239.

43. H. Hofmeier and U. S. Schubert, *Chem. Soc. Rev.*, 2004, **33**, 373.

44. L. Öhrström and K. Larsson, *Dalton Trans.*, 2004, 347.

45. Y. Bai, D. Guo, C. Duan, D. Dang, K. Pang and Q. Meng, *Chem. Commun.*, 2004, 186.

46. (*a*) D. Armentano, G. D. Munno, T. F. Matropietro, M. Julve and F. Lloret, *Chem. Commun.*, 2004, 1160; (*b*) D. J. Price, A. K. Powell and P. T. Wood, *Dalton Trans.*, 2003, 2478; (*c*) D. J. Price, S. Tripp, A. K. Powell and P. T. Wood, *Chem. Eur. J.*, 2001, **7**, 200; (*d*) D. J. Price, A. K. Powell and P. T. Wood, *J. Chem. Soc., Dalton. Trans.*, 2000, 3566; (*e*) M. Molinier, D. J. Price, P. T. Wood and A. K. Powell, 1997, *J. Chem. Soc., Dalton. Trans.*, 4061.

47. (*a*) G. Ercolani, *J. Am. Chem. Soc.*, 2003, **125**, 16097; (*b*) I. Goldberg, *Chem. Commun.*, 2005, 1243.

48. (*a*) P. Kögerler and L. Cronin, *Angew. Chem. Int., Ed. Engl.*, 2005, **44**, 844; (*b*) L. Ruhlmann, J. Canny, J. Vaissermann and R. Thouvenot, *Chem. Commun.*, 2004, 794.

49. M. Du, X.-J. Zhao and Y. Wang, *Dalton Trans.*, 2004, 2065.

50. (*a*) B. Moulton, J. Lu, R. Hajndl, S. Harharan and M. J. Zawarotko, *Angew. Chem. Int. Ed., Engl.*, 2002, **41**, 2821; (*b*) G. Paul, A. Choudhury and C. N. R. Rao, *Chem. Commun.*, 2002, 1904.

51. P. V. Solntsev, J. Sieler, A.N. Chernega, J. A. K. Howard, T. Gelbrich and K. V. Domasevitch, *Dalton Trans.*, 2004, 695.

52. (*a*) G. S. Papaefstathiou, S. P. Perlepes, A. Escuer, R. Vicente, M. Font-Bardia and X. Solans, *Angew. Chem. Int. Ed., Engl.*, 2001, **40**, 884; (*b*) P. Manikandan, R. Muthukumaran, K. R. J. Thomas, B. Varghese, G. V. R. Chandramouli and P. T. Monoharan, *Inorg. Chem.*, 2001, **40**, 2378; (*c*) G. S. Papaefstathiou, A. Escuer, R. Vicente, M. Font-Bardia, X. Solans and S. P. Perlepes, *Chem. Commun.*, 2001, 2414; (*d*) S. Martín, M. G. Barandika, L. Lezama, J. L. Pizarro, Z. E. Serna, J. I. R. de Larramendi, M. I. Arriortua, T. Rojo and R. Cortés, *Inorg. Chem.*, 2001, **40**, 4109; (*e*) L. Li, D. Liao, Z. Zhang and S. Yan, *Inorg. Chem.*, 2002, **41**, 1019; (*f*) A. Escuer, R. Vicente, F. A. Mautner, M. A. S. Goher and M. A. M. Abu-Youssef, *Chem. Commun.*, 2002, 64; (*g*) S. Koner, S. Saha, K. Moto and J.-P. Tuchagues, *Inorg. Chem.*, 2003, **42**, 4668; (*h*) L.-Y. Wang, B. Zhao, C.-X. Zhang, D.-Z. Liao, Z.-H. Jiang and S.-P. Yan, *Inorg. Chem.*, 2003, **42**, 5804; (*i*) E. Gao, S.-Q. Bai, C.-F. Wang, Y.-F. Yue and C.-H. Yan, *Inorg. Chem.*, 2003, **42**, 8456; (*j*) S. Koner, E. Zangrando, M. G. B. Drew, T. Mallah, J. Ribas and N. R. Chaudhuri, *Inorg. Chem.*, 2003, **42**, 5966; (*k*) E.-Q. Gao, S.-Q. Bai, Y.-F. Yue, Z.-M. Wang and C.-H. Yan, *Inorg. Chem.*, 2003, **42**, 3642; (*l*) F. Meyer, P. Kircher and H. Pritzkow, *Chem. Commun.*, 2003, 774; (*m*) E.-Q. Gao, Z.-M. Wang and C.-H. Yan, *Chem. Commun.*, 2003, 1748; (*n*) M. S. Ray, A. Ghosh, R. Bhattacharya, G. Mukhopadhyay, M. G. B. Drew and J. Ribas, *Dalton Trans.*, 2004, 252; (*o*) A. Escuer, M. Font-Bardia, S. S. Massoud, F. A. Mautner, E. Peñalba, X. Solans and R. Vicente, *New. J. Chem.*, 2004, **28**, 681; (*p*) S. Koner, S. Saha, T. Mallah and K. Okamoto, *Inorg. Chem.*, 2004, **43**, 840; (*q*) S. Wang, G.-M. Yang, D. Liao and L. Li, *Inorg. Chem.*, 2004, **43**, 852; (*r*) B. Woodward, R. D. Willett, S.

Haddad, B. Twamley, C. J. Gomez-Garcia and E. Coronado, *Inorg. Chem.*, 2004, **43**, 1822; (*s*) K. Ghosh, D. Ghoshal, E. Zangrando, J. Ribas and N. R. Chaudhuri, *Inorg. Chem.*, 2005, **44**, 1786.

53. *Mn-based* (*a*) V. S. Mironov, L. F. Chibotaru and A. Ceulemans, *J. Am. Chem. Soc.*, 2003, **125**, 9750; (*b*) Z. J. Zoang, H. Seino, Y. Mizobe, M. Hidai, A. Fujishima, S.-i. Ohkoshi and K. Hashimoto, *J. Am. Chem. Soc.*, 2000, **122**, 2952; (*c*) Y. Song, S.-i. Ohkoshi, Y. Arimoto, H. Seino, Y. Mizobe and K. Hashimoto, *Inorg. Chem.*, 2003, **42**, 1848; (*d*) J. Lorinova, M. Gross, M. Pilkington, H. Andres, H. Stœckli-Evans, H.-U. Güdel and S. Decurtins, *Angew. Chem. Int. Ed., Engl.*, 2000, **39**, 1605; (*e*) D. Li, L. Zheng, Y. Zhang, J. Huang, S. Gao and W. Tang, *Inorg. Chem.*, 2003, **42**, 6123; (*f*) W. Dong, L.-N. Zhu, H.-B. Song, D.-Z. Liao, Z.-H. Jiang, S.-P. Yan, P. Cheng and S. Gao, *Inorg. Chem.*, 2004, **43**, 2465; (*g*) H. Tokoro, S. Ohkoshi, T. Matsuda and K. Hashimoto, *Inorg. Chem.*, 2003, **43**, 5231.

54. *Fe-based* (*a*) J. Jiang and S. A. Koch, *Chem. Commun.*, 2002, 1724; (*b*) L. M. Toma, F. S. Delgado, C. Ruiz-Pérez, R. Carrasco, J. Cano, F. Lloret and M. Julve, *Dalton Trans.*, 2004, 2836; (*c*) P. Alborés, L. D. Slep, T. Weyhermüller and L. M. Baraldo, *Inorg. Chem.*, 2004, **43**, 6762; (*d*) C. P. Berlinguette, A. Dragalescu-Andrasi, A. Sieber, J. R. Galán-Mascarós, H.-U. Güdel, C. Achim and K. R. Dunbar, *J. Am. Chem. Soc.*, 2004, **126**, 6222; (*e*) D. R. Roesseinsky, L. Glasser and H. D. B. Jenkins, *J. Am. Chem. Soc.*, 2004, **126**, 10472; (*f*) A. Widmann, H. Kahlert, I. Petrovic-Prelevic, H. Wulff, J. V. Yakhmi, N. Bagkar and F. Scholz, *Inorg. Chem.*, 2002, **41**, 5706; (*g*) R. Lescouëzec, J. Vaissermann, F. Lloret, M. Julve and M. Verdaguer, *Inorg. Chem.*, 2002, **41**, 5943; (*h*) E. Coronado, C. Gómez-García, A. Nuez, F. M. Romero, E. Rusanov and H. Stœckli-Evans, *Inorg. Chem.*, 2002, **41**, 4615; (*i*) H.-Z. Kou, B. C. Zhou, D.-Z. Liao, R.-J. Wang and Y. Li, *Inorg. Chem.*, 2002, **41**, 6887; (*j*) H. Oshio, M. Yamamoto and T. Ito, *Inorg. Chem.*, 2002, **41**, 5817; (*k*) R. Lescouëzec, F. Lloret, M. Julve, J. Vaissermann and M. Verdaguer, *Inorg. Chem.*, 2002, **41**, 818; (*l*) R. Lescouëzec, J. Vaissermann, L. M. Toma, R. Carrasco, F. Loret and M. Julve, *Inorg. Chem.*, 2004, **43**, 2234; (*m*) C. Michaut, L. Ouahab, P. Bergerat, O. Kahn and A. Bousseksou, *J. Am. Chem. Soc.*, 1996, **118**, 3610; (*n*) Y. Liao, W. W. Shum and J. S. Miller, *J. Am. Chem. Soc.*, 2002, **124**, 9336; (*o*) M. K. Saha, F. Lloret and I. Bernal, *Inorg. Chem.*, 2004, **43**, 1969; (*p*) J. Y. Yang, M. P. Shores, J. J. Sokol and J. R. Long, *Inorg. Chem.*, 2003, **42**, 1403; (*q*) H. Miyasaka, H. Ieda, N. Matsumoto, K. Sugiura and M. Yamashita, *Inorg. Chem.*, 2003, **42**, 3509; (*r*) C. P. Berlinguette, J. R. Galán-Mascarós and K. R. Dunbar, *Inorg. Chem.*, 2003, **42**, 3416; (*s*) W. Dong, L.-N Zhu, Y.-Q. Sun, M. Liang, Z.-Q. Liu, D.-Z. Liao, Z.-H. Jiang, S.-P. Yan and P. Cheng, *Chem. Commun.*, 2003, 2544.

55. *Co-based* (*a*) L. G. Beauvais and J. R. Long, *J. Am. Chem., Soc.*, 2002, **124**, 12096; (*b*) Y. Arimoto, S.-i. Ohkoshi, Z. J. Zhong, H. Seino, Y. Mizobe and K. Hashimoto, *J. Am. Chem., Soc.*, 2003, **125**, 9240; (*c*) R. Lescouëzec, J. Vaissermann, C. Ruiz-Pérez, F. Lloret, R. Carrasco, M. Julve, M. Verdaguer, Y. Dromzee, D. Gatteschi and W. Wernsdorfer, *Angew. Chem. Int. Ed., Engl.*, 2003, **42**, 1480.

56. *Other CN-based complexes* (*a*) H.-Z. Kou, S. Gao, C.-H. Li, D.-Z. Liao, B.-C. Zhou, R.-J. Wang and Y. Li, *Inorg. Chem.*, 2002, **41**, 4756; (*b*) O. Kahn, J. Larionova and L. Ouahab, *Chem. Commun.*, 1999, 945; (*c*) J. J. Sokol, M. P. Shores and J. R. Long, *Inorg. Chem.*, 2002, **41**, 3052; (*d*) F. Bonadio, M. Gross, H. Stœckli-Evans and S. Decurtins, *Inorg. Chem.*, 2002, **41**, 5891; (*e*) S. K. Dey, N. Mondal, M. S. E. Fallah, R. Vicente, A. Escuer, X. Solans, M. Font-Bardía, T. Matsushita, V. Gramlich and S. Mitra, *Inorg. Chem.*, 2004, **43**, 2427; (*f*) R. Garde, F. Villain and M. Verdaguer, *J. Am. Chem. Soc.*, 2002, **124**, 10531; (*g*) R. Pradhan, C. Desplanches, P. Guionneau and J.-P. Sutter, *Inorg. Chem.*, 2003, **42**, 6607; (*h*) F. Thétiot, S. Triki, J. S. Pala, C. J. Gómez-García and S. Golhen, *Chem. Commun.*, 2002, 1078; (*i*) M. L. Kuhlman, H. Yao and T. B. Rauchfuss, *Chem. Commun.*, 2004, 1370; (*j*) R. Podgajny, T. Korzeniak, M. Balanda, T. Wasiutynski, W. Errington, T. J. Kemp, N. W. Alcock and B. Sieklucka, *Chem. Commun.*, 2002, 1138; (*k*) Y.-Z. Zhang, S. Gao, H.-L. Sun, G. Su, Z.-M. Wang and S.-W. Zhang, *Chem. Commun.*, 2004, 1906; (*l*) I. S. Lee and J. R. Long, *Dalton Trans.*, 2004, 3434; (*m*) *latest review* L. M. C. Beltran and J. R. Long, *Acc. Chem. Res.*, 2005, **38**, 325.

57. (*a*) B. Vandal, J. Carranza, F. Lloret, M. Julve and J. Sletten, *J. Chem. Soc., Dalton Trans.*, 2002, 566; (*b*) A. M. Kutsai, S. R. Batten, B. Moubaraki and K. S. Murray, *J. Chem. Soc., Dalton Trans.*, 2002, 819; (*c*)

J. Carranza, C. Brennan, J. Sletten, F. Lloret and M. Julve, *J. Chem. Soc., Dalton Trans.*, 2002, 3164; (*d*) P. Jensen, S. R. Batten, B. Moubaraki and K. S. Murray, *J. Chem. Soc., Dalton Trans.*, 2002, 3712; (*e*) S. Martín, M. G. Barandika, J. M. Ezpeleta, R. Cortés, J. I. R. de Larramendi, L. Lezama and T. Rojo, *J. Chem. Soc., Dalton Trans.*, 2002, 4275; (*f*) S. R. Marshall, C. D. Incarvito, W. W. Shum, A. L. Rheingold and J. S. Miller, *Chem. Commun.*, 2002, 3006; (*g*) E.-Q. Gao, S.-Q. Bai, Z.-M. Wang and C.-H. Yan, *Dalton Trans.*, 2003, 1759; (*h*) A. Escuer, N. Sanz, R. Vicente and F. A. Mautner, *Inorg. Chem.*, 2003, **42**, 541; (*i*) J. L. Mason, J. Gu, J. A. Schlueter and H.-H. Wang, *Inorg. Chem.*, 2003, **42**, 3950; (*j*) H.-L. Sun, S. Gao, B.-Q. Ma and G. Su, *Inorg. Chem.*, 2003, **42**, 5399; (*k*) J. A. Schlueter, J. L. Manson, K. A. Hyzer and U. Geiser, *Inorg. Chem.*, 2004, **43**, 4100; (*l*) J. L. Manson, J. A. Schlueter, H.-J. Koo and M.-H. Whangbo, *Inorg. Chem.*, 2004, **43**, 4100; (*m*) A.-Q. Wu, F.-K. Zheng, W.-T. Chen, L.-Z. Cai, C.-C. Guo, J.-S. Huang, Z.-C. Dong and Y. Takano, *Inorg. Chem.*, 2004, **43**, 4839; (*n*) S. Triki, F. Thétiot, F. Vandevelde, J. Sala-Pala and J. Gómez-García, *Inorg. Chem.*, 2005, **44**, 4086.

58. (*a*) E. Coronado and P. Dey, *Chem. Rev.*, 2004, **104**, 5419; (*b*) T. Enoki and A. Miyazaki, *Chem. Rev.*, 2004, **104**, 5449.

59. (*a*) A. Caneschi, D. Gatteschi and R.Sessoli, *Acc. Chem. Res.*, 1989, **22**, 392; (*b*) A. Caneschi, D. Gatteschi, N. Laliolti, R.Sessoli, L. Sorace, V. Tangoulis and A. Vindigni, *Chem. Eur. J.*, 2002, **8**, 286.

60. *See references therein* (*a*) M. R. Bürgstein, M. T. Gamer and P. W. Roesky, *J. Am. Chem. Soc.*, 2004, **126**, 5213.

61. C. Benelli and D. Gatteschi, *Chem. Rev.*, 2002, **102**, 2369.

62. *See references therein* D. Drewes, E. M. Lemanski and B. Krebs, *Dalton Trans.*, 2004, 2087.

63. (*a*) A. Caneschi, D. Gatteschi, N. Lalioti, G. Sangregorio, R. Sessoli, G. Venturi, A. Vindigni, A. Rettori, M. G. Pini and M. A. Novak, *Angew. Chem. Int. Ed., Engl.*, 2001, **40**, 1760; (*b*) L. Li, D. Liao, Z. Jiang and S. Yan, *Inorg. Chem.*, 2002, **41**, 421; (*c*) Y. Sukahara, A. Iino, T. Yoshida, T. Suzuki and S. Kaizaki, *J. Chem. Soc., Dalton Trans.*, 2002, 181; (*d*) D. Zhang, L. Ding, W. Xu, H. Hu, D. Zhu, Y. Huang and D. Fang, *Chem. Commun.*, 2002, 44; (*e*) L. M. Field, P. M. Lahti and F. Palacio, *Chem. Commun.*, 2002, 636; (*f*) L. Li, D. Liao, Z. Jiang and S. Yan, *J. Chem. Soc., Dalton Trans.*, 2002, 1350; (*g*) T. Tsukuda, T. Suzuki and S. Kaizaki, *J. Chem. Soc., Dalton Trans.*, 2002, 1721; (*h*) Y. Sukahara, T. Kamatani, A. Iiono, T. Suzuki and S. Kaizaki, *Inorg. Chem.*, 2002, **41**, 4363; (*i*) C. Aoki, T. Ishida and T. Nogami, *Inorg. Chem.*, 2003, **42**, 7616; (*j*) T. Ise, T. Ishida, D. Hashizume, F. Iwasaki and T. Nogami, *Inorg. Chem.*, 2003, **42**, 6106; (*k*) L. M. Field and P. M. Lahti, *Inorg. Chem.*, 2003, **42**, 7447; (*l*) K. Okada, O. Nagao, H. Mori, M. Kozkai, D. Shiomi, K. Sato, T. Takui, Y. Kitigawa and K. Yamaguchi, *Inorg. Chem.*, 2003, **42**, 3221; (*m*) G. Champion, N. Lalioti, V. Tangoulis, M.-A. Arrio, P. Sainctavit, F. Villain, A. Caneschi, D. Gatteschi, C. Giorgetti, F. Baudelet, M. Verdaguer and C. C. dit Moulin, *J. Am. Chem. Soc.*, 2003, **125**, 837; (*n*) Y. Sukahara, T. Kamatani, T. Suzuki and S.. Kazkai, *Dalton Trans.*, 2003, 1276; (*o*) P. Taylor, P. R. Serwinski and P. M. Lahti, *Chem. Commun.*, 2003, 1400; (*p*) A. Iino, T. Suzuki and S. Kaizkai, *Dalton Trans.*, 2003, 4604; (*q*) S. Yamada, T. Ishida and T. Nogami, *Dalton Trans.*, 2004, 898; (*r*) H. Wang, Z. Liu, C. Liu, D. Zhang, Z. Lü, H. Geng, Z. Shuai and D. Zhu, *Inorg. Chem.*, 2004, **43**, 4091; (*s*) Z. Liu, Z. Lü, D. Zhang, Z. Jiang, L. Li, C. Liu and D. Zhu, *Inorg. Chem.*, 2004, **43**, 6620; (*t*) S. Hiroaka, T. Okamoto, M. Kozaki, D. Shiomi, K. Sato, T. Takui and K. Okada, *J. Am. Chem. Soc.*, 2004, **126**, 58.

64. (*a*) A. Kamiyama, T. Noguchi, T. Kajiwara and T. Ito, *Inorg. Chem.*, 2002, **41**, 507; (*b*) H. Miyasaka, T. Nezu, F. Iwahori, S. Furukawa, K. Sugimoto, R. Clérac, K. Sugiura and M. Yamashita, *Inorg. Chem.*, 2003, **42**, 4501; (*c*) J. L. Manson, *Inorg. Chem.*, 2003, **42**, 2602; (*d*) S. Osa, Y. Sunatsuki, Y. Yamamoto, M. Nakamura, T. Shimamoto, N. Matsumoto and N. Re, *Inorg. Chem.*, 2003, **42**, 5507.

65. (*a*) T. C. Higgs, S. Parsons, A. C. Jones, P. J. Bailey and P. A. Tasker, *J. Chem. Soc., Dalton Trans.*, 2002, 3427; (*b*) C. W. Baxter, T. C. Higgs, A. C. Jones, S. Parsons, P. J. Bailey and P. A. Tasker, . *Chem. Soc., Dalton Trans.*, 2002, 4395; (*c*) Q.-H. Wei, G.-Q. Yin, L.-Y. Zhang, L.-X. Shi, Z.-W. Mao and Z.-N. Chen, *Inorg. Chem.*, 2004, **43**, 3484.

66. (*a*) K. I. Pokhodnya, N. Petersen and J. S. Miller, *Inorg. Chem.*, 2002, **41**, 1996; (*b*) A. M. Madalan, H. W. Roesky, M. Andruh, M. Noltemeyer and N. Stanica, *Chem. Commun.*, 2002, 1638; (*c*) E. B. Vickers, T. D. Salby, M. S. Thorum, M. L. Taliaferro and J. S. Miller, *Inorg. Chem.*, 2004, **43**, 6416.

67. (*a*) H. Chun, C. N. Verani, P. Chaudhuri, E. Bothe, E. Bill, T. Weyhermüller and K. Wieghardt, *Inorg. Chem.*, 2001, **40**, 4157; (*b*) L. Bensivey, A. J. Blake, D. Collison, E. S. Davis, C. D. Garner, E. J. L. McInnes, J. McMaster, G. Whittaker and C. Wilson, *Dalton Trans.*, 2003, 1975; (*c*) S. Mukherjee, T. Weyhermüller, K. Wieghardt and P. Chaudhuri, *Dalton Trans.*, 2003, 3483; (*d*) K. S. Min, T. Weyhermüller and K. Wieghardt, *Dalton Trans.*, 2004, 178.

68. (*a*) R. Bŏca, M. Bŏca, l. Dlháň, K. Falk, H. Fuess, W. Haase, R. Jaroščiak, B. Papánaková, F. Renz, M. Vrbová and R. Werner, *Inorg. Chem.*, 2001, **40**, 3025; (*b*) S. G. Telfer, B. Bocquet and A. F. Williams, *Inorg. Chem.*, 2001, **40**, 4818; (*c*) A. F. Stassen, E. Dova, J. Ensling, H. Schenk, P. Gütlich, J. Haasnoot and J. Reedijk, *Inorg. Chim. Acta*, 2002, **335**, 61; (*d*) D. L. Reger, C. A. Little, M. D. Smith and G. J. Long, *Inorg. Chem.*, 2002, **41**, 4453; (*e*) M. Reiher, *Inorg. Chem.*, 2002, **41**, 6928; (*f*) N. Moliner, M. C. Muñoz, S. Létard, L. Salmon, J.-P. Tuchagues, A. Bousseksou and J. A. Real, *Inorg. Chem.*, 2002, **41**, 6997; (*g*) K. H. Sugiyarto, W.-A. McHale, D. C. Craig, A. D. Rae, M. L. Scudder and H. A. Goodwin, *Dalton Trans.*, 2003, 2443; (*h*) D. M. Jenkins and J. C. Peters, *J. Am. Chem. Soc.*, 2003, **125**, 1162; (*i*) V. Niel, A. B. Gaspar, M. C. Muñoz, B. Abarca, R. Ballesteros and J. A. Real, *Inorg. Chem.*, 2003, **42**, 4782; (*j*) W. Hibbs, P. J. van Koningsbruggen, A. M. Arif, W. W. Shum and J. S. Miller, *Inorg. Chem.*, 2003, **42**, 5645; (*k*) S. Floquet, M.-L. Boillot, E. Rivière, F. Varret, K. Boukheddaden, D. Mourineau and P. Négrier, *New J. Chem.*, 2003, **27**, 341; (*l*) Y. Sunatsuki, Y. Ikuta, N. Matsumoto, H. Ohta, M. Kojima, S. Iijima, S. Hayami, Y. Maeda, S. Kaizaki, F. Dahan and J.-P. Tuchagues, *Angew. Chem. Int. Ed., Engl.*, 2003, **42**, 1614; (*m*) V. A. Money, J. Elhaïk, I. R. Evans, M. A. Halcrow and J. A. K. Howard, *Dalton Trans.*, 2004, 65; (*n*) S. Hayami, K. Hashiguchi, G. Juhász, M. Ohba, H. Ōkawa, Y. Maeda, K. Kato, K. Osaka, M. Takata and K. Inoue, *Inorg. Chem.*, 2004, **43**, 4124; (*o*) S Sunatsuki, H. Ohta, M. Kojima, Y. Ikuta, Y. Goto, N. Matsumoto, S. Iijima, H. Akashi, S. Kaizaki, F. Dahan and J.-P. Tuchagues, *Inorg. Chem.*, 2004, **43**, 4154; (*p*) C. Brady, P. L. Callaghan, Z. Ciunik, C. G. Coates, A. Døssing, A. Hazell, J. J. McGarvey, S. Schenker, H. Toftlund, A. X. Trautwein, H. Winkler and J. A. Wolny, *Inorg. Chem.*, 2004, **43**, 4289.

69. (*a*) Z. Wang, B. Zhang, T. Otsuka, K. Inoue, H. Kobayashi and M. Kurmoo, *Dalton Trans.*, 2004, 2209; (*b*) Z. Wang, B. Zhang, M. Kurmoo, M. A. Green, H. Fujiwara, T. Otsuka and H. Kobayashi, *Inorg. Chem.*, 2005, **44**, 1230.

70. R. E. P. Winpenny, *J.Chem. Soc., Dalton Trans.*, 2002, 1.

71. *Ni complexes:* (*a*) E. K. Brechin, S. G. Harris, S. Parsons and R. E. P. Winpenny, *J. Chem. Soc., Dalton Trans.*, 1997, 1665; (*b*) E. K. Brechin, L. M. Gilby, R. O. Gould, S. G. Harris, *J. Chem. Soc., Dalton Trans.*, 1998, 2657; (*c*) C. Benelli, A. J. Blake, E. K. Brechin, S. J. Coles, A. Graham, S. G. Harris, S. Meier, A. Parkin, S. Parsons, A. M. Seddon and R. E. P. Winpenny, *Chem. Eur. J.*, 2000, **6**, 883; (*d*) E. K. Brechin, A. Graham, S. G. Harris, S. Parsons and R. E. P. Winpenny, *J. Chem. Soc., Dalton Trans.*, 1997, 3405; (*e*) C. Caddiou, R. A. Coxall, A. Graham, A. Harrison, M. Helliwell, S. Parsons and R. E. P. Winpenny, *Chem. Commun.*, 2002, 1106; (*f*) J. Pérez, L. García, A. G. Orpen, M. D. Santana, P. Saez and G. García, *New J. Chem.*, 2002, **26**, 726; (*g*) E. K. Brechin, S. G. Harris, S. Parsons and R. E. P. Winpenny, *Angew. Chem., Int. Ed. Engl.*, 1997, **36**, 1967; *Co complexes:* (*h*) A. J. Blake, L. M. Gilby, S. Parsons, J. M. Rawson, D. Reed, G. A. Solan and R. E. P. Winpenny, *J. Chem. Soc., Dalton Trans.*, 1996, 3575; (*i*) E. K. Brechin, R. A. Coxall, A. Parkin, S. Parsons, P. A. Tasker and R. E. P. Winpenny, *Angew. Chem., Int. Ed. Engl.*, 2001, **40**, 2700; (*j*) E. K. Brechin, S. Parsons and R. E. P. Winpenny, *J. Chem. Soc., Dalton Trans.*, 1996, 3745; (*k*) W. Clegg, D. Garner and M. H. Al-Samman, *Inorg. Chem.*, 1983, **22**, 1543; (*l*) E. K. Brechin, A. Graham, A. Parkin, S. Parsons, A. M. Seddon and R. E. P. Winpenny, *J. Chem. Soc., Dalton Trans.*, 2000, 3242; (*m*) E. K. Brechin, S. G. Harris and R. E. P. Winpenny, *Chem. Commun.*, 1996, 1439; (*n*) E. K. Brechin, O. Cador, A. Caneschi, C. Cadiou, S. G. Harris, S. Parsons, M.

Vonci and R. E. P. Winpenny, *Chem. Commun.*, 2002, 1860; *Cu complexes:* (*o*) A. J. Blake, C. M. Grant, C. I. Gregory, S. Parsons, J. M. Rawson, D. Reed and R. E. P. Winpenny, *J. Chem. Soc., Dalton Trans.*, 1995, 163; (*p*) A. J. Blake, P. E. Y. Milne and R. E. P. Winpenny, *J. Chem. Soc., Dalton Trans.*, 1993, 3727; (*q*) A. J. Blake, R. O. Gould, C. M. Grant, P. E. Y. Milne, S. Parsons and R. E. P. Winpenny, *J. Chem. Soc., Dalton Trans.*, 1997, 485; (*r*) E. K. Brechin, S. G. Harris, S. Parsons and R. E. P. Winpenny, *J. Chem. Soc., Dalton Trans* ., 1997, 3403; (*s*) A. J. Blake, C. M. Grant, E. J. L. McInnes, F. E. Mabbs, P. E. Y. Milne, S. Parsons, J. M. Rawson and R. E. P. Winpenny, *J. Chem. Soc., Dalton Trans.*, 1996, 4077; (*t*) A. J. Blake, R. O. Gould, P. E. Y. Milne and R. E. P. Winpenny, *J. Chem. Soc., Chem. Commun.*, 1992, 522; (*u*) A. J. Blake, S. Parsons, J. M. Rawson and R. E. P. Winpenny, *Polyhedron*, 1995, **14**, 1895; (*v*) A. J. Blake, R. O. Gould, J. M. Rawson and R. E. P. Winpenny, *J. Chem. Soc., Dalton Trans.*, 1994, 2005; (*w*) S.-C. Cheng and H.-H. Wei, *Inorg. Chim. Acta*, 2002, **340**, 105; (*x*) *Mn complexes* N. C. Harden, M. A. Bolcar, W. Wernsdorfer, K. A. Abboud, W. E. Streib and G. Christou, *Inorg. Chem.*, 2002, **42**, 7067 *and references therein.*

72. *See references and patents therein* (*a*) ACS, *SciFinder Scholar*, Substance Database, 2005; (*b*) I. Spasojević, H. Boukhalfa, R. D. Stevens and A. L. Crumbliss, *Inorg. Chem.*, 2001, **40**, 49; (*c*) S. Hati, R. J. Batchelor, F. W. B. Einstein and A. S. Tracey, *Inorg. Chem.*, 2001, **40**, 6258; (*d*) C. Redshaw, M. R. J. Elsegood, K. E. Holmes, *Angew. Chem. Int. Ed., Engl.*, 2005, **44**, 1850; (*e*) A. Abdurahman, H. Izumisawa, H. Saito and Y. Hasegawa, *Proc. Symp. Solvent Extr.*, 1987, 49; (*f*) Y. Hasegawa, M. Tanaka, Miho, A. Ishimori, *Journal of Trace and Microprobe Techniques*, 1998, 16, 1; (*g*) D. Zhou, D. Feng, Y. Xie, R. Qiu and B. Jin, *Fenxi Huaxue*, 1986, **14**, 650.

73. (*a*) P. Chaudhuri, E. Rentschler, F. Birkelbach, C. Krebs, E. Bill, T. Weyhermüller and U. Flörke, *Eur. J. Inorg. Chem.*, 2003, 541; (*b*) B. P. Baranwal, S. S. Das, P. Singh and T. Gupta, *Indian J. Chem. Soc., Sect. A*, 2001, **40**, 320; (*c*) B. P. Baranwal, S. S. Das and P. Singh, *Indian J. Chem. Soc., Sect. A*, 1998, **28**, 1689; (*d*) Y. M. Issa, W. F. El-Hawary, H. A. Abdel-Salam and M. R. Issa, *Transition Metal Chem.*, 1995, **20**, 423; (*e*) S.-X. Liu and X. Wang, *Gaodeng Xue Xiao Huaxue Xuebao*, 1996, **17**, 169; (*f*) S. K. Agarwal and D. Goel, *Oriental J. Chem.*, 1989, **5**, 261; (*g*) R. Carballo, B. Covelo, S. Balboa, A. Castiñeiras and J. Niclós, *Z. Anorg. Allg. Chem.*, 2001, **627**, 948; (*h*) R. Carballo, A. Castineiras, B. Covelo, E. Garcia-Martinez, J. Niclos and E. M. Vazquez-Lopez, *Polyhedron* , 2004, **23**, 1505; (*i*) B. K. Mohanty, B. C. Samantary, G. Sahu, B. K. Mohapatra, *J. Indian Chem. Soc.*, 1987, **64**, 570.

74. *Isopthalate containing complexes* (*a*) Y. Wan, L. Zhang, L. Jin, S. Gao and S. Lu, *Inorg. Chem.*, 2003, **42**, 4985; (*b*) R. García-Zarracino, J. Ramos-Quiñones and H. Höpfl, *Inorg. Chem.*, 2003, **42**, 3835; (*c*) J.-F. Ma, J. Yang, G.-L. Zheng and J.-F. Liu, *Inorg. Chem.*, 2003, **42**, 7531; (*d*) H.-P. Xiao, X.-H. Li and M.-L. Hu, *Acta Crystallogr., Sect. E*, 2004, **60**, 468; (*e*) N. J. Burke, A. D. Burrows, A. S. Donovan, R. W. Harrington, M. F. Mahon and C. E. Price, *Dalton Trans.*, 2003, 3840; (*f*) B. Moulton, H. Abourahma, M. W. Bradner, J. Lu, G. J. McManus and M. J. Zawortko, *Chem. Commun.* 2003, 1342; (*g*) J. Tao, Y. Zhang, M.-L. Tong, X.-M. Chen, T. Yuen, C. L. Lin, X. Huang and J. Li, *Chem. Commun.*, 2002, 1342; (*h*) S. J. Yang, L. S. Long, R. B. Huang and L. S. Zheng, *Chem. Commun.*, 2002, 472; (*i*) H.-X. Zhang, B.-S. Kang, A.-W. Xu, Z.-N. Chen, Z.-Y. Zhou, A. S. Chan, K.-B. Yu and C. Ren, *J. Chem. Soc., Dalton Trans.*, 2001, 2559; (*j*) B. Moulton, J. Lu, R. Hajndl, S. Hariharan and M. J. Zawrotko, *Angew. Chem. Int Ed., Engl.*, 2002, **41**, 2821; (*k*) M. Eddaoudi, J. Kim, D. Vodak, A. Sudik, J. Wachter, M. O.'Keeffe and O. M. Yaghi, *Proc. Nat. Acad. Sci.*, USA, 2002, **99**, 4900; (*l*) A. C. Sudik, A. P. Côté and O. M. Yaghi, *Inorg. Chem.*, 2005, **44**, 2998; (*m*) Q. Zhang, B.-H. Ye, C.-X. Ren and X.-M. Chen, *Z. Anorg. Allg. Chem.*, 2003, **629**, 2053; (*n*) S. A. Bourne, A. Mondal and M. J. Zawarotko, *Cryst. Eng.*, 2001, **4**, 25; (*o*) X.-M. Chen and G.-F. Liu, *Chem. Eur. J.*, 2002, **8**, 4811; (*p*) P. Cheng, S.-P. Yan, C.-Z. Xie, B. Zao, X.-Y. Chen, X.-W. Liu, C.H. Li, D.-Z. Liao, Z.-H. Jiang and G.-L. Wang, *Eur. J. Inorg. Chem.*, 2004, 2369; (*q*) J. Tao, X. Yin, R. Huang and L. Zheng, *Inorg. Chem. Commun.*, 2002, **5**, 1000; (*r*) W.-Z. Shen, X.-Y. Chen, P. Cheng, S.-P. Yan, B. Zhai, D.-Z. Liao and Z.-H. Jiang, *Eur. J. Inorg. Chem.*, 2005, 2297.

75. *Isopthalate paddle wheel-based complexes* (*a*) S. Masaoka, D. Tanaka, Y. Nakanishi and S. Kitigawa, *Angew. Int. Ed., Engl.*, 2004, **43**, 2530; (*b*) S. A. Bourne, J. Lu, A. Mondal, B. Moulton and M. J. Zawarotko, *Angew. Chem. Int. Ed., Engl.*, 2001, **40**, 2111; (*c*) H. Abourahma, G. J. Bodwell, J. Lu, B. Moulton, I. R. Pottie, R. B. Walsh and M. J. Zawarotko, *Cryst. Growth Des.*, 2003, **3**, 513. (*d*) L. Gao, B. Zhao, G. Li, Z. Shi and S. Feng, *Inorg. Chem. Commun.*, 2003, **6**, 1249;

76. *Isopthalate-based nanoballs* (*a*) M. Eddaoudi, J. Kim, J. B. Wachter, H. K. Chae, M. O'Keeffe and O. M. Yaghi, *J. Am. Chem. Soc.*, 2001, **123**, 4368; (*b*) B. Moulton, J. Liu, A. Mondal and M. J. Zaworotko, *Chem. Commun.*, 2001, 863; (*c*) G. J. McManus, Z. Wang and M. J. Zawarotko, *Crystal Growth and Design*, 2004, **4**, 11.

77. (*a*) P. Angaridis, F. A. Cotton, C. A. Murillo, D. Villagrán and X. Wang, *J. Am. Chem. Soc.*, 2005, **127**, 5008; (*b*) F. A. Cotton, C. Lin and C. A. Murillo, *Inorg. Chem.*, 2001, **40**, 5886; (*c*) M. L. Cole, G. B. Deacon, P. C. Junk and K. Konstas, *Chem. Commun.*, 2005, 1581; (*d*) P. Angaridis, F A. Cotton, C. A. Murillo, D. Villagrán and X. Wang, *Inorg. Chem.*, 2004, **43**, 8290.

78. D. Gatteschi, A. Caneschi, L. Pardi and R. Sessoli, *Nature*, 1994, **265**, 1054.

79. D. Kurtz, *Chem. Rev.*, 1990, **90**, 585.

80. W. H. Armstrong and S. J. Lippard, *Inorg. Chem*, 1985, **24**, 981.

81. F. A. Cotton, G. Wilkinson, C. A. Murillo and M. Bochmann, in *Advanced Inorganic Chemistry*, eds., F. A. Cotton, G. Wilkinson, Wiley-Interscience, New York, 6th Edn., 1999, (*a*) p. 465; (*b*) *ibid.* p. 363; (*c*) W. A. Nugent and B. L. Haymore, *Coord. Chem. Rev.*, 1980, **31**, 123.

82. (*a*) P. J. Nichols, G. D. Falton, K. S. Murray and B. O. West, *Inorg. Chem.*, 1988, **27**,.2795; (*b*) T. A. Hanna, A. M. Baranger and R. G. Bergman, *Angew. Chem. Int. Ed., Engl.*, 1996, **35**, 653; (*c*) X. Dai, P. Kapoor and T. H. Warren, *J. Am. Chem. Soc.*, 2004, **126**, 4798.

83. (*a*) C. Lorber, R. Choukroun and B. Donnadieu, *Inorg. Chem.*, 2003, **42**, 673; (*b*) Y. Li, Y. Shi and A. L. Odom, *J. Am. Chem. Soc.*, 2004, **126**, 1794.

84. J. S. Duncan, T. M. Nazif, A. K. Verma and S. C. Lee, *Inorg. Chem.*, 2003, **42**, 1211.

85. (*a*) A. Decker, D. Fenske and K. Maczek, *Angew. Chem. Int. Ed., Engl.*, 1996, **35**, 2863; (*b*) P. Reiß and D. Fenske, *Z. Anorg. Allg. Chem.*, 2000, **626**, 1317.

86. M. L. Green and K. J. Moynihan, *Polyhedron*, 1986, **5**, 921.

87. A. K. Verma and S. C. Lee, *J. Am. Chem. Soc.*, 1999, **121**, 10838; (*b*) C.T.-W. Chu, R. S. Gall and L. F. Dahl, *J. Am. Chem. Soc.*, 1982, **104**, 737.

88. (*a*) C. S. Aluarez, A. D. Bond, E. A. Harron, R. A. Layfield, J. A. McAllister, C. M. Pask, J. M. Rawson and D. S. Wright, *Organometallics*, 2001, **20**, 4135; (*b*) C. A. Alvarez, A. Bashall, A. D. Bond, D. Cave, E. A. Harron, R. A. Layfield, M. E. Mosquera, M. McPartlin, J. M. Rawson, P. T. Wood and D. S. Wright, *Dalton Trans.*, 2003, 3002.

89. (*a*) H. Link, A. Decker and D. Fenske, *Z. Anorg. Allg. Chem.*, 2000, **626**, 1567; (*b*) H. Link and D. Fenske, *Z. Anorg. Allg. Chem.*, 1999, **625**, 1878; (*c*) H. Link, P. Reiss, S. Chitsaz, H. Pfistner and D. Fenske, *Z. Anorg. Allg. Chem.*, 2003, **629**, 744; (*d*) A. Danapoulos, G. Wilkinson, T. K. N. Sweet and M. B. Hursthouse, *J. Chem. Soc. Dalton Trans.*, 1995, 205.

90. (*a*) W. J. Grigsby and P. P. Power, *J. Chem. Soc., Dalton Trans.*, 1996, 4613; (*b*) W. J. Grigsby, M. M. Olmstead and P. P. Power, *J. Organomet. Chem.*, 1996, 513, 173; (*c*) P. T. Gomes, M. L. H. Green, A. M. Martins and P. Mountford, *J. Organomet. Chem.*, 1997, **541**, 121.

91. *Recent studies on {Mn_{12}}-based SMMs* (*a*) A. G. Harter, N. E. Chakov, B. Roberts, R. Achey, A. Reyes, P. Kuhns, G. Christou and N. S. Dalal, *Inorg. Chem.*, 2005, **44**, 2122; (*b*) L. Zobbi, M. Mannini, M. Pacchioni, G. Chastanet, D. Bonacchi, C. Zanardi, R. Biagi, U. D. Pennino, D. Gatteschi, A. Cornia and R. Sessoli, *Chem. Commun.*, 2005, 1640; N. E. Chakov, L. N. Zakharov, A. L. Rheingold, K. A. Abboud and G. Christou, *Inorg. Chem.*, 2005, **44**, 4555.

92. *Fe-based 2-pyridine akoxide complexes* (*a*) C. Cañada-Vilalta, T. A. O'Brien, M. Pink, E. R. Davidson and G. Christou, *Inorg. Chem.*, 2003, **42**, 7819; (*b*) C. Cañada-Vilalta, E. Rumberger, E. K. Brechin, W.

Wernsdorfer, K. Folting, E. R. Davidson, D. N. Hendrickson and G. Christou, *J. Chem. Soc., Dalton Trans.*, 2002, 4005; (*c*) C. Cañada-Vilalta, T. A. O'Brien, E. K. Brechin, M. Pink, E. R. Davidson and G. Christou, *Inorg. Chem.*, 2004, **43**, 5505; (*d*) E. K. Brechin, M. J. Knapp, J. C. Huffman, D. N. Hendrickson and G. Christou, *Inorg. Chim. Acta*, 2000, **297**, 389.

93. *See references therein* C. E. Dubé, S. Mukhopadhyay, P. J. Bonitatebus Jr., R. J. Staples and W. H. Armstrong, *Inorg. Chem.*, 2005, **44**, 5161.

94. A. K. Boudalis, N. Lalioti, G. A. Spyroulias, C. P. Raptopoulou, A. Terzis, A. Bousseksou, V. Tangoulis, J.-P. Tuchagues and S. P. Perlepes, *Inorg. Chem.*, 2002, **41**, 6477.

Chapter 2

2.0 Blending 2-Pyridine Alcohols on a Ni(II) or Cu(II) Centre

In this chapter the synthetic, structural and physical studies of complexes prepared from the reactions of metal acetates with ligand combinations involving 2-pyridinols and 2-pyridine alcohols of the generic formula 2-{$(CH_2)_nOH$}-6-X-C_5H_3N [X = Cl, n = 0, Hchp; X = H, n = 1, hmpH; X = H, n = 2, hepH; X = H, n = 3, hppH] are described (Table 1).

Table 1 2-pyridine alcohols to be employed

Abbreviation	Hchp	hmpH	hepH	hppH
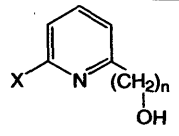	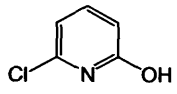	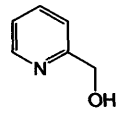	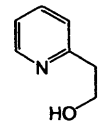	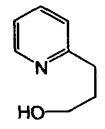
X	Cl	H	H	H
n	0	1	2	3
pK_a[5]	0.10	5.01	5.17	5.62

Hchp, hmpH and hepH each have an independent track record for the synthesis of polymetallic complexes (Chapter 1, section 1.2.1)[1-3,6,7,9-12] and can be neutral or monoanionic binding through the oxygen and/or nitrogen atoms. On the other hand, there are no examples of complexes containing hppH. Bonding modes featuring the deprotonated ligands can be classified using the Harris notation and this will be used to describe structural bonding modes throughout this work (Scheme 1).[1,4] Notably, the reactivity of blends of 2-pyridine alcohols towards metal acetates has not, to the knowledge of the author, been examined.

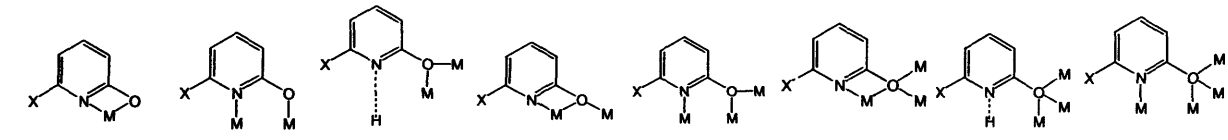

1.11	2.11	2.20	2.21	3.21	3.31	3.30	4.31

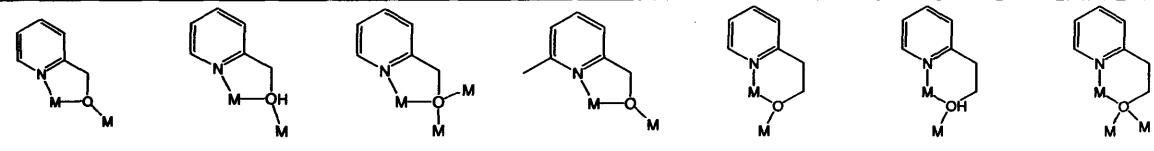

2.21	2.21	3.31	2.21	2.21	2.21	3.31

Scheme 1 Reported bonding modes of 2-pyridine alkoxides and the Harris notation.

The main aim of this chapter is to focus on the coordination chemistry of divalent nickel and copper ions supported by combinations of 2-pyridine alcohols or ligands derived from 2-pyridine alcohols. In particular, the effect of the pyridine alcohol methylene chain length (n = 0 – 3) of the participating ligands is systematically examined (sections 2.1 and 2.2). Spectroscopic/spectrometric data and magnetic measurements are used to support and complement the single crystal X-ray determinations. Scheme 2 shows the general synthetic strategy to be employed and stoichiometry of reagents and the solvents used for all reactions.

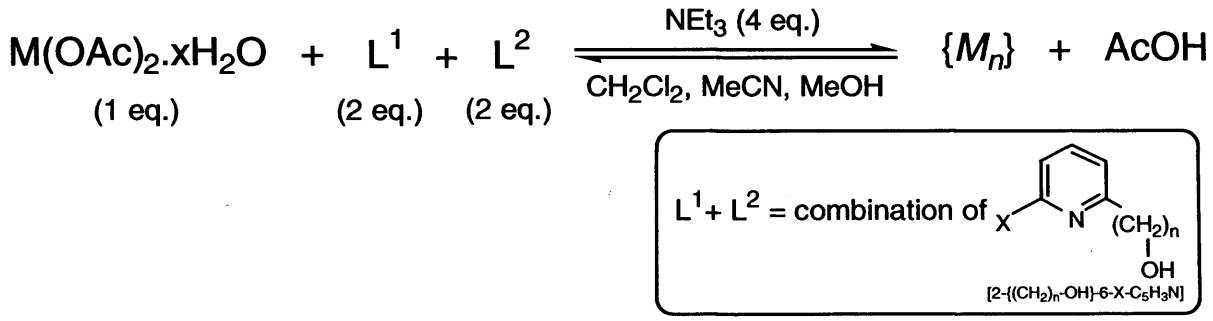

Scheme 2 Synthetic strategy employed.

2.1 Blending 2-Pyridine Alcohols on a Ni(II) Centre

2.1.1 M = Ni, L^1 = Hchp, L^2 = hmpH

The reaction of nickel acetate tetrahydrate with Hchp and hmpH in a trisolvent mixture comprising CH_2Cl_2, MeCN and MeOH gave, on crystallisation, $[Ni(chp)_2(hmpH)_2]$ (**1a**) in low yield (Scheme 3). Complex **1a** has been characterised by elemental analysis, IR and ^1H NMR spectroscopy (Table 13) along with positive FAB spectrometry. In addition, a single crystal of **1a** was subject to an X-ray diffraction study. The molecular structure of **1a** is shown in Figure 1(a); selected bond lengths and angles are given in Table 2.

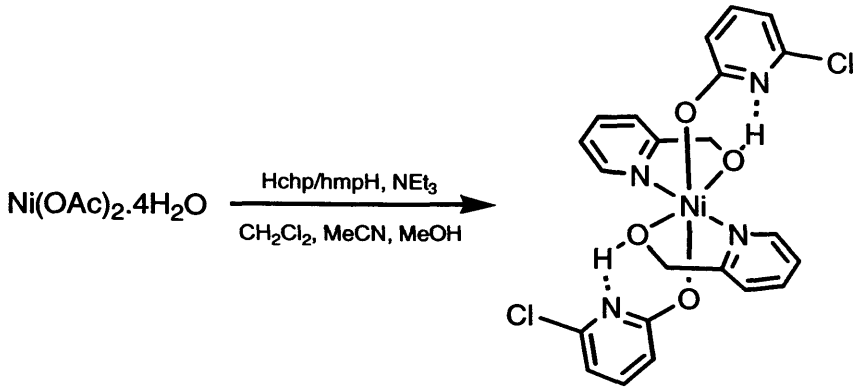

Scheme 3 Synthesis of **1a**.

Table 2 Selected bond length (Å) and angle (°) data for **1a** and **1b**

1a		**1b**			
Ni(1)-O(1)	2.0642(11)	Ni(1)-O(1)	2.130(11)	Ni(1)-N(2)	2.039(12)
Ni(1)-N(1)	2.0356(14)	Ni(1)-N(1)	2.115(12)	Ni(1)-O(3)	2.035(12)
Ni(1)-O(2)	2.0785(12)	Ni(1)-O(2)	2.084(11)	Ni(1)-O(4)	2.057(11)
N(1)-Ni(1)-O(1)	81.32(5)				
		N(1)-Ni(1)-O(1)	89.7(5)	O(3)-Ni(1)-N(2)	88.8(5)
N(1)-Ni(1)-O(1)#1	98.68(5)	O(2)-Ni(1)-O(1)	179.2(4)	O(4)-Ni(1)-O(1)	92.1(4)
N(1)-Ni(1)-O(2)	90.47(5)	N(2)-Ni(1)-N(1)	178.9(5)	O(4)-Ni(1)-O(1)	88.7(5)
N(1)-Ni(1)-O(2)#1	89.53(5)	O(2)-Ni(1)-N(1)	90.9(5)	O(4)-Ni(1)-O(2)	87.4(4)
O(1)-Ni(1)-O(2)#1	91.97(5)	N(2)-Ni(1)-O(1)	90.5(5)	O(4)-Ni(1)-O(2)	90.2(4)
O(1)#1-Ni(1)-O(2)#1	88.03(5)	O(3)-Ni(1)-O(1)	88.1(4)	O(3)-Ni(1)-O(4)	178.9(5)
		O(3)-Ni(1)-N(1)	92.4(5)	N(2)-Ni(1)-O(4)	90.2(4)
		O(3)-Ni(1)-O(2)	92.4(5)		

Symmetry transformations used to generate equivalent atoms: **1a** #1 ($-x, -y+2, -z$).

The molecular structure of **1a** reveals an octahedral Ni(II) ion surrounded by two chp ligands and two hmpH ligands. The chp oxygen atoms are *trans* axially coordinated as monodentate η^1-pyridine alkoxides adopting a 1.10 bonding mode. Two *trans* hmpH ligands form five-membered chelate rings with the Ni(II) ion, with the ligand adopting a 1.11 *N,O*-chelating bonding mode. The close proximity of the hmpH hydroxyl moiety with the chp nitrogen atom in **1a** results in an intramolecular inter-ligand hydrogen bonding interaction [$O_{hmpH}(1)\cdots N_{chp}(2)$ = 2.5595(18) Å].

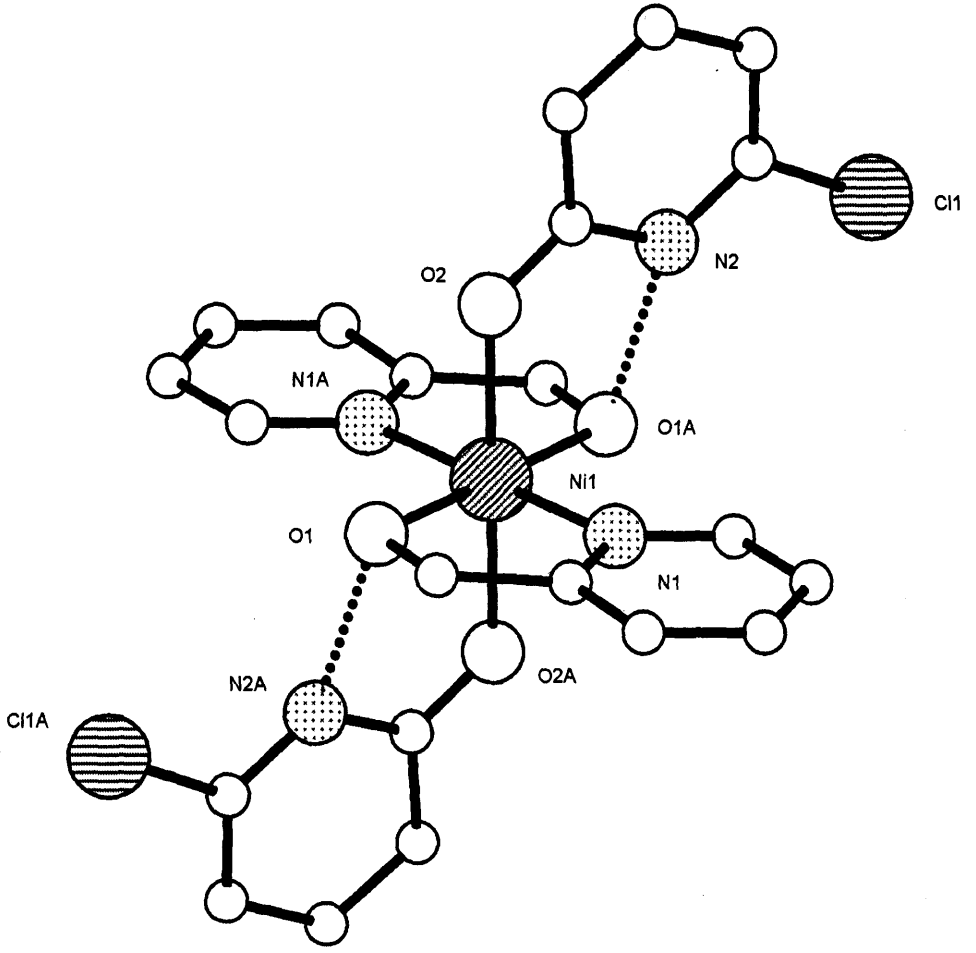

(a)

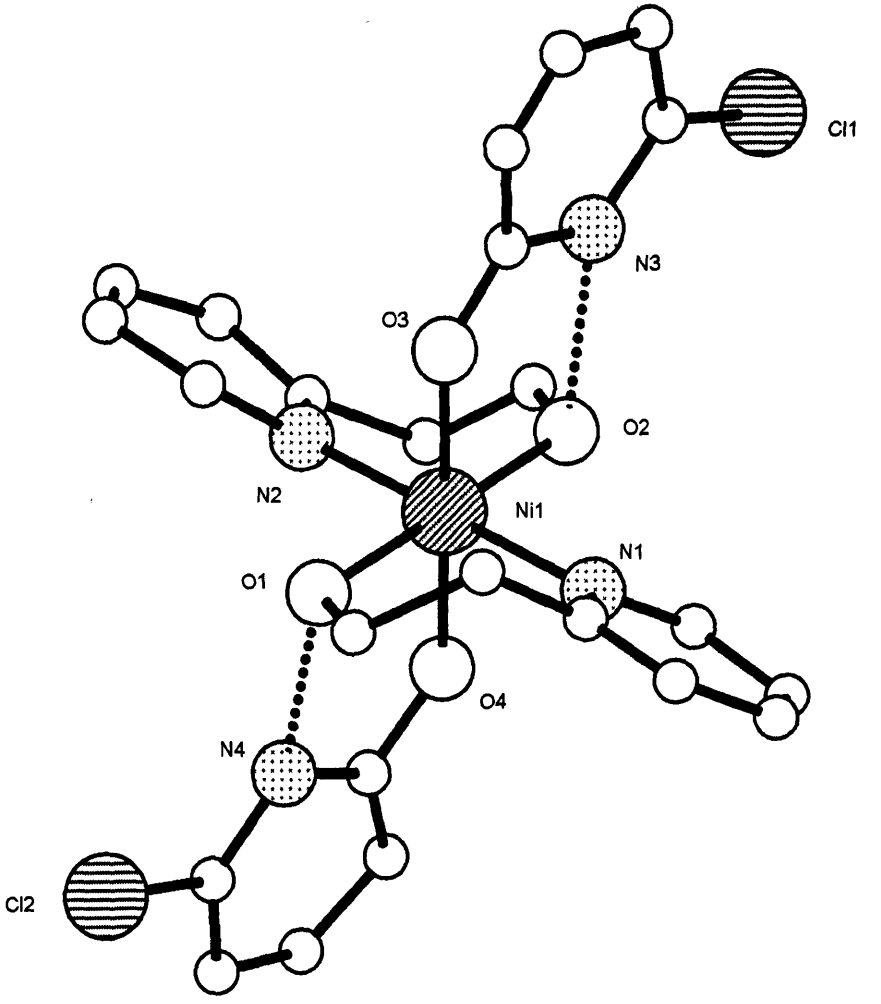

(b)

Figure 1 Molecular structures of (a) **1a** and (b) **1b**. Letter labelled atoms are generated by symmetry. Hydrogen atoms are excluded and carbon atoms are unlabelled for clarity. Dotted bonds indicate hydrogen bonding interactions.

The IR spectrum of **1a** exhibits a strong pyridyl ν(C=N) stretching band at 1596 cm^{-1}.[28,29] The room temperature magnetic moment for **1a** at 2.69 BM ($\chi_M T$ = 0.90 emu K mol^{-1}) is slightly less than compared to a single paramagnetic divalent nickel ion possessing two unpaired electrons (2.83 BM, $\chi_M T$ = 1.00 emu K mol^{-1}, ***SEE NOTE***).[24c,24e] The FAB mass spectrum of **1a** shows a $[M - 2chp]^+$ peak at 277 Da.

2.1.2 M = Ni, L^1 = Hchp, L^2 = hepH

When hmpH is replaced by hepH in the above reaction, crystals of $[Ni(chp)_2(hepH)_2]$ (**1b**) are obtained in low yield (Scheme 4). Complex **1b** was characterised by elemental analysis, IR and ^1H NMR spectroscopy (Table 13) along with positive FAB mass spectrometry. A single crystal of **1b** was subject to an X-ray diffraction study. The molecular structure of **1b** is shown in Figure 1(b); selected bond lengths and angles are given in Table 2.

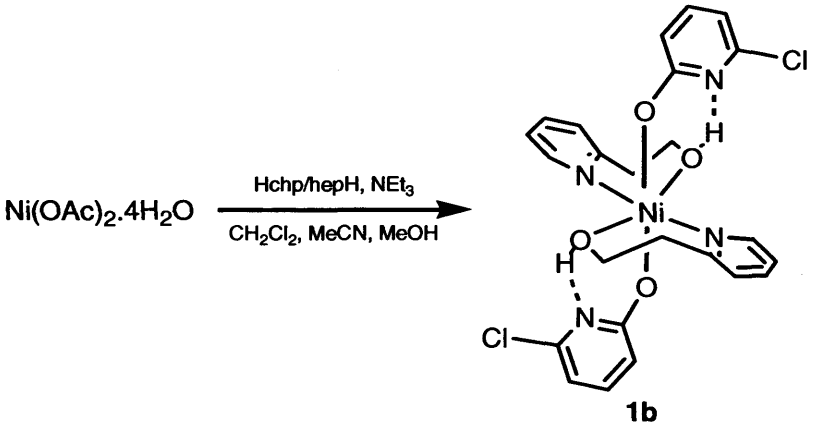

Scheme 4 Synthesis of **1b**.

Two different molecules crystallise within the same unit cell of **1b**; herein, only one of these molecules will be considered. The molecular structure of **1b** reveals an octahedral Ni(II) ion surrounded by two chp and two hepH ligands. The *trans N,O*-chelating hepH ligands form puckered boat-shape six-membered chelate rings with the metal centre and adopt a 1.11 bonding mode; the 1.10 chp ligands are η^1-bound in a similar fashion to **1a**. An intramolecular hydrogen inter-ligand bonding interaction is obtained between the chp

nitrogen atom and hepH hydroxyl group [$O_{hepH}(1)\cdots N_{chp}(4)$ = 2.511(16) Å $O_{hepH}(2)\cdots N_{chp}(3)$ = 2.634(15)].

The hepH-containing chelate bite angle of $N_{hepH}(1)$-Ni(1)-$O_{hepH}(1)$ opens up by a few degrees to 89.7(5)° in **1b** compared to 81.32(5)° for **1a**. The longest nickel-ligand bond length in **1a** of Ni(1)-O(2) at 2.0785(12) Å is obtained from the chp alkoxide. In contrast, the longest bond length in **1b** is from a hepH hydroxy oxygen atom [Ni(1)-O(1) at 2.130(11) Å]. The flexibility of the six-membered chelate in **1b** is also reflected by a longer Ni(1)-N(1) bond length at 2.115(12) Å, which is shorter in **1a** at 2.0356(14) Å. The second chelating hepH ligand in **1b** has shorter Ni(1)-O(2) and Ni(1)-N(2) bond lengths which are closer to the values found for the hmpH ligands in **1a** (Table 2).

The η^1 Ni-O_{chp} bond length values in **1a** and **1b** are comparable to those found in the pentacoordinated monomeric salt [Ni(2,4,4-trimethyl-1,5,9-triazacyclododec-1-ene)(chp)][ClO_4].[6] The reported complex contains a chelating 1.11 chp ligand coordinated to a square pyramidal nickel ion with the bond lengths for the *N,O*-chelated pyridine alkoxide being Ni-O_{chp} = 2.074(3) Å and Ni-N_{chp} = 2.103(3) Å. A heptanuclear complex [$Ni_7(chp)_{12}(MeOH)_6Cl_2$], again containing 1.11 chp ligands bound to octahedral Ni(II) ions, shows Ni-O_{chp} bond lengths in the 1.976 – 2.198 Å range. These values have been attributed to a non-sterically crowded molecule and fall within the same bond length range found for compounds **1a** and **1b**.[7]

The IR spectrum of **1b** exhibits a strong pyridyl ν(C=N) band at 1572 cm^{-1}.[28,29] The room temperature magnetic moment for **1b** at 2.93 BM ($\chi_M T$ = 1.07 emu K mol^{-1}) is slightly more than compared to a single paramagnetic divalent nickel ion (***SEE NOTE***).[24c,24e] The FAB mass spectrum of **1b** shows a base peak of [*M* – hepH – chp]$^+$ at 310 Da.

2.1.3 M = Ni, L^1 = Hchp, L^3 = hppH

Using a ligand blend consisting of Hchp and the least acidic hppH, gave crystals that were unsuitable for an X-ray diffraction study. The crystalline material was primarily characterised by elemental analysis and is tentatively ascribed the empirical formula $[Ni(chp)_2(hppH)_2]$ (**1c**) (Scheme 5). Additionally, complex **1c** was characterised by IR spectroscopy and by positive FAB mass spectrometry.

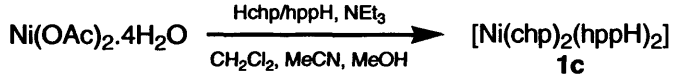

Scheme 5 Synthesis of **1c**.

2.1.4 M = Ni, L^1 = hmpH, L^3 = hepH or hppH

Reaction of a combination of hmpH and hppH with nickel acetate tetrahydrate, results in incomplete displacement of acetate ligands giving $[Ni(hmpH)_2(CH_3COO)_2]$ (**2a**) in low yield (Scheme 6). **2a** was also obtained when a combination of hmpH and hepH was employed. Complex **2a** was characterised using elemental analysis, IR and ^1H NMR spectroscopy (Table 13) along with positive FAB mass spectrometry. A single crystal of **2a** was subject to an X-ray diffraction study. The molecular structure of **2a** is depicted in Figure 2(a); selected bond lengths and angles are shown in Table 3.

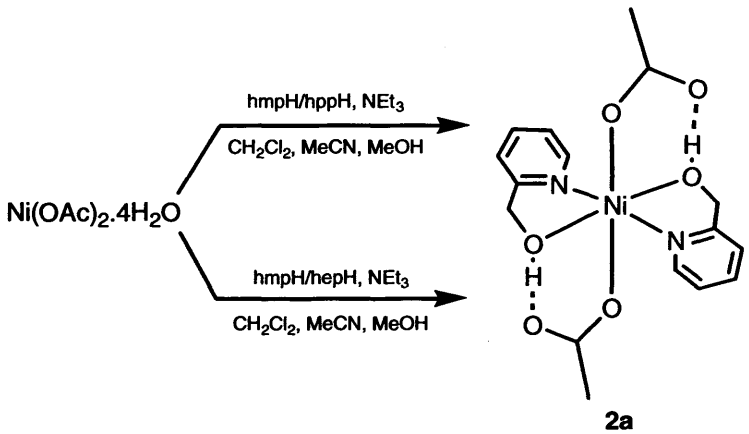

Scheme 6 Synthesis of **2a**.

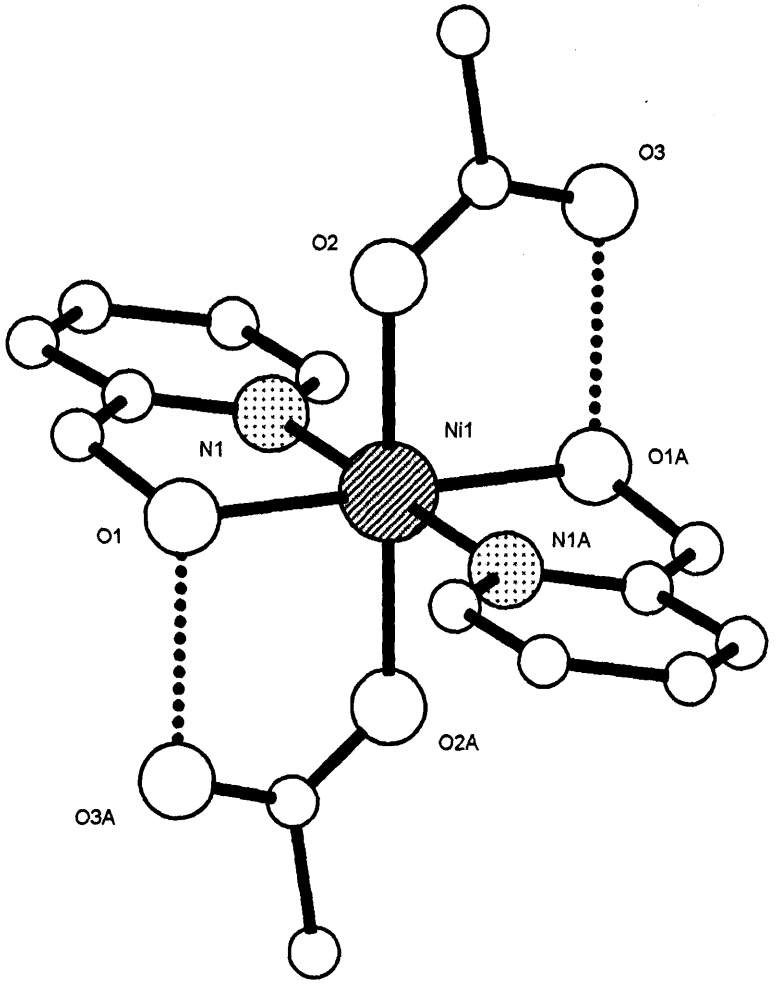

(a)

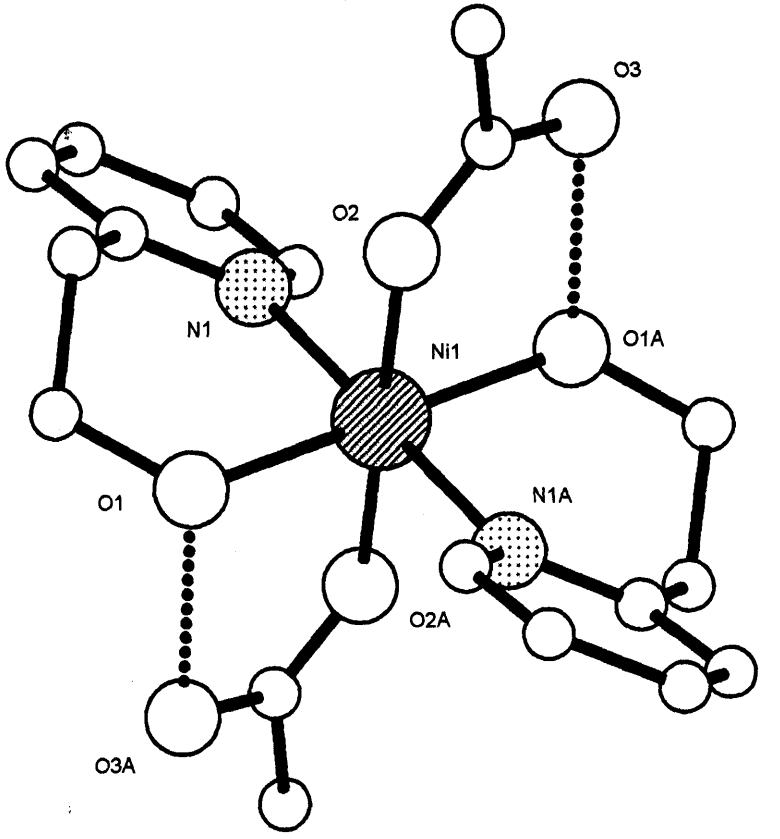

(b)

Figure 2 Molecular structures of (a) **2a** and (b) **2b**. Hydrogen atoms and carbon atom labels are removed for clarity. Letter labelled atoms are generated by symmetry. Dotted bonds show hydrogen bonding interactions.

In the molecular structure of **2a**, an octahedral Ni(II) ion is bound to two intact η^1-*trans* axial acetates and two *trans*-bound 1.11 *N,O*-chelating hmpH ligands in a fashion similar to that found in **1a** (Figure 1). The longest bond length in **2a** is from the bound acetate oxygen atom of Ni(1)-$O_{acetate}$(2) at 2.0950(14) Å, while the shortest bond length is from the hmpH nitrogen atom [Ni(1)-N_{hmpH}(1) = 2.0395(17) Å].

The ionic nature of the acetate to metal bonds in **2a** are suggested by the following acetate C-O bond lengths; 1.251(3) Å (bound), 1.265(3) Å (unbound) [for Ni(II): range ~ 1.263 – 1.268 Å ⇒ ~15 – 20% covalent C-O bond character].[8] The hmpH hydroxyl unit undergoes a intramolecular inter-ligand hydrogen bonding interaction with a neighbouring unbound carboxylate oxygen atom [O_{hmpH}(1)···$O_{acetate}$(3A) = 2.497(3) Å].

Table 3 Selected bond length (Å) and angle (°) data for **2a** and **2b**

2a		**2b**	
Ni(1)-O(1)	2.0654(14)	Ni(1)-O(1)	2.1009(12)
Ni(1)-N(1)	2.0395(17)	Ni(1)-N(1)	2.0863(15)
Ni(1)-O(2)	2.0950(14)	Ni(1)-O(2)	2.0604(12)
N(1)-Ni(1)-O(1)	81.45(6)	N(1)-Ni(1)-O(1)	89.24(5)
N(1)-Ni(1)-O(1)#1	98.55(6)	N(1)#1-Ni(1)-O(1)	90.76(5)
O(1)-Ni(1)-O(2)#1	91.61(6)	O(2)-Ni(1)-O(1)#1	91.06(5)
O(1)-Ni(1)-O(2)	88.39(6)	O(2)-Ni(1)-O(1)	88.94(5)
N(1)-Ni(1)-O(2)	87.88(6)	N(1)-Ni(1)-O(2)	92.07(5)
N(1)#1-Ni(1)-O(2)	92.12(6)	O(2)-Ni(1)-N(1)#1	87.93(5)

Symmetry transformations used to generate equivalent atoms: **2a** and **2b** #1 ($-x, -y, -z$).

The IR spectrum of **2a** exhibits a strong $\nu(CO_2)_{symm}$ band at 1405 cm^{-1}.[28] The room temperature magnetic moment for complex **2a** at 2.88 BM ($\chi_M T$ = 1.03 emu K mol^{-1}) is consistent with a single divalent nickel ion (***SEE NOTE***).[24c,24e] The FAB mass spectrum of **2a** shows a $[M]^+$ peak at 395 Da.

2.1.5 M = Ni, L^1 = hepH, L^2 = hppH

Use of a ligand blend made up of hppH and hepH, again results in ligand competition. The more acidic hepH ligand dominates the reaction and affords $[Ni(hepH)_2(CH_3COO)_2]$ (**2b**) in low yield (Scheme 7). Complex **2b** was characterised by elemental analysis, IR and ^1H NMR spectroscopy (Table 13) along with positive FAB mass spectrometry. A single crystal of **2b** was subject to an X-ray diffraction study. The molecular structure of **2b** is depicted in Figure 2(b); selected bond lengths and angles are shown in Table 3.

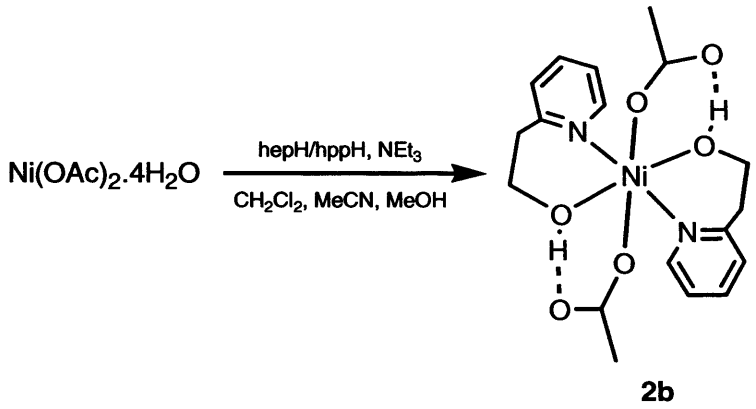

2b

Scheme 7 Synthesis of **2b**.

The structure of **2b** reveals an octahedral Ni(II) ion coordinated by two intact *trans* η^1-acetates and two 1.11 bound hepH ligands which form two six-membered *N,O*-chelate rings. The hepH-containing chelates are distorted and puckered in a similar fashion to **1b**. The chelate bite angle around the nickel ion of N(1)-Ni(1)-O(1) opens up from **2a** to **2b** with values of 81.45(6)° and 89.24(5)°, respectively. Both **2a** and **2b** have internal ligand to metal to ligand atom bond angles that denote a distorted octahedral environment around the Ni(II) ions. The ionic nature of the acetate to metal bonds in **2b** are suggested by the following acetate C-O bond lengths; 1.260(2) Å (bound), 1.255(2) Å (unbound).[8] In **2b**, there is an intramolecular inter-ligand hydrogen bonding interaction from the hepH towards the pendant carboxylate oxygen atom [$O_{hepH}(1)\cdots O_{acetate}(3)$ = 2.523(2) Å].

The IR spectrum of **2b** exhibits a strong $\nu(CO_2)_{symm}$ band at 1411 cm^{-1}.[28] The room temperature magnetic moment for complex **2b** at 3.22 BM ($\chi_M T$ = 1.30 emu K mol^{-1}) is

slightly more than compared to a monometallic divalent nickel (***SEE NOTE***).[24c,24e] The FAB mass spectrum of **2b** shows a $[M]^+$ peak at 423 Da.

2.2 Blending 2-Pyridine Alcohols on a Cu(II) Centre

2.2.1 M = Cu, L^1 = Hchp, L^2 = hmpH

The combination of Hchp and hmpH as the ligand blend with copper acetate affords, on crystallisation, the polymeric species $[Cu(chp)(hmp)]_n$ (**3**) in moderate yield (Scheme 8). Use of mehmpH (pK_a 5.25),[5] in place of hmpH also affords a polymeric species of composition $[Cu(chp)(mehmp)]_n$ (**3'**). Complexes **3** and **3'** were characterised by IR and ^1H NMR spectroscopy (**3**, Table 14) along with positive FAB mass spectrometry. A single crystal of **3** was subject to an X-ray diffraction study. The molecular structure of **3** is depicted in Figure 3; selected bond lengths and angles are given in Table 4.

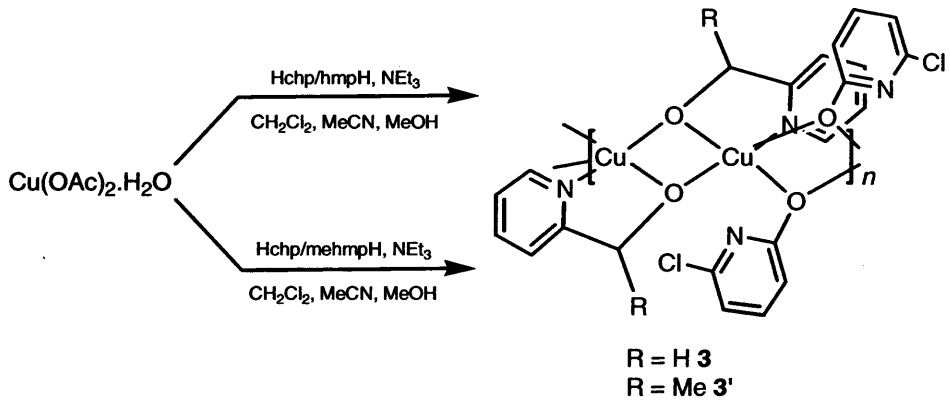

Scheme 8 Synthesis of **3** and **3'**.

The molecular structure of **3** consists of a polymeric chain of trigonal bipyramidal Cu(II) ions coordinated by monoanionic chp and hmp ligands. The chp and hmp ligands are disposed *trans* to one another. The chp ligand is 2.20 bound, in which the chp oxygen bridges over two metal centres (η^1, μ_2). The 2.21 bound hmp ligand is both *N,O*-chelating and bridging (η^1, μ_2). Penta-coordination around each copper ion comprises a nitrogen atom from hmp, two oxygen atoms from two separate η^1- or μ_2-bound chp bridges and two η^1- or μ_2-bound (bridging and chelating) oxygen atoms from separate hmp bridges.

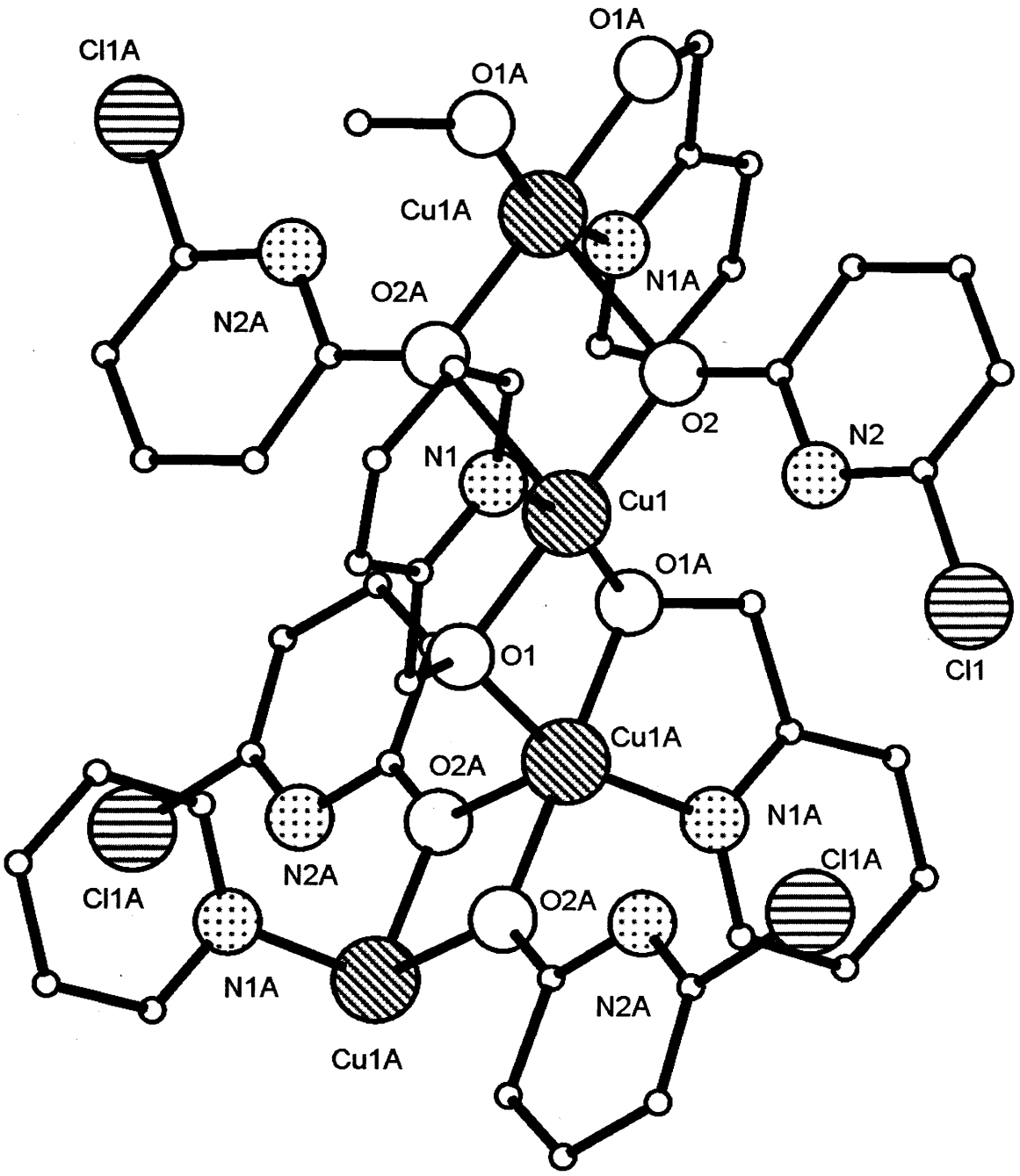

Figure 3 Molecular structure of part of the chain structure of **3**. Hydrogen atoms and carbon atom labels are excluded for clarity. Letter labelled atoms are generated by symmetry.

Table 4 Selected bond length (Å) and angle (°) data for **3**

3					
Cu(1)-O(1)	1.942(2)	O(1)-Cu(1)#1	1.947(3)	Cu(1)-N(1)	1.975(3)
Cu(1)-O(2)	1.928(2)	Cu(1)-O(2)#2	2.402(3)	Cu(1)···Cu(1)#1	2.9075(11)
O(1)-Cu(1)-O(1)#1	79.80(11)	O(1)-Cu(1)-N(1)	82.73(11)	O(1)-Cu(1)-Cu(1)#1	41.68(7)
O(1)-Cu(1)-O(2)#2	104.10(10)	Cu(1)-O(2)-Cu(1)#2	103.35(11)	O(1)#1-Cu(1)-Cu(1)#1	41.56(7)
O(1)#1-Cu(1)-O(2)#2	105.52(10)	O(1)#1-Cu(1)-N(1)	159.63(11)	O(2)-Cu(1)-Cu(1)#1	137.87(8)
O(2)-Cu(1)-O(1)	179.25(11)	O(2)-Cu(1)-N(1)	97.35(12)	O(2)#2-Cu(1)-Cu(1)#1	122.44(6)
O(2)-Cu(1)-O(1)#1	99.98(11)	N(1)-Cu(1)-O(2)#2	88.82(11)	N(1)-Cu(1)-Cu(1)#1	118.37(9)
O(2)-Cu(1)-O(2)#2	76.65(11)				

Symmetry transformations used to generate equivalent atoms: **3** #1 ($-x, y, -z+3/2$), #2 ($-x, -y, -z+2$).

The copper to ligand atom bond lengths in **3** are all relatively short in comparison to the previously described nickel complexes (see section 2.1). The longest bond length of Cu(1)-O(2A) at 2.402(3) Å, belongs to the μ_2-chp bridging oxygen atom. Copper(II) ions within the polymer are separated at a distance of 2.9075(11) Å [Cu(1)···Cu(1A)].

A related dimeric copper complex $[Cu_2(chp)_4]$, displaying square planar copper ions arranged in a paddle wheel arrangement possessing 2.11 chp bridging ligands, has been reported.[9a-b] The Cu-O_{chp} bond lengths in $[Cu_2(chp)_4]$ average to 1.929 Å, the corresponding bond length found in complex **3** is very close to this value at 1.928(2) Å. However, a monomeric complex [Cu{2-(pyridyl-2-amino)-pyridine}$(chp)_2$] containing chelating 1.11 and pendant 1.01 chp ligands has a longer Cu-O_{chp} bond length at 1.963(4) Å.[10]

Other reported square-based pyramidal copper complexes containing chp ligands include $[Cu(chp)_2(2,2\text{-bipyridine})(H_2O)]$ and $[Cu(chp)_2(bipy)]_2$.[11] The monomeric complex has 1.10 chp bonding mode with a Cu-O_{chp} bond length averaging to 1.936 Å. The dimeric complex has 1.10 pendant and 2.20 bridging chp bonding modes, with corresponding bond lengths of Cu_{chp}-O = 1.928(2) Å and Cu_{chp}-O = 1.942(2) Å, respectively. These bond length values are comparable to those in complex **3** despite their structural differences.

A binuclear copper complex $[Cu(hmp)(NCS)]_2$ containing a 2.21 bridging and chelating hmp ligand has been investigated.[12] The Cu-N_{hmp} and Cu-O_{hmp} bond lengths in this complex average to 1.924 Å and 1.989 Å, respectively. In complex **3**, the η^1 Cu(1)-

$O_{hmp}(1)$ and Cu(1)-$N_{hmp}(1)$ bond lengths are 1.942(2) Å and 1.975(3) Å, respectively. Therefore, these values only differ slightly from the reported complex.

The IR spectra of **3** and **3'** exhibit strong pyridyl ν(C=N) stretching bands at 1585 cm^{-1} and 1570 cm^{-1}, respectively.[28,29] Complexes **3** and **3'** exhibit room temperature magnetic moments at 1.37 BM ($\chi_M T$ = 0.23 emu K mol^{-1}) and 1.63 BM ($\chi_M T$ = 0.33 emu K mol^{-1}), respectively (298 K). These values are slightly less than compared to a single non-interacting divalent copper ion possessing one unpaired electron (1.73 BM, $\chi_M T$ = 0.38 emu K mol^{-1}, ***SEE NOTE***).[24c,24e] The FAB mass spectra of **3** and **3'** show fragmentation peaks associated with the asymmetric (monomeric) unit as $[M_{(n=1)} + Cu]^+$ at 363 Da. (**3**) and 377 Da. (**3'**).

2.2.2 M = Cu, L^1 = Hxhp, L^2 = hepH

Reactions of a ligand blend composed of Hxhp [HxpH = Hchp or Hbhp (pK_a 0.10)[5]] and hepH and copper acetate monohydrate leads, on crystallisation, to the binuclear complexes $[Cu(xhp)(hep)]_2$ [xhp = chp (**4a**); bhp (**4b**)] in moderate yield (Scheme 9). Complexes **4a** and **4b** were characterised by elemental analysis, IR and ^1H NMR spectroscopy (**4a**, Table 14) along with positive FAB mass spectrometry. Single crystals of **4a** and **4b** were subject to X-ray diffraction studies. The molecular structures of **4a** and **4b** are depicted in Figure 4; selected bond lengths and angles are shown in Table 5.

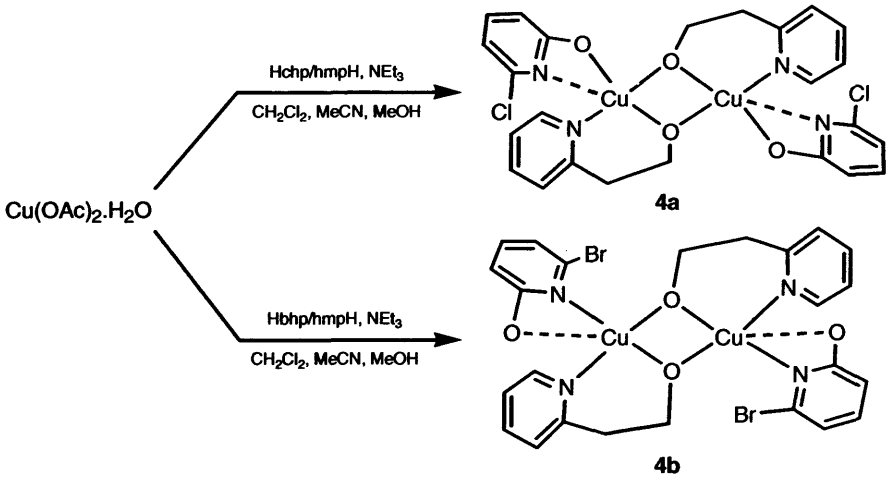

Scheme 9 Synthesis of **4a** and **4b**.

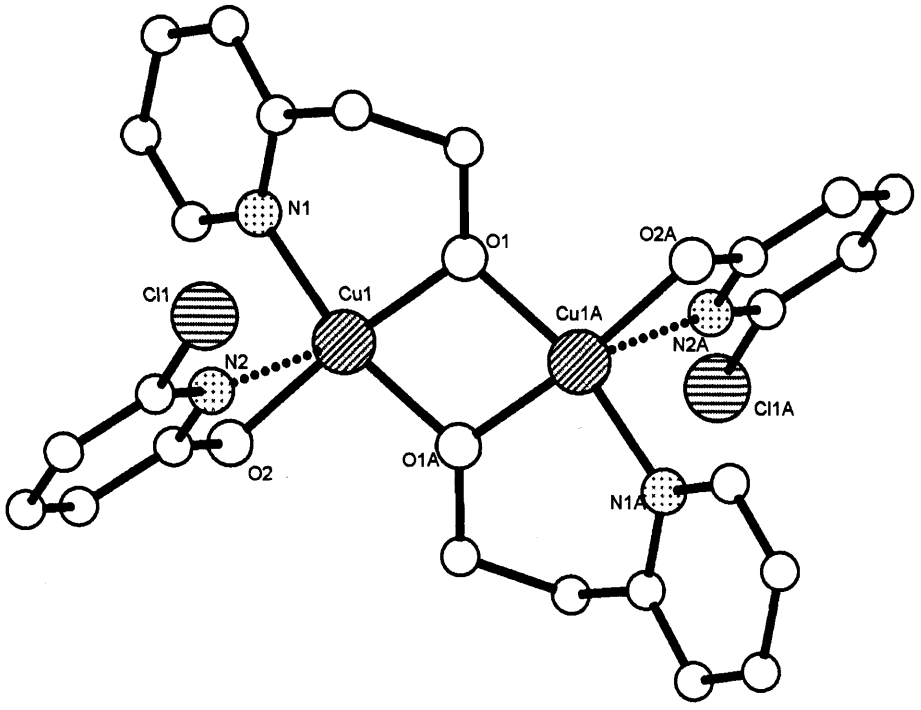

(a)

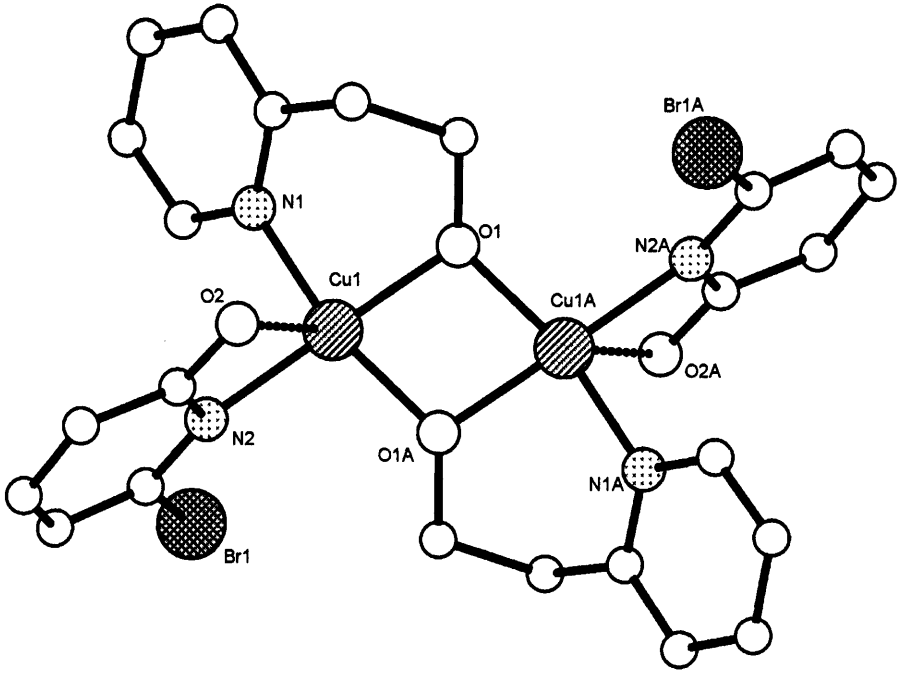

(b)

Figure 4 Molecular structures of (a) **4a** and (b) **4b**. Hydrogen atoms and carbon atom labels are excluded for clarity. Letter labelled atoms are generated by symmetry. Dotted lines indicate pseudo-axial interactions.

The molecular structure of **4a** reveals a dimeric unit in which the two pseudo-square planar Cu(II) ions are coordinated by two chp and hep ligands. In **4a**, there are two *trans* 1.10 η^1-bound chp molecules as monodentate ligands from the alkoxide oxygen atom. The two hep moieties are bound as 2.21 *N,O*-chelating and bridging (η^1, μ_2) ligands in a similar fashion to the hmp ligands in complex **3**. The hep bridge in **4a** leads to the formation of a discrete $[Cu_2O_2]$ rhombic core. The Cu(1)-O_{chp}(2) bond length is 1.940(3) Å and is consistent with values previously stated for the monodentate pyridine alkoxide bonds.[10,11] There are many examples of *N,O*-bridged dimeric complexes which have been extensively studied for biological applications, including catacholase activity,[12,13,14a-b] other metalloproteins,[15a-d] and for their interesting magnetic properties.[16a-e, 18h]

Table 5 Selected bond length (Å) and angle (°) data for **4a** and **4b**

	4a	**4b**
Cu(1)-O(1)	1.922(3)	1.999(2)
Cu(1)-O(1)#1	1.930(3)	1.962(2)
Cu(1)-N(1)	1.991(3)	2.005(3)
Cu(1)-O(2)	1.940(3)	2.605(3)
Cu(1)···N(2)	2.537(3)	2.079(3)
Cu(1)···Cu(1)#1	3.0305(10)	3.0935(10)
O(1)-Cu(1)-O(1)#1	76.21(11)	77.28(10)
O(1)-Cu(1)-N(1)	93.07(12)	90.28(10)
O(1)#1-Cu(1)-N(1)	160.27(12)	162.18(10)
O(1)-Cu(1)-O(2)	171.95(10)	168.44(10)
O(1)#1-Cu(1)-O(2)	97.29(11)	100.42(9)
O(2)-Cu(1)-N(1)	94.50(12)	94.24(10)
Cu(1)-O(1)-Cu(1)#1	103.79(11)	102.72(10)
O(1)-Cu(1)-Cu(1)#1	38.20(7)	
O(1)#1-Cu(1)-Cu(1)#1	38.01(7)	
N(1)-Cu(1)-Cu(1)#1	129.30(9)	
O(2)-Cu(1)-Cu(1)#1	135.12(8)	

Symmetry transformations used to generate equivalent atoms: #1 **4a** $(-x, y+1, -z)$, **4b** $(-x, -y+1, -z+1)$.

The molecular structure of **4b** also reveals a dimeric unit in which two pseudo-square planar Cu(II) ions are bound by two bhp and hep ligands. However, bhp exhibits a 1.01 bonding mode by η^1 coordination from the pyridyl nitrogen atom rather than from the

oxygen (*e.g.*, **4a**). It is uncertain as to why a different coordination mode is exhibited by the bhp ligand but could originate from a change in electronegativity.

The Cu(1)-N_{bhp}(2) bond length at 2.079(3) Å in **4b** is slightly longer than the corresponding reported values for the paddlewheel complex $[Cu_2(bhp)_4]$, in which case the 2.11 bound bhp ligands result in an average Cu-N_{bhp} bond length of 2.036 Å.[9a] The hep chelate bite angle formed in **4a** around the Cu(II) ions of O(1)-Cu(1)-N(1) is 93.07(12)°, whereas, the same angle decreases to 90.28(1)° in **4b**.

Copper dimers containing hep as a bridging and chelating ligand have featured in one report.[12] The complex $[Cu(hep)(NCO)]_2$ is bound to a 2.21 hep ligand, with the Cu-O_{hep} and Cu-N_{hep} bond lengths in this complex being Cu-η^1-O = 1.919(3) Å, Cu-μ_2-O = 1.947(3) Å and Cu-μ-N = 2.032(4) Å, respectively. Complexes **4a** and **4b** display corresponding bond lengths of Cu-η^1-O = 1.922(3) Å, Cu-μ_2-O = 1.930(3) Å, Cu-μ_1-N = 1.991(3) Å (**4a**) and Cu-η^1-O = 1.962(2) Å, μ_2-O = 1.999(2) Å, μ-N = 2.005(3) Å (**4b**). It can be concluded that there are no significant differences between the values found for both complexes, any deviations can be accounted for by ligand variation. In addition, the hep chelate bite angle in $[Cu(hep)(NCO)]_2$ at 93.42(14)° is similar to the hep chelate angle in complex **4a**.[12]

The IR spectra of **4a** and **4b** exhibit strong pyridyl ν(C=N) stretching bands at ~ 1605 cm^{-1}.[28,29] The room temperature magnetic moment for complex **4a** at 1.87 BM ($\chi_M T$ = 0.44 emu K mol^{-1}) is less than expected for two non-interacting divalent copper ions with each possessing one unpaired electron (2.45 BM, $\chi_M T$ = 0.75 emu K mol^{-1}, ***SEE NOTE***).[24c,24e] The FAB mass spectra for the dimeric complexes include $[M]^+$ peaks at 626 Da. (**4a**) and 716 Da. (**4b**).

2.2.3 M = Cu, L^1 = Hxhp, L^2 = hppH

Reaction of a ligand blend consisting of hppH and Hxhp [Hxhp = Hchp or Hbhp] with copper acetate monohydrate forms, on work-up, crystals of $[Cu(xhp)(hpp)]_2 \cdot mMeOH$ [xhp = chp, m = 0 (**5a**); m = 2, bhp, (**5b**)] in good yield (Scheme 10). Complexes **5a** and **5b** were characterised by elemental analysis, IR and ^1H NMR spectroscopy (**5a**, Table 14) along with positive FAB mass spectrometry. Single crystals of **5a** and **5b** were subject to X-ray diffraction studies. The molecular structures of **5a** and **5b** are depicted in Figure 5; selected bond lengths and angles are shown in Table 6.

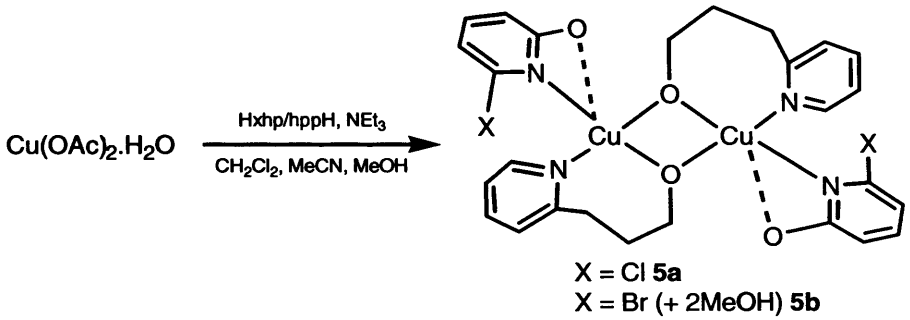

Scheme 10 Synthesis of **5a** and **5b**.

The molecular structures of **5a** and **5b** consist of two pseudo-square planar Cu(II) ions bound to two xhp and hpp ligands. The η^1-*N*-bound xhp ligands adopt a 1.01 bonding mode and the hpp ligands are 2.21 bound as both bridging and *N,O*-chelating ligands. The larger chelate bite angles created by the more flexible hpp ligands in **5a** and **5b** of O(1)-Cu(1)-N(1) are identical at 95.0(2)° and 95.0(5)°, respectively. The Cu(1)-N_{bhp}(2) bond length in **5b** at 1.988(14) Å is ~ 0.02 Å longer than the corresponding bond length found within **5a**.

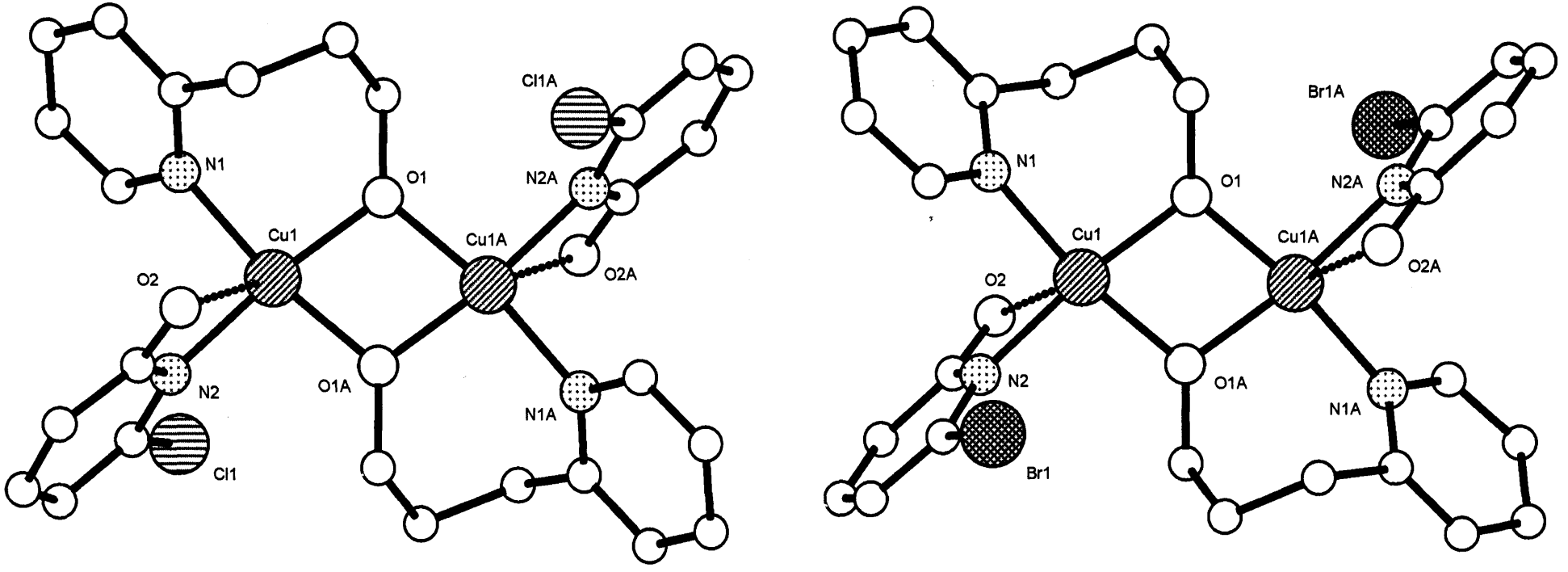

(a) (b)

Figure 5 Molecular structures of (a) **5a** and (b) **5b**. Hydrogen atoms and carbon atom labels are excluded for clarity. The solvent (MeOH) molecules found in **5b** are omitted. Letter labelled atoms are generated by symmetry. Dotted lines indicate pseudo-axial interactions.

Complex **5a** differs from **4a** by adopting a 1.01 chp bonding mode rather than a 1.10 chp bonding mode. A rational explanation for the change in bonding mode from hep-containing **4a** to hpp-containing **5a** could be that the large and flexible seven-membered chelate ring favours the 1.01 chp bonding mode (as the extra methylene group on hpp may be pushing chp away). There is a significant decrease in the bond length of Cu(1)-N_{chp}(2) = 1.978(4) Å in **5a** compared to **4b**. Another feature is that the transannular metal-metal ion distance in **5a** is large at 3.044 Å, thus, ruling out any direct copper to copper interactions.

Table 6 Selected bond length (Å) and angle (°) data for **5a** and **5b**

	5a	**5b**
Cu(1)-O(1)	1.924(5)	1.925(11)
Cu(1)-O(1)#1	1.928(5)	1.929(11)
Cu(1)-N(1)	2.020(5)	2.016(14)
Cu(1)-N(2)	1.978(5)	1.988(14)
Cu(1)···O(2)	2.621(6)	2.566(13)
Cu(1)···Cu(1)#1	3.0440(15)	3.036(4)
O(1)-Cu(1)-O(1)#1	75.6(2)	76.0(5)
O(1)-Cu(1)-N(1)	95.0(2)	95.0(5)
O(1)#1-Cu(1)-N(1)	168.7(2)	170.5(5)
O(1)-Cu(1)-N(2)	170.9(2)	171.7(5)
O(1)#1-Cu(1)-N(2)	97.0(2)	96.2(5)
N(2)-Cu(1)-N(1)	92.9(2)	92.9(6)
Cu(1)-O(1)-Cu(1)#1	129.3(4)	104.0(5)
O(1)-Cu(1)-Cu(1)#1	37.84(13)	38.1(3)
O(1)#1-Cu(1)-Cu(1)#1	37.74(14)	38.0(3)
N(1)-Cu(1)-Cu(1)#1	132.58(15)	133.0(4)
N(2)-Cu(1)-Cu(1)#1	134.49(16)	134.1(4)

Symmetry transformations used to generate equivalent atoms: #1 **5a** ($-x, -y+1, -z+1$), **5b** ($-x+1, -y+2, -z$).

The IR spectra of **5a** and **5b** show strong pyridyl ν(C=N) stretching bands at 1604 cm^{-1} and 1603 cm^{-1}, respectively.[28,29] The room temperature magnetic moments for complexes **5a** and **5b** at 1.58 BM ($\chi_M T$ = 0.31 emu K mol^{-1}) and 2.17 BM ($\chi_M T$ = 0.59 emu K mol^{-1}), respectively, are less than expected for two non-interacting divalent copper ions

(***SEE NOTE***).[24c,24e] The FAB mass spectra for the dimeric complexes include peaks of $[M]^+$ at 655 Da. (**5a**) and $[M - \text{bhp}]^+$ at 571 Da. (**5b**).

A selection of distances involving the polar atoms from chp/bhp on complexes **4a**, **4b**, **5a** and **5b** are summarised in Table 7. In general, as the pyridine alkoxide bonding mode changes from 1.10 to 1.01 the M···Halide distances decrease and the M···O_{xhp} distances increase. In addition, there are various X_{halide}···H-$C_{methylene}$ distances arising from hep/hpp methylene protons closest to the 1.01-bound chp or bhp halide atoms. For example, the Br···H distance at 2.901 Å in **4b** is the shortest and the corresponding Cl···H distance in **4a** is the longest (5.868 Å).[17] In conclusion, from this investigation, it is uncertain as to why **4a** and **4b** adopt different xhp bonding modes.

Table 7 Halide (chp or bhp) to nearest (hep or hpp) H or Cu and Cu to (chp or bhp) O atom distances (Å)

4a		**4b**		**5a**		**5b**	
Cu···Cl	~ 4.607	Cu···Br	3.803(2)	Cu···Cl	3.477(2)	Cu···Br	3.556(4)
Cu···O_{chp}	1.922(3)	Cu···O_{bhp}	2.605(3)	Cu···O_{chp}	2.621(6)	Cu···O_{bhp}	2.566(13)
Cl···$H_{methylene}$	5.868	Br···$H_{methylene}$	2.901	Cl···$H_{methylene}$	3.409	Br···$H_{methylene}$	3.743

The Cu···O_{xhp} and X_{halide}···H-$C_{methylene}$ distances of **4b**, **5a** and **5b** suggest the presence of a pseudo-square based pyramidal geometry and van der Waals interactions, respectively. The third row distances show no esd values as H-atoms are fixed.

2.2.4 M = Cu, L^1 = hmpH, L^2 = hepH

Interaction of hepH and hmpH with copper acetate monohydrate gave, on work-up, crystals of a tetranuclear compound $[Cu(hmp)(CH_3COO)]_4 \cdot 2H_2O$ (**6**) in low yield (Scheme 11). Complex **6** was characterised by elemental analysis, IR and ^1H NMR spectroscopy (Table 11) along with positive FAB mass spectrometry. A single crystal of **6** was subject to an X-ray diffraction study. The molecular structure of **6** is depicted in Figure 6; selected bond lengths and angles are given in Table 8.

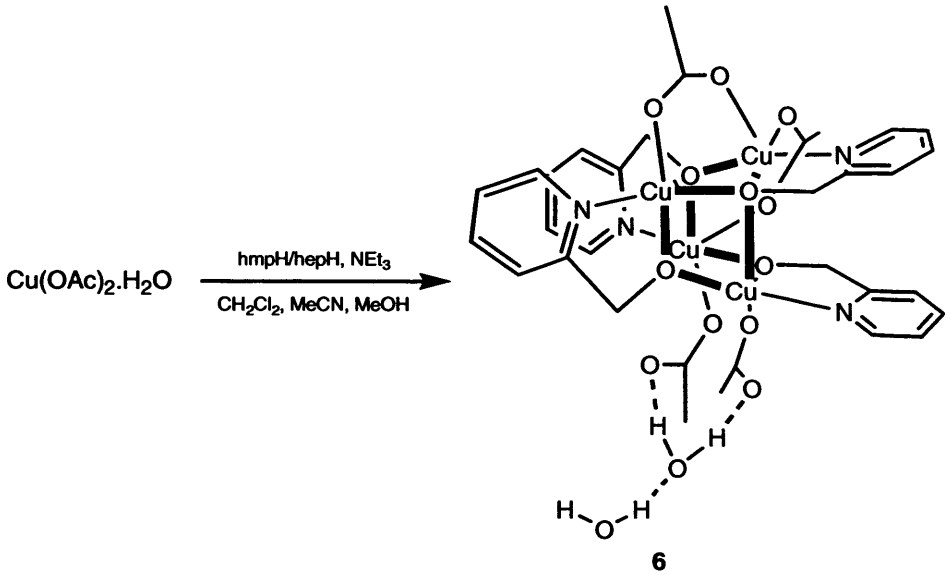

6

Scheme 11 Synthesis of **6**.

The molecular structure of **6** consists of an open-cubane containing four types of distorted square-based pyramidal Cu(II) ions with the coordination sites completed by four hmp and four acetate ligands. The bridging and *N,O*-chelating hmp ligands in **6** are either; 3.31-bound [Cu(1) and Cu(4)] on the closed edges of the cube [N_{hmp}-Cu-O_{hmp} bite angle = av. 82.79°] or 2.21-bound [Cu(2) and Cu(3)] on the open edges of the cube [N_{hmp}-Cu-O_{hmp} bite angle = av. 81.41°]. Cu(3) and Cu(4) each possess an η^1-bound acetate whereas, Cu(1) and Cu(3) are each coordinated to a 1,3-bridging acetate that bridges over to Cu(2).

The average Cu-N_{hmp} bond length in complex **6** is 1.9895 Å, whereas the Cu-O_{hmp} bond lengths range from 1.9220(17) Å – 2.3735(17) Å. The bond lengths and angles of **6** are as expected for a distorted cubic structure.[20] The longest bond lengths found are as follows; Cu(2)-$O_{acetate}$(6) = 2.2650(17) Å, Cu(1)-O_{hmp}(3) = 2.3549(17) Å, Cu(4)-O_{hmp}(2) = 2.3735(17) Å and Cu(3)-$O_{acetate}$(8) = 2.3984(18) Å.

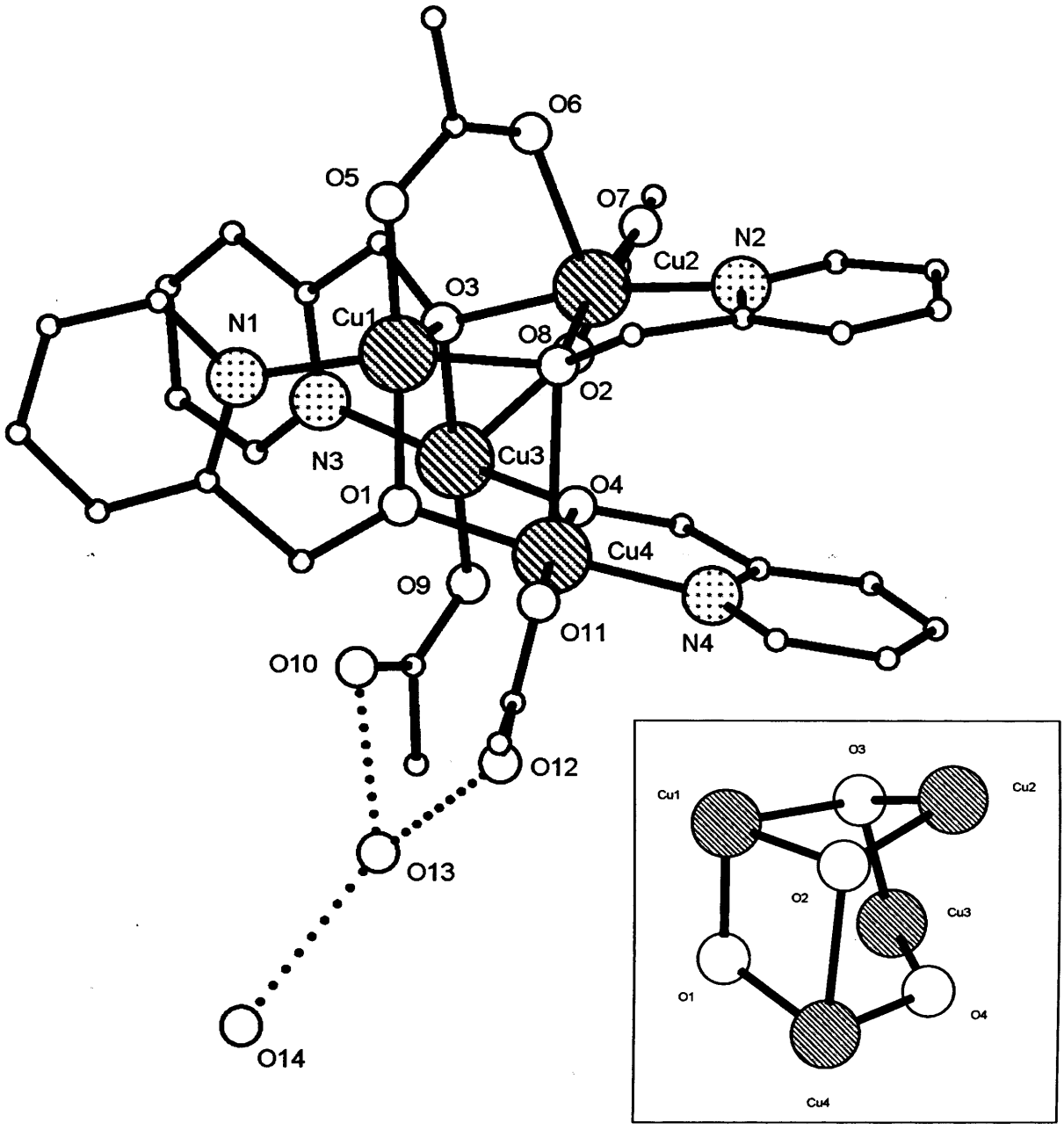

Figure 6 Molecular structure of **6**. Inset shows core. Hydrogen atoms and carbon atom labels are excluded for clarity. Dotted bonds show hydrogen bonding interactions (including an intermolecular water molecule).

Table 8 Selected bond length (Å) and angle (°) data for **6**

6							
Cu(1)-O(1)	1.9220(17)	Cu(2)-O(2)	1.9785(17)	Cu(3)-O(3)	1.9869(16)	Cu(4)-O(1)	1.9413(16)
Cu(1)-O(2)	1.9441(16)	Cu(2)-N(2)	2.000(2)	Cu(3)-O(4)	1.9253(16)	Cu(4)-O(2)	2.3735(17)
Cu(1)-O(3)	2.3549(17)	Cu(2)-O(3)	1.9647(16)	Cu(3)-N(3)	1.984(2)	Cu(4)-O(4)	1.9327(17)
Cu(1)-N(1)	1.975(2)	Cu(2)-O(6)	2.2650(17)	Cu(3)-O(8)	2.3984(18)	Cu(4)-N(4)	1.999(2)
Cu(1)-O(5)	1.9218(17)	Cu(2)-O(7)	1.9462(18)	Cu(3)-O(9)	1.9617(17)	Cu(4)-O(11)	1.9511(17)
O(1)-Cu(1)-N(1)	83.24(8)	O(3)-Cu(2)-N(2)	167.05(8)	N(3)-Cu(3)-O(8)	92.12(7)	N(4)-Cu(4)-O(2)	102.75(7)
O(1)-Cu(1)-O(2)	85.66(7)	O(2)-Cu(2)-O(6)	87.70(7)	O(4)-Cu(3)-O(8)	92.83(7)	O(4)-Cu(4)-N(4)	82.24(8)
O(2)-Cu(1)-N(1)	166.44(8)	N(2)-Cu(2)-O(6)	96.22(7)	O(9)-Cu(3)-O(3)	172.78(7)	O(4)-Cu(4)-O(11)	175.87(7)
O(1)-Cu(1)-O(3)	84.59(7)	O(3)-Cu(2)-O(6)	90.92(7)	O(9)-Cu(3)-N(3)	94.26(8)	O(11)-Cu(4)-N(4)	94.37(8)
N(1)-Cu(1)-O(3)	107.79(7)	O(7)-Cu(2)-O(2)	88.30(7)	O(4)-Cu(3)-O(9)	94.57(7)	Cu(1)-O(2)-Cu(2)	98.87(7)
O(2)-Cu(1)-O(3)	78.79(6)	O(7)-Cu(2)-N(2)	93.98(8)	O(9)-Cu(3)-O(8)	90.21(7)	Cu(1)-O(1)-Cu(4)	107.66(8)
O(5)-Cu(1)-O(1)	176.71(7)	O(7)-Cu(2)-O(3)	95.60(7)	O(1)-Cu(4)-O(2)	74.30(6)	Cu(2)-O(3)-Cu(1)	86.74(6)
O(5)-Cu(1)-N(1)	93.48(8)	O(7)-Cu(2)-O(6)	98.71(7)	O(4)-Cu(4)-O(1)	89.66(7)	Cu(1)-O(2)-Cu(4)	91.95(6)
O(5)-Cu(1)-O(2)	97.62(7)	N(3)-Cu(3)-O(3)	81.59(7)	O(1)-Cu(4)-N(4)	171.74(8)	Cu(3)-O(3)-Cu(1)	113.14(7)
O(5)-Cu(1)-O(3)	96.28(7)	O(4)-Cu(3)-O(3)	90.13(7)	O(4)-Cu(4)-O(2)	81.69(7)	Cu(2)-O(2)-Cu(4)	108.99(7)
O(2)-Cu(2)-N(2)	81.22(8)	O(4)-Cu(3)-N(3)	169.86(8)	O(1)-Cu(4)-O(11)	93.66(7)	Cu(2)-O(3)-Cu(3)	106.11(7)
O(3)-Cu(2)-O(2)	88.30(7)	O(3)-Cu(3)-O(8)	84.07(6)	O(11)-Cu(4)-O(2)	96.84(7)		

In **6**, the η^1-acetate-based carbonyl C-O bond lengths average to 1.277 Å and 1.235 Å from the bound and unbound carbonyls, the former value suggesting mainly ionic metal to carboxylate bonds [for Cu(II): range ~ 1.248 – 1.256 Å ⇒ ~ 0 – 5% covalent C-O bond character].[8]

There are five types of intermolecular hydrogen bonding interactions in **6** these are shown in Figure 7 and summarised in Table 9. Firstly, the η^1-bound acetates act as 'pincer' ligands that accommodate a *trapped* [$H_2O(13)$] water molecule by hydrogen bonding (entries 1 and 2). Secondly, the *trapped* water molecule and a *lattice* [$H_2O(14)$] water molecule hydrogen bond (entry 3). Thirdly, the *lattice* water molecule undergoes a further intermolecular hydrogen bonding interaction with a neighbouring molecule of **6** *via* an acetate oxygen atom [$CH_3COO(11)$] (entry 4). Finally, two separate *lattice* water molecules hydrogen bond with each other (entry 5). Therefore, the molecular structure of **6** can be considered as an extended hydrogen bonded network of tetramers (entries 4 and 5).

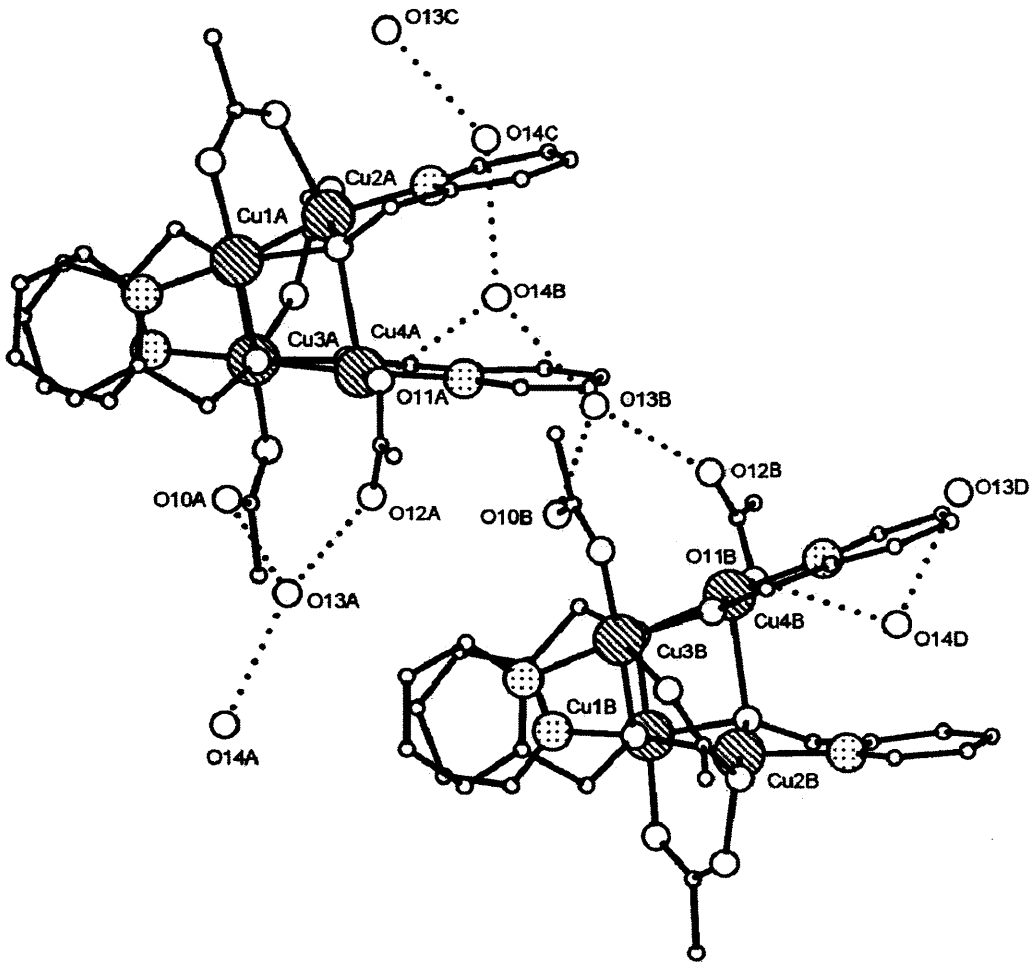

Figure 7 Hydrogen bonding interactions from two molecules of **6** (labelled with atoms A and B), part of the 2,2,2 packed hydrogen bonded network is shown. H atoms are omitted for clarity and neighbouring lattice network H_2O molecules are labelled C and D (see Table 9).

Table 9 Intermolecular hydrogen bonding distances (Å) in **6**

H_2O Type			H_2O Type		
(i) Trapped	$O_{acetate}(10A)\cdots O_{water}(13A)$	2.781(3)	*(iii) Lattice*	$O_{water}(13A)\cdots O_{water}(14A)$	2.762(4)
	$O_{acetate}(10B)\cdots O_{water}(13B)$			$O_{water}(13B)\cdots O_{water}(14B)$	
(ii) Trapped	$O_{acetate}(12A)\cdots O_{water}(13A)$	2.852(3)		$O_{water}(13C)\cdots O_{water}(14C)$	
	$O_{acetate}(12B)\cdots O_{water}(13B)$			$O_{water}(13D)\cdots O_{water}(14D)$	
(iv) Lattice	$O_{acetate}(11A)\cdots O_{water}(14B)$	2.909(4)	*(v) Lattice*	$O_{water}(14B)\cdots O_{water}(14C)$	~ 2.976(4)
(Network)	$O_{acetate}(11B)\cdots O_{water}(14D)$		*(Network)*		

The positive FAB mass spectrum of **6** (dehydrated) shows a fragmentation peak of $[M - CH_3CO_2]^+$ at 861 Da. The IR spectrum of **6**, shows a weak $\nu(OH)_{water}$ stretching band at 3416 cm^{-1} and a strong pyridyl $\nu(C{=}N)$ stretching band at 1585 cm^{-1}.[28,29] The room temperature magnetic moment for **6** at 4.06 BM ($\chi_M T$ = 2.06 emu K mol^{-1}) is more than

expected for four non-interacting divalent copper ions with each possessing one unpaired electron (3.46 BM, $\chi_M T$ = 1.50 emu K mol^{-1}, ***SEE NOTE***).[24c,24e]

There are several examples of tetrameric copper cubane complexes that contain oxygen bridges forming cubic corners as part of a multifunctional *N,O*-donor ligand. These ligands akin to pyridine alcohols are able to create cubic geometries.[13,15a,18] An additional example of a magnetically interesing octanuclear dicubane complex $[Cu_8(dpk{\cdot}OH)_8(O_2CMe)_4]{\cdot}9H_2O$ is based on two complete and separate copper cubes held together by two bridging acetates from a single copper ion vertex on each cube.[19]

The Cu···Cu distances in complex **6** are; Cu(1)···Cu(2) = 2.980 Å, Cu(1)···Cu(3) = 3.629 Å, Cu(1)···Cu(4) = 3.119 Å, Cu(2)···Cu(3) = 3.158 Å, Cu(2)···Cu(4) = 3.550 Å and Cu(3)···Cu(4) = 3.063 Å, these values conforming to previously reported tetra-copper open-cubane structures.[20] Complex **6** indicates the presence of stronger intermolecular hydrogen bonding interactions when compared to the complex $[Cu_4L_2(\mu_{1,1}\text{-}N_3)_2]{\cdot}5H_2O$ (H_3L = *N,N'*-2-Hydroxylpropane-1,3-diyl)bis-salicylideneimine).[20a] The latter complex contains a $Cu_4N_2O_2$ core induced by azido vertices that form the open-face of a cube, whereby, two intermolecular water molecules bind towards the open-face copper ion ligands donor atoms at distances of 3.1 Å and 3.2 Å.

2.2.5 M = Cu, L^1 = hmpH, L^2 = hppH

Reaction of hmpH and hppH with copper acetate monohydrate gave, on work-up, $[Cu(hmpH)_2(CH_3COO)_2]$ (**7**) in low yield (Scheme 12). Complex **7** was characterised by elemental analysis, IR and ^{1}H NMR spectroscopy (Table 11) along with positive FAB mass spectrometry. Complex **7** is isostructural to the nickel containing complex **2a**. A single crystal of **7** was subject to an X-ray diffraction study. The molecular structure of **7** is shown in Figure 8; selected bond lengths and angles are given in Table 10.

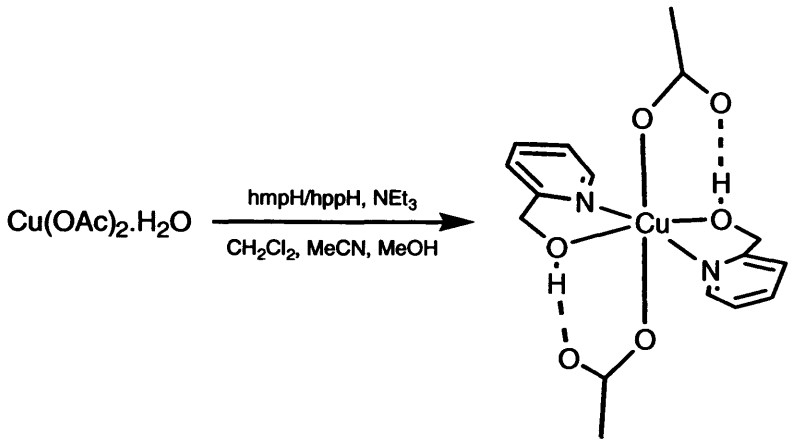

7

Scheme 12 Synthesis of **7**.

The molecular structure of **7** reveals an octahedral Jahn-Teller distorted Cu(II) ion surrounded by two *trans*-acetate and two *trans N,O*-chelating hmpH ligands. The hmpH ligands are 1.11 bound and the acetate ligands are η^1-coordinated. The hmpH ligands form five membered chelate rings with the Cu(II) ion and display a bite angle of $O_{hmpH}(1)$-Cu(1)-$N_{hmpH}(1)$ = 83.34(9)°. The bound and unbound C-O carboxylate carbonyl bond lengths of **7** are 1.231(4) Å and 1.284(4) Å,[28] respectively differing by ~ 0.05 Å, thus, the former suggests mainly ionic metal to carboxylate bonds.[8] On comparison of these values with **2a** and **2b** there is a large bound *vs.* unbound C-O bond length discrepancy.

Table 10 Selected bond length (Å) and angle (°) data for **7**

7					
Cu(1)-O(1)	1.9753(19)	Cu(1)-O(2)	2.414(2)	Cu(1)-N(1)	1.978(2)
O(1)-Cu(1)-N(1)	83.34(9)	O(1)-Cu(1)-O(2)	87.05(7)	N(1)-Cu(1)-O(2)	93.45(8)
O(1)-Cu(1)-N(1)#1	96.66(9)	O(1)-Cu(1)-O(2)#1	92.95(7)	N(1)-Cu(1)-O(2)#1	86.46(8)

Symmetry transformations used to generate equivalent atoms: **7** #1 (– *x*, – *y*, – *z*).

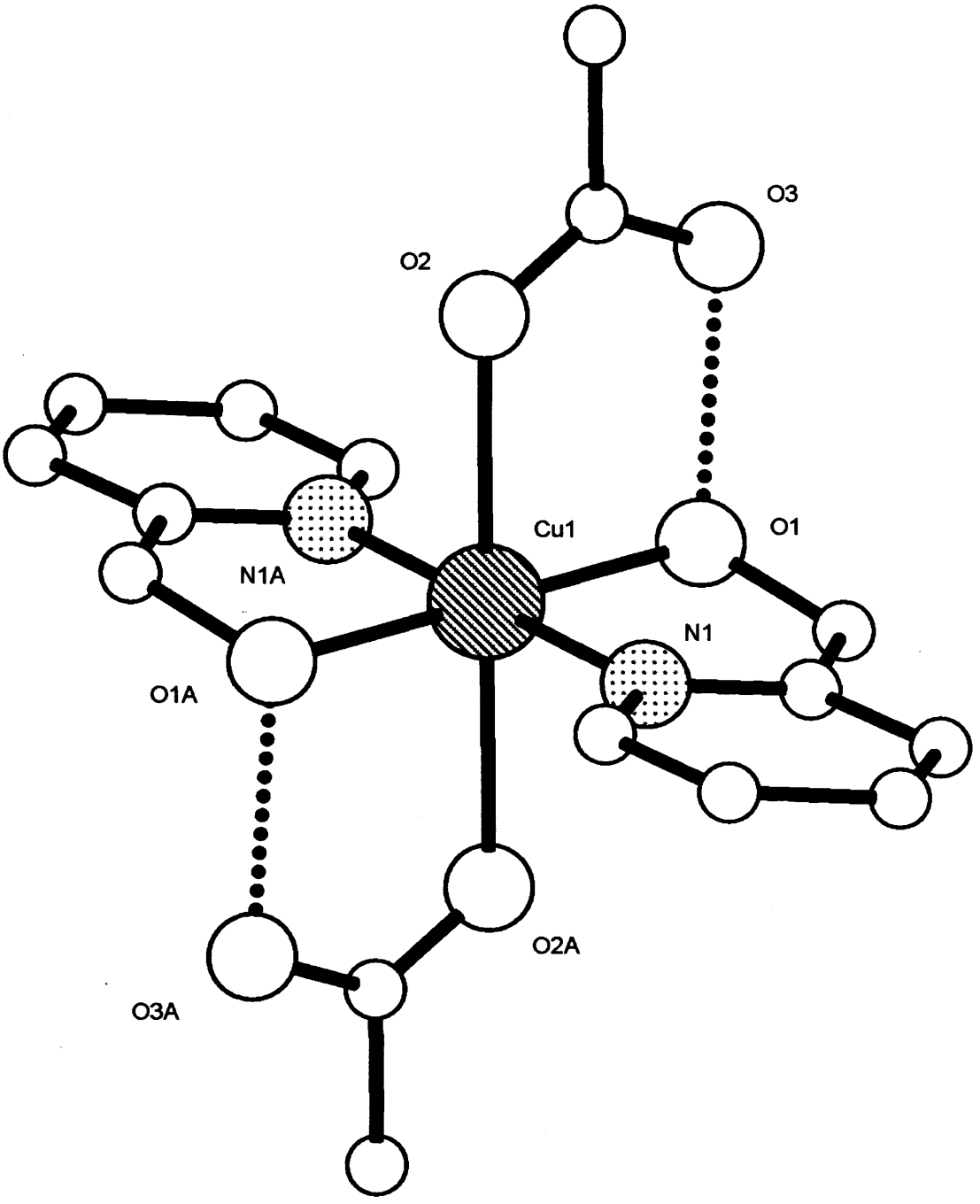

Figure 8 Molecular structure of **7**. Letter labelled atoms are generated by symmetry. Hydrogen atoms and carbon atom labels are excluded for clarity.

The unbound acetate oxygen atoms of **7** undergo an intramolecular inter-ligand hydrogen bonding interaction with a neighbouring hmpH hydroxyl group [$O_{hmpH}(1)\cdots O_{acetate}(3)$ = 2.435(4) Å].

While there are numerous reports of *N,O*-chelated Schiff-ligand based copper complexes,[22a-22b] there is one previous report of a mononuclear hmpH-containing species. In [Cu(salicylate)$_2$(hmpH)$_2$],[21] the Cu-O_{hmpH} and Cu-N_{hmpH} bond lengths at 2.331(1) Å and 1.981(1) Å, respectively are comparable to those found in **7** whereas, the hmpH chelate bite angle is narrower at 77.62(7)°.

The IR bands spectrum of **7** shows a characteristic $\nu(CO_2)_{asymm}$ stretching band at 1651 cm^{-1}.[28,29] The positive FAB mass spectrum of **7**, includes a $[M - 2CH_3CO_2]^+$ peak at 281 Da. The room temperature magnetic moment for **7** at 1.86 BM ($\chi_M T$ = 0.43 emu K mol^{-1}) is more than expected for a single divalent copper ion (***SEE NOTE***).[24c,24e]

Complexes **6** and **7** were analysed using ^{1}H NMR spectroscopy (Chapter 7, section 7.0). The spectra (recorded in $CDCl_3$) show broad paramagnetically shifted peaks (Table 11). Peak assignments have been made on the basis of their chemical shifts, relaxation times and on a comparison of these parameters between complexes in this work and with previously related complexes.[23] Complexes **6** and **7** in $CDCl_3$ show similar ^{1}H NMR spectra (Table 11). It is uncertain as to the reason for this observation, but may be that **6** readily undergoes protonolysis in solution to give **7** (Scheme 13). Similarly, the tetrameric complex $[Cu_4(L)(LH_2)_4](ClO_4)_6\cdot 1.5H_2O\cdot 3.5EtOH$ [LH_2 = 1,2-bis(benzimidazol-2-yl)-1,2-diethanol],[18d] dissociates completely in the solution-state (MeOH/DMSO) to form the dimeric species $[Cu_2(LH)_2]^{2+}$ as observed from ^{1}H NMR spectroscopic studies. The stability of the tetramer in the solid-state has been attributed to the lower solubility or greater crystallinity when compared to the dimeric species.

$$\underset{\mathbf{6}}{[Cu_4(hmp)_4(CH_3CO_2)_4]} + 2H_2O \rightleftharpoons \underset{\mathbf{7}}{2[Cu(hmpH)_2(CH_3CO_2)_2]} + 2Cu^{2+} + 2O^{2-}$$

Scheme 13 Possible equilibrium conditions of **6** towards the formation of **7** in $CDCl_3$.

Table 11 ^{1}H NMR chemical shifts (δ) and relaxation times (T_1 ms, in parentheses) for complexes **6** and **7** (spectra recorded in $CDCl_3$)

Complex in solid-state	H_α	$H_{\beta/\beta'}$	H_γ	α-CH_2 $H_{(eq.)}$	α-CH_2 $H_{(ax.)}$	Me
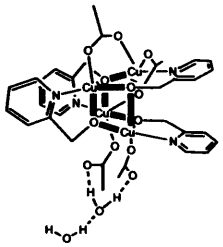 **6**	133.6 (4.26)	40.4 (10.27), 34.3 (17.99)	13.5 (10.37)	115.7 (1.90)	66.0 (0.78)	12.5 (30.46)
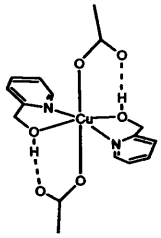 **7**	133.8 (2.96)	40.4 (6.30), 34.7 (8.01)	9.7 (6.49)	116.3 (0.82)	63.4 (0.58)	11.5 (19.61)

The H_α, pyridyl protons from **6** and **7** are assigned with the most downfield chemical shifts. The H_α protons (~ 133 ppm, 3 – 4 ms) are closest to the unpaired electron density of the metal ions and experience more deshielding, therefore, require a higher magnetic field to be brought to resonance. Consequently, H_α protons experience faster relaxation times or lower inversion times and are broader compared to $H_{\beta/\beta'}$ (~ 34 – 40 ppm, 6 – 18 ms) and H_γ (~ 10 – 14 ppm, 6 – 10 ms) protons.[23a] The most positive upfield chemical shifts (~ 12 – 13 ppm, 20 – 30 ms) belong to the acetate methyl groups. The geminal methylene α-CH_2 chemical shifts of **7** appear as resonances at ~ 116 ppm [$H_{(eq.)}$] (0.8 – 1.9 ms) and ~ 63 ppm [$H_{(ax)}$] (0.58 – 0.78 ms) due to the smaller contributions towards pseudo-contact isotropic shifting from Cu(II) ions (see section 2.4).[23e,231]

2.2.6 M = Cu, L^1 = hepH, L^2 = hppH

Interaction of hepH and hppH and copper acetate monohydrate gave, on work-up, the dimeric complex $[Cu(hep)(CH_3COO)]_2$ (**8**) in low yield (Scheme 14). Complex **8** was characterised by elemental analysis, IR and ^{1}H NMR spectroscopy (Table 14) along with positive FAB mass spectrometry. A single crystal of **8** was subject to an X-ray diffraction

study. The molecular structure of **8** is shown in Figure 9; selected bond lengths and angles are given in Table 12.

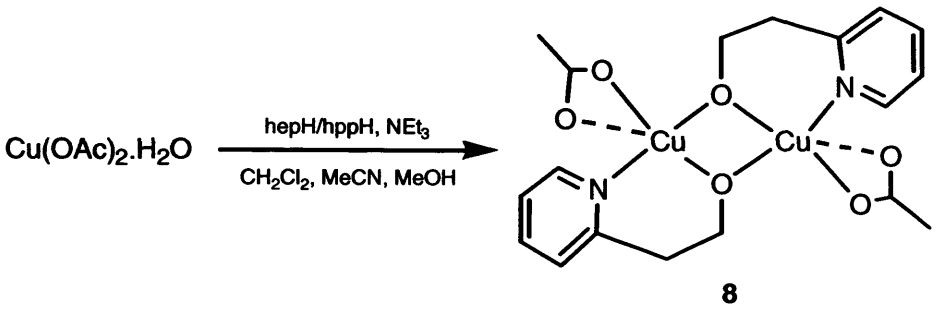

8

Scheme 14 Synthesis of **8**.

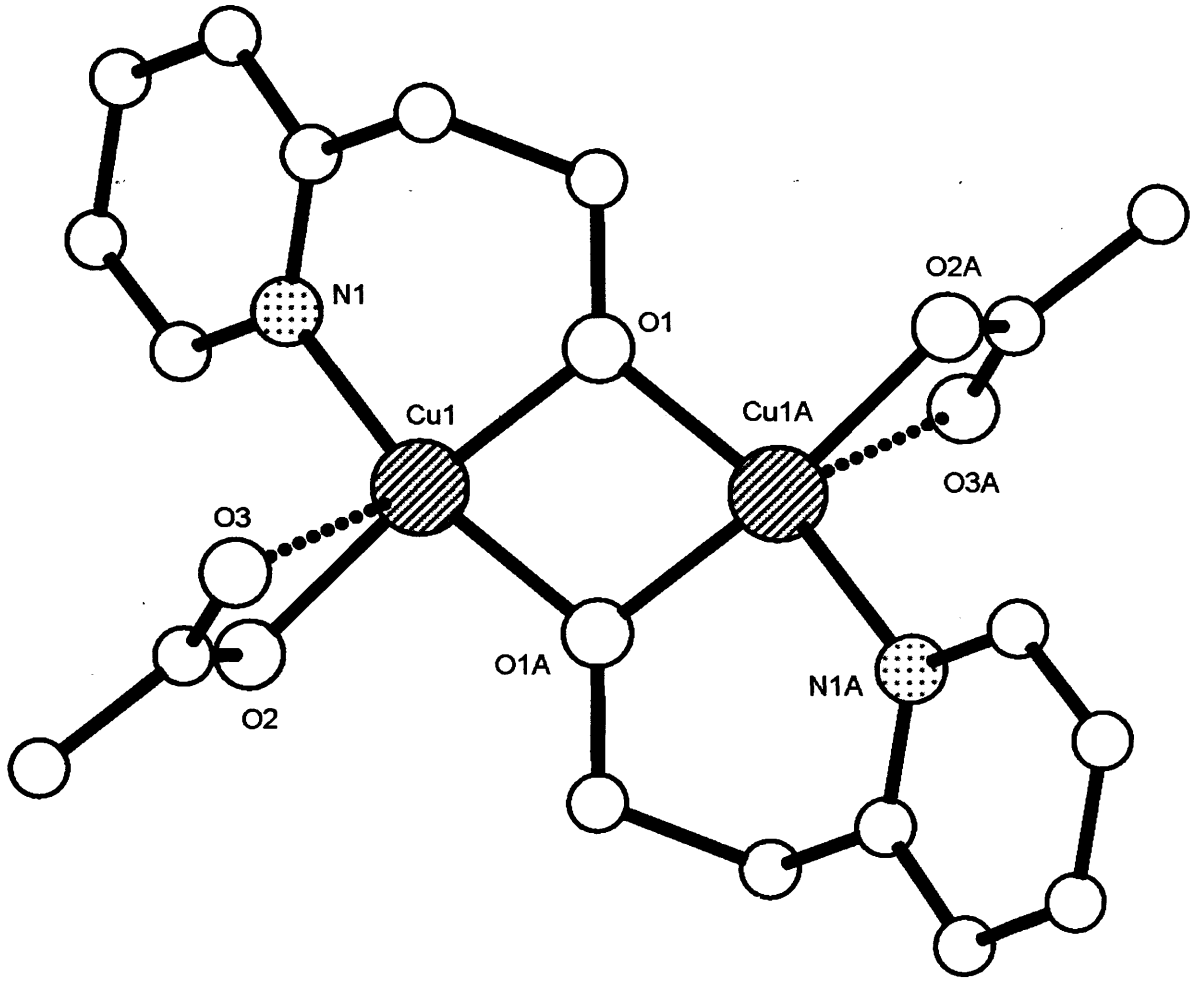

Figure 9 Molecular structure of **8**. Letter labelled atoms are generated by symmetry. Hydrogen atoms and carbon atom labels are excluded for clarity. Dotted lines indicate pseudo-axial interactions.

The molecular structure of **8** consists of a dimer in which the two pseudo-square planar Cu(II) ions are coordinated to two hep and acetate ligands. The deprotonated 2.21 hep ligands bridge and *N,O*-chelate, while the acetate ligands are η^1-bound. Notably, hppH ligands do not feature in **8**. The unbound oxygen atoms on the terminal acetates are located at a distance of 2.491(3) Å from the nearest copper ion, thus suggesting a pseudo-square based pyramidal geometry as an alternative description of the geometry. The longer C-O bond length for the bound carbonyl at 1.274(5) Å [1.228(5) Å for the unbound C-O] suggests that the acetate ligand is bound to Cu(II) with predominantly electrostatic interactions.[8]

In a similar complex $[Cu(hep)(NCO)]_2$,[12] the hep bond lengths are Cu-O_{hep} = 1.919(3) Å or 1.947(3) Å and Cu-N_{hep} = 2.032(4) Å. In **8**, the corresponding bond lengths of Cu(1)- η^1-O_{hep}(1) = 1.903(3) Å, Cu(1)-μ_2-O_{hep}(1A) = 1.920(3) Å and Cu(1)-N_{hep}(1) = 1.987(3) Å are found. The O_{hep}(1)-Cu(1)-N_{hep}(1) chelate bite angle in **8** at 93.82(13)°, is comparable to the hep chelate angle observed in $[Cu(hep)(NCO)]_2$ at 93.42(14)°.[12] In [Cu(6-methyl-2-pyridinemethanol)$(CH_3CO_2)]_2 \cdot 2H_2O$, the Cu-$O_{acetate}$ bond lengths of 1.910(4) Å and 1.926(4) Å, compare with Cu(1)-$O_{acetate}$(3) at 1.959(3) Å found in **8**.

The IR spectrum of **8** exhibits a strong $\nu(CO_2)_{symm}$ band at 1392 cm^{-1} and a pyridyl ν(C=N) stretching band at 1585 cm^{-1}.[28,29] The room temperature magnetic moment for complex **8** at 2.09 BM ($\chi_M T$ = 0.55 emu K mol^{-1}) is less than expected for two non-interacting copper ions (***SEE NOTE***).[24c,24e] The FAB mass spectrum of **8** includes a $[M - CH_3CO_2]^+$ peak at 429 Da.

Table 12 Selected bond length (Å) and angle (°) data for **8**

8					
Cu(1)-O(1)	1.903(3)	Cu(1)-N(1)	1.987(3)	Cu(1)-O(2)	1.959(3)
Cu(1)-O(1)#1	1.920(3)			Cu(1)···Cu(1)#1	3.0119(10)
O(1)-Cu(1)-N(1)	93.82(13)	O(2)-Cu(1)-N(1)	94.97(13)	N(1)-Cu(1)-Cu(1)#1	130.45(10)
O(1)-Cu(1)-O(1)#1	76.04(13)	O(1)#1-Cu(1)-O(2)	96.32(12)	O(1)#1-Cu(1)-Cu(1)#1	37.82(8)
O(1)#1-Cu(1)-N(1)	162.14(13)	Cu(1)-O(1)-Cu(1)#1	103.96(13)	O(2)-Cu(1)-Cu(1)#1	133.90(9)
O(1)-Cu(1)-O(2)	170.56(11)	O(1)-Cu(1)-Cu(1)#1	38.22(8)		

Symmetry transformations used to generate equivalent atoms: **8** #1 ($-x+1, -y+1, -z+1$).

2.3 Transformations of Complexes

From the previous section it has been observed that ligand blends containing 2-pyridine alcohols favour complexation of the most acidic ligands. The extra driving force for reactivity is the ability of the incoming ligand to displace any ligands present on the precursor transition metal complex. For example, pyridine alcohols with sufficiently high acidity can readily displace acetate (in the form of acetic acid) during complexation with transition metal acetate hydrates. In cases where less acidic pyridine alcohol combinations are employed, incomplete acetate displacement results.

On treatment of the monomeric copper acetate-pyridine alcohol complex **7** with Hchp at ambient room temperature, the corresponding mixed pyridinol polymeric copper complex **3** is obtained (Scheme 15). In contrast, treatment of the monomeric nickel acetate-pyridine alcohol complexes **2a** and **2b** with Hchp in the presence of excess base or at higher temperatures were not so successful. The terminal acetate ligands in **8** can also be displaced to yield the mixed pyridine alkoxide dimer complex **4a** (Scheme 16).

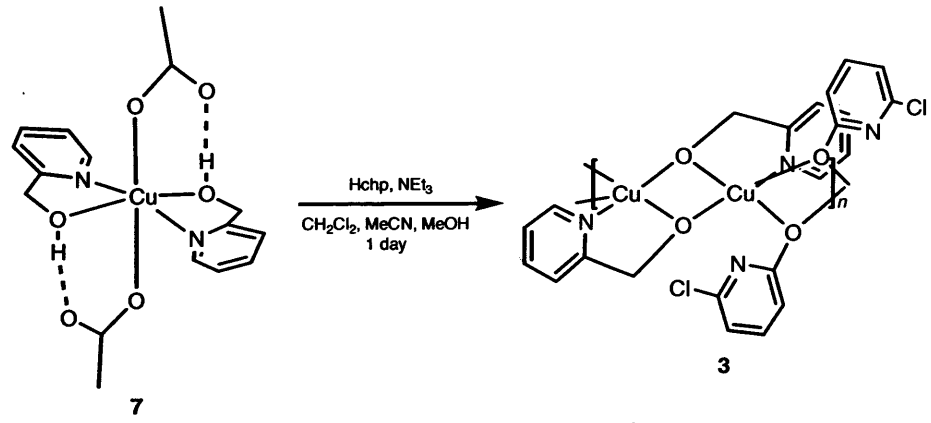

Scheme 15 Conversion of **7** to **3**.

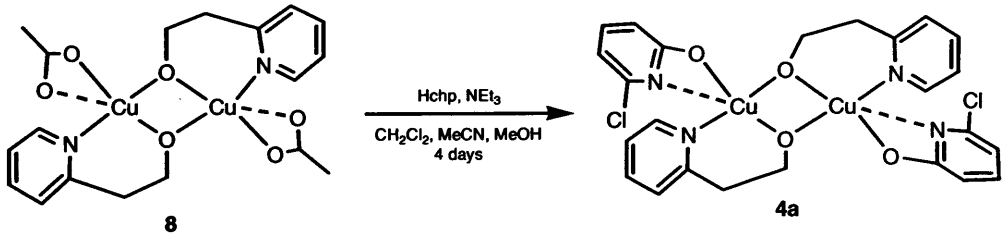

Scheme 16 conversion of **8** to **4a**.

It is also possible to convert the monomeric copper acetate complex **7** into the tetrameric complex **6** by refluxing **7** at 70 °C in excess base (triethylamine) (Scheme 17). The converted products were characterised unequivocally by elemental analysis and solid-state IR spectroscopy (for all transformations in Chapter 2, see Chapter 7, section 7.2 and Table 4).

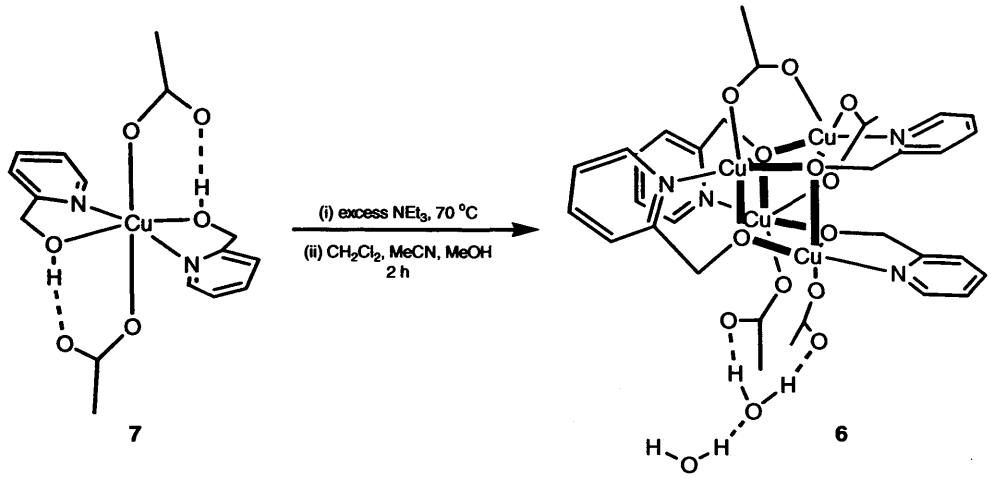

Scheme 17 Conversion of **7** to **6**.

2.4 Paramagnetic ^{1}H NMR Spectroscopic Studies on 1a, 1b, 2a, 2b, 3, 4a, 5a and 8

Most of the complexes in this chapter were analysed using ^{1}H NMR spectroscopy (Chapter 7, section 7.0). As with **6** and **7** (see section 2.2.5), all the spectra (recorded in $CDCl_3$) show broad paramagnetically shifted peaks (Tables 13 and 14). Peak assignments have been made on the basis of their chemical shifts, relaxation times and on a comparison of these parameters between complexes in this work and with previously related complexes.[23]

The H_α, pyridyl protons from the octahedral monomeric nickel complexes **1a**, **1b**, **2a** (Figure 11) and **2b**, are assigned to the most downfield chemical shifts. The H_α protons (~ 116 – 140 ppm, 0.16 – 0.99 ms) are closest to the unpaired electron density of the metal ions and experience more deshielding, therefore, require a higher magnetic field to be brought to resonance. Consequently, H_α protons experience faster relaxation times or lower inversion times and are broader compared to $H_{\beta/\beta'}$ (~ 12 – 46 ppm, 1 – 8 ms) and H_γ (~ 13 – 25 ppm, 5 – 14 ms) protons.[23a] In the case of **1a** and **1b** the chp pyridyl protons are

assigned to the peaks with lower chemical shift values as they are further from the metal ions. The most positive upfield chemical shifts (~ 12 ppm, 3 ms) belong to the acetate methyl groups on complexes **2a** and **2b**.

The closest protons to the metal ions of **1a**, **1b**, **2a** and **2b** are the alkyl methylene chains of alkylated pyridine alcohols (the hydroxyl protons were not detected), these were assigned according to the extent of isotropic shifting effects. Isotropic effects provide an indication about the structural and electronic properties of the complex when paramagnetic NMR spectroscopy is employed.[23b,23l] The pseudo-contact isotropic shift contribution originates from dipolar coupling of unpaired electrons with nuclei of neighbouring unbound atoms, this being a particularly useful technique for octahedral Ni(II) complexes. Notably, EPR characterisation is not possible due to large magnetoanistropic (zero-field splitting) effects which, in contrast, enhances NMR shifting.[23d,23h,23l]

Variation of the pseudo-contact shift is attributed to the dihedral angle dependence of the atom (proton) towards the metal ion. For example, geminal CH_2 axial [$H_{(ax.)}$] and equatorial [$H_{(eq.)}$, Ni-N-C-H ~ 180°] protons experience upfield and downfield shifts, respectively. The α-CH_2 [$H_{(ax.)}$] protons are closer to the paramagnetic ion and usually have broader linewidths, shorter relaxation times and negative chemical shift peaks (Figure 10).[23c,23g,23h,23l]

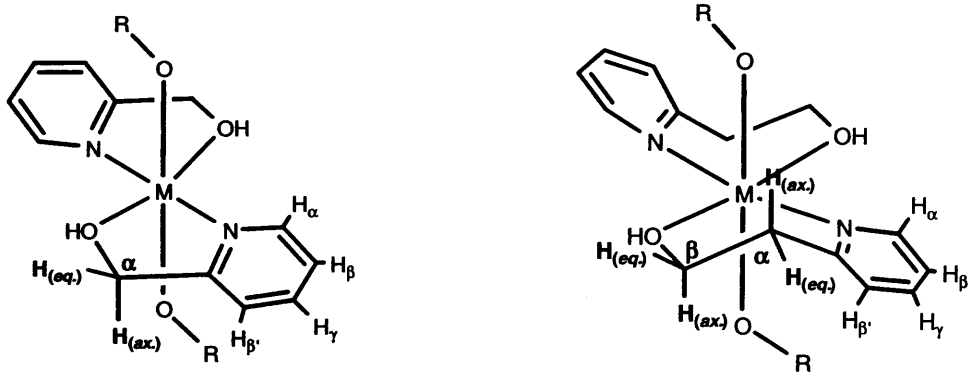

(a) (b)

Figure 10 Geminal axial (*ax.*) and equatorial (*eq.*) methylene protons [(a) hmpH and (b) hepH, R = -COMe or -2-C_5H_3N-6-Cl].

The pseudo-contact isotropic shift effect is enhanced by methylene protons of hmpH/hepH-containing chelate rings. In addition, puckering of methylene rings [*e.g.*, from 1.10 bound hepH rings, Figure 10(b)] may force the $H_{(eq.)}$ protons into an axial position and increase upfield shifting. For example, in **1b**, α-CH_2 $H_{(ax.)}$ = – 12.9 ppm and $H_{(eq.)}$ = – 10.1 ppm (Table 13).[23d,23l] The ^{1}H NMR spectrum of the octahedral copper complex **7** (see section 2.2.5) has been assigned in a similar way to **2a** (Figure 11) and **2b** (Table 13). The α-CH_2 chemical shifts of **7** appear as a single resonance region at ~ 63 ppm due to the smaller contributions of Cu(II) ions towards pseudo-contact isotropic shifting.[23e,23l]

Table 13 ^{1}H NMR chemical shifts (δ) and relaxation times (T_1 ms, in parentheses) for complexes **1a**, **1b**, **2a** and **2b** (spectra recorded in $CDCl_3$)

Complex in solid-state	H_α	$H_{\beta/\beta'}$	H_γ	α-CH_2 $H_{(eq.)}$	α-CH_2 $H_{(ax.)}$	β-CH_2 $H_{(eq.)}$	β-CH_2 $H_{(ax.)}$	Me
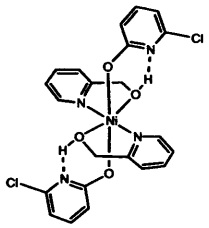 **1a**	138.9 (0.16)	42.9 (2.53),[c] 39.3 (2.79),[c] 15.4 (7.56), 11.9 (3.01)	25.0 (13.5)	90.9 (0.61), 87.7 (0.60)[e]	– 5.0 (0.35)[a]	N/A	N/A	N/A
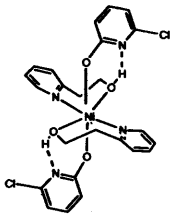 **1b**	140.7 (26.58),[a] 131.6 (0.10),[a,e]	45.6 (2.27),[c] 38.5 (2.12),[c] 34.9 (2.31), 31.6 (1.11)	18.7 (8.87), 16.8 (12.6), 12.7 (4.52)[e]	65.4 (3.17)	– 7.9 (8.96),[a]	– 10.1 (16.32),[a]	– 12.9 (8.83)[a]	N/A
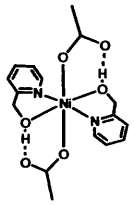 **2a**	139.4 (0.13)[a]	42.6 (2.44), 39.4 (2.73)	15.4 (7.20)	90.8 (0.60)	– 5.3 (1.00)[a]	N/A	N/A	11.9 (2.95)
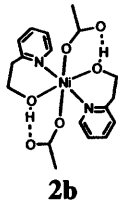 **2b**	115.5 (0.99)	44.7 (2.32), 32.6 (2.43)	17.7 (7.32)	107.9 (0.98)[f]	107.9 (0.98)[f]	49.6 (0.36)	– 12.3 (1.07)[a]	12.7 (2.67)

[a]Unreliable. [b]Could not be observed/determined. [c]From higher alkylated pyridinol. [d]Sharp resonance on normal NMR timescale. [e]Extra resonance. [f]Single broad resonance for several peaks.

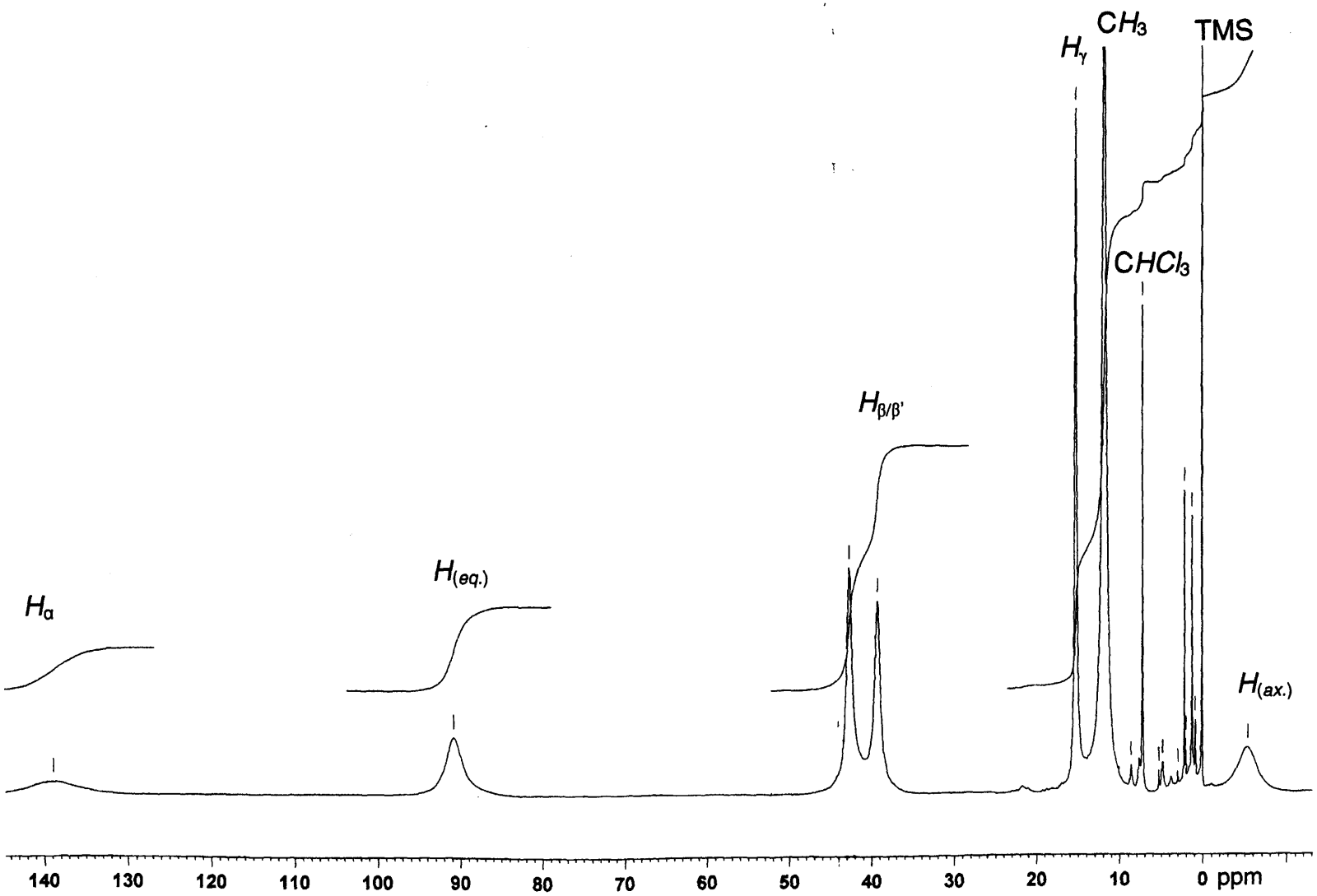

Figure 11 NMR spectrum of complex **2a**.

The dimeric complexes (**4a**, **5a** and **8**) show a significant change in the ^{1}H NMR spectra in contrast to the spectra of the monomers (Table 14). The Cu(II) ions in the dimeric molecules are too far apart to be directly involved in metal-metal interactions and the near diamagnetic state approaching $S = 0$ results in ^{1}H NMR spectra with smaller chemical shift ranges even if the coupling is weak.[18d,23f] Antiferromagnetic interactions between the two copper ions of the dimers are accounted for by pairing up of single d^9 electrons that experience superexchange interactions over the chelating and bridging pyridine alkoxide ligand oxygen atoms.

Table 14 ^{1}H NMR chemical shifts (δ) and relaxation times (T_1 ms, in parentheses) for complexes **3**, **4a**, **5a** and **8** (spectra recorded in $CDCl_3$)

Complex in solid state	H_α	$H_{\beta/\beta'}$	H_γ	α-CH_2 $H_{(eq.)}$	α-CH_2 $H_{(ax.)}$	β-CH_2 $H_{(eq.)}$	β-CH_2 $H_{(ax.)}$	γ-CH_2	Me
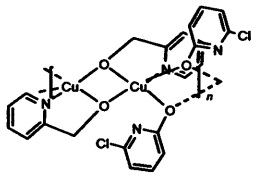 **3**	61.3 (1.93)[a,c]	25.7 (17.90),[c] 16.4 (33.70),[c] 12.7 (14.13), 10.9 (35.05)	9.4 (50.12),[c] 6.00 (d)	31.3 (12.85)[f]	31.3 (12.85)[f]	N/A	N/A	N/A	N/A
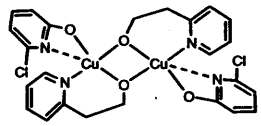 **4a**	20.2 (6.78)[c]	12.7 (8.84),[c] 9.7 (68.22),[c] 8.29 (d) 7.73 (d)	9.3 (65.76), 8.81 (d)	15.3 (5.61)[f]	15.3 (5.61)[f]	13.8 (9.73)[f]	13.8 (9.73)[f]	N/A	N/A
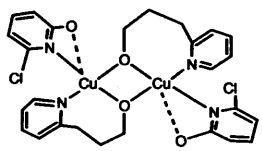 **5a**	16.4 (7.82)[c]	7.93 (d), 4.35 (d), 3.66 (d), 2.95 (d)	2.19 (d), 1.27 (d)	13.6 (6.63)[f]	13.6 (6.63)[f]	9.2 (87.32)[f]	9.2 (87.32)[f]	8.74 (86.99)[f]	N/A
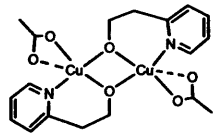 **8**	27.1 (4.92)	10.6 (65.62), 10.2 (61.70)	8.62 (d)	18.5 (4.32)[f]	18.5 (4.32)[f]	18.5 (4.32)[f]	18.5 (4.32)[f]	N/A	3.65 (d)

[a]Unreliable. [b]Could not be observed/determined. [c]From higher alkylated pyridinol. [d]Sharp resonance on normal NMR timescale. [e]Extra resonance. [f]Single broad resonance for several peaks.

The most downfield chemical H_α shifts of the dimeric molecules have a significantly lower range (maximum downfield shift ~30 ppm) in comparison to the monomers. Some peaks sharpen in the 0-10 ppm range,[16e,23f] therefore relaxation time values have not been assigned to these protons (Table 14). Other proton peaks from the dimeric complexes have been assigned similarly to the monomeric complexes starting with the H_α, methylene, $H_{\beta/\beta'}$, H_γ and then any methyl protons.

The ^{1}H NMR spectrum of polymeric complex **3** has a most downfield H_α chemical shift at 61.3 ppm. This value is not as high as observed for the corresponding monomeric copper complex (**7**) and not as low as the most downfield shifts for the dimeric copper complexes (**4a**, **5a** and **8**). Overall, it can be suggested that the unpaired electrons of the copper ions in **3** have slight interactions with the nuclei of neighbouring protons and that any interactions between the metal ions of **3** are antiferromagnetic in origin.[16e,18d,23f]

2.5 Solid-State EPR Spectroscopic and Variable Temperature SQUID Magnetic Characterisation of Selected Complexes

A selection of the multinuclear copper-based compounds **3**, **4a**, **5a**, **6** and **8** described in this chapter were analysed by EPR spectroscopy and accompanied, in many cases, by variable temperature SQUID magnetic measurements (Chapter 7, section 7.0). The EPR spectra of **3**, **4a**, **5a**, **6** and **8** were recorded in the solid-state using Q-band microwave frequencies (~ 34.0 GHz) at 290 K, 120 K and 5 K. ***IMPORTANT NOTE*** *All SQUID magnetic measurements are only part of a preliminary investigation undertaken by Prof. A. Harrison (Edinburgh) therefore, there is a large uncertainty in the data e.g., due to the presence of several parameters and/or parameters with unreliable/inconsistent values.*

The EPR spectrum of the polymeric copper complex $[Cu(chp)(hmp)]_n$ (**3**) shows four different g values of; $g_1 = 2.220$, $g_2 = 2.042$, $g_3 = 2.029$ and $g_{(impurity)} \sim 2.02$ at 295 K (Figure 12). Splitting of the g_3 tensor specifies rhombic (x, y axis) distortions along a non-

interacting monometallic copper(II) ion (Figure 13). The signals broaden at lower temperatures (120 K and 5 K) and no hyperfine coupling from $^{63,65}Cu$ was resolved due to magnetic dilution.[32]

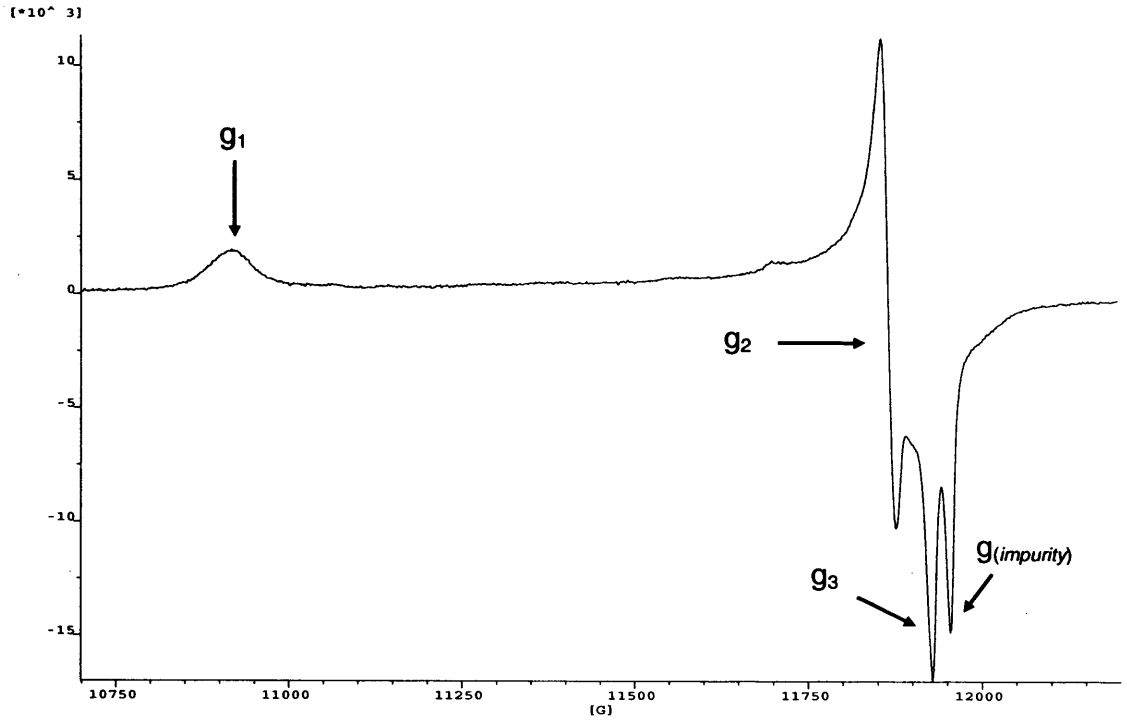

Figure 12 EPR spectrum of **3** taken at 5 K.

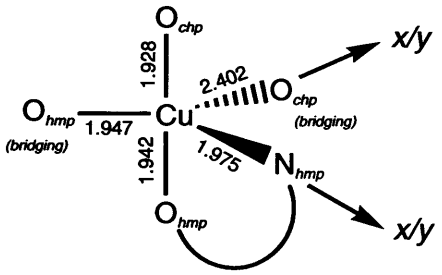

Figure 13 Trigonal bipyramidal copper ion distortions of **3**, bond lengths (Å) are shown (150 K).

There are two different Cu···Cu distances within the polymer chain of **3** at 2.908 Å [Cu(1)···Cu(1A)] and 3.410 Å [Cu(1A)···Cu(1A)], these arising from the μ-O_{hmpH} and μ-O_{chp} bridged ions, respectively (Figure 14). The two values suggest that the Cu(II) ions within the polymer chain of **3** possesses two different exchange interactions (x and αx) and thus, behaves as an alternating chain.

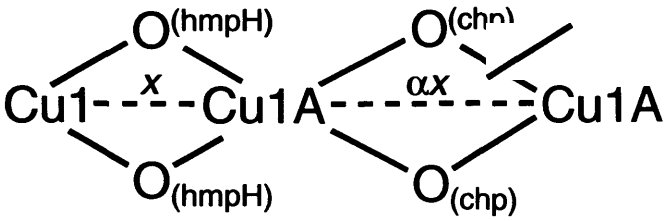

Figure 14 Magnetic interactions within **3**.

Preliminary fitting of the variable temperature magnetic susceptibility data of **3** was modelled using the alternating spin chain model ($S = 0.5$) equation using a six parameter fit including, a temperature independent term and a Curie-Weiss paramagnetic impurity term (Equation 1).[31] The following parameters were obtained from the fit {per Cu(II) ion}; χ_{TIP} = 7.00 × 10^{-5} (± 2.00 × 10^{-5}) emu mol^{-1}, x = – 109.77 (± 0.54) K, α = 0.20 (fixed) K, [⇒ αx = – 21.95 (± 0.54) K], g = 2.45 (fixed), a Curie constant (C') = 2.33 ×10^{-2} (± 2.80 × 10^{-4}) emu K mol^{-1} and a Curie-Weiss constant (θ') = – 1.02 × (± 3.94 × 10^{-2}) K [Figure 15]. The positive value of x and alteration parameter of $\alpha \leq 1$ confirms the presence of an alternating chain with antiferromagnetic interactions.[24d] In **3**, the antiferromagnetic interaction from Cu1···Cu1A is stronger (x ~ – 110 K) than the interaction from Cu1A···Cu1A (αx ~ – 22 K). The fitted data also provides evidence for a small amount of paramagnetic impurity (6%) from the additional Curie-Weiss terms. The deviation from a perfect fit of the data can be attributed to imperfections in the model.

$$\chi = \frac{C}{T} \cdot \frac{A + By + Cy^2}{1 + Dy + Ey^2 + Fy^3} + \frac{C'}{T - \theta'} + \chi_{TIP}$$

Equation 1 Alternating ($S = 0.5$) chain model.[31] A = 0.25, B = – 0.062836 + 0.11376α, C = 0.0047778 – 0.033268α + 0.12742α^2 + 0.32918α^3 + 0.25203α^4, D = 0.05386 + 0.70960α, E = – 0.00071302 – 0.10598α + 0.54883α^2 – 0.20603α^3, F = 0.047193 – 0.0083778α + 0.87256α^2 – 2.7098α^3 + 1.9798α^4. $C = Ng^2\beta^2/kT$; N = Avogadro's number, β = Bohr magneton, k = Boltzmann constant, g = Landé splitting factor, T = temperature, CT = ~ $Ng^2/8$ and χ_{TIP} = temperature independent background susceptibility. The coupling constants are suggested from; $J/k = x$ and $\alpha J/x = \alpha x$ whereby, $y = x/\alpha x$ and α = alteration parameter. Paramagnetic impurity terms are; C' = Curie-constant and θ' = Curie-Weiss constant.

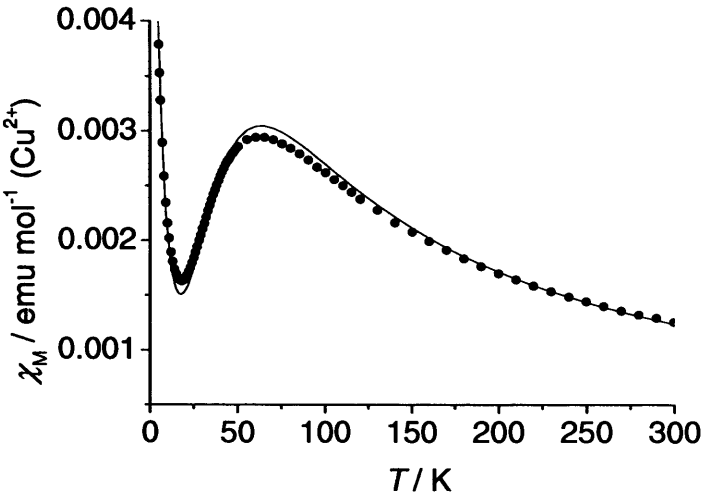

Figure 15 Plot of χ_M against T (closed circles) for **3**; fitted plot in solid line.

The ^{1}H NMR chemical shift range for **3** is smaller when compared to the monometallic copper complex **7** (Table 14), thus supporting the antiferromagnetic interactions indicated from the EPR and magnetic SQUID studies. The variable temperature magnetic susceptibility data of **3** was also fitted using regular spin-chain model[25] and dimer-dimer model.[26,24b] However, these provided unsuitable fits/data parameters. It can be concluded that **3** behaves as an antiferromagnetically coupled chain of alternating $S = 0.5$ Cu(II) ions.

The EPR spectra of the dimeric complexes $[Cu(chp)(hep)]_2$ (**4a**), $[Cu(chp)(hpp)]_2$ (**5a**) and $[Cu(hep)(CH_3CO_2)]_2$ (**8**) exhibit a broad half-field signal at 295 K, whereby g is approximately 5.2 (**4a**) (Figure 16), 5.7 (**5a**) and 4.0 (**8**). This signal arises from a $S = 1$ triplet state for the two copper(II) ions within the dimer and disappears at 5 K due to depopulation on approaching the ground spin state. The monomeric impurity signals [$g_{(impurity)}$] were observed at ~ 2.04 (**4a**), 2.09 (**5a**) and 2.26 (**8**).

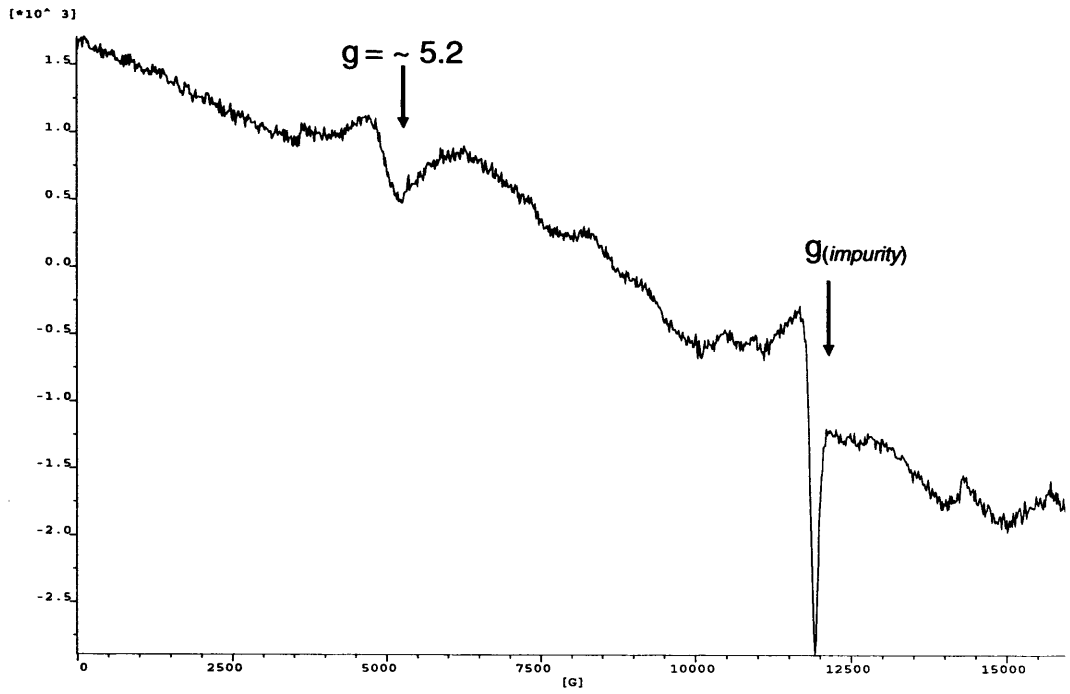

Figure 16 EPR spectra of **4a** at 295 K.

The Cu-O-Cu angle from the bridging hep/hpp alkoxides at 103.79(11)° (**4a**), 129.3(4)° (**5a**) and 103.96(13)° (**8**) are obtuse, this being a common feature present in copper dimers undergoing antiferromagnetic exchange interactions.[16a,16b] These can be represented by a single negative coupling constant (x) from a dimeric Cu_2O_2 core (Figure 17).

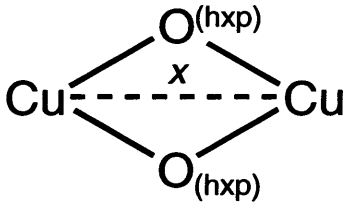

Figure 17 [Cu_2O_2] core of **4a**, **5a** and **8**.

The preliminary variable temperature magnetic susceptibility data of **4a** was modelled using the Bleaney-Bowers equation for a dimer (S = 0.5) using a five parameter fit including a temperature independent term and Curie-Weiss paramagnetic impurity terms (Equation 2).[26,24b] The following parameters were obtained from the fit {per Cu(II) ion}; χ_{TIP} = 6.40 × 10^{-4} (± 2.90 × 10^{-6}) emu mol^{-1}, x = – 300.29 (± 2.67) K, g = 2.45 (fixed), a Curie constant (C') = 4.29 × 10^{-3} (± 4.00 × 10^{-5}) emu K mol^{-1} and a Curie-Weiss constant

(θ') = – 2.60 × 10^{-2} (± 2.01 × 10^{-2}) K [Figure 18]. A large negative coupling constant (x) suggests the presence of strong antiferromagnetic interactions. The fitted data also provides evidence for a small amount of paramagnetic impurity (1%) from the additional Curie-Weiss terms. Both EPR and magnetic SQUID data of **4a** are supported by solution state ^{1}H NMR spectra with a relatively smaller chemical range shift due to the presence of antiferromagnetic interactions when compared to the monometallic complexes (Table 14).[16e]

$$\chi = \frac{C}{T} \cdot \frac{2e^{\left(\frac{2J_1}{kT}\right)}}{1+3e^{\left(\frac{2J_1}{kT}\right)}} + \chi_{TIP} + \frac{C'}{T-\theta'}$$

Equation 2 Bleaney-Bowers S = 0.5 dimer equation. $C = Ng^2\beta^2/k$; N = Avagadro's number, β = Bohr magneton, g = Landé splitting factor, k = Boltzmann constant, T = temperature, $CT = \sim Ng^2/8$ and χ_{TIP} = temperature independent background susceptibility. The coupling constant is suggested from; $J_1/k = x$. Paramagnetic impurity terms; C' = Curie-constant and θ' = Curie-Weiss constant.

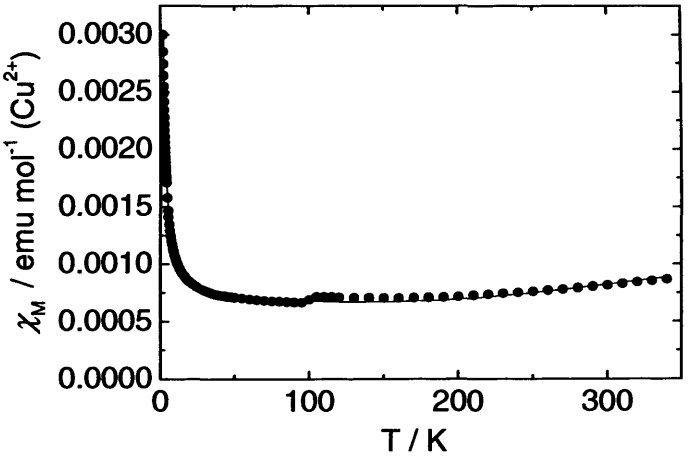

Figure 18 Plot of χ_M against T (closed circles) for **4a** [per Cu(II) ion]; fitted plot in solid line.

In comparison to the dimer $[Cu(hep)_2(NCO)_2]$,[12] **4a** has a larger coupling constant value indicating the presence of stronger antiferromagnetic coupling between the Cu(II) ions [Cu-O-Cu = 105.78(14)°, $2J_1$ = – 98 cm^{-1} (x = – 208.72 cm^{-1} **4a**), g = 2.02 (g = 2.45 **4a**]. The variable temperature inverse magnetic susceptibility plot of **4a** could not be modelled using the Curie-Weiss law due to the presence of a significant temperature independent susceptibility.

The EPR spectrum of the tetrameric complex $[Cu(hmp)(CH_3CO_2)]_4$ (**6**) is complicated. The splitting of the signal lines indicate the presence of both $S = 2$ and $S = 1$ ground spin states (5 K), this behaviour being consistent with the presence of four and two non-interacting copper(II) ions, respectively (Figure 19). Preliminary EPR investigations by data simulation show; $g_1 = 2.27$, $g_2 = 2.26$, $g_3 = 2.24$, a zero field splitting parameter of D at 0.140 cm^{-1}, x, y coupling parameter (E) = 0.0112 cm^{-1} ($S = 2$, 30%) and $g_1 = 2.21$, $g_2 = 2.20$, $g_3 = 2.18$, $D = 0.500$ cm^{-1}, $E = 0.055$ cm^{-1} ($S = 1$, 70%). The EPR signals in the spectrum of **6** broaden as the temperature is increased (295 K).[30] The room temperature magnetic moment of **6** at 4.06 BM ($\chi_M T = 2.06$ emu K mol^{-1}), is slightly higher than expected for four non-interacting Cu(II) ions.[24c]

The previously reported closed cubane $[\{Cu(HL)\}_4]$ [(H_3L = *N,N'*-(2-hydroxypropane-1,3-diyl)bis(acetylacetoneimine)] exhibits a moment value of 3.51 BM at 300 K and possesses ferromagnetic interactions,[18f] this being consistent with the room temperature moment of **6**.

Compared to **6**, the X-band EPR spectrum of tetrakis-{3-[*N*-(2-oxycyclohexyl)aminomethylene]-2,4-pentanedione(2-)$O^{2'}$,*N*,O^2}tetracopper(II) at 4 K also displays $S = 2$ and $S = 1$ spin-states [$g_{zz} = 2.97$, $g_{yy} = 2.80$, $g_{xx} = 2.80$] and exhibits a room temperature moment of 3.86 BM.[13] The X-band and high frequency (HF) simulated EPR spectra for $[Cu_4(NH_3)_4(diethanolaminate)_4][CdBr_4]Br_2 \cdot 3DMF \cdot H_2O$ provides the following parameters ($\geq$ 4 K, 9 – 94 GHz); $S = 2$, $g_{yy} = 2.142$, $g_{xx} = 2.138$, $g_{zz} = 2.067$, $D = -0.3529$ cm^{-1} and $E = -0.0469$ cm^{-1} with a maximum moment of 2.60 BM per Cu(II) ion at 10 K.[18g] The latter matches the $S = 2$ parameters obtained from preliminary analysis of **6**. The sign of D for **6**, may be determined from HFEPR analysis at low temperature when its magnitude is expected to increase.[18g]

The presence of four different copper(II) ion environments in the distorted Cu_4O_4 cubic core of **6** imply the presence of six possible exchange interactions (Figure 20); a

more detailed magnetic investigation into **6** is yet to be undertaken to account for all the types of interactions present. In addition, spin frustration effects due to the triangular arrangement of Cu(II) ions within this cubic complex cannot be excluded.[27]

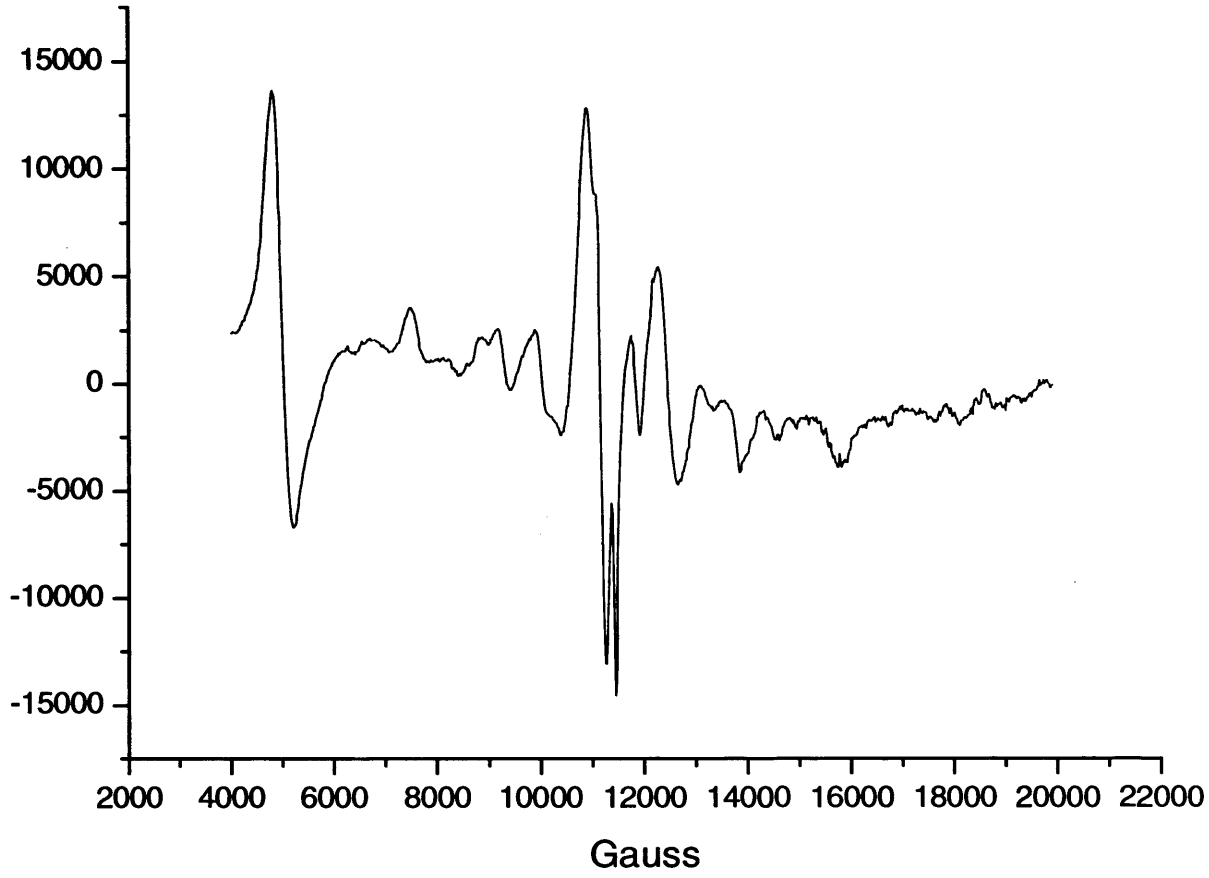

Figure 19 EPR simulated spectrum of **6** at 5 K.

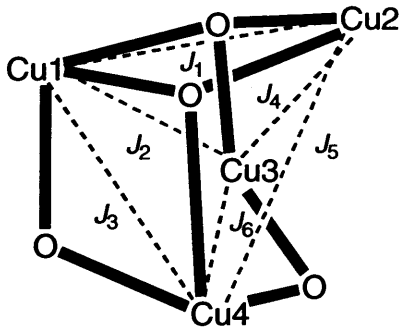

Figure 20 [Cu_4O_4] cubic core of **6**; J_1 Cu(1)···Cu(2), J_2 Cu(1)···Cu(3), J_3 Cu(1)···Cu(4), J_4 Cu(2)···Cu(3), J_5 Cu(2)···Cu(4) and J_6 Cu(3)···Cu(4).

2.6 Summary and Conclusions

Reactions of ligand blends involving combinations of 2-pyridinols/2-pyridine alcohols [2-{$(CH_2)_nOH$}-6-X-C_5H_3N] with nickel acetate tetrahydrate or copper acetate monohydrate in the presence of triethylamine afford a range of complexes displaying a variety of nuclearities and structural types (complexes **1** – **8**). Scheme 18 depicts the synthetic work undertaken in this chapter.

A series of complexes including mononuclear **1a**, **1b**, **2a**, **2b** (M = Ni), **7** (M = Cu), binuclear **4a**, **4b**, **5a**, **5b** and **8**, tetranuclear **6** (M = Cu) and polymeric **3** (M = Cu) have been synthesised and fully characterised.

In conclusion, the factors governing 2-pyridine alcohol complexation in this work would appear to depend on a combination of variables. Firstly, *the nature of the precursor transition metal ion* affects the structural geometry and final nuclearity. Secondly, *the methylene chain length of the 2-pyridine alcohol* influences the nuclearity as a chelating/non-chelating ligand. Finally, *the pK_a values of the ligand blends* manipulate ligand competition by favouring or disfavouring complexes containing mixed 2-pyridine alcohols/alkoxides thus, influencing the numbers and types of bonding modes present and resulting non-covalent interactions.

Transformations involving acetate ligand displacement from complexes **7** and **8** have been undertaken successfully by addition of Hchp, resulting in the formation of **3** and **4a**, respectively. Notably, chp features in all the complexes containing blends of mixed pyridine alcohols. In addition, mononuclear **7** can be converted into the tetrameric **6** through deprotonation under strongly basic conditions. Conversely, **6** undergoes protonolysis to form **7** in solution as detected by ^{1}H NMR spectroscopy.

Chemical shift and relaxation time data obtained from ^{1}H NMR studies has allowed an estimation of the degree of paramagnetic behaviour exhibited by the complexes. Monomeric complexes exhibit significant paramagnetic chemical shifts ranges, while the binuclear complexes have decreased chemical shifting due to the presence of antiferromagnetic coupling.

In polymeric complex **3** the chemical shift range falls between those observed from the mononuclear copper complex **7** and binuclear copper complexes (**4a**, **5a** and **8**). In addition, EPR measurements of the multinuclear complexes **3**, **4a**, **5a**, **6** and **8** have been investigated. Preliminary EPR and SQUID variable temperature magnetic measurements on complex **3** are consistent with the presence of an alternating (S = 0.5) chain and the dimers **4a** and **5a** show evidence for the presence of strong antiferromagnetic behaviour. The tetrameric complex **6** displays interesting EPR signals indicative of the presence of two spin states at low temperatures. These results are to be supported by possible future variable temperature magnetic and EPR studies.

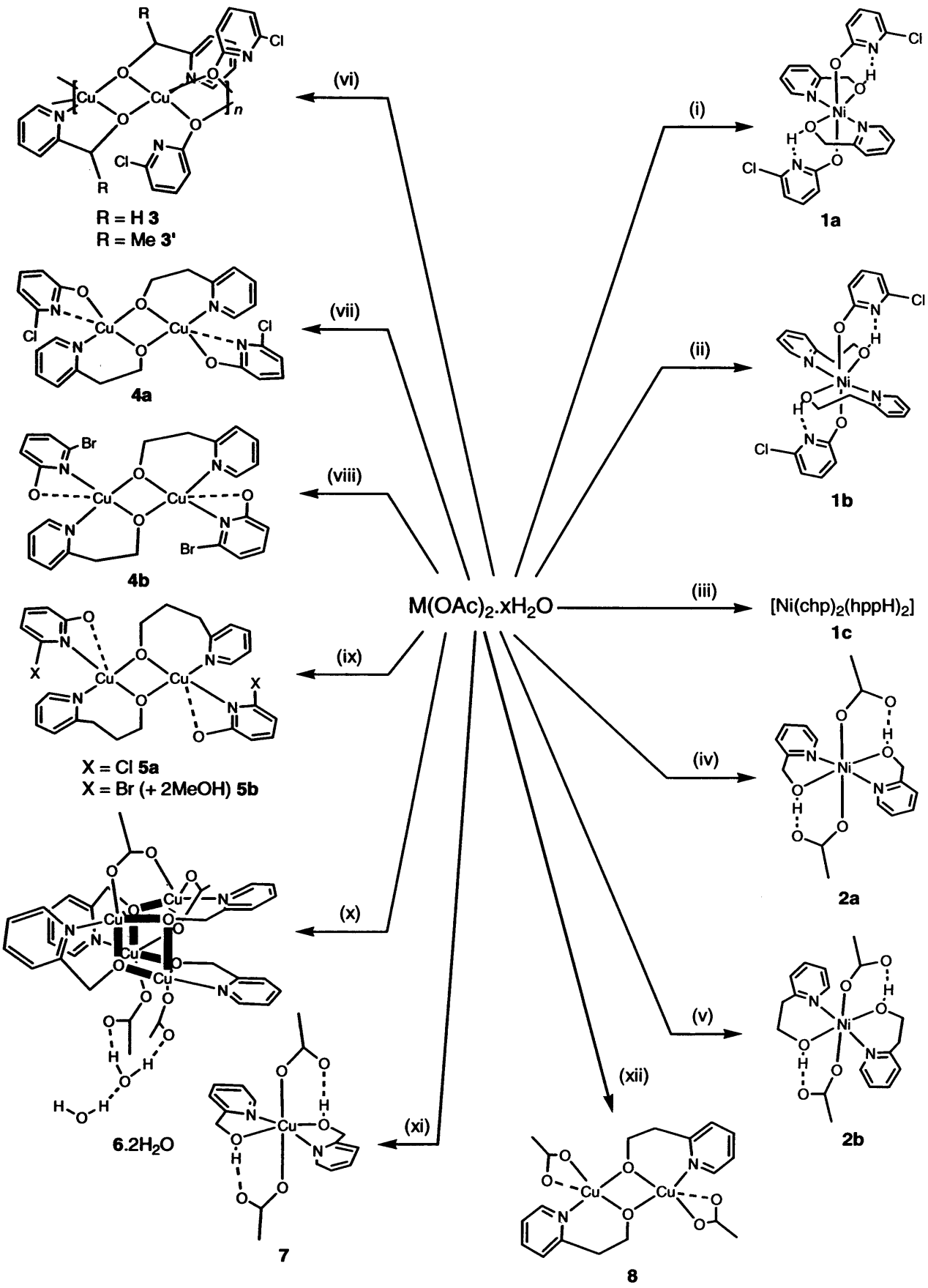

Scheme 18 Overview of chemistry carried out in Chapter 2. General reagents: $M(OAc)_2 \cdot xH_2O$, 2-{$(CH_2)_nOH$}-6-X-C_5H_3N, NEt_3 and $MeCN/CH_2Cl_2/MeOH$; (i) – (v) M = Ni, x = 4; (vi) – (xii) M = Cu, x = 1.

2.7 References

1. R. E. P. Winpenny, *J.Chem. Soc., Dalton Trans.*, 2002, 1.
2. *Ni complexes:* (*a*) E. K. Brechin, S. G. Harris, S. Parsons and R. E. P. Winpenny, *J. Chem. Soc., Dalton Trans.*, 1997, 1665; (*b*) E. K. Brechin, L. M. Gilby, R. O. Gould, S. G. Harris, *J. Chem. Soc., Dalton Trans.*, 1998, 2657; (*c*) C. Benelli, A. J. Blake, E. K. Brechin, S. J. Coles, A. Graham, S. G. Harris, S. Meier, A. Parkin, S. Parsons, A. M. Seddon and R. E. P. Winpenny, *Chem. Eur. J.*, 2000, **6**, 883; (*d*) E. K. Brechin, A. Graham, S. G. Harris, S. Parsons and R. E. P. Winpenny, *J. Chem. Soc., Dalton Trans.*, 1997, 3405; (*e*) C. Caddiou, R. A. Coxall, A. Graham, A. Harrison, M. Helliwell, S. Parsons and R. E. P. Winpenny, *Chem. Commun.*, 2002, 1106; *Co complexes:* (*f*) A. J. Blake, L. M. Gilby, S. Parsons, J. M. Rawson, D. Reed, G. A. Solan and R. E. P. Winpenny, *J. Chem. Soc., Dalton Trans.*, 1996, 3575; (*g*) E. K. Brechin, R. A. Coxall, A. Parkin, S. Parsons, P. A. Tasker and R. E. P. Winpenny, *Angew. Chem., Int. Ed. Engl.*, 2001, **40**, 2700; (*h*) E. K. Brechin, S. Parsons and R. E. P. Winpenny, *J. Chem. Soc., Dalton Trans.*, 1996, 3745; (*i*) W. Clegg, D. Garner and M. H. Al-Samman, *Inorg. Chem.*, 1983, **22**, 1543; (*j*) E. K. Brechin, A. Graham, A. Parkin, S. Parsons, A. M. Seddon and R. E. P. Winpenny, *J. Chem. Soc., Dalton Trans.*, 2000, 3242; (*k*) E. K. Brechin, S. G. Harris and R. E. P. Winpenny, *Chem. Commun.*, 1996, 1439; (*l*) E. K. Brechin, O. Cador, A. Caneschi, C. Cadiou, S. G. Harris, S. Parsons, M. Vonci and R. E. P. Winpenny, *Chem. Commun.*, 2002, 1860; *Cu complexes:* (*m*) A. J. Blake, C. M. Grant, C. I. Gregory, S. Parsons, J. M. Rawson, D. Reed and R. E. P. Winpenny, *J. Chem. Soc., Dalton Trans.*, 1995, 163; (*n*) A. J. Blake, P. E. Y. Milne and R. E. P. Winpenny, *J. Chem. Soc., Dalton Trans.*, 1993, 3727; (*o*) A. J. Blake, R. O. Gould, C. M. Grant, P. E. Y. Milne, S. Parsons and R. E. P. Winpenny, *J. Chem. Soc., Dalton Trans.*, 1997, 485; (*p*) E. K. Brechin, S. G. Harris, S. Parsons and R. E. P. Winpenny, *J. Chem. Soc., Dalton Trans* ., 1997, 3403.
3. *See references therein* N. C. Harden, M. A. Bolcar, W. Wernsdorfer, K. A. Abboud, W. E. Streib and G. Christou, *Inorg. Chem.*, 2002, **42**, 7067.
4. R. A. Coxall, S. G. Harris, D. K. Henderson, S. Parsons, P. A. Tasker and R. E. P. Winpenny, *J.Chem. Soc., Dalton Trans.*, 2000, 2349.
5. ACS, *SciFinder Scholar*, Substance database, 2004.
6. J. Pérez, L. García, A. G. Orpen, M. D. Santana, P. Saez and G. García, *New J. Chem.*, 2002, **26**, 726.
7. E. K. Brechin, S. G. Harris, S. Parsons and R. E. P. Winpenny, *Angew. Chem., Int. Ed. Engl.*, 1997, **36**, 1967.
8. R. K. Hocking and T. W. Hambley, *Inorg. Chem.*, 2003, **42**, 2833. [For Ni(II): range ~ 1.263 – 1.268 Å ⇒ ~15 – 20% covalent C-O bond character; for Cu(II): range ~ 1.248 – 1.256 Å ⇒ ~ 0 – 5% covalent C-O bond character].
9. (*a*) A. J. Blake, C. M. Grant, E. J. L. McInnes, F. E. Mabbs, P. E. Y. Milne, S. Parsons, J. M. Rawson and R. E. P. Winpenny, *J. Chem. Soc., Dalton Trans.*, 1996, 4077; (*b*) A. J. Blake, R. O. Gould, P. E. Y. Milne and R. E. P. Winpenny, *J. Chem. Soc., Chem. Commun.*, 1992, 522.
10. A. J. Blake, S. Parsons, J. M. Rawson and R. E. P. Winpenny, *Polyhedron*, 1995, **14**, 1895.
11. A. J. Blake, R. O. Gould, J. M. Rawson and R. E. P. Winpenny, *J. Chem. Soc., Dalton Trans.*, 1994, 2005.
12. S.-C. Cheng and H.-H. Wei, *Inorg. Chim. Acta*, 2002, **340**, 105.
13. R. Wagner, M. Gottschaldt, H. Görls, E.-G. Jäger and D. Klemm, *Chem. Eur. J.*, 2001, **7**, 2143.
14. (*a*) S. P. Foxon, D. Utz, J. Astner, S. Schindler, F. Thaler, F. W. Heinemann, G. Lieher, J. Mukherjee, V. Balamurugan, D. Ghosh and R. Mukherjee, *Dalton Trans.*, 2004, 2321. (*b*) C.-T. Yang, M. Vetrichelvan, X. Yang, B. Moubaraki, K. S. Murray and J. J. Vittal, *Dalton Trans.*, 2004, 113.
15. (*a*) Y. Xe, H. Jiang, A. S.-C. Chan, Q. Liu, X. Xu., C. Du and Y. Zhu, *Inorg. Chim. Acta*, 2002, **333**, 138; (*b*) G. Rajsekhar, A. K. Sah, C. P. Rao, P. Guionneau, M. Bharathy and T. N. GuruRow, *Dalton Trans.*, 2003, 3126; (*c*) H. Arii, Y. Funahashi, K. Jitsukawa and H. Masuda, *Dalton Trans.*, 2003, 2115; (*d*) E. Berti, A. Caneschi, C. Daiguebonne, P. Dapporto, M. Formica, V. Fusi, L. Giorgi, A. Guerri, M. Micheloni, P. Paoli, R. Pontellini and P. Rossi, *Inorg. Chem.*, 2003, **42**, 348.
16. (*a*) L. K. Thompson, S. K. Mandal, S. S. Tandon, J. N. Bridson and M. K. Park, *Inorg. Chem.*, 1996, **35**, 3117; (*b*) C. R. Choudhury, S. K. Dey, R. Karmakar, C.-D. Wu, C.-Z. Lu, M. S. E. Fallah and S. Mitra, *New J. Chem.*,

2003, **27**, 1360; (*c*) S. Laborda, R. Clérac, C. E. Anson and A. K. Powell, *Inorg. Chem.*, 2004, **43**, 5931; (*d*) H. Saimiya, Y. Sunatsuki, M. Kojima, S. Kashino, T. Kambe, M. Hirotsu, H. Akashi, K. Nakijima and T. Tokii, *J. Chem. Soc., Dalton Trans.*, 2002, 3737; (*e*) I. Koval, K. Schliden, A. M. Schuitema, P. Gamez, C. Belle, J.-L. Pierre, M. Lüken, B. Krebs, O. Roubeau and J. Reedijk, *Inorg. Chem.*, 2005, **44**, 4372.

17. F. A. Cotton, T. Ren and J. L. Eglin, *J. Am. Chem. Soc.*, 1990, **112**, 3439.
18. (*a*) J. W. Hall, W. E. Estes, E. D. Estes, R. P. Scaringe and W. E. Hatfield, *Inorg. Chem.*, 1977, **16**, 1572; (*b*) L. Merz and W. Haase, *J. Chem. Soc., Dalton Trans.*, 1978, 1594; (*c*) L. Merz and W. Haase, *J. Chem. Soc., Dalton Trans.*, 1980, 875; (*d*) L. Schwabe and W. Haase, *J. Chem. Soc., Dalton Trans.*, 1985, 1909; (*e*) *Angew. Chem., Int. Ed.*, 1997, **36**, 2673; (*f*) A. Mukherjee, M. Nethaji and A. R. Chakravarty, 2004, **43**, 87; (*g*) E. A. Buvaylo, V. N. Kokozay, O. Y. Vassilyeva, B. W. Skelton, J. Jezierska, L. C. Brunel and A. Ozarowski, *Inorg. Chem.*, 2005, **44**, 206; (*h*) K. Isele, P. Franz, C. Ambrus, G. Bernardinelli, S. Decurtins and A. F. Williams, *Inorg. Chem.*, 2005, **44**, 3896.
19. V. Tangoulis, C. P. Raptopoulou, A. Terzis, S. Paschalidou, S. P. Perlepes and E. G. Bakalbassis, *Inorg. Chem.*, 1997, **36**, 3996.
20. (*a*) Y. Song, C. Massera, O. Roubeau, P. Gamez, A. M. M. Lanfredi and J. Reedijk, *Inorg. Chem.*, 2004, **43**, 6842; (*b*) X. S. Tan, Y. Fujii, R. Nukada, M. Mukirya and Y. Nakano, *J. Chem. Soc., Dalton Trans.*, 1999, 2415.
21. N. N. Hoang, F. Valach, M. Dunaj-Jurčo and M. Melník, *Acta Crystallogr., Sect. C*, 1992, **48**, 443.
22. (*a*) M. K. Saha, D. K. Dey, B. Samanta, A. J. Edwards, W. Clegg and S. Mitra, *Dalton Trans.*, 2003, 488; (*b*) C.-T. Yang, B. Moubaraki, K. S. Murray and J. J. Vittal, *Dalton Trans.*, 2003, 880.
23. (*a*) E. Szajna, P. Dobrowolski, A. L. Fuller, A. M. Arif and L. M. Berreau, *Inorg. Chem.*, 2004, **43**, 3988; (*b*) R. H. Holm, *J. Magn. Resonance*, 1970, **2**, 307; (*c*) F. F.-L. Ho, L. E. Erickson, S. R. Watkins and C. N. Reiley, *Inorg. Chem.*, 1970, **9**, 1139; (*d*) R. V. Snyder and R. J. Angelici, *Inorg. Chem.*, 1974, **13**, 14; (*e*) M. N. Murthy, K. D. Karlin, I. Bertini and C. Luchinat, *J. Am. Chem. Soc.*, 1997, **119**, 2156; (*f*) T. C. Higgs, N. S. Dean and C. J. Carrano, *Inorg. Chem.*, 1998, **37**, 1473; (*g*) C. Belle, C. Bougault, M.-T. Averbuch, A. Durif, J.-L. Pierre, J.-M. Latour and L. L. Pape, *J. Am. Chem. Soc.*, 2001, **123**, 8053; (*h*) I. Bertini, I. C. Felli and C. Luchinat, *J. Magn. Resonance*, 1998, **134**, 360; (*i*) I. Bertini, S. Ciurli, A. Dikiy, R. Gasanov, C. Luchinat, G. Martini and N. Safarov, *J. Am. Chem. Soc.*, 1999, **121**, 2037; (*j*) C. O Fernández, J. A. Cricco, J. H. Richards, H. B. Gray and A. J. Vila, *J. Am. Chem. Soc.*, 2001, **123**, 11678; (*k*) J. Park, J. Y. Kim, H. So and J. Liu, *Inorg. Chim. Acta*, 2001, **319**, 8; (*l*) G. N. La Mar, W. DeW. Horrocks, Jr. and R. H. Holm, in *NMR of Paramagnetic Molecules; Principles and Applications*, Academic Press, London, 1973, pp. 243 – 332.
24. (*a*) O. Kahn, in *Molecular Magnetism*, VCH publishers, USA, 1993, pp. 251 – 261; (*b*) *ibid.*, p. 104; (*c*) *ibid.*, Chapter 2. [Calculated spin-only values: expected Ni(II) 2.83 BM, $\chi_M T$ = 1.00 emu K mol^{-1} possessing two unpaired electrons; Cu(II) 1.73 BM, $\chi_M T$ = 0.38 emu K mol^{-1}; 2 × Cu(II) 2.45 BM, $\chi_M T$ = 0.75 emu K mol^{-1}; 3.46 BM, 4 × Cu(II) $\chi_M T$ = 1.50 emu K mol^{-1} with each possessing one unpaired electron]; (*d*) *ibid.* pp. 263 – 269; (*e*) ***PLEASE NOTE*** the Evans balance is sometimes ineffective at measuring accurate magnetic data which is mainly due to environmental effects *e.g.*, fluctuations in temperature.
25. J. C. Bonner and M. E. Fisher, *Phys. Rev., Sect. A.*, 1964, **135**, 640.
26. B. Bleaney and K. D. Bowers, *Proc. Roy. Soc., Sect. A*, 1952, **214**, 451.
27. O. Kahn, *Chem. Phys. Lett.*, 1997, **265**, 109.
28. D. H. Williams and I. Fleming, in *Spectroscopic Methods in Organic Chemistry*, 5th Edn., McGraw Hill, 1995, Gt. Britain.
29. Compared to solid-state IR spectrum of the precursor 2-pyridine alcohol.
30. F. Nepveu, *Inorg. Chim. Acta*, 1987, **134**, 43.
31. J. W. Hall, W. E. Marsh, R. R. Weller and W. E. Hatfield, *Inorg. Chem.*, 1981, **20**, 1033.
32. A. F. Orchard, in *Magnetochemistry*, Oxford Chemistry Primers, Oxford University Press, No. 75, UK, 2003, p. 9.

Chapter 3

3.0 Blending Benzilic Acid and 2-Pyridine Alcohols on a Ni(II) or Cu(II) Centre

The reactivity of combinations of 2-pyridine alcohols towards metal acetates was explored in the previous chapter. In this chapter an investigation into the synthetic, structural and physical studies of complexes prepared from the reactions of ligand blends composed of benzilic (diphenylglycolic) acid, 2-pyridine alcohols [2-{$(CH_2)_n$-OH}-6-X-C_5H_3N] and a source of a 3*d* ion is described.

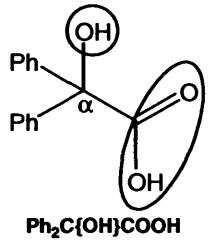

Figure 1 Benzilic acid; binding domains are encircled.

Benzilic acid ($bnzH_2$) [pK_a 3.04 reported by cerimetric titration from the carboxylic acid domain only],[1a] belongs to the α-hydroxy carboxylic acid family, and can act as a bifunctional ligand capable of linking transition metal ions through both the carboxylate and hydroxyl binding domains (Figure 1). It has been utilised for several medicinal purposes, physical applications and investigations into biological and enzymatic activity.[1] In terms of the coordination chemistry, most effort has been directed towards its reactions with high oxidation state metals,[1b] while relatively few reports have seen its use with lower valent metal centres, and in particular, with high spin transition metal ions (Chapter 1, section 1.2.2).[2–4] Based on a search of the crystallographic database, benzilate (bnz or bnzH) ligands normally exhibit five types of bonding modes (Figure 2).[5]

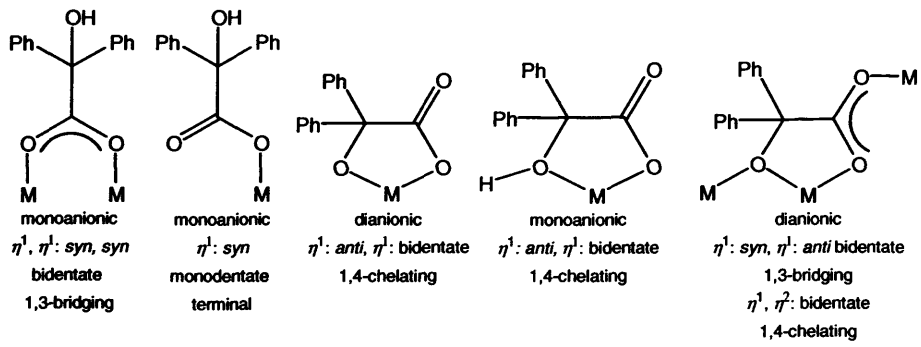

Figure 2 Bonding modes of benzilate (CCDC and SciFinder Scholar search 2005).

An interesting study into the reactivity of $bnzH_2$ towards trivalent iron ions has yielded a dodecanuclear ferric wheel $[Fe(bnzH)(OMe)_2]_{12}$ (Figure 3).[4] In this complex, the monoanionic bnzH ligand 1,3-bridges pairs of iron atoms around the periphery of the wheel. In contrast, if monofunctional carboxylic acids RCO_2H, (R = *p*-Me-C_6H_4-$CO(CH_2)_2$,[6a] Bu^t,[6b] CH_2Cl,[6c] Me,[6d] and H[6e]), are treated with Fe(III) ions in methanol, decanuclear ferric wheels, $[Fe(RCO_2)(OMe)_2]_{10}$, result.[6] It is, thus, likely that the presence of an α-OH group in the bound bnzH ligand influences (*e.g.*, *via* non-covalent interactions) ferric wheel assembly.

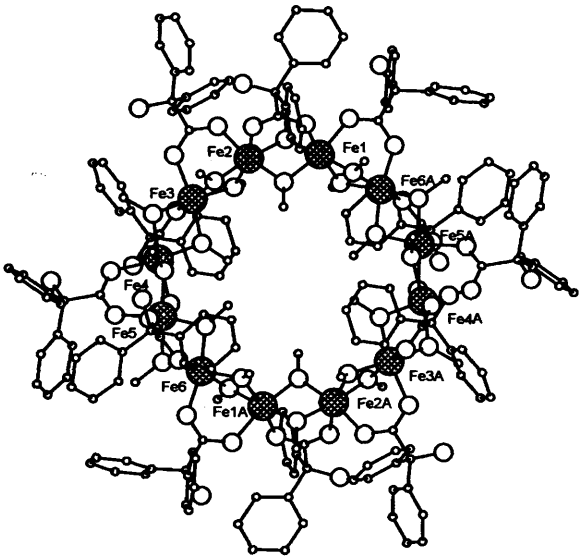

Figure 3 Molecular structure of $[Fe(bnzH)(OMe)_2]_{12}$.[4]

The main aim of this chapter is to focus on the coordination chemistry of divalent nickel and copper ions supported by ligands derived from both $bnzH_2$ and 2-pyridine alcohols (sections 3.1 and 3.2). In particular, the effect of the pyridine alcohol methylene chain length (n = 0 – 3) is systematically probed as is the potential for covalent and non-covalent interaction of the α-OH moiety in the benzilate ligand.

In many cases, the synthesis of the corresponding complexes containing the non-hydroxyl counterpart of $bnzH_2$, diphenylacetic acid [$Ph_2C\{H\}COOH$, pK_a = 3.81],[7] is also reported for comparison. Furthermore, spectroscopic/spectrometric data and magnetic measurements are used to support and complement the single crystal X-ray determinations.

Scheme 1 shows the general synthetic strategy to be employed and the stoichiometry of reagents and the solvents used for all reactions. In addition, the use of an ionic base (NaOMe) in place of triethylamine is also examined.

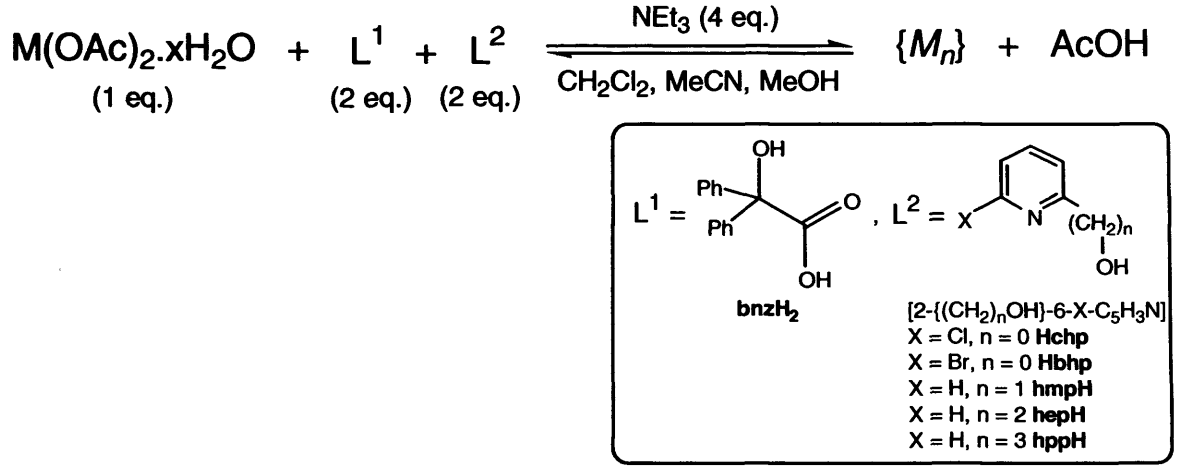

Scheme 1 Synthetic strategy employed.

3.1 Blending Benzilic Acid and 2-Pyridine Alcohols on a Ni(II) Centre

3.1.1 M = Ni, L^1 = $bnzH_2$, L^2 = Hxhp (n = 0, X = Cl or Br)

The reaction of nickel acetate tetrahydrate with a blend of Hxhp (Hxhp = Hchp or Hbhp) and $bnzH_2$, in a trisolvent mixture composed of CH_2Cl_2, MeCN and MeOH, in the presence of triethylamine gave, on work-up, $[Ni_4(xhp)_4(bnzH)_4(MeO)_2(ROH)_2][NEt_3H]_2 \cdot 2MeCN$ [xhp = chp; R = H **9a**, R = Me **9b**] or $[Ni_4(xhp)_4(bnzH)_4(MeO)_2(ROH)_2][NEt_3H]_2 \cdot 2MeCN$ [xhp = bhp; R = H **10a**, R = Me **10b**] in moderate yield (Scheme 2). Complexes **9a/9b** and **10a/10b** were characterised by elemental analysis, IR spectroscopy and positive FAB mass spectrometry. In addition, a single crystal of co-crystallised **9a/9b** was subject to an X-ray diffraction study. The molecular structure of co-crystallised **10a/10b** was also obtained and shows similar features to that for **9a/9b**. The structure of the dianionic unit in **9a** is shown in Figure 4; selected bond lengths and angles of **9a/9b** are listed in Table 1.

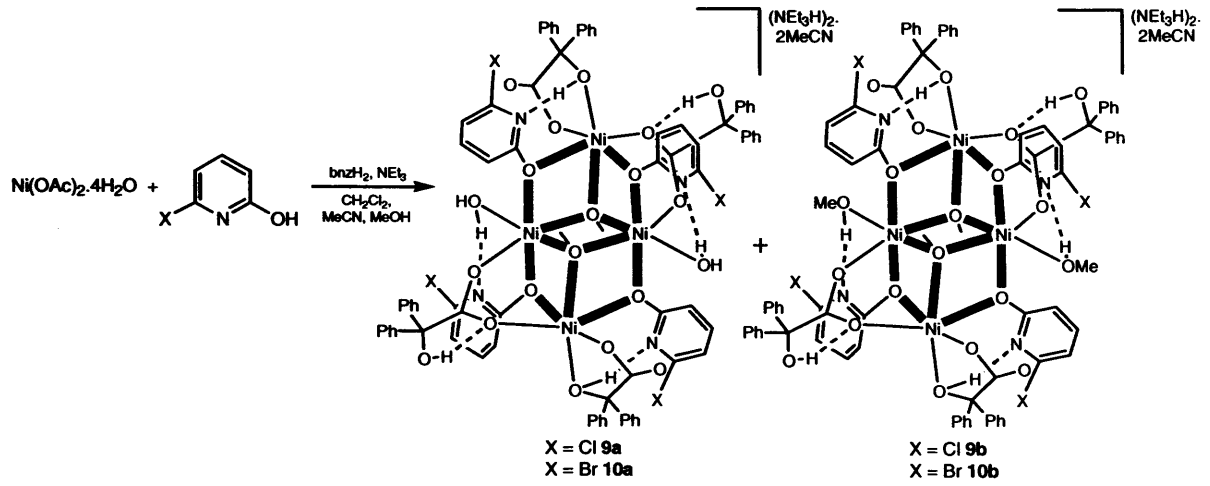

Scheme 2 Synthesis of **9** and **10**.

The molecular structure of **9a/9b** is based on the triethylammonium salts of two independent anionic units which both contain four octahedrally coordinated Ni(II) ions surrounded by four bnzH, four chp, two methoxide and two ROH ligands. The dianionic units in **9a** and **9b** are essentially the same with the two terminally bound water molecules in **9a** being replaced by methanol ligands in **9b**. The structures of **9a** and **9b** can be described as open di-cubanes formed from two fused cubes with missing vertices arranged in a chair-like fashion. Four 2.20 chp ligands (η^1, μ_2) and two μ_3-methoxide (η^1, μ_3) ligands form the defective corners of the cubes. The bnzH ligands either 1,3-bridge or 1,4-chelate to the Ni(II) ions, the latter forms a five-membered ring, whereby, the α-OH group remains protonated (Figure 5). The chelate bite angle (α) from the bnzH ligand at 79.72(14)° is acute.

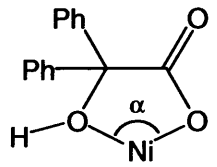

Figure 5 1,4-Chelating monoanionic bnzH bonding mode.

The longest metal to ligand bonds in **9a** arise from the chp oxygen atoms [Ni(1)-O_{chp}(2A) = 2.101(4) Å, Ni(2)-O_{chp}(1) = 2.092(4) Å] and the shortest from OMe [Ni(1)-O_{MeO}(9A) = 2.001(4) Å and Ni(2)-O_{MeO}(9A) = 2.019(4) Å].

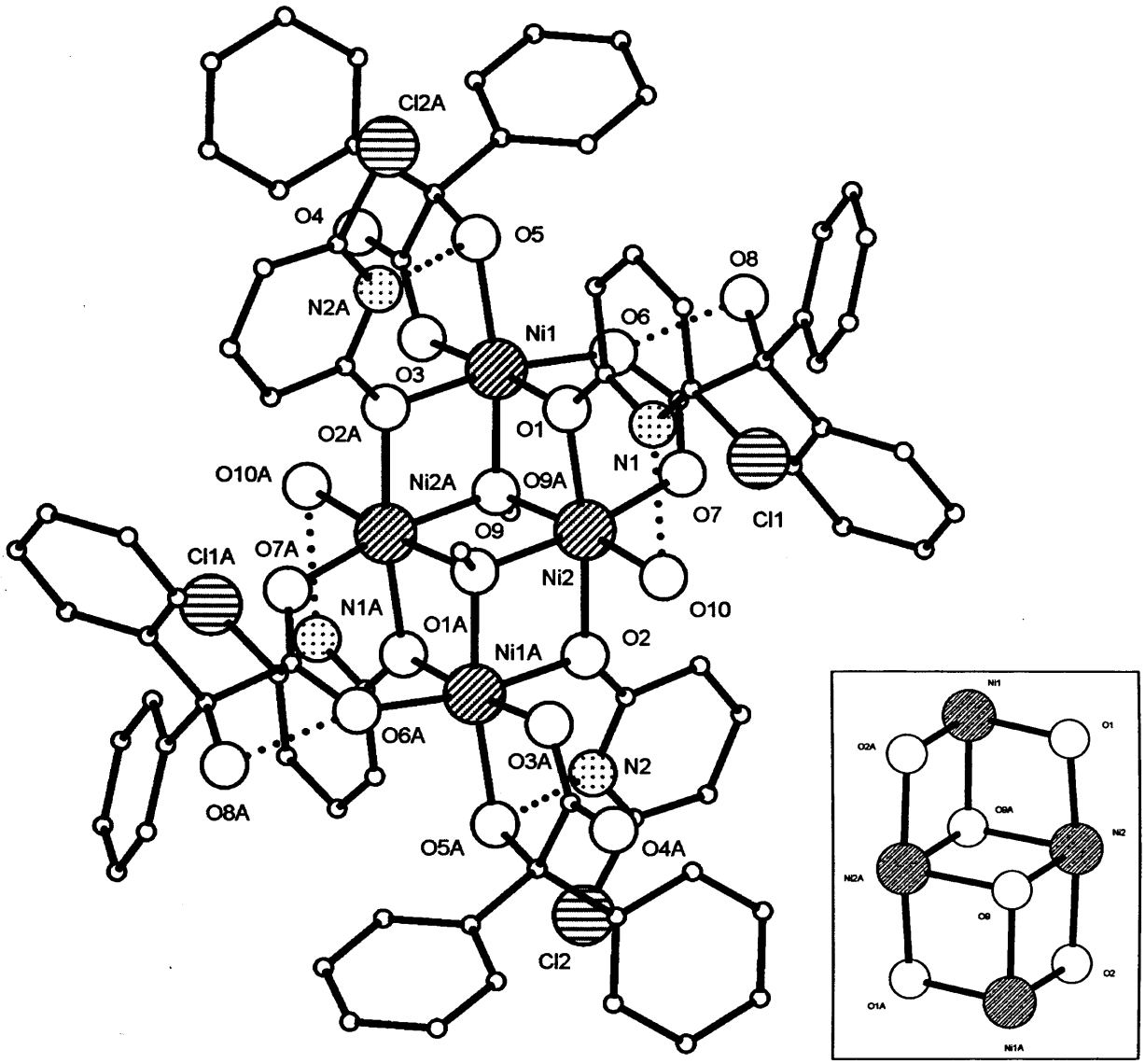

Figure 4 Molecular structure of the dianionic unit in **9a**. Inset shows Ni_4O_6 core. Hydrogen atoms, labels for carbon atoms, triethylammonium cations and solvent (MeCN) molecules are excluded for clarity. Letter labelled atoms were generated by symmetry. Dotted bonds indicate hydrogen bonding interactions.

Table 1 Selected bond length (Å) and angle (°) data for co-crystallised **9a/9b**

9a				**9b**							
Ni(1)-O(1)	2.066(4)	Ni(1)-Ni(2)	2.9694(12)	Ni(2)-O(7)	2.053(4)	Ni(3)-O(11)	2.111(4)	Ni(3)-O(16)	2.071(2)	Ni(4)-O(19)	2.052(4)
Ni(1)-O(2)#1	2.101(4)	Ni(1)-O(9)#1	2.001(4)	Ni(2)-O(9)	2.045(5)	Ni(3)-O(12)	2.070(4)	Ni(4)-O(11)#2	2.097(4)	Ni(4)-O(20)	2.031(4)
Ni(1)-O(3)	2.032(4)	Ni(2)-O(1)	2.092(4)	Ni(2)-O(9)#1	2.019(4)	Ni(3)-O(13)	2.021(4)	Ni(4)-O(12)	2.114(4)	Ni(4)-O(20)#2	2.035(4)
Ni(1)-O(5)	2.096(4)	Ni(2)-O(2)	2.087(4)	Ni(2)-O(10)	2.053(4)	Ni(3)-O(15)	2.084(2)	Ni(4)-O(17)	2.069(2)		
Ni(1)-O(6)	2.051(5)										
O(1)-Ni(1)-O(2)#1	94.12(14)	O(9)#1-Ni(1)-O(1)	86.33(14)	O(9)#1-Ni(2)-O(2)	93.03(14)	O(12)-Ni(3)-O(11)	86.00(15)	O(20)-Ni(3)-O(15)	170.65(12)	O(20)-Ni(4)-O(12)	83.54(14)
O(3)-Ni(1)-O(1)	175.64(15)	O(9)#1-Ni(1)-O(2)#1	81.92(14)	O(10)-Ni(2)-O(1)	96.33(14)	O(13)-Ni(3)-O(11)	97.76(16)	O(20)-Ni(3)-O(16)	91.94(12)	O(20)#2-Ni(4)-O(12)	89.36(15)
O(3)-Ni(1)-O(2)#1	90.50(15)	O(9)#1-Ni(1)-O(3)	90.08(15)	O(10)-Ni(2)-O(2)	84.41(14)	O(16)-Ni(3)-O(11)	169.10(12)	O(20)-Ni(3)-O(20)#2	80.59(15)	O(19)-Ni(4)-O(17)	92.53(14)
O(1)-Ni(1)-O(5)	103.68(14)	O(9)#1-Ni(1)-O(5)	169.05(14)	O(9)-Ni(2)-O(7)	170.81(15)	O(20)-Ni(3)-O(11)	80.85(14)	Ni(4)#2-O(11)-Ni(3)	96.51(15)	O(20)-Ni(4)-O(17)	91.84(12)
O(3)-Ni(1)-O(5)	79.72(14)	O(9)#1-Ni(1)-O(6)	89.99(15)	O(9)#1-Ni(2)-O(7)	91.53(15)	O(13)-Ni(3)-O(12)	176.13(16)	Ni(3)-O(12)-Ni(4)	91.64(15)	O(20)#2-Ni(4)-O(17)	171.75(12)
O(6)-Ni(1)-O(1)	86.13(14)	Ni(2)-O(2)-Ni(1)#1	96.07(15)	O(7)-Ni(2)-O(10)	95.43(15)	O(12)-Ni(3)-O(15)	101.68(12)	O(11)#2-Ni(4)-O(12)	169.63(15)	O(20)-Ni(4)-O(19)	174.59(16)
O(6)-Ni(1)-O(5)	95.03(14)	Ni(1)#1-O(2)-Ni(2)#1	95.21(15)	O(9)-Ni(2)-O(10)	92.77(15)	O(12)-Ni(3)-O(16)	85.29(13)	O(17)-Ni(4)-O(11)#2	103.85(12)	O(20)#2-Ni(4)-O(19)	94.85(16)
O(5)-Ni(1)-O(2)#1	86.55(14)	O(2)-Ni(2)-O(1)	171.08(14)	O(9)#1-Ni(2)-O(9)	80.36(16)	O(20)-Ni(3)-O(12)	85.53(15)	O(19)-Ni(4)-O(11)#2	86.21(16)	O(20)-Ni(4)-O(20)#2	80.59(15)
O(6)-Ni(1)-O(2)#1	169.42(14)	O(7)-Ni(2)-O(1)	85.18(15)	O(9)-Ni(2)-O(10)	92.77(15)	O(13)-Ni(3)-O(15)	79.08(13)	O(20)-Ni(4)-O(11)#2	95.83(14)	O(3)-O(20)-O(4)	96.32(15)
O(6)-Ni(1)-O(5)	95.03(14)	O(7)-Ni(2)-O(2)	103.62(15)	O(9)#1-Ni(2)-O(10)	172.97(15)	O(13)-Ni(3)-O(16)	90.87(14)	O(20)#2-Ni(4)-O(11)#2	80.34(14)	O(3)-O(20)-O(1)#2	102.29(16)
Ni(1)-O(1)-Ni(2)	91.16(14)	O(9)-Ni(2)-O(1)	89.82(14)	Ni(1)#1-O(9)-Ni(2)	100.64(15)	O(20)-Ni(3)-O(13)	94.13(15)	O(17)-Ni(4)-O(12)	86.52(12)	O(4)-O(2)-O(4)#2	99.41(15)
		O(9)-Ni(2)-O(2)	81.26(14)	Ni(1)#1-O(9)-Ni(2)	99.64(16)	O(16)-Ni(3)-O(15)	94.55(9)	O(19)-Ni(4)-O(12)	93.55(16)		

Symmetry transformations used to generate equivalent atoms: #1 ($-x+2, -y+2, -z+1$), #2 ($-x+1, -y, -z+2$).

The nickel to nickel ion distances in **9a** are Ni(1)···Ni(2) = 2.9693(16) Å, Ni(1A)···Ni(2) = 3.1141(16) Å and Ni(2A)···Ni(2) = 3.1051(16) Å. The bridging carboxylate C-O bond lengths of **9a** are 1.261(6) Å and 1.263(6) Å, whereas, the C-$O_{\alpha\text{-}OH}$ bond length at 1.412 Å is as expected for a sp^3 bound oxygen. The chelating bnzH bound and unbound carbonyl oxygen atoms have C-O bond lengths of 1.270(6) Å and 1.241(6) Å, respectively and C-$O_{\alpha\text{-}OH}$ = 1.426(6) Å. The C-O bond lengths of the metal bound carboxylates suggest the presence of some covalent character from the metal-ligand bond [for Ni(II): range ~ 1.263 – 1.268 Å ⇒ ~15 – 20% covalent C-O bond character].[12]

In **9a/9b**, the bnzH hydroxyl groups undergo intramolecular intra-ligand and inter-ligand hydrogen bonding interactions with carboxylate oxygen atoms and neighbouring chp nitrogen atoms, respectively. The water (**9a**) and methanol (**9b**) ligands undergo inter-ligand hydrogen bonding interactions with neighbouring chp nitrogen atoms. In addition, the anionic unit participates in hydrogen bonding with one of the triethylammonium cations. The hydrogen bonding distances in **9a** are summarised in Table 2.

Table 2 Hydrogen bond distances (Å) in co-crystallised **9a/9b**

Type	9a		9b	
Inter-ligand, chelating bnzH	$N_{chp}(2)\cdots O_{\alpha\text{-}OH}(5A)$	2.639(6)	$N_{chp}(3A)\cdots O_{\alpha\text{-}OH}(15A)$	2.588(5)
Intra-ligand, bridging bnzH	$O_{COO}(6)\cdots O_{\alpha\text{-}OH}(8)$	2.581(5)	$O_{COO}(16)\cdots O_{\alpha\text{-}OH}(18)$	2.554(7)
Inter-ligand	$N_{chp}(1)\cdots O_{water}(10)$	2.667(6)	$N_{chp}(4A)\cdots O_{water}(19A)$	2.605(7)
Intermolecular	$N_{triethylammonium}(5)\cdots O_{COO}(4)$	2.725(7)		

There are a number of reported tetrameric di-cubane nickel complexes.[8–11] In $[Ni_4(\mu_3\text{-}OMe)_2(H_2O)_6(ntp)_2]$ [H_3ntp = $N(CH_2CH_2COOH)_3$], the Ni-O_{MeO} bond lengths range from 2.040 – 2.079 Å.[11] In comparison, **9** has shorter Ni-O_{MeO} bond lengths. Furthermore, in $[Ni_4(\mu_3\text{-}OMe)_2(H_2O)_6(ntp)_2]$ the Ni···Ni distances range from 3.089 – 3.126 Å, these bond distance values are comparable to those found in **9a/9b**. In the closed cubane complex $[Ni_4(\mu_3\text{-}OMe)_4(\eta^1\text{-}chp)(chp)_4(MeOH)_7)]$,[14a] the bond lengths of Ni-O_{chp} = 2.062 – 2.091 Å, Ni-O_{OMe} = 2.023 – 2.074 Å, Ni-O_{MeOH} = 2.068 – 2.115 Å (Ni-O_{MeOH} = 2.031 – 2.035 Å in **9b**) are also comparable to those found in **9a/9b**.

The IR spectra of **9a/9b** and **10a/10b** show two strong bands corresponding to $\nu(CO_2)_{asymm}$ and $\nu(CO_2)_{symm}$ stretches for the bnzH ligand at ~ 1591 cm^{-1}, 1446 cm^{-1} (**9a/9b**) and 1585 cm^{-1}, 1443 cm^{-1} (**10a/10b**), respectively, overlapping in each case with the ν(C=N) pyridyl stretching bands.[25,26] The FAB mass spectra of **9** and **10** revealed several peaks associated with the anionic portion of the complex including [**9a** – $2NEt_3H$ – bnzH – chp]$^+$ at 1400 Da., [**9a** – $2NEt_3H$ – 2bnzH – chp]$^+$ at 1173 Da. and [**10a** – $2NEt_3H$ – 2bnzH]$^+$ at 1480 Da., respectively. Magnetic susceptibility measurements of **9a/9b** (desolvated) will be described in more depth later on (section 3.3).

3.1.2 M = Ni, L^1 = $bnzH_2$, L^2 = hmpH (n = 1, X = H)

The reaction of nickel acetate tetrahydrate with a blend of hmpH and $bnzH_2$ in the presence of triethylamine gave, on work-up, green $[Ni_4(hmp)_4(bnzH)_4(MeOH)_2]$ (**11a**) in high yield along with the pale-blue mononuclear complex $[Ni(hmpH)_2(bnzH)_2]$ (**12a**) in lower yield (Scheme 3). To complement the studies, $bnzH_2$ was substituted for $Ph_2C\{H\}CO_2H$ giving $[Ni_4(hmp)_4(Ph_2C\{H\}CO_2)_4(MeOH)_2]$ (**11b**) and $[Ni(hmpH)_2(Ph_2C\{H\}CO_2)_2]$ (**12b**). Complexes **11** and **12** were characterised by elemental analysis, IR and ^1H NMR spectroscopy (Tables 5 and 6) along with positive FAB mass spectrometry. In addition, single crystals of **11a** and **12a** were subject to X-ray diffraction studies. The molecular structures of **11a** and **12a** are depicted in Figures 6 and 7, respectively; selected bond lengths and angles of **11a** and **12a** are listed in Tables 3 and 4, respectively.

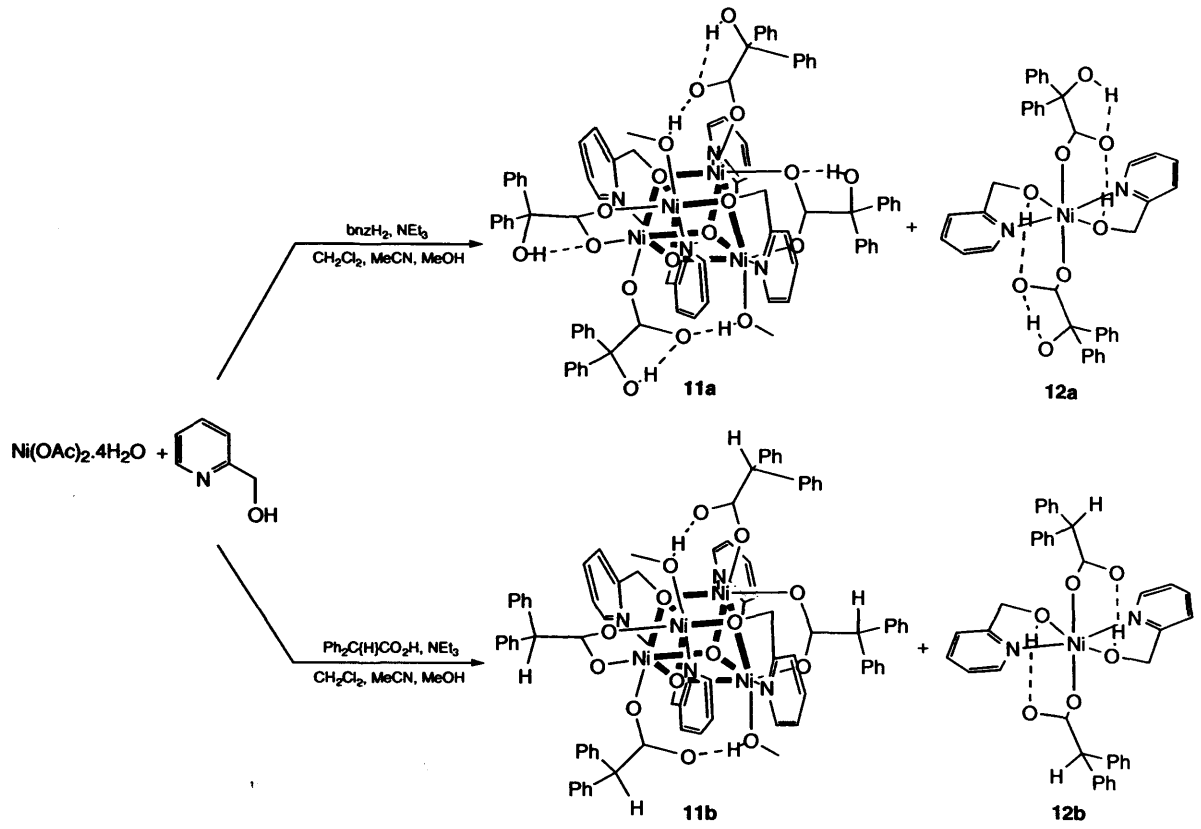

Scheme 3 Synthesis of **11** and **12**.

The structure of **11a** consists of four octahedral nickel(II) ions arranged on the vertices of a cube, these are coordinated to four hmp, four bnzH and two MeOH ligands. The 3.31-hmp ligands bridge the nickel ions and complete the vertices of the cube. The bnzH ligands are bound as either η^1-monodentate or 1,3-bridging carboxylates with the Ni(II) ions.

The longest and shortest metal to donor ligand atom bond lengths in **11a** are observed from the hmp alkoxide and η^1-bnzH ligands [Ni(1)-O_{hmp}(1) = 2.054(4) Å, Ni(2)-O_{hmp}(2) = 2.069(3) Å and Ni(2)-O_{bnzH}(6) = 1.994(3) Å]. The metal to metal ion distances within this complex are Ni(1)···Ni(2) = 2.8988(19) Å Ni(1)···Ni(1A) = 3.110(2) Å, Ni(1)···Ni(2A) = 3.160(2) Å and Ni(2)···Ni(2A) = 3.140(2) Å.

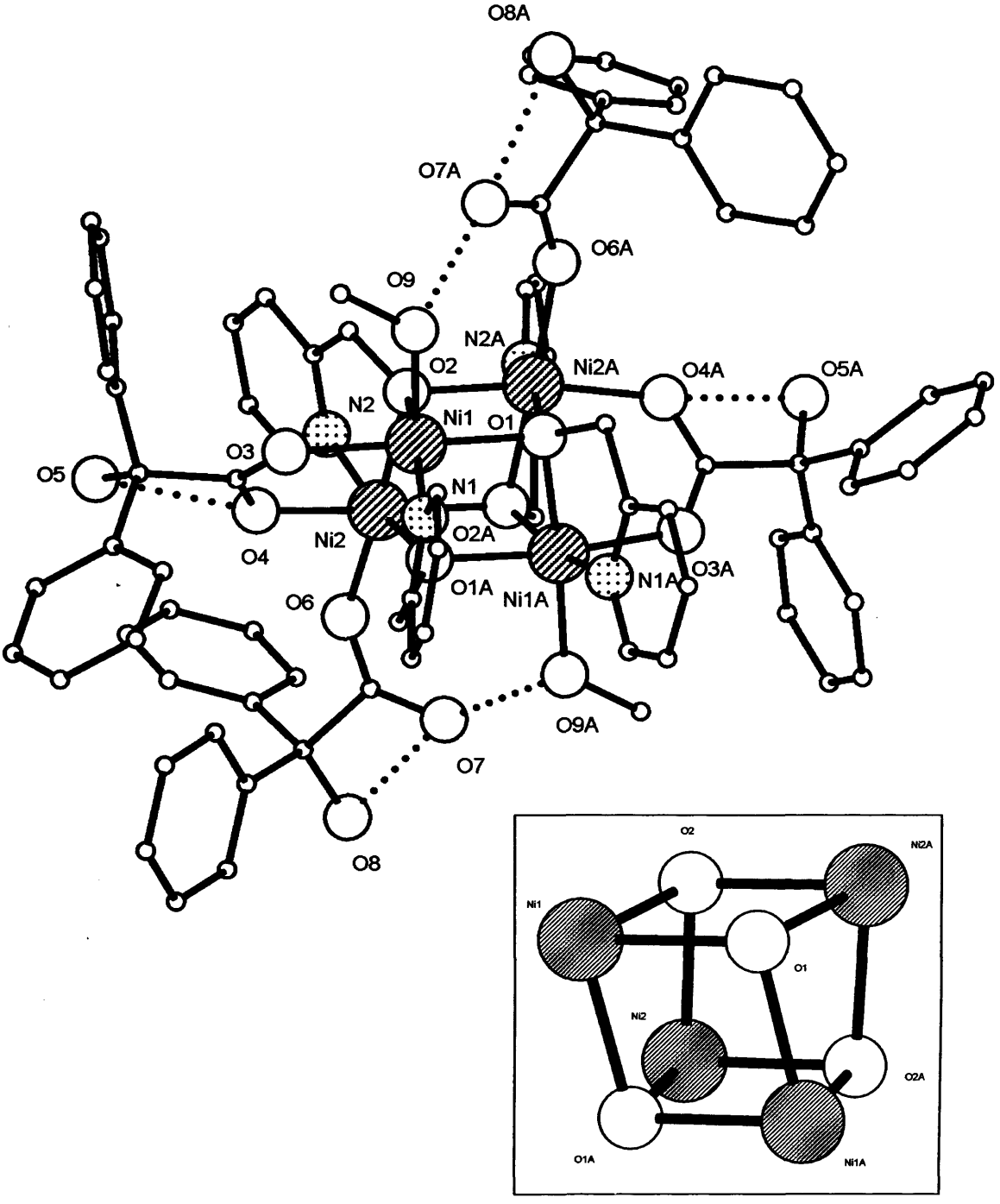

Figure 6 Molecular structure of **11a**. Inset shows the Ni_4O_4 core. Hydrogen atoms and carbon atom labels are excluded for clarity. Dotted bonds show hydrogen bonding interactions.

Table 3 Selected bond length (Å) and angle (°) data for complex **11a**

11a							
Ni(1)-O(1)	2.054(4)	Ni(1)-O(3)	2.037(3)	Ni(2)-O(2)	2.069(3)	Ni(2)-O(4)	2.067(3)
Ni(1)-O(1)#1	2.047(3)	Ni(1)-O(9)	2.031(3)	Ni(2)-O(2)#1	2.042(3)	Ni(2)-O(6)	1.994(3)
Ni(1)-N(1)	2.038(3)	Ni(2)-O(1)#1	2.059(3)	Ni(2)-N(2)	2.064(3)	Ni(1)···Ni(2)	2.8989(14)
Ni(1)-O(2)	2.050(3)						
O(1)#1-Ni(1)-O(1)	81.32(11)	O(9)-Ni(1)-O(1)	174.29(11)	O(4)-Ni(2)-O(2)	93.31(110	O(1)-Ni(1)-Ni(2)	89.53(7)
N(1)-Ni(1)-O(1)	100.15(11)	O(9)-Ni(1)-N(1)	96.47(12)	O(2)#1-Ni(2)-O(4)	168.88(11)	O(1)#1-Ni(1)-Ni(2)	45.27(7)
N(1)-Ni(1)-O(1)#1	81.10(11)	O(9)-Ni(1)-O(2)	94.76(11)	N(2)-Ni(2)-O(4)	85.67(13)	N(1)-Ni(1)-Ni(2)	123.46(10)
O(2)-Ni(1)-O(1)	79.21(10)	O(9)-Ni(1)-O(3)	90.63(12)	O(6)-Ni(2)-O(1)#1	100.62(10)	O(2)-Ni(1)-Ni(2)	45.53(8)
O(1)#1-Ni(1)-O(2)	87.73(10)	O(2)#1-Ni(2)-O(1)#1	79.29(10)	O(6)-Ni(2)-O(2)	172.47(10)	O(3)-Ni(1)-Ni(2)	81.10(9)
N(1)-Ni(1)-O(2)	168.77(12)	O(1)#1-Ni(2)-N(2)	165.86(13)	O(6)-Ni(2)-O(2)#1	100.67(11)	O(9)-Ni(1)-Ni(2)	138.58(8)
O(3)-Ni(1)-O(1)	169.97(11)	O(1)#1-Ni(2)-O(2)	86.90(10)	O(6)-Ni(2)-N(2)	93.03(13)	O(1)#1-Ni(2)-Ni(1)	44.91(8)
O(3)-Ni(1)-O(1)#1	94.44(11)	O(2)#1-Ni(2)-O(2)	80.29(11)	O(6)-Ni(2)-O(4)	86.87(12)	O(2)-Ni(2)-Ni(1)	45.00(7)
O(3)-Ni(1)-N(1)	88.09(12)	N(2)-Ni(2)-O(2)	79.48(12)	Ni(1)#1-O(1)-Ni(1)	98.63(11)	O(2)#1-Ni(2)-Ni(1)	88.76(7)
O(3)-Ni(1)-O(2)	91.59(11)	O(2)#1-Ni(2)-N(2)	101.93(12)	Ni(1)-O(1)-Ni(2)#1	100.38(11)	N(2)-Ni(2)-Ni(1)	120.96(11)
O(9)-Ni(1)-O(1)	94.09(11)	O(1)#1-Ni(2)-O(4)	168.88(11)	Ni(1)-O(1)-Ni(1)#1	89.82(10)	O(4)-Ni(2)-Ni(1)	80.33(9)
						O(6)-Ni(2)-Ni(1)	142.19(8)

Symmetry transformations used to generate equivalent atoms: #1 ($-x+2, y, -z+1$).

The average bridging bnzH C-O bond lengths in **11a** are 1.242(5) Å and 1.249(5) Å. The C-$O_{\alpha\text{-}OH}$ bond length is longer at 1.409(6) Å as expected for C(sp^3)-O. The η^1-bnzH ligands have C-O bond lengths at 1.234(3) Å and 1.249(4) Å for the bound and unbound carbonyls, respectively. The former value indicates the presence of a mainly ionic metal-ligand bond.[12] The η^1-bnzH C-$O_{\alpha\text{-}OH}$ bond length at 1.420(3) Å is similar to the corresponding bond length value found in **9a** (1.426 Å).

The two methanol ligands in **11a** undergo intramolecular inter-ligand hydrogen bonding interactions with adjacent η^1-bnzH carboxylate oxygen atoms [O(7)···O_{MeOH}(9A) = 2.614(4) Å]. Both bridging and η^1-bnzH ligands undergo intra-ligand hydrogen bonding interactions from the α-OH group with the carboxylate oxygen atom [O_{COO}(4)···$O_{\alpha\text{-}OH}$(5) 2.548(5) Å and O_{COO}(7) ··$O_{\alpha\text{-}OH}$(8) at 2.569(4) Å].

There are many examples of tetrameric nickel cubane-type complexes.[13] However, there are only a limited number that contain hmp ligands.[14,15] In $[Ni_4(hmp)_4Cl_4(MeOH)_4]$ and $[Ni_4(hmp)_4(N_3)_4(MeOH)_4]$,[15a] the chelating N_{hmp}-Ni-O_{hmp} bite angles are 81.0°/80.5°

(80.29° **11a**) with average bond lengths of Ni-N_{hmp} = 2.039 Å/2.043 Å (2.051 Å **11a**) and Ni-O_{hmp} = 2.084 Å/1.977 Å (2.062 Å **11a**), are comparable to **11a**. The methanol ligands in $[Ni_4(hmp)_4Cl_4(MeOH)_4]$ and $[Ni_4(hmp)_4(N_3)_4(MeOH)_4]$ have average Ni-O_{MeOH} bond lengths at 2.071 Å/2.139 Å; in **11a** the corresponding bond length is shorter (2.031 Å). The recently reported complex $[Ni_4(hmp)_4$(3,3-dimethyl-1-butanol)$_4Cl_4]$[15b] also possesses hmp bond length and bite-angle values similar to those found in **11a** at 2.0648 Å [Ni-N_{hmp}], 2.0893 Å [Ni-O_{hmp}] and 80.73° [N_{hmp}-Ni-O_{hmp}], respectively.

The molecular structure of **12a** consists of an octahedrally distorted Ni(II) ion bound by two *trans* η^1-bound bnzH ligands and two *N,O*-chelating hmpH ligands. The 1.11 hmpH ligands have bond lengths of Ni-N_{hmpH} = 2.035 Å and Ni-O_{hmpH} = 2.073 Å accompanied by a chelate bite angle of N_{hmpH}(1)-Ni(1)-O_{hmpH}(1) at 80.28°.

Table 4 Selected bond length (Å) and angle (°) data for complex **12a**

12a					
Ni(1)-O(1)	2.0730(18)	Ni(1)-O(2)	2.0800(18)	Ni(1)-N(1)	2.035(2)
N(1)-Ni(1)-O(1)	80.28(8)	O(1)-Ni(1)-O(2)	87.07(7)	N(1)-Ni(1)-O(2)	86.50(9)
N(1)#1-Ni(1)-O(1)	99.72(8)	O(1)-Ni(1)-O(2)#1	92.93(7)	N(1)-Ni(1)-O(2)#1	93.50(9)

Symmetry transformations used to generate equivalent atoms: #1 (– x + 1/2, – y + 1/2, – z + 1).

In **12a**, the metal ion bound and unbound carboxylate (bnzH) C-O bond lengths are 1.241(3) Å and 1.254(3) Å, respectively, the former value suggests the presence of an ionic metal-bnzH bond.[12] The C-$O_{\alpha\text{-}OH}$ bond length is longer at 1.414(4) Å.

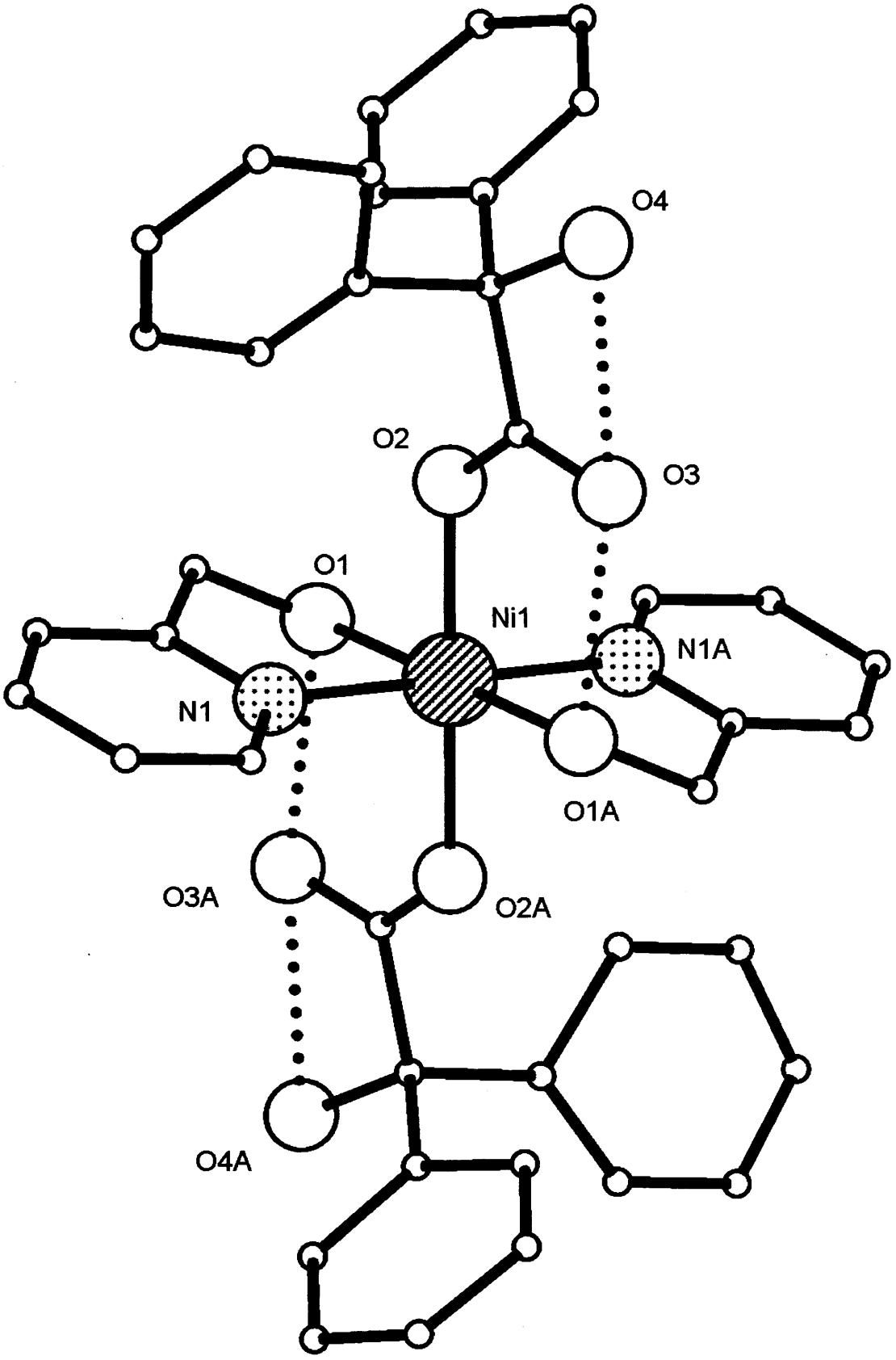

Figure 7 Molecular structure of **12a**. Hydrogen atoms and carbon atom labels are excluded for clarity. Letter labelled atoms were generated by symmetry. Dotted bonds indicate hydrogen bonding interactions.

Complex **12a** contains intra- and inter-ligand hydrogen bonding interactions from the bnzH α-OH groups and adjacent carboxylate oxygen atoms and from the hmpH hydroxyl groups with nearby carboxylate oxygen atoms, respectively [$O_{\alpha\text{-}OH}(4)\cdots O_{COO}(3)$ = 2.558(3) Å, $O_{hmpH}(1)\cdots O_{COO}(3)$ = 2.589(3) Å].

Complex **12a** can be synthesised exclusively and in high yield by replacing methanol by ethanol in the tri-solvent mixture. It is uncertain as to why a change of solvent disallows formation of a tetrameric molecule analogous to **11a** but it may be due to steric reasons. Furthermore, **11a** can be synthesised as the sole reaction product by refluxing the reagents in excess triethylamine (in the absence of the tri-solvent mixture) and subsequent extraction in methanol (Chapter 7, section 7.3).

The IR spectra of **11a, 11b, 12a**, and **12b** show $\nu(CO_2)_{asymm}$ bands at 1606 cm^{-1}, 1576 cm^{-1}, 1591 cm^{-1}, 1571 cm^{-1}, respectively and $\nu(CO_2)_{symm}$ stretching bands at 1386 cm^{-1}, 1382 cm^{-1}, 1380 cm^{-1} and 1387 cm^{-1}, respectively. These bands overlap with ν(C=N) pyridyl stretching bands while ν(OH) stretching bands appear at ~ 3400 cm^{-1}.[25,26] The FAB mass spectra of **11a** and **11b** include $[M - 2MeOH]^+$ peaks at 1575 Da. and 1512 Da., respectively, whereas the spectra of **12a** and **12b** show peaks of $[M - hmpH]^+$ at 622 Da. and $[M]^+$ at 699 Da., respectively. The room temperature magnetic moments for mononuclear **12a** and **12b** at 3.60 BM ($\chi_M T$ = 1.62 emu K mol^{-1}) and 2.83 BM ($\chi_M T$ = 1.00 emu K mol^{-1}), respectively, are higher than/consistent with single Ni(II) ions possessing two unpaired electrons (2.83 BM, $\chi_M T$ = 1.00 emu K mol^{-1}, ***SEE NOTE***).[22b,22c] The magnetic properties of tetrameric **11a** are discussed later on in this Chapter (section 3.3).

Complexes **11a**, **11b** (Table 6), **12a** and **12b** (Table 5) were characterised by ^1H NMR spectroscopy (Chapter 7, section 7.0). All the spectra (recorded in $CDCl_3$) are broad and paramagnetically shifted. Peak assignment has been made on the basis of a comparison of previously reported data,[27] direct comparison of complexes in this work (Chapter 2, section 2.4) and by inspection of the relaxation times.

Assignment of the spectra involving monomers **12a** and **12b** are given in Table 5. The H_α hmpH pyridyl proton peaks appear at ~ 140 ppm (broad), hmpH $H_{\beta/\beta'}$ proton peaks are observed from ~ 39 – 43 ppm (~ 2 ms) and H_γ protons are observed at ~ 15 ppm (~ 6 ms). The sharper aromatic bnzH/diphenylacetate aromatic proton peaks are found in the 5 – 10 ppm region. A sharp Ph_2CH methine proton peak from **12b** appears at ~ 27 ppm (~ 1.7 ms). The hmpH α-CH_2 [$H_{(eq.)}$] proton peaks are chemically shifted in the ~ 95 ppm (~ 0.6 ms) region, the broader α-CH_2 [$H_{(ax.)}$] pseudo-contact shifted peaks appear at ~ – 9 ppm and – 10 ppm (~ 0.2 ms) (Figure 8).[27a,27b,27l]

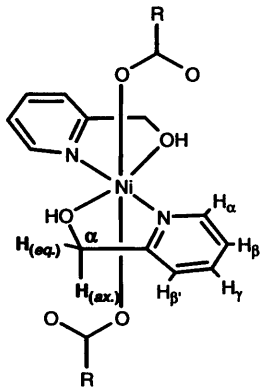

Figure 8 Geminal axial (*ax.*) and equatorial (*eq.*) methylene protons of hmpH.

Table 5 ^{1}H NMR chemical shifts (δ) and relaxation times (T_1 ms, in parentheses) for complexes **12a** and **12b** (spectra recorded in $CDCl_3$)

Complex in solid-state	H_α	$H_{\beta/\beta'}$	H_γ	α-CH_2 $H_{(eq.)}$	α-CH_2 $H_{(ax.)}$	Me	C*H*	Ar-*H*
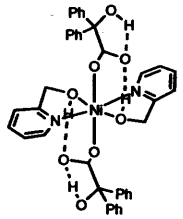 **12a**	140.6 (1.78×10^6)[a]	43.0 (2.02), 39.0 (2.22)	15.6 (6.50)	94.7 (0.57)	– 10.2 (0.24)	N/A	N/A	5 – 10
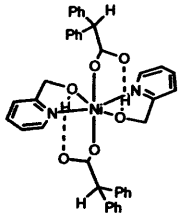 **12b**	140.5 (broad)[b]	42.9 (2.08), 38.7 (2.31)	15.4 (6.76)	95.1 (0.59)	– 8.6 (61.45)[a]	N/A	27.8 (1.71)	5 – 10

[a]Unreliable. [b]Could not be observed/determined.

In the ^{1}H NMR spectra of tetrameric **11a** and **11b**, there are several collections of broad peaks in various regions. The appearance and number of signals in the spectra can be attributed to the presence of four high spin Ni(II) ions (Table 6). The hmp pyridine ring H_α protons are observed as broad and downfield chemically shifted peaks in the range of 193 – 143 ppm (~ 0.48 – 0.28 ms). As an example, the H_α (pyridyl ligand-based) peak has been reported to appear as downfield as 171 ppm (0.16 ms) for a dimeric high spin Ni(II) complex,[27g] the H_α protons are close to the nickel ions and experience the greatest amount of deshielding having faster relaxation times and lower T_1 values. The $H_{\beta/\beta'}$ pyridyl proton peaks are found in the region of ~ 37 – 46 ppm (2.6 – 5.0 ms) and the pyridyl H_γ proton peaks are assigned within the region of ~ 16 – 18 ppm (6.3 – 7.3 ms).

Table 6 ^{1}H NMR chemical shifts (δ) and relaxation times (T_1 ms, in parentheses) for complexes **11a** and **11b** (spectra recorded in $CDCl_3$)

Complex in solid-state	H_α	$H_{\beta/\beta'}$	H_γ	α-CH_2 $H_{(eq.)}$	α-CH_2 $H_{(ax.)}$	CH_3OH	C*H*	Ar-*H*
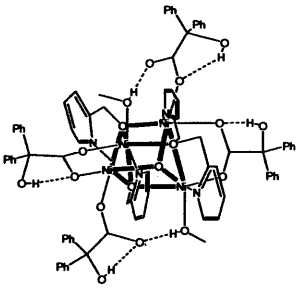 **11a**	193.9 (0.30),[a,c] 151.0 (0.47),[a] 146.2 (0.28)[a]	44.9 (2.64),[c] 43.0 (2.44),[c] 41.1 (3.85),[c] 38.9 (2.86),[c] 37.9 (4.47)[c]	17.5 (7.31),[c] 15.6 (6.25)[c]	~ 237.0 (broad),[b] 225.8 (0.47),[a] 216.3 (0.42),[a] 94.6 (0.49)	~ – 10.0 (broad),[b] – 46.8 (0.73),[a] – 52.7 (0.84)[a,c]	See text	N/A	5 – 8
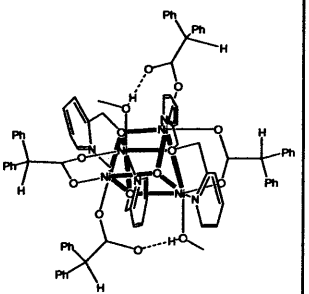 **11b**	190.5 (0.29),[c] 148.0 (0.34), 143.2 (0.48)	46.1 (2.29),[c] 43.2 (3.02),[c] 40.6 (4.46),[c] 37.0 (5.03)[c]	18.3 (6.29),[c] 17.0 (6.52)[c]	234.1 (0.76),[a] 222.6 (0.29), 211.6 (0.31), 158.3 (0.53)	– 2.6 (66.52),[a] – 51.2 (0.29),[c] – 97.2 (broad)[b]	See text	43.2 (3.02)[c]	5 – 8

[a]Unreliable. [b]Could not be observed/determined. [c]Single broad resonance on several peaks.

The methylene α-CH_2 hmp [$H_{(eq.)}$] proton peaks in **11** are significantly downfield chemically shifted in the range of ~ 237 – 94 ppm (0.76 – 0.29 ms). For example, a pyridyl α-CH_2 [$H_{(eq.)}$] proton is reported to appear as downfield as 245 ppm (0.6 ms) from a dinuclear high spin Ni(II) complex.[27g] In contrast, the broader α-CH_2 hmp [$H_{(ax.)}$] pseudo-

contact shifted peaks are observed from – 2.6 to – 97 ppm (very broad) (see Chapter 2, section 2.4). The aromatic bnzH/diphenylacetate protons cause sharp peaks in the 5 – 10 ppm region. Methanolic C*H*$_3$OH protons have been reported to appear as very broad peaks between 20 – 43 ppm in [Ni$_4$(dbm)$_4$(OMe)$_4$(MeOH)$_4$][13f] which undergo intramolecular inter-ligand hydrogen bonding interactions in a similar way to **11**. However, in **11a** and **11b**, the region ~ 30 – 50 ppm is dominated by several intense peaks therefore, methanolic proton peaks have not been assigned. The ^{1}H NMR spectrum of **11b** has an intense Ph$_2$C*H* proton peak at ~ 43.2 ppm (3.02 ms) which is found amongst the $H_{\beta/\beta'}$ proton peaks. Most of the peak resonances in **11a** and **11b** overlap and additional broadness made peak assignments difficult.[13l]

3.1.3 M = Ni, L^1 = bnzH$_2$, L^2 = hepH (n = 2, X = H)

Interaction of nickel acetate tetrahydrate, bnzH$_2$ and hepH gave, on work-up, a mixture of both *trans*-[Ni(hepH)$_2$(bnzH)$_2$] (**13a**) and *cis*-[Ni(hepH)$_2$(bnzH)$_2$] (**14a**) (Scheme 4) in moderate yield. Use of diphenylacetic acid in place of bnzH$_2$ also affords the *cis*- and *trans*-species [Ni(hepH)$_2$(Ph$_2$C{H}CO$_2$)$_2$] (**13b** and **14b**). Complexes **13** and **14** were characterised by elemental analysis, IR and ^{1}H NMR spectroscopy (Table 8) along with positive FAB mass spectrometry. In addition, single crystals of both **13a** and **14a** were subject to X-ray diffraction studies. The molecular structures of **13a** and **14a** are shown in Figure 9; selected bond lengths and angles of **13a** and **14a** are listed in Table 7.

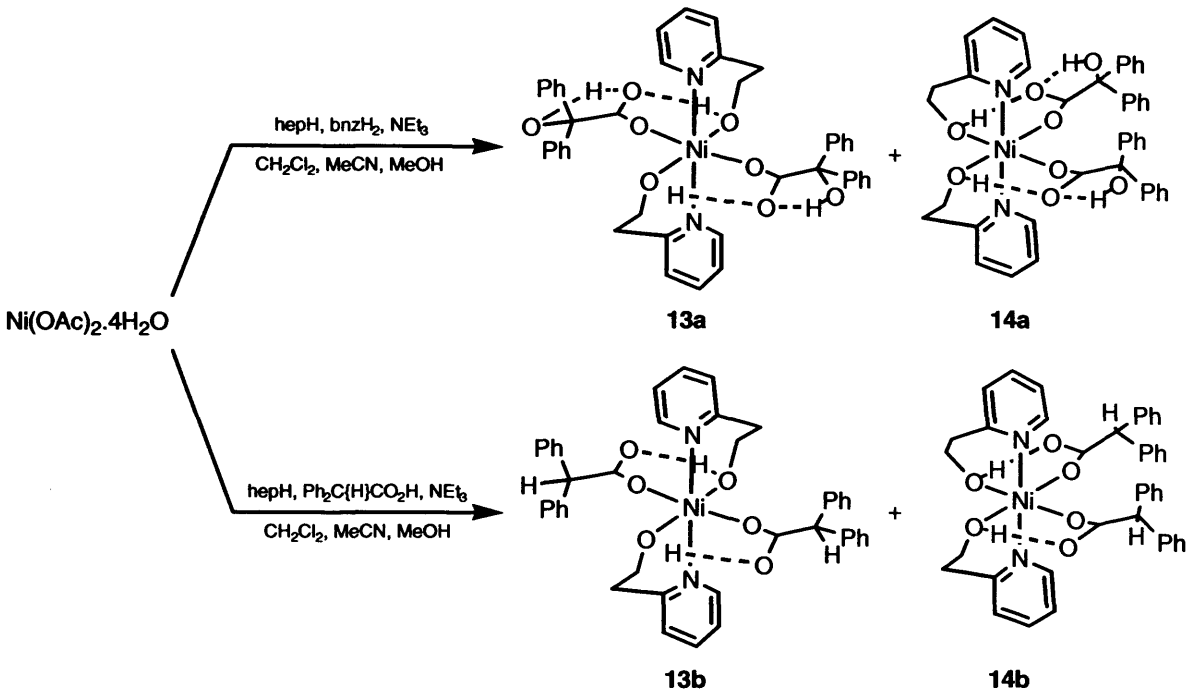

Scheme 4 Synthesis of **13** and **14**.

The molecular structure of **13a** consists of an octahedral Ni(II) centre bound by two *trans* η^1-bound bnzH and two *N,O*-chelating 1.11 hepH ligands, whereas, in **14a** the octahedral Ni(II) ion is bound by two *cis* η^1-bound bnzH and two *N,O*-chelating 1.11 hepH ligands.

In **13a** and **14a**, the nickel bound and unbound C-O carboxylate bond lengths of the bnzH ligands are 1.250(4) Å and 1.263(4) Å (**13a**), 1.249(5) Å and 1.257(5) Å (**14a**), respectively. The nickel bound C-O bond length values suggest the presence of predominantly ionic metal-carboxylate bonds.[12] In comparison, the C-$O_{\alpha\text{-}OH}$ bond lengths are longer at 1.422(4) Å (**13a**) and 1.427(4) Å (**14a**). Intra- and inter-ligand hydrogen bonding interactions are found in complexes **13a** and **14a**, these being similar to those found in complex **12a** [$O_{hepH}(1)\cdots O_{COO}(3)$ = 2.589(4) Å, $O_{\alpha\text{-}OH}(4)\cdots O_{COO}(3)$ = 2.579(4) **13a**, and $O_{hepH}(1)\cdots O_{COO}(7)$ = 2.581(4) Å, $O_{hepH}(2)\cdots O_{COO}(4)$ = 2.585(4) Å; $O_{\alpha\text{-}OH}(8)\cdots O_{COO}(7)$ = 2.537(4), $O_{\alpha\text{-}OH}(5)\cdots O_{COO}(4)$ = 2.555(4) **14a**].

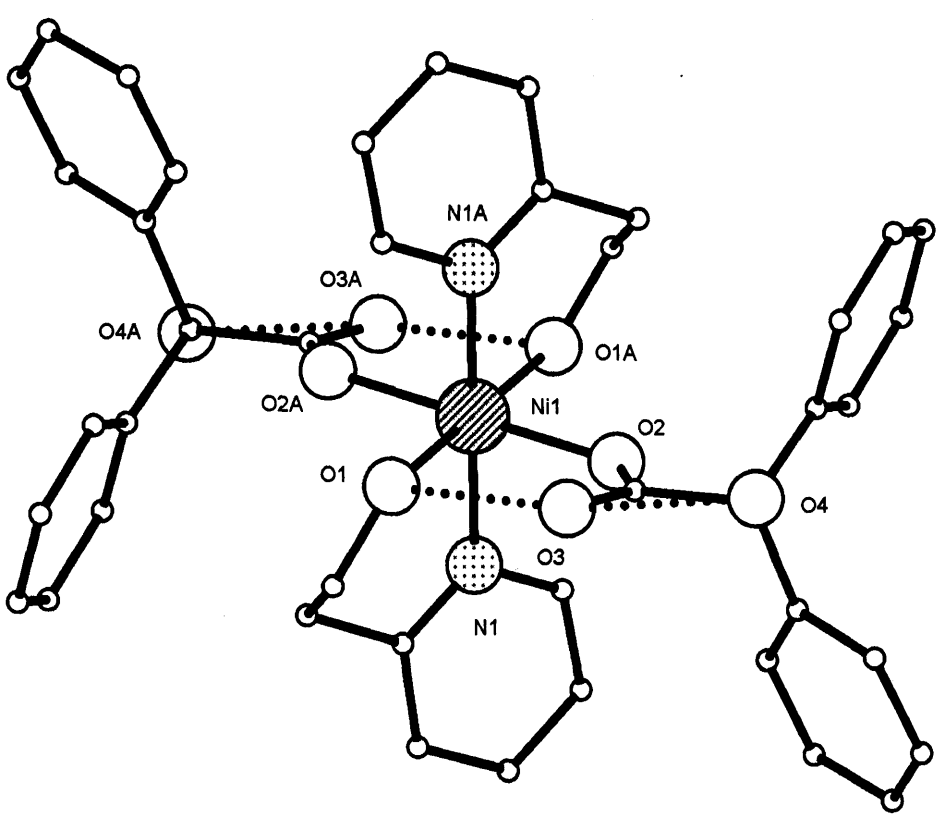

(a)

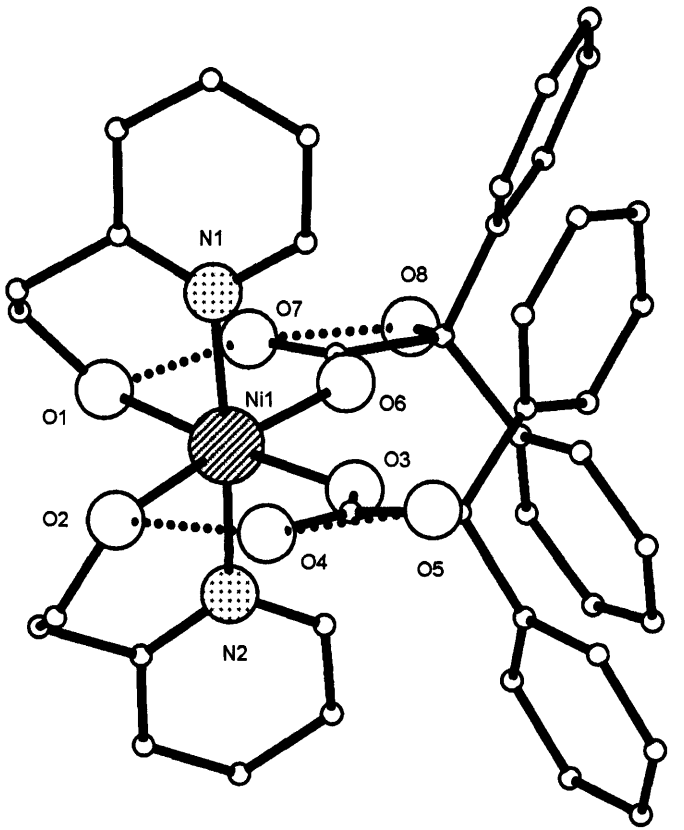

(b)

Figure 9 Molecular structures of (a) **13a** and (b) **14a**. Hydrogen atoms and carbon atom labels are excluded for clarity. Letter labelled atoms in **13a** were generated by symmetry. Dotted bonds show hydrogen bonding interactions. Only one of the two unique molecules of **14a** is shown as both of these are essentially similar.

Table 7 Selected bond length (Å) and angle (°) data for complexes **13a** and **14a**

13a		**14a**			
Ni(1)-O(1)	2.085(2)	Ni(1)-O(1)	2.099(3)	Ni(1)-N(2)	2.079(3)
Ni(1)-N(1)	2.079(3)	Ni(1)-N(1)	2.076(3)	Ni(1)-O(3)	2.057(3)
Ni(1)-O(2)	2.075(2)	Ni(1)-O(2)	2.097(3)	Ni(1)-O(6)	2.077(3)
N(1)-Ni(1)-O(1)	89.46(10)	N(1)-Ni(1)-O(1)	86.55(12)	O(3)-Ni(1)-O(2)	90.62(11)
N(1)#1-Ni(1)-O(1)	90.54(10)	O(2)-Ni(1)-O(1)	93.79(11)	O(3)-Ni(1)-N(2)	93.23(12)
O(1)-Ni(1)-O(2)	90.71(9)	N(2)-Ni(1)-O(1)	88.94(12)	O(6)-Ni(1)-O(1)	90.43(11)
O(1)-Ni(1)-O(2)#1	89.29(9)	N(1)-Ni(1)-O(2)	92.52(12)	N(1)-Ni(1)-O(6)	90.66(12)
N(1)-Ni(1)-O(2)	86.51(11)	N(1)-Ni(1)-N(2)	175.47(14)	O(6)-Ni(1)-O(2)	174.86(11)
N(1)-Ni(1)-O(2)#1	93.49(11)	N(2)-Ni(1)-O(2)	87.38(12)	O(6)-Ni(1)-N(2)	89.77(12)
		O(3)-Ni(1)-O(1)	175.17(11)	O(3)-Ni(1)-O(6)	85.27(10)
		O(3)-Ni(1)-N(1)	91.30(12)		

Symmetry transformations used to generate equivalent atoms: #1 **13a** $(-x+2, -y+2, -z)$.

In **13a** and **14a**, the longest bond lengths arise between the nickel to hepH hydroxyl oxygen atoms [Ni(1)-O_{hepH}(1) = 2.085 Å in **13a** and Ni(1)-O_{hepH} = av. 2.098 Å in **14a**] and those to the carboxylate oxygen atoms are relatively shorter [Ni(1)-O_{bnzH}(2) = 2.075(2) Å and av. Ni(1)-O_{bnzH} = 2.067 Å in **14a**]. In contrast, the elongated bond lengths in the analogous complex **12a** arise from the coordinated hmpH hydroxyl group rather than from the bnzH ligand. The corresponding chelate bite angles from the hepH ligands are O_{hepH}(1)-Ni(1)-N_{hepH}(1) = 89.46(10)° for **13a** and N_{hepH}(1)-Ni(1)-O_{hepH}(1) = 86.55(12)° and N_{hepH}(2)-Ni(1)-O_{hepH}(2) = 87.38(12)° for **14a**. The values of the chelate bite angles signify a more regular octahedral geometry around the nickel ions of **13a** and **14a**. In comparison, **12a** has a tighter chelate bite angle (*ca.* 9°).

The IR absorption bands corresponding to $\nu(CO_2)_{asymm}$ and $\nu(CO_2)_{symm}$ stretches in the spectra of **13/14** are observed at ~ 1590 cm^{-1}, 1445 cm^{-1} (**13a/14a**) and 1604 cm^{-1}, 1446 cm^{-1} (**13b/14b**), these bands overlapping with the ν(C=N) pyridyl stretching region.[25,26] The FAB mass spectra of **13a/14a** and **13b/14b** include a $[M - 2hepH]^+$ peak at 513 Da. and $[M - diphenylacetate]^+$ at 516 Da., respectively. The room temperature magnetic moments for **13/14** at 3.28 BM [$\chi_M T$ = 1.35 emu K mol^{-1} (**13a/14a**)] and 3.50 BM [$\chi_M T$ =

1.53 emu K mol^{-1} (**13a/14a**), ***SEE NOTE***], are higher than expected when compared to a single paramagnetic Ni(II) ion.[22b,22c]

Complexes **13a**, **14a**, **13b** and **14b** (Table 8) were characterised by ^{1}H NMR spectroscopy (Chapter 7, section 7.0). All the spectra (recorded in $CDCl_3$) are broad and paramagnetically shifted. Peak assignment has been made on the basis of a comparison of previously reported data,[27] direct comparison of complexes in this work (Chapter 2, section 2.4) and by inspection of the relaxation times.

The ^{1}H NMR spectra of crystalline samples of **13a/14a** and **13b/14b** indicate the presence of both *cis* and *trans* isomers in the solution state (Table 8, Figure 11). The H_α proton peaks coincide for both isomers (shifted upfield) at 111 ppm (0.44 ms) for **13b/14b** and 121 ppm, (0.28 ms) for **13a/14a**. In comparison, the H_α protons from **12a** and **12b** are shifted more downfield (~ 140 ppm). The H_γ peaks for the *cis* and *trans* isomers appear closely at 18.1 ppm (5.06 ms) [*trans*-**13a**] and 18.5 ppm (5.09 ms) [*cis*-**14a**]. In **13b/14b**, both H_γ *cis* and *trans* peaks overlap at 17.9 ppm (~ 5.42 ms). Four $H_{\beta/\beta'}$ proton peaks are found between ~ 31 – 46 ppm (~ 1.7 ms) for both **13a/14a** and **13b/14b**, the two peaks with lower integration intensity are assigned as *cis*- proton peaks in an approximately 1(*cis*): 1.5(*trans*) ratio (Figure 11).

In **13** and **14**, the geminal hepH α-CH_2 and β-CH_2 protons are seen as a single resonance for both isomers, β-CH_2 pseudo-contact shifted peaks are observed at ~ – 10 ppm [$H_{(eq.)}$] and – 13 ppm [$H_{(ax.)}$], the former value denotes that $H_{(eq.)}$ is possibly forced into an axial position by a puckered hepH ring (Figure 10).[27c,27d,27g,27l] The Ph_2CH proton peak in **13b/14b** appears at 26.9 ppm (1.71 ms) similar to that found in **12b**.

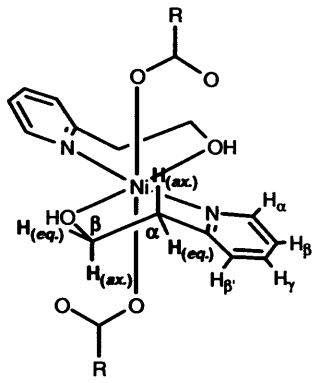

Figure 10 Geminal axial (*ax.*) and equatorial (*eq.*) methylene protons for hepH.

Table 8 ^{1}H NMR chemical shifts (δ) and relaxation times (T_1 ms, in parentheses) for complexes **13** and **14** (spectra recorded in $CDCl_3$)

Complex	H_α	$H_{\beta/\beta'}$	H_γ	α-CH_2 $H_{(eq.)}$	α-CH_2 $H_{(ax.)}$	β-CH_2 $H_{(eq.)}$	β-CH_2 $H_{(ax.)}$	CH	Ar-H
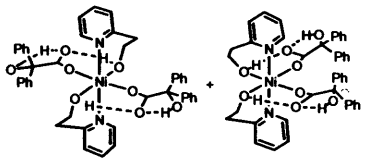 **13a/14a**	121.4 (0.28)[c]	46.1 (1.69), 31.4 (1.75) 44.2 (1.73), 33.3 (1.74)	18.1 (5.06) 18.5 (5.09)	40.7 (0.26)[c]	24.9 (0.25)[c]	– 10.0 (0.34)[a,c]	– 13.0 (42.09)[a,c]	N/A	5 – 8
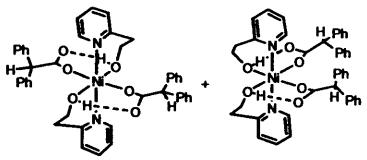 **13b/14b**	111.8 (0.44)[c]	45.4 (1.78), 31.2 (1.80) 43.9 (1.86), 33.1 (1.60)	17.9 (5.42)[c]	49.6 (0.28)[c]	36.9 (1.34)[c]	– 10.9 (0.38)[a,c]	– 13.7 (0.16)[a,c]	26.9 (1.71)	5 – 8

[a]Unreliable. [b]Could not be observed/determined. [c]Single broad resonance for several peaks (both isomers).

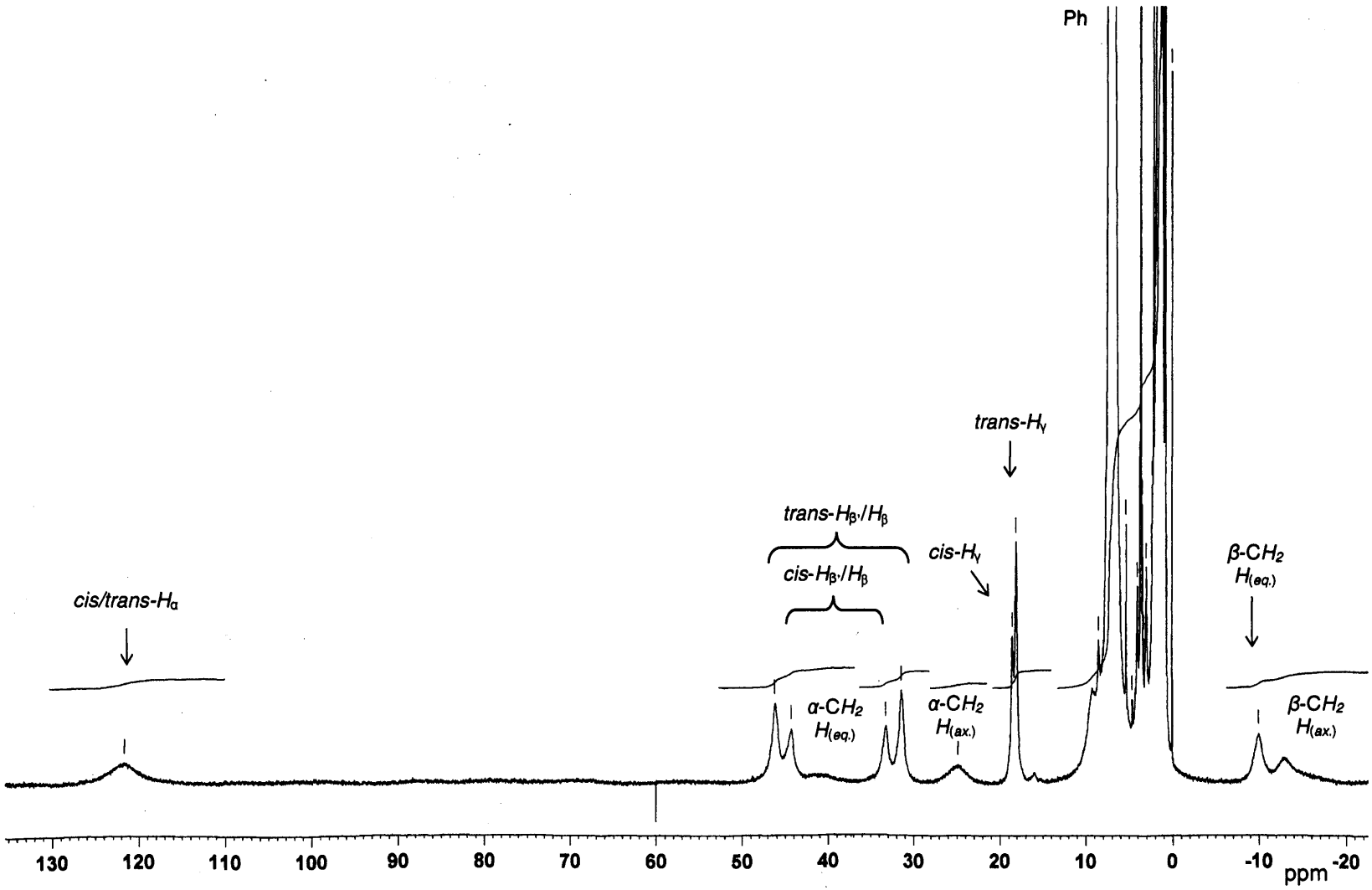

Figure 11 ^{1}H NMR spectrum of **13a/14a** in $CDCl_3$.

3.1.4 M = Ni, L^1 = $bnzH_2$, L^2 = hppH (n = 3, X = H)

Reaction of nickel acetate tetrahydrate with a ligand blend composed of bnzH and hppH, in the presence of triethylamine gave, on work-up, a pale green product in low yield. The resulting powder was characterised by elemental analysis, IR spectroscopy and positive FAB mass spectrometry. Using the latter technique, a $[M]^+$ peak is found at 787 Da. which tentatively supports the presence of a monometallic complex of composition $[Ni(hppH)_2(bnzH)_2]$ (**15**) (Scheme 5).

$$Ni(OAc)_2.4H_2O \xrightarrow[CH_2Cl_2,\ MeCN,\ MeOH]{hppH,\ bnzH_2,\ NEt_3} [Ni(hppH)_2(bnzH_2)_2]\ \mathbf{15}$$

Scheme 5 Synthesis of **15**.

3.2 Blending 2-Pyridine Alcohols and Benzilic Acid on a Cu(II) Centre

3.2.1 M = Cu, L^1 = $bnzH_2$, L^2 = Hxhp (n = 0, X = Cl or H)

Interaction of a ligand blend composed of Hxhp [Hxhp = Hchp or Hhp (pK_a 0.70)[7]], $bnzH_2$ with copper acetate monohydrate in the presence of triethylamine gave, on work-up, $[Cu_3(xhp)_4(bnz)(bnzH)][NEt_3H]\cdot mMeOH$ [xhp = chp, m = 4 (**16a**) as green crystals; hp as pine-green microcrystals, m = 0 (**16b**)] in good yield (Scheme 6). Complexes **16a** and **16b** were characterised by elemental analysis, IR spectroscopy and positive FAB mass spectrometry. In addition, a single crystal of **16a** was subject to an X-ray diffraction study. The molecular structure of **16a** is shown in Figure 12; selected bond lengths and angles are listed in Table 9.

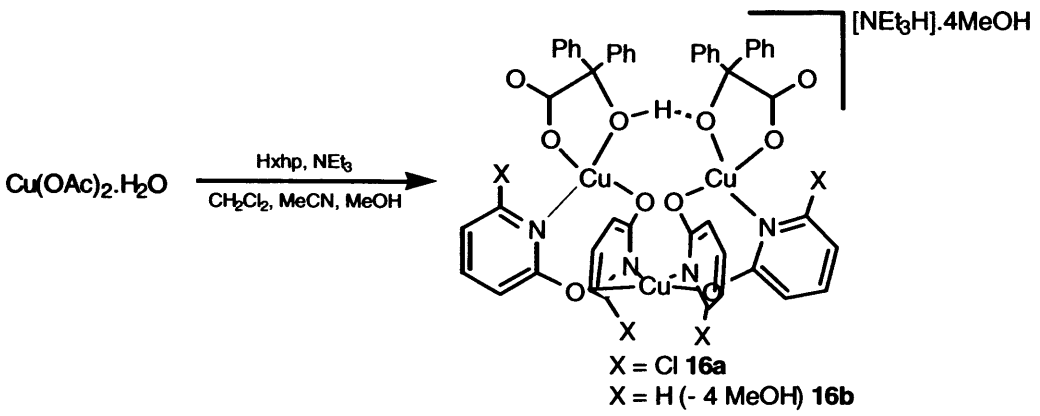

Scheme 6 Synthesis of **16a** and **16b**.

The molecular structure of **16a** is based on a triethylammonium salt in which the anion contains three Cu(II) ions each displaying distorted square planar environments and bound by bnzH, a bnz and four chp ligands. All chp ligands are bound as 2.11 bridging ligands. The central copper ion (bottom of figure) in **16a** is coordinated to two η^1-O_{chp} and two μ-N_{chp} ligands. The terminal copper ions are bound to two separate η^1-O_{chp} and μ-N_{chp} ligands and a protonated [Cu(2)] or deprotonated [Cu(3)] 1,4-chelating benzilate ligand. The Cu···Cu distances in **16a** are Cu(1)···Cu(2) = 3.2777(8) Å, Cu(1)···Cu(3) = 3.3812(8) Å and Cu(2)···Cu(3) = 3.6500(9) Å.

In **16a**, the shortest copper-ligand atom bond lengths are Cu(2)-$O_{\alpha\text{-}OH}$(5) and Cu(3)-O_{COO}(10) = 1.908(2) Å from the benzilate ligands. The longest bond length arises from the chp nitrogen atom of Cu(2)-N_{chp}(3) at 2.009(3) Å. The benzilate five-membered chelate bite angles around the terminal copper ions confirm the presence of distorted square planar Cu(II) environments [O_{bnz}(5)-Cu(2)-O_{bnz}(7) = 83.91(10)°, O_{bnzH}(8)-Cu(3)-O_{bnzH}(10) = 84.61(10)°]. The square planar geometry around the central copper ion is also revealed from the angle N_{chp}-Cu(1)-O_{chp} averaging to 90.553° which is obtained from the four neighbouring chp ligand donor atoms.

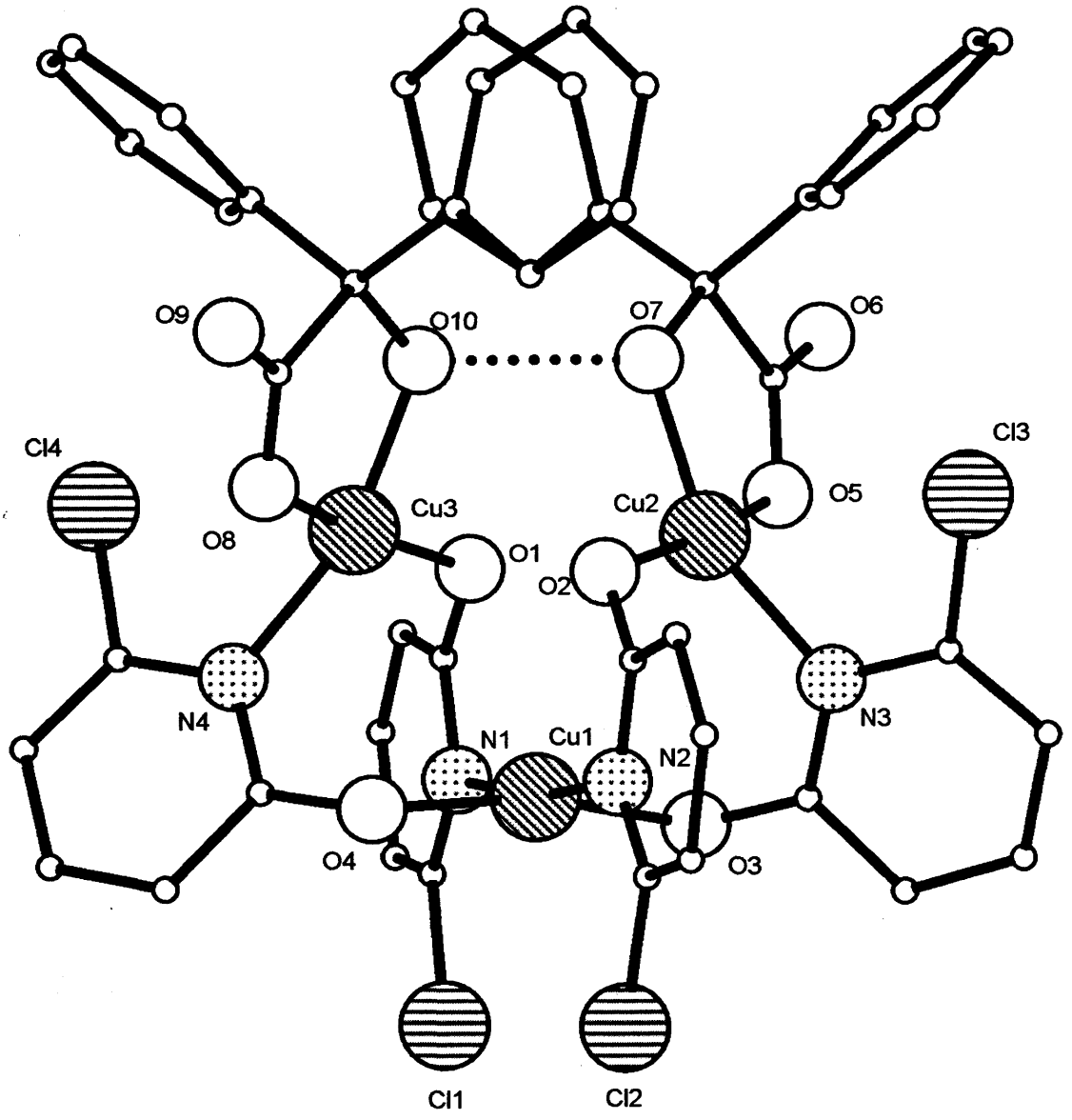

Figure 12 Molecular structure of the anionic unit in **16a**. Hydrogen atoms, carbon atom labels, solvent molecules (one disordered and three ordered molecules of methanol) and the triethylammonium cation are excluded for clarity. Dotted bonds indicate hydrogen bonding interactions.

Table 9 Selected bond length (Å) and angle (°) data for complex **16a**

16a					
Cu(1)-O(3)	1.914(2)	Cu(2)-O(2)	1.931(2)	Cu(3)-O(1)	1.935(2)
Cu(1)-N(1)	1.996(3)	Cu(2)-N(3)	2.009(3)	Cu(3)-N(4)	2.005(3)
Cu(1)-N(2)	1.985(3)	Cu(2)-O(5)	1.908(2)	Cu(3)-O(8)	1.918(2)
Cu(1)-O(4)	1.916(2)	Cu(2)-O(7)	1.947(2)	Cu(3)-O(10)	1.908(2)
O(3)-Cu(1)-N(1)	86.59(11)	O(2)-Cu(2)-N(3)	96.35(11)	O(1)-Cu(3)-N(4)	96.56(11)
O(3)-Cu(1)-N(2)	93.76(11)	O(5)-Cu(2)-O(2)	170.71(11)	O(8)-Cu(3)-O(1)	170.78(11)
O(4)-Cu(1)-N(1)	94.24(11)	O(5)-Cu(2)-N(3)	90.77(11)	O(8)-Cu(3)-N(4)	89.93(11)
O(4)-Cu(1)-N(2)	87.62(11)	O(2)-Cu(2)-O(7)	91.88(10)	O(10)-Cu(3)-O(1)	91.19(10)
O(3)-Cu(1)-O(4)	167.45(11)	O(7)-Cu(2)-N(3)	156.01(11)	O(10)-Cu(3)-O(8)	84.61(10)
N(2)-Cu(1)-N(1)	169.89(12)	O(5)-Cu(2)-O(7)	83.91(10)		

In **16a**, the α-hydroxyl [bnzH] and α-alkoxide [bnz] moieties participate in a strong inter-ligand intramolecular hydrogen bonding interaction. The bnzH to bnz hydrogen bond pushes the two terminal copper ions in close proximity while being pivoted by the central chp bound Cu(II) ion, thus resulting in a triangular structure. The two terminal benzilate ligands also undergo intermolecular hydrogen bonding interactions with external methanol molecules (Table 10).

Table 10 Hydrogen bond distances (Å) in complex **16a**

Type		**Distance**
Intramolecular	$O_{\alpha\text{-}OH}(10)\cdots O_{\alpha\text{-}O}(7)$	2.420(3)
Intermolecular	$O_{MeOH}(11)\cdots O_{COO}(6)$	2.709(4)
Intermolecular-intermolecular	$O_{MeOH}(11)\cdots O_{MeOH}(12)$	2.726(6)
Intermolecular	$O_{MeOH}(13)\cdots O_{COO}(9)$	2.738(7)
	O_{MeOH}*(13')$\cdots O_{COO}(9)$	2.839(12)

*Primed atom indicates methanol disordered over two sites.

In the IR spectra of **16**, there are two strong $\nu(CO_2)_{asymm}$ and $\nu(CO_2)_{symm}$ bands found at 1591 cm^{-1} (**16a**), 1603 cm^{-1} (**16b**), respectively and 1442 cm^{-1} (**16a**), 1428 cm^{-1} (**16b**) respectively, these overlapping with the ν(C=N) pyridyl bands.[25,26] The FAB mass spectra of **16a** and **16b** have several fragmentation peaks including $[M - chp]^+$ at 1129 Da. and $[M - NEt_3H - bnz - C_6H_5]^+$ at 714 Da., respectively. There are many examples of magnetically and biologically interesting copper-based homotrinuclear triangular-based,[16]

or linear-based trinuclear complexes.[17] Complex **16a**, to the knowledge of the author, is the only example of a triangular copper chain held together by a hydrogen bonding interaction.

It is worthy of note that, like **9a/9b** and **10a/10b** (section 3.1), complex **16a** represents an example of product formation driven by salt formation initiated by the addition of the tertiary amine base. The magnetic characterisation with respect to **16a** (desolvated) will be discussed later on in this chapter (section 3.3).

3.2.2 M = Cu, L^1 = $bnzH_2$, L^2 = hmpH (n = 1, X = H)

Interaction of hmpH, $bnzH_2$ and copper acetate monohydrate, in the presence of triethylamine gave, on work-up, blue crystals of a mononuclear complex $[Cu(hmpH)_2(bnzH)_2]$ (**17a**) (Scheme 7) in moderate yield. Use of mehmpH in place of hmpH also affords a mononuclear complex of composition $[Cu(mehmpH)_2(bnzH)_2]$ (**17a'**). On substitution of $bnzH_2$ with $Ph_2C\{H\}CO_2H$, the complex $[Cu(hmpH)_2(Ph_2C\{H\}CO_2)_2]$ (**17b**) was also synthesised and characterised (Scheme 7). Complexes **17a**, **17a'** and **17b** were characterised by elemental analysis, IR and ^1H NMR spectroscopy (Table 13 for **17a**) along with positive FAB mass spectrometry. Single crystals of **17a** and **17a'** were subject to X-ray diffraction studies. The molecular structures of **17a** and **17a'** are shown in Figure 13; selected bond lengths and angles of **17a** and **17a'** are given in Table 11. The structures **17a** and **17a'** are very similar and only **17a** will be discussed in any detail.

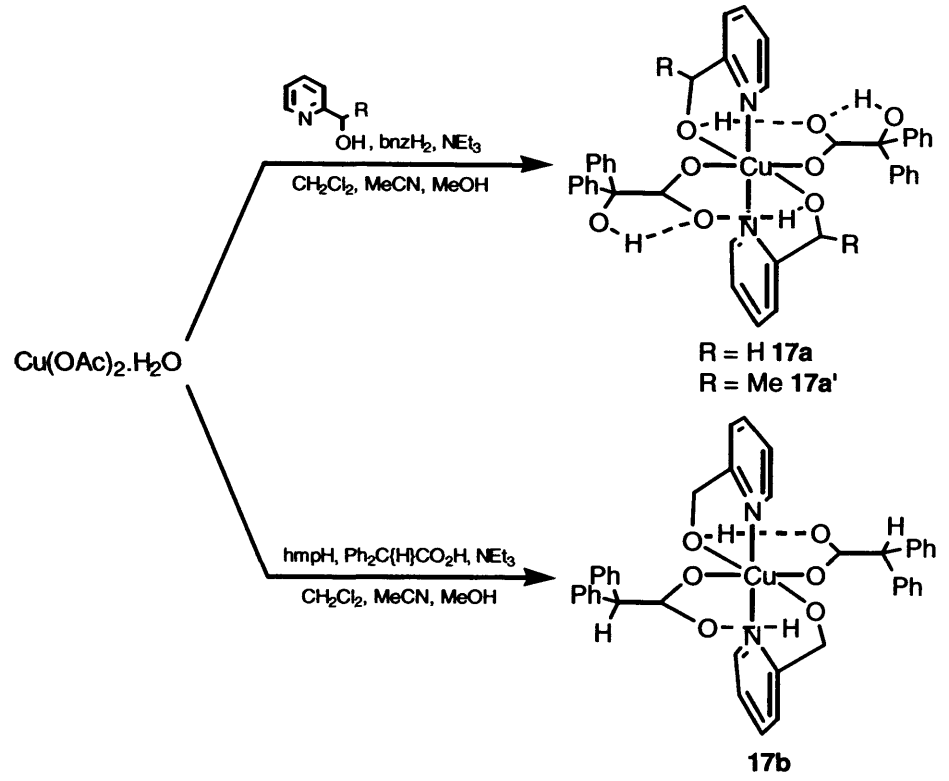

Scheme 7 Synthesis of **17**.

Complex **17a** contains an octahedral Jahn-Teller distorted copper(II) ion bound by two *trans* η^1-bound bnzH ligands and two *trans N,O*-chelating 1.11 hmpH ligands. The molecular structure of **17a** is analogous to the nickel complex **12a**. In **17a**, the hmpH hydroxyl oxygen atom is bound to the copper ion at a Cu(1)-O(1) bond length of 2.3720(12) Å, this bond length being significantly longer (*ca.* 0.3 Å) than the corresponding Ni(1)-O(1) distance in **12a** (2.073 Å). The bond lengths of Cu(1)-N_{hmpH}(1) = 1.9864(15) Å and Cu(1)-O_{bnzH}(2) = 1.9767(15) Å are shorter than those in **12a** (2.035 Å and 2.080 Å, respectively). The five-membered chelate bite angle imposed by hmpH is acute at 76.41(5)°.

The metal bound bnzH carboxylate oxygen atoms from **17a** and **17a'** provide C-O_{COO}(2) bond distances of 1.256(2) Å and 1.268(3) Å, respectively. These bond length values coincide with predominantly ionic metal ion-ligand interactions [for Cu(II): range ~ 1.248 – 1.256 Å ⇒ ~ 0 – 5% covalent C-O bond character].[12]

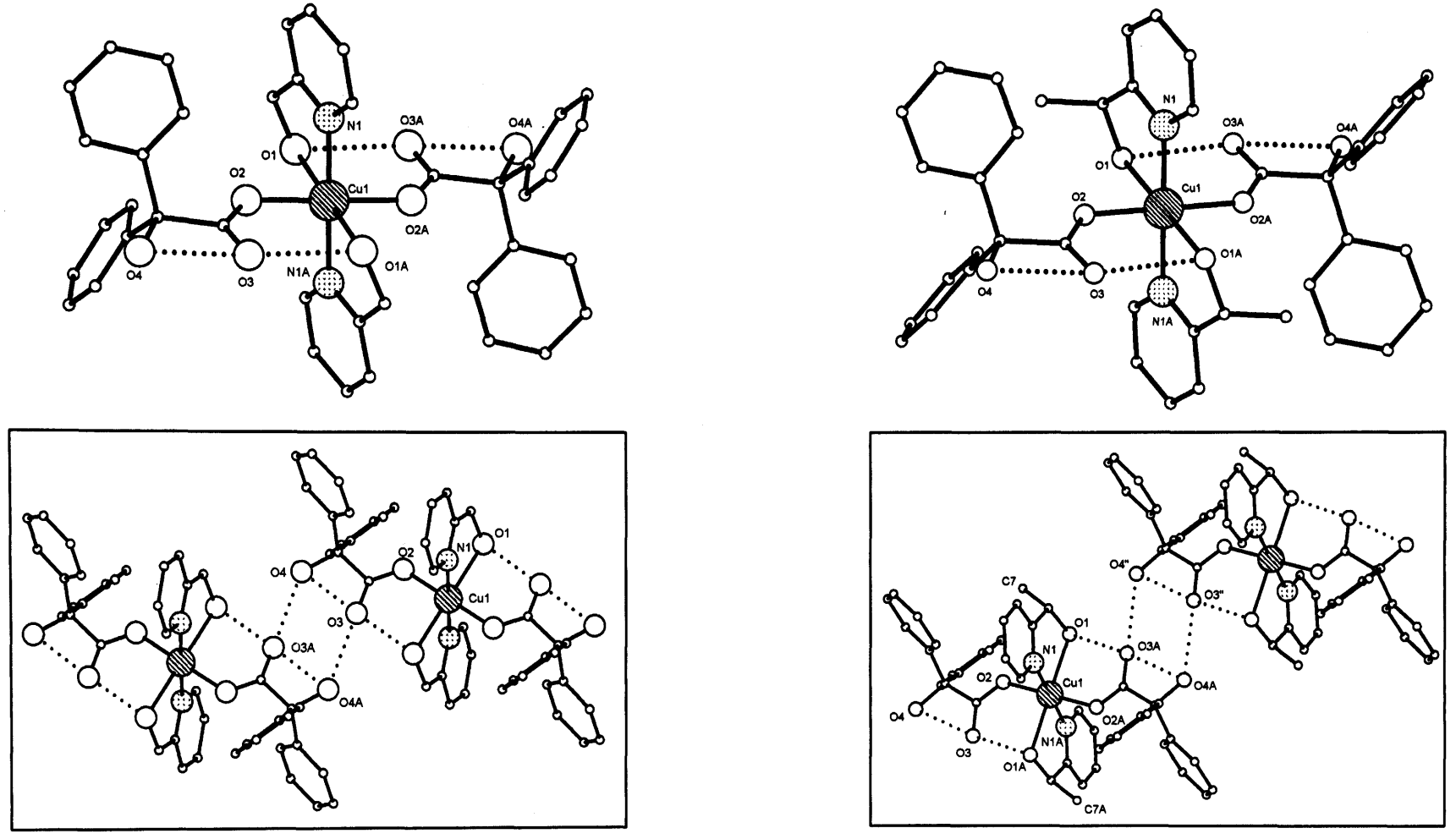

(a) (b)

Figure 13 Molecular structures of (a) **17a** and (b) **17a'**. Insets show parts of the hydrogen bonded polymeric networks. Letter labelled atoms were generated by symmetry. Hydrogen atoms and carbon atom labels are excluded for clarity. An occupancy of 80% methyl (mehmpH): 20% oxygen (2-PyCO_2H) was located on C(7/7A) (see b).[18] Dotted bonds indicate hydrogen bonding interactions.

Table 11 Selected bond length (Å) and angle (°) data for complexes **17a** and **17a'**

	17a	**17a'**
Cu(1)-O(1)	2.3720(12)	2.385(2)
Cu(1)-O(2)	1.9767(12)	1.9866(19)
Cu(1)-N(1)	1.9864(15)	1.990(2)
N(1)-Cu(1)-O(1)	76.41(5)	75.63(9)
N(1)#1-Cu(1)-O(1)	103.59(5)	104.37(9)
O(2)-Cu(1)-O(1)	82.18(5)	86.00(8)
O(2)#1-Cu(1)-O(1)	97.82(5)	94.00(8)
O(2)-Cu(1)-N(1)	86.69(6)	88.26(9)
O(2)#1-Cu(1)-N(1)	93.31(6)	91.74(9)

Symmetry transformations used to generate equivalent atoms: #1 **17a** $(-x+1/2, -y+3/2, -z)$; **17a'** $(-x+2, -y, -z)$.

The monomeric unit of **17a** extends into an intermolecularly hydrogen bonded network with other neighbouring monomers by means of the bnzH α-hydroxyl subsitituent linking with a neighbouring unbound carboxylate oxygen atom [Figure 13(a), inset]. Other intra- and inter-ligand hydrogen bonding interactions are observed between the benzilate α-OH and carboxylate oxygen atom or from the carboxylate oxygen atom and hmpH hydroxyl, respectively (Table 12).

Table 12 Hydrogen bond distances (Å) in complexes **17a** and **17a'**

Type	**17a**		**17a'**	
Intramolecular	$O_{\alpha\text{-}OH}(4)\cdots O_{COO}(3)$	2.6803(17)	$O_{\alpha\text{-}OH}(4)\cdots O_{COO}(3)$	2.594(3)
Intramolecular	$O_{hmpH}(1)\cdots O_{COO}(3)$	2.5682(18)	$O_{hmpH}(1)\cdots O_{COO}(3)$	2.691(3)
Intermolecular	$O_{\alpha\text{-}OH}(4)\cdots O_{COO}(3)$	2.7730(19)	$O_{\alpha\text{-}OH}(4)\cdots O_{COO}(3)$	2.896(3)

The IR spectra of **17a** and **17a'** are essentially similar, with both complexes exhibiting ν(OH) stretching bands in the ~ 3403 – 3418 cm^{-1} region, as well as, $\nu(CO_2)_{asymm}$ and $\nu(CO_2)_{symm}$ stretching bands at ~ 1600 cm^{-1} (**17a**) and ~ 1330 cm^{-1} (**17a'**), these latter bands overlapping with the ν(C=N) pyridyl stretches.[25,26] The FAB mass spectra of **17a** and **17a'** gave mass peaks corresponding to $[M - \text{bnzH}]^+$ at 508 Da. and $[M - \text{mehmpH} - \text{bnzH}]^+$ at 413 Da., respectively.

The room temperature magnetic moments for **17a** and **17a'** are 2.14 BM ($\chi_M T$ = 0.57 emu K mol^{-1}) and 2.16 BM ($\chi_M T$ = 0.58 emu K mol^{-1}), respectively, are higher than expected for a single paramagnetic Cu(II) ion possessing one unpaired electron (1.73 BM,

$\chi_M T$ = 0.38 emu K mol^{-1}, ***SEE NOTE***).[22b,22c] The EPR data of **17a** will be discussed later on in this chapter (section 3.3).

Complexes **17a** and **17b** were analysed by ^{1}H NMR spectroscopy (Chapter 7, section 7.0). All the spectra (recorded in $CDCl_3$) are broad and paramagnetically shifted. Peak assignment has been made on the basis of a comparison of previously reported data, direct comparison of complexes in this work and by inspection of the relaxation times.[27]

Assignment of the ^{1}H NMR spectra for monomers **17a** and **17b** are shown in Table 13. The H_α hmpH pyridyl proton peaks appear at ~ 125 – 140 ppm (very broad), $H_{\beta/\beta'}$ proton peaks are observed in the region of ~ 34 – 42 ppm (~ 3 – 4 ms). The hmpH methylene $H_{(eq.)}$ proton peaks are chemically shifted around ~ 120 ppm (very broad) and $H_{(ax.)}$ proton peaks are observed at ~ 65 – 68 ppm (very broad). The sharper aromatic bnzH/diphenylacetate proton peaks are found in the 5 – 8 ppm region. In **17b**, the intense Ph_2CH methine proton peak appears at 15.3 ppm (0.49 ms). The ^{1}H NMR spectrum of complex **17a** displayed very broad peak resonances that could not be assigned with relaxation times.[27k,27l]

Table 13 ^{1}H NMR chemical shifts (δ) and relaxation times (T_1 ms, in parentheses) for Cu complexes **17a** and **17b** (spectra recorded in $CDCl_3$)

Complex	H_α	$H_{\beta/\beta'}$	H_γ	α-CH_2 $H_{(eq.)}$	α-CH_2 $H_{(ax.)}$	CH	Ar-H
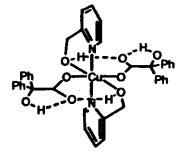 **17a**	125.0 (weak)[b]	42.5 (weak),[b] 35.1 (weak)[b]	13.0 (b)	broad[b]	65.3 (weak)[b]	N/A	5 – 8
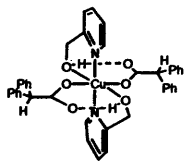 **17b**	140.2 (192.97)[a]	41.6 (3.38), 34.4 (4.42)	12.1 (9.03)	120.9 (0.89)[a]	68.8 (0.65)[a]	15.3 (0.49)	5 – 8

[a]Unreliable. [b]Could not be observed/determined.

3.2.3 M = Cu, L^1 = $bnzH_2$, L^2 = hepH (n = 2, X = H)

Reaction of hepH and $bnzH_2$ with copper acetate monohydrate in the presence of triethylamine gave, on work-up, dimeric $[Cu(hep)(bnzH)]_2$ (**18a**) in moderate yield (Scheme 8). Use of diphenylacetic acid in place of $bnzH_2$ also affords a dimeric complex of composition $[Cu(hep)(Ph_2C\{H\}CO_2)]_2$ (**18b**). Complexes **18a** and **18b** were characterised by elemental analysis, IR and ^1H NMR spectroscopy (Table 16) along with positive FAB mass spectrometry. In addition, a single crystal of **18a** was subject to an X-ray diffraction study. The molecular structure of **18a** is shown in Figure 14(a); selected bond lengths and angles are given in Table 14.

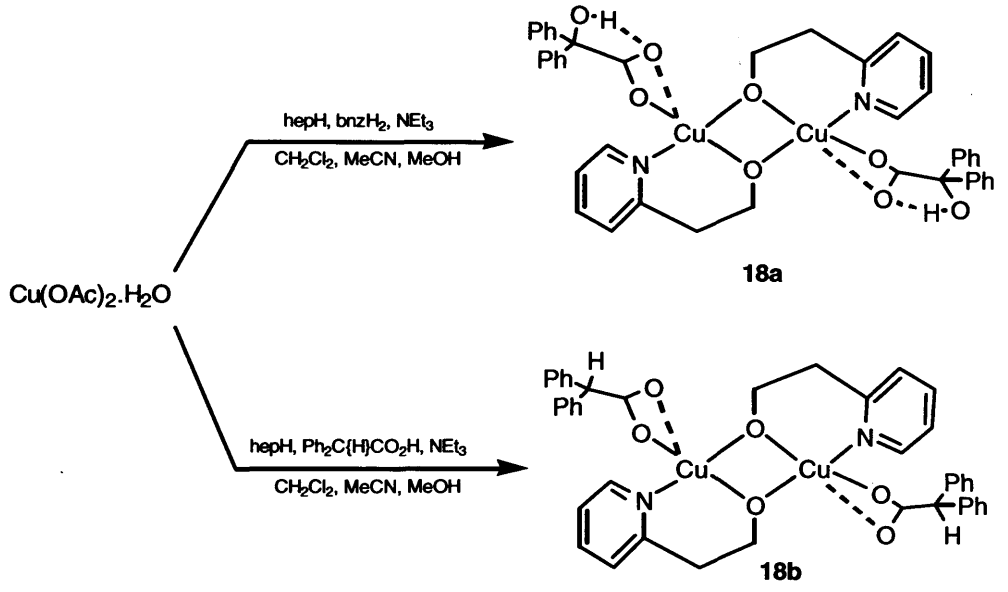

Scheme 8 Synthesis of **18**.

The molecular structure of **18a** consists of two square planar Cu(II) ions each bound by an η^1-bound bnzH and two bridging hep ligands. The hep alkoxide moieties are 2.21 bound as both bridging and *N,O*-chelating (η^1, μ_2) ligands. Alternatively, there is an axial interaction from the unbound bnzH oxygen atom towards the nearest copper ion resulting in a geometry better described as pseudo-square based pyramidal [Cu(1)···O_{coo}(3) = 2.8049(15) Å].

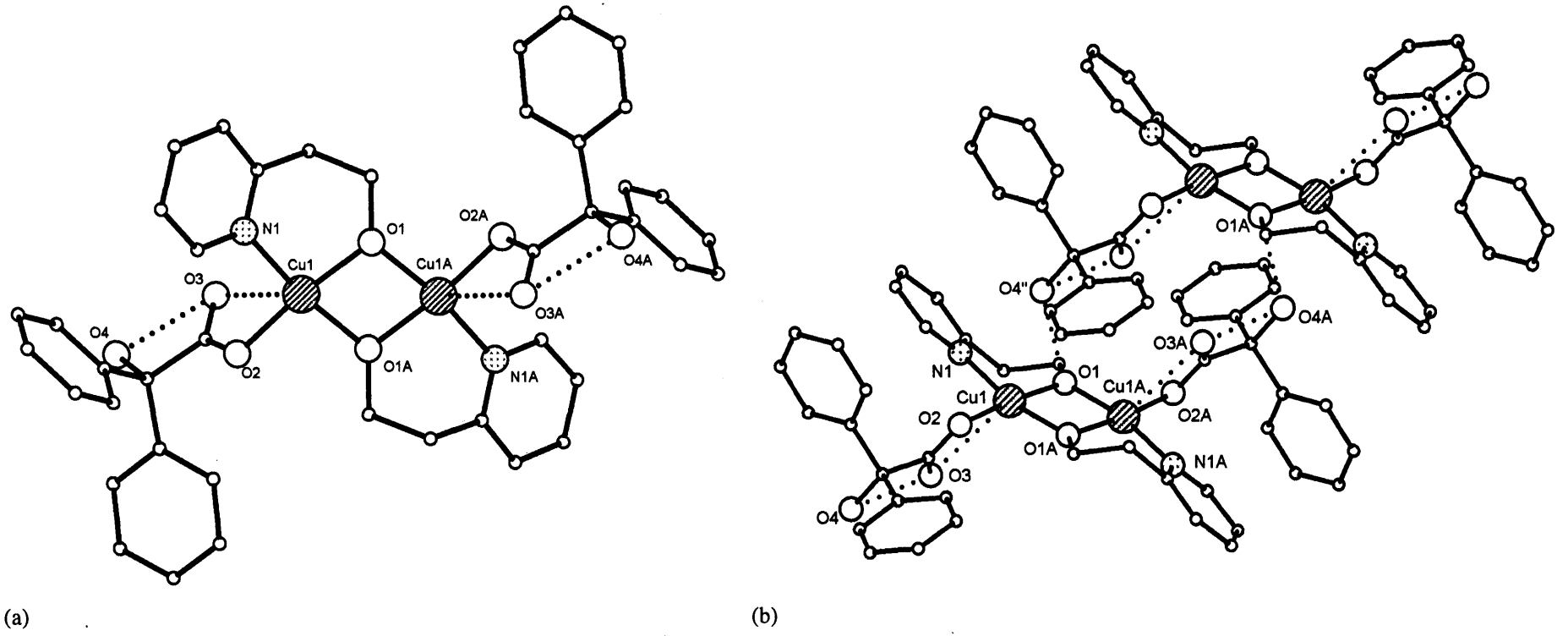

(a) (b)

Figure 14 (a) Molecular structure and (b) hydrogen bonding interactions in the packed structure of **18a**. Dotted lines indicate hydrogen bonding/pseudo-axial interactions.

The longest metal ion to ligand atom bond length arises from the hep nitrogen atom at 1.9816(18) Å and the shortest is from the μ_2-bound hep alkoxide oxygen atom at 1.9222(15) Å. The chelate bite angle from the six-membered hep ring is 92.99(7)°. The bound carboxylate oxygen atom has a carbonyl bond length of C(8)-O(2) = 1.290(3) Å, this being consistent with a metal-ligand bond with some covalent character.[12] The copper ions in **18a** are too far apart to be considered for direct metal-metal interactions [Cu(1)···Cu(1A) = 3.0138(5) Å].

Table 14 Selected bond length (Å) and angle (°) data for complex **18a**

18a					
Cu(1)-O(1)	1.9244(15)	Cu(1)-N(1)	1.9816(18)	Cu(1)···Cu(1)#1	3.0138(5)
Cu(1)-O(1)#1	1.9222(15)	Cu(1)-O(2)	1.9250(15)		
O(1)#1-Cu(1)-O(1)	76.84(7)	Cu(1)#1-O(1)-Cu(1)	103.16(7)	O(1)#1-Cu(1)-O(2)	96.15(6)
O(1)-Cu(1)-N(1)	92.99(7)	O(1)-Cu(1)-O(2)	172.94(6)	O(2)-Cu(1)-N(1)	94.07(7)
O(1)#1-Cu(1)-N(1)	166.94(7)				

Symmetry transformations used to generate equivalent atoms: #1 $(-x+1, -y, -z+2)$.

In **18a**, the bnzH ligands undergo hydrogen bonding interactions. These include an intra-ligand interaction involving the α-hydroxyl substituent with an unbound carboxylate (bnzH) oxygen atom and an intermolecular interaction from the α-hydroxyl substituent with a hep bridging alkoxide oxygen atom from a neighbouring molecule [$O_{\alpha\text{-}O}(3)\cdots O_{COO}(4)$ = 2.594(2) Å, $O_{\alpha\text{-}O}(4)\cdots O_{hep}(1')$ = 2.885(2) Å, respectively]. Therefore, **18a** can be considered as a hydrogen bonded network of dimers [Figure 14(b)].

The IR spectrum of **18a** shows an intense ν(OH) stretching band at ~ 3384 cm^{-1}. For **18a** and **18b** two strong stretching bands are observed corresponding to $\nu(CO_2)_{asymm}$ and $\nu(CO_2)_{symm}$ stretches at ~ 1625 cm^{-1} (**18a**), 1593 cm^{-1} (**18b**) and $\nu(CO_2)_{symm}$ stretches at 1323 cm^{-1} (**18a**), 1366 cm^{-1} (**18b**), these overlapping with the ν(C=N) pyridyl stretching bands.[25,26] The FAB mass spectra of **18a** and **18b** include a $[M]^+$ peak at 824 Da. and a $[M - Ph]^+$ peak at 717 Da., respectively.

The room temperature magnetic moment for **18a** at 2.03 BM ($\chi_M T$ = 0.52 emu K mol^{-1}) and **18b** at 2.42 BM ($\chi_M T$ = 0.73 emu K mol^{-1}) are slightly less than expected for two non-interacting copper(II) ions with each possessing one unpaired electron (2.45 BM, $\chi_M T$ = 0.75 emu K mol^{-1}, ***SEE NOTE***).[22b,22c] The EPR and variable temperature magnetic characterisation of **18a** will be discussed later on in this chapter.

3.2.4 M = Cu, L^1 = $bnzH_2$, L^2 = hppH (n = 3, X = H)

The reaction of copper acetate monohydrate with a blend composed of hppH and $bnzH_2$ in the presence of triethylamine gave, on work-up, pine green crystals of $[Cu(hppH)(bnzH)]_2$ (**19**) (Scheme 9) in low yield. Use of diphenylacetic acid in place of $bnzH_2$ also affords a dimeric complex but of composition $[Cu(hpp)(Ph_2C\{H\}CO_2)]_2$ (**20**). Complexes **19** and **20** were characterised by elemental analysis, IR and ^{1}H NMR spectroscopy (Table 16) along with positive FAB mass spectrometry. Single crystals of both **19** and **20** (blue) were subject to X-ray diffraction studies. The molecular structures of **19** and **20** are shown in Figure 15; selected bond lengths and angles of **19** and **20** are given in Table 15.

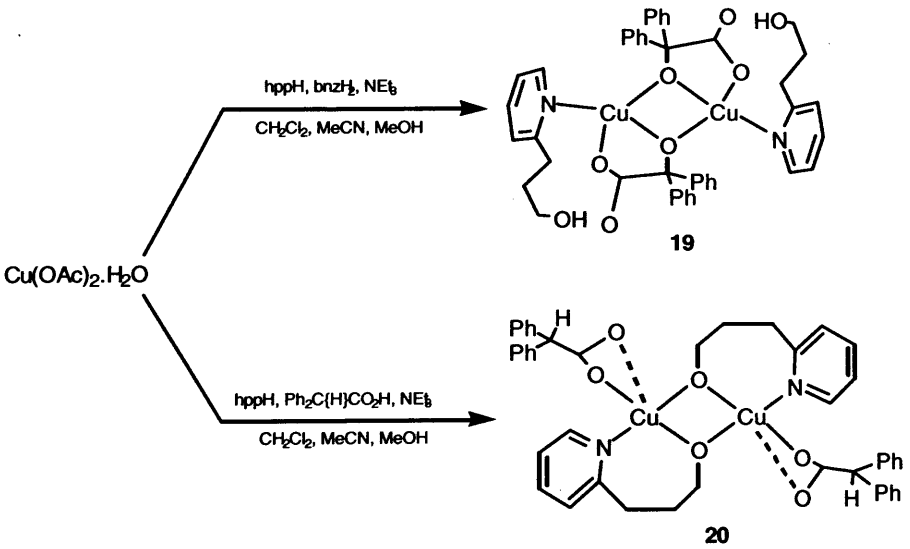

Scheme 9 Synthesis of **19** and **20**.

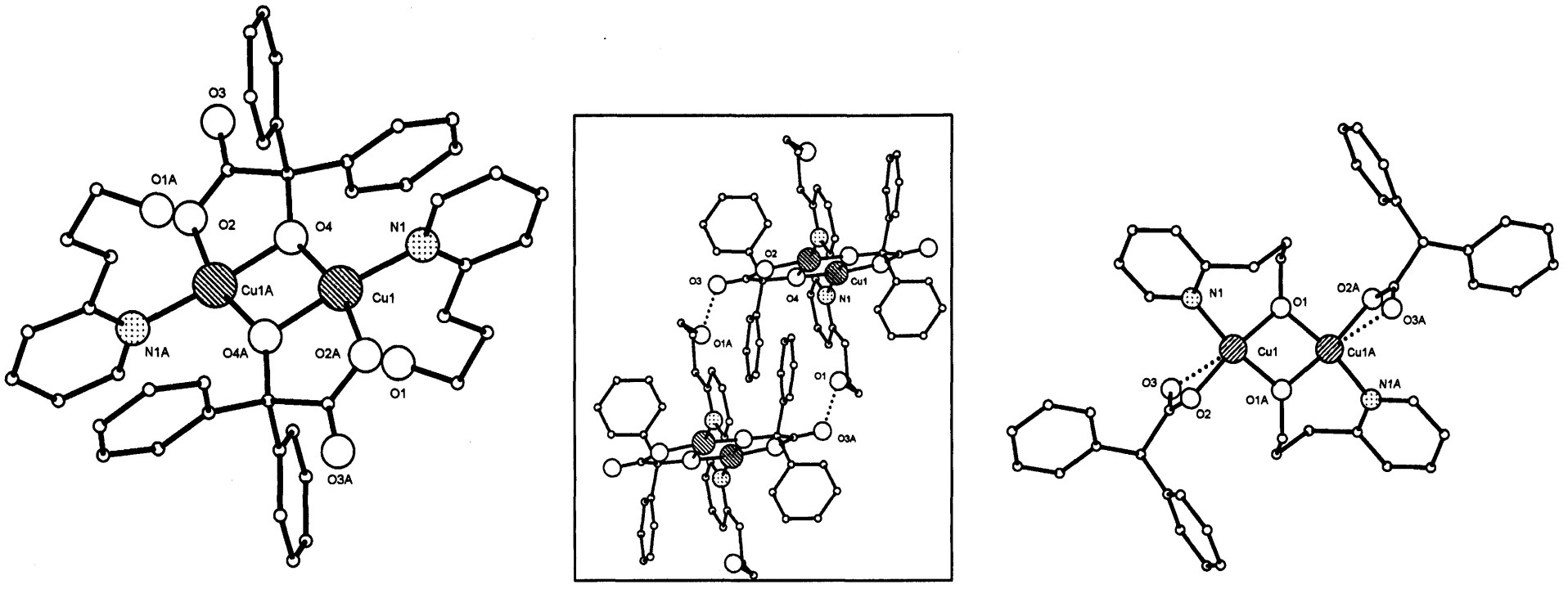

(a) (b) (c)

Figure 15 (a) Molecular structure of **19**, inset (b).shows part of the hydrogen bonded polymer of **19** and (c) the molecular structure of **20**. Hydrogen atoms and carbon atom labels are excluded for clarity. Letter labelled atoms are generated by symmetry. Dotted lines indicate hydrogen bonding/pseudo-axial interactions [**20** Cu(1)···O(3) = 2.7661(13) Å].

The molecular structure of **19** reveals a bimetallic species in which two square planar Cu(II) ions are bridged and chelated by bnz ligands *via* the α-alkoxide and carboxylate binding domains [Figure 15(a)]. The hppH ligand is 1.01-bound through the pyridyl nitrogen atom [Cu(1)-N_{hppH}(1) = 1.962(4) Å] with the OH group pendant.

In **19**, the bond length of Cu(1)-$O_{\alpha\text{-}O}$ = 1.903(3) Å, represents the shortest metal ion to ligand atom bond length found within **19**. The 1,4-chelating bnz bite angle of $O_{\alpha\text{-}OH}$(4)-Cu(1)-O_{COO}(2) at 83.41(14)°, is acute. The copper ions of **19** are separated at a distance of 2.9894(12) Å which is slightly shorter than the Cu···Cu distance in **18a** (3.0138(5) Å).

Table 15 Selected bond length (Å) and angle (°) data for complexes **19** and **20**

19				**20**			
Cu(1)-N(1)	1.962(4)	Cu(1)-O(4)#1	1.903(3)	Cu(1)-O(1)	1.9094(12)	Cu(1)-O(2)	1.9327(11)
Cu(1)-O(2)#1	1.906(3)	Cu(1)···Cu(1)#1	2.9894(12)	Cu(1)-O(1)#1	1.9147(11)	Cu(1)···Cu(1)#1	3.0091(5)
Cu(1)-O(4)	1.938(3)			Cu(1)-N(1)	1.9999(14)		
O(2)#1-Cu(1)-N(1)	95.61(14)	O(2)#1-Cu(1)-O(4)	161.19(13)	O(1)-Cu(1)-O(1)#1	76.21(6)	O(1)-Cu(1)-O(2)	170.47
O(4)-Cu(1)-N(1)	103.10(14)	O(4)#1-Cu(1)-O(2)#1	83.41(13)	O(1)-Cu(1)-N(1)	95.18(5)	O(1)#1-Cu(1)-O(2)	94.74(5)
O(4)#1-Cu(1)-N(1)	174.00(15)	Cu(1)#1-O(4)-Cu(1)	102.23(14)	O(1)#1-Cu(1)-N(1)	169.20(5)	O(2)-Cu(1)-N(1)	95.18(5)

Symmetry transformations used to generate equivalent atoms: #1 **19** (− *x*, − *y*, − *z*); **20** (− *x*, − *y* + 1, − *z* + 1).

Interestingly, the molecular structure of **20** reveals that the monoanionic hpp ligand (instead of bnz) 2.21 bridges the two Cu(II) centres and the diphenylacetate acts as a η^1-terminal ligand [Figure 15(c)]. The seven-membered chelate bite angle displayed by the hpp ligand in **20** [N_{hpp}(1)-Cu(1)-O_{hpp}(1) = 95.18(5)°] is significantly larger than the acute chelating bnz bite angle found in **19** (83.41°). This variation in structural type illustrates a case in which the α-OH group present in $bnzH_2$ affects product type.

In **19**, the pendant hppH hydroxyl groups undergo intermolecular hydrogen bonding interactions with carboxylate oxygen atoms from neighbouring molecules so as to generate a hydrogen bonded network of dimers [O_{hppH}(1)···O_{COO}(3') at 2.742(6) Å] [Figure 15(b)].

The IR spectrum of **19** features a hppH ν(OH) stretching band at ~ 3417 cm^{-1} and $\nu(CO_2)_{asymm}$ and $\nu(CO_2)_{symm}$ stretching bands at 1637 cm^{-1} and 1315 cm^{-1}, respectively, these latter bands overlapping with the ν(C=N) pyridyl stretching bands.[25,26] The FAB mass spectrum of **19** reveals peaks associated with the ligand loss and a $[M]^+$ peak at 852 Da.

The IR spectrum of **20** exhibits intense bands of $\nu(CO_2)_{asymm}$/pyridyl ν(C=N) at 1592 cm^{-1} and $\nu(CO_2)_{symm}$ at 1355 cm^{-1}.[25,26] The room temperature magnetic moments for **19** and **20** are 2.42 BM ($\chi_M T$ = 0.73 emu K mol^{-1}) and 2.26 BM ($\chi_M T$ = 0.64 emu K mol^{-1}), respectively, are slightly less than expected for two independent non-interacting copper(II) ions (***SEE NOTE***).[22b,22c] Magnetic characterisation of these complexes will be discussed in greater detail later on in this chapter (section 3.3).

Complexes **18a**, **18b**, **19** and **20** were analysed by ^{1}H NMR spectroscopy (Chapter 7, section 7.0). All the spectra (recorded in $CDCl_3$) are broad and paramagnetically shifted. Peak assignment has been made on the basis of a comparison of previously reported data, direct comparison of complexes in this work and by inspection of the relaxation times.[27]

The dimeric copper complexes **18a**, **18b**, **19** and **20** exhibit smaller proton chemical shift changes and slower relaxation rates (larger T_1 times) when compared to the monomeric copper complexes **12a**, **12b**, **13a/14a**, **13b/14b**, **17a** and **17b** (Table 16). As the copper ions of the dimers approach a S = 0 spin state the peaks become less shifted and sharper, whereby, the Cu(II) unpaired electrons couple and undergo antiferromagnetic superexchange rather than participation in paramagnetic deshielding (Chapter 2, section 2.4).[27e,27f] The H_α protons are assigned as the most downfield peaks, in **19** this proton is the least chemically shifted at 8.6 ppm (27.72 ms) in contrast to 27.0 ppm (2.61 ms) for **20**. $H_{\beta/\beta'}$ protons are observed from 17.1 ppm (1.75 ms) for **20** to 7.1 ppm (28.84 ms) for **18b** and H_γ are observed from 1.2 ppm (199.62 ms) for **18b** to 8.7 ppm (83.37 ppm) for **18a**. The α-CH_2, β-CH_2 and γ-CH_2 [$H_{(ax.)}$ and $H_{(eq.)}$] geminal protons all appear as a single

resonance.[27e,271] The Ph_2CH protons of **18b** and **20** are shifted at 1.3 ppm (343.98 ms) and 3.67 ppm (63.89 ms), respectively.

Table 16 ^{1}H NMR chemical shifts (δ) and relaxation times (T_1 ms, in parentheses) for Cu complexes **18a** – **20** (spectra recorded in $CDCl_3$)

Complex	H_α	$H_{\beta/\beta'}$	H_γ	α-CH_2	β-CH_2	γ-CH_2	C*H*	Ar-*H*
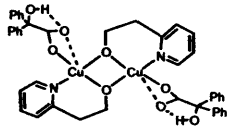 **18a**	20.6 (6.40)	9.9 (82.87), 9.3 (76.83)	8.7 (83.37)	15.4 (5.69)[c]	12.8 (8.03)[c]	N/A	N/A	8.3 (172.66), 7.5 (69.5)
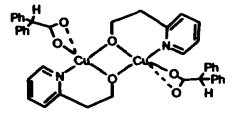 **18b**	10.3 (12.32)	7.3 (56.66),[c] 7.1 (28.84)[c]	1.2 (199.62)	3.7 (16.68)[c]	3.0 (72.62)[c]	N/A	1.3 (343.98)	7.3 (56.66),[c] 7.1 (28.84)[c]
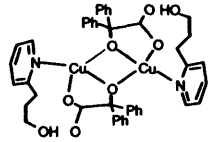 **19**	8.6 (27.72)	7.7 (377.13), 7.6 (925.76)	2.0 (61.64)	3.8 (31.55)[c]	3.0 (21.37)[c]	1.7 (41.88), 1.3 (371.18)[d]	N/A	7.1 (9.94)
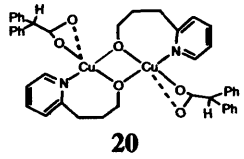 **20**	27.0 (2.61)	17.1 (1.75), ~ 14 (b)	4.1 (2.62)	10.7 (29.24)[c]	9.5 (23.69)[c]	8.4 (43.63)[c]	3.67 (63.89)	7.1 (41.88), 6.9 (46.84)

[a]Unreliable. [b]Could not be observed/determined. [c]Single resonance for several peaks. [d]Possibly axial proton.

3.2.5 M = Cu, L^1 = $bnzH_2$, in the Absence of a 2-Pyridine Alcohol

The reaction of $bnzH_2$ with copper acetate monohydrate in a 3:1 molar ratio, in the presence of triethylamine, results in the formation of $[Cu(bnzH)_3][NEt_3H]$ (**21**) (Scheme 10) in low yield. Complex **21** was characterised by elemental analysis, IR spectroscopy and both positive and negative FAB mass spectrometry. A single crystal of **21** was subject to an X-ray diffraction study. The molecular structure of **21** is shown in Figure 16, selected bond lengths and angles and angles are listed in Table 17.

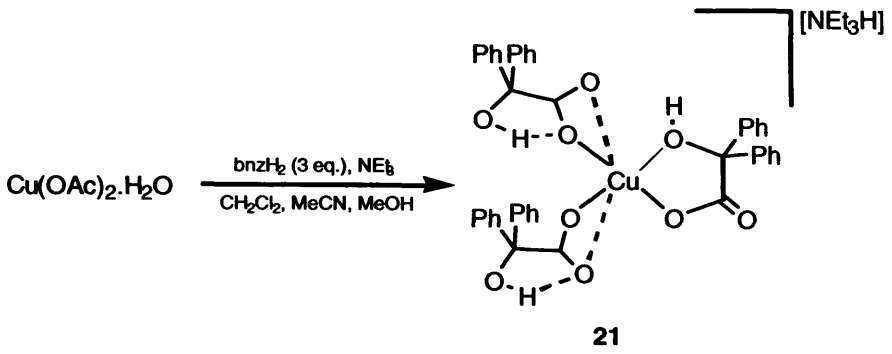

Scheme 10 Synthesis of **21**.

The anionic unit in **21** contains a copper(II) ion located in a distorted pseudo-square planar geometry and coordinated to three bnzH ligands. There are two types of benzilate bonding mode namely, either as a η^1-bonded carboxylate or as a 1,4-chelating bnzH ligand. In addition, the orientation of α-OH substituent in the η^1-bonded mode differs in that the copper-bound carboxylate oxygen atom is either *cis* or *trans* to the α-OH group (Figure 17).

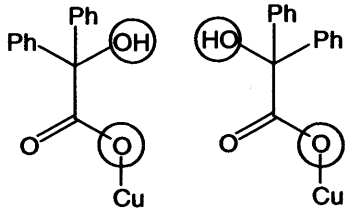

Figure 17 Benzilate bonding mode of *cis*-η^1-bnzH-α-OH (left) and *trans*-η^1-bnzH-α-OH (right).

The Cu(II) ion in **21** can also be considered to have a Jahn-Teller distorted pseudo-octahedral geometry in which the pseudo-*trans* axial bond lengths from the unbound bnzH carboxylate oxygen atoms bonds are Cu(1)···O_{COO}(5) = 2.695(7) Å and Cu(1)···O_{COO}(8) = 2.663(13) Å. Complex **21** possesses a short Cu(1)-$O_{\alpha\text{-}OH}$(3) bond length at 1.898(6) Å, whereas the chelating carboxylate oxygen to copper bond length Cu(1)-O_{COO}(1) is longer at 1.922(7) Å, with a corresponding five-membered chelate bite angle at 85.1(2)°. The carboxylate C-O bond lengths for the *trans*- and *cis*- bnzH moieties are 1.39(2) Å and 1.288(11) Å, respectively, both suggesting the presence of metal-carboxylate bonds with some covalent character.[12]

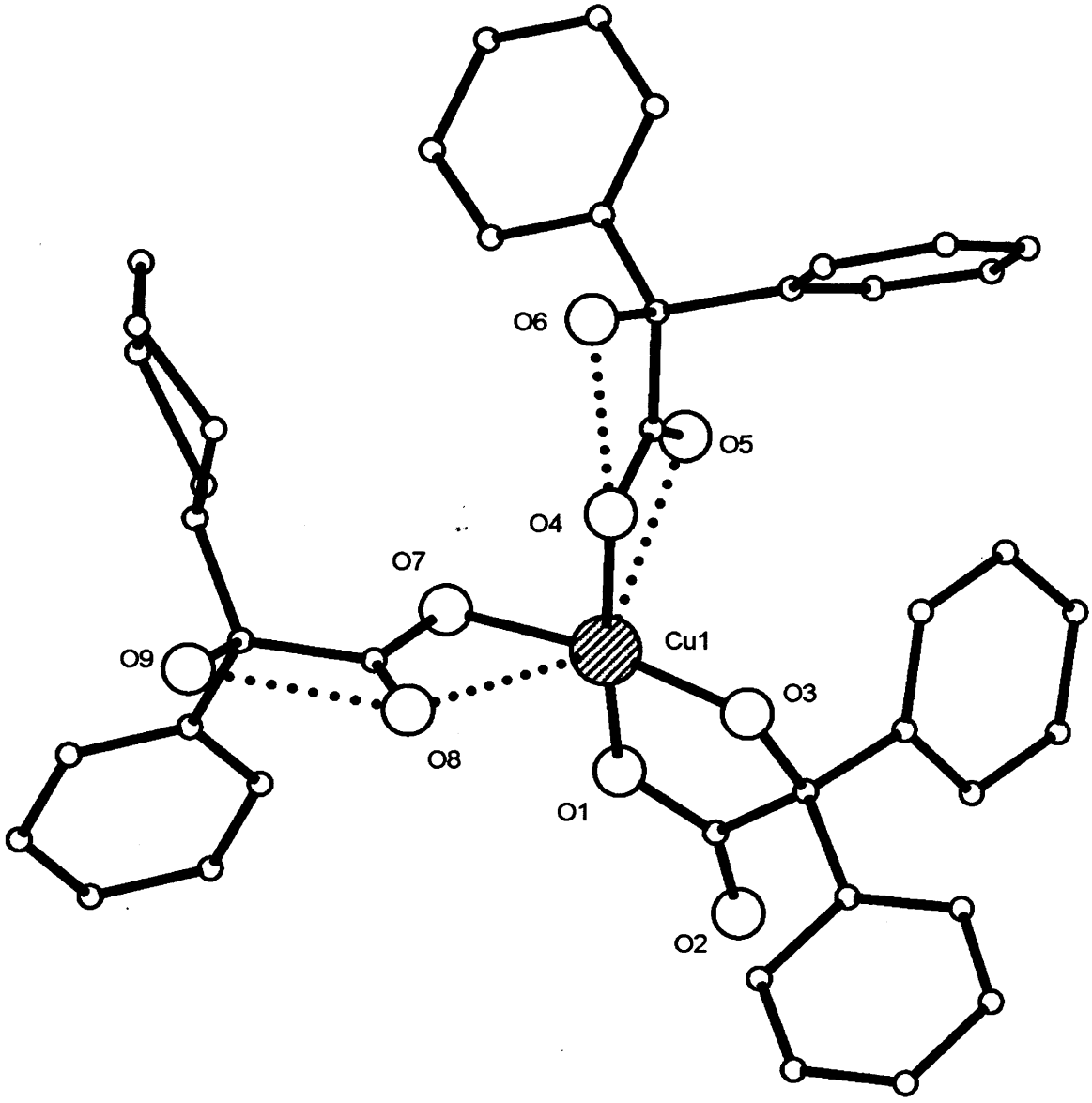

Figure 16 Molecular structure of the anionic unit in **21**. Hydrogen atoms were excluded from refinement. Carbon atom labels and a triethylamine molecule are excluded for clarity. Dotted lines indicate hydrogen bonding/pseudo-axial interactions.

Table 17 Selected bond length (Å) and angle (°) data for complex **21**

21					
Cu(1)-O(1)	1.922(7)	Cu(1)-O(4)	1.979(6)	Cu(1)-O(7)	1.951(8)
Cu(1)-O(3)	1.898(6)				
O(3)-Cu(1)-O(1)	85.1(2)	O(1)-Cu(1)-O(7)	91.8(3)	O(3)-Cu(1)-O(7)	169.9(3)
O(1)-Cu(1)-O(4)	171.3(3)	O(3)-Cu(1)-O(4)	92.7(2)	O(7)-Cu(1)-O(4)	91.8(3)

The α-OH and neighbouring carboxylate oxygen atoms in **21** undergo intra-ligand hydrogen bonding interactions and indicate the presence of a stronger hydrogen bonding interaction from the unbound η^1 *trans*-bnzH oxygen atom with the adjacent α-OH group [$O_{trans\text{-}\alpha\text{-}OH}\cdots O_{COO}$ = ~ 2.522(7) Å and $O_{cis\text{-}\alpha\text{-}OH}\cdots O_{COO}$ = ~ 2.558(13) Å].

The *trans*- and *cis*-η^1 α-hydroxyl to carboxylate bnzH ligands in **21** are bound to the copper ions with bond lengths of Cu(1)-$O_{trans\text{-}\alpha\text{-}OH}$(7) = 1.951(8) Å and Cu(1)-$O_{cis\text{-}\alpha\text{-}OH}$(4) = 1.979(6) Å, respectively. Complex **9a** also contains protonated 1,4-chelating bnzH ligands, in which, the bnzH bond lengths are longer [Ni-$O_{\alpha\text{-}OH}$ = 2.096 Å and Ni-O_{COO} = 2.032 Å].

In the IR spectrum of **21**, there are strong $\nu(CO_2)_{asymm}$ and $\nu(CO_2)_{symm}$ bands at 1597 cm^{-1} and 1327 cm^{-1}, respectively.[25] The room temperature magnetic moment value for **21** at 1.76 BM ($\chi_M T$ = 0.39 emu K mol^{-1}) is consistent with a single copper(II) ion.[22b] The positive and negative FAB mass spectra of **21** shows fragmentation peaks of $[M - NEt_3H]^+$ and $[M - NEt_3H]^-$ at 744 Da.

The formation of **21**, demonstrates that a second ligand component (in addition to $bnzH_2$), is beneficial for multinuclear copper cluster formation under these reaction conditions. Notably, the isolation and full characterisation of a homoleptic Ni-based complex proved illusive using the same synthetic approach.

3.2.6 Effect of Base, M = Cu, L^1 = $bnzH_2$, Featuring no Pyridine Alcohol Ligand

In this section the effect of a change of base on product type is examined. On reaction of copper acetate monohydrate with $bnzH_2$ and hepH/hppH in the presence of sodium methoxide gave, on work-up, $[CuNa_2(bnz)_2(MeOH)_4(MeCN)_2]_n$ (**22**) (Scheme 11) as purple-blue blocks in low yield. Complex **22** was characterised by elemental analysis, IR spectroscopy and positive FAB mass spectrometry. A single crystal of **22** was subject to an X-ray diffraction study. The molecular structure of **22** is shown in Figure 18; selected bond lengths and angles are given in Table 18.

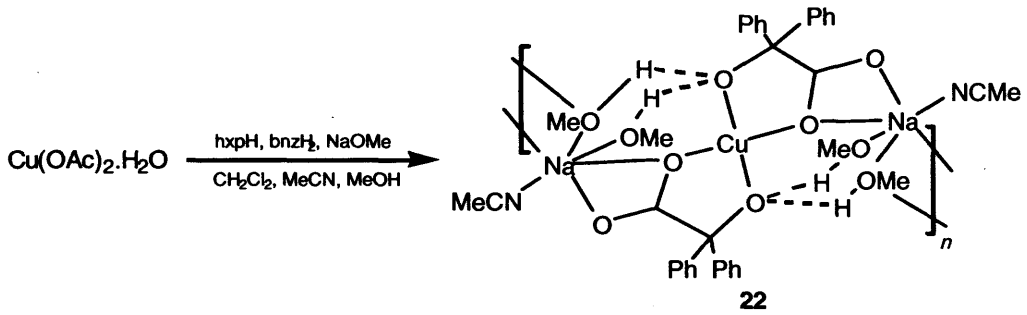

22

Scheme 11 Synthesis of **22**.

The molecular structure of **22** consists of a one dimensional $CuNa_2$ polymer in which each square planar copper ion is coordinated by two 1,4-chelating bnz ligands and the sodium ions by a bnz, two methanol and acetonitrile ligands. The bnz carboxylate functionality also 1,1-chelates with a sodium cation (on the octahedral axial and equatorial sites). Therefore, bnz is involved in a novel bis-chelating bonding mode (Figure 19). In addition, the sodium atoms are bridged by a molecule of methanol. In **22**, the chelate $O_{\alpha\text{-}O}$-Cu-O_{COO} bite angle (α) due to the doubly deprotonated bnz ligand is acute at 85.73(6)°, as is the O_{COO}-Na-O_{COO} bite (β) angle at 53.86(5)°.

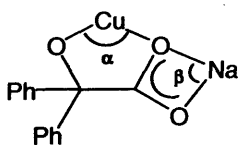

Figure 19 Novel bis-chelating 1,4; 1,1-bnz bonding mode.

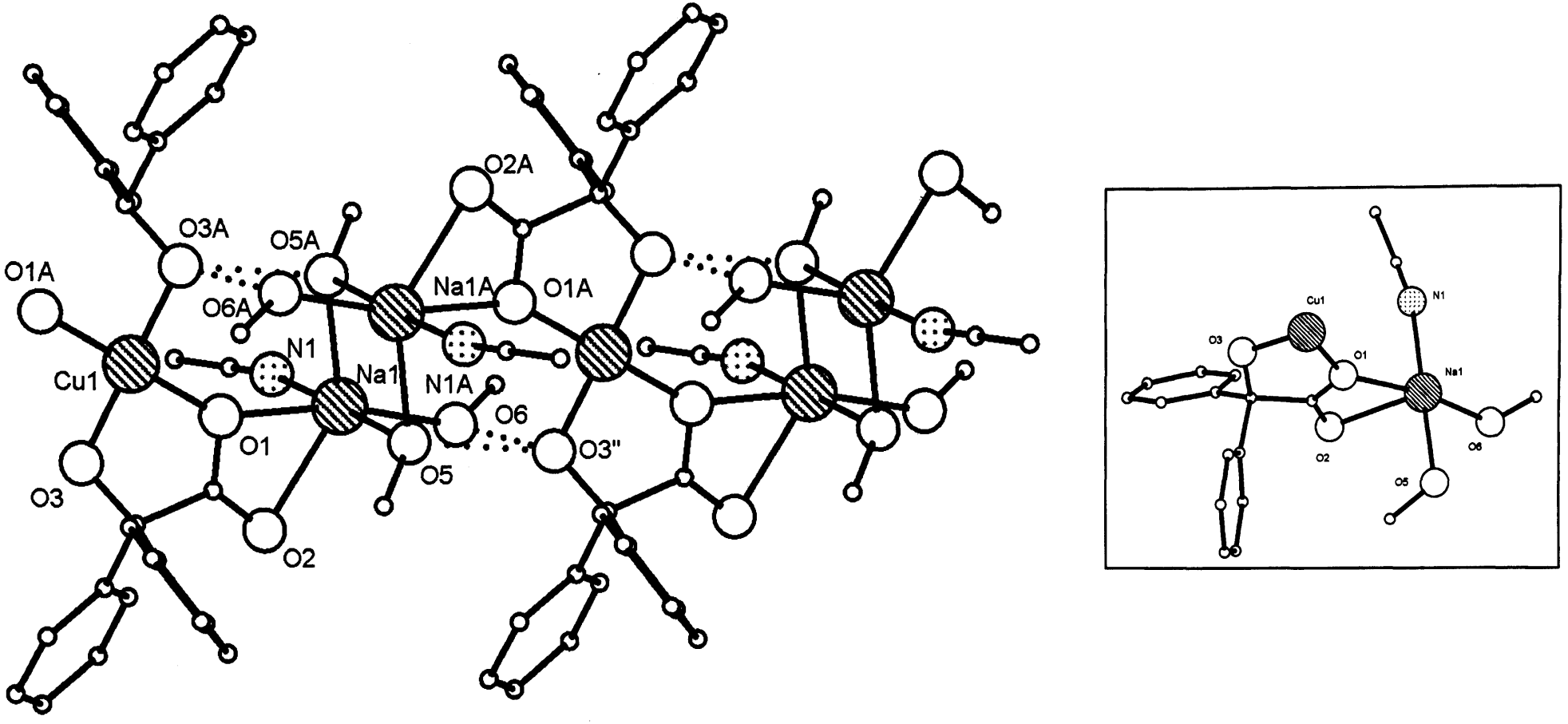

Figure 18 Molecular structure of **22**. Part of the polymeric chain is shown. Inset shows the asymmetric unit. Hydrogen atoms and carbon atom labels are excluded for clarity. Dotted lines indicate hydrogen bonding interactions.

Table 18 Selected bond length (Å) and angle (°) data for complex **22**

22					
Cu(1)-O(1)	1.8961(13)	Na(1)-N(1)	2.529(2)	Na(1)-O(5)#2	2.3868(17)
Cu(1)-O(3)	1.9116(13)	Na(1)-O(2)	2.5343(17)	Na(1)-O(6)	2.2921(16)
Na(1)-O(1)	2.3273(16)	Na(1)-O(5)	2.4654(16)	Na(1)-Na(1)#1	3.4473(16)
O(1)-Cu(1)-O(3)	85.73(6)	O(5)#2-Na(1)-N(1)	93.12(7)	O(6)-Na(1)-N(1)	93.23(7)
O(1)-Cu(1)-O(3)#1	94.27(6)	O(5)-Na(1)-O(2)	86.39(5)	O(6)-Na(1)-O(2)	113.94(6)
O(1)-Na(1)-N(1)	89.35(7)	O(5)#2-Na(1)-O(2)	133.96(6)	O(6)-Na(1)-O(5)	84.60(5)
O(1)-Na(1)-O(2)	53.86(5)	O(5)#2-Na(1)-O(5)	89.47(6)	O(6)-Na(1)-O(5)#2	80.60(5)
N(1)-Na(1)-O(2)	92.75(7)	O(6)-Na(1)-O(1)	167.68(7)	Na(1)#2-O(5)-Na(1)	90.53(5)
O(5)-Na(1)-N(1)	177.10(7)				

Symmetry transformations used to generate equivalent atoms: #1 $(-x, -y, -z+2)$; #2 $(-x+1, -y+1, -z+2)$.

In **22**, intramolecular inter-ligand hydrogen bonding interactions take place between the terminal and bridging methanolic molecules and bnz alkoxide oxygen atoms [$O_{MeOH}\cdots O_{\alpha\text{-}O}$ = ~ 2.679(2) Å and μ_2-$O_{MeOH}\cdots O_{\alpha\text{-}O}$ = ~ 2.768(2) Å].

Complex **22** can be compared to the previously reported three dimensional $CuNa_2$ hydrogen-bonded polymeric complex $[Na_2Cu(CH_3CO_2)_4(H_2O)]\cdot H_2O$.[19] In this species, hydrogen bonding interactions between the water molecules and neighbouring acetate oxygen atoms link the polymer together. The copper ions in **22** are separated at a distance of ~ 8.264 Å which is longer in comparison to 6.899 Å for $[Na_2Cu(CH_3CO_2)_4(H_2O)]\cdot H_2O$.

Complex **22** represents a novel polymeric chain developed by incorporation of the base (NaOMe) into the final structure. Significantly, there is no participation of the pyridine alcohol ligands (hmpH/hepH) in **22**. The IR spectrum of **22** possesses a very broad methanolic ν(OH) stretching band at ~ 3397 cm^{-1}. The benzilate $\nu(CO_2)_{asymm}$ and $\nu(CO_2)_{symm}$ stretching bands are observed at 1600 cm^{-1} and 1380 cm^{-1}, respectively.[25] The FAB mass spectrum of **22** includes a fragmentation peak of $[M_{(n=1)} - MeOH]^+$ at 737 Da. The room temperature magnetic moment for **22** at 2.11 BM ($\chi_M T$ = 0.56 emu K mol^{-1}) is less than expected for a paramagnetic molecule containing non-interacting copper(II) ions (***SEE NOTE***).[22b,22c]

3.3 Solid-State EPR and Variable Temperature SQUID Magnetic Characterisation of Selected Complexes

Preliminary variable temperature SQUID magnetic experiments have been undertaken or are presently being carried out on the multinuclear complexes **9a/9b**, **11a**, **11b**, **16a**, **18a**, **19** and **22** (Chapter 7.0, section 7.0). The copper complexes **16a**, **18a**, **19** and **22** along with **17a**, have been analysed by solid-state EPR spectroscopy (Chapter 7, section 7.0). No EPR data were recorded on the Ni(II) complexes due to their integer spin-states (S = 1) and large magnetoanisotropic effects (ZFS).[30a] ***IMPORTANT NOTE*** *All SQUID magnetic measurements are only part of a preliminary investigation undertaken by Prof. A. Harrison (Edinburgh) therefore, there is a large uncertainty in the data e.g., due to the presence of several parameters and/or parameters with unreliable/inconsistent values.*

3.3.1 Magnetic and/or EPR Spectroscopic Data for Selected Cu(II) Complexes

3.3.1.1 Complex 22

The Q- and X-band EPR spectra obtained for $[CuNa_2(bnz)_2(MeOH)_4(MeCN)_2]_n$ (**22**) indicates axial distortions [$g_{(II)zz} > 2.1$, $g_{(\perp)xx,yy} > 2.00$], in which the unpaired electron of the Cu(II) ion is localised on the $d_{x^2-y^2}$ orbital.[29] The g-values for **22** are $g_1 = 2.253$ and $g_2 = g_3 = 2.054$ with a hyperfine coupling constant from $^{63,65}Cu$ of A_1 =178 G (Figure 20).[16j] The Q-band spectrum also shows a weak signal due to a second species.

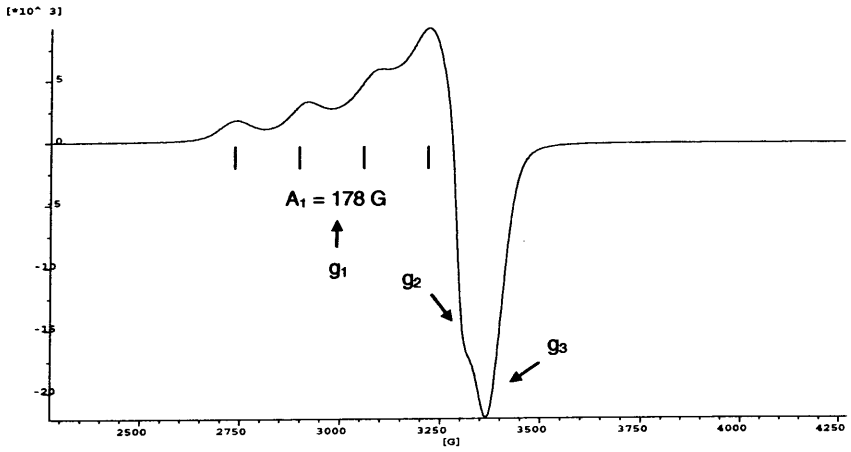

Figure 20 X-band EPR spectrum of **22** recorded at 110 K ($A_1 = A_{(II)}$).

The variable temperature magnetic susceptibility SQUID data for **22**, fitted using the Curie-Weiss law (Equation 1), provides the following parameters; $\chi_{TIP} = 3.16 \times 10^{-3}$ ($\pm$ 3.0 $\times 10^{-5}$) emu mol^{-1}, Curie constant (C) = 0.106 ($\pm$ 4.6 $\times 10^{-4}$) emu K mol^{-1} and Curie-Weiss constant (θ) = – 9.86 $\times 10^{-3}$ ($\pm$ 1.0 $\times 10^{-2}$) K (Figure 21). The small negative value of θ suggests the presence of very weak antiferromagnetic coupling which coincides with the > 8 Å separation between the Cu(II) ions within the polymer chain.

$$\chi = \frac{C}{T-\theta} + \chi_{TIP}$$

Equation 1 Curie-Weiss law for a paramagnet. $C = Ng^2\beta^2/k$; N = Avogadro's number, g = Landé splitting factor, β = Bohr magneton, k = Boltzmann constant, T = temperature, $CT = \sim Ng^2/8$ (g fixed at 2.00) and χ_{TIP} = temperature independent background susceptibility.

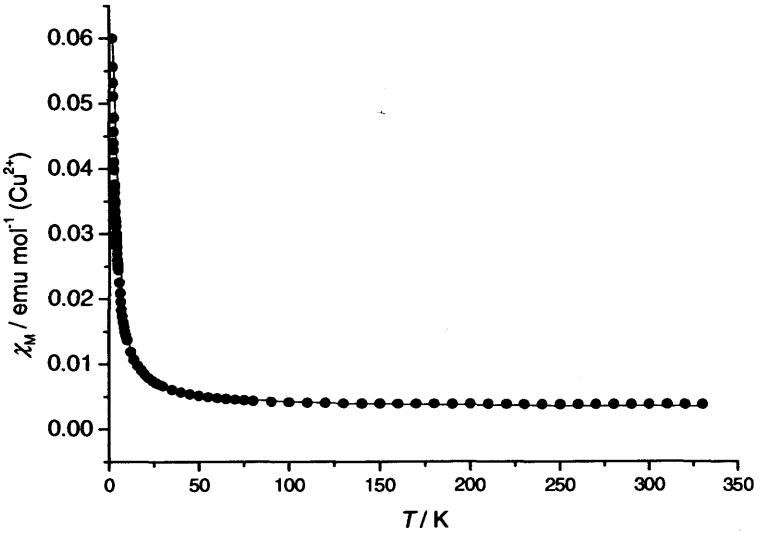

Figure 21 Plot of χ_M against T for **22** (fit in solid line).

3.3.1.2 Complexes 18a and 19

Q- and X-band EPR spectra obtained for [Cu(hep)(bnzH)]$_2$ (**18a**) and [Cu(hppH)(bnz)]$_2$ (**19**) (Figure 22) each possess three g-values and hyperfine coupling for ^{63,65}Cu [g_1 = 2.292, g_2 = 2.069 and g_3 = 2.054, A_1 = 78 G (**18a**); g_1 = 2.234, g_2 = 2.040 and g_3 = 2.025, A_1 = 194 G (**19**)]. The g_3 tensor is split in both **18a** and **19** which signifies reduction of axial symmetry (rhombic distortions).[16w] In **18a**, the presence of a triplet S = 1 signal from the two copper(II) ions and a very small zero field splitting parameter (D) is possible. However, the EPR spectra of **19** exhibits broadened peaks with the absence of additional

features or a triplet state signal at lower temperatures (120 K and 5 K). The latter implies the presence of depopulated spin states even at these temperatures and is consistent with the room temperature ^{1}H NMR spectrum which demonstrates a maximum downfield chemical shift of 8.6 ppm as the molecule favours a diamagnetic-like $S = 0$ state.

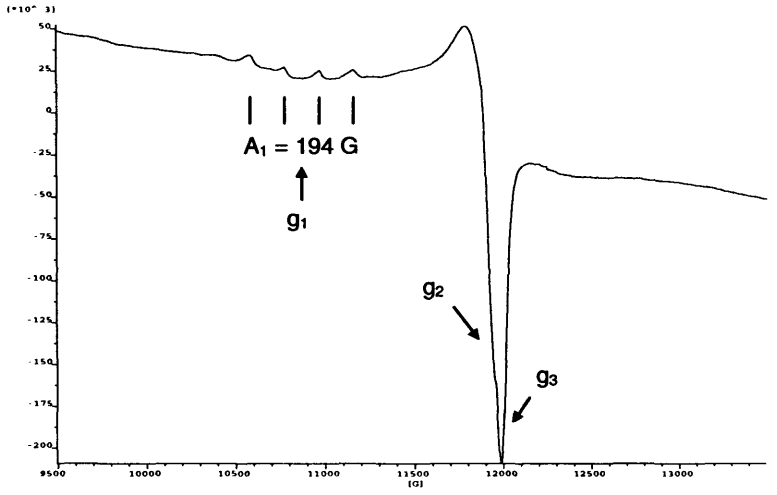

Figure 22 Q-band EPR spectrum of **19** at 295 K.

The preliminary variable temperature magnetic susceptibility data of **18a** (25 – 300 K) was modelled using the Bleaney-Bowers equation for a dimer ($S = 0.5$) using a five parameter fit including a temperature independent term and Curie-Weiss paramagnetic impurity terms (Equation 2).[20] The following parameters were obtained from the fit {per Cu(II) ion}; $\chi_{TIP} = 9.1\times 10^{-4}$ ($\pm$ 2.0 $\times$ 10^{-5}) emu mol^{-1}, $x = -$ 8.37 ($\pm$ 0.17) K, g = 2.26 ($\pm$ 0.35), a Curie constant (C') = 2.44 $\times$ 10^{-2} ($\pm$ 7.5 $\times$ 10^{-4}) emu K mol^{-1} and a Curie-Weiss constant (θ') = – 1.89 ($\pm$ 0.12) K [Figure 23].

The negative value for x confirms the presence of a moderate antiferromagnetic coupling interaction by superexchange through the hep alkoxide bridge between the copper ions {Cu-O-Cu = 103.16(7)° **18a**}. The additional Curie-Weiss term indicates the presence of a small amount of paramagnetic impurity (6%). The presence of antiferromagnetic coupling within **18a** is supported by the ^{1}H NMR data which has a downfield chemical shift peak maximum of 20.6 ppm as a diamagnetic-like $S = 0$ spin state is approached.

$$\chi = \frac{C}{T} \cdot \frac{2e^{\left(\frac{2J_1}{kT}\right)}}{1+3e^{\left(\frac{2J_1}{kT}\right)}} + \chi_{TIP} + \frac{C'}{T-\theta'}$$

Equation 2 Bleaney-Bowers S = 0.5 dimer equation. $C = Ng^2\beta^2/k$; N = Avogadro's number, g = Landé splitting factor, β = Bohr magneton, k = Boltzmann constant, T = temperature, CT = ~ $Ng^2/8$ and χ_{TIP} = temperature independent background susceptibility. The coupling constant is suggested from; $J_1/k = x$. Paramagnetic impurity terms; C' = Curie-constant and θ' = Curie-Weiss constant.

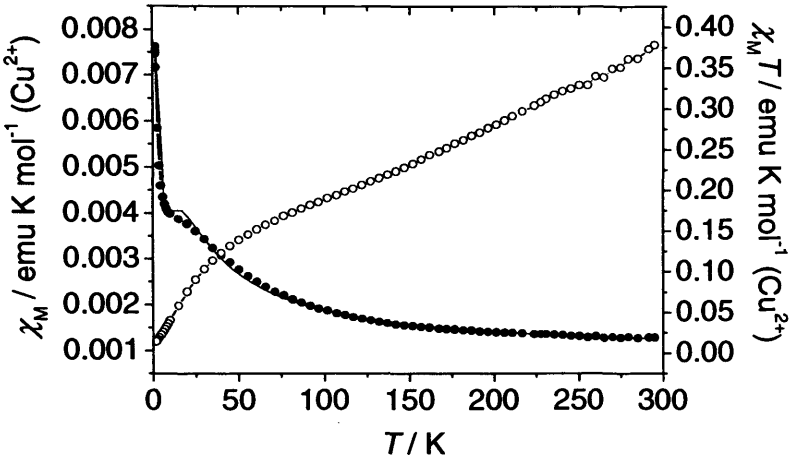

Figure 23 Plot of χ_M against T (closed circles) and $\chi_M T$ against T (open circles) for **18a** [per Cu(II) ion]; fitted plot in solid line.

3.3.1.3 Complex 16a

The Q- and X-band EPR spectra of $[Cu_3(chp)_4(bnz)(bnzH)][NEt_3H]$ (**16a**) (desolvated) exhibit very broad signals at $g_1 = g_2 = g_3 =$ ~ 2.114 from a S = 3/2 state and a half field signal at g ~ 3.955 due to the superimposition of all S = 0.5 spin states (Figure 24). The appearance of the EPR spectra recorded at 4 K is very similar to the spectra obtained at higher temperatures, therefore exchange coupling (x) is very weak. The presence of a small zero field splitting parameter (D) prevented resolution of the fine structure. In comparison, EPR analysis on $[Cu_3(talen)]$ [H_6talen = 2,4,6-tris(1-(2-salicylaldimino-methylpropylimino)-ethyl)-1,3,5-trihydroxybenzene] [2.7 K, X-band] results in signals of S = ½, g = ~ 2 and a half-field signal of S = 3/2, g = ~ 4 and, in which hyperfine coupling was resolved.[16g]

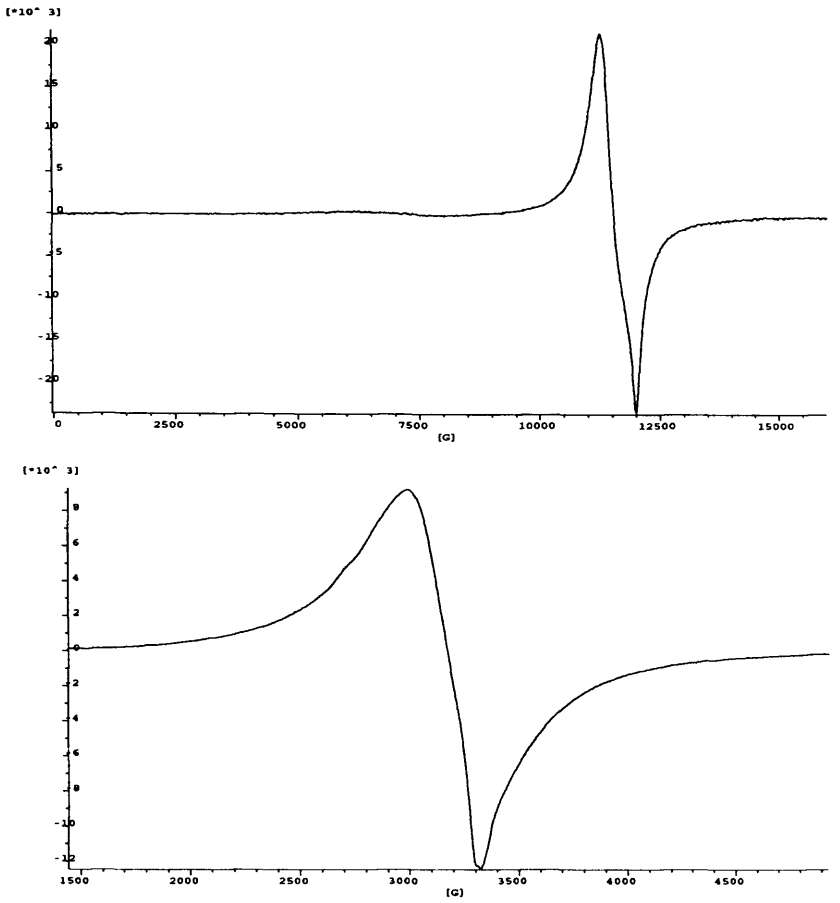

Figure 24 EPR spectra of **16a** Q-band 136 K, $S = 0.5$, g = 2 (above) and X-band 110 K, $S = 1.5$, g = 3.995 (below).

In **16a** (desolvated), there are three possible coupling constants (x_n) which denote the different types of exchange interactions between the copper ions of the trimer, these may be calculated by modelled fits of the magnetic data using a derived equation.[22,23] Herein, we have employed the 'isoceles' trimer fit to model the magnetic data for **16a**. This model was viewed as appropriate because of the variation in the Cu···Cu distances [Cu(2)···Cu(3) = 3.656 Å *vs.* Cu(1)···Cu(3) = 3.381 Å *vs.* Cu(1)···Cu(2) = 3.277 Å] (Figure 25, Equation 3).[24]

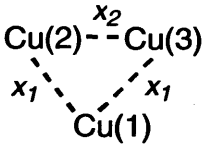

Figure 25 Isosceles triangle-based arrangement of copper ions in **16a**.

Preliminary fitting and parameterisation of the variable temperature magnetic susceptibility data of **16a** using Equation 3 is presently under progress. The data, so far,

displays evidence for moderate antiferromagnetic behaviour in the lower temperature range (2 – 50 K). However, the higher temperature data (50 – 325 K) is consistent with paramagnet-like behaviour and can be modelled suitably by using the Curie-Weiss law (Equation 1).

$$\chi = \frac{Ng^2\beta^2}{4kT}\left[\frac{1+e\left(\frac{-2J_1+2J_2}{kT}\right)+10e\left(\frac{J_1+2J_2}{kT}\right)}{1+e\left(\frac{-2J_1+2J_2}{kT}\right)+2e\left(\frac{J_1+2J_2}{kT}\right)}\right]$$

Equation 3 Spin-isosceles trimer model; χ_{TIP} = temperature independent background susceptibility; N = Avogadro's number, β = Bohr magneton, g = Landé splitting factor, k = Boltzmann constant and T = temperature. The coupling constants are suggested from; $J_1/k = x_1$ and $J_2/k = x_2$.

The isosceles trimer model has been employed on other trinuclear copper complexes including, $[Cu_3(NH_2C\{Me\}_2CH_2C\{Me\}=NO)_6(O)(OH)_2]Cl_2$ [J_1 = – 60 cm^{-1}, J_2 = – 170 cm^{-1}, g = 2.0][16x] and $[Cu_3L{\cdot}2H_2O]{\cdot}2NO_3$ {H_4L = 4,7,13,16-tetrakis(2-carboxybenzyl)-1,10-dioxa-4,7,13,16-tetraazacyclooctadecane} [J_1 = 8.08 cm^{-1}, J_2 = – 0.40 cm^{-1}, g = 2.04][16z] these complexes exhibiting both strong and weak exchange interactions, respectively. Other Cu(II) trimers have been fitted with different models, for example, $[Cu_3(4\text{-}O_2N\text{-}pz)_3Br_5](Bu_4N)_2$ [J = + 3.1 cm^{-1} and g_{zz} = 2.42, $g_{yy} = g_{xx}$ = 2.46; X-band EPR, 77 K, S = 3/2, g_{zz} = 2.08, $g_{yy} = g_{xx}$ = 2.01],[16d] and $[Cu_3(talen)]$ [J = + 1.52 cm^{-1}, g = 2.14],[16h] which exhibit weak ferromagnetic exchange interactions. In general, modelled fits on copper trimers commonly provide weak ferromagnetic or antiferromagnetic coupling constants.[16]

3.3.1.4 Complex 17a

The X-band EPR spectrum of monometallic $[Cu(hmpH)_2(bnzH)_2]$ (**17a**) shows the presence of Cu(II) axial (z axis) elongation.[29] However, the Q-band spectrum has three g values at g_1 = 2.316, g_2 = 2.071 and g_3 = 2.062. The g_3 tensor is split, thus indicating the presence of slight rhombic (x, y) distortions around the octahedral (S = 0.5) copper complex. No hyperfine coupling from $^{63,65}Cu$ was resolved due to magnetic dilution.[30b]

3.3.2 Magnetic Data for Selected Ni(II) Complexes

3.3.2.1 Complex 9a/9b

The variable temperature magnetic moment SQUID plot of co-crystallised $[Ni_4(chp)_4(bnzH)_4(MeO)_2(ROH)_2][NEt_3H]_2$ [R = H **9a**, R = Me **9b**] (desolvated), shows a slightly elevated magnetic moment of ~ 3.75 BM (~ 1.76 emu K mol^{-1}; expected ~ 2.83 BM, 1.00 emu K mol^{-1}) per Ni(II) ion at low temperature which implies the possibility of weak ferromagnetic interactions or spin frustration effects due to the triangular arrangement of the interacting Ni(II) ions (Figure 26).[21] At ~ 325 K the magnetic moment per Ni(II) ion of **9a/9b** approaches a maximum value of ~ 3.40 BM (~ 1.45 emu K mol^{-1}). The variable temperature inverse susceptibility (χ_M^{-1}) data of **9a/9b** can be extrapolated to give a Curie-Weiss intercept at ~ + 4 K therefore, indicating weak overall antiferromagnetic coupling. However, in the lower temperature region the overall coupling appears to favour a low-spin ground state.

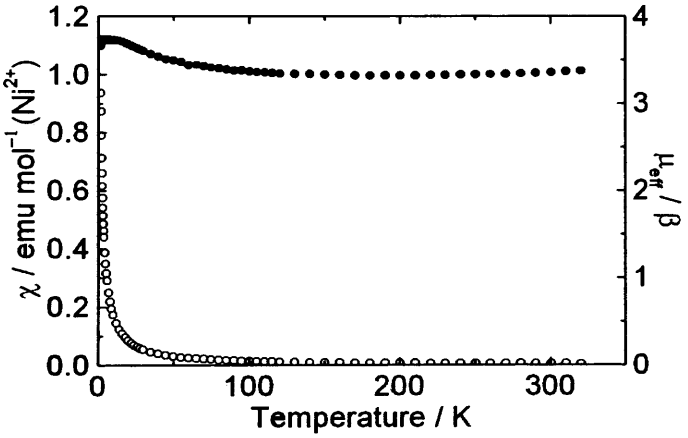

Figure 26 χ_M against T (open circles) and moment / μ_{eff} against T plot (closed circles) for **9a/9b**.

The variable temperature magnetic SQUID susceptibility data of **9a/9b** were modelled using a derivation of the van Vleck equation using spin Hamiltonians based on theoretical simplification and on the assumption that three competing pairwise exchange interactions (J_1, J_2 and J_3) exist between the nickel(II) ions (Figure 27) [Complex **9a/9b** actually has three possible exchange pathways since it adopts an open-di-cubane-based core structure generated from an inversion centre (Figure 28)].[13d] Preliminary modelling,

by fitting the variable temperature magnetic susceptibility data of **9a/9b** (Figure 29), indicates that interactions within this complex are very weak in origin. Thus the best fit is obtained when coupling constants x_1 and x_3 are fixed to zero resulting in a weak antiferromagnetic interaction of $x_2 = -0.17\ (\pm 8.9 \times 10^{-3})$ K (Table 19).

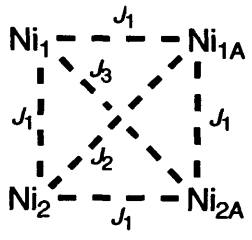

Figure 27 Model based on three pairwise exchange interactions.[13d]

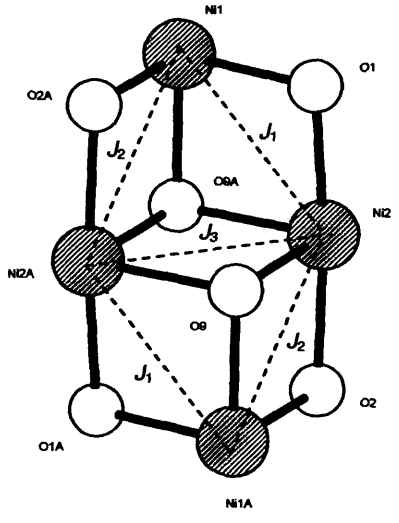

Figure 28 Ni_4O_6 core and possible exchange coupling interactions in **9a**.

Table 19 Preliminary fitting of variable temperature magnetic susceptibility data for **9a/9b** and **11a**

	9a/9b	**11a**
$\chi_{TIP} \times 10^{-4}$ / emu mol^{-1}	0*	1.60 (± 1.20)
x_1 / K	0*	– 5.93 (± 1.17)
x_2 / K	$-0.17\ (\pm 8.9 \times 10^{-3})$	$7.47\ (\pm 4.7 \times 10^{-2})$
x_3 / K	0*	0*
ρ / K	$0.011\ (\pm 2.5 \times 10^{-3})$	$0.035\ (\pm 4.7 \times 10^{-4})$
g	2.36*	2.34 (± 0.23)

*Fixed during fitting, ρ = weak coupling of impurity phase, χ_{TIP} = temperature independent background susceptibility. [13d] The coupling constants are suggested from; $J_1/k = x_1$, $J_2/k = x_2$ and $J_3/k = x_3$.

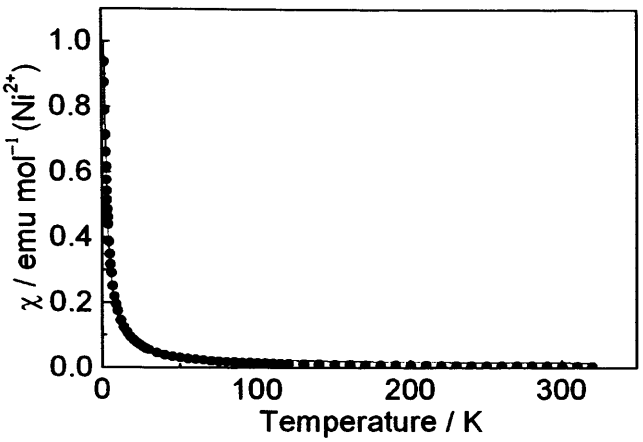

Figure 29 Modelled variable temperature magnetic susceptibility fit (solid line) for **9a/9b**.

3.3.2.2 Complex 11a

The variable temperature inverse susceptibility (χ_M^{-1}) data of the closed-cubane complex **11a**, can be extrapolated to give a Curie-Weiss intercept at ~ – 15 K which is consistent with the presence of net antiferromagnetic coupling. At ~ 325 K the magnetic moment per Ni(II) ion of **11a** approaches a maximum value of ~ 3.30 BM (~ 1.36 emu K mol^{-1}). Preliminary modelling of the variable temperature magnetic susceptibility data of **11a** using the previous model (Figure 30)[13d] yields a combination of antiferromagnetic [x_1 = – 5.93 (± 1.17) K] and ferromagnetic [x_2 = + 7.47 (± 4.7× 10^{-2}) K] exchange interactions (Table 19). [The closed-cubane complex **11a** actually has four possible exchange interactions (Figure 31)].

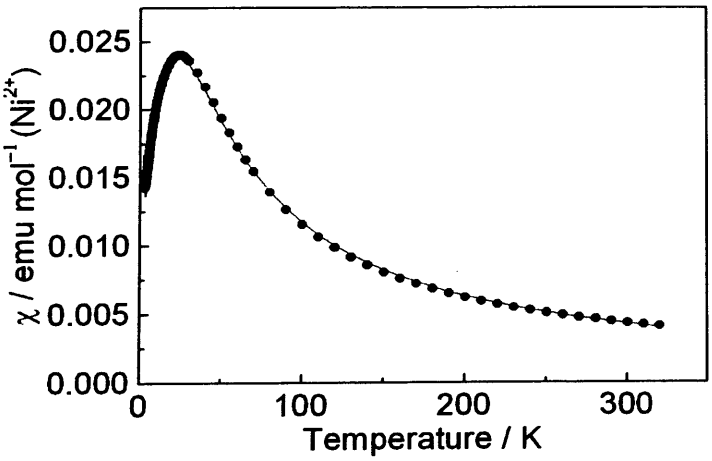

Figure 30 Modelled variable temperature magnetic susceptibility fit (solid line) for **11a**.

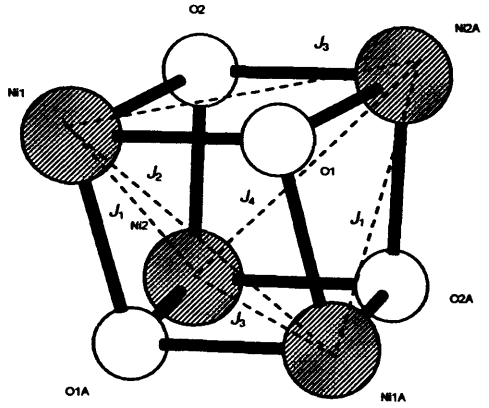

Figure 31 Ni_4O_4 core and possible exchange coupling interactions in **11a**.

3.3.2.3 General Comments

The preliminary magnetic properties of **9a/9b** and **11a** have been compared to a selection of similar tetrameric Ni(II) cubanes, these are summarised in Table 20. Open di-cubane-based tetramers often exhibit moderate coupling constants, such as **9a/9b** (first three entries). These values often increase when azide ligands are incorporated into the complex (entry 3). It is common for closed cubane complexes to possess both ferro- and anti-ferromagnetic interactions as observed in **11a** (last five entries). The ferromagnetic interaction predominates in the presence of a SMM species (entries 4 and 5). An in-depth investigation into the magnetic modelling of **9a/9b** and **11a** is currently in progress.

Table 20 Selected magnetic coupling constants from reported $\{Ni_4\}$-based cubane complexes

Complex	x_1 / cm^{-1}	x_2 / cm^{-1}	x_3 / cm^{-1}	x_4 / cm^{-1}	g	Ref.
$[Ni_4(OMe)_2(H_2O)_6(ntp)_2]^a$	+ 11.9	+ 3.0	-	-	2.19	11
$[Ni_4(dpkOH)_2(dpkOMe)_2(N_3)_2(H_2O)_2](ClO_4)_2{}^a$	+ 18.0	+ 15.3	+ 27.1	− 1. 6	2.1	9
$[Ni_4(enzbipy)_2(N_3)_4]^a$	+ 15.8	+ 15.8	+ 14.6	-	2.15	10
$[Ni(hmp)(MeOH)Cl]_4{}^b$	+ 0.4	+ 5.3	-	-	2.11	15a
$[Ni(hmp)(MeOH)N_3]_4{}^b$	+ 9.8	+ 2.4	-	-	2.21	15a
$[Ni_4(chp)_4(OMe)_4(MeOH)_7]^b$	+ 7.8	+ 13.0	- 9.6	-	2.15	14a
$[Ni_4(LH_2)_2(OMe)_2(CH_3CO_2)_2(MeOH)_2]^b$	+ 0.5	+ 4.3	− 1.45	-	2.12	13k
$[Ni_4(C\{Me\}_3CO_2)_4(8\text{-hydroxyquinaldine})_4]^b$	+ 3.4	− 1.1	-	-	2.24	13l
$[Ni_4(L')_4(MeOH)_4]^b$	− 3.5	8.8	-	-	2.18	13o
$[Ni_4(L')_4(EtOH)_4]^b$	− 2.9	+ 7.8	-	-	2.20	13o

[a]Open di-cubane, [b]closed cubane, dpk = dipyridylketone, enzbipy = [*N,N*-[bis(pyridin-2-yl)benzylidene]ethane-1,2-diamine, LH_3 = pentadentate phenol containing Schiff-base ligand with *O,N,O,N,O* donor atoms, $L'H_2$ = salicylidene-2-ethanolamine. The coupling constants are suggested from; $J_1/k = x_1$, $J_2/k = x_2$, $J_3/k = x_3$ and $J_4/k = x_4$.

3.4 Summary and Conclusions

It has been shown that reactions of ligand blends composed of $bnzH_2$ and 2-pyridine alcohols [2-{$(CH_2)_nOH$}-6-X-C_5H_3N] with nickel acetate tetrahydrate or copper acetate monohydrate in the presence of triethylamine, furnish a range of novel complexes displaying a variety of nuclearities and structural types (**9** – **22**). Scheme 12 depicts the synthetic work undertaken in this chapter.

A series of complexes including; the open di-cubanes **9a/9b** (M = Ni, n = 0, X = Cl), **10a/10b** (M = Ni, n = 0, X = Br), the closed cubane **11a** (M = Ni, n = 1, X = H), the trimers **16a** (M = Cu, n = 0, X = Cl), **16b** (M = Cu, n = 0, X = H), the hydrogen bonded network of dimers **18a** (M = Cu, n = 2, X = H), **19** (M = Cu, n = 3, X = H), the hydrogen bonded network of monomers **17a**, **17a'** (M = Cu, n = 1, X = H) and, the monometallic complexes **12a** (M = Ni, n = 1, X = H), *trans*-**13a** and *cis*-**14** (M = Ni, n = 2, X = H) have been synthesised and fully characterised. However, the reaction of only $bnzH_2$ with copper acetate yields a monometallic complex **21** and the reaction of $bnzH_2$ with copper acetate in the presence of sodium methoxide (change of base), results in the copper-disodium polymer **22**.

If $bnzH_2$ (possessing α-OH) is replaced with diphenylacetic acid (possessing α-H) in the ligand blend, significant changes in the structural type, nuclearity, bonding modes and non-covalent interactions of the resulting complexes are found. For example; (*i*) *there are fewer bonding modes e.g.*, 1,4-chelating bonding modes are only obtained from benzilate ligands which possess a second α-hydroxide/alkoxide binding domain, (*ii*) *there are different bonding modes observed from the co-ligands e.g.*, 1.01-*N*-bound chp in **19** *vs.* 2.21-bound hppH in **20**, (*iii*) *the availability of intramolecular intra-ligand hydrogen bonding interactions e.g.*, α-O···O_{COO} is established in **11a**, **12a**, **13a**, **14a**, **17a** and **18a**, however, this interaction cannot be found in **11b**, **12b**, **13b**, **14b**, **17b** and **18b** and (*iv*) *the*

availability of intermolecular hydrogen bonding interactions e.g., α-O···O_{COO} present in **17a** not **17b**, α-O···O_{hep} exhibited in **18a** not **18b** and O_{hppH}···O_{COO} shown in **19** not **20**.

In conclusion, the factors governing benzilate complexation in this work would appear to depend on a combination of factors. Firstly, *the nature of the precursor transition metal ion* affects the structural geometry and final nuclearity. Secondly, *the pK_a values of the ligand blend* influences the numbers and types of bonding modes present, as well as non-covalent interactions. For example, the benzilate moiety displays several bonding modes and hydrogen bonding interactions from both carboxylate and α-hydroxyl bonding domains depending on the type of 2-pyridine alcohol employed. Thirdly, *the methylene chain length of the 2-pyridine alcohol* influences the nuclearity as a chelating/non-chelating ligand. Fourthly, *the type of base employed* in directing complexation with or without self-incorporation *e.g.*, NEt_3 in some cases leads to the formation of a salt. In contrast, the ionic base NaOMe can dissociate and incorporate itself within the final complex (*e.g.*, **22**). Fifthly, *the solvents employed* influence solubility and crystallisation with solvent incorporation as in **22** or without self-incorporation as observed in most cases. Finally, *the general reaction conditions* determine the final product type, for example, monomer **12a** and tetramer **11a** co-crystallise under standard reaction conditions. However, these can be synthesised exclusively by modifying the reaction environment.

Preliminary ^{1}H NMR, EPR spectroscopic and variable temperature magnetic SQUID measurements reveal several types of interesting magnetic behaviour from the complexes and will be the subject of further possible investigations.

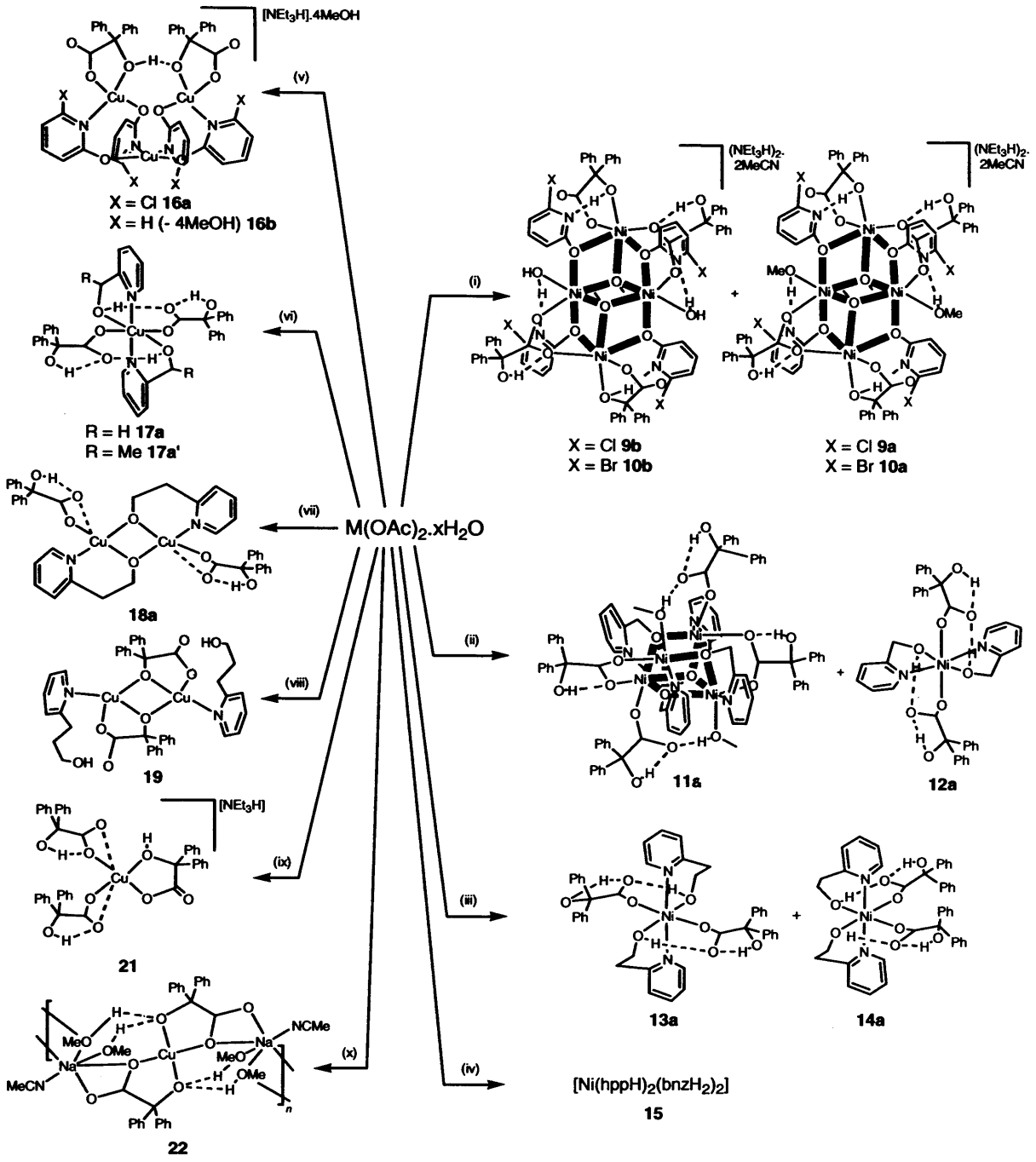

Scheme 12 Overview of chemistry carried out in Chapter 3. General reagents: $M(OAc)_2 \cdot xH_2O$, $bnzH_2$, 2-$\{(CH_2)_n$-OH$\}$-6-X-C_5H_3N, NEt_3 and $MeCN/CH_2Cl_2/MeOH$; M = Ni, x = 4; [(i) X = Cl, n = 0 or X = Br, n = 0; (ii) X = H, n = 1; (iii) X = H, n = 2; (iv) X = H, n = 3] M = Cu, x = 1 [(v) X = Cl, n = 0 or X = H, n = 0; (vi) X = H, n = 1; (vii) X = H, n = 2; (viii) X = H, n = 3]. (ix) $Cu(OAc)_2 \cdot H_2O$, $bnzH_2$, NEt_3 and $MeCN/CH_2Cl_2/MeOH$. (x) $Cu(OAc)_2 \cdot H_2O$, $bnzH_2$, 2-$\{(CH_2)_n$-OH$\}$-6-X-C_5H_3N,.NaOMe and $MeCN/CH_2Cl_2/MeOH$.

3.5 References

1. *See references and patents therein* (*a*) S. B. Hanna and S. A. Serac, *J. Org. Chem.*, 1977, **42**, 2069; (*b*) ACS, *SciFinder Scholar*, Substance Database, 2005; (*c*) I. Spasojević, H. Boukhalfa, R. D. Stevens and A. L. Crumbliss, *Inorg. Chem.*, 2001, **40**, 49; (*d*) S. Hati, R. J. Batchelor, F. W. B. Einstein and A. S. Tracey, *Inorg. Chem.*, 2001, **40**, 6258; (*e*) C. Redshaw, M. R. J. Elsegood, K. E. Holmes, *Angew. Chem. Int. Ed., Engl.*, 2005, **44**, 1850; (*f*) A. Abdurahman, H. Izumisawa, H. Saito and Y. Hasegawa, *Proc. Symp. Solvent Extr.*, 1987, 49; (*g*) Y. Hasegawa, M. Tanaka, Miho, A. Ishimori, *Journal of Trace and Microprobe Techniques*, 1998, 16, 1; (*h*) D. Zhou, D. Feng, Y. Xie, R. Qiu and B. Jin, *Fenxi Huaxue*, 1986, **14**, 650; (*i*) S. B. Hanna and S. A. Serac, *J. Org. Chem.*, 1977, **42**, 2069.
2. (*a*) P. Chaudhuri, E. Rentschler, F. Birkelbach, C. Krebs, E. Bill, T. Weyhermüller and U. Flörke, *Eur. J. Inorg. Chem.*, 2003, 541; (*b*) B. P. Baranwal, S. S. Das, P. Singh and T. Gupta, *Indian J. Chem. Soc., Sect. A*, 2001, **40**, 320; (*c*) B. P. Baranwal, S. S. Das and P. Singh, *Indian J. Chem. Soc., Sect. A*, 1998, **28**, 1689; (*d*) Y. M. Issa, W. F. El-Hawary, H. A. Abdel-Salam and M. R. Issa, *Transition Metal Chem.*, 1995, **20**, 423; (*e*) S.-X. Liu and X. Wang, *Gaodeng Xue Xiao Huaxue Xuebao*, 1996, **17**, 169; (*f*) S. K. Agarwal and D. Goel, *Oriental J. Chem.*, 1989, **5**, 261; (*g*) B. K. Mohanty, B. C. Samantary, G. Sahu, B. K. Mohapatra, *J. Indian Chem. Soc.*, 1987, **64**, 570.
3. (*a*) R. Carballo, B. Covelo, S. Balboa, A. Castiñeiras and J. Niclós, *Z. Anorg. Allg. Chem.*, 2001, **627**, 948; (*b*) R. Carballo, A. Castineiras, B. Covelo, E. Garcia-Martinez, J. Niclos and E. M. Vazquez-Lopez, *Polyhedron* , 2004, **23**, 1505.
4. C. P. Raptopoulou, V. Tangoulis and E. Devlin, *Angew. Chem., Int. Ed. Engl.*, 2002, **41**, 2386.
5. *CCDC, Cambridge Crystallographic Database*, search, 2005.
6. (*a*) M. Frey, S. G. Harris, J. M. Holmes, D. A. Nation, S. Parsons, P. A. Tasker and R. E. P. Winpenny, *Chem. Eur. J.*, 2000, **6**, 1407; (*b*) C. Cañada-Vilalta, T. A. O'Brien, M. Pink, E. R. Davidson and G. Christou, *Inorg. Chem.*, 2003, **42**, 7819; (*c*) K. L. Taft, C. D. Delfs, G. C. Papaefthymiou, S. Foner, D. Gatteschi and S. J. Lippard, *J. Am. Chem. Soc*, 1994, **116**, 823; (*d*) C. Benelli, S. Parsons, G. A. Solan and R. E. P. Winpenny, *Angew. Chem. Int. Ed., Engl.*, 1996, **35**, 1825; (*e*) *Personal Communication*, G. A. Solan, 2005.
7. ACS, *SciFinder Scholar*, Substance database, 2004.
8. *Polyoxometallate-based open di-cubanes* (*a*) J. M. Clemente-Juan, E. Coronado, J. R. Galán-Mascarós and C. J. Gómez-García, *Inorg. Chem.*, 1999, **38**, 55; (*b*) T. Kurata, A. Uehara, Y. Hayashi and K. Isobe, *Inorg. Chem.*, 2005, **44**, 2524.
9. Z. E. Serna, L. Lezama, M. K. Urtiaga, M. I. Arriortua, M. G. Barandika, R. Cortés and T. Rojo, *Angew. Chem., Int. Ed. Engl.*, 2000, **39**, 344.
10. T. K. Karmakar, S. K. Chandra, J. Ribas, G. Mostafa, T. H. Liu and B. K. Ghosh, *Chem. Commun.*, 2002, 2364.
11. P. King, R. Clérac, W. Wernsdorfer, C. E. Anson and A. K. Powell, *Dalton Trans.*, 2004, 2670.
12. R. K. Hocking and T. W. Hambley, *Inorg. Chem.*, 2003, **42**, 2833. [For Ni(II): range ~ 1.263 – 1.268 Å ⇒ ~15 – 20% covalent C-O bond character; for Cu(II): range ~ 1.248 – 1.256 Å ⇒ ~ 0 – 5% covalent C-O bond character].
13. (*a*) J. E. Andrew and A. B. Blake, *J. Chem. Soc., Sect. A*, 1969, 1456; (*b*) J. A. Bertrand, A. P. Ginsberg, R. I. Kaplan, C. E. Kirkwood, R. L. Martin and R. C. Sherwood, *Inorg. Chem.*, 1971, **10**, 240; (*c*) B. Aurivillius, *Acta Chemica Scandinavica, Sect. A*, 1977, **31**, 501; (*d*) W. L. Gladfelter, M. W. Lynch, W. P. Schaefer, D. N. Hendrickson and H. B. Gray, *Inorg. Chem.*, 1981, **20**, 2390; (*e*) F. Paap, E. Bouwman, W. L. Driessen, R. A. G. de Graaf and J. Reedijk, *J. Chem. Soc., Dalton Trans.*, 1985, 737; (*f*) M. A. Halcrow, J.-S. Sun, J. C. Huffman and G. Christou, *Inorg. Chem.*, 1995, **34**, 4167; (*g*) M. S. E. Fallah, E. Rentschler, A. Caneschi and D. Gatteschi, *Inorg. Chim. Acta*, 1996, **247**, 231; (*h*) M.-L. Tong, H. K. Lee, S.-L. Zhang and X.-M. Chen, *Chem. Lett.*, 1999, 1087; (*i*) J. M. Clemente-Juan, B. Chansou, B. Donnadieu and J.-P. Tuchagues, *Inorg. Chem.*, 2000, **39**, 5515; (*j*) M.-L. Tong, S.-L. Zheng, J.-X. Shi,

Y.-X. Tong, H. K. Lee and X. M. Chen, *J. Chem. Soc., Dalton Trans.*, 2002, 1727; (*k*) S. Mukherjee, T. Weyhermüller, E. Bothe, K. Wieghardt and P. Chaudhuri, *Eur. J. Inorg. Chem.*, 2003, 853; (*l*) G. Aromi, A. S. Batsanov, P. Christian, M. Helliwell, O. Roubeau, G. A. Timco and R. E. P. Winpenny, *Dalton Trans.*, 2003, 4466; (*m*) *example of a vertex sharing di-cubane* T. D. Keene, M. B. Hursthouse and D. J. Price, *New J. Chem.*, 2004, 558; (*n*) M. Moragues-Cánovas, M. Helliwell, L. Ricard, E. Rivière, W. Wernsdorfer, E. Brechin and T. Mallah, *Eur. J. Inorg. Chem.*, 2004, 2219; (*o*) A. Sieber, C. Boskovic, R. Bircher, O. Waldemann, S. T. Ochsenbein, G. Chaboussant, H. U. Güdel, N. Kirchner, J. van Slageren, W. Wernsdorfer, A. Neels, H. Stœckli-Evans, S. Janssen, F. Juranyi and H. Mutka, *Inorg. Chem.*, 2005, **44**, 4315.

14. (*a*) A. J. Blake, E. K. Brechin, A. Codron, R. O. Gould, C. M. Grant, S. Parsons, J. M. Rawson and R. E. P. Winpenny, *J. Chem. Soc., Chem. Commun.*, 1995, 1983; (*b*) K. Bizilj, S. G. Hardin, B. F. Hoskins, P. J. Oliver, E. R. Tiekink and G. Winter, *Aust. J. Chem.*, 1986, **39**, 1035.

15. (*a*) A. Escuer, M. Font-Bardía, S. B. Kumar, X. Solans and R. Vicente, *Polyhedron*, 1999, **18**, 909; (*b*) E.-Che, C. Kirman, J. Lawrence, L. N. Zakharov, A. L. Rheingold, S. Hill and D. N. Hendrickson, *Inorg. Chem.*, 2005, **44**, 3827; (*c*) E.-C. Yang, W. Wernsdorfer , S. Hill, R. S. Edwards, M. Nakano, S. Maccagnano, L. N. Zakharov, A. L. Rheingold, G. Christou and D. N. Hendrickson, *Polyhedron*, 2003, **22**, 1727.

16. (*a*) S. Ferrer, F. Lloret, I. Bertomeu, G. Alzuet, J. Borrás, S. García-Granda, M. L.-González and J. G. Haasnoot, *Inorg. Chem.*, 2002, **41**, 5821; (*b*) G. A. van Albada, O. Roubeau, I. Mutikainen, U. Turpeinen and J. Reedijk, *New. J. Chem.*, 2003, **27**, 1693; (*c*) G. Dong, Q. Chun-qi, D: Chun-ying, P. Ke-liang and M. Qing-jin, *Inorg. Chem.*, 2003, **42**, 2024; (*d*) R. Boča, L. Dlháň, G. Mezei, T. Ortiz-Pérez, R. G. Raptis and J. Telser, *Inorg. Chem.*, 2003, **42**, 5801; (*e*) A. Mukherjee, I. Rudra, S. G. Naik, S. Ramasesha, M. Nethaji and A. R. Chakravarty, *Inorg. Chem.*, 2003, **42**, 5660; (*f*) M. I. Belinsky, *Inorg. Chem.*, 2004, **43**, 739; (*g*) T. Glaser, M. Heidemeier, S. Grimme and E. Bill, *Inorg. Chem.*, 2004, **43**, 5192; (*h*) M. Casarin, C. Corvaja, C. di Nicola, D. Falcomer, L. Franco, M. Monari, L. Pandolfo, C. Pettinari, F. Piccinelli and P. Tagliatesta, *Inorg. Chem.*, 2004, **43**, 5865; (*i*) J. Yoon, L. M. Mirica, D. P. Stack and E. I. Solomon, *J. Am. Chem. Soc.*, 2004, **126**, 12586; (*j*) B. Lucchese, K. J. Humphreys, D.-H. Lee, C. D. Incarvito, R. D. Sommer, A. L. Rheingold and K. D. Karlin, *Inorg. Chem.*, 2004, **43**, 5987; (*k*) H. López-Sandoval, R. Contreras, A. Escuer, R. Vicente, S. Bernès, H. Nöth, G. J. Leigh and N. Barba-Behrens, *J. Chem. Soc., Dalton Trans.*, 2002, 2648; (*l*) Q.-Y. Chen, Z.-Q. Pan, Q.-H. Luo, L.-M. Zhen, X.-L. Hu, Z.-L. Wang, Z.-Y. Zhou and C.-H. Yeung, *J. Chem. Soc., Dalton Trans.*, 2002, 1315; (*m*) J. Sanmartín, M. R. Bermejo, A. M. García-Deibe, O. R. Nascimento, L. Lezama and T. Rojo, *J. Chem. Soc., Dalton Trans.*, 2002, 1030; (*n*) B. Graham, L. Spiccia, G. D. Fallon, M. T. W. Hearn, F. E. Mabbs, B. Moubaraki and K. S. Murray, *J. Chem. Soc., Dalton Trans.*, 2002, 1226; (*o*) L. Santagostini, M. Gullotti, R. Pagliarin, E. Monzani and L. Casella, *Chem. Commun.*, 2003, 2186; (*p*) G. Seeber, P. Kögerler, B. M. Kariuki and L. Cronin, *Chem. Commun.*, 2004, 1580; (*q*) R. S. Rarig, Jr. and J. Zubieta, *Dalton Trans.*, 2004, 1861; (*r*) J. K. Clegg, L. F. Lindoy, B. Moubaraki, K. S. Murray and J. C. McMurtrie, *Dalton Trans.*, 2004, 2417; (*s*) M. C. Mimmi, M. Gulloti, L. Santagostini, J. Battaini, E. Monzani, R. Pagliarin, G. Zoppellaro and L. Casella, *Dalton Trans.*, 2004, 2192; (*t*) J.-K. Cheng, Y.-G. Yao, J. Zhang, Z.-J. Li, Z.-W. Cai, X.-Y. Zhang, Z.-N. Chen, Y.-B. Chen, Y. Kang, Y.-Y. Qin and Y.-H. Wen, 2004, **126**, 7796; (*t*) X. Liu, M. P. de Miranda, E. J. L. McInnes, C. A. Kilner and M. A. Halcrow, *Dalton Trans.*, 2004, 59; (*u*) F. Tuna, J. Hamblin, A. Jackson, G. Clarkson, N. W. Alcock and M. J. Hannon, *Dalton Trans.*, 2003, 2141; (*v*) S. Demeshko, G. Leibeling, S. Dechert and F. Meyer, *Dalton Trans.*, 2004, 3782; (*w*) B. Cage, F. A. Cotton, N. S. Dalal, E. A. Hillard, B. Rakvin and C. M Ramsey, *J. Am. Chem. Soc.*, 2003, **125**, 5270; (*x*) Y.-B. Jiang, H.-Z. Kou, R.-J. Wang, A.-L. Cui and J. Ribas, *Inorg. Chem.*, 2005, **44**, 709; (*y*) Z. Mao, J.-S. Huang, C.-M. Che, N. Zhu, S. K.-Y. Leung and Z.-Y. Zhou, *J. Am. Chem. Soc.*, 2005, **127**, 4562; (*z*) S.-L. Ma, W.-X. Zhu, S. Gao, Q.-L. Guo and M-Q. Xu, *Eur. J. Inorg. Chem.*, 2004, 1311.

17. (*a*) J. Tercero, C. Diaz, M. S. E. Fallah, J. Ribas, X. Solans, M. A. Maestro and J. Mahía, *Inorg. Chem.*, 2001, **40**, 3077; (*b*) J. Tercero, C. Diaz, J. Ribas, J. Mahía and M. A. Maestro, *Inorg. Chem.*, 2002, **41**, 5373; (*c*) J. F. Berry, F. A. Cotton, P. Lei and C. A. Murillo, *Inorg. Chem.*, 2003, **42**, 377; (*d*) J. F. Berry, F. A. Cotton, L. M. Daniels, C. A. Murillo and X. Wang, *Inorg. Chem.*, 2003, **42**, 2418; (*e*) P. King, R. Clérac, C. E. Anson, C. Coulon and A. K. Powell, *Inorg. Chem.*, 2003, **42**, 3492; (*f*) M. Wei, R. D. Willett and C. J. Gómez-García, *Inorg. Chem.*, 2004, **43**, 4534; (*g*) I. Castro, M. L. Calatayud, F. Lloret, J. Sletten and M. Julve, *J. Chem. Soc., Dalton Trans.*, 2002, 2397; (*h*) J. Tercero, C. Diaz, J. Ribas, J. Mahía, M. Maestro and X. Solans, *J. Chem. Soc., Dalton Trans.*, 2002, 2040; (*i*) S. L. Jain, P. Bhattacharyya, H. L. Milton, A. M. Z. Slawin, J. A. Crayston and J. D. Woolins, *Dalton Trans.*, 2004, 862.

18. J. M. Rowland, M. M. Olmstead and P. K. Mascharak, *Inorg. Chem.*, 2002, **41**, 2754.

19. A. C. Warden, M. T. W. Hearn and L. Spiccia, *Inorg. Chem.*, 2003, **42**, 7037.

20. B. Bleaney and K. D. Bowers, *Proc. Roy. Soc., Sect. A*, 1952, **214**, 451.

21. O. Kahn, *Chem. Phys. Lett.*, 1997, **265**, 109.

22. (*a*) O. Kahn, in *Molecular Magnetism*, VCH publishers, USA, 1993, pp. 211 – 218.; (*b*) *ibid.*, Chapter 2, [Calculated spin-only values: expected Ni(II) 2.83 BM possessing two unpaired electrons, $\chi_M T$ = 1.00 emu K mol^{-1}; Cu(II) 1.73 BM, $\chi_M T$ = 0.38 emu K mol^{-1}; 2 × Cu(II) 2.45 BM, $\chi_M T$ = 0.75 emu K mol^{-1} with each possessing one unpaired electron]; (*c*) ***PLEASE NOTE*** the Evans balance is sometimes ineffective at measuring accurate magnetic data which is mainly due to environmental effects *e.g.*, fluctuations in temperature.

23. C. A. Koch, C. A. Reed, G. Brewer, N. P. Rath, W. R. Scheidt, G. P. Gupta and G. Lang, *J. Am. Chem. Soc.*, 1989, **111**, 7645.

24. A. Bencini, C. Benelli, A. Dei and D. Gatteschi, *Inorg. Chem.*, 1985, **24**, 695.

25. D. H. Williams and I. Fleming, in Spectroscopic Methods in Organic Chemistry, 5th Edn., 1995, McGraw Hill, Gt. Britain.

26. Compared to solid-state IR spectrum of the precursor 2-pyridine alcohol.

27. (*a*) E. Szajna, P. Dobrowolski, A. L. Fuller, A. M. Arif and L. M. Berreau, *Inorg. Chem.*, 2004, **43**, 3988; (*b*) R. H. Holm, *J. Magn. Resonance*, 1970, **2**, 307; (*c*) F. F.-L. Ho, L. E. Erickson, S. R. Watkins and C. N. Reiley, *Inorg. Chem.*, 1970, **9**, 1139; (*d*) R. V. Snyder and R. J. Angelici, *Inorg. Chem.*, 1974, **13**, 14; (*e*) M. N. Murthy, K. D. Karlin, I. Bertini and C. Luchinat, *J. Am. Chem. Soc.*, 1997, **119**, 2156; (*f*) T. C. Higgs, N. S. Dean and C. J. Carrano, *Inorg. Chem.*, 1998, **37**, 1473; (*g*) C. Belle, C. Bougault, M.-T. Averbuch, A. Durif, J.-L. Pierre, J.-M. Latour and L. L. Pape, *J. Am. Chem. Soc.*, 2001, **123**, 8053; (*h*) I. Bertini, I. C. Felli and C. Luchinat, *J. Magn. Resonance*, 1998, **134**, 360; (*i*) I. Bertini, S. Ciurli, A. Dikiy, R. Gasanov, C. Luchinat, G. Martini and N. Safarov, *J. Am. Chem. Soc.*, 1999, **121**, 2037; (*j*) C. O Fernández, J. A. Cricco, J. H. Richards, H. B. Gray and A. J. Vila, *J. Am. Chem. Soc.*, 2001, **123**, 11678; (*k*) J. Park, J. Y. Kim, H. So and J. Liu, *Inorg. Chim. Acta*, 2001, **319**, 8; (*l*) G. N. La Mar, W. DeW. Horrocks, Jr. and R. H. Holm, in *NMR of Paramagnetic Molecules; Principles and Applications*, Academic Press, London, 1973, 243 – 332.

28. *Example of a typical Cu(II)-based polymer* fitted *to Curie-Weiss law* R. C. Finn, J. Sims, C. J. O'Connor and J. Zubieta, *J. Chem. Soc., Dalton Trans.*, 2002, 159.

29. M. A. Halcrow, *Dalton Trans.*, 2003, 4375.

30. (*a*) A. F. Orchard, in *Magnetochemistry*, Oxford Chemistry Primers, Oxford University Press, No. 75, UK, 2003, pp. 157 – 159; (*b*) *ibid.* p. 9.

Chapter 4

4.0 Blending Isopthalic Acid and L^2 (L^2 = 2-Pyridine Alcohols, α-Diimines or Formamidines) on a Ni(II) or Cu(II) Centre

In this chapter, the synthetic, structural and physical studies of complexes prepared from the reactions of ligand blends composed of isopthalic acid [1,3-$(CO_2H)_2$-C_6H_4] and an *N,O*- or *N,N'*-donor (section 4.3) with transition metal ions are reported.

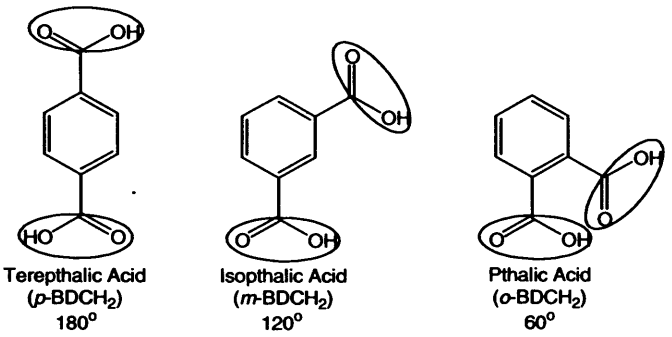

Figure 1 Benzenedicarboxylic acids; angles between encircled binding domains are shown.

Isopthalic acid (*m*-$BDCH_2$) [pK_a 3.53; pK_1 4.78, pK_2 5.98][6a,6b] belongs to a family of benzenedicarboxylic acids that have been widely used to synthesise supramolecular complexes, polymeric coordination networks[1,2] and have also featured in the formation of discrete paramagnetic complexes (Chapter 1, section 1.2.3).[3-5] *m*-$BDCH_2$ itself possesses two potential coordination sites (*viz.*, carboxylic acid groups) subtended by an angle of 120° for binding transition metal ions (Figure 1).

Based on a search of the crystallographic database, the deprotonated forms of isopthalic acid, isopthalate (*m*-BDC^{2-}/*m*-$BDCH^{1-}$), can exhibit several types of bonding mode (Figure 2). Isopthalate ligands are usually classified as being bound either *syn-* or *anti-* with respect to the carboxylate oxygen lone pairs.[31] Furthermore, the metal ion may be coordinated either adjacent to C(4)/C(6) or C(2) on the *m*-BDC phenyl ring, therefore, these will be described as either type 1 or type 2 bonding modes, respectively in this work [Figure 2 and Scheme 1].

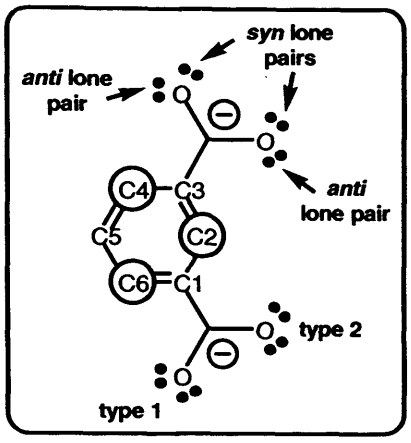

Figure 2 Isopthalate bonding mode convention to be employed for the structural descriptions with C(2) and C(4)/C(6) encircled.

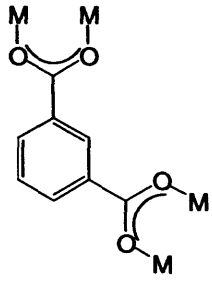	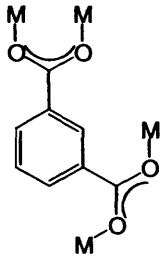	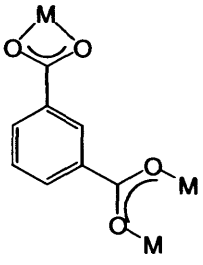	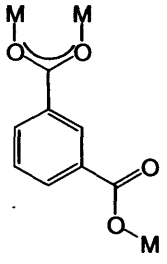	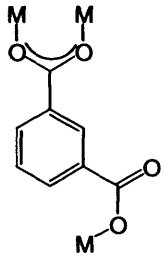	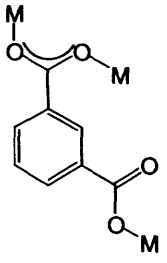
dianionic	dianionic	dianionic	dianionic	dianionic	dianionic
bis-η^1, η^1: *syn, syn*	η^1, η^1: *syn, syn* and η^1, η^1: *anti, anti*	η^1, η^1: *syn, syn*	η^1, η^1: *syn, syn* and type 1, η^1: *syn*	η^1, η^1: *syn, syn* and type 1, η^1: *anti*	type 1, η^1: *syn,* type 2, η^1: *anti* and type 1, η^1 : *syn*
bis-1,3-bridging	bis-1,3-bridging	chelating and 1,3-bridging	1,3-bridging and monodentate	1,3-bridging and monodentate	1,3-bridging and monodentate
(a)	(b)	(c)	(d)	(e)	(f)
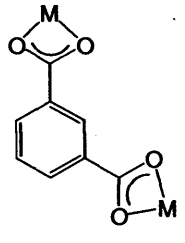	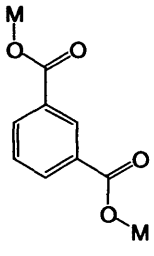	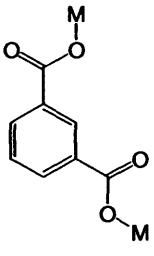	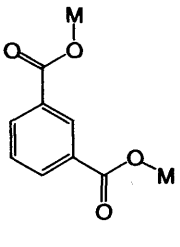	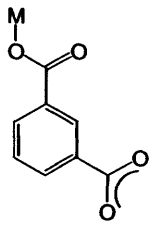	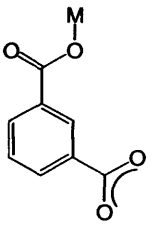
dianionic	dianionic	dianionic	dianionic	dianionic	dianionic	monoanionic
bis-η^1, η^1: *syn-syn*	bis-type 1, η^1: *syn*	type 1, η^1: *syn* and type 2, η^1: *syn*	bis-type 2, η^1: *syn*	type 1, η^1: *syn*	type 2, η^1: *syn*	type 1, η^1: *syn,* type 2, η^1: *anti*
bis-chelating	bis-monodentate	bis-monodentate	bis-monodentate	monodentate	monodentate	1,3-bridging
(g)	(h)	(i)	(j)	(k)	(l)	(m)

Scheme 1 Reported bonding modes for *m*-BDC (a – m) using the convention described in Figure 2 [CCDC database search 2005].

The main aim of this chapter is to focus on the coordination chemistry of divalent nickel and copper ions supported by ligands derived from both *m*-$BDCH_2$ and 2-pyridine alcohols [2-{$(CH_2)_nOH$}-C_5H_4N]. As in previous chapters, a key objective is to systematically examine the effect of the pyridine alcohol methylene chain length (n = 1 – 3) on product type (sections 4.1 and 4.2). As a secondary aim, reactions of ligand blends based on combinations of *m*-$BDCH_2$/α-diimine and *m*-$BDCH_2$/formamidine (HDLF) with copper acetate monohydrate will also be probed (section 4.3). Steric and electronic variation of the HDLF aryl substituents in the latter combinations are investigated as an additional sub-section. Spectroscopic/spectrometric data and magnetic measurements are used, in many cases, to support and complement the single crystal X-ray determinations. Scheme 2 shows the general synthetic strategy to be employed along with the stoichiometry of reagents and the solvents used.

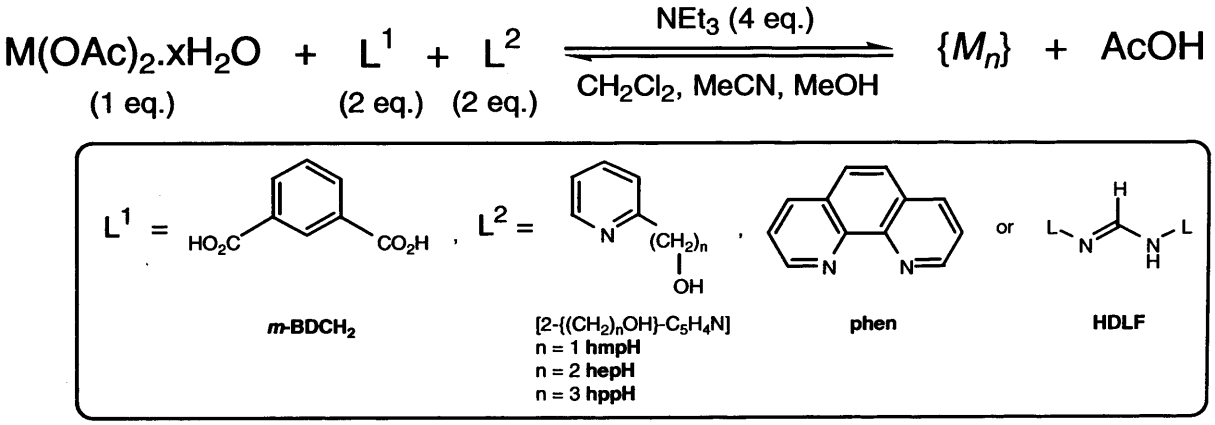

Scheme 2 General synthetic strategy to be employed.

4.1 Blending Isopthalic Acid and 2-Pyridine Alcohols on a Ni(II) Centre

4.1.1 M = Ni, L^1 = *m*-$BDCH_2$, L^2 = hmpH (n = 1)

The reaction of nickel(II) acetate tetrahydrate with *m*-$BDCH_2$ and hmpH in the presence of triethylamine gave, on work-up, crystals of the binuclear complex $[Ni_2(hmpH)_4(m\text{-}BDC)_2]\cdot 1.5MeCN$ (**23a**) in low yield (Scheme 3). Use of mehmpH in place of hmpH also affords a dimeric species of composition $[Ni_2(mehmpH)_4(m\text{-}BDC)_2]$ (**23a'**). Complexes

23a and **23a'** were characterised by elemental analysis, IR spectroscopy, variable temperature SQUID magnetometry (see Appendices, Table 1) and positive FAB mass spectrometry. A single crystal of **23a** was subject to an X-ray diffraction study. The molecular structure of **23a** is shown in Figure 3(a); selected bond lengths and angles are given in Table 1.

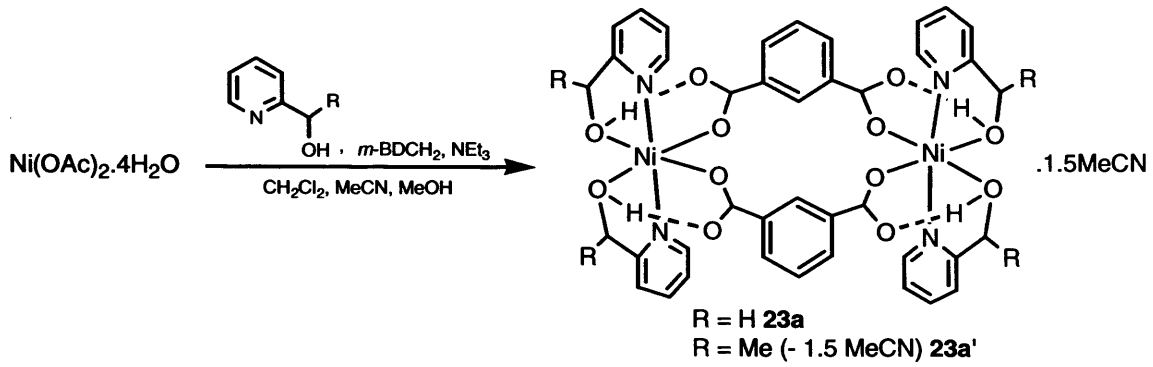

Scheme 3 Synthesis of **23**.

Two independent molecules were found within the unit cell of **23a**, only one of these will be considered as they are essentially similar. The molecular structure of **23a** reveals a bimetallic species in which two distorted octahedral Ni(II) ions are bridged by two *m*-BDC ligands, and each bound terminally by two *N,O*-chelating hmpH ligands. The two 1.11 hmpH ligands form five-membered chelate rings with each Ni(II) centre, with the pyridine moieties of each hmpH positioned mutually *trans*. One of the hmpH ligands at each metal centre is bound more strongly than the other as indicated by the bond lengths of Ni(1)-$O_{hmpH}(2)$ = 2.070(6) Å and Ni(1)-$N_{hmpH}(2)$ = 2.033(8) Å, which are shorter than Ni(1)-$O_{hmpH}(1)$ = 2.091(5) Å and Ni(1)-$N_{hmpH}(1)$ = 2.051(8) Å from the second hmpH ligand. The hmpH-containing chelate bite angle averaging to 84.6(2)° is acute. The bridging *m*-BDC carboxylate oxygen atoms adopt the bis-type 2, η^1: *syn*, monodentate bonding mode with Ni-O bond lengths of 2.024(5) Å [Ni(1)-$O_{m\text{-}BDC}(3)$] and 2.019(5) Å [Ni(1A)-$O_{m\text{-}BDC}(5)$] [Scheme 1(j)].[31].

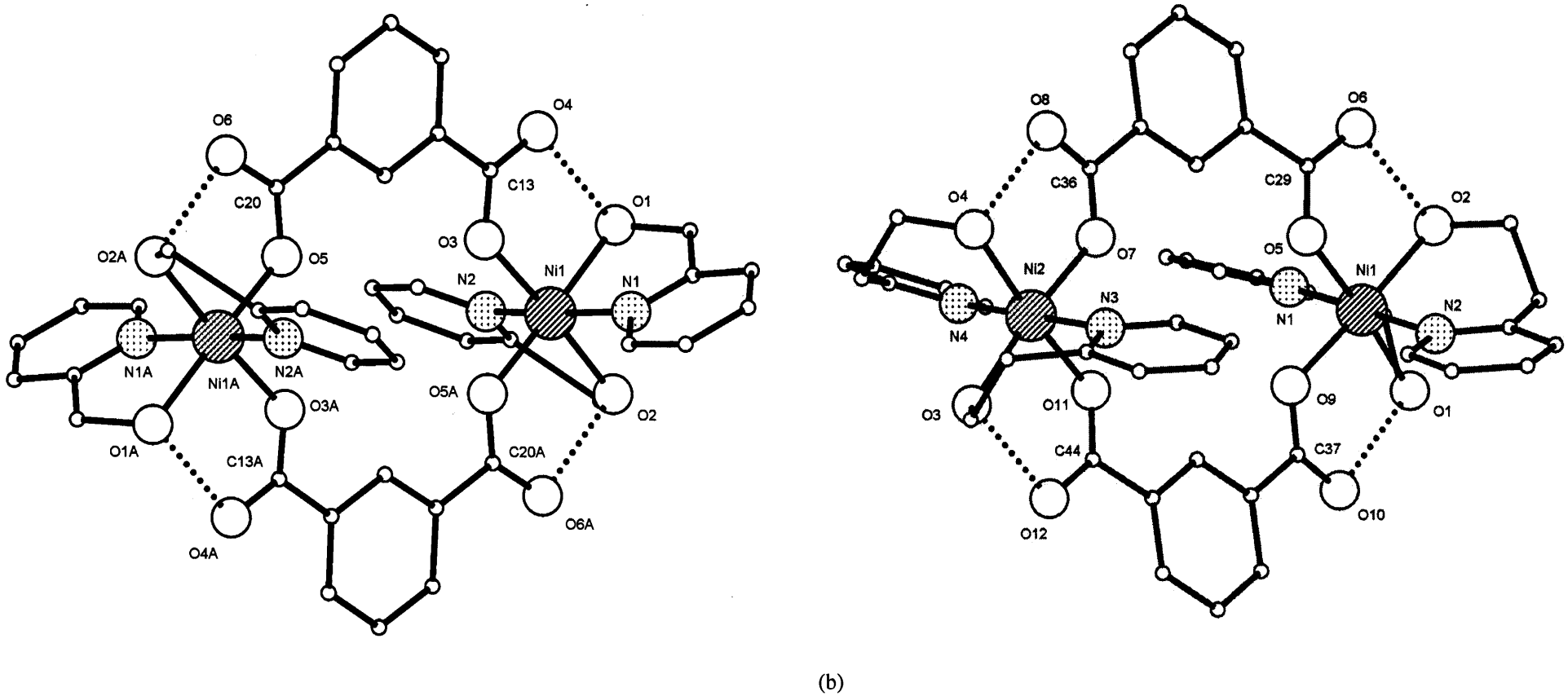

(a) (b)

Figure 3 Molecular structures of (a) **23a** and (b) **23b**. Hydrogen atoms and solvent molecules are excluded for clarity. Dotted lines indicate hydrogen bonding interactions.

Table 1 Selected bond length (Å) and angle (°) data for complex **23a**

23a							
Ni(1)-O(1)	2.091(5)	Ni(1)-O(5)#1	2.019(5)	Ni(2)-O(9)	2.017(6)	Ni(1)-N(2)	2.033(8)
Ni(1)-O(2)	2.070(6)	Ni(2)-O(7)	2.088(6)	Ni(2)-O(11)#2	2.014(5)	Ni(2)-N(3)	2.072(7)
Ni(1)-O(3)	2.024(5)	Ni(2)-O(8)	2.058(6)	Ni(1)-N(1)	2.051(8)	Ni(2)-N(4)	2.048(7)
O(2)-Ni(1)-O(1)	90.8(2)	O(8)-Ni(2)-O(7)	91.3(2)	O(3)-Ni(1)-N(1)	93.1(2)	O(8)-Ni(2)-N(3)	88.7(3)
O(3)-Ni(1)-O(1)	91.5(2)	O(11)#2-Ni(2)-O(7)	92.5(2)	O(3)-Ni(1)-N(2)	93.7(3)	O(9)-Ni(2)-N(3)	92.7(2)
O(5)#1-Ni(1)-O(1)	175.2(2)	O(11)#2-Ni(2)-O(8)	175.7(2)	O(5)#1-Ni(1)-N(1)	96.1(3)	O(9)-Ni(2)-N(4)	94.3(2)
O(3)-Ni(1)-O(2)	176.4(2)	O(11)#2-Ni(2)-O(9)	85.5(2)	O(5)#1-Ni(1)-N(2)	92.5(3)	O(11)#2-Ni(2)-N(3)	93.9(3)
O(5)#1-Ni(1)-O(2)	91.7(2)	N(1)-Ni(1)-O(1)	81.0(2)	N(3)-Ni(2)-O(7)	81.8(2)	O(11)#2-Ni(2)-N(4)	93.5(2)
O(5)#1-Ni(1)-O(3)	84.8(2)	N(1)-Ni(1)-O(2)	88.2(2)	N(4)-Ni(2)-O(7)	91.4(3)	N(2)-Ni(1)-N(1)	169.5(2)
O(9)-Ni(2)-O(7)	174.0(2)	N(2)-Ni(1)-O(1)	90.8(2)	N(4)-Ni(2)-N(8)	84.3(3)	N(4)-Ni(2)-N(3)	170.2(3)
O(9)-Ni(2)-O(8)	90.8(2)	N(2)-Ni(1)-O(2)	85.5(3)				

Symmetry transformations used to generate equivalent atoms; #1 (– *x*+2, – *y*+2, – *z* + 1), #2 (– *x*, – *y* + 1, – *z*).

The *m*-BDC C-O bonds lengths involving the bound and unbound oxygen atoms in **23a** are similar with C-O distances averaging to 1.240 Å (bound) and 1.245 Å (unbound). The former distance indicates that the carboxylate-metal bonds have mainly ionic character [for Ni(II): range ~ 1.263 – 1.268 Å ⇒ ~ 15 – 20% covalent C-O bond character].[9] Intramolecular inter-ligand hydrogen bonding interactions in **23a** are observed between the oxygen atom of the unbound carboxylate oxygen atom and the hmpH hydroxyl substituents [$O_{hmpH}(1)\cdots O_{m\text{-}BDC}(4)$ = 2.514(8) Å and $O_{hmpH}(2)\cdots O_{m\text{-}BDC}(6A)$ = 2.495(9) Å].

Complex **23a** represents the first example of a crystallographically characterised bimetallic nickel complex containing isopthalate bridging ligands.[7] The Ni···Ni distance at 7.789(5) Å is at the top end of the range for $\{Ni(II)_2\}$ complexes. For example, complexes $[Ni\{(Dtox)_2(o\text{-}C_6H_4(CNH)_2\}]_2(ClO_4)_4$ [Dtox = $(ON=\{Me\}CCH_2SCH_2CH_2SCH_2\text{-}C\{Me\}=NO)^{2-}$][7a] and $[Ni_2(L1)_2(H_2O)_2](NO_3)_4$ (L1 = $C_6H_5N\text{-}C(NH_2)=N\text{-}NH\text{-}C_8H_4NN\text{-}C_6H_5N\text{-}C(NH_2)=N\text{-}NH$),[8b] display M···M distances of ~ 6 Å.

The IR spectrum of **23a** shows a broad ν(OH) stretching band at 3449 cm^{-1} along with two strong bands corresponding to $\nu(CO_2)_{asymm}$ (1605 cm^{-1}) and $\nu(CO_2)_{symm}$ (1382 cm^{-1}) stretches.[13] Similarly, the IR spectrum of **23a'** shows a broad ν(OH) stretching band

at 3363 cm^{-1} along with $\nu(CO_2)_{asymm}$ (1603 cm^{-1}) and $\nu(CO_2)_{symm}$ (1385 cm^{-1}) stretches.[13] The FAB mass spectra of **23a** and **23a'** exhibit $[M]^+$ peaks at 882 Da. and 938 Da., respectively. The variable temperature SQUID data for **23a** and **23a'** was fitted using the Curie-Weiss law and the resulting Curie constant (C), the latter was more than expected for two non-interacting Ni(II) ions each possessing two unpaired electrons with $\chi_M T$ = 1.05 emu K mol^{-1} (**23a**) and 1.47 emu K mol^{-1} (**23a'**) (expected $\chi_M T$ = 1.00 emu K mol^{-1}, ***SEE NOTE*** Appendices, Table 1).[26b,26d]

4.1.2 M = Ni, L^1 = *m*-$BDCH_2$, L^2 = hepH (n = 2)

Replacement of hmpH for hepH in the ligand blend also resulted, on work-up, in a dimeric species $[Ni_2(hepH)_4(m\text{-}BDC)_2]\cdot CH_2Cl_2$ (**23b**) in low yield (Scheme 4). Complex **23b** was characterised by elemental analysis, IR spectroscopy, variable temperature SQUID magnetometry (see Appendices, Table 1) and FAB positive mass spectrometry. A single crystal of **23b** was subject to an X-ray diffraction study. The molecular structure of **23b** is shown in Figure 3(b); selected bond lengths and angles are given in Table 2.

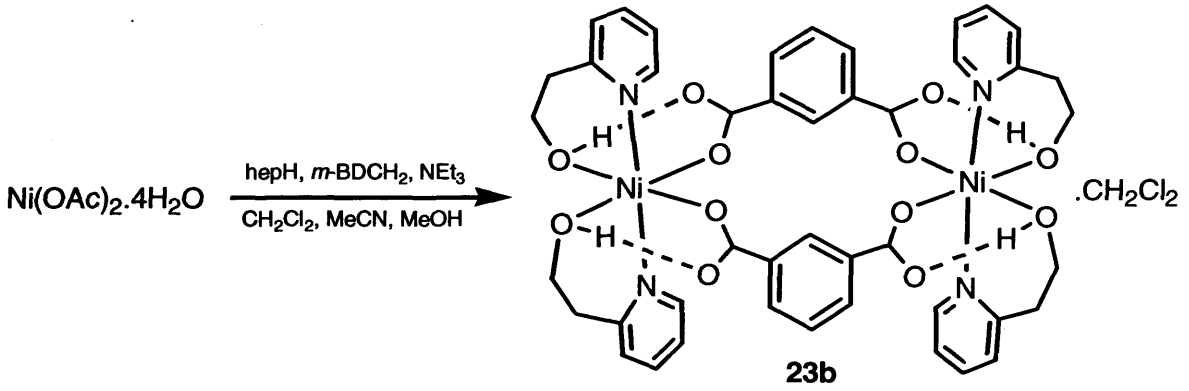

Scheme 4 Synthesis of **23b**.

The molecular structure of **23b** consists of two octahedral Ni(II) ions bridged by two mutually *cis*-*m*-BDC ligands and each bound terminally by two *N,O*-chelating hepH ligands to give a bimetallic complex similar to that for **23a**. The 1.11 hepH ligands are bound with their pyridine moieties *trans* to one another with bond lengths averaging to Ni-

O_{hepH} = 2.110 Å and Ni-N_{hepH} = 2.080 Å. The bridging *m*-BDC carboxylate oxygen atoms are bound in the bis-type 2, η^1: *syn* monodentate bonding fashion [Scheme 1(j)] with the Ni-$O_{m\text{-}BDC}$ bond lengths averaging to 2.047 Å. The hepH-containing six-membered chelate rings are puckered with an average O_{hepH}-Ni-N_{hepH} bite angle of 89.74(13)°, resulting in a less distorted octahedral geometry in comparison to **23a** (~ 85°). The nickel(II) ions in **23b** are separated by a distance of 7.9116(9) Å (*cf.* 7.789 Å in **23a**). As with **23a**, the *m*-BDC C-O bond length involving the coordinated oxygen atom in **23b** (av. 1.255), suggests some covalent metal ion to ligand character.[9] Intramolecular inter-ligand hydrogen bonding interactions between the *m*-BDC non-coordinated carboxylate oxygen atom with the neighbouring hepH hydroxyl group (similar to **23a**) are apparent in **23b** [$O_{hepH}(1)\cdots O_{m\text{-}BDC}(10)$ = 2.548(4) Å, $O_{hepH}(2)\cdots O_{m\text{-}BDC}(6)$ = 2.546(4) Å, $O_{hepH}(3)\cdots O_{m\text{-}BDC}(12)$ = 2.522(4) Å and $O_{hepH}(4)\cdots O_{m\text{-}BDC}(8)$ = 2.529(4) Å].

Table 2 Selected bond length (Å) and angle (°) data for complex **23b**

23b							
Ni(1)-O(1)	2.095(3)	Ni(1)-O(9)	2.037(3)	Ni(2)-O(7)	2.049(3)	Ni(1)-N(2)	2.092(3)
Ni(1)-O(2)	2.098(3)	Ni(2)-O(3)	2.125(3)	Ni(2)-O(11)	2.055(3)	Ni(2)-N(3)	2.067(3)
Ni(1)-O(5)	2.047(3)	Ni(2)-O(4)	2.120(3)	Ni(1)-N(1)	2.090(3)	Ni(2)-N(4)	2.071(3)
O(1)-Ni(1)-O(2)	93.87(12)	O(7)-Ni(2)-O(4)	88.87(10)	O(5)-Ni(1)-N(1)	89.66(12)	N(4)-Ni(2)-O(4)	87.34(11)
O(5)-Ni(1)-O(1)	174.90(10)	O(11)-Ni(2)-O(3)	89.08(10)	O(5)-Ni(1)-N(2)	91.27(12)	O(7)-Ni(2)-N(3)	91.10(12)
O(9)-Ni(1)-O(5)	84.77(11)	O(11)-Ni(2)-O(4)	173.91(10)	O(9)-Ni(1)-N(1)	90.41(12)	O(7)-Ni(2)-N(4)	87.98(12)
O(9)-Ni(1)-O(1)	90.69(10)	O(7)-Ni(2)-O(11)	85.20(12)	O(9)-Ni(1)-N(2)	89.68(12)	O(11)-Ni(2)-N(3)	87.80(12)
O(5)-Ni(1)-O(2)	90.74(10)	N(1)-Ni(1)-O(1)	88.05(12)	N(3)-Ni(2)-O(3)	87.30(11)	O(11)-Ni(2)-N(4)	91.06(12)
O(9)-Ni(1)-O(2)	175.07(10)	N(1)-Ni(1)-O(2)	91.62(12)	N(4)-Ni(2)-O(3)	93.51(12)	N(1)-Ni(1)-N(2)	179.06(13)
O(4)-Ni(2)-O(3)	96.88(11)	N(2)-Ni(1)-O(1)	91.03(13)	N(3)-Ni(2)-O(4)	93.70(11)	N(3)-Ni(2)-N(4)	178.60(13)
O(7)-Ni(2)-O(3)	174.11(10)	N(2)-Ni(1)-O(2)	88.26(12)				

The IR spectrum of **23b** shows broad ν(OH) bands at 3667 cm^{-1} and 3089 cm^{-1} along with strong $\nu(CO_2)_{asymm}$ and $\nu(CO_2)_{symm}$ stretching bands at 1604 cm^{-1} and 1388 cm^{-1}, respectively.[13] The FAB mass spectrum of **23b** includes a molecular ion peak $[M]^+$ at 938 Da. The variable temperature SQUID data for **23b** was fitted using the Curie-Weiss law

and the resulting Curie constant (C) is consistent with two non-interacting Ni(II) ions with $\chi_M T$ = 1.17 emu K mol^{-1} (see Appendices, Table 1, ***SEE NOTE***).[26b,26d]

The reaction of a 1: 1: 2 ratio of nickel(II) acetate tetrahydrate: hepH: *m*-$BDCH_2$, in the presence of triethylamine gave, on work-up, crystals of {[Ni(hepH)$_2$(*m*-BDC)]·MeOH}$_n$ (**24**) in moderate yield (Scheme 5). Complex **24** was characterised by elemental analysis, IR spectroscopy, variable temperature SQUID magnetometry (see Appendices, Table 1) and positive FAB mass spectrometry. A single crystal of **24** was subject to an X-ray diffraction study. The molecular structure of **24** is shown in Figure 4(a); selected bond lengths and angles are given in Table 3.

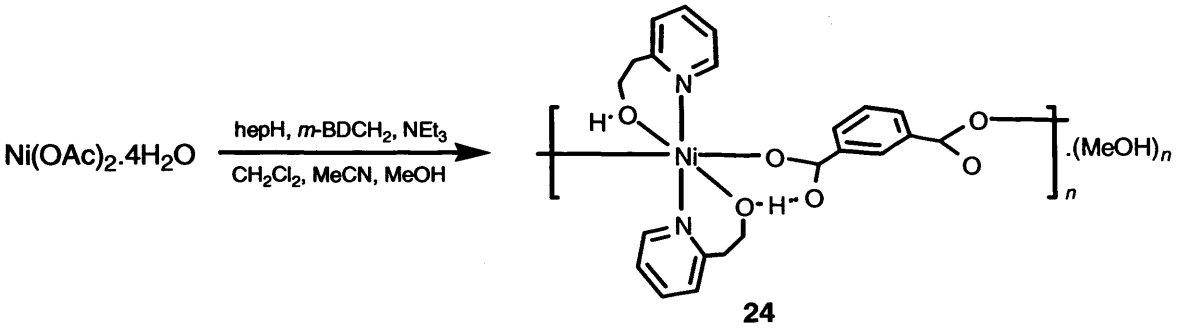

24

Scheme 5 Synthesis of **24**.

The molecular structure of **24** reveals a polymeric chain, in which the octahedral Ni(II) ions are linked by *trans*-*m*-BDC ligands and bound terminally by two *N,O*-chelating hepH ligands. The two mutually *trans*-hepH ligands are 2.11 bound and form six-membered chelate rings with the metal centre. Each of the bridging *m*-BDC carboxylate groups are bound in a bis-type 1, η^1: *syn* monodentate bonding mode [Scheme 1(h)].

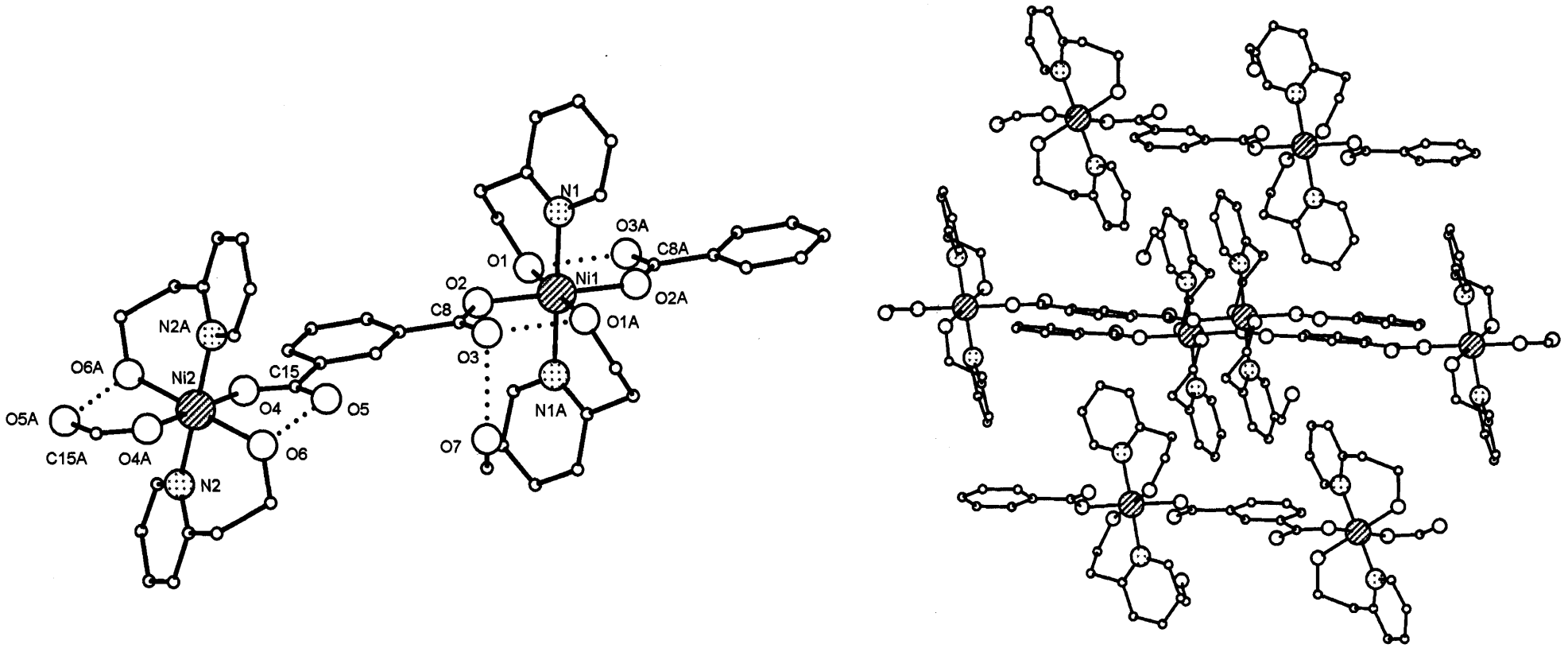

(a) (b)

Figure 4 (a) Part of the polymeric molecular structure and (b) crystal packing (viewed down 1,1,1 *b*-axis) of **24**. Hydrogen atoms and carbon atom labelling is omitted for clarity. Dotted bonds show hydrogen bonding interactions.

Table 3 Selected bond length (Å) and angle (°) data for complex **24**

24					
Ni(1)-O(1)	2.0845(16)	Ni(2)-O(4)	2.0459(15)	Ni(1)-N(1)	2.0802(19)
Ni(1)-O(2)	2.0562(15)	Ni(2)-O(6)	2.0977(15)	Ni(2)-N(2)	2.0747(19)
O(2)-Ni(1)-N(1)	93.12(7)	N(2)-Ni(2)-O(6)	89.40(7)	O(4)-Ni(2)-O(6)	90.61(6)
O(2)-Ni(1)-N(1)#1	86.88(7)	N(2)#2-Ni(2)-O(6)	90.60(7)	O(4)-Ni(2)-O(6)#2	89.39(6)
O(4)-Ni(2)-N(2)	88.60(7)	O(2)-Ni(1)-O(1)	89.02(6)	N(1)-Ni(1)-O(1)	88.61(7)
O(4)-Ni(2)-N(2)#2	91.40(7)	O(2)#1-Ni(1)-O(1)	90.98(6)	N(1)#1-Ni(1)-O(1)	91.39(7)

Symmetry transformations used to generate equivalent atoms; #1 $(-x+1, -y, -z+1)$; #2 $(-x, -y+1, -z)$.

In complex **24**, the Ni-O and Ni-N bond lengths involving the two hepH ligands differ [Ni(1)-O_{hepH}(1) = 2.0845(16) Å and Ni(1)-N_{hepH}(1) = 2.0802(19) Å *vs.* Ni(2)-O_{hepH}(6) = 2.0977(15) Å and Ni(2)-N_{hepH}(2) = 2.0747(19) Å] as do the Ni-$O_{m\text{-}BDC}$ bond lengths [2.0459(15) Å and 2.0562(15) Å]. The Ni(1)···Ni(2) distance in **24** at 10.9884(9) Å is larger in comparison to the corresponding distances in **23a** and **23b** (*ca.* 3.0 Å). This difference may be attributed to the relative positions of the *syn*-bound carboxylate oxygen atoms. The bound *m*-BDC carboxylate C-O bond lengths averaging to 1.257 Å are indicative of mainly ionic metal-carboxylate bonds.[9]

There are two types of hydrogen bonding interactions in complex **24**. Firstly, intramolecular inter-ligand hydrogen bonding interactions between the hepH hydroxyl groups and the unbound *m*-BDC carboxylate oxygen atoms [$O_{m\text{-}BDC}$(6)···O_{hepH}(5) = 2.550 (2)Å, O_{hepH}(1)···$O_{m\text{-}BDC}$(3A) = 2.576(2) Å] and secondly, an intermolecular hydrogen bonding interaction from a molecule of methanol with a neighbouring *m*-BDC carboxylate oxygen atom [$O_{m\text{-}BDC}$(3)···O_{MeOH}(7) = 2.772(3) Å].

In the previously reported isopthalate-bridged polymeric species [Ni(*m*-BDC)$(MeOH)_4]_n$, the bridging *m*-BDC ligands adopt the bis-type 2, η^1: *syn* monodentate *m*-BDC bonding mode (as with **23**), which results in an undulating/zig-zag 1-D polymer with hydrogen bonding and π···π-stacking interactions.[1t] In contrast, **24** is a linear polymer [Figure 4(b)] which may be attributed to a different *m*-BDC bonding mode [*viz.* bis-type 1, η^1: *syn* monodentate (**24**)] adopted. The average Ni-$O_{m\text{-}BDC}$ bond length in [Ni(*m*-

BDC)(MeOH)$_4$]$_n$ at ~ 2.05 Å is similar to the corresponding bond lengths in **24** (av. ~ 2.05 Å) and **23** (~ av. 2.03 Å). The intramolecular $O_{m\text{-}BDC}\cdots O_{MeOH}$ hydrogen bonding interaction in [Ni(*m*-BDC)(MeOH)$_4$]$_n$ at ~ 2.6 Å is comparable to the $O_{m\text{-}BDC}\cdots O_{pyridinol}$ distance found in complexes **23** (> 2.5 Å) and is shorter than the intermolecular methanolic hydrogen bonding interaction in **24** (~ 2.8 Å).

The IR spectrum of **24** shows a very broad ν(OH) stretching band at 3423 cm^{-1} along and stronger $\nu(CO_2)_{asymm}$ and $\nu(CO_2)_{symm}$ stretching bands at 1604 cm^{-1} and 1358 cm^{-1}, respectively.[13] The FAB mass spectrum of **24** shows fragmentation peaks related to ligand loss from a monomeric unit including a $[M_{(n=1)}$ – hepH$]^+$ peak at 346 Da. (no peaks are found > ~ 400 Da. *cf.* **23b**). The variable temperature SQUID data from **24** was fitted using the Curie-Weiss law and the resulting Curie constant (C) is consistent with a single non-interacting Ni(II) ion with $\chi_M T$ = 1.18 emu K mol^{-1} (see Appendices, Table 1, ***SEE NOTE***).[26b,26d]

It is uncertain why the variation of molar equivalents of hepH affects the structural type of the product (i.e. dimer **23b** *vs.* polymer **24**). Attempts to generate a crystalline product for the corresponding hmpH polymer [Ni(hmpH)$_2$(*m*-BDC)]$_n$ using the same molar quantities of starting materials as in **24** proved to be unsuccessful.

4.1.3 M = Ni, L^1 = *m*-$BDCH_2$, L^2 = hppH (n = 3)

Work-up of the reaction of nickel acetate tetrahydrate with hppH and *m*-$BDCH_2$, in the presence of triethylamine, did not afford a crystalline product. Nevertheless, elemental analysis tentatively suggests the presence of [Ni(hppH)$_2$(*m*-BDC)]$_n$ (**25**) (Scheme 6).

$$Ni(OAc)_2.4H_2O \xrightarrow[CH_2Cl_2,\ MeCN,\ MeOH]{hppH,\ m\text{-}BDCH_2,\ NEt_3} \underset{\mathbf{25}}{[Ni(hppH)_2(m\text{-}BDC)]_n}$$

Scheme 6 Synthesis of **25**.

4.2 Blending Isopthalic Acid and 2-Pyridine Alcohols on a Cu(II) Centre

4.2.1 M = Cu, L^1 = *m*-$BDCH_2$, L^2 = hmpH (n =1)

Reaction of hmpH, *m*-$BDCH_2$ with copper(II) acetate monohydrate in the presence of triethylamine, results in the formation of corn-blue crystals of the polymeric complex $[Cu(hmpH)_2(m\text{-}BDC)]_n \cdot CH_2Cl_2$ (**26**) in low yield (Scheme 7). Use of mehmpH in place of hmpH also affords a polymeric species of composition $[Cu(mehmpH)_2(m\text{-}BDC)]_n$ (**26'**). Complexes **26** and **26'** were characterised by elemental analysis, IR spectroscopy, variable temperature SQUID magnetometry (see Appendices, Table 1 for **26**) and positive FAB mass spectrometry. A single crystal of **26** was subject to an X-ray diffraction study. The molecular structure of **26** is shown in Figure 5; selected bond lengths and angles are given in Table 4.

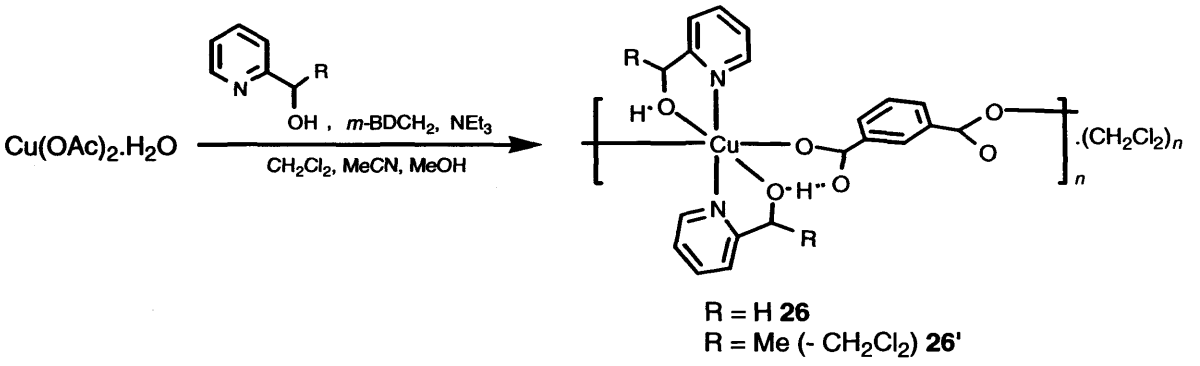

R = H **26**
R = Me (- CH_2Cl_2) **26'**

Scheme 7 Synthesis of **26**

The molecular structure of **26** reveals a polymeric chain in which the Jahn-Teller distorted octahedral Cu(II) ions are bridged by *m*-BDC ligands and bound terminally by two *N,O*-chelating 1.11 hmpH ligands. The hmpH ligands in **26** are coordinated mutually *trans*. Each of the bridging η^1-*m*-BDC carboxylate ligands adopt a bis-type 1, η^1: *syn* monodentate bonding mode and are positioned *trans* to one another [Scheme 1(h)].

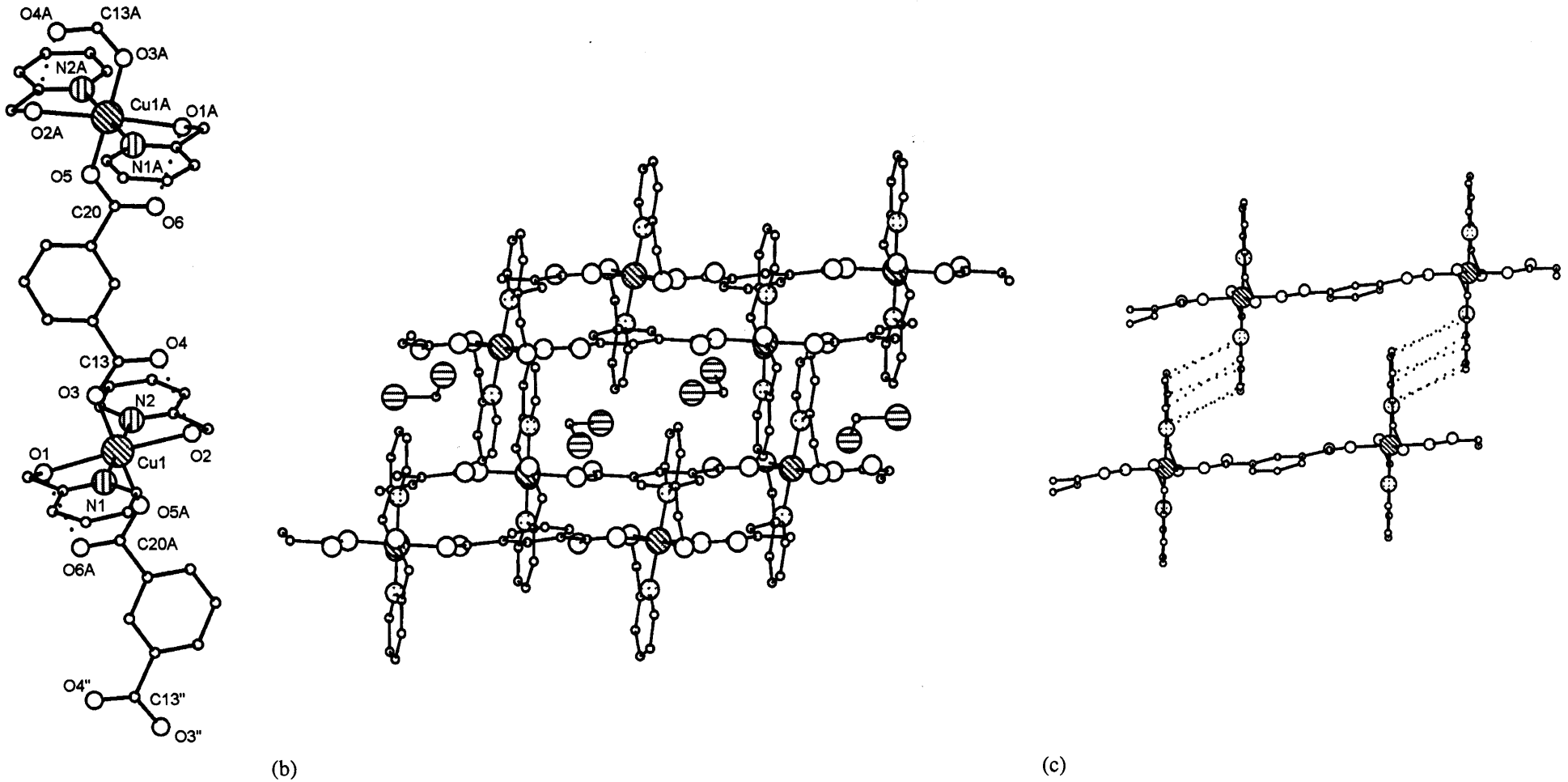

(a) (b) (c)

Figure 5 (a) Part of polymeric chain (viewed down the 001 *a*-axis), (b) crystal packing (viewed down 111 *b*-axis) and (c) part of stacked polymer of **26**. Hydrogen atoms and atom labelling is excluded from the polymer fragments for clarity. Dotted lines show hydrogen bonding or van der Waals stacking interactions.

In **26**, the hmpH-containing chelate bite angle of $O_{hmpH}(1)$-Cu(1)-$N_{hmpH}(1)$ = 76.75(10)°, is acute. The corresponding Cu(II) to hmpH nitrogen and hydroxyl oxygen bond lengths average to 1.995(3) Å and 2.359(2) Å, respectively. The two η^1 : *syn* bound *m*-BDC carboxylate oxygen atoms display Cu-$O_{m\text{-}BDC}$ bond lengths averaging to 1.984 Å, while the *m*-BDC C-O bond length involving the coordinated oxygen atom in **26** at 1.269(4) Å [O(3)-C(13)] is indicative of a slightly covalent metal-carboxylate bond.[9]

Table 4 Selected bond length (Å) and angle (°) data for complex **26**

26					
Cu(1)-O(1)	2.368(2)	Cu(1)-O(3)	1.992(2)	Cu(1)-N(1)	1.996(3)
Cu(1)-O(2)	2.349(2)	Cu(1)-O(5)#1	1.975(2)	Cu(1)-N(2)	1.993(3)
O(2)-Cu(1)-O(1)	177.38(7)	O(3)-Cu(1)-N(2)	90.90(10)	N(2)-Cu(1)-O(2)	77.57(10)
O(3)-Cu(1)-O(1)	88.25(9)	O(5)#1-Cu(1)-N(1)	92.74(10)	N(2)-Cu(1)-N(1)	179.66(11)
O(3)-Cu(1)-O(2)	94.09(9)	O(5)#1-Cu(1)-N(2)	87.29(10)	C(1)-O(1)-Cu(1)	104.1(2)
O(5)#1-Cu(1)-O(1)	92.46(9)	N(1)-Cu(1)-O(1)	76.75(10)	C(7)-O(2)-Cu(1)	103.99(19)
O(5)#1-Cu(1)-O(2)	85.23(9)	N(1)-Cu(1)-O(2)	102.09(10)	C(13)-O(3)-Cu(1)	126.7(2)
O(5)#1-Cu(1)-O(3)	178.17(9)	N(2)-Cu(1)-O(1)	103.59(10)	C(20)-O(5)-Cu(1)#2	129.1(2)
O(3)-Cu(1)-N(1)	89.07(10)				

Symmetry transformations used to generate equivalent atoms; #1 ($x - 0.5, -y + 1.5, z + 0.5$), #2 ($x + 0.5, -y + 1.5, z - 0.5$).

The copper ions in **26** are separated by distances of 10.873(2) Å (intramolecular) and ~ 8.118 Å (intermolecular/chain···chain), these being comparable to the corresponding distances in **24** [Ni···Ni = 10.9884(9) Å (intramolecular) and ~ 8.764 Å (intermolecular/chain···chain), respectively]. Complexes **24** and **26** are both linear 1-D polymers, with both exhibiting similar bis-type 1, η^1: *syn* monodentate bonding modes for the *m*-BDC ligands. Complex **26** exhibits offset, intermolecular hmpH-based dipole-dipole (pyridine ring to pyridine ring) van der Waals/non-π···π stacking interactions [centroid-centroid C···C = 3.985(2) Å, offset ~ 22° (nearest atom···atom = 3.661 Å)] [Figure 5(c)].[32] Intramolecular hydrogen bonding interactions in **26** arise between the hmpH hydroxyl groups and the nearest *m*-BDC carboxylate oxygen atoms [$O_{hmpH}(2)$···$O_{m\text{-}BDC}(4)$ = 2.587(3) Å and $O_{hmpH}(1)$···$O_{m\text{-}BDC}(6A)$ = 2.604(4) Å]. In **26**, molecules of dichloromethane sandwich between neighbouring polymer chains in a regular pattern throughout the entire lattice and

are likely to be influencing crystal packing [Figure 5(b)].[34] Indeed, weak intermolecular hydrogen bonding or van der Waals interactions (all > 3 Å) are apparent from CH_2Cl_2 with neighbouring hmpH or *m*-BDC ligands [Figure 6 and Table 5].[33]

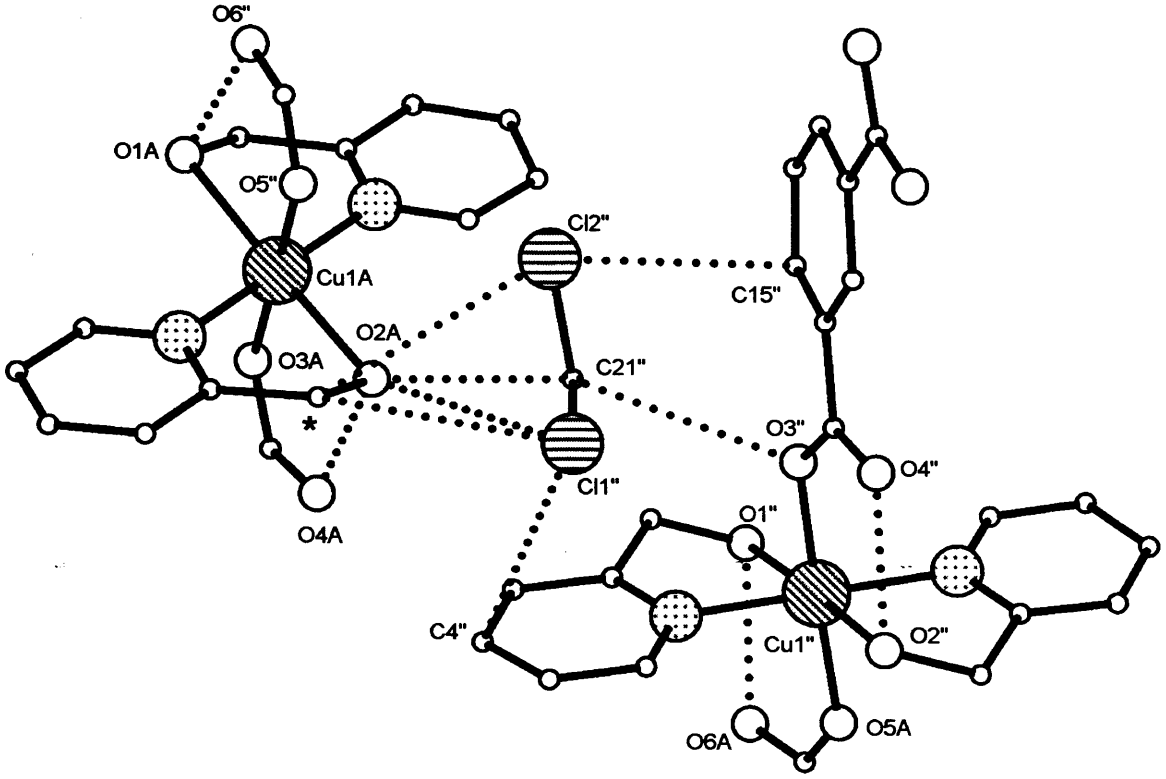

Figure 6 Intermolecular non-covalent interactions in part of the 1.1.1 packed structure of **26** (dotted lines). Atoms involved in these interactions are labelled. H-atoms and parts of ligands are excluded for clarity.

Table 5 Non-covalent interaction-based intermolecular distances (Å) for CH_2Cl_2 molecules in complex **26**

Type		
Bifurcated CH_2Cl_2-hmpH	C(21'')···O(2A)	3.211(7)
Bifurcated CH_2Cl_2-hmpH	Cl(2'')···O(2A)	3.505(7)
CH_2Cl_2-m-BDC	C(21'')···O(3'')	3.525(7)
Bifurcated CH_2Cl_2-hmpH	Cl(2)···C(7A)*	3.828(7)
Bifurcated CH_2Cl_2-hmpH	Cl(1'')···C(7A)*	4.065(7)

In the previously reported copper *N*-pyridine/*m*-BDC-based 1-D polymers $\{[Cu(m\text{-}BDC)(py)_2]\cdot 1.5H_2O\}_n$ and $\{[Cu(m\text{-}BDC)(py)_3]\cdot H_2O\cdot MeOH\}_n$, the bridging *m*-BDC ligand binds as both type 1, η^1: *syn* monodentate and type 2, η^1: *syn* monodentate [Scheme 1(i)]. In comparison, the non-solvated polymer $\{[Cu(m\text{-}BDC)(py)_2]\}_n$ possesses type 1, η^1: *syn* monodentate and type 2, η^1: *anti* bidentate, 1,3-bridging *m*-BDC ligands [Scheme 1(f)].[1t] The Cu-N_{py} and Cu(1)-$O_{m\text{-}BDC}$ bond lengths from both the pyridyl (non-substituted) and *m*-

BDC ligands in the latter three complexes, averaging to 2.087 Å and 1.958 Å, respectively, are similar to those found for the corresponding pyridyl containing hmpH and *m*-BDC ligands in **26** [Cu-N_{hmpH} = av. 1.995 Å and Cu(1)-$O_{m\text{-}BDC}$ = 1.984 Å].

The IR spectra of **26** and **26'** reveal ν(OH) stretching bands at 3421 cm^{-1} and 3080 cm^{-1}, along with $\nu(CO_2)_{asymm}$ and $\nu(CO_2)_{symm}$ stretching bands at 1607 cm^{-1}, 1605 cm^{-1} and 1480 cm^{-1}, 1400 cm^{-1}, respectively.[13] The FAB mass spectra of **26** and **26'** show fragmentation peaks at $[M_{(n=1)} - \text{hmpH}]^+$ = 336 Da. (**26**) and $[M_{(n=1)} - \text{mehmpH} - m\text{-BDC}]^+$ = 186 Da. (**26'**). The variable temperature SQUID data of **26** was fitted using the Curie-Weiss law and the resulting Curie constant (*C*) was consistent with a single non-interacting Cu(II) ion possessing one unpaired electron with $\chi_M T$ = 0.32 emu K mol^{-1} (see Appendices, Table 1, ***SEE NOTE***).[26b,26d]

Attempted incorporation of azide into the framework of **26** by carrying out the reaction with an additional equivalent of NaN_3 resulted in the unexpected formation of mononuclear complex [Cu(hmpH)$_2$(*m*-BDC)] (**27**), as dark-blue crystals in low yield (Scheme 8). Complex **27** was characterised by elemental analysis, IR spectroscopy, variable temperature SQUID magnetometry (see Appendices, Table 1) and positive FAB mass spectrometry. A single crystal of **27** was subject to an X-ray diffraction study. The molecular structure of **27** is shown in Figure 7(a); selected bond lengths and angles are given in Table 6.

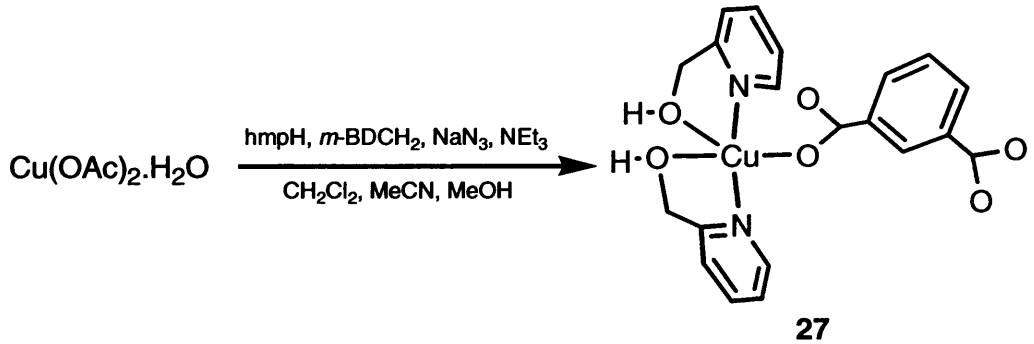

27

Scheme 8 Synthesis of **27**.

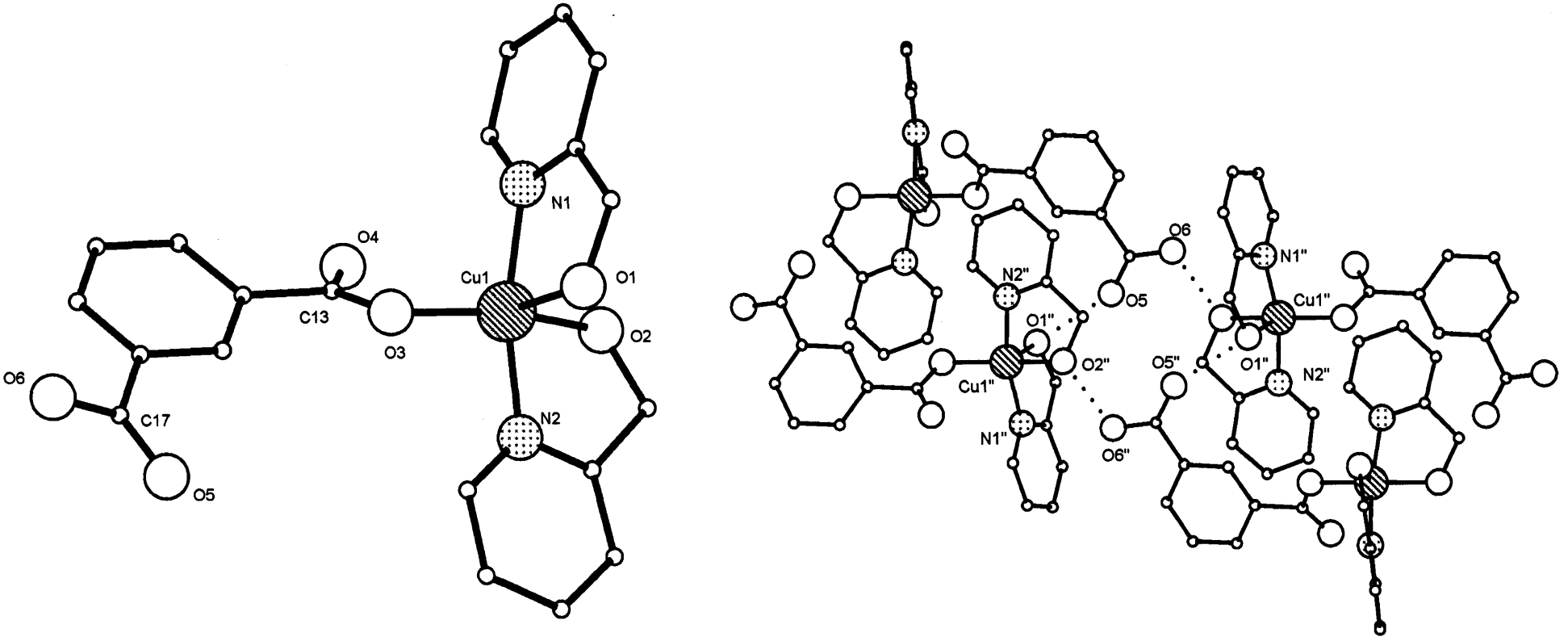

(a) (b)

Figure 7 (a) Molecular structure and (b) view of the hydrogen bonded network (111 *b*-axis) of **27**. Atoms and carbon atom labels are excluded for clarity. Dotted bonds indicate Hydrogen intermolecular hydrogen bonding interactions.

The molecular structure of **27** reveals a distorted trigonal bipyramidal copper(II) ion surrounded by a *m*-BDC and two *N,O*-chelating 1.11 hmpH ligands. The *m*-BDC ligand is coordinated in the type 2, η^1: *syn* monodentate bonding mode to a single copper ion, while, the second carboxylate moiety is negatively charged and remains unbound [Scheme 1(l)].

In **27**, the two hmpH nitrogen atoms are *trans* bound, with the two hmpH hydroxyl oxygen atoms sitting in the equatorial plane of the trigonal bipyramid along with the oxygen atom from a *m*-BDC ligand [Cu(1)-$O_{m\text{-}BDC}$(3) = 1.923(2) Å]. The two Cu-O_{hmpH} bond lengths differ [Cu(1)-O_{hmpH}(1) = 2.255(2) Å, Cu(1)-O_{hmpH}(2) = 1.952(2) Å] whereas the Cu-N_{hmpH} bond lengths are comparable [Cu(1)-N_{hmpH}(1) = 1.984(2) Å, Cu(1)-N_{hmpH}(2) = 1.965(3) Å]. The hmpH-containing chelate bite angles at the copper ions within **27** average to 79.42°, which is not as acute as the corresponding chelate bite angle found in **26** (*ca.* 0.3°).[12]

Table 6 Selected bond length (Å) and angle (°) data for complexes **27**

27					
Cu(1)-O(1)	2.255(2)	Cu(1)-O(3)	1.923(2)	Cu(1)-N(2)	1.965(3)
Cu(1)-O(2)	1.952(2)	Cu(1)-N(1)	1.984(2)		
O(2)-Cu(1)-O(1)	98.38(9)	O(2)-Cu(1)-N(2)	80.93(9)	N(1)-Cu(1)-O(1)	77.90(9)
O(3)-Cu(1)-O(1)	103.28(8)	O(3)-Cu(1)-N(1)	98.52(9)	N(2)-Cu(1)-O(1)	92.06(9)
O(3)-Cu(1)-O(2)	157.73(9)	O(3)-Cu(1)-N(2)	93.10(10)	N(2)-Cu(1)-N(1)	166.09(10)
O(2)-Cu(1)-N(1)	90.94(9)				

In **27**, the two unbound *m*-BDC oxygen atoms, O(4) and O(5), have shorter and presumably stronger C-O bond lengths averaging to 1.228 Å, suggesting some double bond character. In contrast, the C-O bond distance [C(17)-O(6) = 1.259(4) Å] from the non-coordinated carboxylate oxygen atom [O(6)] is comparable to the metal bound carboxylate oxygen atom distance [C(13)-O(3) = 1.267(3) Å]. The latter value indicates the presence of some covalent character from the metal-carboxylate bond.[9]

There is no evidence for the presence of intramolecular hydrogen bonding interactions in **27**. However, **27** exhibits significant intermolecular hydrogen bonding

interactions and indeed the structure could be described as part of a hydrogen bonded network of monomers [$O_{hmpH}(1')\cdots O_{m\text{-}BDC}(5)$ = 2.587(3) Å and $O_{hmpH}(2')\cdots O_{m\text{-}BDC}(6)$ = 2.427(3) Å] [Figure 7(b)]. Notably, the intermolecular Cu···Cu bond distance at ~ 6.984 Å in this hydrogen bonded network is much shorter in comparison to the intramolecular Cu···Cu distance found in **26** (10.872 Å).

The related monodentate Schiff complex [$Cu(salea)_2$] (Hsalea = N-{2-hydroxybenzyl}-2-amino-1-ethanol) has been reported to form a 2-D hydrogen bonded network of monomers.[11a] [$Cu(salea)_2$] possesses two *N,O*-chelated Schiff-base ligands bound in a similar fashion to the hmpH ligands in **27**, with the Cu(II) ion exhibiting pseudo-octahedral geometry. The intermolecular Cu···Cu distance in this species is 6.309 Å (*cf.* 6.984 Å in **27**).[11b]

The IR spectrum of **27** exhibits a strong carbonyl ν(C=O) stretching band at 1714 cm^{-1}, in addition to bands corresponding to ν(OH), $\nu(CO_2)_{asymm}$ and $\nu(CO_2)_{symm}$ stretches at ~ 2985 cm^{-1} (broad), 1600 cm^{-1} and 1382 cm^{-1}, respectively.[13] The FAB mass spectrum of **27** shows a $[M]^+$ peak at 445 Da. The variable temperature SQUID data for **27** was fitted using the Curie-Weiss law and the resulting Curie constant (*C*) is consistent with a single non-interacting Cu(II) ion with $\chi_M T$ = 0.38 emu K mol^{-1} (see Appendices, Table 1).[26b]

The role of sodium azide in the formation of **27** is uncertain, but notably its role as a base for the formation of a related polymeric network has been previously reported.[10]

4.2.2 M = Cu, L^1 = *m*-$BDCH_2$, L^2 = hepH (n = 2)

On extension of the 2-pyridinol alkyl chain length by the use of hepH within the ligand blend, the polymeric species $[Cu(hepH)_2(m\text{-}BDC)]_n$ (**28**) was isolated in low yield (Scheme 9). Complex **28** was characterised by elemental analysis, IR spectroscopy, variable temperature SQUID magnetometry (see Appendices, Table 1) and positive FAB mass spectrometry. A single crystal of **28** was subject to an X-ray diffraction study. The

molecular structure of **28** is shown in Figure 8(a); selected bond lengths and angles are given in Table 7.

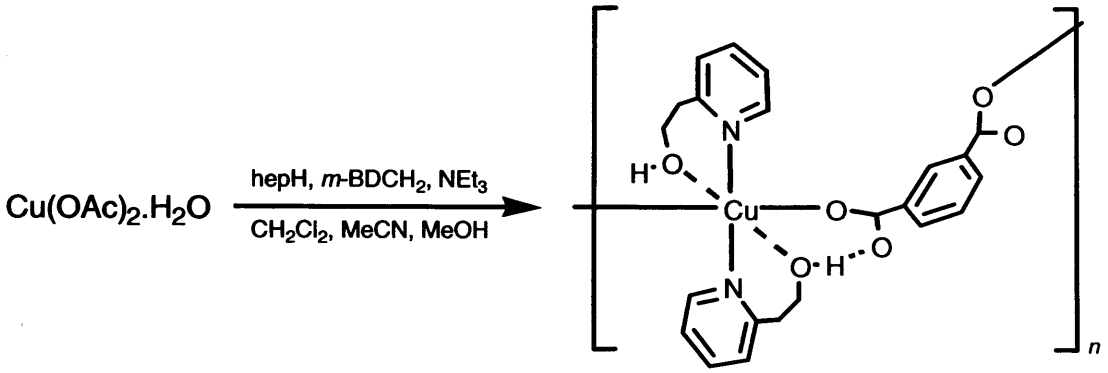

28

Scheme 9 Synthesis of **28**.

The molecular structure of **28** reveals a 1-D polymer with each Cu(II) ion bridged by a *m*-BDC ligand and bound terminally by two hepH ligands. Each monomeric unit of **28** comprises a pseudo-square planar copper centre coordinated by two 1.01 *trans*-bound hepH nitrogen atoms and two *trans*-bound *m*-BDC oxygen atoms in a bis-type 2, η^1: *syn* monodentate bonding mode [Scheme 1(j)]. In compound **28**, the elongated Cu(1)···O_{hepH}(1) = 2.4665(13) Å bond distance suggests the presence of a pseudo-axial interaction due to the Jahn-Teller effect thus, the coordination geometry of **28** could also be described as octahedral.

The copper ions within the polymer chain of **28** are separated by a distance of 7.8703(9) Å, this being much shorter than the corresponding bond distance within **26** (~ >10 Å). The relatively shorter Cu···Cu distance can be attributed to the *m*-BDC bis-type 2, η^1: *syn* monodentate bonding mode which is similar to those found in the dimers **23a** and **23b** [Scheme 1(j)]. The intermolecular Cu···Cu distance in **26** is longer at 8.417 Å. In contrast, the *m*-BDC bonding modes found in **24** and **26** result in longer M···M distances. Complex **28** forms part of a undulating/zig-zag chain polymer with offset, intermolecular hepH-based dipole-dipole (pyridine ring to pyridine ring) van der Waals/non-π···π stacking interactions [centroid-centroid C···C = 4.446(13) Å, offset ~ 35° (nearest atom···atom = 3.611 Å)] [Figure 8(b)].[32]

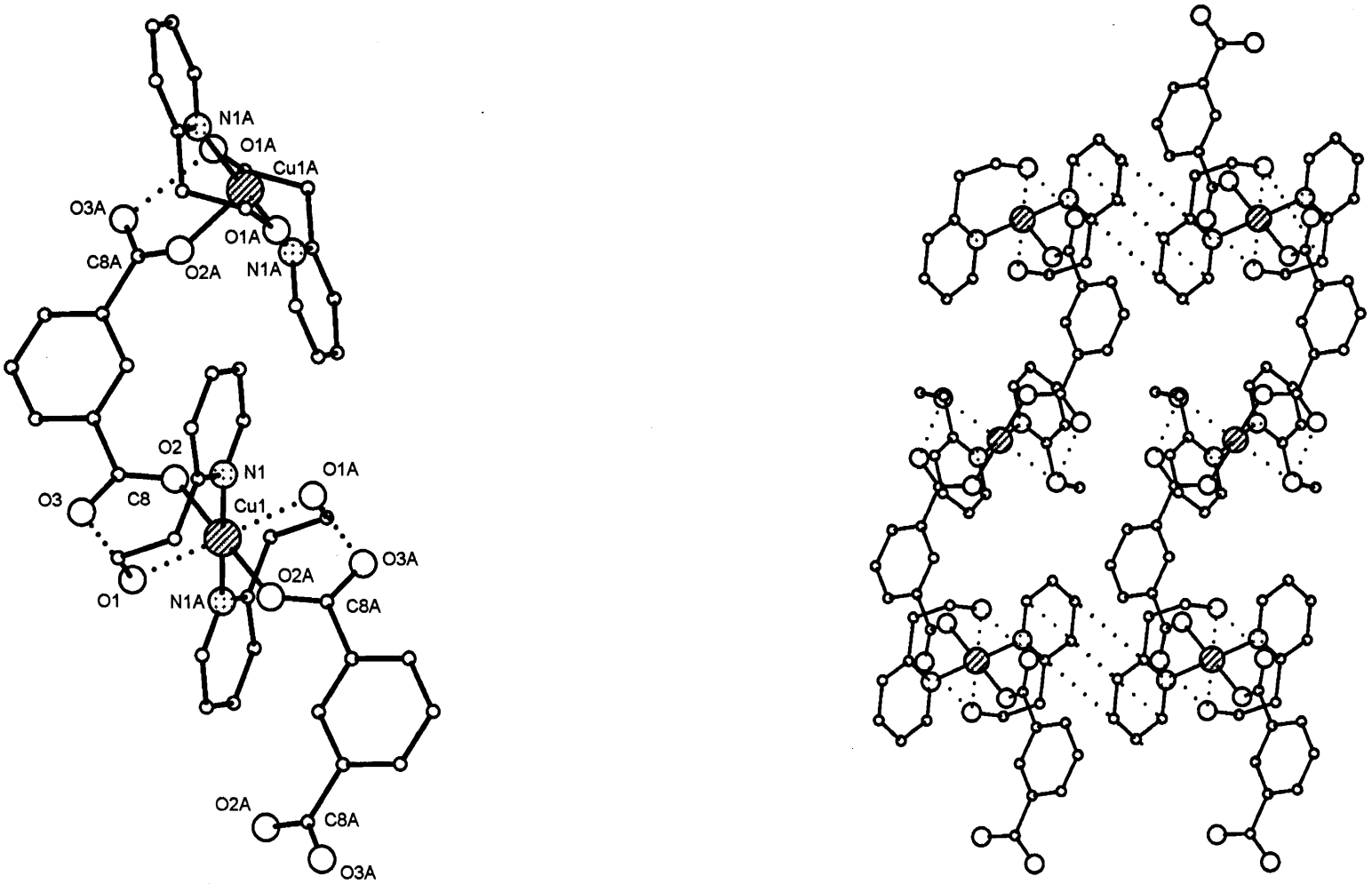

(a) (b)

Figure 8 (a) Part of the polymer chain and (b).crystal packing (viewed mid-way down *c*-axis 1,1,1) of **28**. Hydrogen atoms and most carbon atom labels are omitted for clarity. Dotted lines indicate van der Waals stacking/hydrogen bonding/pseudo-axial interactions.

The bound and non-coordinated *m*-BDC carboxylate oxygen atoms display the following C-O bond lengths of C(8)-O(2) = 1.260(2) Å and C(8)-O(3) = 1.236(2) Å, respectively. The former value (bound) is consistent with an essentially ionic metal ion to carboxylate bond.[9] In **28**, each hepH hydroxyl group is involved in intramolecular inter-ligand hydrogen bonding interactions with neighbouring *m*-BDC ligands [$O_{hepH}(1)\cdots O_{m\text{-}BDC}(3)$ = 2.5752(18) Å].

Table 7 Selected bond length (Å) and angle (°) data for complex **28**

28			
Cu(1)-O(2)	1.9750(11)	Cu(1)-N(1)	2.0000(14)
C(1)-N(1)-Cu(1)	114.26(11)	O(2)-Cu(1)-N(1)	85.58(6)
C(5)-N(1)-Cu(1)	126.07(12)	O(2)#1-Cu(1)-N(1)	94.42(6)
		C(8)-O(2)-Cu(1)	127.57(11)

Symmetry transformations used to generate equivalent atoms; #1 (1 – *x*, – y + 1, – z + 1).

The IR spectrum of **28** shows ν(OH), $\nu(CO_2)_{asymm}$ and $\nu(CO_2)_{symm}$ stretching bands at 3388 cm^{-1} (broad), 1601 cm^{-1} and 1360 cm^{-1}, respectively.[13] The FAB mass spectrum of **28** includes a $[M_{(n=1)} - hepH]^+$ peak at 350 Da. The variable temperature SQUID data from **28** was fitted using the Curie-Weiss law and the resulting Curie constant (*C*) is consistent with a single non-interacting Cu(II) ion with $\chi_M T$ = 0.36 emu K mol^{-1} (see Appendices, Table 1, ***SEE NOTE***).[26b,26d]

4.2.3 M = Cu, L^1 = *m*-$BDCH_2$, L^2 = hppH (n = 3)

Attempts to grow crystals of the product obtained from the reaction of a ligand blend composed of hppH, *m*-$BDCH_2$ with copper acetate monohydrate proved to be unsuccessful. However, the resulting turquoise-green coloured amorphous powder was tentatively assigned as $[Cu(hppH)_2(m\text{-}BDC)]_n$ (**29**) and was obtained in low yield (Scheme 10). Complex **29** was characterised by elemental analysis, IR spectroscopy and positive FAB mass spectrometry. The FAB mass spectrum of **29** shows a $[M_{(n=1)} - m\text{-}BDC]^+$ peak at 377 Da.

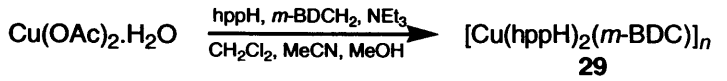

Scheme 10 Synthesis of **29**.

Although complex **29** did not afford crystals of a quality suitable for X-ray diffraction studies, it could be transformed into polymeric **26** by the addition of hmpH to a suspension of **29** in MeCN, CH_2Cl_2 and MeOH (see Scheme 11 and Chapter 7, section 7.4). The resulting blue crystals gave spectroscopic and analytical data consistent with **26** (Chapter 7, section 7.4, Table 18).

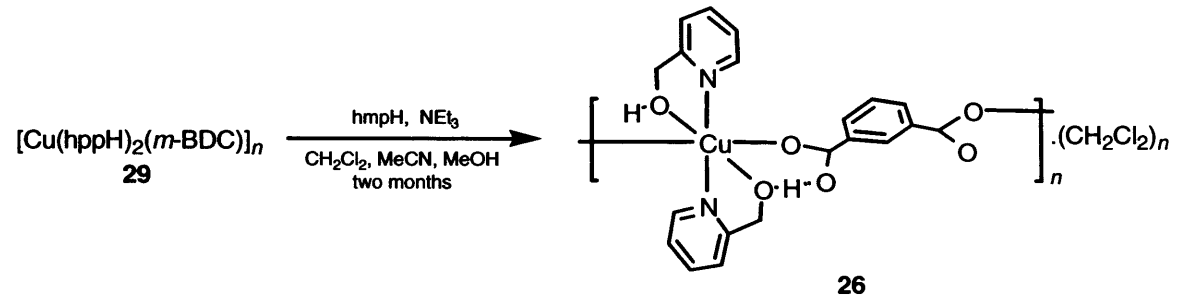

Scheme 11 Conversion of **29** into **26**.

Similarly, successful conversion of the polymer **26** to **3** could be achieved by refluxing **26** and Hchp, in the presence of triethylamine in MeCN, CH_2Cl_2 and MeOH [see Scheme 12, Chapter 2, section 2.2 (**3**) and Chapter 7, section 7.4]. The resulting blue crystals gave spectroscopic and analytical data consistent with **3** (Chapter 7, section 7.4, Table 18).

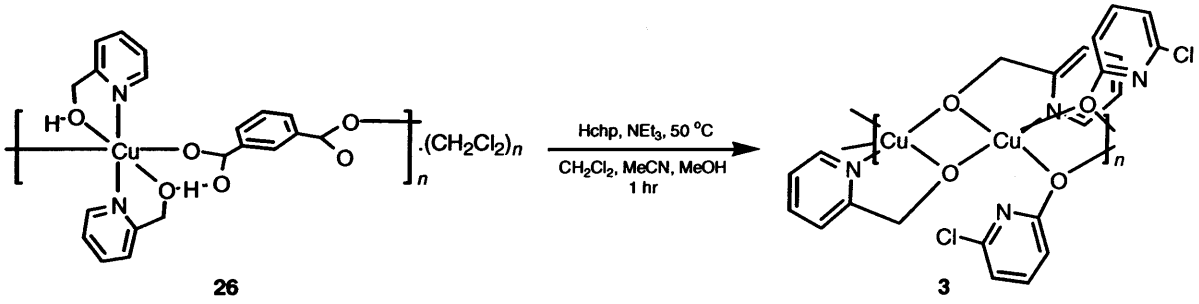

Scheme 12 Conversion of **26** into **3**.

Notably, reactions of ligand blends composed of *m*-$BDCH_2$ and Hchp (n = 0) with either nickel(II) acetate tetrahydrate or copper(II) acetate monohydrate, using the synthetic strategy employed in this work, proved to be unsuccessful in terms of well-characterised

products. It is worthy of note that reactions of combinations of *o*-$BDCNa_2$ (*o*-BDC = 1,2-benzenedicarboxylate) and Nachp with metal salts have proved successful for the formation of a number of complexes including $[Co_{13}(chp)_{20}(o\text{-}BDC)_2(OH)_2]$[5b] and $[Ni_{16}Na_6(chp)_4(o\text{-}BDC)_{10}(o\text{-}BDCH)_2(MeO)_{10}(OH)_2(MeOH)_{20}]$.[5c]

4.3 Blending Isopthalic Acid and α-Diimines or Formamidines on a Cu(II) Centre

4.3.1 M = Cu, L^1 = *m*-$BDCH_2$, L^2 = phen

The reaction of *m*-$BDCH_2$ and 1,10-*N,N*-phenanthroline (phen) with copper acetate monohydrate in the presence of triethylamine gave, on work-up, crystals of $[Cu(phen)_2(m\text{-}BDC)]\cdot 6H_2O\cdot CH_2Cl_2$ (**30**) in moderate yield (Scheme 13). Complex **30** was characterised by elemental analysis, IR spectroscopy and FAB mass spectrometry. In addition, a single crystal of **30** was subject to X-ray diffraction study. The molecular structure of **30** is depicted in Figure 9; selected bond lengths and angles are given in Table 8.

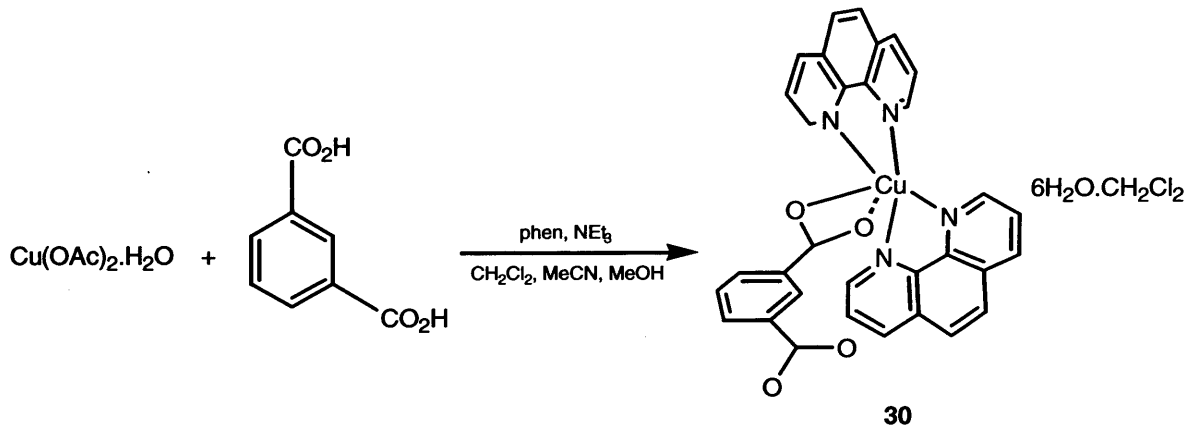

30

Scheme 13 Synthesis of **30** (picture excludes a CH_2Cl_2 and a water molecule).

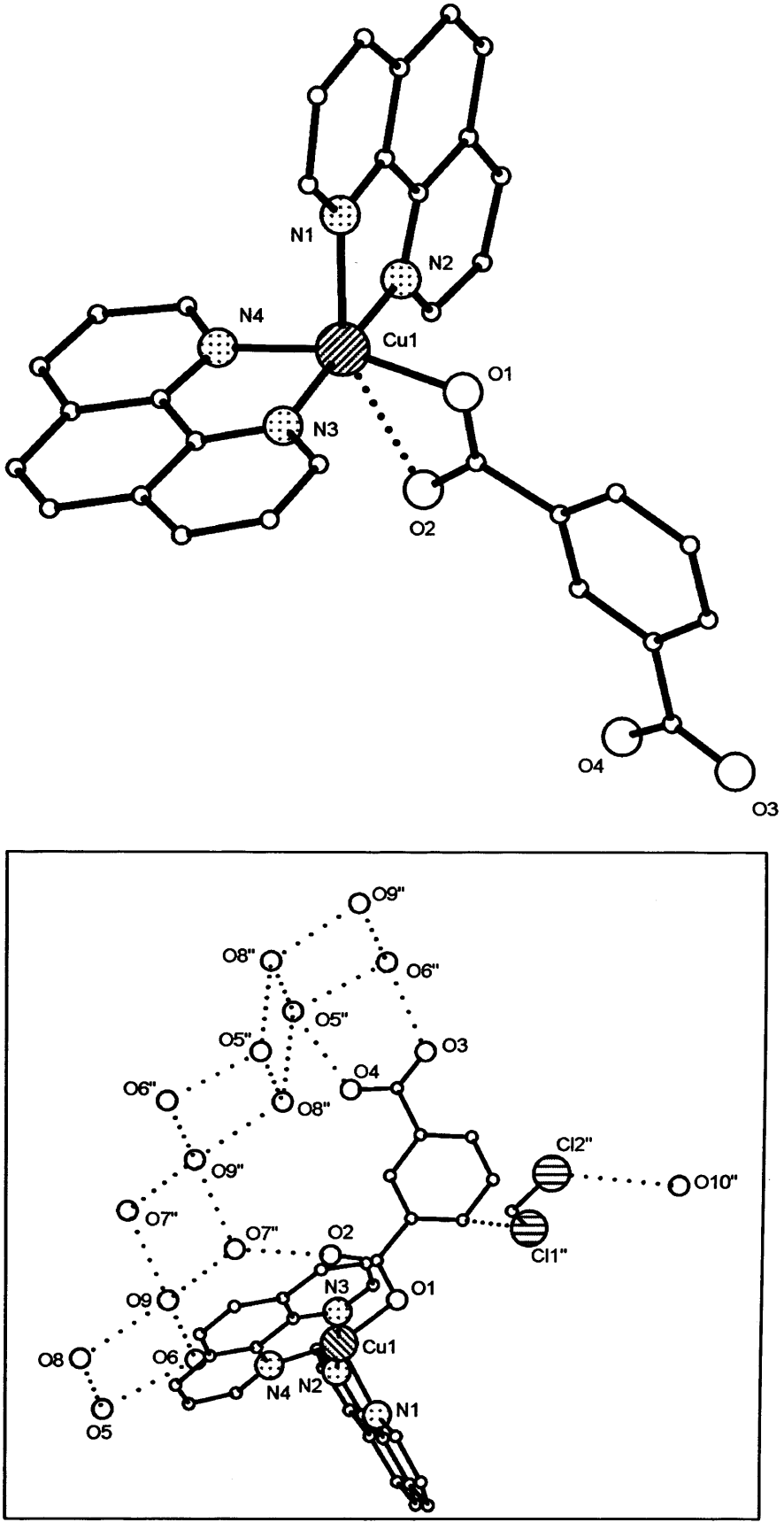

Figure 9 Molecular structure of **30** (excluding solvent molecules). The asymmetric unit is labelled. Hydrogen atoms and carbon atom labels have been excluded for clarity. Dotted lines indicate hydrogen bonding/pseudo-axial interactions. Inset shows part of the 2,2,2 packed hydrogen bonded network, in which primed atoms denote atoms from neighbouring/lattice packed molecules.

The molecular structure of **30** consists of a single Cu(II) ion displaying a distorted square-based pyramidal geometry and coordinated by two phen ligands and an *m*-BDC ligand. The basal sites are occupied by one phen ligand, one oxygen atom from a *m*-BDC ligand and one nitrogen of the second phen, while the apical site is filled by the remaining nitrogen atom [N(1)] of the second phen ligand. The *N,N*-bound phen ligands form five-membered chelate rings with the metal ion and the *m*-BDC ligand adopts a type 1, η^1: *syn* monodentate, terminal bonding mode [Figure 1(k)].

Table 8 Selected bond length (Å) and angle (°) data for complex **30**

30					
Cu(1)-O(1)	2.001(11)	Cu(1)-N(1)	2.200(3)	Cu(1)-N(3)	1.994(3)
Cu(1)-N(2)	2.008(3)	Cu(1)-N(4)	2.029(3)		
O(1)-Cu(1)-N(1)	101.11(10)	N(3)-Cu(1)-O(1)	91.03(11)	N(3)-Cu(1)-N(2)	175.57(11)
O(1)-Cu(1)-N(2)	89.58(11)	O(1)-Cu(1)-N(4)	161.06(10)	N(2)-Cu(1)-N(4)	96.36(11)
N(2)-Cu(1)-N(1)	79.54(11)	N(4)-Cu(1)-N(1)	97.66(11)	N(3)-Cu(1)-N(4)	81.71(11)
N(3)-Cu(1)-N(1)	104.63(11)				

In **30**, the longest metal-ligand bond length arises from a phen nitrogen atom situated at the apex of the square-based pyramid [Cu(1)-N_{phen}(1) = 2.200 Å]. The coordinated *m*-BDC oxygen atom-based C-O bond length at 1.274(4) Å indicates the presence of mainly ionic metal ion-ligand interactions.[9] A Jahn-Teller distorted pseudo-octahedral geometry at the Cu(II) ion in **30** could also be used to describe the geometry on consideration of the pseudo-axial Cu(1)···$O_{m\text{-}BDC}$(1) bond distance at 2.616(2) Å.

The asymmetric unit in **30** additionally contains six water molecules and a molecule of dichloromethane. Five of the water molecules undergo hydrogen bonding interactions with each other and the non-coordinated *m*-BDC carboxylate oxygen atoms [O(3) and O(4)]. In addition, a molecule of dichloromethane undergoes a very weak interaction with an adjacent *m*-BDC aryl proton and a sixth water molecule. Thus, complex **30** can be regarded as a network of hydrogen bonded monomers held collectively by predominantly weak intermolecular hydrogen bonding interactions from interpenetrating molecules of

water (Figure 9, inset). All hydrogen bonding interactions present in **30** are summarised in Table 9.

Table 9 Intermolecular hydrogen bonding distances (Å) for complex **30**

Type			Type		
Water-water	O(5)···O(6)	2.8143	*m-BDC-packed lattice*	$O_{m\text{-}BDC}(2)\cdots O_{water}(7'')$	2.7856
Water-water	O(5)···O(8)	2.7911	*m-BDC-packed lattice*	$O_{m\text{-}BDC}(3)\cdots O_{water}(6'')$	2.7386
Water-water	O(6)···O(9)	2.763	*m-BDC-packed lattice*	$O_{m\text{-}BDC}(4)\cdots O_{water}(5'')$	2.7072
Water-water	O(8)···O(9)	2.7632	CH_2Cl_2-*m-BDC*	$Cl(1'')\cdots C_{m\text{-}BDC}(4)$	3.1639
water-packed lattice	O(9)···O(7'')	2.770	CH_2Cl_2-*packed lattice*	$Cl(2'')\cdots O_{water}(10)$	3.866

All esd values are less than the sum – 0.2 Å.

In the, previously reported isopthalate-bridged/phen complex $\{[Cu(phen)(m\text{-}BDC)_2(H_2O)]\cdot H_2O\cdot DMF\}_n$ the Cu(II) ions also displays a square-based pyramidal geometry.[14] However, in this complex, a *N,N*-phen chelating ligand, and two *m*-BDC ligands {type 1, η^1: *syn*, monodentate and type 2, η^1: *syn*, monodentate, terminal} [Scheme 1(i)] are each bound to the square base (vertices) of the pyramid and the apical site of the pyramid is occupied by a water ligand. The average bond lengths in $\{[Cu(phen)(m\text{-}BDC)_2(H_2O)]\cdot H_2O\cdot DMF\}_n$ with $Cu\text{-}N_{phen}$ = 2.018 Å and $Cu\text{-}O_{m\text{-}BDC}$ = 2.137 Å are comparable to those found in **30** [2.058 Å and 2.001Å, respectively].

Other recent reports on square planar Cu(II) ion-based polymers supported by *N,N*-chelating phen and isopthalate ligands include $[Cu_3(phen)_2(m\text{-}BDCH)_2(m\text{-}BDC)_2]_n$[1u] and $[Cu_2(phen)_2(m\text{-}BDC)_2(H_2O)]_n$.[1s] These contain bis-type 1, η^1: *anti*, monodentate, terminal and type 2, η^1: *syn* bidentate, 1,3-bridging *m*-BDC and *m*-BDCH ligands [Scheme 1(m)] or bis-type 2, η^1: *syn*, monodentate, terminal *m*-BDC ligands [Scheme 1(j)], respectively. $[Cu_3(phen)_2(m\text{-}BDCH)_2(m\text{-}BDC)_2]_n$, adopts a two-dimensional zig-zag polymeric structure [$Cu\text{-}N_{phen}$ = av. 2.005 Å and $Cu\text{-}O_{m\text{-}BDC/m\text{-}BDCH}$ = av. 2.024 Å] while $[Cu_2(phen)_2(m\text{-}BDC)_2(H_2O)]_n$ is a zipper-like helical double-stranded polymer [$Cu\text{-}N_{phen}$ = av. 2.048 Å and $Cu\text{-}O_{m\text{-}BDC}$ = av. 1.964 Å].[1u] The bond lengths in these two complexes are comparable with those found in **30**. However, unlike these complexes, **30** shows no evidence for $\pi\cdots\pi$

stacking interactions as the monomers in the crystal packed lattice are separated by intervening molecules of water.

The IR spectrum of **30** exhibits a strong $\nu(CO_2)_{symm}$ stretching band at 1388 cm^{-1}.[13] The FAB mass spectrum of **30** includes a $[M]^+$ peak at 588 Da. The room temperature magnetic moment for **30** at 2.4 BM ($\chi_M T$ = 0.74 emu K mol^{-1}) is slightly higher than expected for a single paramagnetic Cu(II) ion (***SEE NOTE***).[26b,26d]

4.3.2 M = Cu, L^1 = *m*-$BDCH_2$, L^2 = HDLF

4.3.2.1 HDLF (L = mes or *o*-tol)

As a variation on the molar ratios employed in Scheme 1, equimolar amounts of *m*-$BDCH_2$ and a formamidine (HDLF) were treated with with copper(II) acetate monohydrate in the presence of triethylamine in a solvent mixture composed of MeCN, CH_2Cl_2 and MeOH, resulting in green crystals of $[Cu_{24}(m\text{-}BDC)_{24}(HDLF)_{12}(H_2O)_{12}]\cdot 2MeCN\cdot 12H_2O$ [L = mes (**31a**), L = *o*-tol (– 2MeCN, – $12H_2O$) (**31b**)] in good yield (Scheme 14). Complexes **31a** and **31b** were characterised by elemental analysis, IR spectroscopy, variable temperature SQUID magnetometry (for **31a**) and MALDI mass spectrometry. Single crystals of **31a** and **31b** were subject to X-ray diffraction studies. The molecular structure of **31a** is shown in Figure 10; selected bond lengths and angles are given in Table 10.

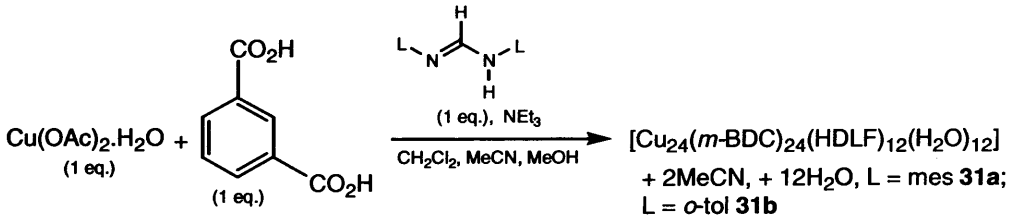

Scheme 14 Synthesis of **31**.

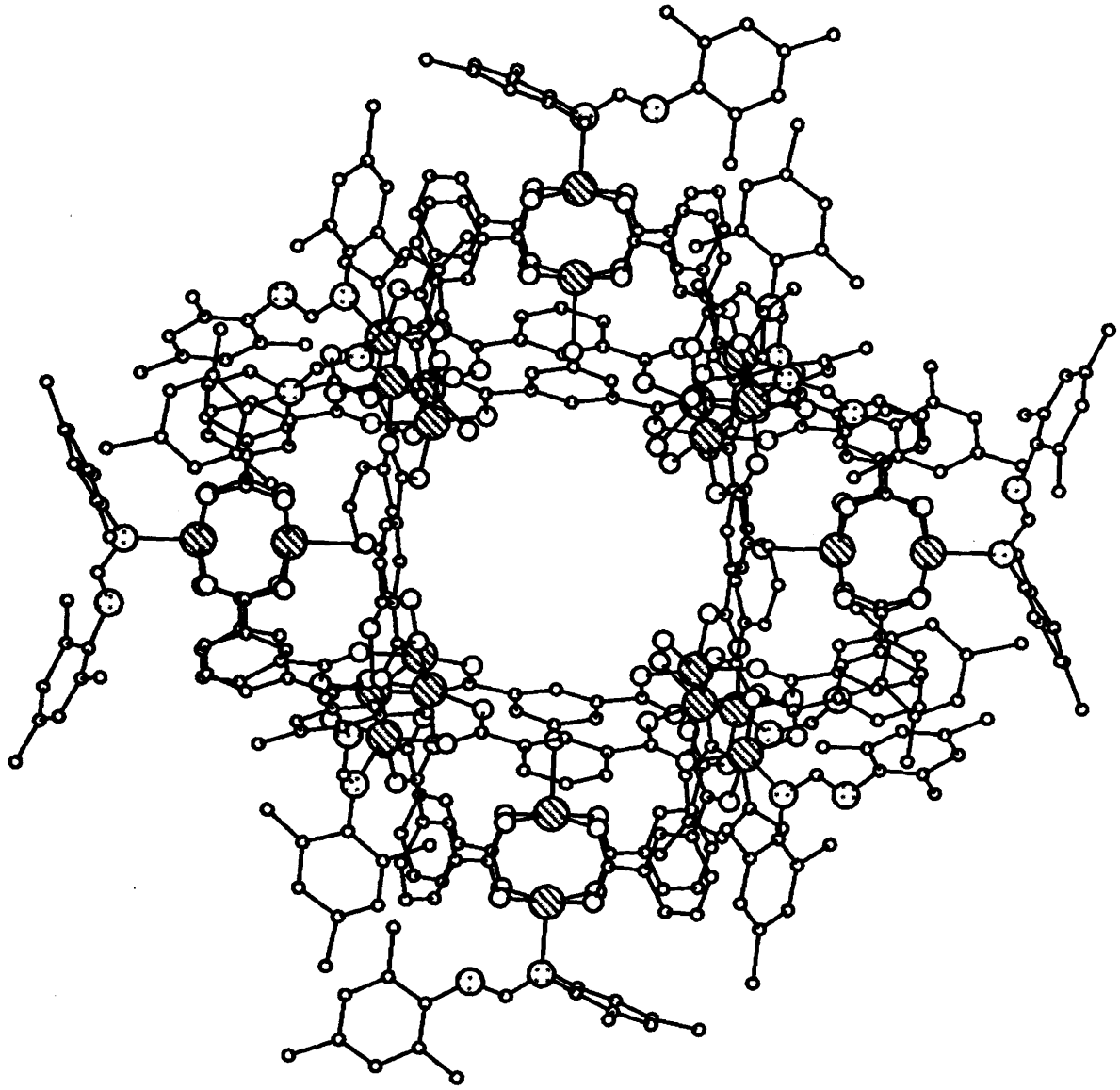

Figure 10 Molecular structure of **31a**. Hydrogen atoms, solvent molecules and atom labelling have been removed for clarity.

Table 10 Selected bond length (Å) and angle (°) data for complex **31a**

31a											
Cu(1)-O(1)	2.220(11)	Cu(2)-O(3)	1.941(10)	Cu(3)-O(12)	2.246(7)	Cu(4)-O(16)	1.966(9)	Cu(2)-N(1)	2.104(12)	Cu(1)···Cu(2)	2.669(2)
Cu(1)-O(2)	1.961(10)	Cu(2)-O(5)	1.947(11)	Cu(3)-O(13)	1.952(9)	Cu(4)-O(18)	1.952(9)	Cu(4)-N(3)	2.208(15)	Cu(3)···Cu(4)	2.678(2)
Cu(1)-O(4)	1.931(11)	Cu(2)-O(7)	1.956(11)	Cu(3)-O(15)	1.944(9)	Cu(5)-O(21)	2.208(15)	Cu(6)-N(5)	2.136(16)	Cu(5)···Cu(6)	2.683(2)
Cu(1)-O(6)	1.957(11)	Cu(2)-O(9)	1.935(11)	Cu(3)-O(15)	1.953(10)	Cu(7)-O(30)	2.237(7)	Cu(8)-N(7)	2.209(5)	Cu(7)···Cu(8)	2.689(2)
Cu(1)-O(8)	1.971(11)	Cu(3)-O(10)	1.957(9)	Cu(4)-O(11)	1.943(7)	Cu(9)-O(39)	2.333(7)	Cu(10)-N(9)	2.186(11)	Cu(9)···Cu(10)	2.686(2)
				Cu(4)-O(14)	1.970(9)	Cu(11)-O(48)	2.314(6)	Cu(12)-N(11)	2.196(11)	Cu(11)···Cu(12)	2.688(2)
O(3)-Cu(2)-N(1)	94.3(5)	O(11)-Cu(4)-N(3)	101.4(5)	O(22)-Cu(6)-N(5)	97.5(6)	O(29)-Cu(8)-N(7)	98.1(3)	O(38)-Cu(10)-N(9)	97.2(4)	O(47)-Cu(12)-N(11)	103.2(4)
O(5)-Cu(2)-N(1)	94.2(5)	O(14)-Cu(4)-N(3)	94.2(5)	O(24)-Cu(6)-N(5)	92.6(5)	O(32)-Cu(8)-N(7)	101.0(3)	O(41)-Cu(10)-N(9)	101.5(4)	O(50)-Cu(12)-N(11)	100.1(4)
O(7)-Cu(2)-N(1)	96.8(5)	O(16)-Cu(4)-N(3)	99.9(5)	O(27)-Cu(6)-N(5)	96.7(5)	O(34)-Cu(8)-N(7)	94.8(3)	O(43)-Cu(10)-N(9)	82.8(3)	O(52)-Cu(12)-N(11)	93.2(4)
O(9)-Cu(2)-N(1)	98.2(5)	O(18)-Cu(4)-N(3)	91.3(5)	O(20)-Cu(6)-N(5)	99.8(5)	O(36)-Cu(8)-N(7)	93.6(4)	O(45)-Cu(10)-N(9)	91.5(4)	O(54)-Cu(12)-N(11)	92.3(4)
O(2)-Cu(1)-O(1)	96.4(3)	O(10)-Cu(3)-O(12)	95.9(3)	O(19)-Cu(5)-O(21)	95.1(4)	O(28)-Cu(7)-O(30)	96.8(4)	O(37)-Cu(9)-O(39)	93.0(3)	O(46)-Cu(11)-O(48)	94.5(3)
O(4)-Cu(1)-O(1)	96.9(3)	O(13)-Cu(3)-O(12)	96.5(3)	O(23)-Cu(5)-O(21)	95.5(4)	O(31)-Cu(7)-O(30)	94.9(4)	O(40)-Cu(9)-O(39)	93.9(3)	O(51)-Cu(11)-O(48)	93.7(3)
O(6)-Cu(1)-O(1)	96.5(3)	O(15)-Cu(3)-O(12)	93.9(3)	O(25)-Cu(5)-O(21)	96.2(4)	O(33)-Cu(7)-O(30)	95.7(4)	O(42)-Cu(9)-O(39)	99.6(3)	O(53)-Cu(11)-O(48)	96.3(3)
O(8)-Cu(1)-O(1)	95.2(3)	O(17)-Cu(3)-O(12)	97.8(3)	O(26)-Cu(5)-O(21)	96.7(4)	O(35)-Cu(7)-O(30)	97.4(4)	O(44)-Cu(9)-O(39)	98.9(3)		

The molecular structure of **31a** reveals a spheroidal cluster (nanoball) containing twenty four Cu(II) ions. The structure of **31a** is constructed from the self assembly of twelve dimeric units or Secondary Building Units (SBUs) (Figure 11).[17] These SBUs comprise pairs of copper ions 1,3-bridged by four bis-η^1, η^1: *syn, syn* bidentate (μ_2) *m*-BDC ligands [Scheme 1(a)] so as to generate twelve paddle wheel units [{$Cu_2(RCO_2)_4(HDmesF)(H_2O)$}, R = $0.5C_6H_4$].

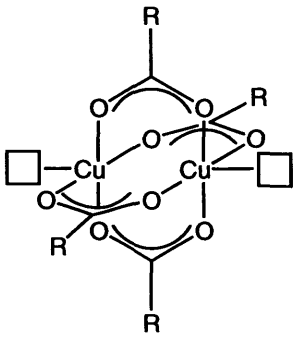

Figure 11 SBU paddle wheel-based motif with two vacant apical sites.

The axial sites of the paddle wheel-based SBUs are occupied by either an η^1-bound HDmesF or a water ligand. The first type of SBU is based on a *cis-N,N'*-imine bound HDmesF ligand, of which there are five of this type [Figure 12(a)]. The second type of SBU contains a *trans-N,N'*-imine bound HDmesF ligand located on Cu(1/1A) and Cu(2/2A) [Figure 12(b)].

The HDmesF ligands in **31a**, are found on the surface of the nanoball as part of a hydrophobic exterior (bound to outer copper ions) while, the water ligands are encased within the nanoball as the hydrophilic interior (bound to inner copper ions). The imine-bound HDmesF and water ligands have bond lengths averaging to Cu-N_{imine} = 2.173 Å and Cu-O_{water} = 2.260 Å, respectively.

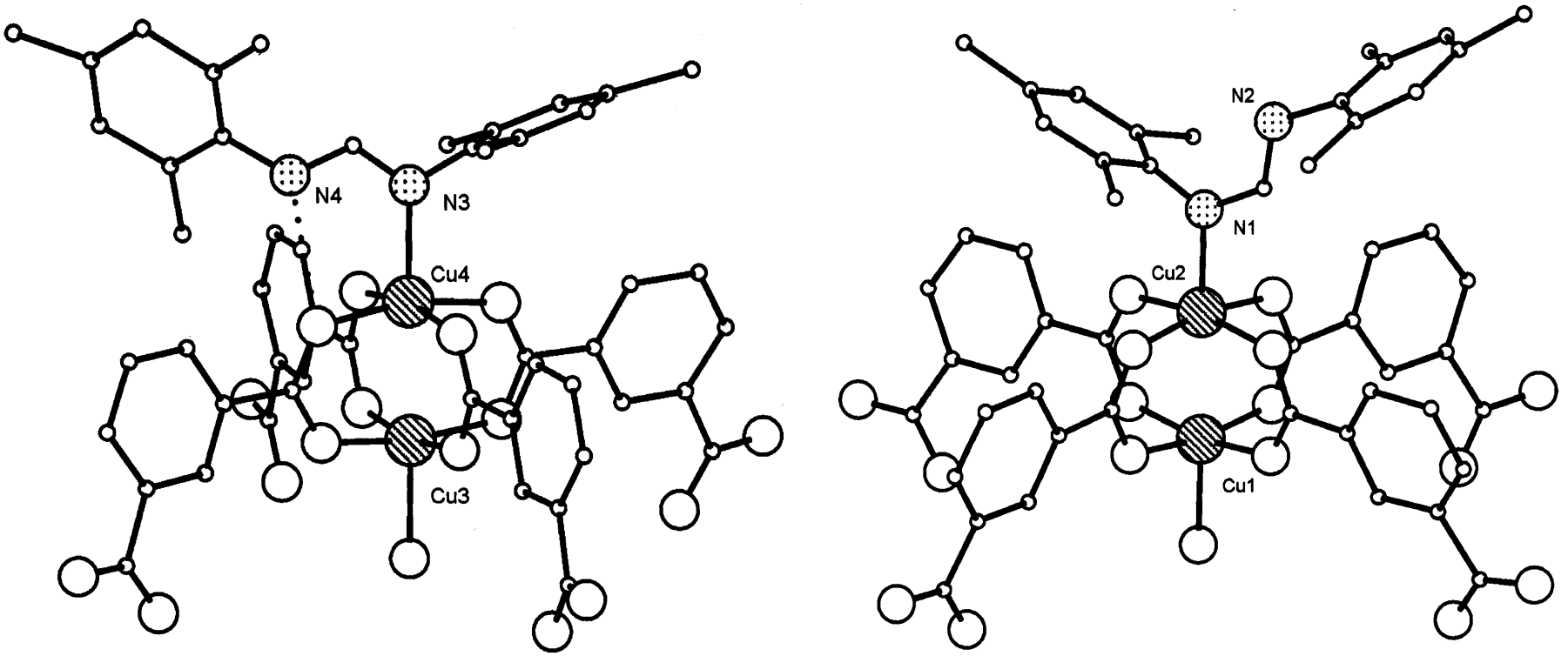

(a) (b)

Figure 12 Examples of SBU fragments in **31a**, containing (a) *cis-N,N'*-HDmesF and (b) *trans-N,N'*-HDmesF. Dotted lines show hydrogen bonding interactions.

In **31a**, the five *cis*-HDmesF ligands have C-N bond lengths of C(H)=N_{imine} = 1.301 Å and C(H)-NH_{amine} = 1.310 Å, with corresponding C-N-C average bond angles of C_{Mes}-N_{imine}=C(H) = 114.62°, C_{Mes}-$N(H)_{amine}$-C(H) = 121.78° and N_{amine}-C(H)=N_{imine} = 120.14°. In comparison, the two *trans*-HDmesF ligands have C-N bond lengths of C(H)=N_{imine} = 1.352 Å and C(H)-NH_{amine} = 1.317 Å, with corresponding C-N-C average bond angles of C_{Mes}-N_{imine} =C(H) = 116.6°, C_{Mes}-$N(H)_{amine}$-C(H) = 125.2° and N_{amine}-C(H)=N_{imine} = 125.6°. These values suggest the presence of C=N bonds and sp^2-hybridised carbon-atoms.[16] The Cu-$O_{m\text{-}BDC}$ bond lengths in **31a** average to 1.956 Å while the average C-O *m*-BDC bond length at 1.256 Å indicates the presence of mainly ionic metal-carboxylate bonds.[9]

In **31a**, the *cis-N,N'* imine-bound HDmesF ligands undergo inter-ligand hydrogen bonding interactions *via* the protonated amine towards a neighbouring *m*-BDC oxygen atom [av. $N_{amine}\cdots O_{m\text{-}BDC}$ = 2.876 Å] (Table 11). The *trans-N,N'* imine-bound HDmesF ligands are not involved in hydrogen bonding interactions.

Table 11 Hydrogen bond distances (Å) from the five *cis-N,N'*-HDmesF SBUs in **31a**

Type		Type		Type	
$O_{m\text{-}BDC}(16)\cdots N_{amine}(4)^a$	2.88(2)	$O_{m\text{-}BDC}(29)\cdots N_{amine}(8)^c$	2.9138(3)	$O_{m\text{-}BDC}(47)\cdots N_{amine}(12)^e$	2.909(16)
$O_{m\text{-}BDC}(27)\cdots N_{amine}(6)^b$	2.89(3)	$O_{m\text{-}BDC}(38)\cdots N_{amine}(10)^d$	2.785(17)		

From HDmesF on [a]Cu(4), [b]Cu(6), [c]Cu(8), [d]Cu(10) or [e]Cu(12).

An estimate to the void space in **31a** can be appreciated by consideration of the maximum Cu(II)···Cu(II) ion distances averaging to 10.70 Å between the HDmesF bound ions (outer) and 7.98 Å between the water bound ions (inner). Connection of the copper ions along the direction of the planes of the *m*-BDC phenyl rings results in six 2-D square and eight 2-D triangular faced polygons, which in-turn connect to form a cuboctahedron [12 vertices, 8_3 + 6_4 = 14 faces, 24 edges] (Figures 13 and 14).[30a,17b] The maximum distance between two opposing copper ions within the coordination sphere is 21.573 Å (outer polyhedra) [16.208 Å (inner polyhedra)].

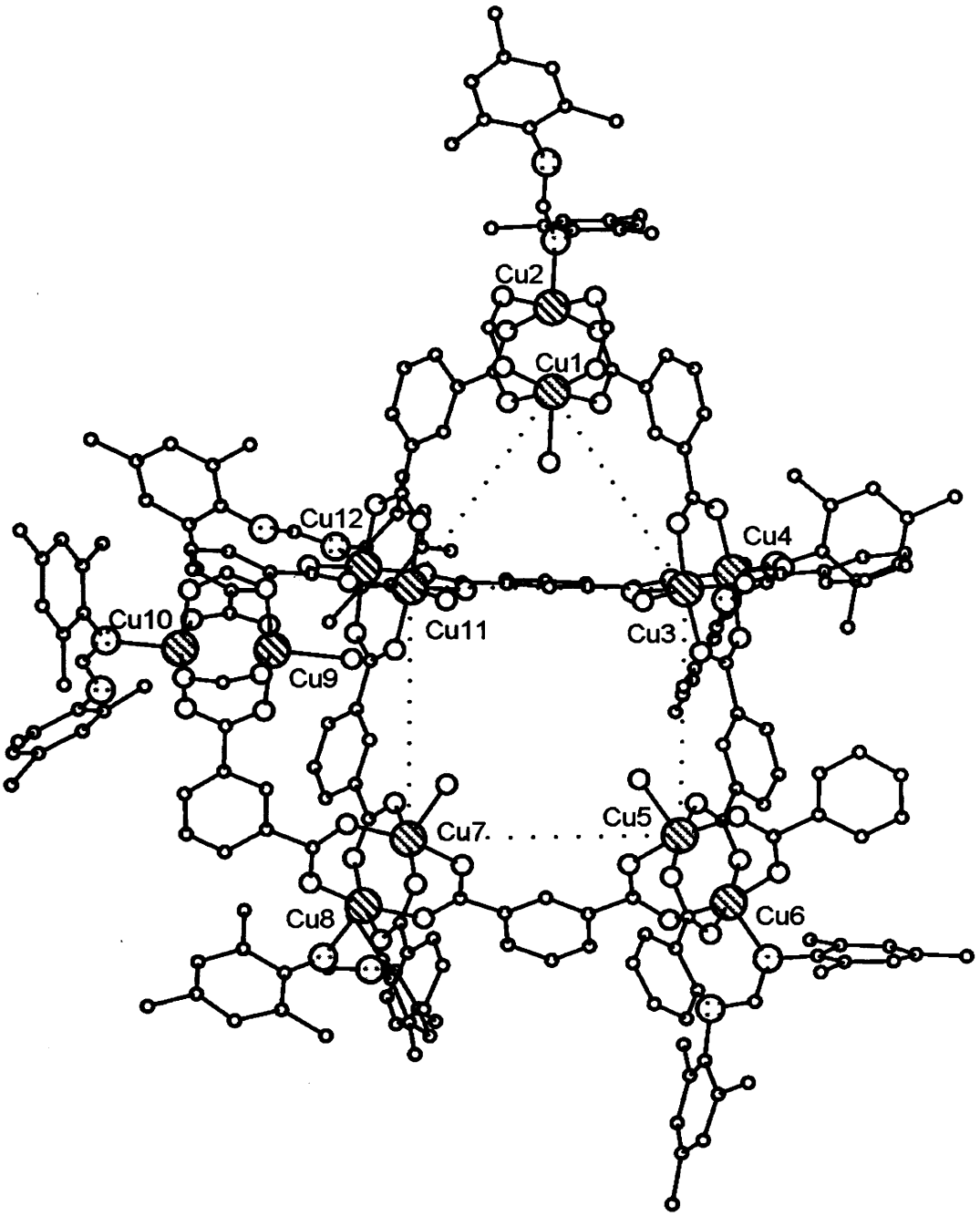

Figure 13 The asymmetric unit of **31a** containing six different types of SBUs. Only copper ions are labelled for clarity. Hydrogen atoms and solvent molecules are omitted for clarity. Dotted lines depict the square and triangular faces that form the part of the cuboctahemihedra (inner).

The oxygen atoms of the *m*-BDC ligands in **31** can be linked to form outer and enclosed inner truncated cuboctahedra [48 vertices, $12_4 + 8_6 + 6_8$ = faces, 72 edges].[30a] The truncated cuboctahedral frameworks resemble a portion of the zeolitic framework structure of faujasite (Figure 15).[30b] The basic geometrical polyhedral structures obtained from **31a** and **31b** have been reported previously and more recently classified as supramolecular MOFs (see section Chapter 1, sections 1.1.6 and 1.2.3).[1,2,17,23-25]

In **31a**, the largest distances observed between the furthest opposing *p*-Me mesityl carbon atoms average to 35.432 Å ($H_{HDmesF}\cdots H_{HDmesF}$ = 36.921 Å) with a maximum distance of $C_{HDmesF}\cdots C_{HDmesF}$ = 36.961 Å ($H_{HDmesF}\cdots H_{HDmesF}$ = 38.449 Å). The largest diameters for the reported spheroidal clusters *viz.* $[Cu_{24}(m\text{-}BDC)_{24}(DMF)_{14}(H_2O)_{10}]\cdot 50H_2O\cdot 6DMF\cdot C_2H_5OH$ [3.4 nm diameter from opposing DMF atoms (non H)] and $\{[Cu_2(5\text{-}SO_3\text{-}BDC)_2(4\text{-methoxypyridine})_{0.5}(MeOH)_x(H_2O)_{1.5-x}]_{12}\}^{24-}$ [3.6 nm diameter from opposing 4-methoxypyridine atoms (non H)], are slightly smaller in size when compared with **31a**.[17a,17c]

There are a few recent reports of other copper clusters having nuclearities of ≥ $\{Cu_{24}\}$, for example; an aggregate of $\{Cu_{44}\}$, [20] a spheroidal $\{Cu_{36}\}$ cluster,[21a] a $\{Cu_{36}\}$ cluster encapsulating a $\{KCl_6\}^{5-}$ unit,[21b] heteronuclear clusters of $\{Cu_{24}Ln_6\}$,[22a-b] $\{Mg_{35}Cu_{24}Ga_{53}\}$ and,[22c] $\{Cu_{29}Se_{15}\}$, $\{Cu_{30}Se_{15}\}$, $\{Cu_{36}Se_{18}\}$, $\{Cu_{70}Se_{35}\}$,[22d,22e] and an imido cluster $[Cu_{24}(NPh)_{14}]$ $[Li(THF)_4]_4$.[22f]

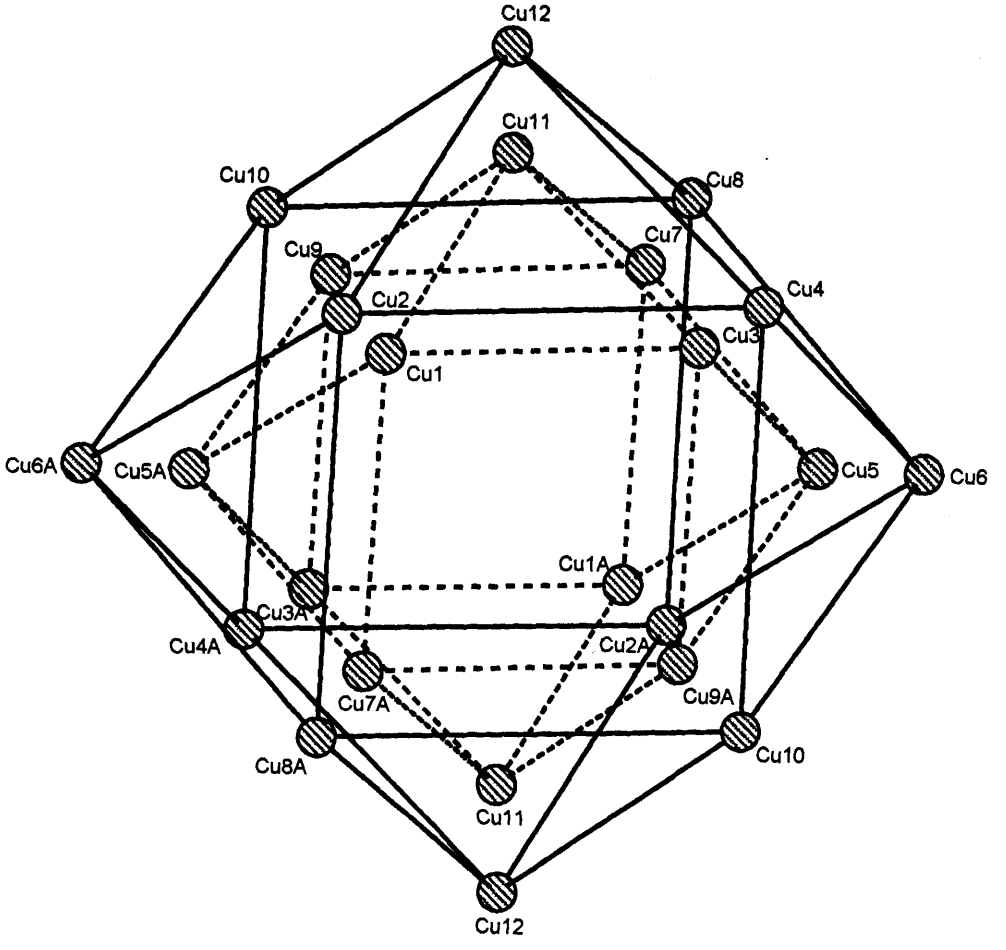

Figure 14 Copper connected squares and triangles forming inner (dashed lines) and outer (solid lines) cuboctahedra within **31a**.

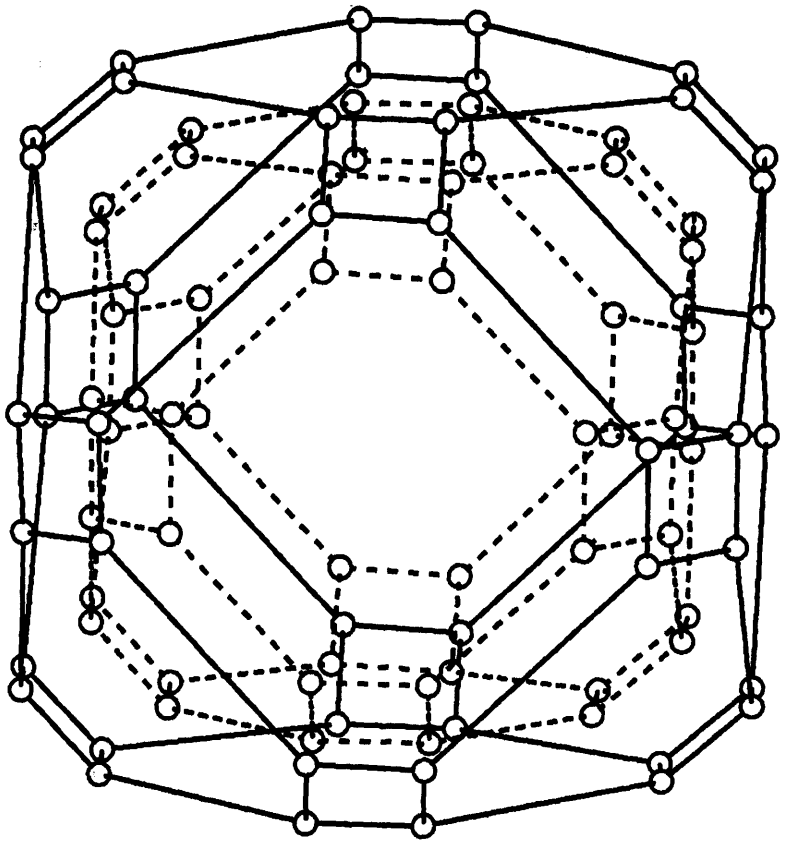

Figure 15 Truncated cuboctahedral core of **31a** formed by intra- and inter-connecting *m*-BDC ligand donor oxygen atoms. The inner polyhedron is depicted by the dotted lines and the outer polyhedron is shown by the connected dotted lines.

The MALDI mass spectra of desolvated **31a** (9024 Da.) and **31b** (8352) display peaks associated with complete removal of apical ligands (H_2O and HDLF)[18] along with selected fragmentation peaks associated with the loss of copper ions and *m*-BDC ligands (Table 12). Thermogravimetric (TGA) analysis has recently provided a better method for determining the composition of the nanoballs within the research group.[15]

Table 12 MALDI mass spectrum peaks (Da.) of **31**

31a		**31b**[b]	
[*M* – 12HDmesF – 12H_2O – 7Cu – 9*m*-BDC]$^+$	3540	[*M* – 12HD*o*-tolF – 12H_2O – 14Cu – 2*m*-BDC]$^+$	4238
[*M* – 12HDmesF – 12H_2O – 7Cu – 12*m*-BDC]$^+$	3048	[*M* – 12HD*o*-tolF – 12H_2O – 16Cu – 8*m*-BDC]$^+$	3128
[*M* – 12HDmesF – 12H_2O – 13Cu – 13*m*-BDC]$^+$	2502	[*M* – 12HD*o*-tolF – 12H_2O – 16Cu – 12*m*-BDC]$^+$	2472
[*M* – 12HDmesF – 12H_2O – 9Cu – 15*m*-BDC]$^+$	2429	[*M* – 12HD*o*-tolF – 12H_2O – 19Cu – 18*m*-BDC]$^+$	1299
[*M* – 12HDmesF – 12H_2O – 13Cu – 18*m*-BDC]$^{+a}$	2011	[*M* – 12HD*o*-tolF – 12H_2O – 20Cu – 18*m*-BDC]$^+$	1236
[*M* – 12HDmesF – 12H_2O – 14Cu – 18*m*-BDC]$^+$	1619	[*M* – 12HD*o*-tolF – 12H_2O – 20Cu – 19*m*-BDC]$^+$	1072
		[*M* – 12HD*o*-tolF – 12H_2O – 21Cu – 19*m*-BDC]$^+$	1009

[a]Base peak. [b]No matrix

The IR spectra of complexes **31** exhibit four distinct stretching bands including, weak bands of $\nu(NH)_{amine}$ 3323 cm^{-1} (**31a**) 3275 cm^{-1} (**31b**), a strong $\nu(C{=}N)_{imine}$ band at ~ 1634 cm^{-1}, a less intense $\nu(CO_2)_{asymm}$ band at ~ 1580 cm^{-1} and a strong $\nu(CO_2)_{symm}$ band at ~ 1388 cm^{-1}.[36] UV-Vis. electronic spectroscopy of the nanoballs in acetonitrile, was attempted but due to a lack of solubility the results were inconclusive.

4.3.2.2 HDLF (L = 2,6-xyl)

Reacting equimolar amounts of a ligand blend composed of *m*-$BDCH_2$ and HD2,6-xylF with copper acetate monohydrate in the presence of triethylamine gave, on work-up, $[Cu_{24}(m\text{-BDC})_{24}(HD2,6\text{-xylF})_{12}(H_2O)_{12}]$ (**31c**), as a green powder in low yield and blue crystals of $[Cu(HD2,6\text{-xylF})_2(m\text{-BDC})]_n$ (**32**) in moderate yield (Scheme 15).[15] Complexes **31c** and **32** were characterised by elemental analysis, IR spectroscopy along with FAB (for **32**) and MALDI mass spectrometry. A single crystal of **32** was subject to an X-ray

diffraction study. The molecular structure of **32** is depicted in Figure 16; selected bond lengths and angles are given in Table 13.

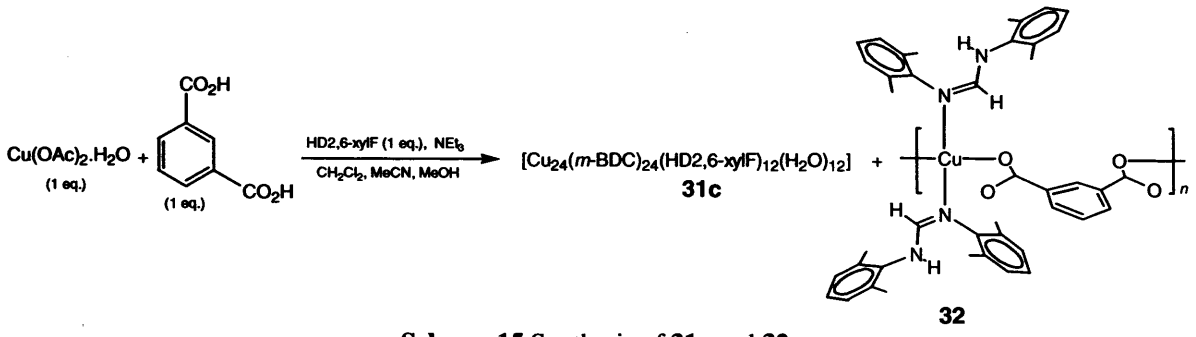

Scheme 15 Synthesis of **31c** and **32**.

The molecular structure of **32** reveals a polymeric structure with each pseudo-square planar Cu(II) ion surrounded by two oxygen atoms from two *m*-BDC dianions and two *N*-atoms from two HD2,6-xylF ligands. In each monomeric unit, two HD2,6-xylF ligands are *trans* bound through the imine nitrogen atoms while the amine moieties remain pendant. The *trans*-disposed *m*-BDC dianions function as bridges between adjacent Cu(II) ions in a bis-type 2, η^1: syn, monodentate bonding mode [Scheme 1(j)], thus, resulting in a 1-D undulating/zig-zag polymer chain similar in type to polymeric **28** [Figure 16(c)].

In **32**, the (H)C=N_{imine} bond length at 1.292(2) Å is typical for an imine C(sp^2)=N bond (~ 1.28 Å) while the amine (H)C-N_{amine} bond length at 1.338(2) Å is shorter than expected for a C(sp^2)-N bond (~ 1.38 Å).[16] The bulky imine- and amine-dimethylphenyl substituents of the HD2,6-xylF ligands in **32**, are positioned almost perpendicular to each other. The *m*-BDC and HD2,6-xylF aryl rings possess offset (skewed), intramolecular (aryl-imine-*m*-BDC aryl) induced dipole-dipole van der Waals/non-$\pi\cdots\pi$ stacking interactions [centroid-centroid; intramolecular C···C = 4.0780(13) Å, offset ~ 10° (nearest atom···atom = 3.411 Å)]. Furthermore, the HD2,6-xylF aryl rings of adjacent polymer chains undergo intermolecular induced dipole-induced dipole (aryl-amine to aryl-amine) Van der Waals/non-$\pi\cdots\pi$ stacking interactions [centroid-centroid; intermolecular C···C = 3.9485(15) Å, offset ~ 9° (nearest atom···atom = 3.611 Å)] [Figure 16(b)].[32]

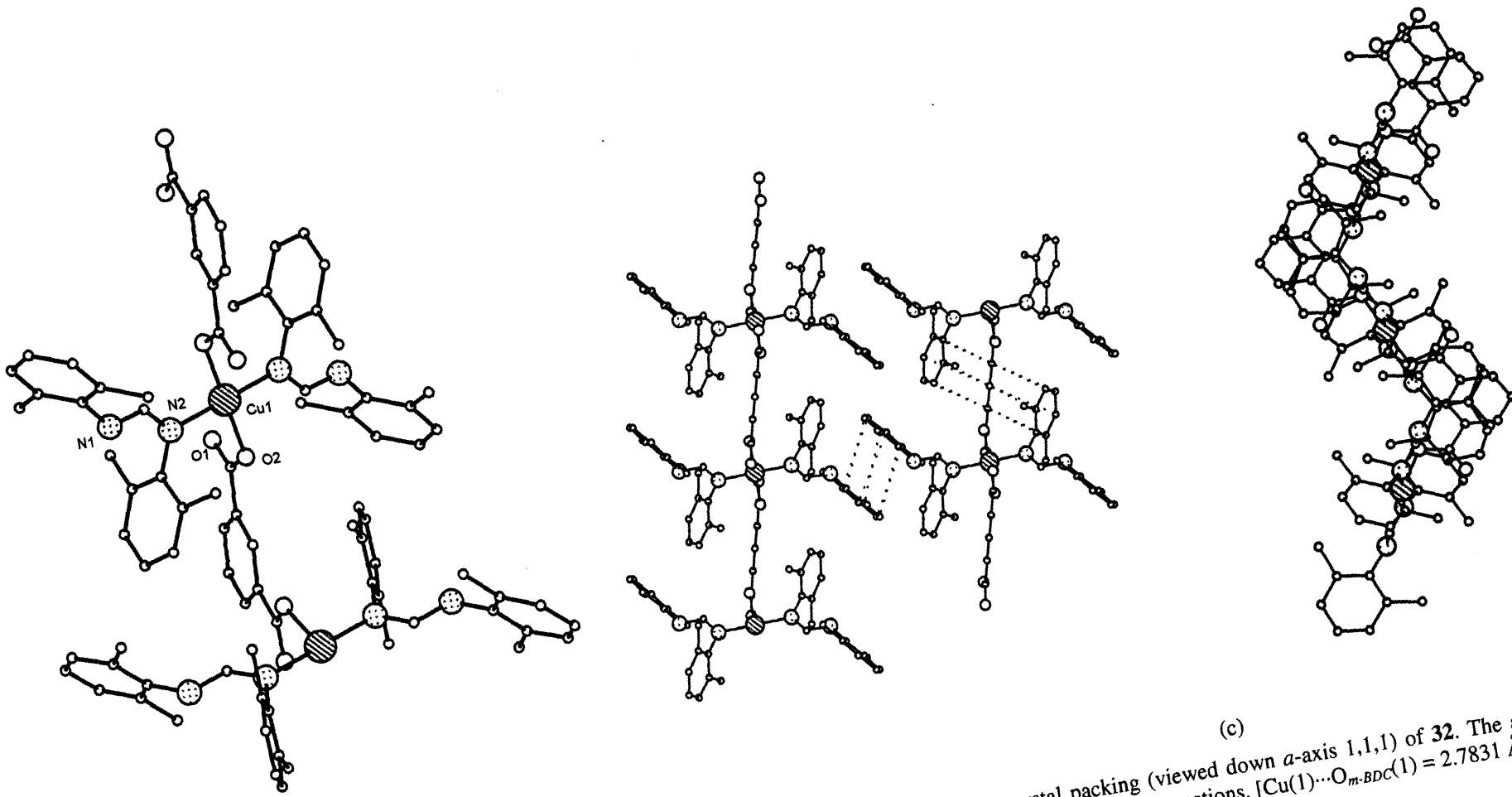

(a) (b) (c)

Figure 16 (a) Part of the polymeric structure, (b) crystal packing (viewed down *b*-axis 1,1,1) and (c) crystal packing (viewed down *a*-axis 1,1,1) of **32**. The asymmetric unit is labelled. Hydrogen atoms and carbon atom labels are excluded for clarity. Dotted bonds indicate van der Waals stacking interactions. [Cu(1)···$O_{m\text{-}BDC}$(1) = 2.7831 Å].

In **32**, the C-O(2) bond length for the bound oxygen atom at 1.291(2) Å indicates the presence of a covalent metal-*m*-BDC interaction.[9] The copper(II) ions within the polymer chain of **32** are separated by ~ 8.13 Å [*cf.* Cu···Cu = 10.872 Å (**26**), 6.984 Å (**27**) and 7.870 Å (**28**)]. No intermolecular hydrogen bonding interactions are apparent between neighbouring chains of **32**. The intermolecular Cu···Cu distance in **32** at ~ 12.82 Å is greater (by *ca.* 4 Å) in comparison to the intermolecular M···M distances in polymers **24**, **26**, **27** and **28**.

Table 13 Selected bond length (Å) and angle (°) data for complex **32**

32	
Cu(1)-O(2)	1.9220(12)
Cu(1)-N(2)	2.0387(15)
C(18)-O(1)	1.238(2)
O(2)-Cu(1)-N(2)	88.67(6)
O(2)#1-Cu(1)-N(2)	91.33(6)

Symmetry transformations used to generate equivalent atoms #1: $(-x+0.5, -y+0.5, -z)$.

The IR spectrum of **31c** exhibits stretching bands of $\nu(NH)_{amine}$ at 3325 cm^{-1} (weak), $\nu(C{=}N)$ at 1635cm^{-1} (strong), $\nu(CO_2)_{asymm}$ at 1557 cm^{-1} and $\nu(CO_2)_{symm}$ at 1389 cm^{-1}.[13] The MALDI mass spectrum of **31c** is similar to **31a** and **31b** and exhibits fragmentation peaks corresponding to the loss of axial ligands along with the selected loss of *m*-BDC ligands and copper ions (Table 14). The IR spectrum of **32** exhibits a strong $\nu(C{=}N)$ stretching band at 1626 cm^{-1}.[13] The FAB mass spectrum of **32** displays a $[M_{(n=1)} - m\text{-BDC}]^+$ peak at 567 Da. and the MALDI mass spectrum (no matrix) displayed peaks including, $[M_{(n=1)} - m\text{-BDC}]^+$ at 567 Da., $[M_{(n=2)} - 2m\text{-BDC}]^+$ at 630 Da. and $[M_{(n=2)} - m\text{-BDC}]^+$ at 794 Da.

Table 14 MALDI mass spectrum peaks (Da.) of **31c**.

31c	**Da.**
$[M - 12HD2,6\text{-xylF} - 12H_2O - 20Cu - 18m\text{-BDC}]^+$	1236
$[M - 12HD2,6\text{-xylF} - 12H_2O - 20Cu - 19m\text{-BDC}]^+$	1072
$[M - 12HD2,6\text{-xylF} - 12H_2O - 21Cu - 20m\text{-BDC}]^+$	845
$[M - 12HD2,6\text{-xylF} - 12H_2O - 22Cu - 20m\text{-BDC}]^+$	782

It is uncertain as to why combinations of *m*-$BDCH_2$ and HDmesF or HD*o*-tolF with copper acetate monohydrate yield exclusively, clusters (**31a** and **31b**), whereas, combinations of *m*-$BDCH_2$ and HD2,6-xylF with copper acetate monohydrate result in both cluster **31c** (similar to **31a** and **31b**) and polymer **32**. This may be attributed to the selective precipitation/crystallisation of the products observed, in which case both polymeric and cluster species may be present in the solution state.

4.3.3 Preliminary Magnetic Characterisation of Complexes 30, 31 and 32

As complexes **31a-c** are constructed from paddle wheel-based SBUs [{$Cu_2(RCO_2)_4(HDLF)(H_2O)$}, R = $0.5C_6H_4$], it was viewed as appropriate to compare their magnetic properties with simple dinuclear copper paddle wheel-based complexes [*e.g.*, $Cu_2(RCO_2)_4 \cdot 2L$, L fills axial sites], which have been exhaustively albeit controversially, investigated.[26,27] The Cu(II)···Cu(II) internuclear ion distances in dinuclear Cu(II) paddle wheel-based complexes range from ~ 2.44 – 2.81 Å, with the corresponding distances comparable in **31a** and **31b**, falling in the range [2.620 – 2.689 Å]. In terms of the magnetochemistry, the Cu(II) ions of paddle wheel units are postulated to couple through the π-orbitals of the 1,3-bridging acetates rather than from overlapping of the contracted Cu(II) $d_{x^2-y^2}$ orbitals.[26]

The room temperature magnetic moments of **31a** (6.5 BM, $\chi_M T$ = 5.28 emu K mol^{-1}) and **31b** (7.0 BM, $\chi_M T$ = 6.07 emu K mol^{-1}) are less than expected for twenty four non-interacting Cu(II) ions (8.5 BM, $\chi_M T$ = 9.00 emu K mol^{-1}) as are the values per copper ion [1.33 BM (**31a**) and 1.43 BM (**31b**) *vs.* 1.73 BM, ***SEE NOTE***].[26d] In the case of **31a**, a variable temperature SQUID magnetic susceptibility study has also been performed. Preliminary results show a maximum magnetic moment at ~ 1.25 BM [$\chi_M T$ = 0.20 emu K mol^{-1}] (325 K) per Cu(II) ion within the nanoball (Figure 17), this value being comparable with the room temperature measurement (*vide infra*).[26b,27] In the temperature range of ~

200 – 100 K, the moment drops rapidly from ~ 1.0 BM – 0.3 BM [$\chi_M T$ = 0.13 emu K mol^{-1} – 0.01 emu K mol^{-1}], suggesting the presence of very strong antiferromagnetic interactions. Below 100 K, it is uncertain as to what is occurring, but could be due to a paramagnetic impurity. Modelling and parameterisation of the data for **31a** is in progress.

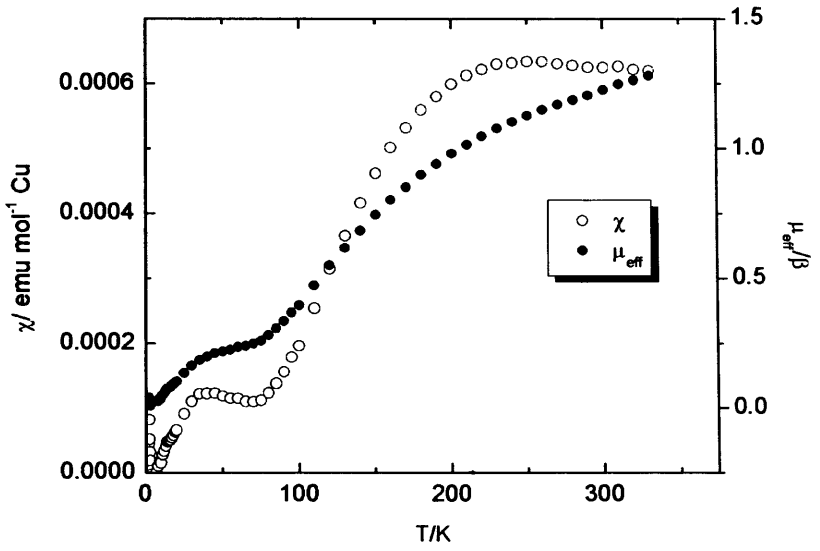

Figure 17 Plots of χ_M against T (open circles) and μ_{eff} against T (closed circles) for **31a** [per Cu(II) ion].

In $Cu_2(CH_3CO_2)_4 \cdot 2H_2O$, the calculated room temperature magnetic moment [per Cu(II) ion] at 1.4 BM [*cf.* 1.33 (**31a**), 1.43 (**31b**)] and the low value being attributed to incomplete antiferromagnetic coupling. The variable temperature magnetic susceptibility measurements of $Cu_2(CH_3CO_2)_4 \cdot 2H_2O$ display maxima at around 300 K and then rapidly decreases at temperatures below 100 K as the Cu(II) ions become strongly antiferromagnetically coupled.[28] Therefore, it is very likely that complexes **31a-c** contain twelve strong antiferromagnetically coupled paddle wheel-based SBUs which collectively accumulate to provide overall antiferromagnetic interactions. The ^{1}H NMR (300 MHz, $CDCl_3$) spectra of **31a** and **31b** recorded at 300 K support the magnetic observations with modestly shifted and broadened peak signals apparent.[35]

In conjunction with magnetic measurements, the EPR spectrum of $Cu_2(CH_3CO_2)_4 \cdot 2H_2O$ exhibits a characteristic S = 1 (average g = 2.159) triplet state signal at higher temperatures of ~ 300 K which disappears at ~ 77 K (S = 0). The triplet and

singlet states of $Cu_2(CH_3CO_2)_4 \cdot 2H_2O$ are significantly separated in energy as a unique feature observed from paddle wheel-based dimers that undergo antiferromagnetic interactions accompanied by a $S = 0$ ground spin state.[28] However, the Q-band EPR spectra for **31a** at 295 K and 5 K did not provide any informative results.

In contrast, the room temperature magnetic moment for the polymer **32** at 1.6 BM [$\chi_M T$ = 0.31 emu K mol^{-1}] is slightly less than expected for a single paramagnetic Cu(II) ion (SEE NOTE).[26b,26d] Therefore, it is apparent that polymer **32** exhibits paramagnetic behaviour similar to polymeric species **24**, **26** and **28**.

4.4 Summary and Conclusions

The reactions of ligand blends composed of *m*-$BDCH_2$ and 2-pyridine alcohols [2-{$(CH_2)_nOH$}-C_5H_4N] with nickel acetate tetrahydrate or copper acetate monohydrate, in the presence of triethylamine, result in the formation of a range of complexes displaying a variety of nuclearities and structural types (Scheme 16).

A series of complexes including; a hydrogen bonded network of monomers **27** (M = Cu, n =1), the discrete dimers **23a** and **23a'** (M = Ni, n = 1), **23b** (M = Ni, n = 2) and 1-D coordination polymers **24** (M = Ni, n = 2), **26** (M = Cu, n = 1), **26'** (M = Cu, n = 1), and **28** (M = Cu, n = 2) have been synthesised and fully characterised. In addition, the reactivity of mixtures of *m*-$BDCH_2$ and an α-diimine or formamidines [HDLF], with copper acetate monohydrate in the presence of triethylamine have also been investigated. The complexes synthesised and characterised from these reactions include, the hydrogen bonded network of monomers (**30**) from the reaction of *m*-$BDCH_2$ and phen, the supramolecular nanoballs $[Cu_{24}(m\text{-}BDC)_{24}(HDLF)_{12}(H_2O)_{12}]$ (+ 2MeCN, + $12H_2O$, L = mes **31a**; L = *o*-tol **31b**) from the reaction of *m*-$BDCH_2$ and formamidine ligands by the self-assembly of twelve paddle wheel-based SBUs of generic formula $[Cu_2(RCO_2)_4(HDLF)(H_2O)]$ (R = $0.5C_6H_4$). In comparison, a ligand blend composed of *m*-$BDCH_2$ and HD2,6-xylF results in the nanoball $[Cu_{24}(m\text{-}BDC)_{24}(HD2,6\text{-}xylF)_{12}(H_2O)_{12}]$ (**31c**) and polymer $[Cu(m\text{-}BDC)(HD2,6\text{-}xylF)_2]$ (**32**).

On inspection, the reactivity studies appear to demonstrate trends in structural type, bonding modes and nuclearities of the resulting complexes. Firstly, *in all cases m-BDC coordinates syn to the metal ion.* The *m*-BDC ligands within the dimers of **23** and polymer **28** are bound in a bis-type 2, η^1: *syn*-bonding mode. However, the polymers **24** and **26** possess bis-type 1, η^1: *m*-BDC *syn*-bound ligands which result in a longer M···M distance. It is also noticeable that monomeric species **27** contains a type 2, η^1: *syn* monodentate, terminal *m*-BDC ligand, whereas, monomer **30** possesses a type 1, η^1: *syn* monodentate,

terminal *m*-BDC ligand. Secondly, *2-pyridine alcohols and phen commonly coordinate as chelating ligands.* As an exception the hepH moiety in **28** acts as a pseudo-chelating ligand. Thirdly, *combinations of 2-pyridinols and m-BDCH$_2$ yield only polymeric copper complexes*, even though a combination of 3-{CH_2OH}-C_5H_4N (3-hmpH) with copper acetate monohydrate is known to form the dinuclear paddle wheel-based copper complex $[Cu_2(CH_3CO_2)_4(3\text{-hmpH})_2]$.[29] In comparison, a combination of *N,N*-phen with *m*-$BDCH_2$ results in a hydrogen bonded network of monomers, although similar ligand combinations under different reaction conditions have been reported before to form polymeric species.[1s,1u,14] Fourthly, *bulky HDLF ligands bind through the imine group*, by adopting either *cis-N,N'* or *trans-N,N'* arrangements with the imine-/amine-aryl groups perpendicular to one another. On modifying L substituents in HDLF changes are observed. For example, HD2,6-xylF in combination with bis-η^1, η^1: *syn*, *syn*-bridging *m*-BDC ligands result in the formation of the paddle wheel SBU-based nanoball **31c** and polymer **32**. Fifthly, *hydrogen bonding interactions commonly involve the oxygen atoms of m-BDC* which may be intramolecular (**23**, **24**, **26** and **31**) or intermolecular (**24**, **27**, **30** and **31**) in origin.

In conclusion, the factors governing isopthalate complexation in this work would appear to depend on a combination of features including; *(i) the nature of the precursor transition metal ion* which influences the structural geometry and final nuclearity, *(ii) the pK_a values of the ligand blends* which influence the numbers and types of bonding modes present as well as non-covalent interactions; *(iii) the methylene chain length of the 2-pyridine alcohol* which influences the nuclearity (as a chelating/non-chelating ligand); *(iv) the type of N,N'-donor ligand employed* (as a precursor to monomeric, polymeric or supramolecular species) and; *(v) the presence of an additional base* which may direct complexation without self-incorporation (*e.g.*, NaN_3 for the synthesis of **27**).

Complexes **23**, **24**, **26**, **27** and **28** display simple paramagnetic behaviour as determined by variable temperature magnetic data fitting using the Curie-Weiss law (Appendices). Preliminary magnetic data of nanoball complexes **31** suggest that they are built up from overall antiferromagnetically coupled SBU dimers. Modelling of variable temperature magnetic measurements is underway in order to understand the underlying magnetic behaviour of the $\{Cu_{24}\}$ complexes in further detail.

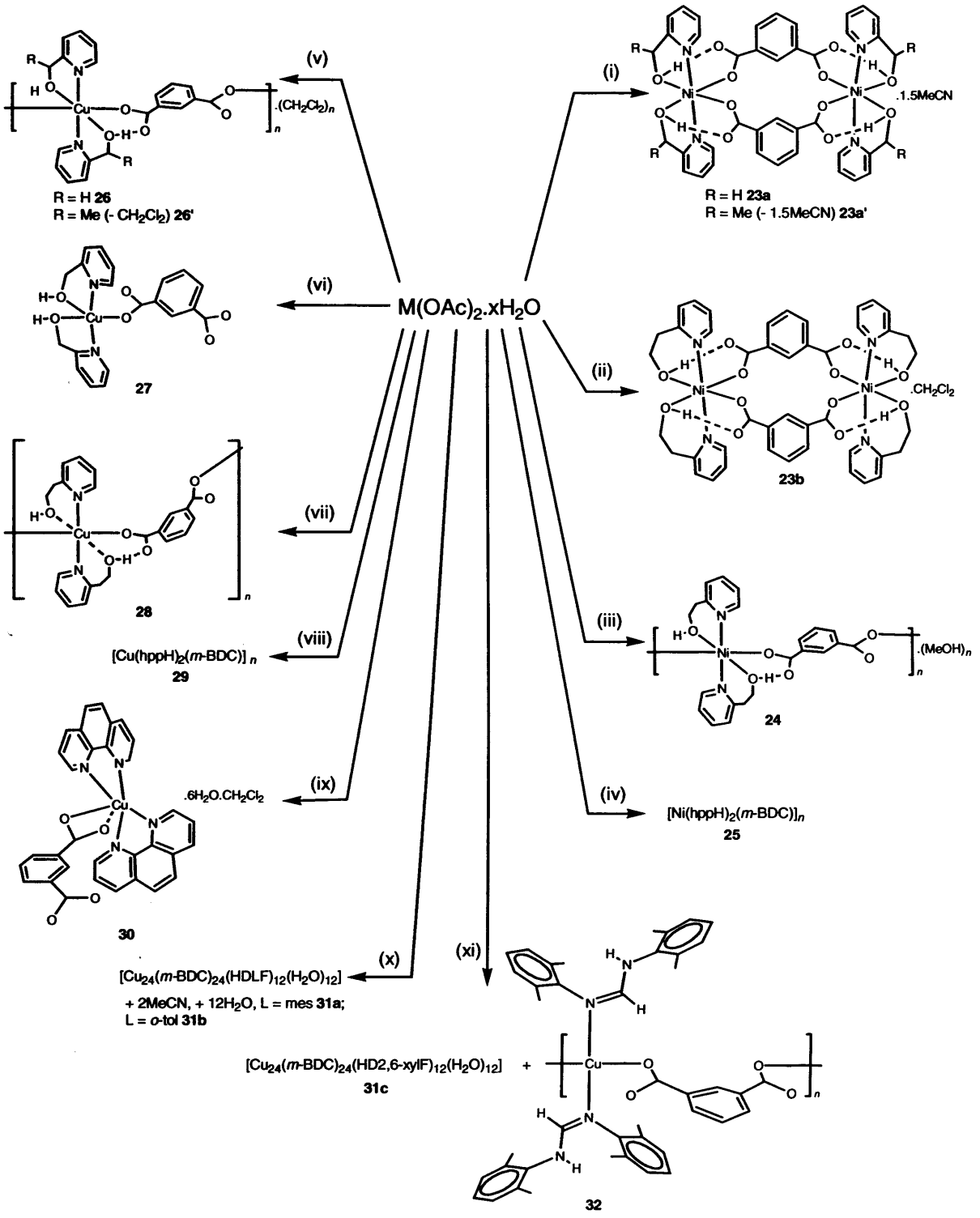

Scheme 16 Overview of chemistry carried out in Chapter 4. General reagents: $M(OAc)_2 \cdot xH_2O$, *m*-$BDCH_2$, 2-$\{(CH_2)_nOH\}$-C_5H_4N, NEt_3 and $MeCN/CH_2Cl_2/MeOH$; M = Ni, x = 4; [(i) n = 1; (ii) n = 2; (iii) n = 2; (iv) n =3] M = Cu, x = 1 [(v) n = 1; (vi) n = 1, NaN_3; (vii) n = 2; (viii) n = 3]. (ix) $Cu(OAc)_2 \cdot H_2O$, *m*-$BDCH_2$, phen, NEt_3 and $MeCN/CH_2Cl_2/MeOH$. (x) $Cu(OAc)_2 \cdot H_2O$, *m*-$BDCH_2$, HDLF, NEt_3 and $MeCN/CH_2Cl_2/MeOH$; desolvated {L = mes pK_a 7.46/L = *o*-tol pK_a 7.31}[6], (xi) {L = 2,6-xyl pK_a 7.22}[6].

4.5 References

1. (*a*) Y. Wan, L. Zhang, L. Jin, S. Gao and S. Lu, *Inorg. Chem.*, 2003, **42**, 4985; (*b*) R. García-Zarracino, J. Ramos-Quiñones and H. Höpfl, *Inorg. Chem.*, 2003, **42**, 3835; (*c*) J.-F. Ma, J. Yang, G.-L. Zheng and J.-F. Liu, *Inorg. Chem.*, 2003, **42**, 7531; (*d*) R.-Q. Zou, X.-H. Bu and R.-H. Zhang, *Inorg. Chem.*, 2004, **43**, 5382; (*e*) N. J. Burke, A. D. Burrows, A. S. Donovan, R. W. Harrington, M. F. Mahon and C. E. Price, *Dalton Trans.*, 2003, 3840; (*f*) J.-C. Dai, X.-T. Wu, Z.-Y. Fu, S.-M. Hu, W.-X. Du, C.-P. Cui, L.-M. Wu, H.-H. Zhang and R.-Q. Sun, *Chem. Commun.*, 2002, 12; (*g*) G. Férey, M. Latroche, C. Serre, F. Millange, T. Loiseau and A. Percheron-Guégan, *Chem. Commun.*, 2003, 2976; (*h*) B. Moulton, H. Abourahma, M. W. Bradner, J. Lu, G. J. McManus and M. J. Zawortko, *Chem. Commun.* 2003, 1342; (*i*) K. Barthelet, D. Riou and G. Férey, *Chem. Commun.*, 2002, 1492; (*j*) K. Barthelet, J. Marrot, G. Férey and D. Riou, *Chem. Commun.*, 2004, 520; (*k*) F. Millange, C. Serre and G. Férey, *Chem. Commun.*, 2002, 822; (*l*) J. Tao, Y. Zhang, M.-L. Tong, X.-M. Chen, T. Yuen, C. L. Lin, X. Huang and J. Li, *Chem. Commun.*, 2002, 1342; (*m*) S. J. Yang, L. S. Long, R. B. Huang and L. S. Zheng, *Chem. Commun.*, 2002, 472; (*n*) H.-X. Zhang, B.-S. Kang, A.-W. Xu, Z.-N. Chen, Z.-Y. Zhou, A. S. Chan, K.-B. Yu and C. Ren, *J. Chem. Soc., Dalton Trans.*, 2001, 2559; (*o*) B. Moulton, J. Lu, R. Hajndl, S. Hariharan and M. J. Zawrotko, *Angew. Chem. Int Ed., Engl.*, 2002, **41**, 2821; (*p*) M. Eddaoudi, J. Kim, D. Vodak, A. Sudik, J. Wachter, M. O.'Keeffe and O. M. Yaghi, *Proc. Nat. Acad. Sci.*, USA, 2002, **99**, 4900; (*q*) *{Cu_4} SBU-based polymer* D. Sun, R. Cao, Y. Sun, W. Bi, D. Yuan, Q. Shi and X. Li, *Chem. Commun.*, 2003, 1528; (*r*) A. C. Sudik, A. P. Côté and O. M. Yaghi, *Inorg. Chem.*, 2005, **44**, 2998; (*s*) Q. Zhang, B.-H. Ye, C.-X. Ren and X.-M. Chen, *Z. Anorg. Allg. Chem.*, 2003, **629**, 2053; (*t*) S. A. Bourne, A. Mondal and M. J. Zawarotko, *Crystal Engineering*, 2001, **4**, 25; (*u*) X.-M. Chen and G.-F. Liu, *Chem. Eur. J.*, 2002, **8**, 4811; (*v*) P. Cheng, S.-P. Yan, C.-Z. Xie, B. Zao, X.-Y. Chen, X.-W. Liu, C.H. Li, D.-Z. Liao, Z.-H. Jiang and G.-L. Wang, *Eur. J. Inorg. Chem.*, 2004, 2369; (*w*) J. Tao, X. Yin, R. Huang and L. Zheng, *Inorg. Chem. Commun.*, 2002, **5**, 1000; (*x*) W.-Z. Shen, X.-Y. Chen, P. Cheng, S.-P. Yan, B. Zhai, D.-Z. Liao and Z.-H. Jiang, *Eur. J. Inorg. Chem.*, 2005, 2297.
2. *Reviews on m-BDC-based and other MOFs* (*a*) C. Janiak, *Dalton Trans.*, 2003, 2781; (*b*) D. Bradshaw, J. B. Claridge, E. J. Cussen, T. J. Prior and M. J. Rosseinsky, *Acc. Chem. Res.*, 2005, **38**; 273 (*c*) N. L. Rosi, J. Kim, M. Eddaoudi, B. Chen, M. O'Keeffe and O. M. Yaghi, *J. Am. Chem. Soc.*, 2005, **127**, 1504; (*d*) N. W. Ockwig, O. Delgado-Friedrichs, M. O'Keeffe and O. M. Yaghi, *Acc. Chem. Res.*, 2005, **38**, 176; (*e*) G. Férey, C. Mellot-Draznieks, C. Serre and F. Millange, *Acc. Chem. Res.*, 2005, **38**, 217.
3. C. Chen, D. Huang, X. Zhang, F. Chen, H. Zu, Q. Liu, C. Zhang, D. Liao, L. Li and L. Sun, *Inorg. Chem.*, 2003, **42**, 3540.
4. D. Li, Z. Liao, Y. Wei, F. Du, M. Wang, W. Chen, W. Li and X. Mao, *Dalton Trans.*, 2003, 2164.
5. (*a*) C. Cañada-Vilalta, M. Pink and G. Christou, *Dalton Trans.*, 2003, 1121; (*b*) E. K. Brechin, A. Graham, A. Parkin, S. Parsons, A. M. Seddon and R. E. P. Winpenny, *J. Chem. Soc., Dalton Trans.*, 2000, 3242; (*c*) E. K. Brechin, R. O. Gould, S. G. Harris, S. Parsons and R. E. P. Winpenny, *J. Am. Chem. Soc.*, 1996, **118**, 11293.
6. (*a*) ACS, *SciFinder Scholar*, Substance database, 2004; (*b*) *Isopthalic acid 50 wt.% aq. MeOH:* J. S. Gumbley and R. Stewart, *J. Chem. Soc., Perkin Trans. (II)*, 1984, **3**, 529.
7. *See for example,* (*a*) E. Pardo, J. Faus, M. Julve, F .Lloret, M. C. Muñoz, J. Cano, X. Ottenwaelder, Y. Journaux, R. Carrasco, G. Bay, I. Fernández and R. Ruiz-García, *J. Am. Chem. Soc.*, 2003, **125**, 10771; (*b*) A. Lavalette, F. Tuna, G. Clarkson, N. W. Alcock and M. J. Hannon, *Chem. Commun.*, 2003, 2666; (*c*) C. Bazzicalupi, A. Bencini, A. Bianchi, C. Duce, P. Fornasari, C. Giorgi, P. Paoletti, R. Pardini, M. Tinè and B. Valtancoli, *Dalton Trans.*, 2004, 463.
8. (*a*) V. V. Pavlischchuck, S. V. Kolotilov, A. W. Addison, M. J. Prushan, R. J. Butler and L. K. Thompson, *Chem. Commun.*, 2002, 468; (*b*) Z. Xu, L. K. Thompson, V. A. Milway, L. Zhao, T. Kelly and D. O. Miller, *Inorg. Chem.*, 2003, **42**, 2950.

9. R. K. Hocking and T. W. Hambley, *Inorg. Chem.*, 2003, **43**, 2833. [For Ni(II): range ~ 1.263 – 1.268 Å ⇒ ~ 15 – 20% covalent C-O bond character; for Cu(II): range ~ 1.248 – 1.256 Å ⇒ ~ 0 – 5% covalent C-O bond character and ~ 1.268 – 1.273 Å ⇒ ~ 20 – 23% covalent C-O bond character].
10. R. Wang, E. Gao, M. Hong, S. Gao, J. Luo, Z. Lin, L. Han and R. Cao, *Inorg. Chem.*, 2003, **42**, 5486.
11. (*a*) Y. Xie, W. Bu, A. S.-C. Chan, X. Xu, Q. Liu, Z. Zhang, J. Yu and Y. Fan, *Inorg. Chim. Acta*, 2000, **310**, 257; (*b*) *Personal Communiction*, Q. Liu, 2005.
12. S. K. Dey, B. Bag, K. M. A. Malik, M. S. E. Fallah, J. Ribas and S. Mitra, *Inorg. Chem.*, 2003, **42**, 4029.
13. D. H. Williams and I. Fleming, in *Spectroscopic Methods in Organic Chemistry*, 5th Edn., McGraw Hill, 1995, Gt. Britain.
14. H.-P. Xiao, X.-H. Li and M.-L. Hu, *Acta Crystallogr., Sect. E*, 2004, **60**, 468.
15. The synthesis of complex **32**, crystals for the analysis of **31b** and further investigations of the nanoballs was carried out by Philip Greenfield (final year MChem student, 2005). Thermogravimetric analysis was investigated by Dr. G. Capper at Leicester University.
16. J. March, in *Advanced Organic Chemistry*, 4th Edn., Wiley-Interscience, 1992, USA, p 21.
17. (*a*) M. Eddaoudi, J. Kim, J. B. Wachter, H. K. Chae, M. O'Keeffe and O. M. Yaghi, *J. Am. Chem. Soc.*, 2001, **123**, 4368; (*b*) B. Moulton, J. Liu, A. Mondal and M. J. Zaworotko, *Chem. Commun.*, 2001, 863; (*c*) G. J. McManus, Z. Wang and M. J. Zawarotko, *Crystal Growth and Design*, 2004, **4**, 11.
18. J. Barker, M. Jones and M. Kilner, *Organic Mass Spectrometry*, 1985, **20**, 619.
19. *Example of aggregated {Cu_{12}} ferrimagnetic clusters;* M. Murugesu, C. E. Anson and A. K. Powell, *Chem. Commun.*, 2002, 1054.
20. M. Murugesu, R. Clérac, C. E. Anson and A. K. Powell, *Inorg. Chem.*, 2004, **43**, 7269.
21. (*a*) T. S. M. Abedin, L. K. Thompson, D. O'Miller and E. Krupicka, *Chem. Commun.*, 2003, 708; (*b*) M. Murugesu, R. Clérac, C. E. Anson and A. K. Powell, *Chem. Commun.*, 2004, 1598.
22. (*a*) J.-J. Zhang, S.-Q. Xia, T.-L. Sheng, S.-M. Hu, G. Leibeling, F. Meyer, X.-T. Wu, S.-C. Xiang and R.-B. Fu, *Chem. Commun.*, 2004, 1186; (*b*) J.-J. Zhang, T.-L. Sheng, G. Leibeling, F. Meyer, S.-M. Hu, R.-B. Fu, S.-C. Xiang and X.-T. Wu, *Inorg. Chem.*, 2004, **43**, 5472; (*c*) Q. Lin and J. D. Corbett, *Inorg. Chem.*, 2005, **44**, 512; (*d*) D. Fenske, H. Krautscheid and S. Balter, *Angew. Chem. Int. Ed., Engl.*, 1990, **29**, 796; (*e*) D. Fenske and H. Krautscheid, *Angew. Chem. Int. Ed., Engl.*, 1990, **29**, 1452; (*f*) A. Decker, D. Fenske and K. Maczek, *Angew. Chem. Int. Ed., Engl.*, 1996, **35**, 2863.
23. (*a*) M. Eddaoudi, D. B. Moler, H. Li, B. Chen, T. M. Reineke, M. O'Keeffe and O. M. Yaghi, *Acc. Chem. Res.*, 2001, **34**, 319; (*b*) J. Kim, B. Chen, T. M. Reineke, H. Li, M. Eddaoudi, D. B. Moler, M. O'Keeffe and O. M. Yaghi, *J. Am. Chem. Soc.*, 2001, **123**, 8239; (*c*) A. C. Sudik, A. P. Côté and O. M. Yaghi, *Inorg. Chem.*, 2005, **44**, 2998.
24. (*a*) M. V. Marhino, M. I. Yoshida, K. J. Guedes, K. Krambrock, A. J. Bortoluzzi, M. Hörner, F. C. Machado and W. M. Teles, *Inorg. Chem.*, 2004, **43**, 1539; (*b*) S. Masaoka, D. Tanaka, Y. Nakanishi and S. Kitigawa, *Angew. Int. Ed., Engl.*, 2004, **43**, 2530; (*c*) E. V. Dikarev, K. W. Andreini and M. A. Petrukhina, *Inorg. Chem.*, 2004, **43**, 3219; (*d*) M. H. Chisolm, P. J. Wilson and P. M. Woodward, *Chem. Commun.*, 2002, 566; (*e*) W. J. Belcher, C. A. Longstaff, M. R. Neckenig and J. W. Steed, *Chem. Commun.*, 2002, 1602; (*f*) *example of a tricarboxylate paddle wheel* M.-L. Tong, L.-J. Lu, K. Mochizuki, H.-C. Chang, X.-M. Chen, Y. Li and S. Kitigawa, *Chem. Commun.*, 2003, 428; (*g*) B. Rather and M. J. Zawortko, *Chem. Commun.*, 2003, 830; (*h*) N. Mercier and M. Riou, *Chem. Commun.*, 2004, 844; (*i*) C. Qin, X. Wang, L. Carlucci, M. Tong, E. Wang, C. Hu and L. Xu, *Chem. Commun.*, 2004, 1876; (*j*) C. B. Aakeröy, A. M. Beatty, J. Desper, M. O'Shea and J. Valdés-Martínez, *Dalton Trans.*, 2003, 3956; (*k*) J. F. Berry, F. A. Cotton, S. A. Ibragimov, C. A. Murillo and X. Wang, *Dalton Trans.*, 2003, 4297; (*l*) *nickel-based* S. Wang, M.-L. Hu and S. W. Ng, *Acta Crystallogr., Sect. E*, 2002, **58**, 242; (*m*) J. J. Perry, G. J. McManus and M. J. Zawarotko, *Chem. Commun.*, 2004, 2354; (*n*) S. A. Bourne, J. Lu, A. Mondal, B. Moulton and M. J. Zawarotko, *Angew. Chem. Int. Ed., Engl.*, 2001, **40**, 2111; (*o*) H. Abourahma, G. J.

Bodwell, J. Lu, B. Moulton, I. R. Pottie, R. B. Walsh and M. J. Zawarotko, *Cryst. Growth Des.*, 2003, **3**, 513. (*p*) L. Gao, B. Zhao, G. Li, Z. Shi and S. Feng, *Inorg. Chem. Commun.*, 2003, **6**, 1249;

25. (*a*) T. E. Vos, Y. Liao, W. W. Shum, J.-H. Her, P. W. Stephens, W. M. Reiff and J. S. Miller, *J. Am. Chem. Soc.*, 2004, **126**, 11630; (*b*) D. Maspoch, D. Ruiz-Molina, K. Wurst, C. Rovira and J. Veciana, *Chem. Commun.*, 2002, 2958; (*c*) *manganese paddle wheel complex* A. Grirrane, A. Pastor, A. Galindo, A. Ienco, C. Mealli and P. Rosa, *Chem. Commun.*, 2003, 512; (*d*) M. J. Byrnes, M. H. Chisolm, D. F. Dye, C. M. Hadad, B. D. Pate, P.J. Wilson and J. M. Zaleski, *Dalton Trans.*, 2004, 523; (*e*) D. Maspoch, D. Ruiz-Molina, J. Vidal-Gancedo, C. Rovira and J. Veciana, *Dalton Trans.*, 2004, 1073; (*f*) S. Furukawa, M. Ohba and S. Kitigawa, *Chem. Commun.*, 2005, 865.

26.(*a*) O. Kahn, in *Molecular Magnetism*, VCH publishers, USA, 1993, pp. 106 – 108; (b) *ibid.*, Chapter 2, [Calculated spin-only values: expected Ni(II) $\chi_M T$ = 1.00 emu K mol^{-1} each possessing two unpaired electrons; Cu(II) $\chi_M T$ = 0.38 emu K mol^{-1} each possessing one unpaired electron]. (*c*) R. S. Drago, in *Physical Methods; for Chemists*, 1992, Saunders College Publishing, Orlando, 2nd International Edn., pp 430 – 432; (*d*) ***PLEASE NOTE*** the Evans balance is sometimes ineffective at measuring accurate magnetic data which is mainly due to environmental effects *e.g.*, fluctuations in temperature.

27.(*a*) F. A. Cotton, G. Wilkinson, C. A. Murillo and M. Bochmann, in *Advanced Inorganic Chemistry*, eds., F. A. Cotton, G. Wilkinson, Wiley-Interscience, New York, 6th Edn., 1999, p 870; (*b*) F. A. Cotton and G. Wilkinson, in *Advanced Inorganic Chemistry: A Comprehensive Treatise*, Wiley, New York, 1988, p 685.

28. A. F. Orchard, in *Magnetochemistry*, Oxford Chemistry Primers, Oxford University Press, No. 75, UK, 2003, pp. 67 – 68.

29. M. Melník, K. Smolander and P. Sharrock, *Inorg. Chim. Acta*, 1985, **103**, 187.

30. (*a*) S. Alvarez, *Dalton Trans.*, 2005, 2209; (*b*), M. T. Weller, in *Inorganic Materials Chemistry*, Oxford Chemistry Primers, Oxford University Press, No. 23, UK, 2002, pp. 72 – 74;

31. *See references therein* (*a*) S. Durot, C. Policar, G. Pelosi, F. Bisceglie, T. Mallah and J.-P. Mahy, *Inorg. Chem.*, 2003, **42**, 8072; (b) R. L. Rardin, W. B. Tolman and S. J. Lippard, *New. J. Chem.*, 1991, **15**, 417.

32. (*a*) C. Janiak, *J. Chem. Soc., Dalton Trans.*, 2000, 3885; (*b*) C. A. Hunter and J. K. M. Sanders, *J. Am. Chem. Soc.*, 1990, **112**, 5525; (*c*) the maximum acceptable centroid-centroid C···C distance for a $\pi\cdots\pi$ interaction is 3.8 Å which is offset by 20° perpendicular to the ring plane [see (*a*)].

33.T. Steiner, *Angew. Chem. Int. Ed., Engl.*, 2002, **41**, 48.

34. G. R. Desiraju, *Acc. Chem. Res.*, 2002, **35**, 565.

35. See *for example* I. A. Koval, K. van der Schilden, A. M., Schuitema, P. Gamez, C. Belle, J.-L. Pierre, M. Lüken, B. Krebs, O. Roubeau and J. Reedijk, *Inorg. Chem.*, 2005, **44**, 4372.

Chapter 5

5.0 Blending Salts of Carboxylates or 2-Pyridonates and L^2 (L^2 = 2-Pyridine Alkoxides, α-Diimines) on a Fe(III) Centre

In Chapters 2 – 4, the base-assisted protonation of a metal acetate by using a ligand blend composed of at least one hydroxyl-containing species had been employed as the synthetic strategy. In this chapter, a complementary metathesis approach is employed whereby a first row transition metal-μ-oxo-bridged halide species (building block) is treated with a blend of s-block salts of the corresponding ligands. In particular, the synthetic and structural studies of complexes prepared from the reactions of combinations of the sodium salts of carboxylates and 2-pyridonates/2-pyridine alkoxides [2-{$(CH_2)_nONa$}-6-X-C_5H_3N] [X = Cl, n = 0, Nachp; X = H, n = 1, Nahmp; X = H, n = 2, Nahep] with the bimetallic iron-oxo salt $[Fe_2OCl_6][NEt_4]_2$ are described (Scheme 1). $[Fe_2OCl_6][NEt_4]_2$ has proved to be a convenient source of the tetra-cationic fragment $\{Fe_2O\}^{4+}$ and a number of reports have seen its use in the assembly of polymetallic iron clusters (Chapter 1, section 1.2.4).[1-3] The considerable flexibility of the oxo-group can be appreciated by the sheer variety of bonding modes it is known to exhibit (Table 1).[3]

Table 1 Reported oxo-bonding modes[3]

μ_2	μ_3	μ_4	μ_5	μ_6
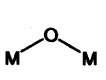	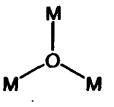	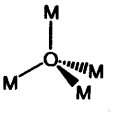	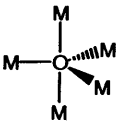	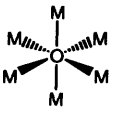
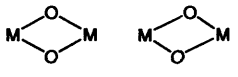	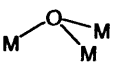	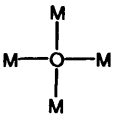	–	–
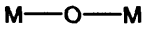	–	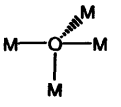	–	–

The main aim of this chapter is to focus on the coordination chemistry of trivalent iron ions supported by blends of carboxylates and 2-pyridonates/2-pyridine alkoxides (section 5.1). In particular, the effect of the pyridine alkoxide methylene chain length (n = 0 – 2) is probed as is the steric and electronic variation of the carboxylate substituents. As a

secondary aim, reactions of ligand blends based on a carboxylate salt and an α-diimine ligand (*viz.* phen) with $[Fe_2OCl_6][NEt_4]_2$ are also investigated (section 5.2). Spectroscopic/spectrometric data and magnetic measurements are used to support and complement the single crystal X-ray determinations. Scheme 1 shows the general synthetic strategy to be employed, reagents types and the solvent used for all reactions.

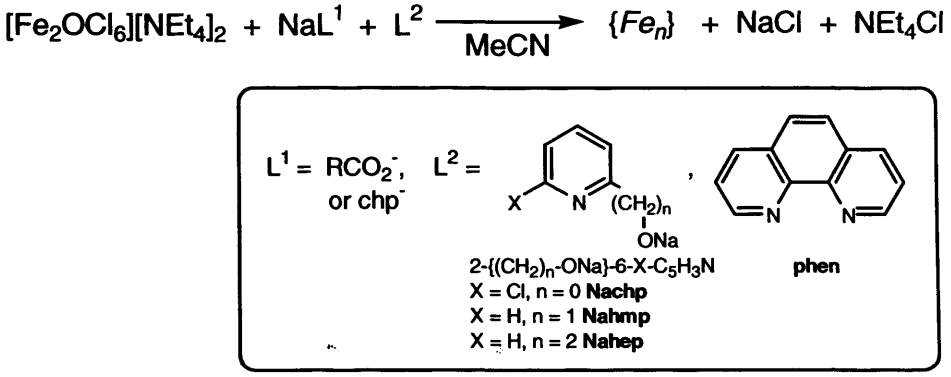

Scheme 1 General synthetic strategy employed.

5.1 Blending Salts of Carboxylates and 2-Pyridine Alkoxides on a Fe(III) Centre

5.1.1 M = Fe, NaL^1 = NaO_2CR (R = $CH_2C_6H_5$, *p*-CH_3-C_6H_4), L^2 = Nachp (n = 0, X = Cl)

The reaction of $[Fe_2OCl_6][NEt_4]_2$ with NaO_2CPh/Nachp is known to form $[Fe_{10}Na_2(\mu_4\text{-}O)_2(\mu_3\text{-}O)_4(\mu_3\text{-}OH)_4(C_6H_5CO_2)_{10}(chp)_6(H_2O)_2(Me_2CO)_2]$ which has shown behaviour consistent with a SMM (Chapter 1, section 1.1.2).[8] However, the relaxation of magnetisation has been found to be more rapid in comparison with other SMMs.[25] In this section, we aim to re-examine this reaction by modifying the electronic and steric properties of the carboxylate being employed by using an alkyl-based carboxylate ($PhCH_2CO_2^-$) and an electron donating aromatic carboxylate (*p*-CH_3-$C_6H_4CO_2^-$).

The reaction of $[Fe_2OCl_6][NEt_4]_2$ with sodium phenylacetate ($C_6H_5CH_2CO_2Na$) and Nachp gave, on work-up, red crystals of $[Fe_{10}Na_2(\mu_4\text{-}O)_2(\mu_3\text{-}O)_4(\mu_3\text{-}OH)_4(C_6H_5CH_2CO_2)_{10}(chp)_6(H_2O)_2(MeCN)_2]\cdot 9MeCN$ (**33**) (– 25 °C, 2d. EtOAc) in moderate yield (Scheme 2). Complex **33** was characterised by elemental analysis, IR

spectroscopy and positive FAB mass spectrometry. A single crystal of **33** was subject to an X-ray diffraction study. The molecular structure of **33** is shown in Figure 1; selected bond lengths and angles are shown in Table 2.

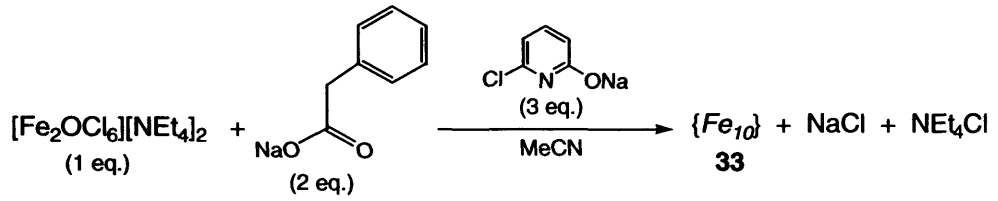

Scheme 2 Synthesis of **33**.

The molecular structure of **33** reveals the presence of ten octahedral Fe(III) ions and two octahedral sodium cations surrounded by ten phenylacetate, six chp, two terminal water and two terminal acetonitrile ligands. The ten phenylacetates 1,3-bridge over the iron ions. The chp ligands are 2.20 bound as either one of four Fe-O_{chp}-Fe-based or two Fe-O_{chp}-Na-based bridging alkoxides. The two terminal acetonitrile molecules are bound to each of the sodium cations on the axial positions of the molecule.

The iron-oxo core within **33** can be described as a double hexagon $[Fe_6O_6]^{8+}$/$[Fe_6(\mu_4\text{-}O)_2(\mu_3\text{-}O)_2(\mu_3\text{-}OH)_2]^{8+}$ fused from a square face [Fe(3)-O(5)-Fe(3A)-O(5A)], resulting in a bi-prismatic cage of $[Fe_{10}O_{12}]^{12+}$/$[Fe_{10}(\mu_4\text{-}O)_2(\mu_3\text{-}O)_4(\mu_3\text{-}OH)_4(O_{chp})_2]^{12+}$. The core is capped by chp oxygen atoms [O(7) and O(7A)] (Figure 2). Complex **33** consists of ten iron(III) ions in three types of environments. Firstly, Fe(3) and Fe(3A), which are bound to ligands of μ_4-O, two μ_3-O, two μ_2-CO_2 and a terminal μ-H_2O. Secondly, Fe(2), Fe(2A), Fe(4) and Fe(4A), which are each bound to the oxygen atoms of a μ_4-O, a μ_3-O, a μ_3-OH, two types of μ_2-O_{chp} and a μ-CO_2 ligand. Finally, the remaining type of iron ions of Fe(1), Fe(1A), Fe(5) and Fe(5A), which are each bound to a μ_3-O, two μ_3-OH and three μ-CO_2 ligands. There are fourteen possible Fe···Fe interactions in **33** (Figure 2).

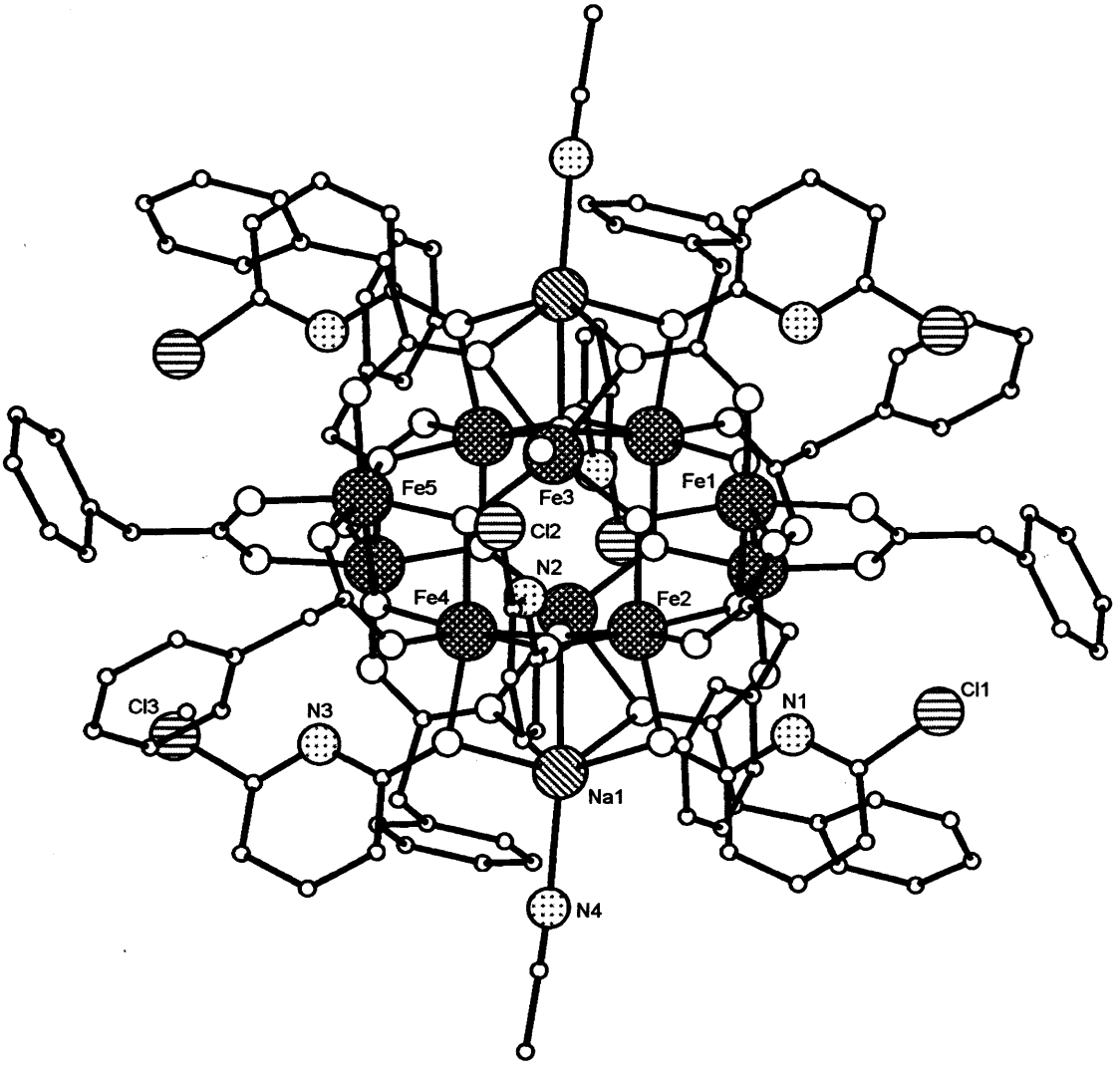

Figure 1 Molecular structure of **33**. Hydrogen atoms, atom labels (except asymmetric unit atoms excluding C) and solvent molecules are omitted for clarity.

Table 2 Selected bond length (Å) and angle (°) data for **33**

33												
Fe(1)-O(1)	2.091(2)	Fe(2)-O(1)	2.035(2)	Fe(2)-O(11)	2.097(2)	Fe(3)-O(16)	2.182(2)	Fe(4)-O(7)	2.029(2)	Fe(5)-O(4)#1	2.152(2)	Na(1)-O(5)#1	2.440(3)
Fe(1)-O(2)	1.910(2)	Fe(2)-O(2)	1.963(2)	Fe(3)-O(2)	1.903(2)	Fe(3)-O(19)	2.123(2)	Fe(4)-O(8)	2.018(2)	Fe(5)-O(13)	2.001(2)	Na(1)-O(6)	2.361(3)
Fe(1)-O(4)	2.032(2)	Fe(2)-O(5)#1	1.940(2)	Fe(3)-O(3)	1.904(2)	Fe(4)-O(3)	1.970(2)	Fe(4)-O(12)	2.083(2)	Fe(5)-O(17)	1.980(2)	Na(1)-O(8)	2.341(3)
Fe(1)-O(9)	2.080(2)	Fe(2)-O(6)	2.040(2)	Fe(3)-O(5)	1.931(2)	Fe(4)-O(4)#1	2.026(2)	Fe(5)-O(1)#1	2.042(2)	Fe(5)-O(18)	2.036(2)	Na(1)-O(15)#1	2.447(3)
Fe(1)-O(10)	1.991(2)	Fe(2)-O(7)	2.007(2)	Fe(3)-O(15)	2.186(2)	Fe(4)-O(5)#1	1.940(2)	Fe(5)-O(3)	1.894(2)	Na(1)-N(4)	2.431(4)	Na(1)-O(16)#1	2.410(3)
Fe(1)-O(14)	1.977(2)												
Fe(2)-O(1)-Fe(1)	91.87(9)	Fe(2)#1-O(5)-Fe(4)#1	100.86(10)	O(2)-Fe(1)-O(14)	99.30(10)	O(5)#1-Fe(2)-O(6)	90.23 (9)	O(3)-Fe(3)-O(16)	91.96(9)	O(4)#1-Fe(4)-O(12)	88.27(9)	O(17)-Fe(5)-O(1)#1	91.39(10)
Fe(5)#1-O(1)-Fe(1)	98.46(9)	Fe(3)-O(5)-Fe(4)#1	126.43(12)	O(10)-Fe(1)-O(4)	165.98(10)	O(5)#1-Fe(2)-O(7)	80.92(9)	O(3)-Fe(3)-O(19)	88.79(9)	O(5)#1-Fe(4)-O(7)	80.35(9)	O(18)-Fe(5)-O(1)#1	84.24(9)
Fe(2)-O(1)-Fe(5)#1	128.95(11)	Fe(2)-O(7)-Fe(4)	95.63(9)	O(14)-Fe(1)-O(4)	91.39(10)	O(7)-Fe(2)-O(6)	95.42(10)	O(5)-Fe(3)-O(15)	84.57(9)	O(5)#1-Fe(4)-O(8)	170.03(9)	O(3)-Fe(5)-O(4)#1	78.14(9)
Fe(1)-O(2)-Fe(2)	99.90(10)	O(2)-Fe(1)-O(1)	79.44(9)	O(10)-Fe(1)-O(9)	83.01(10)	O(5)#1-Fe(2)-O(11)	161.52(9)	O(5)-Fe(3)-O(16)	85.44(9)	O(5)#1-Fe(4)-O(12)	161.17(10)	O(3)-Fe(5)-O(13)	95.10(10)
Fe(3)-O(2)-Fe(1)	130.47(12)	O(2)-Fe(1)-O(4)	96.24(9)	O(14)-Fe(1)-O(9)	94.70(10)	O(6)-Fe(2)-O(11)	84.44(9)	O(5)-Fe(3)-O(19)	165.28(10)	O(8)-Fe(4)-O(7)	94.20(10)	O(3)-Fe(5)-O(17)	101.30(10)
Fe(2)-O(2)-Fe(2)	126.93(12)	O(2)-Fe(1)-O(9)	165.99(10)	O(2)-Fe(2)-O(1)	79.64(9)	O(7)-Fe(2)-O(11)	81.99(9)	O(3)-Fe(4)-O(4)#1	79.58(9)	O(7)-Fe(4)-O(12)	82.20(10)	O(3)-Fe(5)-O(18)	164.62(10)
Fe(3)-O(3)-Fe(4)	128.41(12)	O(2)-Fe(1)-O(10)	96.99(10)	O(5)#1-Fe(2)-O(1)	107.66(9)	O(2)-Fe(3)-O(3)	103.58(10)	O(5)#1-Fe(4)-O(3)	95.11(9)	O(8)-Fe(4)-O(12)	83.70(10)	O(13)-Fe(5)-O(4)#1	80.72(10)
Fe(5)-O(3)-Fe(3)	128.84(12)	O(4)-Fe(1)-O(1)	82.42(9)	O(1)-Fe(2)-O(6)	88.40(9)	O(2)-Fe(3)-O(5)	101.27(10)	O(3)-Fe(4)-O(7)	94.84(9)	O(3)-Fe(5)-O(1)#1	95.07(9)		
Fe(5)-O(3)-Fe(4)	101.34(10)	O(4)-Fe(1)-O(9)	83.03(9)	O(7)-Fe(2)-O(1)	170.64(9)	O(3)-Fe(3)-O(5)	99.02(9)	O(3)-Fe(4)-O(8)	170.03(9)	O(1)#1-Fe(5)-O(4)#1	80.72(9)		
Fe(4)#1-O(4)-Fe(1)	128.94(1)	O(9)-Fe(1)-O(1)	86.61(9)	O(1)-Fe(2)-O(11)	89.90(9)	O(2)-Fe(3)-O(15)	89.82(9)	O(3)-Fe(4)-O(12)	93.36(9)	O(13)-Fe(5)-O(1)#1	168.88(10)		
Fe(1)-O(4)-Fe(5)#1	96.82(9)	O(10)-Fe(1)-O(1)	95.48(9)	O(2)-Fe(2)-O(6)	167.53(9)	O(2)-Fe(3)-O(16)	161.73(9)	O(5)#1-Fe(4)-O(4)	109.79(9)				
Fe(4)#1-O(4)-Fe(5)	91.32(9)	O(14)-Fe(1)-O(1)	173.48(10)	O(2)-Fe(2)-O(7)	95.89(10)	O(2)-Fe(3)-O(19)	88.86(10)	O(4)#1-Fe(4)-O(7)	168.68(9)				
Fe(3)-O(5)-Fe(2)#1	128.57(12)	O(2)-Fe(1)-O(10)	96.99(10)	O(2)-Fe(2)-O(11)	91.96(9)	O(3)-Fe(3)-O(15)	165.74(10)	O(8)-Fe(4)-O(4)#1	90.79(9)				

Symmetry transformations used to generate equivalent atoms: #1 $(-x+2, -y, -z+1)$.

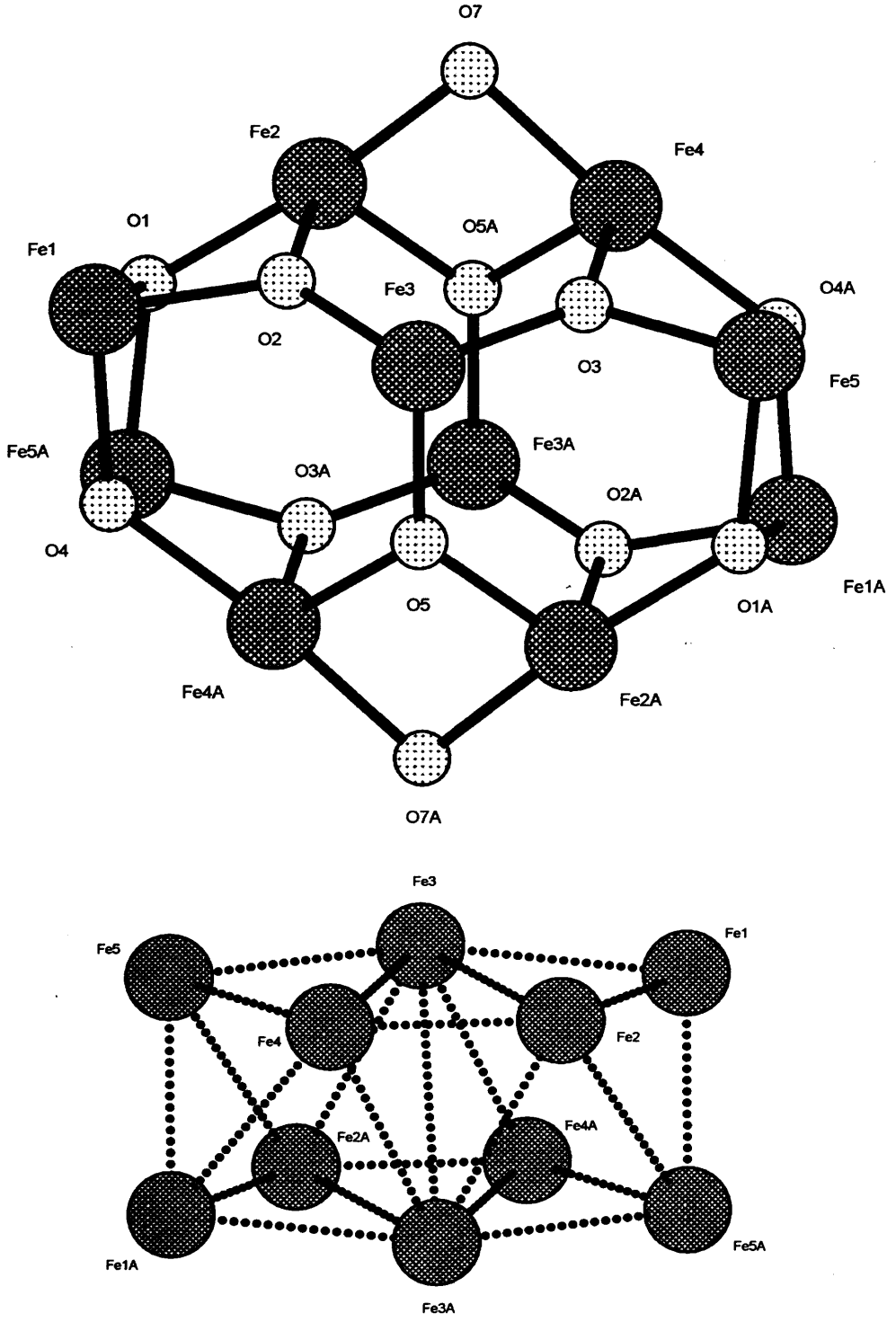

Figure 2 Iron-oxo core (above) and the fourteen different Fe(III)···Fe(III) ion interactions (below) of **33** [in Å; Fe(1)···Fe(2) 2.965(7), Fe(1)···Fe(3) 3.4628(8); Fe(1)···Fe(4A) 3.6616(8), Fe(1)···Fe(5A) 3.130(9), Fe(2)···Fe(3) 3.4589(7), Fe(2)···Fe(4) 2.9903(7), Fe(2)···Fe(5A) 3.6787(8), Fe(3)···Fe(2A) 3.4875(7), Fe(3)···Fe(3A) 4.2580(7), Fe(3)···Fe(4A) 3.4554(8), Fe(3)···Fe(5) 3.4258(8), Fe(4)···Fe(3) 3.4883(7), Fe(4)···Fe(3A) 3.4554(8), Fe(4)···Fe(5) 2.9889(8)].

The average iron to oxygen bond lengths in **33** are as follows, Fe-μ_4-O = 1.937 Å, Fe-μ_3-O = 1.934 Å, Fe-μ_3-OH = 2.063 Å, Fe-μ_2-O_{chp} = 2.013 Å, Fe-μ-CO_2 = 2.061 Å and Fe-μ_4-O_{water} = 2.123 Å. The geometry around each oxo/hydroxide oxygen atom is confirmed by the following average bond angles with, Fe-μ_3-O-Fe = 119.32°, Fe-μ_4-O-Fe = 118.62° and Fe-μ_3-OH-Fe = 106.00° that are consistent with distorted trigonal planar and tetrahedral oxide or hydroxide oxygen atom geometries, respectively. Each sodium atom on the axial position of the molecule is bound to a μ_4-O, two μ_2-O_{chp}, two μ_2-CO_2 and a terminal acetonitrile ligand.

The structure of **33** is essentially similar to $[Fe_{10}Na_2(\mu_4\text{-}O)_2(\mu_3\text{-}O)_4(\mu_3\text{-}OH)_4(C_6H_5CO_2)_{10}(chp)_6(H_2O)_2(Me_2CO)_2]$ and differs in the nature of the bridging carboxylate (Ph *vs.* $PhCH_2$) and donor ligands on sodium (Me_2CO *vs.* MeCN).[8,25] Other types of decanuclear iron complexes include the elaborate ferric wheels of $[Fe(OMe)_2(O_2CR)]_{10}$[6,9,10] and $[Fe_{10}(O)_4(OMe)_{16}(dbm)_6]$ (Hdbm = dibenzoylmethane).[11]

The solid-state IR spectrum of **33** indicates the presence of three absorption bands corresponding to $\nu(CO_2)_{asymm}$ = 1567 cm^{-1}, $\nu(CO_2)_{symm}$ = 1392 cm^{-1} and ν(Fe-O) = 694 cm^{-1} The ESI mass spectrum of **33** exhibits several peaks associated with ligand fragmentation including $[M]^+$ at 3009 Da.

Complex **33** (desolvated) has been subject to preliminary Q-band EPR spectroscopy. The simulations of the resulting spectra display several transitions at temperatures < 20 K, these being indicative for the presence of zero-field splitting (*ca.* 0.1 cm^{-1}) and are attributed to the exclusive population of the molecular ground spin state (Figure 3).[26] Theoretically, there should be 2*S* (*S* = 11) lines in the EPR spectrum of **33** for a given orientation of the molecule to the magnetic field therefore, the resulting spectrum is very complicated. At higher temperatures the transitions transform into a single broad signal due to the population of excited spin states.[30] The EPR spectrum of $[Fe_{10}Na_2(\mu_4\text{-}O)_2(\mu_3\text{-}O)_4(\mu_3\text{-}OH)_4(C_6H_5CO_2)_{10}(chp)_6(H_2O)_2(Me_2CO)_2]$ also exhibits several transitions at low

temperature which is consistent with the presence of a large ground spin state [being one of the requirements for a SMM (Chapter 1, section 1.1.2)].[26]

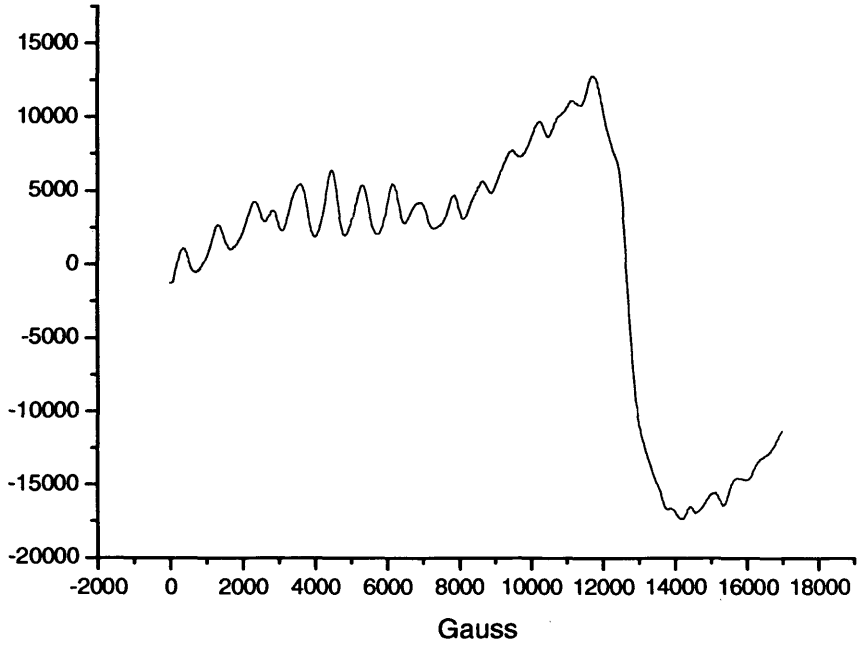

Figure 3 Q-band EPR spectrum of **33** (34 GHz, 5K).

The room temperature magnetic moment of **33** (desolvated) at 17.9 BM ($\chi_M T$ = 40.02 cm^3 K mol^{-1}) is slightly less than expected for ten non-interacting Fe(III) ions each possessing five unpaired electrons (expected 18.7 BM, $\chi_M T$ = 43.75 emu K mol^{-1}, ***SEE NOTE***).[31] In comparison, the SMM $[Fe_{10}Na_2(\mu_4\text{-}O)_2(\mu_3\text{-}O)_4(\mu_3\text{-}OH)_4\text{-}(C_6H_5CO_2)_{10}(chp)_6(H_2O)_2\text{-}(Me_2CO)_2]$ exhibits a high temperature (298 K) magnetic moment at 13.36 BM ($\chi_M T$ = 34.35 emu K mol^{-1}).[4] The preliminary variable temperature magnetic (SQUID) measurements of suggest that **33** (desolvated) is indeed a SMM (to be confirmed by AC magnetic susceptibility data). The $\chi_M T$ against T plot of **33** [Figure 4, per Fe(III)] increases abruptly from $\chi_M T$ ~ 4.81 emu K mol^{-1} at low temperature (~ 2 K) to a peak plateau of $\chi_M T$ ~ 5.00 emu K mol^{-1} (~ 2 – 4 K) [Figure 4(b)] and then reaches a maximum of $\chi_M T$ ~ 5.14 emu K mol^{-1} (~ 50 K). The $\chi_M T$ values then decrease smoothly from > 65 K to a minimum value of $\chi_M T$ ~ 4.43 emu K mol^{-1} at an elevated temperature (300 K) which is consistent with the presence of ten non-interacting Fe(III) ions each possessing five unpaired electrons (expected $\chi_M T$ = 4.38 emu K mol^{-1}). The magnetic data

of **33** is yet to be modelled in order to account for the magnitude of exchange interactions and to confirm the ground spin state. In addition, other magnetic studies need to be undertaken to further support the evidence for SMM characteristics [*e.g.*, AC susceptibility measurements (χ''), U_{eff}, D (see Chapter 1, section 1.1.2)].

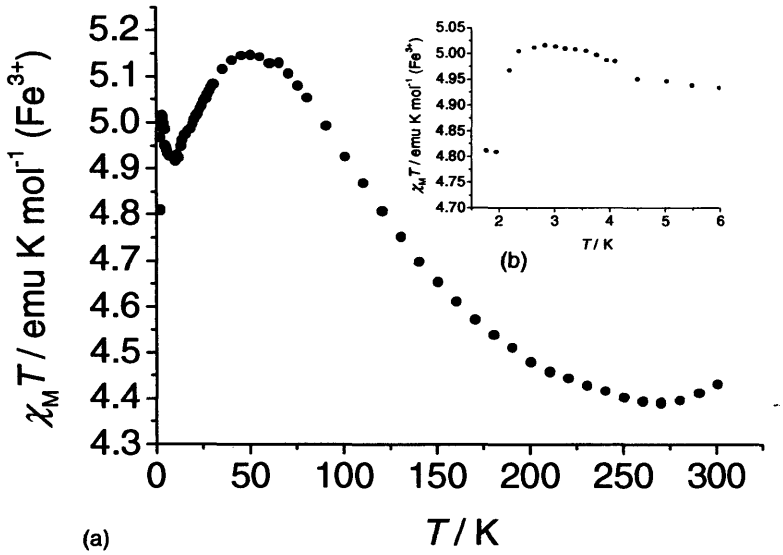

Figure 4 Plots of $\chi_M T$ against T (closed circles); (a) 0 – 350 K and (b) 0 – 6 K (inset) for **33** [per Fe(III) ion].

The reaction of $[Fe_2OCl_6][NEt_4]_2$ with a ligand blend composed of sodium toluate [*p*-CH_3-$C_6H_4CO_2Na$] and Nachp gave, on work-up, small red crystals of the undecanuclear complex $[Fe_{11}(\mu_3\text{-}O)_6(\mu_3\text{-}OH)_6(p\text{-}\{CH_3\}\text{-}C_6H_4CO_2)_{15}]\cdot 15MeCN$ (**34**) (– 25 °C, 2d. EtOAc) in low yield (Scheme 3). Complex **34** was characterised by elemental analysis, IR spectroscopy and positive FAB mass spectrometry. A single crystal of **34** was subject to an X-ray diffraction study. The molecular structure of **34** is shown in Figure 5; selected bond lengths and angles are given in Table 3.

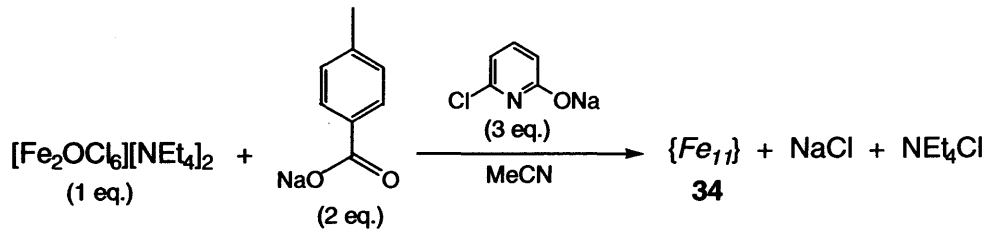

Scheme 3 Synthesis of **34**.

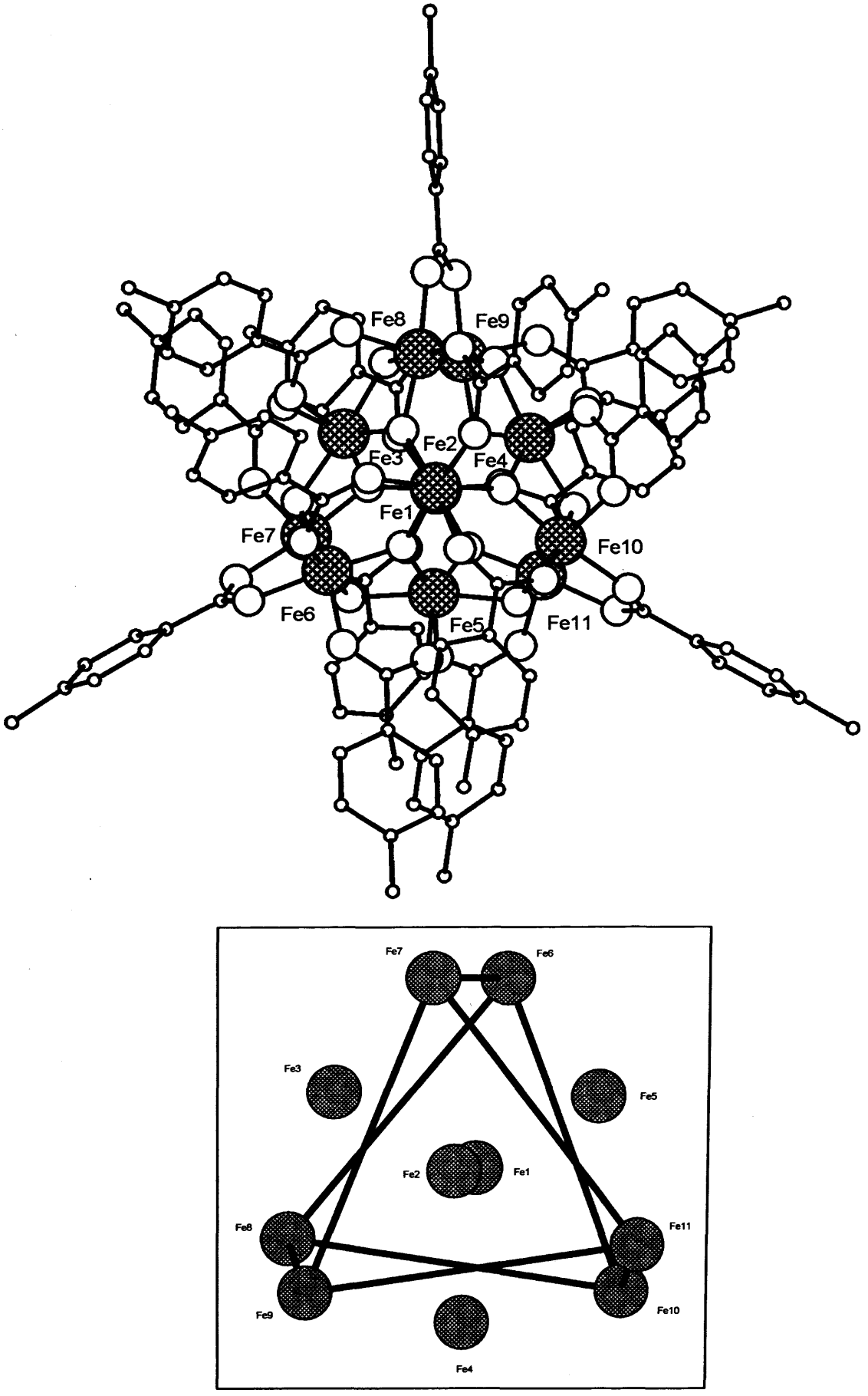

Figure 5 Molecular structure of **34**. Inset shows the pentacapped twisted trigonal prismatic arrangement of iron ions. Hydrogen atoms, solvent molecules and atom labels are omitted for clarity.

Table 3 Selected bond length and angle data for **34**

34							
Fe(1)-O(3)	1.917(3)	Fe(6)-O(1A)	2.052(3)	Fe(3)-O(2M)	2.089(3)	Fe(9)-O(12)	2.139(3)
Fe(1)-O(4)	1.906(3)	Fe(6)-O(1D)	1.951(3)	Fe(4)-O(3)	1.927(3)	Fe(9)-O(2B)	2.025(3)
Fe(1)-O(5)	1.924(3)	Fe(6)-O(1N)	1.995(3)	Fe(4)-O(6)	1.936(3)	Fe(9)-O(2H)	1.988(3)
Fe(1)-O(2D)	2.095(3)	Fe(7)-O(1)	1.894(3)	Fe(4)-O(9)	2.073(3)	Fe(9)-O(2J)	2.023(3)
Fe(1)-O(1E)	2.119(3)	Fe(7)-O(7)	2.142(3)	Fe(4)-O(12)	2.057(3)	Fe(10)-O(3)	1.879(3)
Fe(1)-O(1F)	2.129(3)	Fe(7)-O(11)	2.069(11)	Fe(4)-O(IJ)	2.064(3)	Fe(10)-O(8)	2.084(3)
Fe(2)-O(1)	1.916(3)	Fe(7)-O(2A)	2.040(3)	Fe(4)-O(IK)	2.110(3)	Fe(10)-O(9)	2.124(3)
Fe(2)-O(2)	1.902(3)	Fe(7)-O(1G)	1.974(3)	Fe(5)-O(2)	1.923(3)	Fe(10)-O(2C)	2.034(3)
Fe(2)-O(6)	1.919(3)	Fe(7)-O(1M)	1.973(3)	Fe(5)-O(5)	1.927(3)	Fe(10)-O(2F)	1.947(3)
Fe(2)-O(2G)	2.092(3)	Fe(8)-O(4)	1.900(3)	Fe(5)-O(8)	2.069(3)	Fe(10)-O(2K)	1.975(3)
Fe(2)-O(1H)	2.049(3)	Fe(8)-O(10)	2.137(3)	Fe(5)-O(11)	2.068(3)	Fe(11)-O(2)	1.886(3)
Fe(2)-O(1I)	2.107(3)	Fe(8)-O(12)	2.056(3)	Fe(5)-O(2N)	2.054(3)	Fe(11)-O(8)	2.122(3)
Fe(3)-O(1)	1.915(3)	Fe(8)-O(1B)	2.051(3)	Fe(5)-O(2O)	2.086(3)	Fe(11)-O(9)	2.101(3)
Fe(3)-O(4)	1.934(3)	Fe(8)-O(2E)	1.963(3)	Fe(6)-O(5)	1.893(3)	Fe(11)-O(1C)	2.053(3)
Fe(3)-O(7)	2.065(3)	Fe(8)-O(2L)	1.973(3)	Fe(6)-O(7)	2.085(3)	Fe(11)-O(2I)	1.961(3)
Fe(3)-O(10)	2.082(3)	Fe(9)-O(6)	1.883(3)	Fe(6)-O(11)	2.129(3)	Fe(11)-O(1O)	1.995(3)
Fe(3)-O(1L)	2.081(3)	Fe(9)-O(10)	2.137(3)				
Fe(3)-O(1)-Fe(2)	129.17(17)	Fe(8)-O(12)-Fe(4)	122.30(16)	Fe(9)-O(6)-Fe(2)	124.74(17)	O(2)-Fe(5)-O(8)	78.16(13)
Fe(7)-O(1)-Fe(2)	126.58(17)	Fe(4)-O(12)-Fe(9)	92.04(13)	Fe(9)-O(6)-Fe(4)	104.50(16)	O(5)-Fe(5)-O(8)	105.95(13)
Fe(7)-O(1)-Fe(3)	104.24(15)	Fe(8)-O(12)-Fe(9)	96.46(13)	Fe(3)-O(7)-Fe(6)	125.42(16)	O(5)-Fe(6)-O(7)	92.17(13)
Fe(2)-O(2)-Fe(5)	128.63(17)	O(4)-Fe(1)-O(3)	94.72(14)	Fe(3)-O(7)-Fe(7)	91.22(13)	O(7)-Fe(6)-O(11)	83.99(13)
Fe(11)-O(2)-Fe(2)	127.06(17)	O(4)-Fe(1)-O(5)	95.72(13)	Fe(6)-O(7)-Fe(7)	94.75(13)	O(5)-Fe(6)-O(11)	78.26(13)
Fe(11)-O(2)-Fe(5)	104.30(16)	O(3)-Fe(1)-O(5)	93.42(13)	Fe(5)-O(8)-Fe(10)	121.92(13)	O(1)-Fe(7)-O(7)	76.87(13)
Fe(1)-O(3)-Fe(4)	128.52(17)	O(2)-Fe(2)-O(1)	95.68(14)	Fe(5)-O(8)-Fe(11)	91.72(13)	O(1)-Fe(7)-O(11)	92.98(13)
Fe(10)-O(3)-Fe(1)	127.23(18)	O(2)-Fe(2)-O(6)	94.86(14)	Fe(10)-O(8)-Fe(11)	96.22(13)	O(11)-Fe(7)-O(7)	84.05(13)
Fe(10)-O(3)-Fe(4)	104.25(15)	O(1)-Fe(2)-O(6)	96.87(14)	Fe(4)-O(9)-Fe(10)	91.45(13)	O(4)-Fe(8)-O(10)	78.50(13)
Fe(1)-O(4)-Fe(3)	129.40(17)	O(1)-Fe(3)-O(4)	107.28(14)	Fe(4)-O(9)-Fe(11)	124.90(15)	O(4)-Fe(8)-O(12)	94.22(13)
Fe(8)-O(4)-Fe(1)	128.10(17)	O(1)-Fe(3)-O(7)	78.34(13)	Fe(11)-O(9)-Fe(10)	95.65(13)	O(12)-Fe(8)-O(10)	83.67(13)
Fe(8)-O(4)-Fe(3)	102.50(15)	O(4)-Fe(3)-O(7)	104.77(13)	Fe(3)-O(10)-Fe(8)	90.26(13)	O(6)-Fe(9)-O(10)	91.19(13)
Fe(1)-O(5)-Fe(5)	131.23(17)	O(3)-Fe(4)-O(6)	108.79(13)	Fe(3)-O(10)-Fe(9)	126.84(16)	O(6)-Fe(9)-O(12)	77.17(13)
Fe(6)-O(5)-Fe(1)	125.52(17)	O(3)-Fe(4)-O(9)	78.04(13)	Fe(9)-O(10)-Fe(8)	95.53(13)	O(3)-Fe(10)-O(8)	94.55(13)
Fe(6)-O(5)-Fe(5)	103.24(15)	O(6)-Fe(4)-O(9)	103.32(13)	Fe(5)-O(11)-Fe(6)	91.05(13)	O(3)-Fe(10)-O(9)	77.80(13)
Fe(2)-O(6)-Fe(4)	130.73(18)	O(2)-Fe(5)-O(5)	108.19(13)	Fe(5)-O(11)-Fe(7)	123.54(16)	O(2)-Fe(11)-O(9)	91.95(13)
				Fe(7)-O(11)-Fe(6)	95.65(13)	O(2)-Fe(11)-O(8)	77.63(13)

The molecular structure of **34** consists of eleven octahedral Fe(III) ions surrounded by fifteen toluate ligands. The toluate carboxylates are bound as 1,3-bridging ligands over the iron(III) ions. The iron-oxo core of **34** contains eleven iron ions situated at the corners of a twisted pentacapped trigonal prism (Figure 5, inset). A D_3 axis is determined crystallographically on the distorted trigonal prism whereby, the prismatic triangular faces have C_3 symmetry. In **34**, the iron oxo-hydroxy core comprises $[Fe_{11}(\mu_3\text{-}O)_6(\mu_3\text{-}OH)_6]^{15+}$ and could be described as a regular icosahedron [Figure 6(a)].

There are three types of iron ions in **34**. Firstly, two central ions Fe(1) and Fe(2), which cap the triangular faces of the prism are each bound to three *fac*-μ_3-oxo bridges and three *fac*-μ-CO_2 ligands. Secondly, three iron ions Fe(3), Fe(4) and Fe(5), which cap the square faces of the trigonal prism are each bound to two *cis*-μ_3-O atoms, two *trans*-μ_3-OH and two *cis*-μ-CO_2 ligands. Finally, the remaining six iron ions Fe(6), Fe(7), Fe(8), Fe(9), Fe(10) and Fe(11), are each situated on the vertices of the trigonal prism (on a C_2 axis). Each of these ions is bound to one μ_3-O, two *cis*-μ_3-OH and three *fac*-μ-CO_2 ligands. There are twenty eight possible Fe···Fe interactions in **34** [Figure 6(c)].

The average Fe-O bond lengths and angles are typical for the presence of either trigonal planar oxide- or pyramidal hydroxide-based oxygen atoms [Fe-O_{oxo} = 1.914 Å (type 1), 1.927 Å (type 2), 1.889 Å (type 3), Fe-μ_3-O_{oxide}-Fe angle ~ av. 123.50°; Fe-OH = 2.069 Å (type 2), 2.110 Å (type 3); Fe-μ_3-$O_{hydroxide}$-Fe ~ av. 103.74°].

It is noteworthy that the chp ligand does not, unlike in **33** and $[Fe_{10}Na_2(\mu_4\text{-}O)_2(\mu_3\text{-}O)_4(\mu_3\text{-}OH)_4(C_6H_5CO_2)_{10}(chp)_6(H_2O)_2(Me_2CO)_2]$, coordinate to any of the iron ions of **34**, instead it possibly enables solubility/basicity of the starting materials for subsequent crystallisation. Attempts to reproduce the synthetic pathway by excluding Nachp to synthesise **34** proved to be unsuccessful.

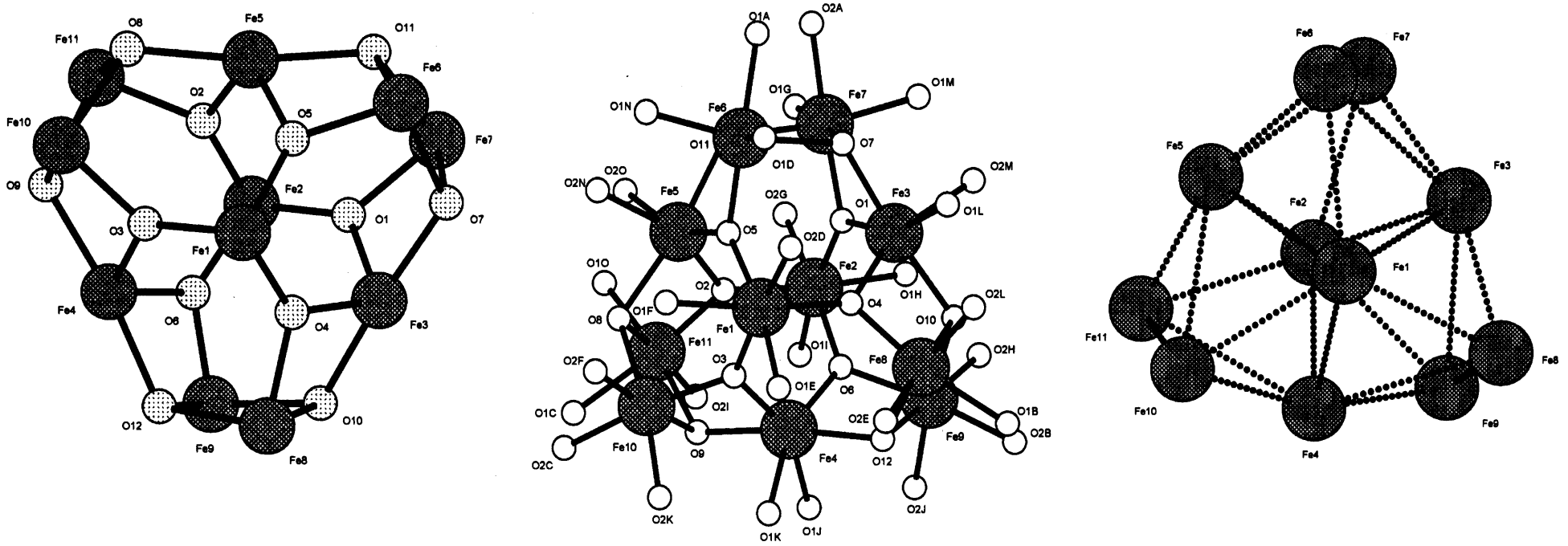

(a) (b) (c)

Figure 6 (a) Icosahedral iron-oxo core, (b) iron-oxo/carboxylate core and (c) the twenty-eight different Fe(III)···Fe(III) ion interactions of **34** [in Å, Fe(1)···Fe(2) 4.691, Fe(1)···Fe(3) 3.472, Fe(1)···Fe(4) 3.463, Fe(1)···Fe(5) 3.508, Fe(1)···Fe(6) 3.393, Fe(1)···Fe(7) 5.036, Fe(1)···Fe(8) 3.422, Fe(1)···Fe(10) 3.401, Fe(1)···Fe(11) 5.088, Fe(2)···Fe(4) 3.504, Fe(2)···Fe(5) 3.447, Fe(2)···Fe(7) 3.404, Fe(2)···Fe(9) 3.368, Fe(3)···Fe(6) 3.688, Fe(3)···Fe(7) 3.007, Fe(3)···Fe(8) 2.990, Fe(3)···Fe(9) 3.730, Fe(4)···Fe(8) 3.602, Fe(4)···Fe(9) 3.020, Fe(4)···Fe(10) 3.005, Fe(4)···Fe(11) 3.701, Fe(5)···Fe(6) 2.995, Fe(5)···Fe(7) 3.644, Fe(5)···Fe(10) 3.631, Fe(5)···Fe(11) 3.007, Fe(6)···Fe(7) 3.111, Fe(8)···Fe(9) 3.129, Fe(10)···Fe(11) 3.131, CIF file not handled by PLATON to generate esd values].

The undecanuclear twisted trigonal prismatic iron ion arrangement of **34** has been reported before in $[Fe_{11}(\mu_3\text{-}O)_6(\mu_3\text{-}OH)_6(RCO_2)_{15}]$ {R = C_6H_5,[4] or 3-(4-methylbenzoyl)-propionate[5]} whereby, the molecular structures only differ in the nature of the bridging carboxylate substituents. $\{Fe_{11}\}$ clusters of this type have been of interest for the understanding of corrosion inhibition,[6a] and bioinorganic iron rust chemistry by controlled nucleation.[6b] In addition, another type of undecanuclear cluster $[Fe_{11}O_3(OH)(MeCO_2)_8(thme)(L)_6]$ [H_2L = 2-{CH=N$(CH_2)_2$OH}-C_6H_4OH] has been reported recently.[7]

The solid-state IR spectrum of **34** exhibits four absorption bands corresponding to $\nu(CO_2)_{asymm}$ = 1598 cm^{-1}/1554 cm^{-1}, $\nu(CO_2)_{symm}$ = 1400 cm^{-1} and ν(Fe-O) = 767 cm^{-1}. The ESI mass spectrum of **34** shows several fragmentation peaks including $[M]^+$ at 2839 Da.

The room temperature magnetic moment of **34** (desolvated) at 8.2 BM ($\chi_M T$ = 8.33 emu K mol^{-1}) is less than expected for eleven non-interacting Fe(III) ions with each possessing five unpaired electrons (expected 19.6 BM, $\chi_M T$ = 48.13 emu K mol^{-1}, ***SEE NOTE***).[31] In $[Fe_{11}(O)_6(OH)_6(PhCO_2)_{15}]$ antiferromagnetic behaviour has been reported with a high temperature magnetic moment at 13.9 BM per molecule (298 K);[4] this type of magnetic behaviour should also be consistent with **34**. The variable temperature magnetic (SQUID) measurements of **34** are still in progress.

5.1.2 M = Fe, NaL^1 = RCO_2Na (R = Ph_2CH), L^2 = Nahmp (n = 1, X = H)

Given the effect of the carboxylate substituent on cluster assembly in section 5.1.1, we decided to examine the reaction of $[Fe_2OCl_6][NEt_4]_2$ with blends composed of Nahmp and $Ph_2C\{H\}CO_2Na$. Previously, the reaction of $FeCl_3$ with ligand combinations based on Nahmp/CH_3CO_2Na or hmpH/CH_3CO_2Na/NaOMe have furnished the octanuclear clusters $[Fe_8(O)_4(hmp)_4(O_2CMe)_{12}]$ and $[Fe_8(O)_4(hmp)_5(O_2CMe)_{11}]$, respectively.[17] In addition, the reaction of $[Fe_3O(RCO_2)_2(H_2O)_3](NO_3)$ with mehmpH or hmpH has been previously

reported to give the hexanuclear species $[Fe_6(O)_2(OH)_2(mehmp)_2(O_2CBu^t)_{10}]$[10,15] and $[Fe_6(O)_2(hmp)_6(O_2CR)_6](NO_3)_2$ (R = Bu^t, Ph), respectively.[17]

The reaction of $[Fe_2OCl_6][NEt_4]_2$ with sodium diphenylacetate ($Ph_2C\{H\}CO_2Na$) and Nahmp gave, on work-up, red crystals of $[Fe_8(\mu_3\text{-}O)_4(\mu_2\text{-}OH)_2(hmp)_4(\eta^2\text{-}Ph_2C\{H\}CO_2)_8(\eta^1\text{-}Ph_2C\{H\}CO_2)_2(MeOH)]\cdot 2MeCN\cdot MeOH$ (**35**) (– 25 °C, 3d THF) in low yield (Scheme 4). Complex **35** was characterised by elemental analysis, IR spectroscopy and positive FAB mass spectrometry. A single crystal of **35** was subject to an X-ray diffraction study. The molecular structure of **35** is shown in Figure 7; selected bond lengths and angles are given in Table 4.

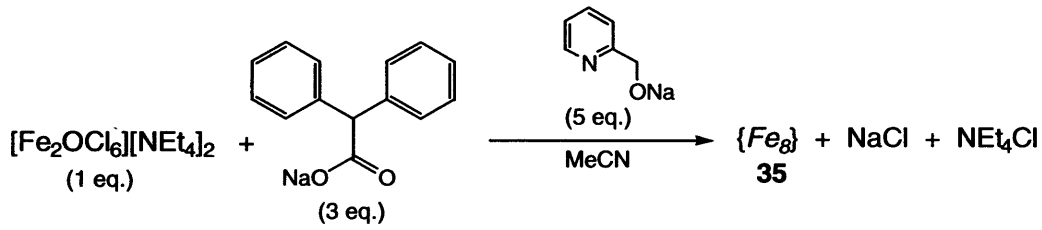

Scheme 4 Synthesis of **35**.

Two unique molecules were found within the asymmetric unit in **35**; only one of these molecules will be described. The molecular structure of **35** consists of eight octahedral Fe(III) ions surrounded by an outer hydrophobic coating based on ten diphenylacetate ligands. Of the ten diphenylacetate ligands two are η^1-bound and eight are 1,3-bridged. In addition, there are four *N,O*-chelating and bridging 2.21 or 3.31 hmp ligands and a terminal methanol ligand (present from the preparation of the Nahmp salt). The donor atom types per iron ion of **35** are shown in Table 5.

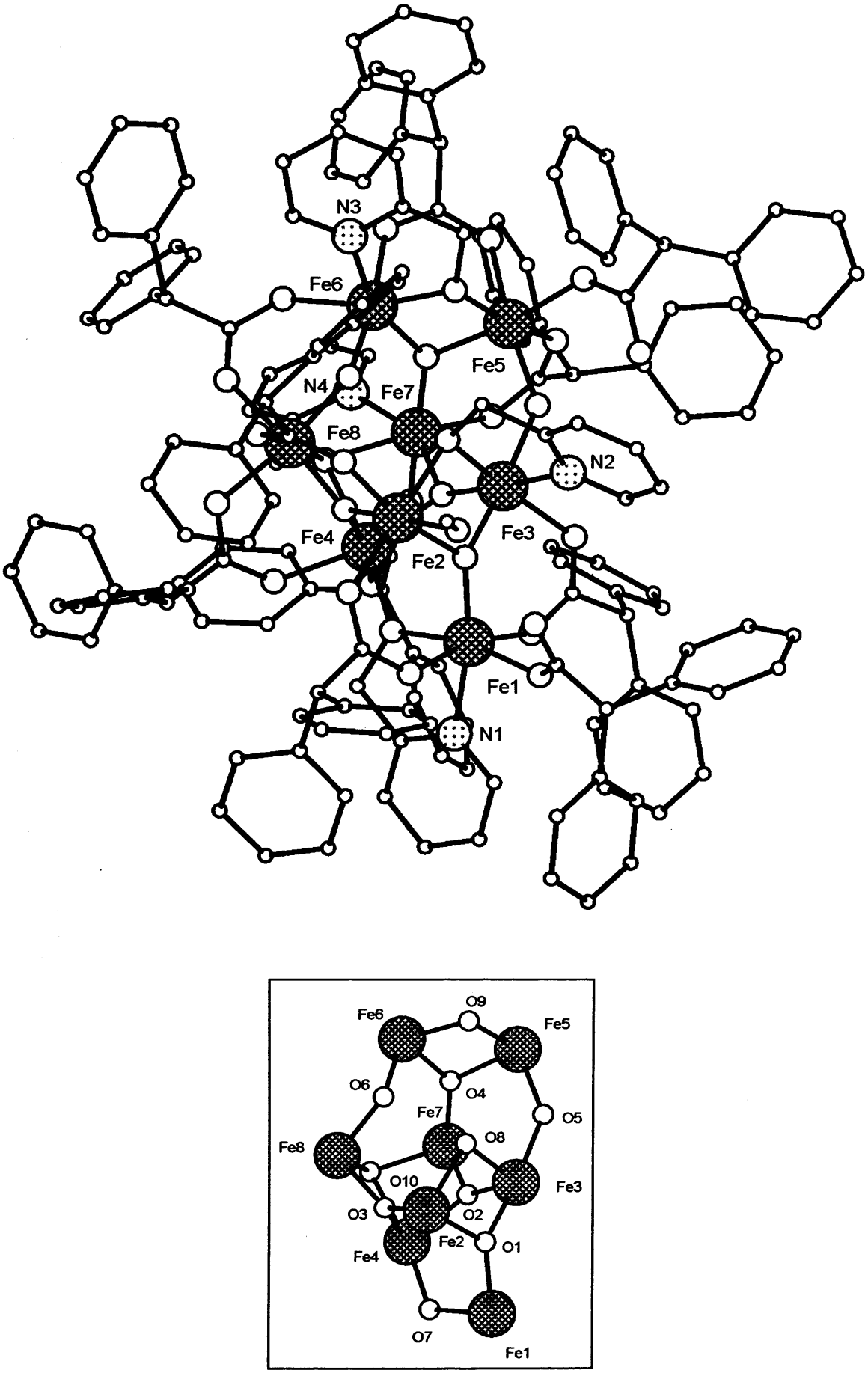

Figure 7 Molecular structure of a unique molecule in **35**. Inset shows the iron-oxo core. Hydrogen atoms, atom labels (except core and N atoms) and solvent (MeCN/MeOH) molecules are omitted for clarity.

Table 4 Selected bond length (Å) and angle (°) data for **35**

35											
Fe(1)-O(1)	1.856(7)	Fe(2)-O(3)	1.881(7)	Fe(3)-O(5)	1.975(7)	Fe(6)-O(26)	2.027(7)	Fe(5)-O(9)	1.998(7)	Fe(7)-O(22)	2.105(7)
Fe(1)-N(1)	2.140(9)	Fe(2)-O(8)	2.047(7)	Fe(3)-O(8)	2.072(7)	Fe(6)-O(29)	2.035(7)	Fe(5)-O(23)	1.987(7)	Fe(7)-O(28)	2.014(7)
Fe(1)-O(7)	2.012(6)	Fe(2)-O(14)	2.029(7)	Fe(3)-O(16)	2.036(7)	Fe(7)-O(2)	1.932(6)	Fe(5)-O(25)	2.077(7)	Fe(8)-O(3)	1.867(6)
Fe(1)-O(11)	1.973(7)	Fe(2)-O(17)	2.039(7)	Fe(4)-O(2)	1.945(6)	Fe(4)-O(10)	2.208(6)	Fe(5)-O(27)	1.996(7)	Fe(8)-O(6)	1.919(6)
Fe(1)-O(13)	2.054(7)	Fe(2)-O(31)	2.084(7)	Fe(4)-O(3)	1.938(7)	Fe(4)-O(19)	2.090(7)	Fe(6)-N(3)	2.165(9)	Fe(8)-O(10)	2.230(7)
Fe(1)-O(15)	2.032(8)	Fe(3)-O(1)	1.982(6)	Fe(4)-O(7)	1.967(6)	Fe(4)-O(21)	2.035(7)	Fe(6)-O(4)	1.913(6)	Fe(8)-O(18)	2.010(7)
Fe(2)-O(1)	1.911(6)	Fe(3)-O(2)	1.913(6)	Fe(6)-O(6)	1.946(6)	Fe(5)-O(4)	1.953(6)	Fe(7)-N(4)	2.178(9)	Fe(8)-O(20)	2.032(7)
		Fe(3)-N(2)	2.205(9)	Fe(6)-O(9)	1.985(7)	Fe(5)-O(5)	1.971(6)	Fe(7)-O(10)	2.141(7)	Fe(8)-O(30)	2.011(6)
Fe(1)-O(1)-Fe(2)	124.6(3)	Fe(8)-O(3)-Fe(4)	106.7(3)	Fe(6)-O(9)-Fe(5)	96.5(3)	O(3)-Fe(2)-O(8)	90.2(3)	O(5)-Fe(3)-N(2)	83.4(3)	O(4)-Fe(6)-O(9)	80.2(3)
Fe(1)-O(1)-Fe(3)	129.0(3)	Fe(6)-O(4)-Fe(5)	100.4(3)	Fe(7)-O(10)-Fe(4)	88.9(2)	O(2)-Fe(3)-O(1)	91.6(3)	O(3)-Fe(4)-O(2)	91.6(3)	O(6)-Fe(6)-O(9)	95.5(3)
Fe(2)-O(1)-Fe(3)	102.2(3)	Fe(7)-O(4)-Fe(5)	122.4(3)	Fe(4)-O(10)-Fe(8)	86.9(2)	O(2)-Fe(3)-O(5)	99.4(3)	O(2)-Fe(4)-O(7)	109.9(3)	O(4)-Fe(6)-N(3)	156.4(3)
Fe(3)-O(2)-Fe(4)	122.1(3)	Fe(7)-O(4)-Fe(6)	134.4(3)	Fe(7)-O(10)-Fe(8)	124.0(3)	O(5)-Fe(3)-O(1)	167.1(3)	O(3)-Fe(4)-O(7)	98.8(3)	O(6)-Fe(6)-N(3)	94.2(3)
Fe(3)-O(2)-Fe(7)	128.1(3)	Fe(5)-O(5)-Fe(3)	140.4(3)	O(1)-Fe(1)-O(7)	88.3(3)	O(1)-Fe(3)-O(8)	78.7(3)	O(4)-Fe(5)-O(5)	92.9(3)	O(4)-Fe(7)-O(2)	104.3(3)
Fe(7)-O(2)-Fe(4)	103.6(3)	Fe(8)-O(6)-Fe(6)	130.1(3)	O(1)-Fe(1)-N(1)	165.7(3)	O(2)-Fe(3)-O(8)	99.4(3)	O(4)-Fe(5)-O(9)	78.9(3)	O(2)-Fe(7)-N(4)	153.4(3)
Fe(2)-O(3)-Fe(4)	120.8(3)	Fe(4)-O(7)-Fe(1)	121.3(3)	O(3)-Fe(2)-O(1)	94.5(3)	O(1)-Fe(3)-N(2)	88.1(3)	O(5)-Fe(5)-O(9)	102.7(3)	O(4)-Fe(7)-N(4)	92.6(3)
Fe(8)-O(3)-Fe(2)	127.6(4)	Fe(2)-O(8)-Fe(3)	94.7(3)	O(1)-Fe(2)-O(8)	81.0(3)	O(2)-Fe(3)-N(2)	176.0(3)	O(4)-Fe(6)-O(6)	92.2(3)	O(3)-Fe(8)-O(6)	96.9(3)

The iron-oxo core of **35**, $[Fe_8(\mu_3\text{-}O)_4(\mu_2\text{-}OH)_2]^{14+}$, is capped with additional hmp oxygen atoms [O(7), O(8), O(9) and O(10)] (Figure 7, inset). The average iron to oxygen bond lengths are Fe-μ_3-O ~ 1.916 Å, Fe-μ_2-OH ~ 1.955 Å, Fe-μ_3-O_{hmp} ~ 2.193 Å and Fe-μ_2-O_{hmp} ~ 2.013 Å. The accompanying bond angles to the aforementioned bond lengths are as follows, Fe-μ_3-O-Fe ~ 118.49°, Fe-μ_2-OH-Fe ~ 135.25°, Fe-μ_3-O_{hmp}-Fe ~ 99.93° and Fe-μ_2-O_{hmp}-Fe ~ 104.17°, these values being consistent with trigonal planar, bent and distorted tetrahedral oxygen environments, respectively.

The hmp chelate bite angles in **35** average to 76.68° therefore, these acute angles lead to distorted octahedral geometries around Fe(1), Fe(3), Fe(6) and Fe(7). The five-membered hmp chelate ring angles display almost regular pentagonal geometries having a discrepancy of > 4° from the interior angles within a perfect pentagon (72°). The bond length of Fe-N_{hmp} ~ av. 2.172 Å is shorter (*ca.* 0.02 Å) than Fe-μ_3-O_{hmp}.

Table 5 Ligand bonding types present in **35**

Description	Fe(1)	Fe(2)	Fe(3)	Fe(4)	Fe(5)	Fe(6)	Fe(7)	Fe(8)
μ_3-O	1	2	2	2	1	1	2	1
μ_2-OH			1	1	1	1		1
μ_3-O_{hmp}				1			1	1
μ_2-O_{hmp}	1	1	1	1		1		
N-μ_3-O_{hmp}							1	
N-μ_2-O_{hmp}	1		1			1		
μ-CO_2	2	2	1	1	3	2	2	3
η^1-CO_2	1				1			
μ-OH_{MeOH}		1						

The iron-oxo core in complex **35** represents to the knowledge of the author, a unique structural type and consists of edge-connected polygons including a $[Fe_4(\mu_3\text{-}O)_2(\mu_2\text{-}OH)_2]^{6+}$ octagon and two hexagons of $[Fe_3(\mu_3\text{-}O)_3]^{3+}$ or $[Fe_3(\mu_3\text{-}O)_2(\mu_2\text{-}OH)]^{4+}$ [Figure 8(a)]. In $[Fe_8(O)_4(hmp)_4(O_2CMe)_{12}]$, $[Fe_8(O)_4(hmp)_5(O_2CMe)_{11}]$,[10,17] the iron-oxo cores are described as four linked $[Fe_3(\mu_3\text{-}O)_4]^{7+}$ units that assemble to form $[Fe_8(\mu_3\text{-}O)_4]^{16+}$ with a central Fe_2O_4 rhombus and are structurally different when compared to **35**. There are

sixteen possible Fe···Fe interactions in **35** [Figure 8(b)]. Other previously reported octanuclear complexes include $[Fe_8(OH)_4(OPh)_8(O_2CR)_{12}]$ (R = Bu^t, Ph),[10,12] $[CsFe_8\{N(CH_2CH_2O)_3\}_8][Cl]$[13] and $[Fe_8O_3(O_2CPh)_9(tea)(teaH)_3]$ ($teaH_3$ = triethanolamine).[14]

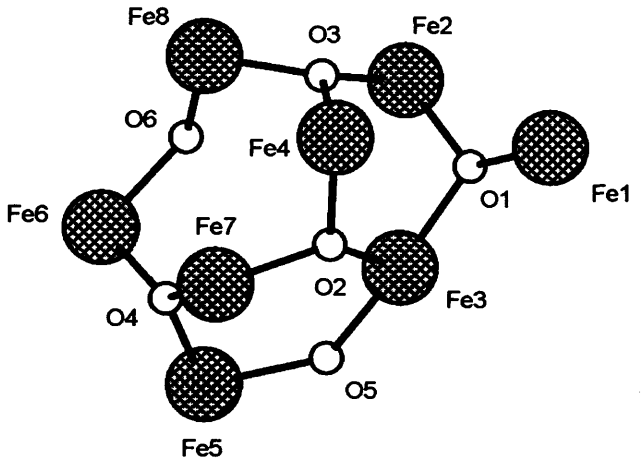

(a)

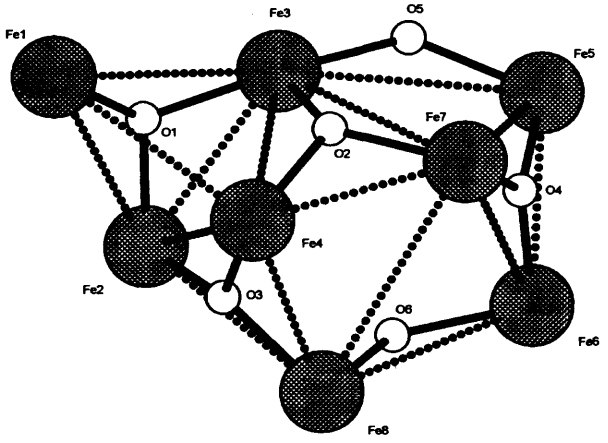

(b)

Figure 8 (a) Connected polygons within the iron-oxo core and (b) the sixteen different Fe(III)···Fe(III) ion interactions of **35** [in Å; Fe(1)···Fe(2) 3.335(2), Fe(1)···Fe(3) 3.465(2), Fe(1)···Fe(4) 3.470(2), Fe(2)···Fe(3) 3.030(2), Fe(2)···Fe(4) 3.321(2), Fe(2)···Fe(8) 3.362(2), Fe(3)···Fe(4) 3.376(2), Fe(3)···Fe(5) 3.712(2), Fe(3)···Fe(7) 3.458(2), Fe(4)···Fe(7) 3.047(2), Fe(4)···Fe(8) 3.053(2), Fe(5)···Fe(6) 2.971(2), Fe(5)···Fe(7) 3.340(2), Fe(6)···Fe(7) 3.475(2), Fe(6)···Fe(8) 3.505(2), Fe(7)···Fe(8) 3.860(2)].

The IR spectrum of **35** shows three significant bands for $\nu(CO_2)_{asymm}$ = 1572 cm^{-1}, $\nu(CO_2)_{symm}$ = 1392 cm^{-1} and ν(Fe-O) = 694 cm^{-1}, these are very close in value to the stretches observed from **34**. The MALDI mass spectrum of **35** exhibits several

fragmentation peaks associated with ligand loss including a [*M* – MeOH – $2Ph_2C\{H\}CO_2]^+$ peak at 2666 Da.

The room temperature magnetic moment of **35** (desolvated) at 9.0 BM ($\chi_M T$ = 10.04 emu K mol^{-1}) is less than expected for eight non-interacting Fe(III) ions with each possessing five unpaired electrons (expected 16.7 BM, $\chi_M T$ = 35.00 emu K mol^{-1}, ***SEE NOTE***).[31] The variable temperature magnetic (SQUID) measurements of **35** are still in progress.

5.1.3 M = Fe, $NaL^1 = RCO_2Na$ (R = Ph_2CH), L^2 = Nahep (n = 2, X = H)

The reaction of $[Fe_3O(RCO_2)_2(H_2O)_3](NO_3)$ with hepH has been previously reported to give the hexanuclear species $[Fe_6(O)_2(OH)_2(hep)_2(O_2CBu^t)_{10}]$.[10,15] In addition, $[Fe_6(O)_2(OH)(hep)_4(O_2CBu^t)_9]$ is obtained from the reaction of $[Fe_6(O)_2(OH)_2(hep)_2(O_2CBu^t)_{10}]$ with excess hepH.[16] Herein, we examine the reaction of $[Fe_2OCl_6][NEt_4]_2$ with a ligand blend composed of $Ph_2C\{H\}CO_2Na$ and Nahep.

Thus, treatment reaction of $[Fe_2OCl_6][NEt_4]_2$ with sodium diphenylacetate and hepH, in the presence of sodium methoxide (forming Nahep *in-situ*) gave, on work-up, brown crystals of $[Fe_6(\mu_3\text{-}O)_2(\mu_2\text{-}OH)_2(hep)_2(Ph_2C\{H\}CO_2)_{10}]\cdot 12MeCN$ (**36**) (– 25 °C, 3d. Et_2O) in low yield (Scheme 5). Complex **36** was characterised by elemental analysis, IR spectroscopy and MALDI mass spectrometry. A single crystal of **36** was subject to an X-ray diffraction study. The molecular structure of **36** is shown in Figure 9; selected bond lengths and angles are given in Table 6.

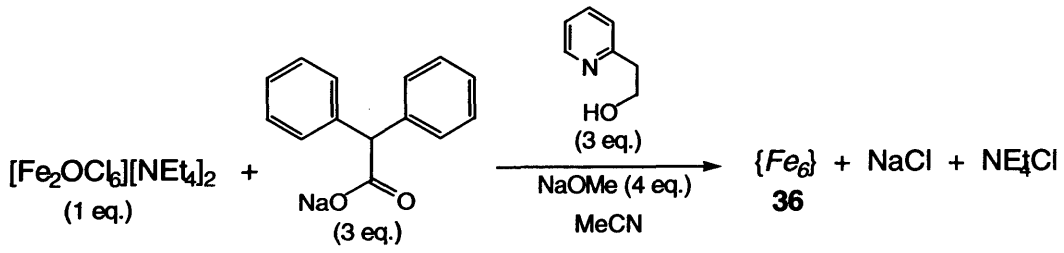

Scheme 5 Synthesis of **36**.

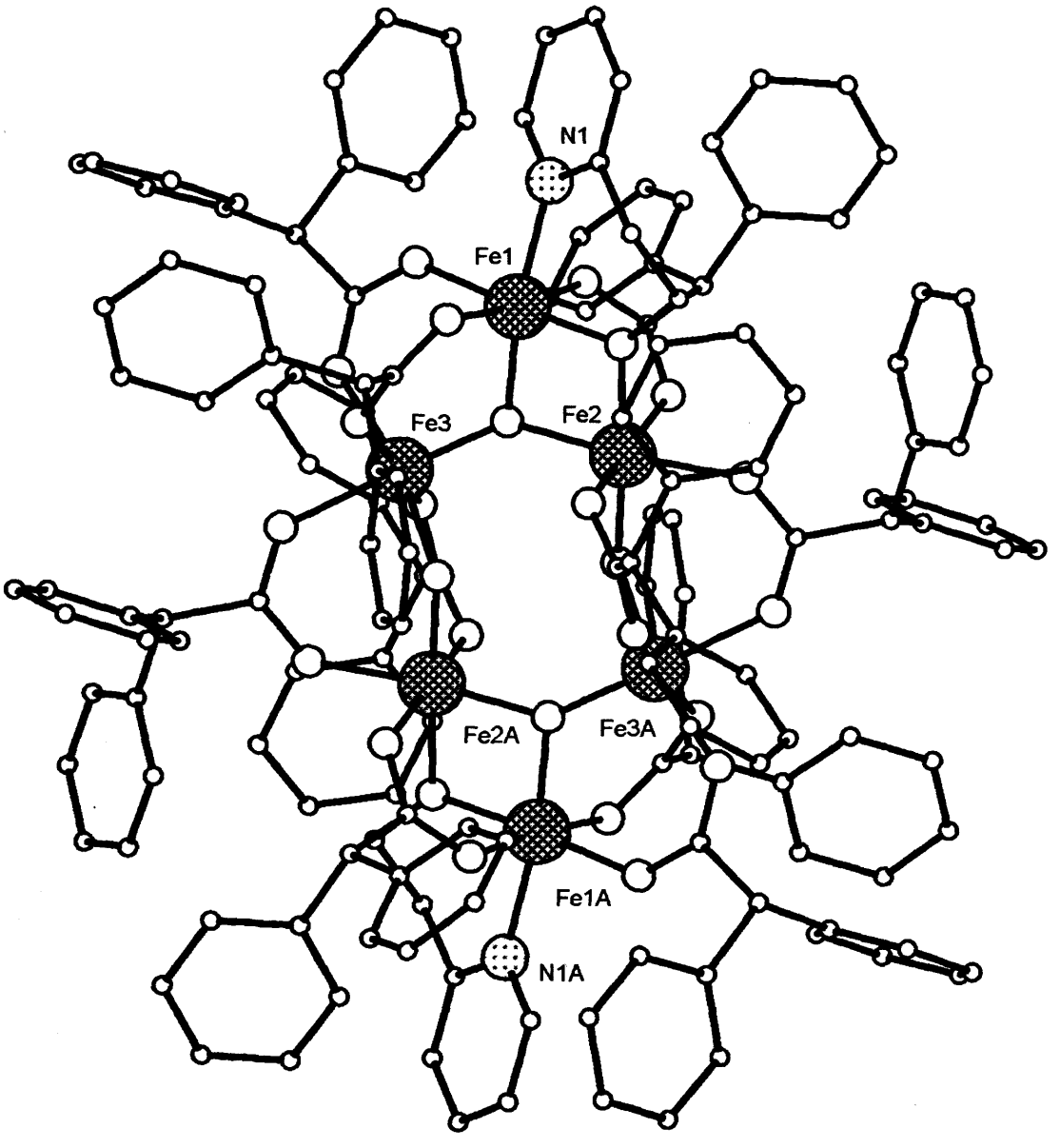

Figure 9 Molecular structure of **36**. Hydrogen atoms, solvent molecules and carbon atom labels (except Fe and N atoms) are omitted for clarity.

Table 6 Selected bond length (Å) and angle (°) data for **36**

36							
Fe(1)-O(1)	1.906(2)	Fe(1)-N(1)	2.152(3)	Fe(2)-O(8)	2.064(2)	Fe(3)-O(7)	2.064(2)
Fe(1)-O(2)	1.939(2)	Fe(2)-O(1)	1.950(2)	Fe(2)-O(13)#1	2.017(2)	Fe(3)-O(9)#1	2.017(2)
Fe(1)-O(4)	2.054(2)	Fe(2)-O(2)	1.979(2)	Fe(3)-O(1)	1.863(2)	Fe(3)-O(11)	2.036(2)
Fe(1)-O(6)	1.977(2)	Fe(2)-O(3)	1.959(2)	Fe(3)-O(3)#1	1.981(2)	Fe(3)-O(12)	2.073(2)
Fe(1)-O(10)	2.054(2)	Fe(2)-O(5)	2.053(2)				
Fe(1)-O(1)-Fe(2)	97.51(9)	O(4)-Fe(1)-O(10)	174.45(8)	O(1)-Fe(2)-O(8)	93.02(9)	O(1)-Fe(3)-O(11)	92.25(9)
Fe(3)-O(1)-Fe(1)	120.51(11)	O(6)-Fe(1)-O(10)	88.99(9)	O(2)-Fe(2)-O(8)	86.77(9)	O(1)-Fe(3)-O(12)	177.18(9)
Fe(3)-O(1)-Fe(2)	139.04(11)	O(1)-Fe(1)-N(1)	171.37(9)	O(3)-Fe(2)-O(8)	93.96(8)	O(3)#1-Fe(3)-O(7)	168.27(8)
Fe(1)-O(2)-Fe(2)	95.42(9)	O(2)-Fe(1)-N(1)	88.86(9)	O(5)-Fe(2)-O(8)	171.56(9)	O(3)#1-Fe(3)-O(9)#1	96.10(9)
Fe(2)-O(3)-Fe(3)#1	123.79(10)	O(4)-Fe(1)-N(1)	85.12(9)	O(1)-Fe(2)-O(13)#1	174.43(8)	O(3)#1-Fe(3)-O(11)#1	93.42(8)
O(1)-Fe(1)-O(2)	83.04(9)	O(6)-Fe(1)-N(1)	88.52(9)	O(2)-Fe(2)-O(13)#1	93.75(9)	O(3)#1-Fe(3)-O(12)	84.88(8)
O(1)-Fe(1)-O(4)	91.79(9)	O(10)-Fe(1)-N(1)	90.23(9)	O(3)-Fe(2)-O(13)#1	89.39(8)	O(9)#1-Fe(3)-O(7)	82.57(9)
O(2)-Fe(1)-O(4)	89.20(9)	O(1)-Fe(2)-O(2)	80.90(8)	O(13)#1-Fe(2)-O(5)	86.77(9)	O(11)-Fe(3)-O(7)	86.86(80
O(1)-Fe(1)-O(6)	99.43(9)	O(1)-Fe(2)-O(3)	95.95(8)	O(13)#1-Fe(2)-O(8)	88.19(9)	O(7)-Fe(3)-O(12)	83.42(8)
O(2)-Fe(1)-O(6)	176.22(9)	O(3)-Fe(2)-O(2)	176.80(9)	O(1)-Fe(3)-O(3)#1	92.59(9)	O(9)#1-Fe(3)-O(11)	168.18(9)
O(6)-Fe(1)-O(4)	87.87(9)	O(1)-Fe(2)-O(5)	91.36(9)	O(1)-Fe(3)-O(7)	99.13(9)	O(9)#1-Fe(3)-O(12)	87.20(9)
O(1)-Fe(1)-O(10)	93.24(8)	O(2)-Fe(2)-O(5)	86.80(9)	O(1)-Fe(3)-O(9)#1	94.31(9)	O(11)-Fe(3)-O(12)	86.86(8)
O(2)-Fe(1)-O(10)	93.73(9)	O(3)-Fe(2)-O(5)	92.75(8)				

Symmetry transformations used to generate equivalent atoms: #1 $(-x, -y, -z+1)$.

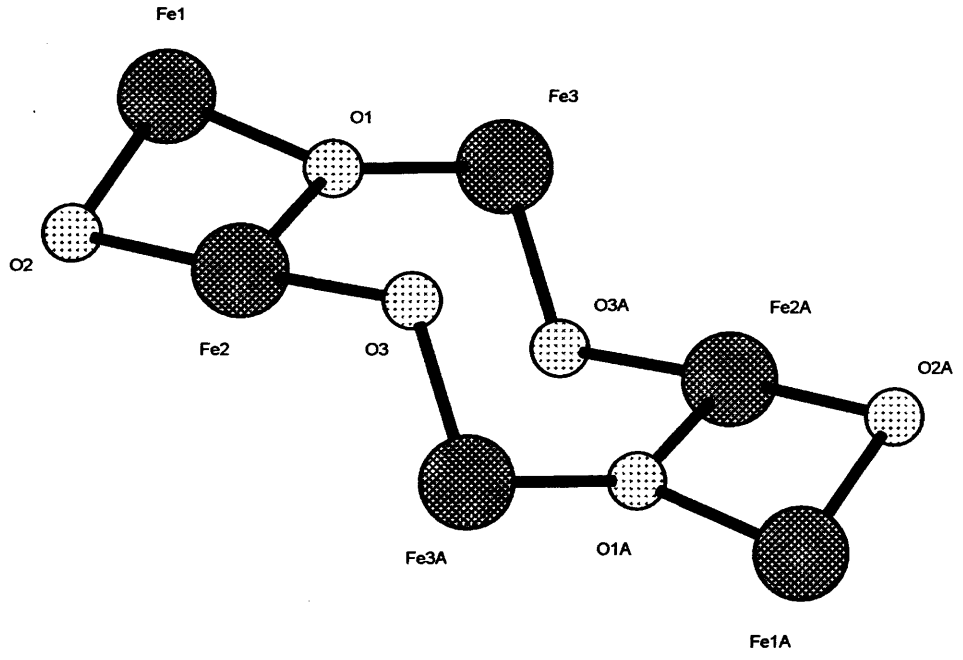

Figure 10 Iron-oxo core of **36**. Fe(III)···Fe(III) interactions (not shown) in Å, Fe(1)···Fe(2) 3.2436(17), Fe(1)···Fe(3) 2.8811(16), Fe(2)···Fe(3) 3.4672(16).

The molecular structure of **36** consists of six octahedral Fe(III) ions. The periphery of the iron-oxo core is surrounded by ten 1,3-bridging diphenylacetate ligands and two 2.21 *N,O*-chelating hep ligands. The $[Fe_6(\mu_3\text{-}O)_2(\mu_2\text{-}OH)_2]^{12+}$ core within **36** is capped by two hep oxygen atoms [O(2) and O(2A)] (Figure 10).

The average iron ion bond lengths and angles to core oxygen donor atoms are as follows, Fe-μ_3-O = 1.885 Å, Fe(1)-μ_3-O(1)-Fe(3) = 120.51° and Fe-μ_2-OH = 1.959 Å, Fe-μ_2-OH-Fe = 123.79°, with the bond angles being indicative of trigonal planar geometries around the μ_3-O and μ_2-OH bound oxygen atoms, with the latter in greater distortion.

The core of **36** can be considered as fused polygons consisting of two edge sharing distorted squares $[Fe_2(\mu_2\text{-}O_{hep})(\mu_3\text{-}O)]^{3+}$ (including capping hep oxygen atoms) and an inner octagonal iron-oxo core of $[Fe_4(\mu_3\text{-}O)_2(\mu_2\text{-}OH)_2]^{6+}$. The following average interior angles of Fe-μ_3-O-Fe = 96.47° and μ_3-O-Fe-O_{hep} = 81.97° confirm the presence of distorted iron-oxo $[Fe_2O_4]$ squares on the edges of the core. The hep bond lengths in **36** average to Fe-O_{hep} = 1.959 Å and Fe-N_{hep} = 2.152 Å. The O_{hep}-Fe-N_{hep} a bite angle at 88.86(9)° is larger in comparison to the hmp chelate bite angle found in **35** (76.68°). The larger bite angle results in a more regular octahedral geometry around the hep bound iron ions of **36**.

The structure of **36** is essentially the same as $[Fe_6(O)_2(OH)_2(hep)_2(O_2CBu^t)_{10}]$ and possesses similar bond length and angle values when compared to **36**.[15] However, **36** is structurally different to the hexanuclear iron clusters $[Fe_6(O)_2(hmp)_6(O_2CR)_6](NO_3)_2$ (R = Bu^t, Ph)[17] and $[Fe_6(O)_2(OH)(hep)_4(O_2CBu^t)_9]$.[16] Other hexanuclear iron clusters have been previously investigated for their properties and structural types[10,18,20] which include, the ferric wheels $[Fe_6(bic)_6]$ ($bicH_3$ = bicine),[14] $[MFe_6(OCH_3)_{12}(L')_6]^+$ (M = Na or Li, $L'H_3$ = dibenzoylmethane and other derivatives),[19a] $[FeF_6(edea)_6]$ (H_2edea = *N*-ethyldiethanol),[19b] [MFe$_6$(*N*-diethanolaminate)$_6$X$_6$],[19c] $[Fe_6L''_6]$ [H_3L'' = N-(2-hydroxy-5-nitrobenzyl)-iminodiethanol][19d] and an open di-cubane-based complex $[Fe_6(L''')_2(\mu\text{-}OMe)_6(\mu_4\text{-}O)_2Cl_4]$ [H_2L''' = *N,N'*-bis(n-butylcarbamoyl)pyridine-2,6-carboxamide][19e]

The solid-state IR spectrum of **36** indicates the presence of three strong absorption bands corresponding to $\nu(CO_2)_{asymm}$ = 1574 cm^{-1}, $\nu(CO_2)_{symm}$ = 1393 cm^{-1} and ν(Fe-O) = 695 cm^{-1}; these are very close to the values found in both iron-oxo clusters **34** and **35**. The MALDI mass spectrum of **36** includes a peak of $[M - 4Ph_2C\{H\}CO_2 - O]^+$ = 1896 Da.

The room temperature magnetic moment of **36** (desolvated) at 12.4 BM ($\chi_M T$ = 19.29 emu K mol^{-1}) is less than expected for six non-interacting Fe(III) ions with each possessing five unpaired electrons (expected 14.5 BM, $\chi_M T$ = 26.25 emu K mol^{-1}). In $[Fe_6(O)_2(OH)_2(hep)_2(O_2CBu^t)_{10}]$ the variable temperature magnetic susceptibility studies are indicative of a S = 5 ground spin state with an elevated temperature (300 K) magnetic moment at 10.8 BM ($\chi_M T$ = 14.63 emu K mol^{-1}, ***SEE NOTE***);[31] this is comparable to the room temperature magnetic moment of **36**.[15] The variable temperature magnetic (SQUID) measurements of **36** are still in progress.

5.1.4 M = Fe, NaL^1 = Nachp (n = 0, X = Cl), L^2 = hmpH (n = 1, X = H)

In chapter 2, the reactions of blends of two different 2-pyridine alcohols were examined. In this section, we investigate the reaction of sodium salts of two different 2-pyridine alcohols with $[Fe_2OCl_6][NEt_4]_2$. Thus, the reaction of $[Fe_2OCl_6][NEt_4]_2$ with a ligand blend composed of Nachp and hmpH gave, on work-up, red crystals of hexanuclear $[Fe_6(\mu_3\text{-}O)_2(hmp)_8Cl_4](Cl)_2{\cdot}4H_2O$ (**37**) (– 25 °C, 3d. Et_2O) in low yield (Scheme 6). Complex **37** was characterised by elemental analysis, IR spectroscopy and positive FAB mass spectrometry. A single crystal of **37** was subject to an X-ray diffraction study. The molecular structure of **37** is shown in Figure 11; selected bond lengths and angles are given in Table 7.

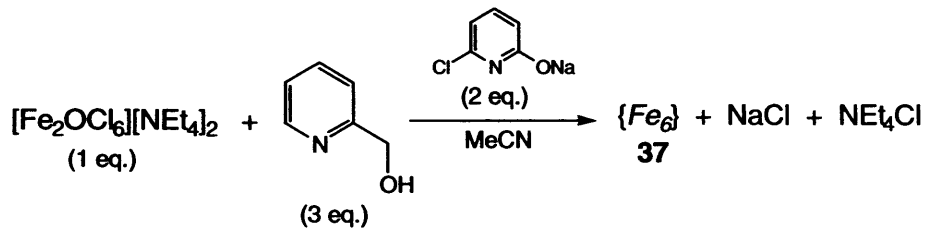

Scheme 6 Synthesis of **37**.

The molecular structure of **37** reveals a hexanuclear cationic unit and two chloride counterions. The cationic unit contains four distorted octahedral and two distorted trigonal bipyramidal Fe(III) ions coordinated by eight hmp and four terminal chloride ligands. The hmp ligands are bound to the four octahedral iron ions in a 2.21 *N,O*-chelating bonding mode. The two remaining trigonal bipyramidal iron ions are coordinated by two intact *cis*-chlorides.

The iron-oxo core in **37** is based on $[Fe_6(\mu_3\text{-}O)_2]^{14+}$. The Fe-$\mu_3$-O bond lengths are 1.926 Å and Fe-μ_3-O-Fe = av. 120°, these values being consistent with a trigonal planar oxo-atom geometry. The core of **37** is formed by the fusing of edge-sharing polygons consisting of two $[Fe_2(\mu_2\text{-}O_{hmp})_2]^{4+}$ and two $[Fe_2(\mu_3\text{-}O)(\mu_2\text{-}O_{hmp})]^{3+}$ rhombic polygons along with a central $[Fe_4(\mu_3\text{-}O)_2(\mu_2\text{-}O_{hmp})_2]^{6+}$ chair-shaped octagon. The corresponding angles forming the vertices of these polygons average to Fe-μ_2-O_{hmp}-Fe = 102.38° and Fe-μ_3-O-Fe = 76.6°. The five-membered chelate bite angles of N_{hmp}-Fe-O_{hmp} average to ~ 75.8°, is smaller than the corresponding angle in **35** (N_{hmp}-Fe-O_{hmp} = 76.68°). The hmp ligands have Fe-O_{hmp} and Fe-N_{hmp} bond lengths within the chelate averaging to 1.975 Å and 2.139 Å, respectively.

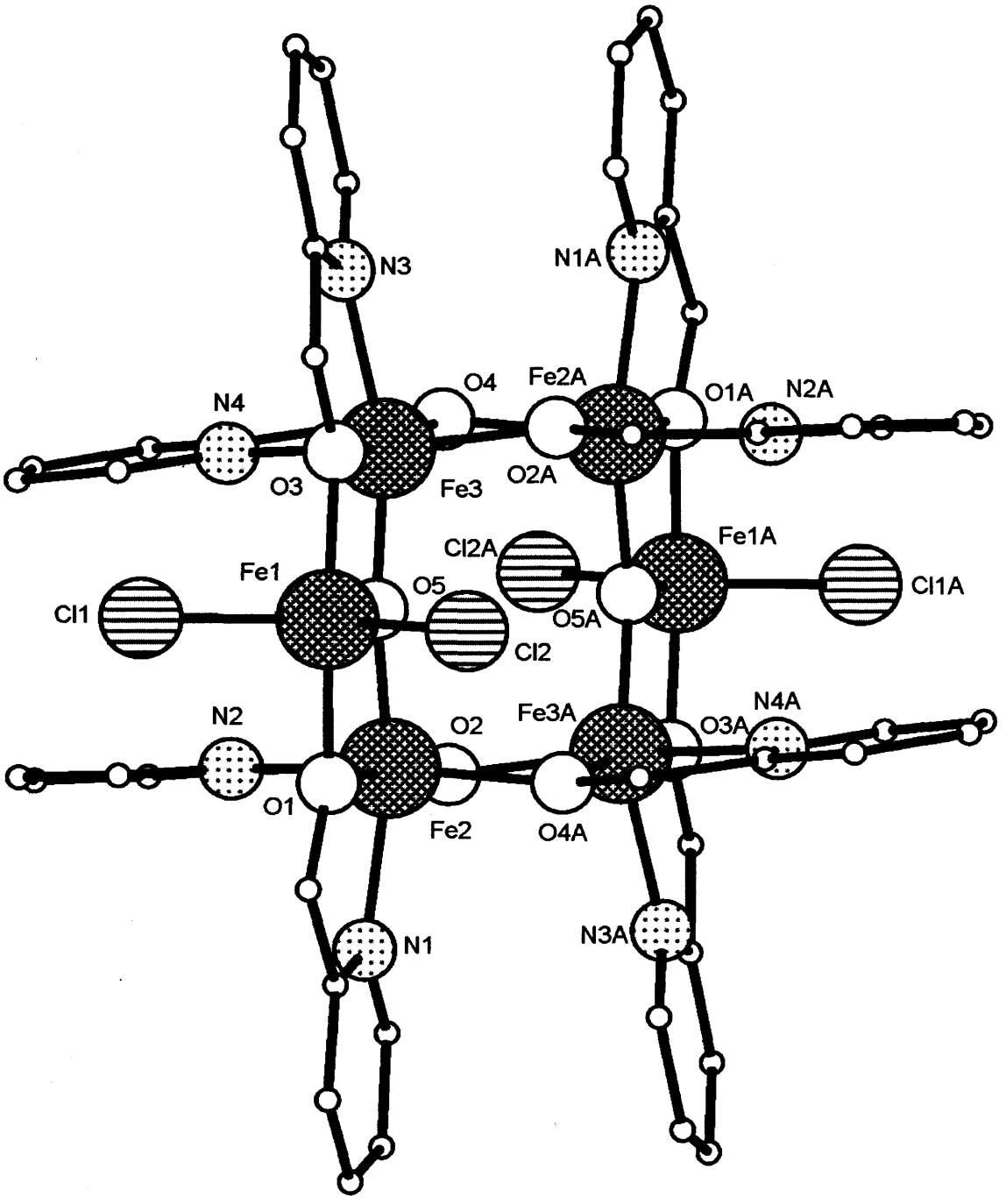

Figure 11 Molecular structure of one of the unique di-cationic units in the unit cell of **37**. Hydrogen atoms, carbon atom labels (except core and ligand donor atoms) external chlorides and solvent molecules are excluded for clarity.

Table 7 Selected bond length (Å) and angle (°) data for **37**

37							
Fe(1)-O(1)	1.982(8)	Fe(2)-O(1)	1.969(9)	Fe(2)-O(4)#1	1.971(9)	Fe(2)-N(3)	2.168(11)
Fe(1)-O(3)	1.968(8)	Fe(2)-N(1)	2.150(10)	Fe(2)-O(5)	1.929(8)	Fe(3)-O(4)	1.976(8)
Fe(1)-O(5)	1.926(8)	Fe(2)-O(2)	1.991(8)	Fe(3)-O(2)#1	1.974(9)	Fe(2)-N(4)	2.123(11)
Fe(1)-Cl(1)	2.234(4)	Fe(2)-N(2)	2.116(11)	Fe(3)-O(3)	1.972(9)	Fe(3)-O(5)	1.900(8)
Fe(1)-Cl(2)	2.244(4)						
Fe(2)-O(1)-Fe(1)	100.1(4)	O(3)-Fe(1)-Cl(2)	97.7(3)	O(4)#1-Fe(2)-N(1)	91.8(4)	O(2)#1-Fe(3)-N(4)	151.5 (4)
Fe(3)#1-O(2)-Fe(2)	104.3(4)	O(5)-Fe(1)-O(1)	77.9 (3)	O(2)-Fe(2)-O(4)#1	73.9(3)	O(3)-Fe(3)-O(4)	170.7(3)
Fe(1)-O(3)-Fe(3)	100.1(4)	O(5)-Fe(1)-Cl(1)	96.3(3)	O(4)#1-Fe(2)-N(2)	150.8(4)	O(4)-Fe(3)-N(3)	96.6(4)
Fe(2)#1-O(4)-Fe(3)	105.0(4)	O(5)-Fe(1)-Cl(2)	118.7(3)	O(5)-Fe(2)-O(1)	78.2(3)	O(3)-Fe(3)-N(4)	77.4(4)
Fe(1)-O(5)-Fe(2)	103.5(4)	O(5)-Fe(1)-O(3)	77.5(3)	O(5)-Fe(2)-N(1)	152.9(4)	N(4)-Fe(3)-N(3)	87.8(4)
Fe(3)-O(5)-Fe(1)	104.3(4)	O(1)-Fe(2)-N(1)	74.9(4)	O(5)-Fe(2)-O(2)	109.2(3)	O(4)-Fe(3)-N(4)	77.4(4)
Fe(3)-O(5)-Fe(2)	152.2(5)	O(1)-Fe(2)-O(2)	109.2(3)	O(5)-Fe(2)-N(2)	95.0(4)	O(5)-Fe(3)-O(2)#1	98.8(4)
O(1)-Fe(1)-Cl(1)	96.3(3)	O(1)-Fe(2)-N(2)	101.8(4)	O(5)-Fe(2)-O(4)#1	98.3(4)	O(5)-Fe(3)-O(3)	78.0(3)
O(1)-Fe(1)-Cl(2)	97.8(3)	O(2)-Fe(2)-N(1)	152.9(4)	O(3)-Fe(3)-O(2)#1	101.6(4)	O(5)-Fe(3)-N(3)	152.0(4)
Cl(1)-Fe(1)-Cl(2)	114.74(16)	N(2)-Fe(2)-N(1)	87.9(4)	O(2)#1-Fe(3)-N(3)	94.6(4)	O(5)-Fe(3)-O(4)	110.6(3)
O(3)-Fe(1)-O(1)	155.1(4)	O(2)-Fe(2)-N(2)	77.3(4)	O(3)-Fe(3)-N(3)	75.2(4)	O(5)-Fe(3)-N(4)	91.8(4)
O(3)-Fe(1)-Cl(1)	94.8(3)	O(1)-Fe(2)-O(4)#1	106.3(4)	O(2)#1-Fe(3)-O(4)	74.1(4)		

Symmetry transformations used to generate equivalent atoms: #1 $(-x+2,-y,-z)$, #2 $(-x+1,-y+1,-z+1)$.

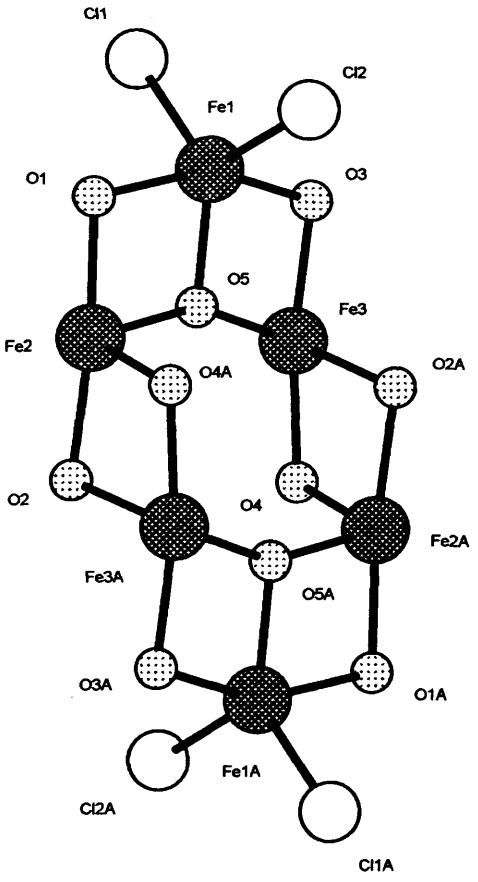

Figure 12 Iron-oxo core of **37**.

The molecular structure of the perchlorate salt of **37** has been reported previously.[18d] The iron-oxo core for this type of structure is described as a chair conformation whereby, the head- and foot-rests of the chair represent the two terminal iron ions of Fe(1) and Fe(1A) while the remaining Fe(III) ions constitute the body of the chair. If the core of **37** is viewed down the terminal iron ions, a grid-like cuboidal box shape is observed (Figure 12). The terminal iron ions possess trigonal bipyramidal coordination geometries and are bound to two *cis*-chlorides, two μ_2-O_{hmp} ligands and a μ_3-O ligand. The central Fe(III) ions are octahedrally coordinated to a μ_3-O ligand, a μ_2-O_{hmp} ligand and two hmp ligands which are further bound to either the nearest terminal Fe(III) or a neighbouring central Fe(III) ion.

In $[Fe_6(\mu_3\text{-}O)_2(hmp)_8Cl_4][ClO_4]_2$, the Fe-$\mu_3$-O, Fe-$N_{hmp}$ and Fe-O_{hmp} bond lengths average to 1.907 Å, 2.155 Å and 1.995 Å, respectively. The corresponding oxo- and hmp angles average to Fe-μ_3-O-Fe = av. 119.9°, Fe-μ_2-O_{hmp}-Fe ~ av.105° and Fe-μ_3-O-Fe ~ av. 74°. The hmp-based chelate bite angles in $[Fe_6(\mu_3\text{-}O)_2(hmp)_8Cl_4][ClO_4]_2$ average to 81.43° and is larger in comparison to **37** (*ca.* 5°). Therefore, there are only slight structural differences between $[Fe_6(\mu_3\text{-}O)_2(hmp)_8Cl_4][ClO_4]_2$ and **37**. It is to be noted that the chp ligand once again, is not involved within the structure of **37**. It is possible that Nachp plays a role as a reagent base (also evident for the formation of complex **34**).

The solid-state IR spectrum of **37** shows stretching bands of ν(C=N) at 1608 cm^{-1} and ν(Fe-O) at 671 cm^{-1}. The FAB mass spectrum of **37** shows a $[M - 4Cl - 4hmp]^+$ peak at 871 Da. The magnetic data of $[Fe_6(\mu_3\text{-}O)_2(hmp)_8Cl_4][ClO_4]_2$ has been fitted by variable temperature magnetic modelling resulting in a $S = 3$ ground spin state with four potential exchange interactions.[18d] Similarly, **37** has four possible metal-metal ion interaction pathways (Figure 13) and a corresponding number of coupling constants (J) (Table 8). The preliminary variable temperature $\chi_M T$ plot (SQUID) of **37** progresses from ~ 1.05 emu K mol^{-1} per Fe(III) ion at the lowest temperature and then decreases to ~ 0.95 emu K mol^{-1} (~ 12 K) probably due to a paramagnetic impurity. From 100 K upwards, the $\chi_M T$ values

increase almost linearly to a maximum of ~ 1.72 emu K mol^{-1} (340 K) per Fe(III) ion which is less than expected for a single non-interacting Fe(III) ion possessing five unpaired electrons [expected $\chi_M T$ = 4.38 emu K mol^{-1} per Fe(III), ***SEE NOTE***] (Figure 14).[31] In comparison, the magnetic moment plot of $[Fe_6(\mu_3\text{-}O)_2(hmp)_8Cl_4][ClO_4]_2$ starts at ~ 6.0 BM [$\chi_M T$ = 4.50 emu K mol^{-1}] and reaches a maximum of ~ 8.5 BM (~ 325 K) [$\chi_M T$ = 9.03 emu K mol^{-1}], these results being similar to the preliminary magnetic results of **37** [6.8 BM, $\chi_M T$ = 5.70 emu K mol^{-1} (~ 12 K) and 9.1 BM $\chi_M T$ = 10.32 emu K mol^{-1} (~ 340 K) per molecule of **37**]. The variable temperature magnetic susceptibility data of **37** is yet to be modelled.

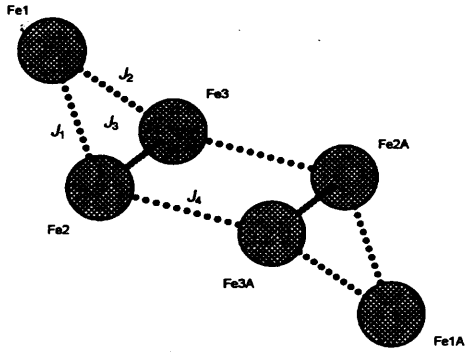

Figure 13 Core Fe···Fe interactions in **37**

Table 8 Possible coupling interactions and distances (Å) in **37**

	Interaction	37
J_1	Fe(1)···Fe(2)	3.028(3)
J_2	Fe(1)···Fe(3)	3.022(3)
J_3	Fe(2)···Fe(3)	3.717(3)
J_4	Fe(2A)···Fe(3)/ Fe(2)···Fe(3A)	3.132(3)

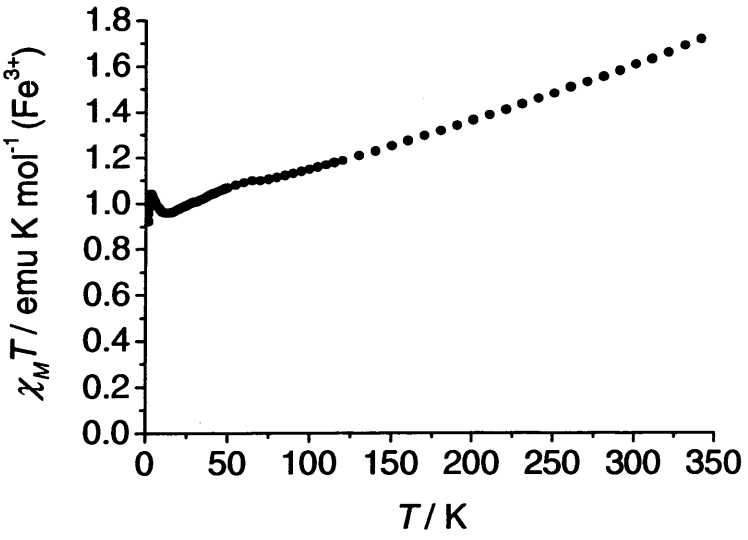

Figure 14 Plot of $\chi_M T$ against T (closed circles) for **37** [per Fe(III) ion].

5.2 Blending Salts of Carboxylates and α-Diimines on a Fe(III) Centre

5.2.1 M = Fe, $NaL^1 = RCO_2Na$, L^2 = phen

The reaction of $[Fe_2OCl_6][NEt_4]_2$ with a ligand blend comprising RCO_2Na and phen gave, on work-up, red-brown crystals of tetranuclear $[Fe_4(\mu_3\text{-}O)_2(phen)_2(RCO_2)_6(Cl)_2]\cdot nMeCN$ [R = Ph_2CH, n = 2 (**38a**), $PhCH_2$, n = 2 (**38b**), CH_3CH_2, n = 0 (**37c**)] [0 °C; 3d. Me_2CO (**38a** and **38c**), 3d. Et_2O (**38b**)] in good yield (Scheme 7). Complexes **38a**, **38b** and **38c** were characterised by elemental analysis, IR spectroscopy and FAB positive mass spectrometry. Single crystals of **38a**, **38b** and **38c**, were subject to single crystal X-ray diffraction studies. The molecular structure of **38c** is shown in Figure 15; selected bond lengths and angles of **38a**, **38b** and **38c** are given in Table 9.

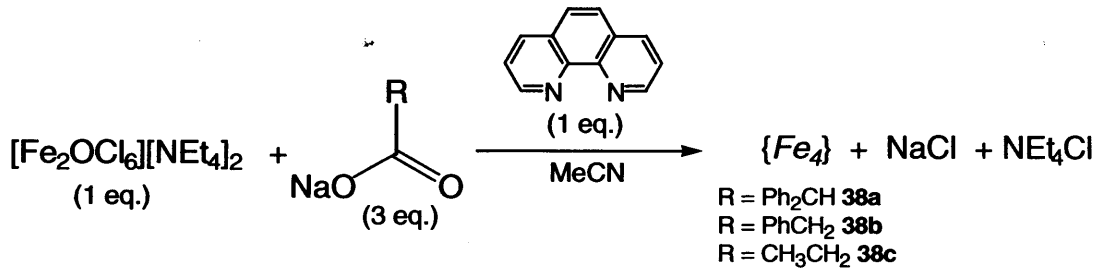

Scheme 7 Synthesis of **38**.

Complexes **38a**, **38b** and **38c** each consist of four octahedral Fe(III) ions coordinated by six peripheral 1,3-bridging carboxylates, two five-membered *N,N*-chelating phen ligands and two terminal chlorides. The iron-oxo core in complexes **38** can be represented as a $[Fe_4(\mu_3\text{-}O)_2]^{8+}$ rhombus consisting of two central [Fe(1) and Fe(3] and two terminal [Fe(2) and Fe(4)] iron ions (Figure 15, inset). The Fe-μ_3-O bond lengths for complexes **38** range from 1.921 – 1.985 Å for the core and 1.824 – 1.845 Å for the two terminal iron ions with corresponding Fe-μ_3-O-Fe angles ranging from 94.9° – 131.9°; these values being indicative of a distorted trigonal planar environment around the μ_3-O atoms. The terminal iron atoms are bound to phen ligands with a five-membered chelate bite angle averaging to ~ 74.72°, which is narrower than those found from the hmp or hep *N,O*-chelated complexes **35**, **36** and **37**.

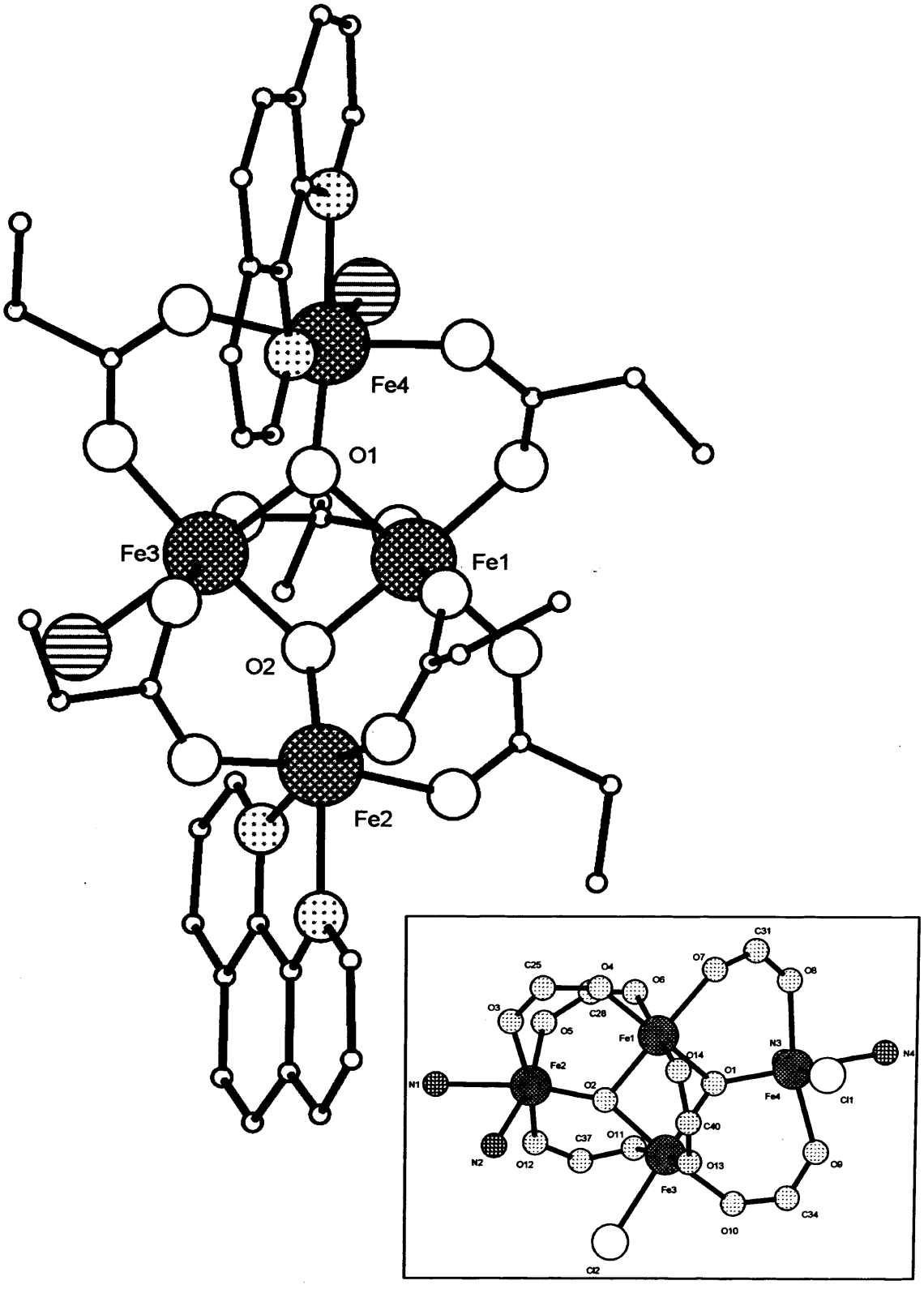

Figure 15 Molecular structure of **38c**. Inset shows iron-oxo carboxylate core. Hydrogen atoms and atom labels outside the core are omitted for clarity.

Table 9 Selected bond length (Å) and angle (°) data for **38a**, **38b** and **38c**

	38a	**38b**	**38c**		**38a**	**38b**	**38c**
Fe(1)-O(1)	1.921(2)	1.975(4)	1.938(5)	Fe(1)-O(1)-Fe(3)	95.01(10)	95.87(18)	94.9(2)
Fe(1)-O(2)	1.941(2)	1.958(4)	1.927(4)	Fe(4)-O(1)-Fe(1)	131.85(13)	131.9(2)	126.6(2)
Fe(1)-O(4)	2.044(3)	2.053(4)	2.005(6)	Fe(4)-O(1)-Fe(3)	129.85(13)	130.1(2)	134.0(3)
Fe-O(6)	2.074(2)	2.048(4)	2.047(5)	Fe(2)-O(2)-Fe(1)	120.06(12)	129.2(2)	119.0(3)
Fe(1)-O(7)	2.006(3)	2.033(5)	2.008(5)	Fe(1)-O(2)-Fe(3)	95.30(10)	95.22(18)	95.9(2)
Fe(1)-O(14)	2.033(2)	2.032(4)	2.031(5)	Fe(2)-O(2)-Fe(3)	129.65(13)	119.0(2)	132.4(3)
Fe(2)-N(1)	2.218(3)	2.195(6)	2.184(6)	O(1)-Fe(1)-O(2)	83.64(10)	80.67(17)	83.9(2)
Fe(2)-O(2)	1.837(2)	1.824(4)	1.837(5)	O(1)-Fe(1)-O(4)	175.69(10)	92.75(16)	178.5(2)
Fe(2)-N(2)	2.129(3)	2.130(6)	2.165(6)	O(2)-Fe(1)-O(4)	92.21(10)	91.79(17)	95.0(2)
Fe(2)-O(3)	2.022(3)	2.024(5)	2.036(6)	O(2)-Fe(2)-O(3)	93.34(11)	96.40(18)	96.8(2)
Fe(2)-O(5)	2.011(3)	2.026(5)	2.007(5)	O(2)-Fe(2)-N(2)	95.79(11)	97.4(2)	90.4(2)
Fe(2)-O(12/11)	2.009(3)	2.037(5)	2.033(5)	O(5)-Fe(2)-O(3)	87.51(11)	90.09(18)	87.0(3)
Fe(3)-O(1)	1.985(2)	1.921(4)	1.973(4)	O(2)-Fe(3)-O(1)	81.59(10)	82.06(18)	82.30(19)
Fe(3)-O(2)	1.956(2)	1.957(4)	1.952(5)	O(1)-Fe(3)-O(10)	171.43(10)	98.24(18)	91.2(2)
Fe-Cl(2)	2.339(11)	2.334(2)	2.370(2)	O(2)-Fe-(3)-O(13)	91.24(10)	93.11(18)	88.3(2)
Fe(3)-O(10)	2.032(3)	2.007(4)	2.019(5)	O(1)-Fe-O(4)-O(8)	95.27(11)	96.93(18)	97.4(2)
Fe(3)-O(11/12)	2.070(3)	2.025(4)	2.033(5)	O(1)-Fe-O(4)-O(9)	96.85(11)	95.18(18)	96.4(2)
Fe(3)-O(13)	2.038(2)	2.033(4)	2.053(5)	O(1)-Fe-O(4)-N(3)	92.93(12)	94.40(18)	92.0(2)
Fe(4)-O(1)	1.844(2)	1.845(4)	1.844(5)	N(1)-Fe(2)-N(2)	75.68(12)	75.7(2)	74.9(2)
Fe-Cl(1)	2.3009(11)	2.3190(18)	2.313(2)	N(3)-Fe(4)-N(4)	73.54(12)	73.98(19)	74.5(2)
Fe(4)-N(3)	2.177(3)	2.179(5)	2.168(6)				
Fe(4)-N(4)	2.257(3)	2.234(5)	2.243(6)				
Fe(4)-O(8)	2.020(3)	2.034(5)	2.048(6)				
Fe(4)-O(9)	2.028(3)	2.030(5)	2.030(5)				
Fe(1)···Fe(3)	2.8798(7)	2.8919(14)	2.8810(16)				

Table 10 Ligand bonding types present in **38a**, bold numbers represent types only present in **38b**.

Description	**Fe(1)**	**Fe(2)**	**Fe(3)**	**Fe(4)**
μ_3-O	2	1	2	1
phen		1		1
η^1-Cl	**1**		1	1
μ-CO_2	**3,4**	3	**4,3**	2

The IR spectra of **38a**, **38b** and **38c** indicate the presence of three strong absorption bands in the ranges for $\nu(CO_2)_{asymm}$ ~ 1536 – 1558, $\nu(CO_2)_{symm}$ ~ 1391 – 1423 cm^{-1} and ν(Fe-O) ~ 696 – 723 cm^{-1}. The FAB mass spectra of **38a** (solvated), **38b** and **38b** show peaks of $[M]^+$ = 2036 Da., $[M - 2Cl]^+$ = 1426 Da. and $[M - CH_3CH_2]^+$ = 1086 Da., respectively.

There have been reports on similar tetranuclear complexes, for example, $[Fe_4(O)_2(picolinate)_2(O_2CMe)_7][NBu^n_4]$,[21] $[Fe_4(OHO)(OH)_2(phen)_4(O_2CMe)_4](ClO_4)_3$, $[Fe_4(O)_2(phen)_2(O_2CPh)_7](ClO_4)$, $[Fe_4(O)_2(phen)_2(O_2CPh)_8]$,[22] $[Fe_4(O)_2(NC_5H_4Me)_2(O_2CCMe_3)_8]$,[23] $[Fe_4(O)_2(2,2\text{-}N,N\text{-bipyridyl})_2(O_2CMe)_6(Cl)_2]$[21] and $[Fe_4(O)_2(phen)_2(O_2CMe)_6(N_3)_2]$.[24] The latter two complexes are structurally related to **38** and their corresponding bond length and angle data is very similar to those found in **38**.

The molecular structures of the reported complexes have been described as adopting butterfly motifs, in which case the body is represented by a Fe_2O_2 rhombic core and the wing tips by two terminally bound iron ions.[21-24] Similarly, complexes **38a-c** also contain this rhombic core with five metal-metal ion distances and the same number of potential coupling exchange constants (J) (Figure 16 and Table 11).

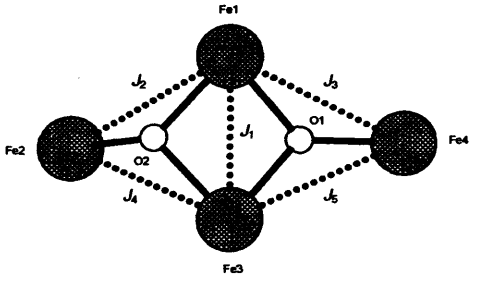

Figure 16 and Rhombic core of **38**

Table 11 Possible coupling interactions and distances (Å) in **38**

	Interaction	38a	38b	38c
J_1	Fe(1)···Fe(3)	2.8798(7)	2.8919(14)	2.8810(16)
J_2	Fe(1)···Fe(2)	3.2731(7)	3.4173(16)	3.2346(17)
J_3	Fe(1)···Fe(4)	3.4371(80	3.4889(19)	3.3791(16)
J_4	Fe(3)···Fe(2)	3.4329(7)	3.2586(16)	3.4672(16)
J_5	Fe(3)···Fe(4)	3.4681(7)	3.4136(15)	3.5141(14)

The tetrameric complexes **38** are expected to act as antiferromagnetically coupled species possessing a S = 0 ground spin state.[21-24] The temperature dependence on the magnetic susceptibility data for **38** and the reported complexes is indicative of strong antiferromagnetic interactions. The $\chi_M T$ values for **38a**, **38b** (desolvated) and **38c** start at

non-zero (due to paramagnetic impurities) and reach a maximum at 1.33 emu K mol^{-1} (Figure 17), 3.19 emu K mol^{-1} and 1.26 emu K mol^{-1} per Fe(III) ion at 340 K, respectively. These values are less than expected for a non-interacting iron(III) ion possessing five unpaired electrons (expected $\chi_M T$ = 4.38 emu K mol^{-1} per Fe(III) ion, ***SEE NOTE***).[31] The variable temperature magnetic data of complexes **38** is yet to be modelled.

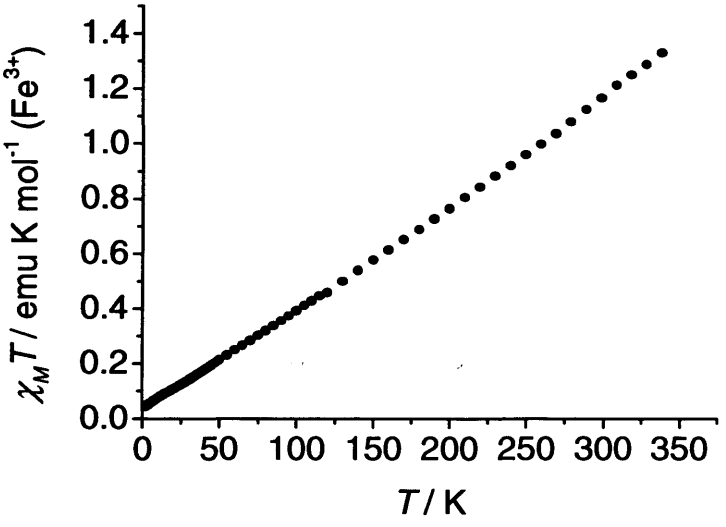

Figure 17 Plot of $\chi_M T$ against T (closed circles) for **38a** [per Fe(III) ion].

It is noteworthy that the reaction of $[Fe_2OCl_6][NEt_4]_2$ with a tri-component ligand blend composed of $PhCH_2CO_2Na$, phen and additionally Nachp results in the dinuclear complex $[Fe_2(O)(chp)_2(PhCH_2CO_2)_2(phen)_2]$ (Scheme 8).[28] This complex exhibits predominantly antiferromagnetic behaviour which is consistent with other extensively studied μ-oxo-bridged diiron species.[1]

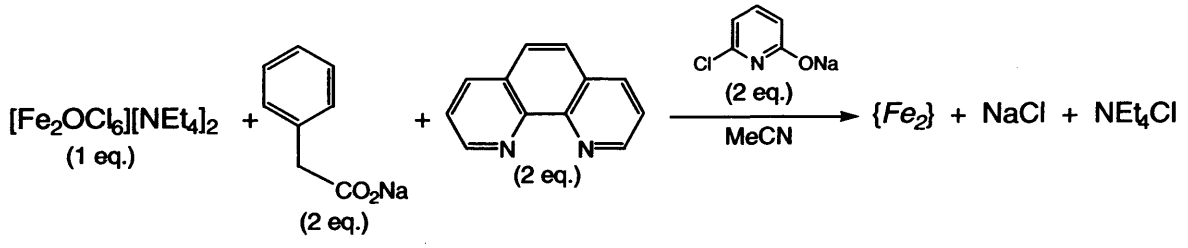

Scheme 8 Synthesis of $[Fe_2(O)(chp)_2(PhCH_2CO_2)_2(phen)_2]$.[28]

On the other hand, the heptadecanuclear cluster $[Fe_{17}O_{15}(OH)_6(OMe)_3(chp)_{12}(phen)_8]$ has been synthesised by the reaction of $[Fe_2OCl_6][NEt_4]_2$ with phen and Nachp (Scheme 9).[29] The preliminary magnetic behaviour of this cluster indicates the presence of an antiferromagnetically coupled species.

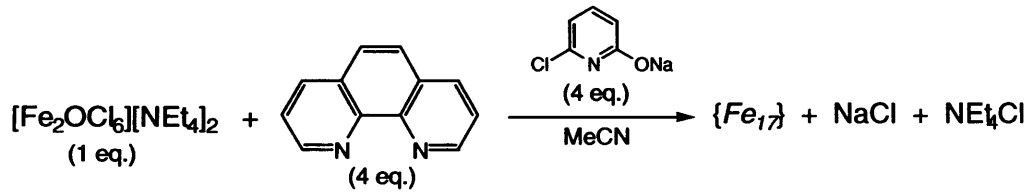

Scheme 9 Synthesis of $[Fe_{17}O_{15}(OH)_6(OMe)_3(chp)_{12}(phen)_8]$.[29]

5.3 Summary and Conclusions

A series of iron-oxo based complexes (**33** – **38**) have been synthesised from the reaction of $[Fe_2OCl_6][NEt_4]_2$ with ligand combinations composed of sodium carboxylate and sodium 2-pyridonates/2-pyridine alkoxides [2-{$(CH_2)_nONa$}-6-X-C_5H_3N] (Scheme 10). The resultant nuclearities of the complexes prepared are dependent on the specific nature of the ligand blends employed. In all cases, discrete cluster-based molecules containing an iron-oxo core surrounded by a coating of organic ligands are obtained.

A number of reactions have been re-examined with different carboxylates by variation of their steric and electronic attributes. Sodium phenylacetate combined with Nachp forms $[Fe_{10}Na_2(\mu_4\text{-}O)_2(\mu_3\text{-}O)_4(\mu_3\text{-}OH)_4(C_6H_5CH_2CO_2)_{10}(chp)_6(H_2O)_2(MeCN)_2]\cdot\text{-}9MeCN$ (**33**). However, sodium *p*-toluate combined with Nachp results in $[Fe_{11}(\mu_3\text{-}O)_6(\mu_3\text{-}OH)_6(p\text{-}\{CH_3\}\text{-}C_6H_4CO_2)_{15}]\cdot 15MeCN$ (**34**) in which no chp ligands are present. The nuclearities of the iron-oxo clusters decrease further on increasing the pyridyl alkyl chain length. For example, use of sodium diphenylacetate and Nahmp leads to $[Fe_8(\mu_3\text{-}O)_4(\mu_2\text{-}O)_2(hmp)_4(\eta^2\text{-}Ph_2C\{H\}CO_2)_8(\eta^1\text{-}Ph_2C\{H\}CO_2)_2(MeOH)]\cdot 2MeCN\cdot MeOH$ (**35**), while use of sodium diphenylacetate and Nahep affords $[Fe_6(\mu_3\text{-}O)_2(\mu_2\text{-}OH)_2(hep)_2(Ph_2C\{H\}CO_2)_{10}]\cdot\text{-}12MeCN$ (**36**). On the other hand, if a ligand blend involving Nachp and hmpH is employed $[Fe_6(\mu_3\text{-}O)_2(hmp)_8Cl_4](Cl)_2\cdot 4H_2O$ (**37**) is furnished. The combination of sodium diphenylacetate, sodium phenylacetate or sodium propionate and phen resulted in the formation of tetrameric $[Fe_4(\mu_3\text{-}O)_2(phen)_2(RCO_2)_6(Cl)_2]\cdot 2MeCN$ [R = Ph_2CH **38a**; $PhCH_2$ **38b**; CH_3CH_2 (- MeCN) **38c**] respectively, showing a further decrease in nuclearity.

In conclusion, the factors governing iron-oxo cluster formation in this work would appear to depend on a number of variables. Firstly, *the type of carboxylate employed*, in terms of the steric and electronic effects. For example, a combination of *p*-{CH_3}-C_6H_4-CO_2Na (containing *para*-directing Me) and Nachp results in $\{Fe_{11}\}$ species (**34**). However, replacement of the carboxylate with $PhCH_2CO_2Na$ in the latter reaction yields a $\{Fe_{10}\}$

species (**33**). Secondly, *the methylene chain length of the N,O-based 2-pyridine alkoxide* appears to influence the nuclearity in which a general decrease is observed as the alkyl chain length is increased. For example, hep (n = 2) and hmp (n = 1) act as *N,O*-chelating ligands for the formation of $\{Fe_6\}$ and $\{Fe_8\}$ complexes, respectively. However, chp (n = 0) has the role of either an *O*-bound alkoxide for the formation of **33**, or as a potential base (Nachp) for the synthesis of **34** and **37**. Thirdly, *the presence of an N,N-based α-diimine e.g.*, 1,10-phenanthroline acts as a chelating/capping ligand and limits core aggregation and thus, results in lower complex nuclearities [$\{Fe_4\}$ **38a-c**]. Finally, *the numbers of ligands employed* also appear to influence the nuclearity. For example, a tri-ligand combination involving phen, Nachp and NaO_2CR results in $\{Fe_2\}$ species[28] while, a combination of phen and Nachp results in a $\{Fe_{17}\}$[29] cluster

Complexes **33** – **38** are expected to behave antiferromagnetically due to their structural similarities with reported complexes. Preliminary EPR spectroscopic and magnetic susceptibility studies have suggested that complex **34** is a SMM.[25] Complex **34** will be subject to in-depth analysis using both EPR simulations and SQUID variable temperature data in the future.

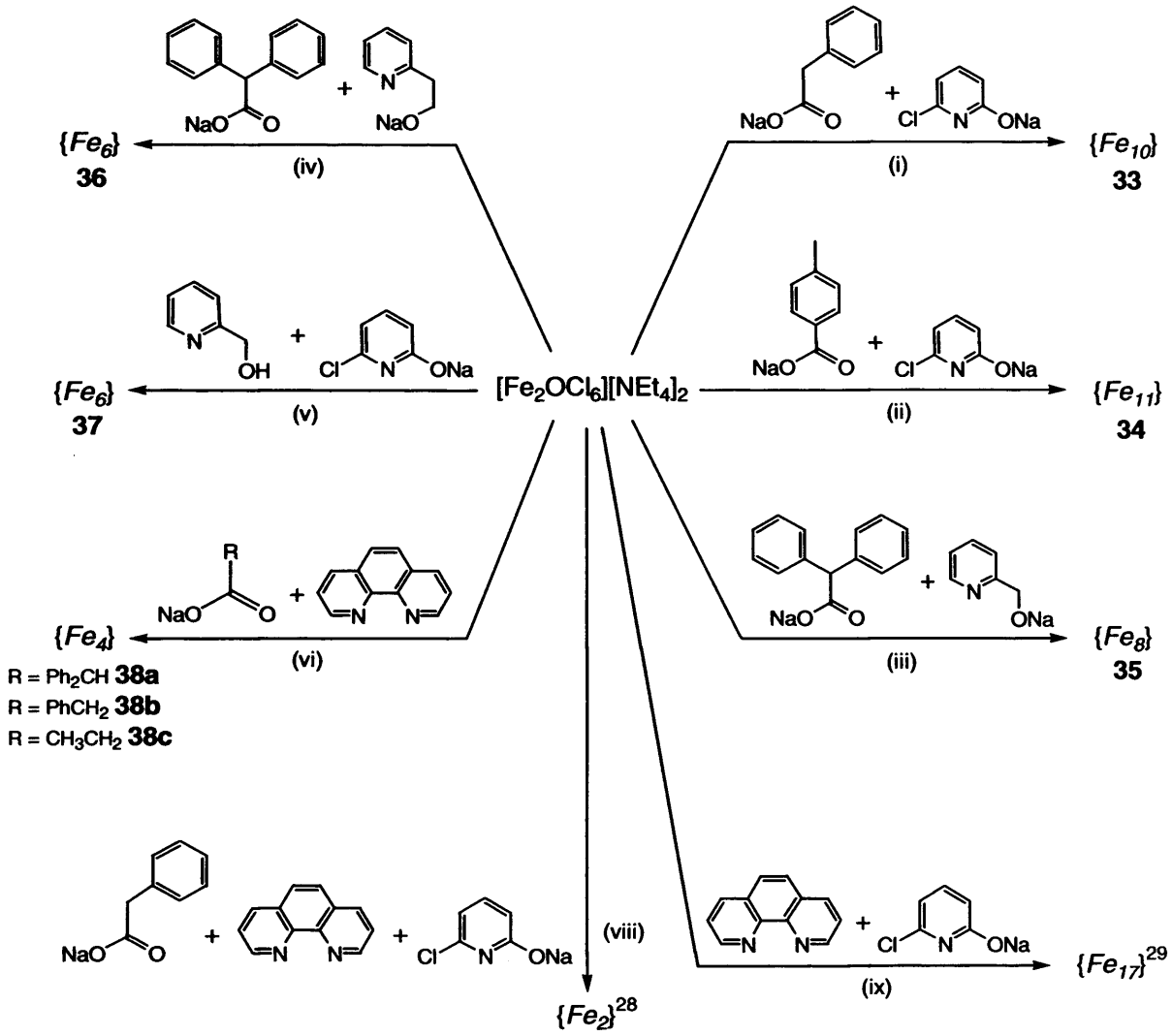

Scheme 10 Overview of chemistry carried out in Chapter 5. General reagents: $[Fe_2OCl_6][NEt_4]_2$ and MeCN.

5.4 References

1. D. Kurtz, *Chem. Rev.*, 1990, **90**, 585.
2. W. H. Armstrong and S. J. Lippard, *Inorg. Chem*, 1985, **24**, 981.
3. F. A. Cotton, G. Wilkinson, C. A. Murillo and M. Bochmann, in *Advanced Inorganic Chemistry*, eds., F. A. Cotton, G. Wilkinson, Wiley-Interscience, New York, 6th Edn., 1999, p. 465.
4. S. M. Gorun, G. C. Papaefthymiou, R. B. Frankel and S. J. Lippard, *J. Am. Chem. Soc.*, 1987, **109**, 3337.
5. M. Frey, S. G. Harris, J. M. Holmes, D. A. Nation, S. Parsons, P. A. Tasker, S. J. Teat and R. E. P. Winpenny, *Angew. Chem. Int. Ed., Engl.*, 1998, **37**, 3246.
6. (*a*) M. Frey, S. G. Harris, J. M. Holmes, D. A. Nation, S. Parsons, P. A. Tasker and R. E. P. Winpenny, *Chem. Eur. J.*, 2000, **6**, 1407; (*b*) S. J. Lippard, *Chem. in Br.*, 1986, March, p. 222.
7. C. Boskovic, H. U. Güdel, G. Labat, A. Neels, W. Wernsdorfer, B. Moubaraki and K. S. Murray, *Inorg. Chem.*, 2005, **44**, 3181.
8. C. Benelli, S. Parsons, G. A. Solan and R. E. P. Winpenny, *Angew. Chem. Int. Ed., Engl.*, 1996, **35**, 1825.
9. K. L. Taft, C. D. Delfs, G. C. Papaefthymiou, S. Foner, D. Gatteschi and S. J. Lippard, *J. Am. Chem. Soc*, 1994, **116**, 823.
10. C. Cañada-Vilalta, T. A. O'Brien, M. Pink, E. R. Davidson and G. Christou, *Inorg. Chem.*, 2003, **42**, 7819.
11. A. Caneschi, A. Cornia, A. C. Fabretti and D. Gatteschi, *Angew. Chem. Int. Ed., Engl.*, 1995, **34**, 2716.
12. C. Cañada-Vilalta, M. Pink and G. Christou, *Chem. Commun.*, 2003, 1240.
13. O. Waldmann, R. Koch, S. Schromm, J. Schülein, P. Müller, I. Bernt, R. W. Saalfrank, F. Hempel and E. Balthes, *Inorg. Chem.*, 2001, **40**, 2986.
14. M. Murugesu, K. A. Abboud and G. Christou, *Dalton Trans.*, 2003, 4552.
15. C. Cañada-Vilalta, E. Rumberger, E. K. Brechin, W. Wernsdorfer, K. Folting, E. R. Davidson, D. N. Hendrickson and G. Christou, *J. Chem. Soc., Dalton Trans.*, 2002, 4005.
16. C. Cañada-Vilalta, T. A. O'Brien, E. K. Brechin, M. Pink, E. R. Davidson and G. Christou, *Inorg. Chem.*, 2004, **43**, 5505.
17. E. K. Brechin, M. J. Knapp, J. C. Huffman, D. N. Hendrickson and G. Christou, *Inorg. Chim. Acta*, 2000, **297**, 389.
18. (*a*) W. Micklitz and S. J. Lippard, *Inorg. Chem.*, 1998, **27**, 3067; (*b*) D. F. Harvey, C. A. Christmas, J. K. McCusker, P. M. Hagen, R. K. Chadha and D. N. Hendrickson, *J. Angew. Chem. Int. Ed., Engl.*, 1991, **30**, 598; (*c*) J. K. McCusker, C. A. Christmas, P. M. Hagen, R. K. Chadha, D. F. Harvey and D. N. Hendrickson, *J. Am. Chem. Soc.*, 1991, **113**, 6114; (*d*) C. A. Christmas, H.-L. Tsai, L. Pardi, J. M. Kesselman, P. K. Gantzel, R. K. Chadha, D. Gatteschi, D. F. Harvey and D. N. Hendrickson, *J. Am. Chem. Soc.*, 1993, **115**, 12483; (e) R. Çelenligil-Çetin, R. J. Staples and P. Stavropoulos, *Inorg. Chem.*, 2000, **39**, 5838.
19. (*a*) A. Caneschi, A. Cornia, A. C. Fabretti, S. Foner, D. Gatteschi, R. Grandi and L. Schenetti, *Chem. Eur. J.*, 1996, 2, 1379; (*b*) E. M. Rumberger, L. N. Zakharov, A. L. Rheingold and D. N. Hendrickson, *Inorg. Chem.*, 2004, **43**, 6531; (*c*) R. W. Saalfrank, C. Deutscher, S. Sperner, T. Nakajima, A. M. Ako, E. Uller, F. Hampel and F. W. Heinemann, *Inorg. Chem.*, 2004, **43**, 4372; (*d*) S. Koizumi, M. Nihei, M. Nakano and H. Oshio, *Inorg. Chem.*, 2005, **44**, 1208; (*e*) H. A. Burkill, N. Robertson, R. Villar, A. J. P. White and D. J. Williams, *Inorg. Chem.*, 2005, **44**, 3337.
20. (*a*) K. Hegetschweiler, H. W. Schmalle, H. M. Streit, V. Gramlich, H.-U. Hund and I. Erni, *Inorg. Chem.*, 1992, **31**, 1299; (*b*) C. M. Grant, M. J. Knapp, W. E. Streib, J. C. Huffman, D. N. Hendrickson and G. Christou, *Inorg. Chem.*, 1998, **37**, 6065; (*c*) C. M. Grant, M. J. Knapp, J. C. Huffman, D. N. Hendrickson and G. Christou, *Chem. Commun.*, 1998, 1753; (*d*) E. J. Seddon, J. Yoo, K. Folting, J. C. Huffman, D. N. Hendrickson and G. Christou, *J. Chem. Soc., Dalton Trans.*, 2000, 3640; (*e*) E. J. Seddon, J. C. Huffman and G. Christou, *J. Chem. Soc., Dalton Trans.*, 2000, 446; (*f*) M. Mikuriya, S. Ikemi and S. Yoo, *Chem. Lett.*, 2000, 538; (*g*) T. Scneppensieper, G. Liehr, R. van Eldik, J. Ensling and P. Gütlich, *Inorg. Chem.*,

2000, **39**, 5565; (*h*) S. Lin, S.-X. Liu and B.-Z. Lin, *Inorg. Chim. Acta*, 2002, **328**, 69; (*i*) E. I. Tolis, M. Helliwell, S. Langley, J. Raftery and R. E. P. Winpenny, *Angew. Chem. Int. Ed., Engl.*, 2003, **42**, 3804; *Keggin ion-based* (*j*) L.-H. Bi, U. Kortz, S. Nellutla, A. C. Stowe, J.van Tol, N. S. Dalal, B. Keita and L. Nadjo, *Inorg. Chem.*, 2005, **44**, 896.

21. M. W. Wemple, D. K. Coggin, J. B. Vincent, J. K. McCusker, W. E. Streib, J. C. Huffman, D. N. Hendrickson and G. Christou, *J. Chem. Soc., Dalton Trans.*, 1998, 719.
22. A. K. Boudalis, N. Lalioti, G. A. Spyroulias, C. P. Raptopoulou, A. Terzis, A. Bousseksou, V. Tangoulis, J.-P. Tuchagues and S. P. Perlepes, *Inorg. Chem.*, 2002, **41**, 6477.
23. J. Overgaard, D. E. Hibbs, E. Rentschler, G. A. Timco and F. K. Larsen, *Inorg. Chem.*, 2003, **42**, 7593.
24. A. K. Boudalis, V. Tangoulis, , C. P. Raptopoulou, J.-P. Tuchagues and S. P. Perlepes, *Inorg. Chim. Acta*, 2004, **357**, 1345.
25. C. Benelli, J. Cano, Y. Journaux, R. Sessoli, G. A. Solan and R. E. P. Winpenny, *Inorg. Chem.*, 2001, **40**, 188.
26. *Personal Communication*, Dr. E. J. McInnes and Dr. J. Wolowska, University of Manchester EPSRC EPR service, 2005.
27. R. S. Drago, in *Physical Methods; for Chemists*, 1992, Saunders College Publishing, Orlando, 2nd International Edn., pp. 559 – 596.
28. P. M. Muirhead, S. Parsons, G. A. Solan and R. E. P. Winpenny, Unpublished results
29. S. Parsons, G. A. Solan and R. E. P. Winpenny, *J. Chem. Soc., Chem. Commun.*, 1995, 1987.
30. A. F. Orchard, in *Magnetochemistry*, Oxford Chemistry Primers, Oxford University Press, No. 75, UK, 2003, p. 151
31. ***PLEASE NOTE*** the Evans balance is sometimes ineffective at measuring accurate magnetic data which is mainly due to environmental effects *e.g.*, fluctuations in temperature. *All SQUID magnetic measurements are only part of a preliminary investigation undertaken by Prof. A. Harrison (Edinburgh) therefore, there is a large uncertainty in the data e.g., due to the presence of several parameters and/or parameters with unreliable/inconsistent values.*

Chapter 6

6.0 Blending Salts of Imides and L (L = Carboxylates, Amides or Amidinates) on a M(III) [and M(II)] Centre

In Chapter 5, synthetic strategies were implemented to synthesise clusters incorporating iron-oxo units. In this chapter, attempts to synthesise transition metal assemblies based on the related metal-imido units are described. Targeting electron rich paramagnetic imido assemblies was viewed as an alternative way of accessing magnetically interesting species that to the knowledge of the author, have not been widely explored (Chapter 1, section 1.2.4). The imido-group $[N(R)^{2-}]$ (R = H, hydrocarbyl) although isolobal and isoelectronic to the oxo-group $[O^{2-}]$ (Figure 1), displays far fewer bonding modes than the latter, this is a feature that can be attributed, in part, to the presence of the R-group and the relative dearth of research activity in this field (Table 1).[2]

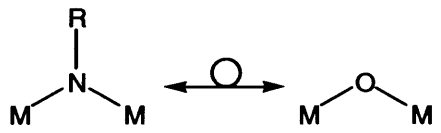

Figure 1 Isolobal relationship of imido and oxo in μ_2-bridged species.

However, the presence of an R-substituent on the imido-moiety offers considerable opportunities to influence several factors. Firstly, *sterics* for example, large R-groups can increase steric contacts leading to the destabilisation of high nuclearity structures.[4] Secondly, *electronics* in which the R-group can influence the stability (*i.e.*, through delocalisation) of an imido-bridged species.[8b] Thirdly, *magnetics* in which the overall magnetic behaviour of an imido-bridged complex is influenced by M-N(R) bond lengths and M-N(R)-M angles which are related to the M···M distances.[9d] Finally, *solubility* wherein the type of R-group can influence the type(s) of solvent(s) required to solubilise the complex and hence affect the capacity to crystallise. Additional importance of preparing and studying metal-imido-bridged complexes is their relationship to biological systems *e.g.*, S-based iron nitrogenase clusters[7a,9] and their resemblance to analogous oxo-based clusters in terms of their structural and physical features.[1,2c]

Table 1 Reported bonding modes exhibited by oxo- and imido-groups[2a,b]

μ_2	μ_3	μ_4	μ_5	μ_6
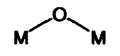	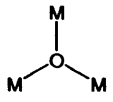	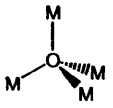	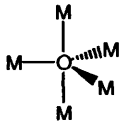	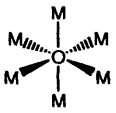
	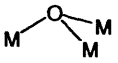	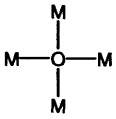	–	–
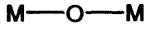	–	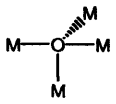	–	–
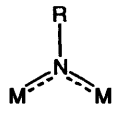	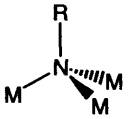		–	–

Previously reported methods of introducing an imido-unit into a transition metal framework have involved a wide range of synthetic strategies but in general involve treatment of the metal ion with a source of the imido fragment (Table 2).[2c] The source of the imido-bridge will hereafter be referred to as an imido transfer reagent (ITR). A general synthetic drawback for the preparation of metal-imido complexes is their air-sensitivity and sometimes redox lability[4] which can lead to the formation of the more stable oxo-species of the type $[M\text{-}\mu\text{-}O]_n$.

The following sections are concerned with describing attempts at generating well-defined paramagnetic-imido-bridged assemblies and, in particular, with trivalent iron as the metal centre. Some of our other efforts at preparing metal-imido clusters are compiled in the Appendices.

Table 2 Exemplary synthetic routes for the preparation of transition metal imido-bridged complexes

Reagents (ITRs are highlighted)	Imido-bridged complex	Ref.
Metathesis-type $MX/MX_2/MX_3$ + **Li_2NR/LiNHR** [M = Fe(III), Co(II), Ni, Cu(I) or Cu(II)]	$[Mn_6(\mu_4\text{-NPh})_3(\mu_3\text{-NPh})_2Cl_6][Li(THF)_4][Li(THF)_2]_3$	9c,
	$[Co_{18}(\mu_4\text{-NPh})_3(\mu_3\text{-NPh})_{12}Cl_3][Li(DME)_3]_2$	9b,9c
	$[Co_6(\mu_4\text{-NPh})(\mu_3\text{-NPh})_6(PPh_2Et)_2][Li(DME)_3]_2$	9b,9c
	$[Co_8(\mu_3\text{-NPh})_6(\mu_2\text{-NPh})_3(PPh_3)_2][Li(THF)_4]$	9b,9c
	$[Co_6(\mu_4\text{-NPh})_3(\mu_3\text{-NPh})_2(NHPh)_6][Li(DME)_3][Li(DME)]_3$	9c
	$[Co_{18}(\mu_4\text{-NPh})_3(\mu_3\text{-NPh})_{12}(NHPh)_3][Li_2(\mu\text{-Cl})(THF)_6]$	9c
	$[Cu_{12}(\mu_3\text{-NPh})_8][Li(DME)_2][\{Li(DME)_3\}_3]$	5b,9c
	$[Cu_6(\mu\text{-NMes})_2(NHMes)_3][Li(DME)_3]$	5b,9c
	$[Ni_{11}Br_6(\mu_3\text{-NBu}^t)_8]$	5a
	$[Cu_{24}(\mu_4\text{-NPh})_6(\mu_3\text{-NPh})_8][Li(THF)_4]_4/[Li(DME)_3]_4$	5a,9c
	*Fe complexes - see Table 3	9a
Metathesis-type $Mn(NBu^t)_3Cl$ + $Li(NHBu^t)$	$[Mn(\mu\text{-NBu}^t)_2(NBu^t)]_2$	9d
$Mn(NBu^t)_3Cl$ + $ZnMe_2$	$[Mn_2R_2(\mu\text{-NBu}^t)_2(NBu^t)_2]$ (R = Me)	9d
	$[Mn_2R_2(\mu\text{-NBu}^t)_2(NBu^t)_2]$ (R = Et, CH_2CMe_3, CH_2CMe_2Ph, CH_2SiMe_3 or CH_2Ph)	9d
$[Mn(\mu\text{-NBu}^t)_2(NBu^t)]_2$ + ZnR_2 (R = Me or CH_2Bu^t)	$[Mn_2(\mu\text{-NBu}^t)_4(NBu^t)_2ZnMe]$	9d
	$[Mn_2(\mu\text{-NBu}^t)_4(NBu^t)_2ZnCH_2Me_3]$	9d
$[Mn(\mu\text{-NBu}^t)_2(NBu^t)]_2$ + Al_2Me_6	$[Mn_2(\mu\text{-NBu}^t)_4(NBu^t)_2AlMe_2]$	9d
$[Li(DME)]_2[Mn(NBu^t)_6]$ + Al_2Me_6	$[Mn(\mu\text{-NBu}^t)_2AlMe_3]_2$	9d
Metathesis-type $[MX_2(L)_2]$ + **$RN(SnMe_3)_2$** [M = Co(II) or Ti(II)]	$[\eta^5\text{-(Cp)Ti}(\mu\text{-NSnMe}_3)]_4$	5a
	$[Co_{11}(\mu_3\text{-NPh})_6(\mu_2\text{-NPh})_6(PPh_3)_3]$	5a
Metathesis-type $MX_2/[MX_2(L)_2]$ + **$[\{Mg(NPh)(THF)\}_6]$** [M = Mn(II), Ti(II) or Zr(II)]	$[Mn_6(\mu_3\text{-NPh})_4Br_4(THF)_6]$	10a
	$\{Mn_6(\mu_3\text{-NPh})_4Br_3(THF)_4\}\{Mg_2(\mu\text{-NHPh})_4(\mu\text{-Br})_3Br_2(THF)_4\}$	10a
	$[(\eta^5\text{-Cp})(Cl)Ti(\mu\text{-NPh})]_2$	10b
	$[(\eta^5\text{-Cp})(Cl)Ti(\mu\text{-NPh})]_2$	10b
	$[(\eta^5\text{-Cp})_2Zr(\mu\text{-NPh})_2]_2$	10b
Addition to nitrile $[Ti\{MeC(2\text{-}C_5H_4N)(CH_2NHSiMe_3)_2\}\text{-}(NBu^t)py]$ + **MeCN**	$[Ti\{MeC(2\text{-}C_5H_4N)(CH_2NHSiMe_3)_2\}\{\mu\text{-}(NCMe)NBu^t\}]_2$	15
Addition of organic azide Fe(Salen)py + ***p*-tolylN$_3$**	*$[(Salen)_2Fe_2(\mu\text{-}p\text{-tolylN})]$	1a
Addition of organic azide $[L']Co(\eta^1\text{-toluene})$ + **ArN_3**	$\{[L']Co(\mu\text{-NAr})\}_2$	1c 1c
Reductive cleavage of nitrobenzene $[L']Co(\eta^1\text{-toluene})$ + **ArNO**	$\{[L']_2Co_2(\mu\text{-NAr})(O)\}$	1c
Deprotonation of primary amine Cp_2Mn + **^{b}$ArNH_2$**	$[\{(\eta\text{-Cp})Mn(2\text{-NH}(4,6\text{-}Me_2pm)\}\{Mn(\mu_3\text{-}2\text{-N}(4,6\text{-}Me_2pm)\}]_4$	8a,8b
	$[\{(\eta\text{-Cp})Mn(2\text{-NH}(4\text{-MeO-}6\text{-Mepm})\}\{Mn(\mu_3\text{-}2\text{-N}(4\text{-MeO-}6\text{-Mepm})\}]_4$	8b
	$[\{(\eta\text{-Cp})Mn(2\text{-NH}(4,6\text{-}Me_2Opm)\}\{Mn(\mu_3\text{-}2\text{-N}(4,6\text{-}Me_2Opm)\}]_4$	8b
Deprotonation of primary amine $MNMe_2$ + **^{a}$ArNH_2$** [M = V(IV) or Ti(II)]	$[V(\mu\text{-NAr})(NMe_2)_2]_2$	3a,3b
	$[(dpma)Ti(\mu\text{-NPh})]_2$	3a,3b
Disproportionation of 1,2-disubstituted hydrazine $Fe[N(SiMe_3)_2]SMes$ + **PhNH-NHPh**	*$[Fe(\mu_3\text{-NPh})(SMes)]_4$	7a
Oxidation of metal carbonyl $Hg[Fe(CO)_3(NO)]_2$ + **$(Me_3CN)_2S$**	*$[Fe(III)_4(\mu_3\text{-NCMe}_3)_2(\mu_3\text{-S})_2(NO)_4]$	7b
Reduction (see entry above) **$[Fe(\mu_3\text{-NCMe}_3)_2(\mu_3\text{-S})_2(NO)_4]$** + Na/Hg + $(Ph_3P)_2NCl$	*$[Fe(II)Fe(III)_3(\mu_3\text{-NCMe}_3)_2(\mu_3\text{-S})_2(NO)_4][(PPh_3)_2N]$	7b
Oxo/imido exchange reactions using an isocynate $CpOMoO_2MoOCp$ + **PhCNO**	$[(\eta\text{-Cp})Mo(\mu\text{-NPh})(=NPh)]_2$	6
Deprotonation of primary amine $FeCl[N(SiMe_3)_2]_2(THF)$ + **$ArNH_2$**	*See Table 3	4

dpma = *N,N*-di(pyrrol-α-methyl)-*N*-ethylamine. [a]Ar = 2,6-*i*$Pr_2C_6H_3$, 2,6-$Me_2C_6H_3$, Ph, 2,6-$Cl_2C_6H_3$ or C_6F_5. [b]Ar = 4,6-dimethylpyrimidine {2-NH_2(4,6-Me_2pm)}, 4-methoxy-6-methylpyrimidine {2-NH_2(4-MeO-6-Mepm)} or 4,6-dimethoxypyrimidine {2-NH_2(4,6-MeO_2pm)}. [c][L'] = *N,N*-bis(2,6-xylyl) substituted β-diketiminato ligand. L = labile ligands.

The general synthetic route employed in this chapter is shown in Scheme 1. This metathesis-type approach involves firstly, the treatment of a transition metal halide (*e.g.*, MX_3) with a s- or p-block salt containing the imido reagent (ITR) resulting in an intermediate species (imido-bridge-based building block) of likely composition $[XM\text{-}N(R)]_n$. Secondly, interaction of $[XM\text{-}N(R)]_n$ with an s-block salt of the chosen ligand ($M'L^1$) allows access to the new organo-functionalised metal-imido-bridged species. The monoanionic ligand types ($[L^1]^-$) to be employed in this work include carboxylates, amides and formamidinates for the provision of an organic periphery around the metal-imido-bridged core. It is to be noted that ligand blends involving co-bridging ligands have been rarely investigated for the preparation/isolation of paramagnetic metal-imido bridged cluster complexes.

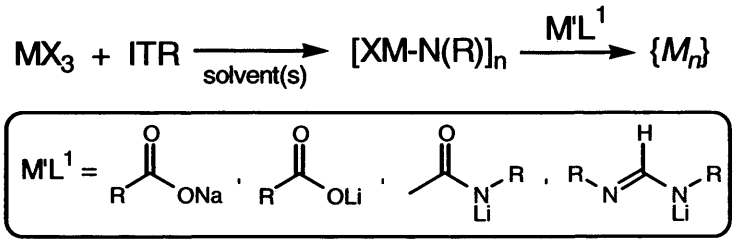

Scheme 1 General synthetic strategy employed in this work to prepare metal(III) imido complexes.

The types of imido-R groups to be employed will include, Mes, Ph or 2-picolyl. The 2-picolyl system was targeted in order to introduce an additional donor that would potentially increase the robustness of the complexes (for related 2-pyridyl systems see Chapters 2, 3, 4 and 5). The aryl group variation was identified in order to modify the steric and electronic properties.[4,8] In addition, the role of the metal in the ITR was examined by using both s- and p-block derivatives of the corresponding ligand.

6.1 Blending Salts of Imides and L (L = Carboxylates, Amides, Amidinates) on a Fe(III) Centre

6.1.1 M = Fe, ITR = MesNHLi, M'L^1 = CH_3CO_2Na

Reaction of anhydrous iron(III) chloride with monolithium 2,4,6-trimethylanilide [MesN(H)Li] in THF led to the formation of the previously reported polymeric complex $\{[Fe(III)_2(\mu\text{-NMes})_2Cl_4][Li(THF)_2]_2\}_n$.[9a] The addition of anhydrous sodium acetate to $\{[Fe_2(\mu\text{-NMes})_2Cl_4][Li(THF)_2]_2\}_n$ gave, on work-up, black crystals of $[Fe_2(\mu\text{-NMes})(CH_3C\{O\}NMes)_2Cl_2]\cdot 2MeCN$ [Mes = 2,4,6-$Me_3C_6H_2$)] (**39**) in low yield (Scheme 2). Complex **39** was characterised by elemental analysis and by single crystal X-ray diffraction. The molecular structure of **39** is shown in Figure 2; selected bond lengths and angles are given in Table 3.

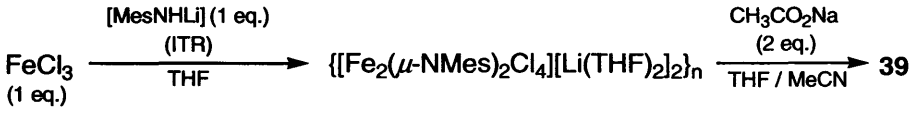

Scheme 2 Synthesis of **39**.

The molecular structure of **39** consists of two distorted tetrahedral iron(III) ions bridged by both a mesityl-imido and two bridging mesitylacetamide ligands with the coordination sphere at each metal centre being completed by two η^1-monodentate chloride ligands. The mesityl-imido group is *N*-bound as a μ_2-1,1 bridging ligand over the two Fe(III) ions. The mesitylacetamide ligands are η^1, η^1-*N*,*O*-bound over the Fe(III) ions, resulting in an incomplete or, a half-paddle wheel structure. Interestingly, mesitylacetamide was not added into the original reaction mixture and is formed *in-situ* during the synthetic process. The mesitylacetamide *N*- and *O*-donor atoms occupy trigonal planar environments possessing interior angles averaging to 120°, accompanied with the following bond lengths C-O_{amide} = 1.342(4) Å and C-N_{amide} = 1.330(4) Å, these values being characteristic for sp^2 hybridised environments around the donor atoms.[14] The C-N_{imido} bond length is slightly longer at 1.412(6) Å.

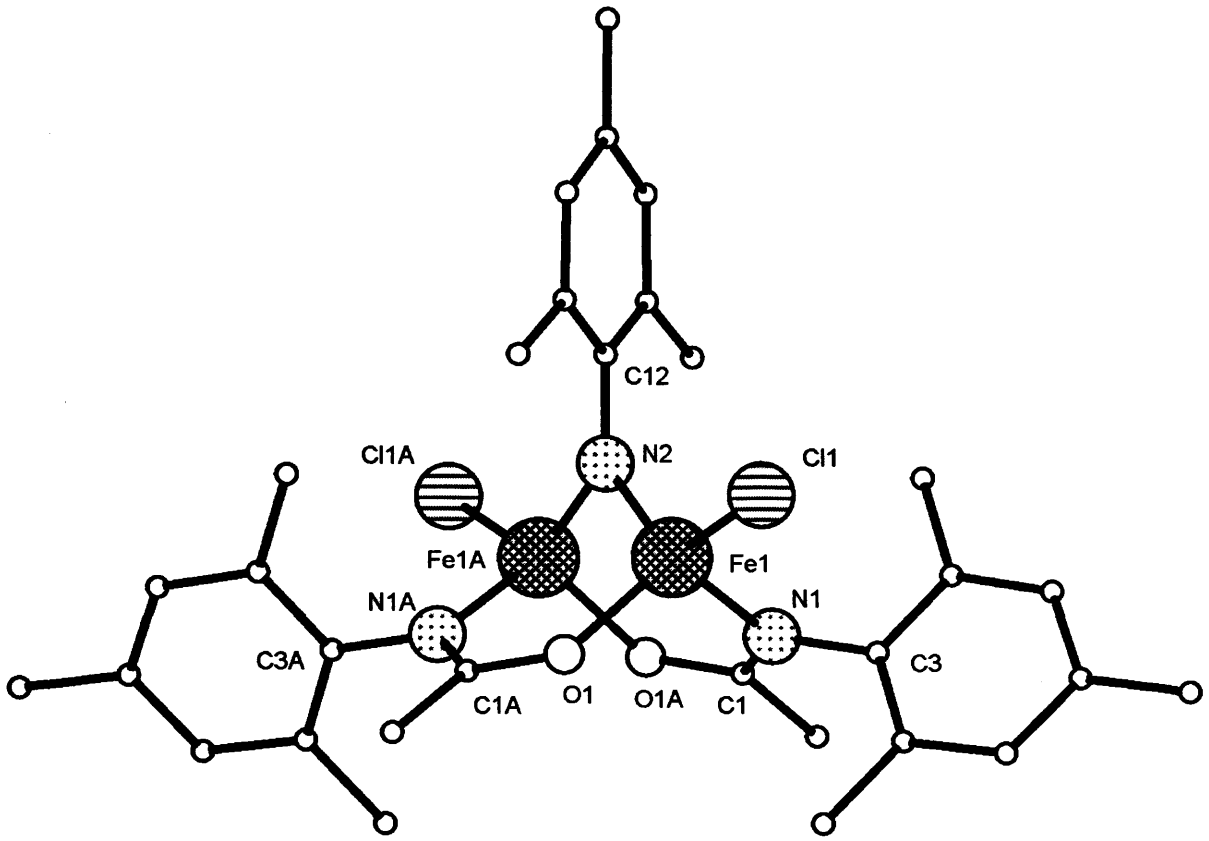

Figure 2 Molecular structure of **39**. Letter labelled atoms were generated by symmetry. Hydrogen atoms and solvent molecules are excluded for clarity.

Table 3 Selected bond length (Å) and angle (°) data for **39**

39					
Fe(1)-O_{amide}(1)	1.977(3)	Fe(1)-N_{imido}(2)	1.837(2)	N_{amide}(1)-C(1)	1.330(4)
Fe(1)-N_{amide}(1)	2.004(3)	Fe(1)···Fe(1)#1	2.7515(9)	N_{amide}(1)-C(3)	1.435(4)
Fe(1)-Cl(1)	2.2160(10)	O_{amide}(1)-C(1)#1	1.342(4)	N_{imido}(2)-C(12)	1.412(6)
Fe(1)-N_{imido}(2)-Fe(1)#1	97.02(18)	N_{imido}(2)-Fe(1)-O_{amide}(1)	107.09(10)	C(1)#1-O_{amide}(1)-Fe(1)	129.6(2)
O_{amide}(1)-Fe(1)-N_{amide}(1)	107.95(11)	N_{imido}(2)-Fe(1)-N_{amide}(1)	106.93(9)	C(1)-N_{amide}(1)-Fe(1)	120.9(2)
O_{amide}(1)-Fe(1)-Cl(1)	110.23(9)	N_{imido}(2)-Fe(1)-Cl(1)	117.14(9)	C(3)-N_{amide}(1)-Fe(1)	119.3(2)
N_{amide}(1)-Fe(1)-Cl(1)	107.15(8)				

Symmetry transformations used to generate equivalent atoms; #1 ($-x+1, y, -z+0.5$).

To the knowledge of the author, **39** is the first example of a co-bridged iron-imido species and the second example of a neutral imido-bridged Fe(III) dimer. In [Fe_2(μ-N-*p*-tolyl)(salen)$_2$], the Fe-N(R)-Fe angle at 129.6° and an internuclear Fe···Fe distance at 3.399 Å are larger than the corresponding values found in **39** (Table 4). It is likely that the constraints of the two bulky co-bridging mesitylacetamide ligands in **39** have the effect of compressing the Fe···Fe distance, in comparison with the Salen complex [Fe_2(μ-N-*p*-tolyl)(salen)$_2$].

On the other hand, the Fe···Fe distances and Fe-N(R)-Fe angles in **39** are considerably larger than those found for other imido-bridged iron complexes (Table 4, entries 1 – 14). For example, in the polymeric Fe(III) salt {[Fe_2(μ-NMes)$_2$$Cl_4$]-[Li(THF)$_2$]$_2$}$_n$, the Fe-$N_{imido}$-Fe = ~ 85.1° angle and Fe···Fe distance at ~ 2.546 Å are much smaller in comparison to **39** [Fe-N_{imido}-Fe = 97.02(18)°, Fe-N_{imido} = 2.7515(9) Å] (Table 4).[9a] However, the Fe-N_{imido} bond length at 1.867 Å is larger than the corresponding bond length in **39** [1.837(2) Å].

Table 4 Iron-imido bridged complex Fe···Fe distances (Å) and Fe-N_{imido}-Fe bond angles (°)

Complex	av. Fe···Fe	av. Fe-N_{imido}-Fe	Ref.
{[Fe(III)$_2$(μ-NMes)$_2$$Cl_4$][Li(THF)$_2$]$_2$}$_n$	2.546	85.1	9a
[Fe(II)$_2$Fe(III)$_2$(μ_3-NPh)$_4$$Cl_4$][Li(THF)$_4$][Li(THF)$_3$]	2.646	81.5	9a
[Fe(III)$_3$Fe(II)(μ_3-N^{t}Bu)$_4$$Cl_4$][Li(DME)$_3$]	2.616	83.65	9a
[Fe_4(μ_3-N^{t}Bu)$_4$$Cl_4$]·$Et_3$PN^{t}Bu	2.609	83.45	9a
[Fe(III)$_3$Fe(II)(NH^{t}Bu)$_4$(μ_3-N^{t}Bu)$_4$][Li(THF)$_4$]	2.688	84.5	9a
[Fe_2(μ-NPh)$_2$$Cl_4$][N^n$Bu_4$]$_2$	2.564	85.8	9a
[Fe_2(μ-NMes)$_2$$Cl_4$][$Li_2(THF)_7$]	2.5347	85.04	4
[Fe(IV)Fe(III)$_2$(μ-NPh)$_4$$Cl_4$][$Fe_2$($\mu$-Cl)$_3(THF)_6$]$_2$	2.587	88.775	4
[Fe(IV)Fe(III)$_2$(μ-N-*p*-tolyl)$_4$$Cl_4$][Li(THF)$_4$]$_2$	2.589	88.925	4
[Fe_2(μ-NPh)$_2$$Cl_4$][Li(DME)$_3$]$_2$	2.5517	85.45	4
[Fe(II)$_2$Fe(III)$_2$(μ_3-NPh)$_4$$Cl_4$][Li(DME)$_3$]$_2$	2.638	83.90	4
[Fe_4(μ_3-NPh)$_4$(SMes)$_4$]	2.630	84.05	7a
[Fe(III)$_3$(μ_3-NCMe$_3$)$_2$(μ_3-S)$_2$(NO)$_4$]	2.562	84.2	7b
[Fe(II)Fe(III)$_3$(μ_3-NCMe$_3$)$_2$(μ_3-S)$_2$(NO)$_4$][(PPh_3)$_2$N	2.574	85.75	7b
[Fe_2(μ-N-*p*-tolyl)(salen)$_2$]	3.399	129.6	1a
39	2.7515	97.02	This work

Scheme 3 describes a proposed pathway to account for the unexpected generation of a mesitylacetamide ligand in **39** [Scheme 3(2)]. Firstly, $\{[Fe_2(\mu\text{-NMes})_2Cl_4][Li(THF)_2]_2\}_n$ reacts with sodium acetate to give $[Fe_2(\mu\text{-NMes})_2Cl_3(CH_3CO_2)][Li(THF)_2]_2$ [Scheme 3(1)].[9a] Secondly, reaction of mesitylacetamide (formed *in-situ* from the reaction of NaOAc and MesNHLi) with $[Fe_2(\mu\text{-NMes})_2Cl_3(CH_3CO_2)][Li(THF)_2]_2$ gives $[Fe_2(\mu\text{-NMes})_2Cl_2(CH_3C\{O\}NMes)(CH_3CO_2)][Li(THF)_2]_2$ [Scheme 3(2)]. $[Fe_2(\mu\text{-NMes})_2Cl_2(CH_3C\{O\}NMes)(CH_3CO_2)][Li(THF)_2]_2$ subsequently rearranges by intramolecular nucleophilic attack to form $[Fe_2(\mu\text{-NMes})Cl_2(CH_3C\{O\}NMes)\text{-}(CH_3CO_2NMes)][Li(THF)_2]_2$ [Scheme 3(3)]. Finally, a molecule of lithium oxide is liberated to give **39** [Scheme 3(4)].

It is noteworthy that attempts at synthesising **39** directly by reacting $\{[Fe_2(\mu\text{-NMes})_2Cl_4][Li(THF)_2]_2\}_n$ with an alkali metal salt of the pre-prepared mesitylacetamide ligand were however, unsuccessful.

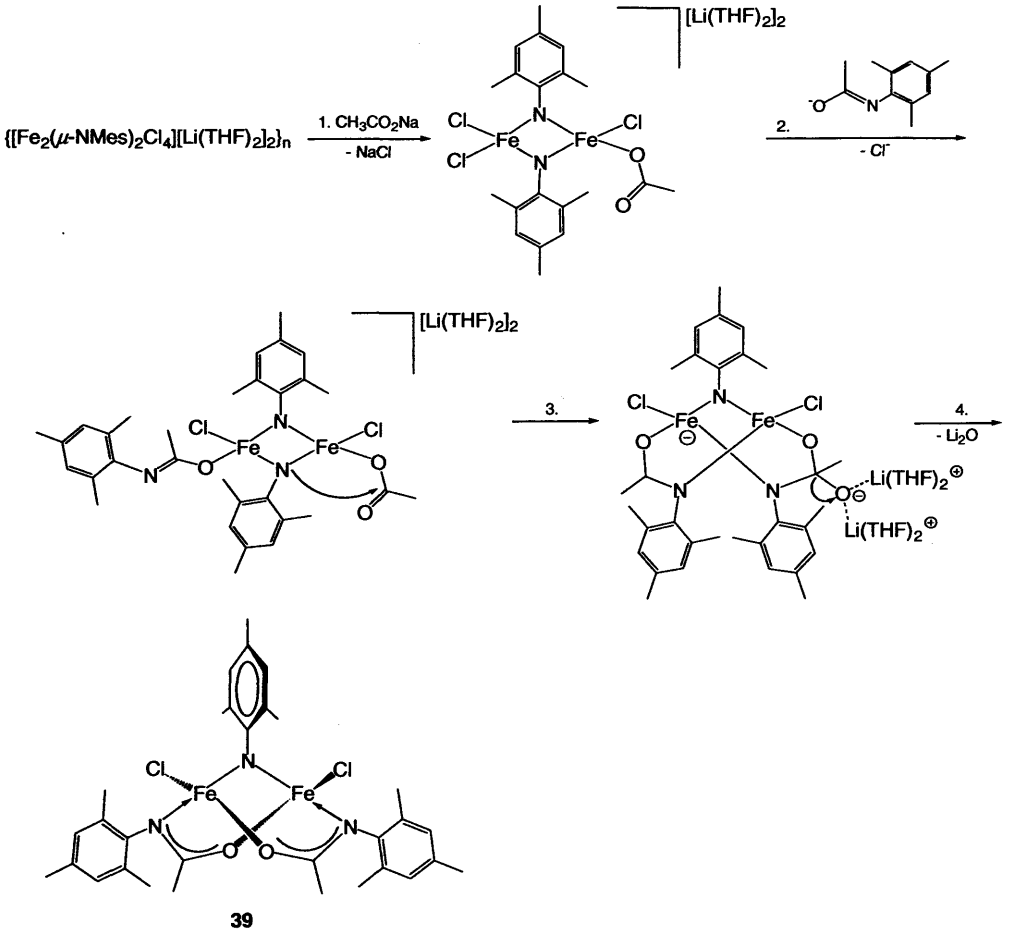

Scheme 3 Proposed route for *in-situ* generation of *N,O*-mesitylacetamide-bridged **39**.

6.1.2 M = Fe, ITR = MesNHLi, $M'L^1$ = MesN{Li}C{H}=NMes

With the intent of developing related structural types to that shown in **39**, other ligands known to form paddle wheel-type structures[13] were investigated. Thus, [MesNC{H}=NMes][Li] was treated with $\{[Fe_2(\mu\text{-NMes})_2Cl_4][Li(THF)_2]_2\}_n$ (generated *in-situ*) (Scheme 4 and Appendices). Unfortunately crystals of the complex suitable for X-ray diffraction could not be obtained.

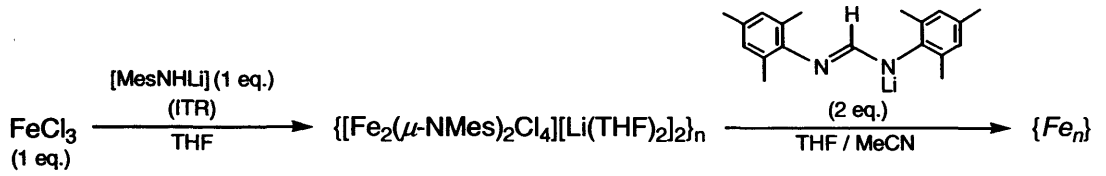

Scheme 4 Proposed route for the synthesis of iron-imido bridged complexes using [MesN{Li}C{H}=NMes].

6.1.3 M = Fe, ITR = $PhNLi_2$, $M'L^1$ = RCO_2Na

The reaction of $FeCl_3$ with $PhNLi_2$ has previously been reported to give $[Fe(II)_2Fe(III)_2(\mu_3\text{-NPh})_4Cl_4][Li(THF)_4][Li(THF)_3]$.[9a] We also examined the reactivity of $[Fe_4(\mu_3\text{-NPh})_4Cl_4][Li(THF)_3][Li(THF)_4]$ towards sodium salts of carboxylates in the attempt to form other imido-bridged species (Scheme 5 and Appendices). However, work-up and crystallisation of the reaction products proved to be unsuccessful.

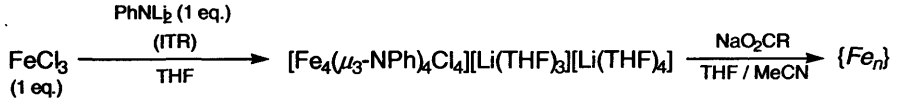

Scheme 5 Proposed route for the synthesis of iron-imido bridged complexes using $PhNLi_2$.

Other research groups have also found the use of lithium-based ITRs for metal imido complexations as challenging and the problems encountered have been attributed to; labile ligand exchange, use of redox-active iron ions and the aggressive reactivity of *N*-based anions.[4]

6.2 Blending Salts of 2-Picolylimides and L (L = Carboxylates, Amides or Amidinates) on a M(II) or M(III) Centre

With the aim of increasing the stability of the imido-containing complexes and to exploit and complement the work studied in chapters 2 – 5, we decided to incorporate the imido moiety into a chelating ligand whereby complexes containing pyridyl alkyl-amides/-imides could be potentially accessed. Notably, it has been reported that the 4,6-substituted pyrimidinimides can be used to prepare the organometallic octanuclear imido-/amido-based manganese clusters *e.g.*, $[\{(\eta\text{-Cp})Mn(\eta^1, \eta^1\text{-2-NH(4,6-Me}_2\text{pm})\}\{Mn(\eta^1, \mu_3\text{-2-N(4,6-Me}_2\text{pm})\}]_4$ (4,6-Me_2pm = 4,6-dimethylpyrimidine) (Figure 3).[8a,8b] In this section we probe the use of s- and p-block sources of $[2\text{-}C_5H_4N\text{-}CH_2N]^{2-}$ (amp^{2-}) in combination with carboxylates, amides or amidinates as a route to imido-bridge-containing multinuclear assemblies (Figure 4). For example, use of the silylated 2-picolyl-amine ampH($SiMe_2Bu^t$) with $ZnMe_2$, affords the dimeric zinc-amido-bridged species $[Zn(Me)(ampSiMe_2Bu^t)_2]_2$.[12] However, to the knowledge of the author, the amp^{2-} framework has not been explored as a support for paramagnetic imido-bridged clusters.

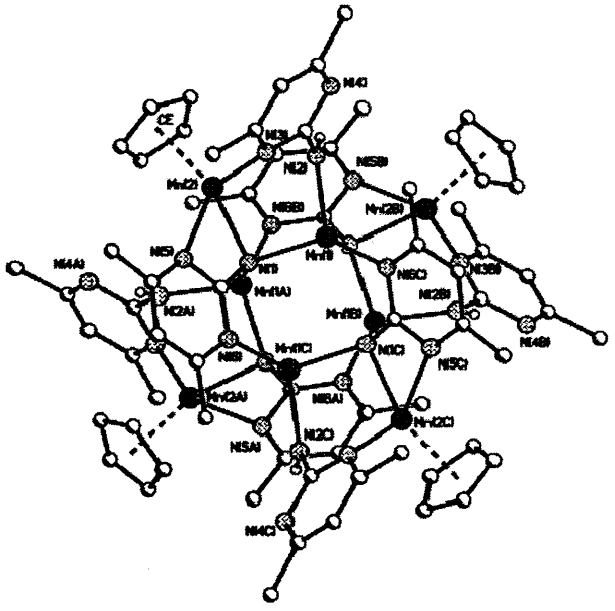

Figure 3 Molecular structure of $[\{(\eta\text{-Cp})Mn(\eta^1, \eta^1\text{-2-NH(4,6-Me}_2\text{pm})\}\{Mn(\eta^1, \eta^1, \mu_3\text{-2-N(4,6-Me}_2\text{pm})\}]_4$.[8]

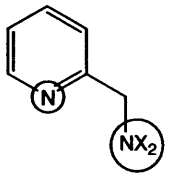

Figure 4 Structure of $ampX_2$ (X = Li, $SiMe_3$ or $SnBu^t_3$); potential binding domains are encircled.

6.2.1 ITR = $ampLi_2$, $M'L^1$ = MesN{Li}C{H}=NMes/$CH_3C\{O\}CN\{Li\}$Mes

Reactions of MX_3 or MX_2 [M = Mn(II), Fe(III), Co(II), Ni(II) or Cu(II)] with $ampLi_2$ were also carried out in the attempt to form metal imido complexes similar to **39** by using potential co-bridging ligand salts such as MesN{Li}C{H}=NMes or $CH_3C\{O\}CN\{Li\}$Mes (Scheme 6 and Appendices). In most cases, reactions were apparent by the dramatic colour changes observed. However, the products gave either too small crystals for potential X-ray diffraction analysis or were amorphous.

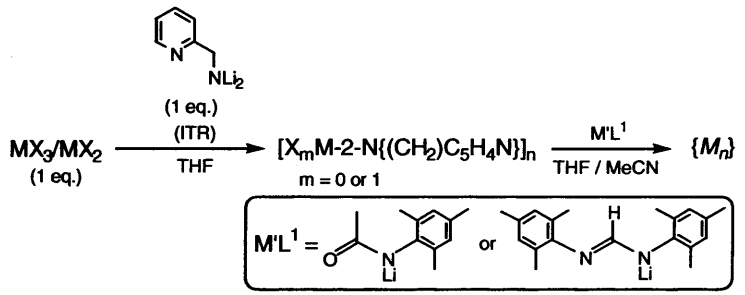

Scheme 6 Proposed route for the synthesis of $ampLi_2$ derived imido bridged complexes.

6.2.2 ITR = $amp(SiMe_3)_2$

In order to explore the role of the source of amp^{2-}, we decided to employ the previously reported p-block amp-based ITR $amp(SiMe_3)_2$.[11] Thus, we decided to investigate the reaction of $amp(SiMe_3)_2$ with a variety of transition metal halides to prepare multinuclear amp-based imido-bridged assemblies (Scheme 7 and Appendices).

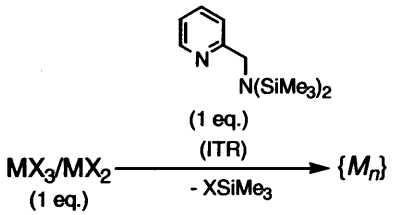

Scheme 7 Proposed route for the synthesis of $amp(SiMe_3)_2$ derived imido bridged complexes.

As was encountered in the previously described synthetic strategies, crystallisation of the resulting solutions to obtain amp-based imido-bridged complexes also proved to be unsuccessful. Similar attempts were also made using tin-based amp^{2-} reagents (see Appendices).

6.3 Summary and Conclusions

Considerable effort was directed towards the development of transition metal imido complexes including the successful synthesis and characterisation of a binuclear iron(III) imido complex $[Fe_2(\mu\text{-NMes})(CH_3C\{O\}NMes)_2Cl_2]$ (**39**). Complex **39** features two tetrahedral iron(III) ions coordinated by a single mesityl imido bridge, two *N,O*-bound mesitylacetamide ligands (formed indirectly during synthesis) and two terminal chlorides.

Several reaction pathways were devised to improve the synthetic strategy, these were seen to be promising from the outset because reactivity was clearly evident *i.e.*, from the apparent colour changes. However, the common recurrence of intractable, amorphous or microcrystalline air sensitive products meant that these could not be characterised and moreover, these species precluded recrystallisation. Other reactions in the attempts to build imido-bridged transition metal ion complexes are summarised in the Appendices.

6.4 References

1. (*a*) P. J. Nichols, G. D. Falton, K. S. Murray and B. O. West, *Inorg. Chem.*, 1988, **27**, 2795; (*b*) T. A. Hanna, A. M. Baranger and R. G. Bergman, *Angew. Chem. Int. Ed., Engl.*, 1996, **35**, 653; (*c*) X. Dai, P. Kapoor and T. H. Warren, *J. Am. Chem. Soc.*, 2004, **126**, 4798.
2. (*a*) F. A. Cotton, G. Wilkinson, C. A. Murillo and M. Bochmann, in *Advanced Inorganic Chemistry*, eds., F. A. Cotton, G. Wilkinson, Wiley-Interscience, New York, 6th Edn., 1999, p. 363; (*b*) *ibid.* p 465; (*c*) W. A. Nugent and B. L. Haymore, *Coord. Chem. Rev.*, 1980, **31**, 123.
3. (*a*) C. Lorber, R. Choukroun and B. Donnadieu, *Inorg. Chem.*, 2003, **42**, 673; (*b*) Y. Li, Y. Shi and A. L. Odom, *J. Am. Chem. Soc.*, 2004, **126**, 1794.
4. J. S. Duncan, T. M. Nazif, A. K. Verma and S. C. Lee, *Inorg. Chem.*, 2003, **42**, 1211.
5. (*a*) A. Decker, D. Fenske and K. Maczek, *Angew. Chem. Int. Ed., Engl.*, 1996, **35**, 2863; (*b*) P. Reiß and D. Fenske, *Z. Anorg. Allg. Chem.*, 2000, **626**, 1317.
6. M. L. Green and K. J. Moynihan, *Polyhedron*, 1986, **5**, 921.
7. (a) A. K. Verma and S. C. Lee, *J. Am. Chem. Soc.*, 1999, **121**, 10838; (*b*) C.T.-W. Chu, R. S. Gall and L. F. Dahl, *J. Am. Chem. Soc.*, 1982, **104**, 737.
8. (*a*) C. S. Aluarez, A. D. Bond, E. A. Harron, R. A. Layfield, J. A. McAllister, C. M. Pask, J. M. Rawson and D. S. Wright, *Organometallics*, 2001, **20**, 4135; (*b*) C. A. Alvarez, A. Bashall, A. D. Bond, D. Cave, E. A. Harron, R. A. Layfield, M. E. Mosquera, M. McPartlin, J. M. Rawson, P. T. Wood and D. S. Wright, *Dalton Trans.*, 2003, 3002.
9. (*a*) H. Link, A. Decker and D. Fenske, *Z. Anorg. Allg. Chem.*, 2000, **626**, 1567; (*b*) H. Link and D. Fenske, *Z. Anorg. Allg. Chem.*, 1999, **625**, 1878; (*c*) H. Link, P. Reiss, S. Chitsaz, H. Pfistner and D. Fenske, *Z. Anorg. Allg. Chem.*, 2003, **629**, 744; (*d*) A. A. Danapoulos, G. Wilkinson, T. K. N. Sweet and M. B. Hursthouse, *J. Chem. Soc. Dalton Trans.*, 1995, 205.
10. (*a*) W. J. Grigsby and P. P. Power, *J. Chem. Soc., Dalton Trans.*, 1996, 4613; (*b*) W. J. Grigsby, M. M. Olmstead and P. P. Power, *J. Organomet. Chem.*, 1996, 513, 173; (*c*) P. T. Gomes, M. L. H. Green, A. M. Martins and P. Mountford, *J. Organomet. Chem.*, 1997, **541**, 121.
11. S. Aldrige, R. J. Calder, D. L. Coombs, C. Jones, J. W. Steed, S. Coles and M. Hursthouse, *New J. Chem.*, 2002, **26**, 677.
12. M. Westerhausen, T. Bollwein, N. Makropoulos, T. M. Rotter, T. Habereder, M. Suter and H. Nöth, *Eur. J. Inorg. Chem.*, 2001, 851.
13. *See for example* P. Angaridis, F. A. Cotton, C. A. Murillo, D. Villagrán and X. Wang, *Inorg. Chem.*, 2004, **43**, 8290.
14. J. March, in *Advanced Organic Chemistry*, 4th Edn., Wiley-Interscience, 1992, USA, p. 21.
15. L. H. Gade and P. Mountford, *Coord. Chem. Rev.*, 2001, **216**, 65.

Chapter 7

Experimental

7.0 General

The FAB, MALDI and ESI mass spectra were recorded by Dr. G. Eaton (University of Leicester) using a Kratos Concept spectrometer [*m*-nitrobenzoic acid (NBA) matrix], an Applied Biosystems Voyager DE-STR spectrometer [2,5-dihydroxybenzoic acid (DHBA) matrix] and a Micromass Quattra LC spectrometer (methanolic solution), respectively. Elemental analyses were performed by Dr S. Boyer (Department of Chemistry, University of North London). The IR spectra were recorded using a Perkin-Elmer Spectrum One FT-IR spectrometer using the universal ATR sampling accessory (solid samples).

^{1}H NMR spectra were recorded on Bruker DRX-400 (400.13 MHz) and Bruker DPX-300 (300 MHz) spectrometers at a temperature of 300 K. Complex samples (~ 5 – 90 mgs) were dissolved in $CDCl_3$ and filtered from any residual solids prior to NMR data collection. All chemical shifts are in ppm referenced to TMS at 0 ppm. Longitudinal relaxation times (T_1) (400 MHz) were measured by Dr. G. Griffith (University of Leicester) using the inversion-recovery pulse sequence method (180-τ-90). Intensity data (Appendices, Equation 1) were analysed using the standard Bruker relaxation analysis package.

Room temperature magnetic measurements were carried out on an Evans balance [***PLEASE NOTE*** the Evans balance is sometimes ineffective at measuring accurate magnetic data which is mainly due to environmental effects *e.g.*, fluctuations in temperature]. The room temperature magnetic susceptibilities (Appendices, Equation 2) were used to determine the effective magnetic moments (Appendices, Equation 3). Magnetic susceptibility corrections for underlying diamagnetism were applied to data using Pascal's constants.[1]

Magnetic data was collected using a Quantum Design $MPMS_2$ DC SQUID magnetometer at the University of Edinburgh by Prof. A. Harrison and his co-workers, the

magnetisation of powdered samples was recorded from 1.8 to 300 K in fields of 100 G/1000 G. Data were corrected for the diamagnetism of the gelatine sample holder and the constituent atoms using Pascal's constants.[1] Non-linear regression lines of best fit on magnetic plots were obtained using the Levenberg-Marquardt method from the computer graphics program ORIGIN.[2] ***IMPORTANT NOTE*** *All SQUID magnetic measurements are only part of a preliminary investigation undertaken by Prof. A. Harrison (Edinburgh) therefore, there is a large uncertainty in the data e.g., due to the presence of several parameters and/or parameters with unreliable/inconsistent values.*

EPR measurements were carried out at the University of Manchester by Dr J. Wolowska. Q-band (~ 34.0 GHz) or X-band (~ 9.5 GHz) microwave frequencies were used for simulations at 290 K, 120 K or 5 K. X-band spectra were collected on an EMX hybrid spectrometer using powdered samples in 3 mm (outer diameter) quartz tubes. Q-band spectra were collected on an ESP300 spectrometer using powdered samples in 2 mm (outer diameter) quartz tubes.

All reactions requiring anaerobic conditions were carried out under an atmosphere of dry, oxygen-free nitrogen using standard Schlenk techniques or in a nitrogen purged glovebox. Anilines/amines were dried and distilled over calcium hydride. Solvents were distilled under nitrogen from appropriate drying agents and were degassed prior to use.[3] The compounds $[Fe_2OCl_6][NEt_4]_2$,[4] mehmpH,[5] Hbhp,[6] $\{[Li(THF)_2]_2[Fe_2(\mu\text{-}NMes)_2Cl_4]\}_n$, $[Fe_4(\mu_3\text{-}NPh)_4Cl_4][Li(THF)_3][Li(THF)_4]$ and $[Fe_4(\mu_3\text{-}NPh)_2Cl_4][N^nBu_4]_2$[7] were prepared according to previously reported procedures. The sodium salts of ligands were prepared by the dropwise addition of an aqueous solution of sodium hydroxide to a methanolic solution of the ligand, and left to stir for at least 3 h before drying to a solid under reduced pressure. Reagents were purchased from Sigma Aldrich Chemicals or commercially from other sources and used without further purification. Percentage yields represent total yields.

7.1 X-Ray Crystallography

All crystallographic data analysis was carried out in collaboration with Dr. J. Fawcett (University of Leicester). The crystallographic data for the complexes characterised by X-ray diffraction methods are shown in Tables 5, 6, 12, 13, 14, 19, 20, 24 and 25. Full spheres of diffraction data were collected on a Bruker APEX 2000 CCD diffractometer. All data were collected using graphite monochromated Mo-K_α radiation (λ = 0.7107 Å) and the reflections were corrected for Lorentz, polarisation and absorption effects. The structures were solved by full-matrix least squares on F^2 using SHELXTL.[8]

In the analysed complexes all carbon bonded hydrogen atoms were included in calculated positions (C-H = 0.96 Å) with isotropic displacement parameters set to $1.2U_{eq}$(C). All non-hydrogen atoms were refined with anisotropic displacement parameters. Further details with respect to crystallographic data are described within the text for the structural descriptions.

7.2 Compounds in Chapter 2

7.2.1 Synthesis of 1

(i) **1a**: $Ni(OAc)_2 \cdot 4H_2O$ (0.40 g, 1.61 mmol) in acetonitrile (10 cm^3) was added to a solution of Hchp (0.43 g, 3.32 mmol), hmpH (0.32 cm^3, 3.32 mmol) and triethylamine (1 cm^3, 7.50 mmol) in dichloromethane (10 cm^3). Methanol (10 cm^3) was added to solubilise the starting materials. After stirring for 30 min., the resulting solution was filtered, layered with *n*-hexane and left to stand. Pale green-blue crystals of **1a** were obtained by slow diffusion at ambient temperature after three weeks (7%, 0.05 g, 0.12 mmol).

(ii) **1b**: The procedure employed for **1a** was adopted to synthesise **1b**, using hepH (0.37 cm^3, 3.31 mmol) in place of hmpH; the ratio of molar equivalents of the reagents was as described for **1a**. Pale green-blue crystals of **1b** were obtained by slow diffusion at ambient temperature after three weeks (7%, 0.06 g, 0.11 mmol).

(iii) **1c**: The procedure employed for **1a** was adopted to synthesise **1c**, using hppH (0.42 cm^3, 3.27 mmol) in place of hmpH; the ratio of molar equivalents of the reagents was as described for **1a**. The resulting solution was concentrated to *ca.* 1 cm^3 and pale green-blue microcrystals of **1c** were obtained at ambient temperature on standing after three months (10%, 0.04 g, 0.12 mmol).

7.2.2 Synthesis of 2

Synthesis of 2

(i) **2a**: $Ni(OAc)_2 \cdot 4H_2O$ (0.40 g, 1.61 mmol) in acetonitrile (10 cm^3) was added to a solution of hmpH (0.32 cm^3, 3.32 mmol), hppH (0.42 cm^3, 3.27 mmol) and triethylamine (1 cm^3, 7.50 mmol) in dichloromethane (10 cm^3). Methanol (10 cm^3) was added to solubilise the starting materials. After stirring for 30 min., the resulting solution was filtered, layered

with *n*-hexane and left to stand. Pale green-blue crystalline blocks of **2a** were obtained by slow diffusion at ambient temperature after three months (8%, 0.05 g, 0.13 mmol).

(ii) **2b**: The procedure employed for **2a** was adopted to synthesise **2b**, using hepH (0.37 cm^3, 3.31 mmol) and hppH (0.42 cm^3, 3.27 mmol); the ratio of molar equivalents of the reagents was as described for **2a**. Pale green-blue crystalline blocks of **2b** were obtained by slow diffusion at ambient temperature after three months (9%, 0.06 g, 0.14 mmol).

7.2.3 Alternative Synthesis of 2 (melt reaction)

(i) **2a**: Ground $Ni(OAc)_2 \cdot 4H_2O$ (1.00 g, 4.02 mmol) and hmpH (1 cm^3, 10.37 mmol) were refluxed at 130 °C under nitrogen for 1 h and then dried under vacuum. After drying for 1 h, the remaining viscous solution was extracted in a 1: 1: 1 solvent mixture of methanol: dichloromethane: acetonitrile (30 cm^3). The resulting solution was filtered, layered with *n*-hexane and left to stand. Large blue crystalline blocks of **2a** were obtained at ambient temperature by slow diffusion after six months (38%, g, 0.60 g, 1.52 mmol).

(ii) **2b**: The procedure employed for **2a** (melt reaction) was adopted to synthesise **2b** (melt), using hepH (1 cm^3, 8.35 mmol); the ratio of molar equivalents of the reagents was as described for **2a**. Pale green-blue crystalline needles of **2b** were obtained at ambient temperature by slow diffusion after six months (15%, g, 0.13 g, 0.31 mmol).

7.2.4 Synthesis of 3

(i) **3**: $Cu(OAc)_2 \cdot H_2O$ (0.32 g, 1.61 mmol) in acetonitrile (10 cm^3) was added to a solution of Hchp (0.43 g, 3.32 mmol), hmpH (0.32 cm^3, 3.32 mmol) and triethylamine (1 cm^3, 7.50 mmol) in dichloromethane (10 cm^3). Methanol (10 cm^3) was added to solubilise the starting materials. After stirring for 30 min., the resulting solution was filtered, layered

with *n*-hexane and left to stand. Dark blue crystalline needles of **3** were obtained by slow diffusion at ambient temperature after three weeks (23%, 0.11 g, 0.37 mmol).

(ii) **3'**: $Cu(OAc)_2 \cdot H_2O$ (0.05 g, 0.25 mmol) in acetonitrile (3 cm^3) was added to a solution of Hchp (0.06 g, 0.47 mmol), mehmpH (0.06 cm^3, 0.54 mmol) and triethylamine (1 cm^3, 7.50 mmol) in dichloromethane (3 cm^3). Methanol (3 cm^3) was added to solubilise the starting materials. After stirring for 30 min., the resulting solution was filtered, layered with *n*-hexane and left to stand. Dark blue microcrystals of **3'** were obtained by slow diffusion at ambient temperature after one day (80%, 0.04 g, 0.13 mmol).

7.2.5 Synthesis of 4

(i) **4a**: $Cu(OAc)_2 \cdot H_2O$ (0.32 g, 1.61 mmol) in acetonitrile (10 cm^3) was added to a solution of Hchp (0.43 g, 3.32 mmol), hepH (0.37 cm^3, 3.31 mmol) and triethylamine (1 cm^3, 7.50 mmol) in dichloromethane (10 cm^3). Methanol (10 cm^3) was added to solubilise the starting materials. After stirring for 30 min., the resulting solution was filtered, concentrated to *ca.* 2 cm^3 and dark blue crystalline blocks of **4a** were obtained at ambient temperature on standing after three weeks (30%, 0.15 g, 0.24 mmol).

(ii) **4b**: $Cu(OAc)_2 \cdot H_2O$ (0.03 g, 0.16 mmol) in acetonitrile (10 cm^3) was added to a solution of Hbhp (0.05 g, 0.28 mmol), hepH (0.04 cm^3, 0.33 mmol) and triethylamine (10 drops) in dichloromethane (10 cm^3). Methanol (10 cm^3) was added to solubilise the starting materials. After stirring for 30 min., the resulting solution was filtered, concentrated to *ca.* 2 cm^3 and dark blue crystalline blocks of **4b** were obtained at ambient temperature on standing after three weeks (26%, 0.02 g, 0.08 mmol).

7.2.6 Synthesis of 5

(i) **5a**: $Cu(OAc)_2 \cdot H_2O$ (0.32 g, 1.61 mmol) in acetonitrile (10 cm^3) was added to a solution of Hchp (0.43 g, 3.32 mmol), hppH (0.42 cm^3, 3.27 mmol) and triethylamine (1 cm^3, 7.50 mmol) in dichloromethane (10 cm^3). Methanol (10 cm^3) was added to solubilise the starting materials. After stirring for 30 min., the resulting solution was filtered, concentrated to ~ 2 cm^3 and dark blue crystalline needles of **5a** were obtained at ambient temperature on standing after three days (40%, 0.20 g, 0.32 mmol).

(ii) **5b**: $Cu(OAc)_2 \cdot H_2O$ (0.03 g, 0.16 mmol) in acetonitrile (10 cm^3) was added to a solution of Hbhp (0.05 g, 0.28 mmol), hppH (0.04 cm^3, 0.33 mmol) and triethylamine (10 drops) in dichloromethane (10 cm^3). Methanol (10 cm^3) was added to solubilise the starting materials. After stirring for 30 min., the resulting solution was filtered, concentrated to ~ 2 cm^3 and dark blue crystalline blocks of **5b** were obtained at ambient temperature on standing after three weeks (98%, 0.06 g, 0.08 mmol).

7.2.7 Synthesis of 6

$Cu(OAc)_2 \cdot H_2O$ (0.32 g, 1.61 mmol) in acetonitrile (10 cm^3) was added to a solution of hmpH (0.32 cm^3, 3.32 mmol), hepH (0.37 cm^3, 3.31 mmol) and triethylamine (1 cm^3, 7.50 mmol) in dichloromethane (10 cm^3). Methanol (10 cm^3) was added to solubilise the starting materials. After stirring for 30 min., the resulting solution was filtered, layered with *n*-hexane and left to stand. Blue crystalline blocks of **6** were obtained by slow diffusion at ambient temperature after three weeks (8%, 0.03 g, 0.03 mmol).

7.2.8 Synthesis of 7

$Cu(OAc)_2 \cdot H_2O$ (0.32 g, 1.61 mmol) in acetonitrile (10 cm^3) was added to a solution of hmpH (0.32 cm^3, 3.32 mmol), hppH (0.42 cm^3, 3.27 mmol) and triethylamine (1 cm^3, 7.50

mmol) in dichloromethane (10 cm^3). Methanol (10 cm^3) was added to solubilise the starting materials. After stirring for 30 min., the resulting solution was filtered, layered with *n*-hexane and left to stand. Blue crystalline blocks of **7** were obtained by slow diffusion at ambient temperature after two weeks (11%, 0.07 g, 0.18 mmol).

7.2.9 Synthesis of 3 from 7

Complex **7** (0.25 g, 0.63 mmol), Hchp (0.08 g, 0.62 mmol) and triethylamine (1 cm^3, 7.50 mmol) in a 1: 1: 1 solvent mixture of acetonitrile: dichloromethane: methanol (15 cm^3). After stirring for 30 min., the resulting solution was filtered, concentrated to 1 cm^3, re-filtered, layered with *n*-hexane and left to stand. Dark-blue crystals of **3** had formed by slow diffusion at ambient temperature after one day (33%, 0.03 g, 0.10 mmol).

7.2.10 Synthesis of 6 from 7

Complex **7** (0.08 g, 0.20 mmol) in triethylamine (5 cm^3, 37.5 mmol) was refluxed with stirring for 2 h at 70 °C. The mixture was cooled, filtered and the remaining solid was extracted by dissolving into a 1: 1: 1 solvent mixture of acetonitrile: dichloromethane: methanol (1 cm^3). The resulting solution was filtered, layered with *n*-hexane and left to stand. Blue crystals of **6** had formed at ambient temperature by slow diffusion after two days (22%, 0.01 g, 10.87 μmol).

7.2.11 Synthesis of 8

$Cu(OAc)_2 \cdot H_2O$ (0.32 g, 1.61 mmol) in acetonitrile (10 cm^3) was added to a solution of hepH (0.37 cm^3, 3.31 mmol), hppH (0.42 cm^3, 3.27 mmol) and triethylamine (1 cm^3, 7.50 mmol) in dichloromethane (10 cm^3). Methanol (10 cm^3) was added to solubilise the starting materials. After stirring for 30 min., the resulting solution was filtered, layered

with *n*-hexane and left to stand. Blue crystalline blocks of **8** were obtained by slow diffusion at ambient temperature after two weeks (10%, 0.04 g, 0.08 mmol).

7.2.12 Synthesis of 4a from 8

Complex **8** (0.01 g, 20.49 μmol), Hchp (4 mg, 31.00 μmol) and triethylamine (1 cm^3, 7.50 mmol) were dissolved in a 1: 1: 1 solvent mixture of acetonitrile: dichloromethane: methanol (1 cm^3). After stirring for 30 min., the resulting solution was filtered, concentrated to 1 cm^3, re-filtered, layered with *n*-hexane and left to stand. Dark-blue crystals of **4a** had formed by slow evaporation at ambient temperature after four days (25%, 3.00 mg, 4.78 μmol).

Table 1 Spectroscopic and analytical data for the new complexes **1a – 2b**

Compound	μ_{eff} (BM)[a]	IR data (cm^{-1})[b]	FAB mass spectrum (Da.)	Formula	Microanalysis (%)[c] C	H	N
1a	2.69	ν(OH) 3061(w), 1868(w), 2455(m), 1868(m), 1596(s), 1522(m), 1488(m), 1460(s), 1435(s), 1396(s), 1368(s), 1339(m), 1290(s), 1242(w), 1218(w), 1168(s), 1160(s), 1070(s), 1062(s), 1043(s), 1026(s), 986(s), 907(s), 892(m), 816(w), 879(s), 787(w), 774(s), 759(s), 744(s), 721(m), 699(s), 666(m)	405 $[M - chp]^+$, 498 $[M - chp - hmpH]^+$, 277 $[M - 2chp]^+$, 168 $[M - 2chp - hmpH]^+$	$NiC_{22}H_{20}O_4Cl_2N_4$	49.65 (49.35)	3.61 (3.74)	10.32 (10.47)
1b	2.93	ν(OH) 2932(w), 2477(w), 1874(w), 1874(w)br, 1597(s), 1572(m), 1523(m), 1467(s), 1445(s), 1412(s), 1396(s), 1370(s), 1340(m), 1317(m), 1301(m), 1237(w), 1196(w), 1153(s), 1135(m), 1113(m), 1069(s), 1034(m), 1023(m), 991(s), 968(m), 908(s), 774(s), 761(s), 755(s), 724(m), 702(m), 688(w), 664(s)	491 $[M - 2Cl]^+$, 433 $[M - chp]^+$, 310 $[M - chp - hepH]^+$	$NiC_{24}H_{24}O_4Cl_2N_4 \cdot AcOH \cdot 0.5CH_2Cl_2$	48.54 (47.86)	3.94 (4.36)	8.07 (8.43)
1c	3.08	ν(OH) 3468(s), 3105(s), 2936(s), 1592(s), 1505(s), 1413(s), 1350(s), 1150(w), 1055(w), 1029(m), 962(w), 905(s), 736(s), 674(s)	645 $[M - OH]^+$, 508 $[M - hppH - OH]^+$, 441 $[M - chp - C_6H_4N - CH_2]^+$, 404 $[M - 2chp]^+$, 379 $[M - hppH - chp - OH]^+$	$NiC_{26}H_{28}O_4Cl_2N_4 \cdot 3CH_2Cl_2$	37.81 (37.95)	4.01 (3.71)	6.63 (6.11)
2a	2.80	ν(OH) 3066(w), 1916(m), 1608(m), 1573(m), 1504(m), 1485(m), 1407(s), 1361(s), 1339(s), 1288(s), 1250(w), 1221(w), 1155(m), 1133(m), 1098(w), 1062(s), 1042(s), 1016(s), 997(s), 913(s), 819(w), 761(s), 666(s)	395 $[M]^+$, 336 $[M - CH_3CO_2]^+$, 277 $[M - 2CH_3CO_2]^+$, 227 $[M - hmpH - 2CH_3CO_2]^+$	$NiC_{16}H_{20}O_6N_2$	48.77 (48.61)	5.13 (5.06)	6.94 (7.09)
2b	3.22	ν(OH) 2926(w), 2322(w), 1991(w), 1606(m), 1572(m), 1530(s), 1481(m), 1467(m), 1449(m), 1411(s), 1361(s), 1336(s), 1314(s), 1252(w), 1188(w), 1157(w), 1113(w), 1077(s), 1062(m), 1023(s), 974(w), 905(s), 896(s), 858(m), 791(s), 772(s), 660(s)	423 $[M]^+$, 360 $[M - CH_3CO_2]^+$, 305 $[M - 2CH_3CO_2]^+$, 241 $[M - hepH - 2CH_3CO_2]^+$	$NiC_{24}H_{26}O_4N_2$	51.21 (51.06)	5.74 (5.67)	6.68 (6.62)

[a]Recorded on an Evans Balance at room temperature. [b]Recorded on a Perkin-Elmer Spectrum One FT-IR spectrometer on solid samples. [c]Calculated values are shown in parentheses.

Table 2 Spectroscopic and analytical data for the new complexes **3 – 5a**

Compound	μ_{eff} (BM)[a]	IR data (cm^{-1})[b]	FAB mass spectrum (Da.)	Formula	Microanalysis (%)[c] C	H	N
3	1.37	3363(w), 3073(w), 2832(w), 1638(m), 1607(m), 1585(s), 1529(m), 1486(m), 1470(w), 1442(s), 1432(s), 1388(s), 1360(m), 1339(s), 1312(s), 1289(s), 1244(w), 1218(w), 1187(w), 1154(s), 1132(m), 1096(w), 1072(s), 1050(s), 1032(s), 974(s), 910(s), 856(w), 817(w), 777(s), 766(s), 718(s), 698(s), 666(s)	363 $[M_{(n=1)} + Cu]^+$	$CuC_{11}H_9O_2Cl_1N_2$	44.04 (44.07)	3.17 (3.01)	9.22 (9.35)
3'	1.63	2979(w), 1607(s), 1570(s), 1479(s), 1443(s), 1392(w), 1373(s), 1336(m), 1307(m), 1281(m), 1257(m), 1257(m), 1150(s), 1132(s), 1071(s), 1052(s), 1021(s), 973(s), 904(s), 836(s), 782(s), 754(s), 726(s), 684(s), 656(s)	314 $[M_{(n=1)}]^+$, 377 $[M_{(n=1)} + Cu]^+$	$CuC_{12}H_{11}O_2Cl_1N_2$	46.16 (46.01)	3.30 (3.51)	8.82 (8.91)
4a	1.87	2951(w), 2813(m), 1605(m), 1589(s), 1531(s), 1481(m), 1436(s), 1417(s), 1388(s), 1356(m), 1339(s), 1306(s), 1242(s), 1214(w), 1179(w), 1149(s), 1138(s), 1069(s), 1047(s), 975(s), 912(s), 893(m), 874(s), 845(s), 786(s), 760(s), 753(s), 721(s), 694(s)	626 $[M]^+$, 504 $[M - hep]^+$, 498 $[M - chp]^+$, 376 $[M - chp - hep]^+$	$Cu_2C_{24}H_{22}O_4Cl_2N_4$	46.10 (46.01)	3.59 (3.51)	8.77 (8.44)
4b	d	3367(w), 3061(w), 2889(w), 2832(m), 1605(s), 1568(s), 1536(s), 1475(s), 1447(s), 1409(s), 1395(s), 1374(m), 1358(s), 1340(m), 1249(w), 1217(w), 1193(m), 1156(s), 1113(s), 1066(s), 1046(s), 1029(s), 988(s), 973(s), 877(s), 834(s), 773(s), 759(s), 715(s), 682(s)	716 $[M]^+$, 594 $[M - hep]^+$, 543 $[M - bhp]^+$, 421 $[M - bhp - hep]^+$	$Cu_2C_{24}H_{22}O_4Br_2N_4$	40.35 (40.22)	3.03 (3.07)	7.67 (7.82)
5a	1.58	2907(w), 2934(w), 2850(w), 1615(s), 1604(s), 1540(s), 1481(s), 1451(s), 1400(s), 1367(m), 1347(w), 1314(w), 1219(w), 1178(m) 1159(s), 1111(w), 1083(s), 1058(s), 1024(w), 1003(s), 946(s), 900(w), 871(w), 835(m), 824(m), 775(s), 762(s), 716(s), 695(s)	655 $[M]^+$	$Cu_2C_{26}H_{26}O_4Cl_2N_4$	47.72 (47.36)	3.75 (3.97)	8.35 (8.55)

[a]Recorded on an Evans Balance at room temperature. [b]Recorded on a Perkin-Elmer Spectrum One FT-IR spectrometer on solid samples. [c]Calculated values are shown in parentheses. [d]Not enough sample for analysis.

Table 3 Spectroscopic and analytical data for the new complexes **5b – 8**

Compound	μ_{eff} (BM)[a]	IR data (cm^{-1})[b]	FAB mass spectrum (Da.)	Formula	Microanalysis (%)[c] C	H	N
5b	2.17	3390(w), 3061(w), 3029(w), 2935(m), 2906(m), 2850(m), 1603(s), 1568(s), 1538(s), 1479(s), 1449(s), 1413(m), 1396(s), 1370(m), 1359(m), 1325(m), 1314(m), 1271(w), 1242(w), 1217(w), 1196(w), 1176(m), 1155(s), 1128(w), 1110(w), 1082(s), 1058(s), 1023(m), 994(s), 970(w), 960(w), 945(s), 900(w), 881(m), 871(w), 834(m), 823(m), 774(s), 759(s), 714(s), 682(s)	608 $[M - hpp]^+$, 571 $[M - bhp]^+$	$Cu_2C_{26}H_{26}O_4Br_2N_4$[d]	42.96 (41.94)	3.35 (3.49)	7.29 (7.53)
6	4.06	ν(OH) 3416(w), 2840(w), 1585(s), 1482(w), 1444(m), 1391(s), 1333(s), 1284(m), 1223(w), 1157(w), 1076(s), 1048(s), 1028(w), 824(w), 781(m), 768(s), 721(m), 666(s), 654(s)	861 $[M - CH_3CO_2]^+$,[d] 802 $[M - 2CH_3CO_2]^+$,[d] 635 $[M - hmp - 3CH_3CO_2]^+$,[d] 576 $[M - hmp - 4CH_3CO_2]^+$,[d] 527 $[M - 2hmp - 3CH_3CO_2]^+$,[d] 397 $[M - 2hmp - 2CH_3CO_2]^+$,[d] 397 $[M - 2hmp - 2CH_3CO_2]^+$,[d] 450 $[2Cu + 3hmp]^+$,[d] 342 $[2Cu + 2hmp]^+$,[d] 171 $[Cu + hmp]^+$[d]	$Cu_4C_{32}H_{36}O_{12}N_4$[d]	41.70 (41.74)	4.56 (3.91)	6.05 (6.09)
7	1.86	ν(OH) 3253(w), 3071(w), 2614(w), 1651(s), 1608(s), 1572(s), 1531(s), 1485(s), 1439(s), 1404(s), 1373(s), 1283(s), 1248(s), 1227(w), 1155(w), 1069(s), 1044(s), 1014(s), 992(m), 965(m), 816(m), 762(s), 724(s), 654(s)	399 $[M]^+$, 340 $[M - CH_3CO_2]^+$, 281 $[M - 2CH_3CO_2]^+$, 172 $[M - 2CH_3CO_2 - hmpH]^+$	$CuC_{16}H_{20}O_6N_2 \cdot 1.1CH_2Cl_2$	41.71 (41.66)	4.33 (4.51)	6.01 (5.69)
8	2.09	3271(w), 3084(w), 2875(m), 2828(m), 1606(s), 1585(s), 1484(s), 1448(s), 1415(s), 1392(s), 1358(m), 1334(s), 1249(m), 1199(w), 1168(w), 1116(s), 1080(s), 1052(s), 1028(m), 1007(m), 978(w), 925(w), 881(m) 788(s), 775(s), 678(s)	429 $[M - CH_3CO_2]^+$, 370 $[M - 2CH_3CO_2]^+$, 307 $[M - hep - CH_3CO_2]^+$, 244 $[M - 2hepH]^+$, 185 $[Cu + hep]^+$	$Cu_2C_{18}H_{22}O_6N_2 \cdot MeCN$	45.48 (45.37)	5.23 (4.73)	6.09 (7.94)

[a]Recorded on an Evans Balance at room temperature. [b]Recorded on a Perkin-Elmer Spectrum One FT-IR spectrometer on solid samples. [c]Calculated values are shown in parentheses. [d]Dehydrated/desolvated sample (*cf.* to crystal structure).

Table 4 Characterisation of conversion products

Compound	Converted from	IR data (cm^{-1})[a]	Formula	Microanalysis (%)[b] C	H	N
3	-	3363(w), 3073(w), 2832(w), 1638(m), 1607(m), 1585(s), 1529(m), 1486(m), 1470(w), 1442(s), 1432(s), 1388(s), 1360(m), 1339(s), 1312(s), 1289(s), 1244(w), 1218(w), 1187(w), 1154(s), 1132(m), 1096(w), 1072(s), 1050(s), 1032(s), 974(s), 910(s), 856(w), 817(w), 777(s), 766(s), 718(s), 698(s), 666(s)	$CuC_{11}H_9O_2Cl_1N_2$	44.04 (44.07)	3.17 (3.01)	9.22 (9.35)
3	**7**	3364(w), 3074(w), 2832(w), 1610(m), 1585(s), 1529(m), 1485(m), 1432(s), 1405(s), 1388(s), 1361(w), 1340(s), 1289(m), 1258(w), 1244(w), 1218(w), 1157(m), 1132(m), 1072(s), 1049(s), 974(s), 910(s), 885(w), 857(w), 823(w), 777(s), 766(s), 718(s), 698(s), 669(s), 653(s)	$CuC_{11}H_9O_2Cl_1N_2$	43.95 (44.07)	2.95 (3.01)	9.35 (9.35)
6	-	ν(OH) 3416(w), 2840(w), 1585(s), 1482(w), 1444(m), 1391(s), 1333(s), 1284(m), 1223(w), 1157(w), 1076(s), 1048(s), 1028(w), 824(w), 781(m), 768(s), 721(m), 666(s), 654(s)	$Cu_4C_{32}H_{36}O_{12}N_4(-H_2O)$	41.70 (41.74)	4.56 (3.91)	6.05 (6.09)
6	**7**	ν(OH) 3416(w), 2838(w), 1585(s), 1482(w), 1444(m), 1380(s), 1330(s), 1285(m), 1223(w), 1158(w), 1078(s), 1049(s), 1027(m), 1015(m), 928(w), 825(w), 782(s), 771(s), 761(s), 721(m), 664(s), 654(s)	$Cu_4C_{32}H_{36}O_{12}N_4{\cdot}CH_2Cl_2{\cdot}H_2O$	38.38 (38.71)	3.71 (3.91)	5.51 (5.47)
4a	-	2951(w), 2813(m), 1605(m), 1589(s), 1531(s), 1481(m), 1436(s), 1417(s), 1388(s), 1356(m), 1339(s), 1306(s), 1242(s), 1214(w), 1179(w), 1149(s), 1138(s), 1069(s), 1047(s), 975(s), 912(s), 893(m), 874(s), 845(s), 786(s), 760(s), 753(s), 721(s), 694(s)	$Cu_2C_{24}H_{22}O_4Cl_2N_4$	46.10 (46.01)	3.59 (3.51)	8.77 (8.44)
4a	**8**	3337(w), 2952(w), 2814(m), 1605(m), 1590(s), 1532(s), 1481(m), 1437(s), 1416(s), 1388(s), 1356(m), 1340(s), 1306(s), 1243(m), 1214(w), 1179(w), 1149(s), 1139(m), 1112(m), 1069(s), 1047(s), 1030(m), 975(s), 912(s), 893(w), 875(m), 845(m), 787(m), 766(s), 753(s), 722(s), 694(s)	$Cu_2C_{24}H_{22}O_4Cl_2N_4{\cdot}NEt_3$	49.29 (49.52)	5.62 (5.69)	10.22 (9.63)

[a]Recorded on a Perkin-Elmer Spectrum One FT-IR spectrometer on solid samples. [b]Calculated values are shown in parentheses.

Table 5 Crystallographic and data processing parameters for complexes **1a – 4b**

Complex	1a	1b	2a	2b	3	4a	4b
J. Fawcett code	04091	04036	04083	04047	03170	04010	04071
Formula	$Ni_{0.5}C_{11}H_{10}ClN_2O_2$	$NiC_{24}H_{24}Cl_2N_4O_4$	$NiC_{16}H_{20}N_2O_6$	$NiC_{18}H_{24}N_2O_6$	$CuC_{11}H_9ClN_2O_2$	$CuC_{12}H_{11}ClN_2O_2$	$Cu_2C_{24}H_{22}Br_2N_4O_4$
M	267.02	562.09	395.05	423.10	300.19	314.22	717.36
Crystal size (mm)	0.32 × 0.21 × 0.10	0.32 × 0.16 × 0.04	0.09 × 0.13 × 0.16	0.27 × 0.20 × 0.15	0.23 × 0.18 × 0.11	0.23 × 0.13 × 0.01	0.22 × 0.17 × 0.05
Temperature (K)	150(2)	150(2)	150(2)	150(2)	150(2)	150(2)	150(2)
Crystal system	Monoclinic	Orthorhombic	Triclinic	Monoclinic	Monoclinic	Triclinic	Triclinic
Space group	$P2_1/c$	$P2_12_12_1$	P-1	$P2_1c$	$C2c$	P-1	P-1
Lattice parameters							
a (Å)	10.9015(7)	14.194(2)	7.7974(7)	8.4068(9)	14.885(4)	7.687(3)	7.6858(19)
b (Å)	13.8221(8)	17.135(3)	7.9314(7)	7.8593(8)	13.747(3)	7.905(3)	8.899(2)
c (Å)	7.6327(5)	20.306(3)	8.4387(7)	15.1140(16)	11.504(3)	11.122(4)	10.263(3)
α (°)	90	90	114.9140(10)	90	90	99.267(5)	67.168(4)
β (°)	102.2440(10)	90	100.4390(10)	104.925(2)	106.042(4)	103.897(5)	89.363(4)
γ (°)	90	90	108.5030(10)	90	90	108.234(5)	84.491(4)
U (Å^3)	1123.95(12)	4938.8(13)	417.69(6)	964.92(18)	2262.5(10)	602.4(3)	643.7(3)
Z	4	8	1	2	8	2	1
D_c (Mg m^{-3})	1.578	1.507	1.571	1.456	1.763	1.732	1.851
F(000)	548	2320	206	444	1208	318	354
μ (Mo-K$_\alpha$) (mm^{-1})	1.139	1.041	1.197	1.042	2.155	2.028	4.794
Reflections collected	8610	24048	3054	7247	7973	4427	4943
Independent reflections	2216	8673	1471	1888	1982	2334	2493
R_{int}	0.0231	0.1306	0.0244	0.0464	0.0363	0.0375	0.0232
Parameters/ restraints	151/0	311/0	116/0	125/0	154/0	163/0	163/0
Final R indices							
R_1; wR_2 [I>2σ(I)]	0.0287; 0.0750	0.0608; 0.0871	0.0277; 0.0698	0.0313; 0.0858	0.0395; 0.1036	0.0487; 0.1217	0.0328; 0.0879
R_1; wR_2 (All data)	0.0304; 0.0758	0.1830; 0.1146	0.0285; 0.0701	0.0353; 0.0877	0.0473; 0.1076	0.0542; 0.1247	0.0374; 0.0910
Goodness of fit on F^2 (all data)	1.053	0.6072	1.070	1.046	1.065	1.019	0.793

Data in common: graphite-monochromated Mo-K$_\alpha$ radiation, λ = 0.71073 Å; $R_1 = \Sigma||F_o| - |F_c||/\Sigma|F_o|$, $wR_2 = [\Sigma w(F_o^2 - F_c^2)^2/\Sigma w(F_o^2)^2]^{1/2}$, $w^{-1} = [\sigma^2(F_o)^2 + (aP)^2]$, $P = [\max(F_o^2,0) + 2(F_c^2)]/3$, where a is a constant adjusted by the program; goodness of fit = $[\Sigma(F_o^2 - F_c^2)2/(n-p)]^{1/2}$ where n is the number of reflections and p the number of parameters.

Table 6 Crystallographic and data processing parameters for complexes **5a – 8**

Complex	5a	5b	6	7	8
J. Fawcett code	04022	04060	04086	04084	04018
Formula	$Cu_2C_{26}H_{22}Cl_2N_4O_4$	$CuC_{14}H_{17}BrN_2O_3$	$Cu_4C_{32}H_{39}N_4O_{13.50}$	$CuC_{16}H_{20}N_2O_6$	$CuC_9H_{11}NO_3$
M	656.49	404.75	949.83	399.88	244.73
Crystal size (mm)	0.21 × 0.06 × 0.03	0.28 × 0.11 × 0.06	0.28 × 0.18 × 0.14	0.24 × 0.14 × 0.12	0.28 × 0.17 × 0.08
Temperature (K)	150(2)	150(2)	150(2)	150(2)	150(2)
Crystal system	Triclinic	Triclinic	Monoclinic	Triclinic	Triclinic
Space group	*P*-1	*P*-1	$P2_1c$	*P*-1	*P*-1
Lattice parameters					
a (Å)	7.6858(19)	7.741(3)	14.1452(7)	7.8035(16)	7.648(2)
b (Å)	8.899(2)	10.435(4)	12.6869(6)	7.9655(16)	7.787(2)
c (Å)	10.263(3)	10.931(4)	20.9799(10)	8.4786(17)	8.602(2)
α (°)	67.168(4)	65.022(6)	90	103.740(3)	100.123(4)
β (°)	89.363(4)	73.919(6)	95.6280(10)	115.224(3)	105.561(4)
γ (°)	84.491(4)	88.051(7)	90	106.476(3)	93.207(4)
U (Å^3)	643.7(3)	765.6(5)	3746.9(3)	416.35(15)	482.9(2)
Z	1	2	4	1	2
D_c (Mg m^{-3})	1.694	1.756	1.684	1.595	1.683
F(000)	334	406	1932	207	250
μ (Mo-K$_\alpha$) (mm^{-1})	1.901	4.046	2.309	1.348	2.239
Reflections collected	4224	5930	28987	2514	3739
Independent reflections	2448	2943	7369	1419	1871
R_{int}	0.0357	0.0575	0.0334	0.0187	0.0456
Parameters/ restraints	172/0	192/0	487/0	116/0	128//0
Final *R* indices					
R_1; wR_2 [$I>2\sigma(I)$]	0.0714; 0.1812	0.1055; 0.3324	0.0306; 0.0725	0.0385; 0.0976	0.0524; 0.1282
R_1; wR_2 (All data)	0.0886; 0.1921	0.1196; 0.3367	0.0374; 0.0749	0.0403; 0.0984	0.0562; 0.1304
Goodness of fit on F^2 (all data)	1.044	1.063	0.999	1.057	1.038

Data in common: graphite-monochromated Mo-K$_\alpha$ radiation, λ = 0.71073 Å; $R_1 = \Sigma||F_o| - |F_c||/\Sigma|F_o|$, $wR_2 = [\Sigma w(F_o^2 - F_c^2)^2/\Sigma w(F_o^2)^2]^{1/2}$, $w^{-1} = [\sigma^2(F_o)^2 + (aP)^2]$, $P = [\max(F_o^2,0) + 2(F_c^2)]/3$, where a is a constant adjusted by the program; goodness of fit = $[\Sigma(F_o^2 - F_c^2)2/(n-p)]^{1/2}$ where n is the number of reflections and p the number of parameters.

7.3 Compounds in Chapter 3

7.3.1 Synthesis of 9a and 9b

$Ni(OAc)_2.4H_2O$ (0.40 g, 1.61 mmol) in acetonitrile (10 cm^3) was added to a solution of $bnzH_2$ (0.75 g, 3.29 mmol), Hchp (0.43 g, 3.33 mmol) and triethylamine (1 cm^3, 7.5 mmol) in dichloromethane (10 cm^3). Methanol (10 cm^3) was added to solubilise the starting materials. After stirring for 30 min., the resulting solution was filtered, layered with *n*-hexane and left to stand. Green crystalline blocks of co-crystallised **9a** and **9b** were obtained at ambient temperature by slow diffusion after 3 weeks (28%, 0.22 g, 0.11 mmol).

7.3.2 Synthesis of 10a and 10b

$Ni(OAc)_2.4H_2O$ (0.04 g, 0.16 mmol) in acetonitrile (10 cm^3) was added to a solution of $bnzH_2$ (0.36 g, 0.16 mmol), Hbhp (0.05 g, 0.28 mmol) and triethylamine (10 drops) in dichloromethane (10 cm^3). Methanol (10 cm^3) was added to solubilise the starting materials. After stirring for 30 min., the resulting solution was filtered, concentrated to 2 cm^3, re-filtered and layered with *n*-hexane. Green crystalline blocks of co-crystallised **10a** and **10b** were obtained at 0 °C on standing after 2 days (23%, 0.02 g, 4.79 μmol).

7.3.3 Synthesis of 11a and 12a

$Ni(OAc)_2.4H_2O$ (0.40 g, 1.61 mmol) in acetonitrile (10 cm^3) was added to a solution of $bnzH_2$ (0.75 g, 3.29 mmol), hmpH (0.32 cm^3, 3.32 mmol) and triethylamine (1 cm^3, 7.50 mmol) in dichloromethane (10 cm^3). Methanol (10 cm^3) was added to solubilise the starting materials. After stirring for 30 min., the resulting solution was filtered, layered with *n*-hexane and left to stand. After a few days green crystals of **11a** (77%, 0.05 g, 0.03 mmol) and pale-blue crystals of **12a** (1%, 0.01 g, 0.02 mmol) were obtained at ambient temperature by slow diffusion.

7.3.4 Synthesis of 11a

Ground $Ni(OAc)_2 \cdot 4H_2O$ (0.40 g, 1.61 mmol), $bnzH_2$ (0.75 g, 3.29 mmol) and hmpH (0.32 cm^3, 3.32 mmol) were added to triethylamine (10 cm^3, 37.5 mmol) and refluxed with stirring at 60 °C. After 1.5 h the remaining viscous solution was extracted by using methanol (20 cm^3), filtered and left to stand. Green crystalline blocks of **11a** were obtained at ambient temperature by slow evaporation after three days (9%, 0.06 g, 0.04 mmol).

7.3.5 Synthesis of 12a

$Ni(OAc)_2 \cdot 4H_2O$ (0.40 g, 1.61 mmol) in acetonitrile (10 cm^3) was added to a solution of $bnzH_2$ (0.75 g, 3.29 mmol), hmpH (0.32 cm^3, 3.32 mmol) and triethylamine (1 cm^3, 7.50 mmol) in dichloromethane (10 cm^3). Ethanol (10 cm^3) was added to solubilise the starting materials. After stirring for 2 h, the resulting solution was filtered and left to stand. Pale-blue crystals of **12a** were obtained by slow diffusion at ambient temperature after two days (26%, 0.30 g, 0.41 mmol).

7.3.6 Synthesis of 11a from 12a

Complex **12a** (0.01 g, 0.02 mmol) in a 1: 1: 1 solvent mixture of acetonitrile: dichloromethane: methanol (1 cm^3) and triethylamine (15 drops) were stirred for 30 min., the remaining solution was filtered and left to crystallise at ambient temperature. A green powder of **11a** had formed after one week (5%, 2.00 mg, 3.97 μmol).

7.3.7 Synthesis of 11b and 12b

$Ni(OAc)_2 \cdot 4H_2O$ (0.40 g, 1.61 mmol) in acetonitrile (10 cm^3) was added to a solution of diphenylacetic acid (0.70 g, 3.32 mmol), hmpH (0.32 cm^3, 3.32 mmol) and triethylamine (1 cm^3, 7.50 mmol) in dichloromethane (10 cm^3). Methanol (10 cm^3) was added to solubilise the starting materials. After stirring for 30 min., the resulting solution was

filtered, layered with *n*-hexane and left to stand. Green crystals of **11b** and pale-blue crystalline blocks of **12b** were obtained at ambient temperature by slow diffusion after two weeks for **11b** (11%, 0.07 g, 0.04 mmol) and after four days for **12b** (71%, 0.80 g, 1.09 mmol).

7.3.8 Synthesis of 13 and 14

(i) **13a** and **14a**: $Ni(OAc)_2.4H_2O$ (0.40 g, 1.61 mmol) in acetonitrile (10 cm^3) was added to a solution of $bnzH_2$ (0.75 g, 3.29 mmol), hepH (0.37 cm^3, 3.31 mmol) and triethylamine (1 cm^3, 7.5 mmol) in dichloromethane (10 cm^3). Methanol (10 cm^3) was added to solubilise the starting materials. After stirring for 30 min., the resulting solution was filtered, layered with hexane and left to stand. Pale-blue crystalline blocks of **13a** and **14a** were obtained by slow diffusion at ambient temperature after a few days (33%, 0.40 g, 0.53 mmol).

(ii) **13b** and **14b**: The procedure employed for **13a** and **14a** was adopted to synthesise **13b** and **14b**, using diphenylacetic acid (0.70 g, 3.32 mmol); the ratio of molar equivalents of the reagents was as described for **13a** and **14b**. Pale-blue crystalline blocks of **13b** and **14b** were obtained by slow diffusion at ambient temperature on standing after a few days (12%, 0.15 g, 0.20 mmol).

7.3.9 Synthesis of 15

$Ni(OAc)_2.4H_2O$ (0.40 g, 1.61 mmol) in acetonitrile (10 cm^3) was added to a solution of $bnzH_2$ (0.75 g, 3.29 mmol), hppH (0.42 cm^3, 3.27 mmol) and triethylamine (1 cm^3, 7.5 mmol) in dichloromethane (10 cm^3). Methanol (30 cm^3) was added to solubilise the starting materials. After stirring for 30 min., the remaining solution was filtered, concentrated to *ca.* 10 cm^3, re-filtered and left to stand. A pale green-yellow powder of **15** was obtained at ambient temperature after several months (6%, 0.07 g, 0.09 mmol).

7.3.10 Synthesis of 16

(i) **16a**: $Cu(OAc)_2 \cdot H_2O$ (0.32 g, 1.61 mmol) in acetonitrile (10 cm^3) was added to a solution of $bnzH_2$ (0.75 g, 3.29 mmol), Hchp (0.43 g, 3.32 mmol) and triethylamine (1 cm^3, 7.50 mmol) in dichloromethane (10 cm^3). Methanol (10 cm^3) was added to solubilise the starting materials. After stirring for 30 min., the remaining solution was filtered, layered with *n*-hexane and left to stand. Large dark-green crystalline blocks of **16a** were obtained by slow diffusion at ambient temperature after two months (60%, 0.40 g, 0.32 mmol).

(ii) **16b**: The procedure employed for **16a** was adopted to synthesise **16b**, using Hhp (0.31 g, 3.3 mmol); the ratio of molar equivalents of the reagents was as described for **16a**. Dark-green microcrystals of **16b** were obtained by slow diffusion at ambient temperature on standing after one day (23%, 0.14 g, 0.13 mmol).

7.3.11 Synthesis of 17

(i) **17a**: $Cu(OAc)_2 \cdot H_2O$ (0.32 g, 1.61 mmol) in acetonitrile (10 cm^3) was added to a solution of $bnzH_2$ (0.75 g, 3.29 mmol), hmpH (0.32 cm^3, 3.32 mmol) and triethylamine (1 cm^3, 7.50 mmol) in dichloromethane (10 cm^3). Methanol (10 cm^3) was added to solubilise the starting materials. After stirring for 30 min., the resulting solution was filtered, layered with *n*-hexane and left to stand. Large blue crystalline blocks of **17a** were obtained by slow diffusion at ambient temperature after one day (27%, 0.32 g, 0.43 mmol).

(ii) **17a'**: $Cu(OAc)_2 \cdot H_2O$ (0.03 g, 0.16 mmol) in acetonitrile (2 cm^3) was added to a solution of $bnzH_2$ (0.09 g, 0.39 mmol), mehmpH (0.06 cm^3, 0.48 mmol) and triethylamine (3 drops) in dichloromethane (2 cm^3). Methanol (2 cm^3) was added to solubilise the starting materials. After stirring for 30 min., the resulting solution was, layered with *n*-

hexane and left to stand. Large blue crystalline blocks of **17a'** were obtained by slow diffusion at ambient temperature after one day (5%, 5.6 mg, 7.34 μmol).

(iii) **17b**: The procedure employed for **17a** was adopted to synthesise **17b**, using diphenylacetic acid (0.70 g, 3.32 mmol); the ratio of molar equivalents of the reagents was as described for **17a**. Large blue crystalline blocks of **17b** were obtained by slow diffusion at ambient temperature on standing after one day (45%, 0.50 g, 0.71 mmol).

7.3.12 Synthesis of 18

(i) **18a**: $Cu(OAc)_2 \cdot H_2O$ (0.320 g, 1.61 mmol) in acetonitrile (10 cm^3) was added to a solution of $bnzH_2$ (0.75 g, 3.29 mmol), hepH (0.37 cm^3, 3.31 mmol) and triethylamine (1 cm^3, 7.50 mmol) in dichloromethane (10 cm^3). Methanol (10 cm^3) was added to solubilise the starting materials. After stirring for 30 min., the resulting solution was filtered, layered with *n*-hexane and left to stand. Large blue crystalline blocks of **18a** were obtained by slow diffusion at ambient temperature after one day (33%, 0.22 g, 0.27 mmol).

(i) **18b**: The procedure employed for **18a** was adopted to synthesise **18b**, using diphenylacetic acid (0.70 g, 3.32 mmol); the ratio of molar equivalents of the reagents was as described for **18a**. Blue microcrystals of **18b** were obtained by slow diffusion at ambient temperature on standing after one day (21%, 0.18 g, 0.23 mmol).

7.3.13 Synthesis of 19

$Cu(OAc)_2 \cdot H_2O$ (0.32 g, 1.61 mmol) in acetonitrile (10 cm^3) was added to a solution of $bnzH_2$ (0.75 g, 3.29 mmol), hppH (0.42 cm^3, 3.27 mmol) and triethylamine (1 cm^3, 7.50 mmol) in dichloromethane (10 cm^3). Methanol (10 cm^3) was added to solubilise the starting materials. After stirring for 30 min., the resulting solution was concentrated to *ca.*

2 cm^3, layered with diethyl ether and left to stand. Green solvent dependant crystals of **19** were obtained by slow diffusion at ambient temperature after four months (4%, 0.03 g, 0.04 mmol).

7.3.14 Synthesis of 20

$Cu(OAc)_2 \cdot H_2O$ (0.32 g, 1.61 mmol) in acetonitrile (10 cm^3) was added to a solution of diphenylacetic acid (0.70 g, 3.32 mmol), hppH (0.42 cm^3, 3.27 mmol) and triethylamine (1 cm^3, 7.50 mmol) in dichloromethane (10 cm^3). Methanol (10 cm^3) was added to solubilise the starting materials. After stirring for 30 min., the resulting solution was filtered, layered with *n*-hexane and left to stand. A blue microcrystalline powder of **20** was obtained by slow diffusion at ambient temperature after three days (3%, 0.02 g, 0.02 mmol).

7.3.15 Synthesis of 21

$Cu(OAc)_2 \cdot H_2O$ (0.32 g, 1.61 mmol) in acetonitrile (10 cm^3) was added to a solution of $bnzH_2$ (1.09 g, 4.78 mmol) and triethylamine (1 cm^3, 7.50 mmol) in dichloromethane (10 cm^3). Methanol (10 cm^3) was added to solubilise the starting materials. After stirring for 30 min., the resulting solution was filtered, concentrated to *ca.* 5 cm^3 and left to stand. Turquoise coloured crystals of **21** were obtained amongst a dark brown viscous solution by slow diffusion at ambient temperature after two months (10%, 0.14 g, 0.47 mmol).

7.3.16 Synthesis of 22

$Cu(OAc)_2 \cdot H_2O$ (0.32 g, 1.61 mmol) in acetonitrile (10 cm^3) was added to a solution of $bnzH_2$ (0.75 g, 3.29 mmol) and sodium methoxide (0.41 g, 7.50 mmol) in dichloromethane (10 cm^3). Methanol (10 cm^3) was added to solubilise the starting materials. After stirring for 30 min., the resulting solution was filtered, layered with *n*-hexane and left to stand.

Large blue-purple blocks of **22** were obtained by slow diffusion at ambient temperature after four days (15%, 0.18 g, 0.23 mmol).

Table 7 Spectroscopic and analytical data for the new complexes **9 – 12**

Compound	μ_{eff} (BM)[a]	IR data (cm^{-1})[b]	FAB mass spectrum (Da.)	Formula	Microanalysis (%)[c] C	H	N
9a/9b	9.70	ν(OH) 3433(w), 2932(w), 2825(w), 2476(w), 1591(s), 1532(m), 1489(w), 1446(s), 1377(s), 1345(s), 1209(w), 1166(s), 1071(w), 1045(s), 990(s), 943(s), 918(s), 873(w), 845(w), 813(w), 784(s), 775(s), 757(s), 735(s), 695(s), 675(s)	1400 [**9a** – $2HNEt_3$ – bnzH – chp]$^+$, 1302 [**9a** – $2HNEt_3$ – 2bnzH]$^+$, 1173 [**9a** – $2HNEt_3$ – 2bnzH – chp]$^+$, 1075 [**9a** – $2HNEt_3$ – 3bnzH]$^+$, 949 [**9a** – $2HNEt_3$ – 3bnzH – chp]$^+$	**9a** $Ni_4C_{90}H_{98}N_6O_{20}Cl_4$· **9b** $Ni_4C_{92}H_{102}N_6O_{20}Cl_4$[e]	54.61 (54.82)	5.17 (5.02)	4.44 (4.22)
10a/10b	d	ν(OH) 3433(w), 2983(w), 2631(w), 2492(w), 1585(s), 1527(m), 1443(s), 1376(s), 1344(s), 1287(w), 1246(w), 1212(w), 1164(s), 1132(w), 1086(w), 1070(w), 1045(s), 985(s), 943(w), 901(s), 856(w), 843(w), 813(w), 800(w), 774(s), 757(s), 684(s), 674(s), 698(s)	1480 [**10a** – $2HNEt_3$ – 2bnzH]$^+$, 1444 [**10a** – $2HNEt_3$ – 2bnzH – $2H_2O$]$^+$, 1307 [**10a** – $2HNEt_3$ – 2bnzH – bhp]$^+$, 1253 [**10a** – $2HNEt_3$ – 3bnzH]$^+$, 1209 [**10b** – $2HNEt_3$ – 2bnzH – Br – bhp – H_2O]$^+$, 1026 [**10a** – $2HNEt_3$ – 4bnzH]$^+$	**10a** $Ni_4C_{90}H_{98}N_6O_{20}Br_4$· **10b** $Ni_4C_{92}H_{102}N_6O_{20}Br_4$[e]	50.88 (50.74)	4.48 (4.65)	3.92 (3.90)
11a	6.23	ν(OH) 3411(w), 3059(w), 1606(s), 1571(s), 1484(s), 1446(s), 1386(s), 1357(s), 1289(s), 1238(w), 1218(w), 1166(s), 1152(s), 1076(s), 1048(s), 1033(s), 1024(s), 972(m), 947(w), 917(w), 846(w), 819(w), 798(w), 755(s), 733(s), 695(s), 673(s)	1575 [*M* – 2HOMe]$^+$, 1468 [*M* – 2HOMe – hmp]$^+$, 1347 [*M* – 2HOMe – bnzH]$^+$	$Ni_4C_{82}H_{76}N_4O_{18}$	59.77 (60.00)	4.63 (4.35)	3.41 (3.38)
11b	8.76	ν(OH) 3026(w), 1576(s), 1492(m), 1438(m), 1382(s), 1286(m), 1238(w), 1153(w), 1079(s), 1049(s), 1031(s), 955(w), 755(s), 739(s), 729(w), 695(w)	1512 [*M* – 2HOMe]$^+$, 1193 [*M* – 2HOMe – $Ph_2C\{H\}CO_2$ – hmp]$^+$, 1085 [*M* – 2HOMe – $Ph_2C\{H\}CO_2$ - hmp]$^+$	$Ni_4C_{82}H_{76}N_4O_{14}·2CH_2Cl_2$	57.58 (57.73)	4.67 (4.58)	3.44 (3.21)
12a	3.60	ν(OH) 3392(m), 3059(w), 2629(w), 1591(s), 1484(s), 1445(s), 1380(s), 1368(s), 1337(s), 1291(s), 1236(w), 1198(w), 1165(s), 1056(s), 1036(s), 997(w), 974(m), 946(m), 904(m), 840(w), 819(w), 798(s), 750(s), 695(s), 673(s)	622 [*M* – hmpH]$^+$, 503 [*M* – bnzH]$^+$	$NiC_{40}H_{36}N_2O_8$	65.61 (65.66)	4.85 (4.92)	3.63 (3.83)

[a]Recorded on an Evans Balance at room temperature. [b]Recorded on a Perkin-Elmer Spectrum One FT-IR spectrometer on solid samples. [c]Calculated values are shown in parentheses. [d]Not enough sample for analysis. [e]Desolvated sample (*cf.* to crystal structure).

Table 8 Spectroscopic and analytical data for the new complexes **12b – 16b**

Compound	μ_{eff} (BM)[a]	IR data (cm^{-1})[b]	FAB mass spectrum (Da.)	Formula	Microanalysis (%)[c] C	H	N
12b	2.83	ν(OH) 2923(w), 1954(w), 1603(m), 1571(s), 1531(s), 1490(s), 1451(m), 1435(s), 1387(s), 1361(s), 1336(m), 1287(s), 1248(m), 1095(s), 1081(s), 1052(s), 1033(s), 1000(s), 959(m), 873(w), 852(w), 823(w), 793(m), 771(s), 751(s), 705(s), 696(s)	699 $[M]^+$	$NiC_{40}H_{36}N_2O_6$	68.17 (68.67)	4.73 (5.15)	4.03 (4.01)
13a/14a	3.28	ν(OH) 3460(m), 3064(w), 2919(w), 2885(w), 2629(w), 2516(w), 1656(m), 1606(s), 1580(s), 1485(s), 1470(s), 1445(s), 1386(s), 1369(s), 1330(s), 1319(s), 1280(m), 1262(m),1234(w), 1202(w), 1183(m), 1168(s), 1158(s), 1109 (m), 1065(s), 1056(s), 1025(s), 1002(w), 988(w), 968(m), 932(m), 854(m), 792(s), 787(s), 768(s), 749(s), 695(s), 673(s)	636 $[M - hepH]^+$, 532 $[M - bnzH]^+$, 513 $[M - 2hepH]^+$, 409 $[M - hepH - bnzH]^+$	$NiC_{42}H_{40}N_2O_8$	66.38 (66.40)	5.45 (5.27)	3.76 (3.69)
13b/14b	3.50	ν(OH) 3062(w), 3023(w), 2583(w), 2423(w), 2289(w), 1604(s), 1572(s), 1549(s), 1506(w), 1492(s), 1481(s), 1446(s), 1384(s), 1365(s), 1318(s), 1288(w), 1257(w), 1236(w), 1189(m), 1107(m), 1078(m), 1064(s), 1027(s), 995(s), 968(w), 943(s), 904(w), 856(s), 809(w), 787(s), 770(s), 755(s), 745(s), 705(s), 695(s)	516 $[M - Ph_2C\{H\}CO_2]^+$	$NiC_{42}H_{40}N_2O_6$	68.88 (69.33)	5.64 (5.50)	3.95 (3.85)
15	4.13	ν(OH) 3058(w), 1568(s), 1488(m), 1411(s), 1343(s), 1168(w), 1050(m), 1031(m), 941(w), 913(w), 817(w), 754(s), 697(s), 674(s)	787 $[M]^+$, 560 $[M - bnzH]^+$, 331 $[M - 2bnzH]^+$	$NiC_{44}H_{44}N_2O_8 \cdot 4.5CH_2Cl_2$	49.88 (49.76)	4.94 (4.53)	2.10 (2.39)
16a	4.05	ν(OH) 3023(w), 2937(w), 2655(w), 1716(w), 1591(s), 1535(m), 1473(s), 1442(s), 1396(s), 1331(s), 1165(s), 1051(m), 1032(m), 1012(m), 983(m), 916(s), 823(m), 788(s), 759(s), 732(s), 695(s)	1139 $[M - NEt_3H - OH]^+$, 1129 $[M - chp]^+$, 1031 $[M - bnz]^+$, 929 $[M - NEt_3H - bnz]^+$, 800 $[M - NEt_3H - chp - bnz]^+$, 384 $[Cu_2 + 2chp]^+$	$Cu_3C_{54}H_{49}N_5O_{10}Cl_4$[d]	51.81 (51.51)	4.17 (3.90)	5.29 (5.56)
16b	3.93	ν(OH) 3037(w), 1654(w), 1603(s), 1568(m), 1554(s), 1544(m), 1477(s), 1428(s), 1342(s), 1278(m), 1246(w), 1157(m), 1112(w), 1043(w), 1010(s), 856s, 841s, 762s, 739s, 676w	714 $[M - NEt_3H - bnz - C_6H_5]^+$, 620 $[M - NEt_3H - bnz - C_6H_5 - hp]^+$	$Cu_3C_{54}H_{53}N_5O_{10} \cdot 2MeCN$	57.66 (57.90)	5.00 (4.91)	8.22 (8.15)

[a]Recorded on an Evans Balance at room temperature. [b]Recorded on a Perkin-Elmer Spectrum One FT-IR spectrometer on solid samples. [c]Calculated values are shown in parentheses. [d]Desolvated sample (*cf.* to crystal structure).

Table 9 Spectroscopic and analytical data for the new complexes **17a – 18b**

Compound	μ_{eff} (BM)[a]	IR data (cm^{-1})[b]	FAB mass spectrum (Da.)	Formula	Microanalysis (%)[c] C	H	N
17a	2.14	ν(OH) 3403(m), 3062(w), 2913(w), 1602(s), 1488(s), 1446(s), 1433(m), 1391(s), 1370(s), 1332(s), 1290(s), 1228(w), 1178(w), 1162(s), 1095(w), 1068(s), 1058(s), 1048(s), 1031(s), 1002(w), 990(w), 970(s), 944(w), 909(w), 894(w), 838(w), 814(w), 753(s), 737(s), 753(s), 710(s), 671(s)	508 $[M - bnzH]^+$	$CuC_{40}H_{36}N_2O_8$	65.22 (65.31)	4.77 (4.90)	3.72 (3.81)
17a'	2.26	ν(OH) 3418(m), 3057(w), 2981(w), 1710(w), 1596(s), 1484(s), 1444(s), 1391(s), 1368(s), 1325(s), 1292(s), 1225(w), 1251(w), 1181(w), 1156(s), 1188(w), 1104(s), 1096(s), 1079(w), 1057(s), 1024(s), 1002(w), 970(s), 943(w), 915(w), 899(w), 837(w), 788(m), 751(s), 736(s), 696(s), 671(s), 655(s)	413 $[M - mehmpH - bnzH]^+$	$0.8CuC_{42}H_{40}N_2O_8 \cdot 0.2CuC_{40}H_{36}N_2O_{10}$	65.96 (65.46)	4.98 (5.14)	3.50 (3.67)
17b	1.92	ν(OH) 3026(w), 2921(w), 2634(w), 1604(w), 1572(s), 1551(s), 1491(s), 1451(m), 1432(m), 1380(s), 1336(m), 1289(s), 1251(w), 1149(m), 1081(w), 1063(s), 1044(s), 1002(w), 979(m), 941(s), 908(w), 871(w), 839(w), 820(w), 791(w), 772(s), 752(s), 732(s), 706(s)	383 $[M - hmpH - Ph_2C\{H\}CO_2]^+$	$CuC_{40}H_{36}N_2O_6$	68.36 (68.28)	5.13 (5.12)	4.01 (3.98)
18a	2.03	ν(OH) 3384(m), 3056(w), 3019(w), 2896(w), 2849(w), 1625(s), 1605(s), 1596(s), 1484(s), 1444(s), 1358(s), 1332(s), 1323(s), 1307(s), 1247(w), 1226(w), 1178(m), 1162(s), 1109(s), 1099(m), 1072(s), 1058(s), 1048(s), 1030(s), 972(s), 941(w), 905(w), 875(s), 852(w), 806(s), 791(w), 765(s), 755(s), 732(s), 701(s), 695(s), 675(s)	824 $[M]^+$, 701 $[M - hepH]^+$, 597 $[M - bnz]^+$, 474 $[M - hepH - bnz]^+$, 370 $[M - 2bnz]^+$, 309 $[Cu + 2hepH]^+$	$Cu_2C_{42}H_{38}N_2O_8$	61.27 (61.17)	4.57 (4.61)	3.36 (3.40)
18b	2.42	ν(OH) 3364(w), 3069(w), 3027(w), 2945(w), 2909(w), 2848(m), 1593(s), 1580(s), 1564(s), 1493(s), 1470(w), 1482(s), 1445(s), 1420(w), 1366(s), 1345(s), 1309(s), 1251(s), 1222(s), 1191(w), 1161(s), 1114(s), 1079(s), 1052(s), 1029(s), 976(m), 956(w), 925(w), 879(s), 856(w), 839(w), 788(s), 775(s), 751(s), 725(s), 705(s), 691(s)	717 $[M - Ph]^+$, 396 $[M - Cu - hepH - Ph_2C\{H\}CO_2]^+$	$Cu_2C_{42}H_{38}N_2O_6 \cdot H_2O$	61.82 (62.22)	4.88 (4.94)	3.59 (3.46)

[a]Recorded on an Evans Balance at room temperature. [b]Recorded on a Perkin-Elmer Spectrum One FT-IR spectrometer on solid samples. [c]Calculated values are shown in parentheses.

Table 10 Spectroscopic and analytical data for the new complexes **19 – 22**

Compound	μ_{eff} (BM)[a]	IR data (cm^{-1})[b]	FAB mass spectrum (Da.)	Formula	Microanalysis (%)[c] C	H	N
19	2.42	ν(OH) 3417(m), 3056(w), 2859(w), 1637(s), 1609(s), 1568(m), 1486(m), 1443(s), 1315(s), 1278(s), 1217(w), 1181(w), 1165(w), 1048(s), 1025(s), 1002(w), 987(m), 940(w), 921(w), 823(s), 779(s), 759(s), 733(s), 700(s), 686(s)	852 $[M]^+$, 716 $[M - \text{hpp}]^+$, 625 $[M - \text{bnz}]^+$, 399 $[M - 2\text{bnz}]^+$	$Cu_2C_{44}H_{42}N_2O_8{\cdot}0.4CH_2Cl_2$	60.29 (60.14)	3.94 (4.83)	3.06 (3.16)
20	2.26	ν(OH) 3064(w), 2945(w), 2860(w), 1592(s), 1486(s), 1449(s), 1355(s), 1239(m), 1163(m), 1154(m), 1082(s), 1057(s), 1025(s), 945(s), 891(w), 823(w), 788(w), 767(s), 757(s), 745(s), 728(s), 706(s), 698(s)	684 $[M - \text{hpp}]^+$, 609 $[M - Ph_2C\{H\}CO_2]^+$, 548 $[M - 2\text{hpp}]^+$, 398 $[M - 2Ph_2C\{H\}CO_2]^+$	$Cu_2C_{44}H_{42}N_2O_6$	64.44 (64.39)	5.24 (5.12)	3.47 (3.41)
21	1.76	ν(OH) 3450(w), 3058(w), 3033(w), 2632(w), 2429(w), 1639(s), 1597(s), 1489(m), 1446(s), 1371(s), 1355(s), 1327(s), 1215(w0, 1163(s), 1157(s), 1087(w), 1048(s), 1031(m), 1003(w), 957(w), 940(w), 916(w), 821(w), 809(w), 775(s), 767(s), 757(s), 735(s), 683(m), 698(s), 671(s)	744 $[M - NEt_3H]^+$, 744 $[M - NEt_3H]^{-d}$	$CuC_{48}H_{49}NO_9{\cdot}NEt_3$	68.59 (68.65)	5.80 (6.86)	3.02 (2.96)
22	2.11	ν(OH) 3397(m), 2932(m), 2902(m), 2847(m), 1637(s), 1606(s), 1562(s), 1483(m), 1438(s), 1389(s), 1356(s), 1273(s), 1273(m), 1220(w), 1156(m), 1079(s), 1060(s), 1025(s), 949(s), 940(s), 867(w), 823(s), 767(s), 747(s), 700(s), 663(s)	737 $[M_{(n=1)} - \text{MeOH}]^+$, 604 $[\text{Cu} + 2\text{bnz} + 2\text{Na} + \text{MeCN}]^+$, 581 $[\text{Cu} + 2\text{bnz} + \text{Na} + \text{MeCN}]^+$, 563 $[\text{Cu} + 2\text{bnz} + 2\text{Na}]^+$, 540 $[\text{Cu} + 2\text{bnz} + \text{Na}]^+$, 517 $[\text{Cu} + 2\text{bnz}]^+$	$CuNa_2C_{36}H_{42}N_2O_{10}{\cdot}CH_2Cl_2{\cdot}H_2O$	50.83 (50.68)	5.19 (5.48)	2.84 (3.20)

[a]Recorded on an Evans Balance at room temperature. [b]Recorded on a Perkin-Elmer Spectrum One FT-IR spectrometer on solid samples. [c]Calculated values are shown in parentheses. [d]FAB negative ion peak.

Table 11 Characterisation of conversion products

Compound	Converted from	IR data (cm^{-1})[a]	NMR data (13 – 55 ppm)[b]	Formula	Microanalysis (%)[c] C	H	N
11a	-	ν(OH) 3411(w), 3059(w), 1606(s), 1571(s), 1484(s), 1446(s), 1386(s), 1357(s), 1289(s), 1238(w), 1218(w), 1166(s), 1152(s), 1076(s), 1048(s), 1033(s), 1024(s), 972(m), 947(w), 917(w), 846(w), 819(w), 798(w), 755(s), 733(s), 695(s), 673(s)	45.0 ($H_{\beta/\beta'}$), 43.0 ($H_{\beta/\beta'}$), 41.0($H_{\beta/\beta'}$), 38.0 ($H_{\beta/\beta'}$), 17.0 (H_{γ}), 14.0 (H_{γ})	$Ni_4C_{82}H_{76}N_4O_{18}$	59.77 (60.00)	4.63 (4.35)	3.41 (3.38)
11a	**12a**	3375(w), 2922(w), 1619(s), 1572(m), 1481(m), 1439(m), 1384(s), 1348(s), 1287(s), 1217(w), 1164(s), 1078(s), 1048(s), 967(w), 938(w), 911(w), 804(w), 749(s), 738(s), 696(s), 672(s)	45.0 ($H_{\beta/\beta'}$), 44.0 ($H_{\beta/\beta'}$), 41.0($H_{\beta/\beta'}$), 38.0 ($H_{\beta/\beta'}$), 17.5 (H_{γ}), 14.5 (H_{γ})	$Ni_4C_{82}H_{76}N_4O_{18}\cdot 2CH_2Cl_2$	55.69 (60.00)	4.73 (4.35)	3.09 (3.38)

[a]Recorded on a Perkin-Elmer Spectrum One FT-IR spectrometer on solid samples. [b]Recorded on a Bruker DPX-300 NMR spectrometer approximate values are shown all peaks are broad. [c]Calculated values are shown in parentheses.

Table 12 Crystallographic and data processing parameters for complexes **9 – 12b**

Complex	9a/9b	10a/10b	11a	11b	12a	12b
J. Fawcett code	03195	04061	03090	03058	03152	03085
Formula	$C_{95}H_{106}Cl_4N_8Ni_4O_{20}$	$C_{95}H_{106}Br_4N_8Ni_4O_{20}$	$C_{41}H_{38}N_2Ni_2O_9$	$C_{84}H_{81}Cl_4N_4Ni_4O_{14.5}$	$C_{40}H_{36}N_2NiO_8$	$C_{40}H_{36}N_2NiO_6$
M	2056.52	2234.36	820.15	877.58	731.42	699.42
Crystal size (mm)	0.24 × 0.19 × 0.08	0.29 × 0.20 × 0.13	0.25 × 0.24 × 0.24	0.30 × 0.28 × 0.19	0.31 × 0.21 × 0.08	0.26 × 0.22 × 0.06
Temperature (K)	150(2)	150(2)	150(2)	293(2)	150(2)	150(2)
Crystal system	Triclinic	Triclinic	Monoclinic	Monoclinic	Monoclinic	Triclinic
Space group	*P*-1	*P*-1	C_2c	C_2c	C_2c	*P*-1
Lattice parameters						
a (Å)	13.179(5)	13.179(5)	21.399(13)	21.9386(16)	15.4179(16)	9.5236(14)
b (Å)	15.834(5)	15.834(5)	16.471(10)	17.3464(16)	9.6183(16)	9.9782(14)
c (Å)	25.738(9)	25.738(9)	22.915(14)	22.5313(18)	23.226(3)	10.0697(14)
α (°)	83.435(7)	83.435(7)	90	90	90	66.022(2)
β (°)	80.451(6)	80.451(6)	99.850(11)	102.454(2)	92.079(3)	84.238(2)
γ (°)	68.085(6)	68.085(6)	90	90	90	68.231(2)
U (Å^3)	4906(3)	4906(3)	7958(8)	8372.7(12)	3442.1(8)	
Z	2	2	8	4	4	1
D_c (Mg m^{-3})	1.392	1.513	1.369	1.392	1.411	1.433
F(000)	2144	2288	3408	3636	1528	366
μ (Mo-K$_\alpha$) (mm^{-1})	0.936	2.456	1.002	1.078	0.622	0.652
Reflections collected	35546	38229	18926	30656	12958	4665
Independent reflections	17115	18995	6890	8207	3370	3003
R_{int}	0.0831	0.0770	0.0535	0.0352	0.0816	0.0191
Parameters/ restraints	1017/0	1114/0	462/0	500/0	280/0	224/0
Final R indices						
R_1; wR_2 [I>2σ(I)]	0.0692; 0.1639	0.0691; 0.1725	0.0546; 0.1373	0.0482; 0.1447	0.0544; 0.1191	0.0372; 0.0858
R_1; wR_2 (All data)	0.1071; 0.1799	0.1169; 0.1883	0.0756; 0.1479	0.0688; 0.1537	0.0599; 0.1219	0.0414; 0.0884
Goodness of fit on F^2 (all data)	0.9304	1.003	1.016	1.005	1.188	1.019

Data in common: graphite-monochromated Mo-K$_\alpha$ radiation, λ = 0.71073 Å; $R_1 = \Sigma||F_o| - |F_c||/\Sigma|F_o|$, $wR_2 = [\Sigma w(F_o^2 - F_c^2)^2/\Sigma w(F_o^2)^2]^{1/2}$, $w^{-1} = [\sigma^2(F_o)^2 + (aP)^2]$, $P = [\max(F_o^2,0) + 2(F_c^2)]/3$, where a is a constant adjusted by the program; goodness of fit = $[\Sigma(F_o^2 - F_c^2)2/(n-p)]^{1/2}$ where n is the number of reflections and p the number of parameters.

Table 13 Crystallographic and data processing parameters for complexes **13a – 17a'**

Complex	13a	14a	16a	17a	17a'
J. Fawcett code	03175	04107	03218	03067	04042
Formula	$C_{42}H_{40}N_2NiO_8$	$C_{42}H_{40}N_2NiO_8$	$C_{58}H_{63}Cl_4Cu_3N_5O_{14}$	$C_{40}H_{36}CuN_2O_8$	$C_{41.6}H_{38.4}N_2O_{8.4}Cu$
M	759.48	759.47	1386.55	736.25	764.28
Crystal size (mm)	0.35 × 0.14 × 0.05	0.22 × 0.13 × 0.12	0.29 × 0.12 × 0.11	0.35 × 0.25 × 0.24	0.38 × 0.10 × 0.05
Temperature (K)	150(2)	150(2)	150(2)	150(2)	150(2)
Crystal system	Monoclinic	Monoclinic	Monoclinic	Monoclinic	Triclinic
Space group	$P2_1/n$	$P2_1c$	$P2_1c$	$C2/c$	P-1
Lattice parameters					
a (Å)	12.892(4)	17.188(2)	11.1442(17)	16.6822(18)	9.1479(18)
b (Å)	10.381(3)	14.9908(17)	15.567(2)	9.0559(10)	9.3222(18)
c (Å)	13.811(4)	28.533(3)	35.368(6)	22.667(3)	12.268(2)
α (°)	90	90	90	90	79.339(3)
β (°)	105.348(5)	94.634(2)	91.329(3)	92.553	78.536(3)
γ (°)	90	90	90	90	64.863(3)
U (Å^3)	1782.5(9)	7327.9(14)	6134.1(16)	3420.9(6)	922.3(3)
Z	2	8	4	4	1
D_c (Mg m^{-3})	1.415	1.377	1.501	1.430	1.376
F(000)	796	3184	2852	1532	398
μ (Mo-K$_\alpha$) (mm^{-1})	0.603	0.587	1.272	0.697	0.650
Reflections collected	12293	45311	47662	13051	6849
Independent reflections	3134	10543	12068	3361	3560
R_{int}	0.0758	0.0961	0.0429	0.0225	0.0387
Parameters/restraints	242/0	955/0	769/0	233/0	251/0
Final R indices					
R_1; wR_2 [$I>2\sigma(I)$]	0.0547; 0.1200	0.0500; 0.0978	0.0491; 0.1316	0.0338; 0.0895	0.0540; 0.1182
R_1; wR_2 (All data)	0.0824; 0.1314	0.0865; 0.1068	0.0644; 0.1380	0.0365; 0.0911	0.0675; 0.1229
Goodness of fit on F^2 (all data)	1.001	0.939	1.032	1.037	1.009

Data in common: graphite-monochromated Mo-K$_\alpha$ radiation, $\lambda = 0.71073$ Å; $R_1 = \Sigma||F_o| - |F_c||/\Sigma|F_o|$, $wR_2 = [\Sigma w(F_o^2 - F_c^2)^2/\Sigma w(F_o^2)^2]^{1/2}$, $w^{-1} = [\sigma^2(F_o)^2 + (aP)^2]$, $P = [\max(F_o^2,0) + 2(F_c^2)]/3$, where a is a constant adjusted by the program; goodness of fit = $[\Sigma(F_o^2 - F_c^2)2/(n-p)]^{1/2}$ where n is the number of reflections and p the number of parameters.

Table 14 Crystallographic and data processing parameters for complexes **17b – 22**

Complex	17b	18a	19	20	21	22
J. Fawcett code	03054	04007	04067	03083	04160	03214
Formula	$C_{40}H_{36}CuN_2O_6$	$C_{21}H_{19}CuNO_4$	$C_{22}H_{21}CuNO_4$	$C_{22}H_{21}CuNO_3$	$C_{48}H_{49}CuNO_9$	$C_{36}H_{42}CuN_2Na_2O_{10}$
M	704.25	412.91	426.94	410.94	847.42	772.24
Crystal size (mm)	0.33 × 0.27 × 0.13	0.22 × 0.16 × 0.15	0.30 × 0.11 × 0.10	0.30 × 0.19 × 0.15	0.20 × 0.16 × 0.10	0.23 × 0.14 × 0.09
Temperature (K)	150(2)	150(2)	150(2)	150(2)	150(2)	150(2)
Crystal system	Triclinic	Monoclinic	Monoclinic	Orthorhombic	Triclinic	Triclinic
Space group	*P*-1	$P2_1/c$	$P2_1/n$	*Pbca*	*P*-1	*P*-1
Lattice parameters						
a (Å)	9.6335(11)	10.6459(8)	9.9606(15)	15.8647(16)	11.2399(17)	8.2637(7)
b (Å)	9.9915(11)	23.8826(19)	9.1471(14)	11.2223(11)	15.201(2)	10.8529(9)
c (Å)	10.0640(11)	7.4625(6)	21.088(3)	20.806(2)	15.710(2)	12.3444(11)
α (°)	67.856(2)	90	90	90	69.555(3)	99.4220(10)
β (°)	84.376(2)	108.5790(10)	95.326(2)	90	77.472(4)	108.0300(10)
γ (°)	65.594(2)	90	90	90	87.369(3)	107.6010(10)
U (Å^3)	815.15(16)	1798.5(2)	1913.1(5)	3704.4(6)	2454.0(7)	962.18(14)
Z	1	4	4	8	2	1
D_c (Mg m^{-3})	1.435	1.525	1.482	1.474	1.147	1.333
F(000)	367	852	884	1704	890	403
μ (Mo-K$_\alpha$) (mm^{-1})	0.723	1.242	1.170	1.201	0.495	0.646
Reflections collected	6458	13504	13864	27332	19425	7030
Independent reflections	3168	3525	3746	3634	9553	3367
R_{int}	0.0211	0.0416	0.0885	0.0306	0.0606	0.0207
Parameters/restraints		245/0	253/0	244/0	502/0	232/0
Final R indices						
R_1; wR_2 [I>2σ(I)]	0.0384; 0.1018	0.0332; 0.0832	0.0670; 0.1503	0.0281; 0.0722	0.1441; 0.3957	0.0344; 0.0859
R_1; wR_2 (All data)	0.0418; 0.1037	0.0377; 0.0852	0.0985; 0.1646	0.0344; 0.0744	0.2040; 0.4274	0.0384; 0.0881
Goodness of fit on F^2 (all data)	1.073	1.062	1.055	0.979	1.271	1.084

Data in common: graphite-monochromated Mo-K$_\alpha$ radiation, λ = 0.71073 Å; $R_1 = \Sigma||F_o| - |F_c||/\Sigma|F_o|$, $wR_2 = [\Sigma w(F_o^2 - F_c^2)^2/\Sigma w(F_o^2)^2]^{1/2}$, $w^{-1} = [\sigma^2(F_o)^2 + (aP)^2]$, $P = [\max(F_o^2,0) + 2(F_c^2)]/3$, where a is a constant adjusted by the program; goodness of fit = $[\Sigma(F_o^2 - F_c^2)2/(n-p)]^{1/2}$ where n is the number of reflections and p the number of parameters.

7.4 Compounds in Chapter 4

7.4.1 Synthesis of 23

(i) **23a**: $Ni(OAc)_2 \cdot 4H_2O$ (0.40 g, 1.61 mmol) in acetonitrile (10 cm^3) was added to a solution of *m*-$BDCH_2$ (0.55 g, 3.31 mmol), hmpH (0.32 cm^3, 3.32 mmol) and triethylamine (1 cm^3, 7.5 mmol) in dichloromethane (10 cm^3). Methanol (10 cm^3) was added to solubilise the starting materials. After stirring for 30 min., the resulting solution was filtered, layered with *n*-hexane and left to stand. Large pale-green crystalline blocks of **23a** were obtained at ambient temperature by slow diffusion after a few days (18%, 0.36 g, 0.04 mmol).

(ii) **23a'**: The procedure employed for **23a** was adopted to synthesise **23a'**, using mehmpH (0.40 cm^3, 3.30 mmol); the ratio of molar equivalents of the reagents was as described for **23a**. Pale green microcrystals of **23a'** was obtained by slow diffusion at ambient temperature on standing after one week (8%, 0.06 g, 0.06 mmol).

(iii) **23b**: The procedure employed for **23a** was adopted to synthesise **23b**, using hepH (0.37 cm^3, 3.31 mmol); the ratio of molar equivalents of the reagents was as described for **23a**. Large blocks of pale-blue crystals of **23b** were obtained at ambient temperature by slow diffusion on standing after five days (35%, 0.26 g, 0.28 mmol).

7.4.2 Synthesis of 24

$Ni(OAc)_2 \cdot 4H_2O$ (0.40 g, 1.61 mmol) in acetonitrile (10 cm^3) was added to a solution of *m*-$BDCH_2$ (0.55 g, 3.31 mmol), hepH (0.20 cm^3, 1.83 mmol) and triethylamine (1 cm^3, 7.5 mmol) in dichloromethane (10 cm^3). Methanol (10 cm^3) was added to solubilise the starting materials. After stirring for 30 min., the resulting solution was filtered, layered

with *n*-hexane and left to stand. Large blocks of pale-blue crystals of **24** were obtained at ambient temperature by slow diffusion after a few days (29%, 0.22 g, 0.47 mmol).

7.4.3 Synthesis of 25

$Ni(OAc)_2 \cdot 4H_2O$ (0.40 g, 1.61 mmol) in acetonitrile (10 cm^3) was added to a solution of *m*-$BDCH_2$ (0.55 g, 3.31 mmol), hppH (0.42 cm^3, 3.27 mmol) and triethylamine (1 cm^3, 7.5 mmol) in dichloromethane (10 cm^3). Methanol (10 cm^3) was added to solubilise the starting materials. After stirring for 30 min., the resulting solution was filtered, layered with *n*-hexane and left to stand. A pale yellow solid of **25** was obtained at ambient temperature by slow diffusion after several months (5%, 0.04 g, 0.08 mmol).

7.4.4 Synthesis of 26

(i) **26**: $Cu(OAc)_2 \cdot H_2O$ (0.32 g, 1.61 mmol) in acetonitrile (10 cm^3) was added to a solution of *m*-$BDCH_2$ (0.55 g, 3.31 mmol), hmpH (0.32 cm^3, 3.32 mmol) and triethylamine (1 cm^3, 7.5 mmol) in dichloromethane (10 cm^3). Methanol (10 cm^3) was added to solubilise the starting materials. After stirring for 30 min., the resulting solution was filtered, layered with *n*-hexane and left to stand. Large blue crystal blocks of **26** were obtained at ambient temperature by slow diffusion after a few days (14%, 0.10 g, 0.22 mmol).

(ii) **26'**: The procedure employed for **26** was adopted to synthesise **26'**, using mehmpH (0.40 cm^3, 3.25 mmol); the ratio of molar equivalents of the reagents was as described for **26**. Large blue crystal blocks of **26'** were obtained at ambient temperature by slow diffusion on standing after a few months (14%, 0.10 g, 0.22 mmol).

7.4.5 Synthesis of 3 from 26

Complex **26** (0.71 g, 0.22 mmol), Hchp (0.43 g, 3.33 mmol), triethylamine (1 cm^3, 7.5 mmol) in a 1: 1: 1 solvent mixture of acetonitrile: dichloromethane: methanol (30 cm^3) was heated to 50 °C and stirred. After 1 h, the solution was filtered and left to stand. Blue crystals of **3** were obtained by slow diffusion at room temperature after two months (6%, 0.03 g, 0.1 mmol).

7.4.6 Synthesis of 27

$Cu(OAc)_2 \cdot H_2O$ (0.32 g, 1.61 mmol) in acetonitrile (10 cm^3) was added to a solution of *m*-$BDCH_2$ (0.55 g, 3.31 mmol), hmpH (0.32 cm^3, 3.32 mmol) sodium azide (0.21 g, 3.23 mmol) and triethylamine (1 cm^3, 7.5 mmol) in dichloromethane (10 cm^3). Methanol (10 cm^3) was added to solubilise the starting materials. After stirring for 30 min., the resulting solution was filtered, layered with *n*-hexane and left to stand. Blue crystalline needles of **27** were obtained at ambient temperature by slow diffusion after two weeks (4%, 0.03 g, 0.06 mmol).

7.4.7 Synthesis of 28

$Cu(OAc)_2 \cdot H_2O$ (0.32 g, 1.61 mmol) in acetonitrile (10 cm^3) was added to a solution of *m*-$BDCH_2$ (0.55 g, 3.31 mmol), hepH (0.37 cm^3, 3.31 mmol) and triethylamine (1 cm^3, 7.5 mmol) in dichloromethane (10 cm^3). Methanol (10 cm^3) was added to solubilise the starting materials. After stirring for 30 min., the resulting solution was filtered, layered with *n*-hexane and left to stand. Large blocks of dark-blue crystals of **28** were obtained at ambient temperature by slow diffusion after one day (13%, 0.15 g, 0.20 mmol).

7.4.8 Synthesis of 29

$Cu(OAc)_2 \cdot H_2O$ (0.32 g, 1.61 mmol) in acetonitrile (10 cm^3) was added to a solution of *m*-$BDCH_2$ (0.55 g, 3.31 mmol), hppH (0.42 cm^3, 3.27 mmol) and triethylamine (1 cm^3, 7.5 mmol) in dichloromethane (10 cm^3). Methanol (10 cm^3) was added to solubilise the starting materials. After stirring for 30 min., the resulting solution was filtered, layered with *n*-hexane and left to stand. A turquoise powder of **29** was obtained at ambient temperature by slow evaporation after one day (9%, 0.06 g, 0.12 mmol).

7.4.9 Synthesis of 26 from 29

Complex **29** (0.06 g, 0.12 mmol), hmpH (0.20 cm^3, 2.08 mmol) and triethylamine (3 drops) was added to a 1: 1: 1 solvent mixture of acetonitrile: dichloromethane: methanol (10 cm^3). After 30 min. of stirring, the resulting blue solution was filtered and left to stand. Blue crystalline blocks of **26** were obtained at ambient temperature by slow evaporation after two months (15%, 0.02 g, 0.04 mmol).

7.4.10 Synthesis of 30

$Cu(OAc)_2 \cdot H_2O$ (0.32 g, 1.61 mmol) in acetonitrile (10 cm^3) was added to a solution of *m*-$BDCH_2$ (0.27 g, 1.63 mmol), 1,10-*N,N*-phenanthroline (0.19 g, 0.93 mmol) and triethylamine (1 cm^3, 7.5 mmol) in dichloromethane (10 cm^3). Methanol (10 cm^3) was added to solubilise the starting materials. After stirring for 30 min., the resulting solution was filtered, layered with *n*-hexane and left to stand. Blue crystalline blocks of **30** were obtained at ambient temperature by slow diffusion after one day (6%, 0.06 g, 0.01 mmol).

7.4.11 Synthesis of 31

(i) **31a**: $Cu(OAc)_2 \cdot H_2O$ (0.32 g, 1.61 mmol) in acetonitrile (10 cm^3) was added to a solution of *m*-$BDCH_2$ (0.27 g, 1.63 mmol), *N,N'*-bis(2,4,6-trimethylphenyl)formamidine

(0.46 g, 1.64 mmol) and triethylamine (1 cm^3, 7.5 mmol) in dichloromethane (10 cm^3). Methanol (10 cm^3) was added to solubilise the starting materials. After stirring for 30 min., the resulting solution was filtered and left to stand. Green crystalline blocks of **31a** suitable for single crystal X-ray diffraction analysis were obtained at ambient temperature by slow diffusion after several months (43%, 0.26 g, 0.03 mmol).

(ii) **31b**: $Cu(OAc)_2 \cdot H_2O$ (0.96 g, 4.83 mmol) in acetonitrile (30 cm^3) was added to a solution of *m*-$BDCH_2$ (0.81 g, 4.89 mmol), *N,N'*-bis(2-methylphenyl)formamidine (1.10 g, 4.92 mmol) and triethylamine (3 cm^3, 22.5 mmol) in dichloromethane (30 cm^3). Methanol (30 cm^3) was added to solubilise the starting materials. After stirring for 30 min., the resulting solution was filtered and left to stand. Green crystalline blocks of **31b** suitable for single crystal X-ray diffraction analysis were obtained at ambient temperature by slow diffusion after one week (57%, 0.96 g, 0.11 mmol).

7.4.12 Synthesis of 31c and 32

$Cu(OAc)_2 \cdot H_2O$ (0.96 g, 4.83 mmol) in acetonitrile (30 cm^3) was added to a solution of *m*-$BDCH_2$ (0.81 g, 4.89 mmol), *N,N'*-bis(2,6-dimethylphenyl)formamidine (1.24 g, 4.92 mmol) and triethylamine (3 cm^3, 22.5 mmol) in dichloromethane (30 cm^3). Methanol (30 cm^3) was added to solubilise the starting materials. After stirring for 30 min., the resulting solution was filtered, layered with *n*-hexane and left to stand. A green powder of **31c** (4 %, 0.07 g, 8.06 μmol) and blue crystalline blocks of **32** (18 %, 0.64 g, 0.88 mmol) suitable for single crystal X-ray diffraction analysis were obtained at ambient temperature by slow diffusion after one week.

Table 15 Spectroscopic and analytical data for the new complexes **23a – 25**

Compound	μ_{eff} (BM)[a]	IR data (cm^{-1})[b]	FAB mass spectrum (Da.)	Formula	Microanalysis (%)[c] C	H	N
23a	4.17	ν(OH) 3449(w), 3031(w), 2413(w), 2923(w), 1992(w), 1605(s), 1573(m), 1538(s), 1477(m), 1430(s), 1382(s), 1359(s), 1288(m), 1267(m), 1239(m), 1154(s), 1059(s), 1039(s), 988(m), 950(m), 889(m), 820(w), 808(m), 757(s), 737(s), 726(s), 656(s)	882 $[M]^+$, 773 $[M - hmpH]^+$, 718 $[M - m\text{-}BDC]^+$, 664 $[M - 2hmpH]^+$, 609 $[M - hmpH - m\text{-}BDC]^+$, 500 $[M - 2hmpH - m\text{-}BDC]^+$	$Ni_2C_{40}H_{36}N_4O_{12}\cdot 2CH_2Cl_2\cdot 0.5H_2O$	47.29 (47.55)	3.76 (3.40)	5.32 (5.28)
23a'	8.26	ν(OH) 3363(w), 2969(w), 1980(w), 1737(w), 1603(s), 1574(m), 1534(m), 1481(w), 1466(w), 1455(w), 1437(s), 1385(s), 1367(s), 1344(s), 1308(w), 1284(m), 1247(w), 1233(w), 1221(w), 1163(m), 1090(s), 1075(m), 1049(s), 1020(s), 901(w), 854(w), 841(w), 803(w), 788(w), 769(m), 746(s), 704(s), 657(s)	938 $[M]^+$, 815 $[M - mehmpH]^+$, 774 $M - m\text{-}BDC]^+$, 692 $[M - 2mehmpH]^+$, 651 $[M - mehmpH - m\text{-}BDC]^+$	$Ni_2C_{44}H_{44}N_4O_{12}\cdot 0.5CH_2Cl_2$	54.60 (54.46)	4.50 (4.59)	5.82 (5.71)
23b	4.75	ν(OH) 4667(w), 3089(w), 2358(w), 2089(w), 1604(s), 1571(m), 1537(s), 1485(m), 1436(s), 1388(s), 1359(s), 1264(m), 1151(m), 1107(w), 1065(s), 1024(s), 897(m), 803(w), 785(m), 767(s), 734(s), 726(s), 657(m)	938 $[M]^+$, 815 $[M - hepH]^+$, 651 $[M - hepH - m\text{-}BDC]^+$	$Ni_2C_{44}H_{44}N_4O_{12}\cdot 0.5CH_2Cl_2\cdot 0.5H_2O$	54.14 (53.97)	4.94 (4.65)	5.52 (5.66)
24	2.78	ν(OH) 3423(s), 2939(w), 2826(w), 2636(w), 1604(s), 1541(s), 1479(m), 1437(m), 1385(s), 1358(s), 1315(s), 1271(m), 1155(m), 1105(w), 1074(m), 1060(m), 1029(s), 966(w), 925(w), 887(w), 841(w), 802(s), 785(s), 763(s), 748(s), 726(s), 658(s)	346 $[M_{(n=1)} - hepH]^+$, 182 $[M_{(n=1)} - hepH - m\text{-}BDC]^+$	$NiC_{22}H_{22}N_2O_6$[d]	56.26 (56.29)	4.85 (4.69)	5.75 (5.97)
25	3.16	ν(OH) 3347(m), 2288(w), 2111(w), 1984(w), 1603(s), 1542(s), 1480(s), 1437(s), 1375(s), 1271(w), 1155(w), 1075(w), 1019(w), 936(w), 884(w), 834(w), 807(m), 744(s), 769(s)	343 $[M - hppH - OH]^+$	$NiC_{24}H_{26}N_2O_6\cdot 5CH_2Cl_2\cdot 4MeOH\cdot 2CH_3CO_2H$	37.76 (37.95)	5.30 (5.47)	1.60 (2.39)

[a]Recorded on an Evans Balance at room temperature. [b]Recorded on a Perkin-Elmer Spectrum One FT-IR spectrometer on solid samples. [c]Calculated values are shown in parentheses. [d]Desolvated sample (*cf.* to crystal structure).

Table 16 Spectroscopic and analytical data for the new complexes **26 – 29**

Compound	μ_{eff} (BM)[a]	IR data (cm^{-1})[b]	FAB mass spectrum (Da.)	Formula	Microanalysis (%)[c] C	H	N
26	2.37	ν(OH) 3421(m), 2812(w), 1607(s), 1566(s), 1480(m), 1441(m), 1350(s), 1283(s), 1272(m), 1226(m), 1154(m), 1070(s), 1061(s), 1046(s), 1028(s), 935(w), 897(w), 838(w), 814(m), 762(s), 742(s), 716(s), 683(s), 659(s)	445 $[M_{(n=1)}]^+$, 336 $[M_{(n=1)} - \text{hmpH}]^+$, 281 $[M_{(n=1)} - m\text{-BDC}]^+$	$CuC_{20}H_{18}N_2O_6 \cdot CH_2Cl_2$	47.29 (47.55)	3.76 (3.40)	5.32 (5.28)
26'	1.75	ν(OH) 3080(w), 2979(w), 2875(w), 2687(w), 2495(w), 1706(w), 1605(s), 1575(m), 1548(s), 1485(m), 1426(s), 1400(s), 1374(s), 1290(s), 1268(w), 1223(w), 1160(s), 1154(s), 1117(m), 1095(m), 1107(w), 1076(m), 1055(m), 1023(m), 949(m), 886(w), 846(w), 809(w), 794(w), 771(s), 755(s), 711(s), 653(s)	186 $[M_{(n=1)} - \text{mempH} - m\text{-BDC}]^+$	$CuC_{22}H_{22}N_2O_6$	55.85 (55.81)	4.61 (4.65)	5.73 (5.92)
27	1.83	ν(OH) 3456(w), 3016(m), 2970(m), 2790(w), 2654(w),ν(C=O) 1738(s), 1600(s), 1574(m), 1542(s), 1489(m), 1435(s), 1382(s), 1293(w), 1266 (w), 1229(s), 1217(s), 1155(w), 1092(w), 1072(m), 1047(s), 997(w), 942(m), 897(w), 802(s), 765(s), 739(s), 712(s), 657(s)	445 $[M]^+$	$CuC_{20}H_{18}N_2O_6 \cdot 0.25CH_2Cl_2 \cdot 0.5H_2O$	51.64 (51.13)	3.23 (4.10)	5.26 (5.89)
28	2.32	ν(OH) 3388(w), 2989(w), 2876(w), 1601(s), 1554(s), 1494(w), 1468(w), 1451(w), 1425(w), 1360(s), 1256(m), 1169(m), 1123(w), 1080(m), 1052(s), 1024(s), 1001(w), 974(w), 929(w), 873(w), 840(m), 785(s), 770(s), 752(s), 700(s), 660(s)	350 $[M_{(n=1)} - \text{hepH}]^+$, 227 $[M_{(n=1)} - 2\text{hepH}]^+$	$CuC_{22}H_{22}N_2O_6$	55.32 (55.82)	4.98 (4.65)	5.62 (5.92)
29	2.96	ν(OH) 3078(w), 2950(w), 2895(w), 2837(w), 1696(m), 1600(s), 1563(s), 1488(m), 1476(w), 1434(m), 1386(s), 1355(s), 1327(s), 1311(s), 1266(s), 1169(m), 1152(m), 1075(s), 1044(s), 1000(w), 970(w), 932(s), 876(w), 842(w), 827(m), 774(s), 746(s), 705(s), 658(s)	337 $[M_{(n=1)} - m\text{-BDC}]^+$, 320 $[M_{(n=1)} - \text{hppH} - CO_2]^+$, 200 $[M_{(n=1)} - m\text{-BDC} - \text{hppH}]^+$	$CuC_{24}H_{26}N_2O_6 \cdot 1.5CH_2Cl_2$	48.99 (48.69)	4.06 (4.61)	3.91 (4.46)

[a]Recorded on an Evans Balance at room temperature. [b]Recorded on a Perkin-Elmer Spectrum One FT-IR spectrometer on solid samples. [c]Calculated values are shown in parentheses.

Table 17 Spectroscopic and analytical data for the new complexes **30 – 32**

Compound	μ_{eff} (BM)[a]	IR data (cm^{-1})[b]	MALDI mass spectrum (Da.)	Formula	Microanalysis (%)[c] C	H	N
30	2.44	3064(w), 1607(s), 1556(s), 1479(w), 1388(s), 1162(w), 1077(w), 1033(w), 873(w), 853(m), 749(s), 726(s), 664(s)	588 $[M]^+$,[d] 423 $[M - m\text{-BDC}]^+$,[d] 408 $[M - \text{phen}]^{+d}$	$CuC_{32}H_{20}N_4O_4{\cdot}4H_2O$[e]	58.11 (58.27)	4.90 (4.25)	8.96 (8.50)
31a	6.50	ν(NH) 3323(w), 2920(w), ν(C=N) 1634(s), 1580(m), 1481(w), 1451(w), 1388(s), 1314(w), 1274(w), 1207(w), 1158(w), 1102(w), 1076(w), 1010(w), 944(w), 895(w), 851(w), 832(w), 803(w), 743(s), 726(s), 664(s)	3540 $[M - 12\text{HDmesF} - 12H_2O - 7\text{Cu} - 9m\text{-BDC}]^+$, 3048 $[M - 12\text{HDmesF} - 12H_2O - 7\text{Cu} - 12m\text{-BDC}]^+$, 2502 $[M - 12\text{HDmesF} - 12H_2O - 13\text{Cu} - 13m\text{-BDC}]^+$, 3429 $[M - 12\text{HDmesF} - 12H_2O - 9\text{Cu} - 15m\text{-BDC}]^+$, 2011 $[M - 12\text{HDmesF} - 12H_2O - 13\text{Cu} - 16m\text{-BDC}]^+$, 1619 $[M - 12\text{HDmesF} - 12H_2O - 14\text{Cu} - 18m\text{-BDC}]^+$	$Cu_{24}C_{420}H_{408}N_{24}O_{108}$[e]	55.93 (55.85)	4.45 (4.52)	3.85 (3.72)
31b	6.97	ν(NH) 3275(w), 2986(w), ν(C=N) 1634(s), 1579(m), 1552(w), 1481(w), 1451(w), 1387(s), 1275(w), 1159(w), 1077(w), 1029(w), 944(w), 832(w), 744(s), 726(s), 664(s)	4238 $[M - 12\text{HD}o\text{-tolF} - 12H_2O - 14\text{Cu} - 2m\text{-BDC}]^+$, 3128 $[M - 12\text{HD}o\text{-tolF} - 12H_2O - 16\text{Cu} - 8m\text{-BDC}]^+$, 2472 $[M - 12\text{HD}o\text{-tolF} - 12H_2O - 16\text{Cu} - 12m\text{-BDC}]^+$, 1299 $[M - 12\text{HD}o\text{-tolF} - 12H_2O - 19\text{Cu} - 18m\text{-BDC}]^+$, 1236 $[M - 12\text{HD}o\text{-tolF} - 12H_2O - 20\text{Cu} - 18m\text{-BDC}]^+$, 1072 $[M - 12\text{HD}o\text{-tolF} - 12H_2O - 20\text{Cu} - 19m\text{-BDC}]^+$, 1009 $[M - 12\text{HD}o\text{-tolF} - 12H_2O - 21\text{Cu} - 19m\text{-BDC}]^+$	$Cu_{24}C_{372}H_{312}N_{24}O_{108}{\cdot}5CH_2Cl_2$	51.60 (51.54)	3.32 (3.67)	3.93 (3.83)
31c	5.46	ν(NH) 3325 (w), 2921 (w), 2666(w), 2327(w), 2115(w), 1996(w), ν(C=N) 1635(s), 1557(m), 1474(w), 1447(w), 1389(s), 1274(w), 1197(w), 1159(w), 1091(w), 1075(w), 1032(w), 944(w), 831(w), 769(w), 743(s), 726(s), 993(w)	1236 $[M - 12\text{HD2,6-xylF} - 12H_2O - 20\text{Cu} - 18m\text{-BDC}]^+$, 1072 $[M - 12\text{HD2,6-xylF} - 12H_2O - 20\text{Cu} - 19m\text{-BDC}]^+$, 845 $[M - 12\text{HD2,6-xylF} - 12H_2O - 21\text{Cu} - 20m\text{-BDC}]^+$, 782 $[M - 12\text{HD2,6-xylF} - 12H_2O - 22\text{Cu} - 20m\text{-BDC}]^+$	$Cu_{24}C_{396}H_{360}N_{24}O_{108}{\cdot}6CH_2Cl_2$	52.51 (52.45)	3.09 (4.04)	3.93 (3.65)
32	1.58	ν(NH) 3364(w), 2919(w), ν(C=N) 1626(s), 1616(s), 1584(s), 1470(m), 1372(s), 1353(s), 1300(s), 1266(w), 1203(w), 1166(m), 1090(w), 1069(w), 1030(w), 9889w), 965(w), 942(w), 924(w), 908(w), 826(w), 791(w), 778(m), 768(m), 742(s), 725(s), 676(w), 664(w)	794 $[M_{(n=2)} - m\text{-BDC}]^+$, 719 $[\text{Cu} + 4m\text{-BDC}]^+$, 567 $[M_{(n=2)} - 2m\text{-BDC}]^+$	$CuC_{42}H_{44}N_4O_4$	69.02 (68.95)	5.85 (6.02)	7.56 (7.66)

[a]Recorded on an Evans Balance at room temperature. [b]Recorded on a Perkin-Elmer Spectrum One FT-IR spectrometer on solid samples. [c]Calculated values are shown in parentheses. [d]Recorded using FAB mass spectrometry. [e]Desolvated sample (*cf.* to crystal structure).

Table 18 Characterisation of conversion products

Compound	Converted from	IR data (cm^{-1})[a]	Formula	Microanalysis (%)[b] C	H	N
3	-	3363(w), 3073(w), 2832(w), 1638(m), 1607(m), 1585(s), 1529(m), 1486(m), 1470(w), 1442(s), 1432(s), 1388(s), 1360(m), 1339(s), 1312(s), 1289(s), 1244(w), 1218(w), 1187(w), 1154(s), 1132(m), 1096(w), 1072(s), 1050(s), 1032(s), 974(s), 910(s), 856(w), 817(w), 777(s), 766(s), 718(s), 698(s), 666(s)	$CuC_{11}H_9O_2Cl_1N_2$	44.04 (44.07)	3.17 (3.01)	9.22 (9.35)
3	**26**	3073(w), 2832(w), 1609(w), 1585(s), 1529(m), 1486(m), 1432(s), 1406(m), 1388(s), 1360(w), 1340(s), 1289(m), 1257(w), 1243(w), 1218(w), 1157(s), 1073(s), 1049(s), 1032(w), 974(s), 910(s), 885(w), 856(w), 823(w), 778(s), 767(s), 718(s), 698(s), 669(s), 653(s)	$CuC_{11}H_9O_2Cl_1N_2 \cdot 0.5NEt_3$	48.17 (47.93)	2.85 (4.71)	9.76 (9.99)
26	-	ν(OH) 3421(m), 2812(w), 1607(s), 1566(s), 1480(m), 1441(m), 1350 (s), 1283(s), 1272(m), 1226(m), 1154(m), 1070(s), 1061(s), 1046(s), 1028(s), 935(w), 897(w), 838(w), 814(m), 762(s), 742(s), 716(s), 683(s), 659(s)	$CuC_{20}H_{18}N_2O_6 \cdot CH_2Cl_2$	47.29 (47.55)	3.76 (3.40)	5.32 (5.28)
26	**29**	ν(OH) 3257(w), 3066(w), 2824(w), 1607(s), 1565(s), 1482(w), 1441(w), 1354(s), 1284(w), 1270(w), 1225(w), 1154(w), 1075(s), 1049(s), 1029(w), 993(w), 941(w), 902(w), 816(w), 806(w), 750(s), 715(s), 673(s), 656(s)	$CuC_{20}H_{18}N_2O_6$	53.62 (53.43)	3.89 (4.04)	6.25 (6.29)

[a]Recorded on a Perkin-Elmer Spectrum One FT-IR spectrometer on solid samples. [b]Calculated values are shown in parentheses.

Table 19 Crystallographic and data processing parameters for complexes **23a – 28**

Complex	23a	23b	24	26	27	28
J. Fawcett code	03142	03071	03114	03042	03105	03080
Formula	$C_{43}H_{39}N_{5.50}Ni_2O_{12}$	$C_{45}H_{46}Cl_2N_4Ni_2O_{12}$	$C_{23}H_{26}N_2Ni_1O_7$	$C_{21}H_{20}Cl_2Cu_1N_2O_6$	$C_{20}H_{18}CuN_2O_6$	$C_{11}H_{11}Cu_{0.5}N_1O_3$
M	942.71	1023.19	501.17	529.82	445.90	336.98
Crystal size (mm)	0.30 × 0.24 × 0.18	0.38 × 0.33 × 0.30	0.23 × 0.14 × 0.08	0.30 × 0.29 × 0.10	0.18 × 0.16 × 0.05	0.26 × 0.25 × 0.10
Temperature (K)	150(2)	150(2)	150(2)	290(2) K	150(2)K	150(2)K
Crystal system	Triclinic	Monoclinic	Monoclinic	Monoclinic	Monoclinic	Monoclinic
Space group	*P*-1	$P2_1/n$	$P2_1/c$	$P2_1/n$	$P2_1/n$	$C2/c$
Lattice parameters						
a (Å)	11.018(7)	14.1506(10)	20.2592(17)	10.004(2)	12.872(2)	14.0138(15)
b (Å)	13.849(9)	22.8058(15)	7.7255(6)	13.418(3)	6.9234(11)	9.3276(10)
c (Å)	15.092(10)	16.6937(11)	15.7326(13)	17.223(3)	20.293(3)	15.7405(11)
α (°)	91.685(11)	90	90	90	90	90
β (°)	102.361(10)	112.4590(10)	111.5990(10)	102.720(3)	93.363(3)	100.901(2)
γ (°)	104.394(11)	90	90	90	90	90
U (Å^3)	2165(2)	4978.7(6)	2289.4(3)	2255.1(8)	1805.4(5)	2020.4(4)
Z	2	4	4	4	4	8
D_c (Mg m^{-3})	1.584	1.509	1.454	1.561	1.641	1.558
F(000)	976	2120	1048	1080	916	980
μ (Mo-K$_\alpha$) (mm^{-1})	0.938	0.925	0.894	1.246	1.253	1.125
Reflections collected	16688	38547	17407	15943	13686	7568
Independent reflections	8368	9787	4512	3953	3554	1998
R_{int}	0.1044	0.0380	0.0400	0.0371	0.0454	0.0218
Parameters/restraints	542/0	613/0	303.0	289.0	262.0	144.0
Final R indices						
R_1; wR_2 [I>2σ(I)]	0.0994; 0.2447	0.0718; 0.2334	0.038; 0.0729	0.0567; 0.1543	0.0417; 0.1006	0.0277; 0.0775
R_1; wR_2 (All data)	0.1567; 0.2748	0.0854; 0.2474	0.0600; 0.0800	0.0608; 0.1579	0.0533; 0.1064	0.0304; 0.0791
Goodness of fit on F^2 (all data)	1.036	1.041	1.065	1.070	0.960	1.101

Data in common: graphite-monochromated Mo-K$_\alpha$ radiation, λ = 0.71073 Å; $R_1 = \Sigma||F_o| - |F_c||/\Sigma|F_o|$, $wR_2 = [\Sigma w(F_o^2 - F_c^2)^2/\Sigma w(F_o^2)^2]^{1/2}$, $w^{-1} = [\sigma^2(F_o)^2 + (aP)^2]$, $P = [\max(F_o^2,0) + 2(F_c^2)]/3$, where a is a constant adjusted by the program; goodness of fit = $[\Sigma(F_o^2 - F_c^2)2/(n-p)]^{1/2}$ where n is the number of reflections and p the number of parameters.

Table 20 Crystallographic and data processing parameters for complexes **30 – 32**

Complex	**30**	**31a**	**31b**	**32**
J. Fawcett code	03030	04025	04200	04193
Formula	$C_{33}H_{34}Cl_2CuN_4O_{10}$	$C_{424}H_{438}Cu_{24}N_{26}O_{120}$	$C_{372}H_{312}Cu_{24}N_{24}O_{108}$	$C_{21}H_{22}Cu_{0.50}N_2O_2$
M	781.08	9343	8371.49	366.18
Crystal size (mm)	0.25 × 0.17 × 0.10	0.33 × 0.31 × 0.29	0.37 × 0.15 × 0.13	0.26 × 0.14 × 0.11
Temperature (K)	150(2)	150(2)	150(2)	150(2)
Crystal system	Triclinic	Triclinic	Triclinic	Monoclinic
Space group	*P*-1	*P*-1	*P*-1	*C2c*
Lattice parameters				
a (Å)	11.2568(8)	25.361(3)	23.803(9)	15.523(2)
b (Å)	11.8253(9)	26.213(3)	25.711(10)	17.594(3)
c (Å)	14.5054(10)	27.684(3)	44.210(16)	14.821(2)
α (°)	73.6670(10)	111.353(2)	88.973(7)	90
β (°)	79.7020(10)	101.272(2)	82.586(7)	115.285(2)
γ (°)	69.5700(10)	112.384(3)	68.432(7)	90
U (Å^3)	1729.4(2)	24608(3)	24939(160	3659.8(10)
Z	2	1	2	8
D_c (Mg m^{-3})	1.500	1.073	1.136	1.329
F(000)	806	4820	8544	1540
μ (Mo-K$_\alpha$) (mm^{-1})	0.849	0.916	1.065	0.645
Reflections collected	12674	105636	195645	14115
Independent reflections	6060	50965	96706	3604
R_{int}	0.0324	0.1140	0.4186	0.0287
Parameters/restraints	433/0	2212/0	1769/0	237/0
Final R indices				
R_1; wR_2 [I>2σ(I)]	0.0539; 0.1536	0.1159; 0.3200	0.1628; 0.3999	0.0344; 0.0914
R_1; wR_2 (All data)	0.0609; 0.1580	0.2709; 0.3743	0.5636; 0.5456	0.0421; 0.0947
Goodness of fit on F^2 (all data)	1.071	0.934	0.756	1.023

Data in common: graphite-monochromated Mo-K$_\alpha$ radiation, λ = 0.71073 Å; $R_1 = \Sigma||F_o| - |F_c||/\Sigma|F_o|$, $wR_2 = [\Sigma w(F_o^2 - F_c^2)^2/\Sigma w(F_o^2)^2]^{½}$, $w^{-1} = [\sigma^2(F_o)^2 + (aP)^2]$, $P = [\max(F_o^2,0) + 2(F_c^2)]/3$, where a is a constant adjusted by the program; goodness of fit = $[\Sigma(F_o^2 - F_c^2)2/(n - p)]^{1/2}$ where n is the number of reflections and p the number of parameters.

7.5 Compounds in Chapter 5

7.5.1 Synthesis of 33

The complex $[Fe_2OCl_6][NEt_4]_2$ (0.25 g, 0.42 mmol), sodium phenylacetate (0.13 g, 0.80 mmol) and sodium 6-chloro-2-pyridonate (0.19 g, 1.25 mmol) in acetonitrile (25 cm^3) were stirred for 2 h. The resulting red solution was filtered into four portions and ethylacetate (3 drops) was added to each portion. Large red rhombic crystals of **33** were obtained on standing after two months of crystallisation at – 25 °C (22%, 0.11 g, 0.05 mmol).

7.5.2 Synthesis of 34

The complex $[Fe_2OCl_6][NEt_4]_2$ (0.25 g, 0.42 mmol), sodium *para*-methylbenzoate (0.13 g, 0.80 mmol) and sodium 6-chloro-2-pyridonate (0.19 g, 1.25 mmol) were stirred in acetonitrile (25 cm^3) for 2 h. The resulting red solution was filtered into four portions and ethylacetate (3 drops) was added to each portion. Red crystalline blocks of **34** were obtained on standing after one week at – 25 °C, (13%, 0.08 g, 0.028 mmol).

7.5.3 Synthesis of 35

The complex $[Fe_2OCl_6][NEt_4]_2$ (0.25 g, 0.42 mmol), sodium diphenylacetate (0.40 g, 1.71 mmol) and sodium 2-hydroxymethylpyridinol (0.83 g, 6.33 mmol) were stirred in acetonitrile for 2 h. The resulting brown-red solution was filtered into four portions and tetrahydrofuran (3 drops) was added to each portion. After one month at – 25 °C, red blocks of crystals of **35** were obtained (17%, 0.05 g, 0.02 mmol).

7.5.4 Synthesis of 36

The complex $[Fe_2OCl_6][NEt_4]_2$ (0.25 g, 0.42 mmol), sodium diphenylacetate (0.28 g, 1.20 mmol), 2-hydroxyethylpyridinol (0.13 cm^3, 1.20 mmol) and sodium methoxide (0.10 g, 1.85 mmol) were stirred in acetonitrile for 2 h. The resulting brown-red solution was

filtered into four portions and diethyl ether (3 drops) was added to each portion. After one month at – 25 °C, brown crystalline blocks of **36** were obtained (10%, 0.04 g, 0.01 mmol).

7.5.5 Synthesis of 37

The complex $[Fe_2OCl_6][NEt_4]_2$ (0.25 g, 0.42 mmol), 2-hydroxymethylpyridinol (0.12 cm^3, 1.20 mmol) and sodium 2-chloro-6-pyridonate (0.12 g, 0.80 mmol) were stirred in acetonitrile for 2 h. The resulting yellow solution was filtered into four portions and diethyl ether (3 drops) was added to each portion. After one week at – 25 °C, red crystalline blocks of **37** were obtained (10%, 0.02 g, 0.01 mmol).

7.5.6 Synthesis of 38

(i) **3a**: The complex $[Fe_2OCl_6][NEt_4]_2$ (0.25 g, 0.42 mmol), sodium diphenylacetate (0.28 g, 1.20 mmol) and 1,10- phenanthroline (0.08 g, 0.44 mmol) were stirred in acetonitrile (25 cm^3) for 2 h. The resulting red solution was filtered into four portions and acetone (3 drops) was added to each portion. After one week at 0 °C, dark-brown crystalline blocks of **38a** were obtained (56%, 0.19 g, 0.10 mmol).

(ii) **38b**: The procedure employed for **38a** was adopted to synthesise **38b**, using sodium phenylacetate (0.19 g, 1.20 mmol); the ratio of molar equivalents of the reagents was as described for **38a**. After one week at 0 °C, dark-brown crystalline blocks of **38b** were obtained (73%, 0.23 g, 0.15 mmol).

(iii) **38c**: The procedure employed for **38a** was adopted to synthesise **38c**, using sodium propionate (0.12 g, 1.20 mmol); the ratio of molar equivalents of the reagents was as described for **38a**. After two months at 0 °C, small dark-brown crystals of **38c** were obtained (8%, 0.02 g, 0.02 mmol).

Table 21 Spectroscopic and analytical data for the new complexes **33** and **34**

Compound	μ_{eff} (BM)[a]	IR data[b] (cm^{-1})	ESI Mass spectrum (Da.)		Formula	Microanalysis (%)[c] C	H	N
33	17.89	1392(s), 1338(w), 1251(w), 1175(w), 1156(w), 1108(w), 1076(w), 1047(w), 1031(w), 1003(w), 968(w), 912(w), 883(w), 844(w), 783(s), ν(Fe-O) 741(s), ν(OH) 3059(w), 3026(w), ν(C≡N) 1951(w), 1567(s), 1493(m), 1451(w), 694(s)	3009 $[M]^+$, 2968 $[M - MeCN]^+$, 2950 $[M - MeCN - H_2O]^+$, 2927 $[M - 2MeCN]^+$, 2981 $[M - 2MeCN - 2H_2O]^+$, 2874 $[M - PhCH_2CO_2]^+$, 2845 $[M - 2MeCN - 2H_2O - 2Na]^+$, 2833 $[M - MeCN - PhCH_2CO_2]^+$, 2775 $[M - 2MeCN - chp - Na]^+$, 2723 $[M - 2MeCN - PhCH_2CO_2 - 2Na]^+$, 2668 $[M - MeCN - 2H_2O - chp - PhCH_2CO_2]^+$, 2616 $[M - MeCN - 2H_2O - 2PhCH_2CO_2 - 2Na]^+$	2536 $[M - MeCN - 2H_2O - chp - 2PhCH_2CO_2]^+$, 2566 $[M - MeCN - 3PhCH_2CO_2]^+$, 1452 $[M - 2MeCN - 6PhCH_2CO_2 - 5chp - Na]^+$, 1228 $[M - 2MeCN - 4chp - 8PhCH_2CO_2 - 2Na]^+$, 1121 $[M - 2MeCN - 4chp - 9PhCH_2CO_2 - 2Na - 2O]^+$, 956 $[M - 2MeCN - H_2O - 6chp - 8PhCH_2CO_2 - 2Na - Fe]^+$, 918 $[M - 2MeCN - 2H_2O - 4chp - 10PhCH_2CO_2 - 2Na - 4O]^+$, 793 $[M - 2MeCN - 5chp - 10PhCH_2CO_2 - 2Na - 6O]^+$, 686 $[M - 2MeCN - H_2O - 6chp - 10PhCH_2CO_2 - 2Na - Fe]^+$, 628 $[M - 2MeCN - 2H_2O - 6chp - 10PhCH_2CO_2 - 2Na - 6O]^+$, 588 $[M - 2MeCN - 2H_2O - 6chp - 10PhCH_2CO_2 - 2Na - 5O - Fe]^+$	$Fe_{10}Na_2C_{114}H_{96}O_{38}Cl_6N_8 \cdot 3H_2O$[d]	44.53 (44.66)	3.19 (3.53)	3.45 (3.66)
34	8.16	ν(OH) 3036, 1738(w), 1649(w), 1598(s), 1554(s), 1513(w), 1473(w), 1438(w), 1400(s), 1295(w), 1248(w), 1229(w), 1216(w), 1182(s), 1151(w), 1117(w), 1078(w), 1032(w), 1019(w), 985(w), 965(w), 919(w), 854(w), ν(Fe-O) 767, 729(w), 693(w)	2839 $[M]^+$, 2659 $[M - p\text{-}CH_3C_6H_4CO_2 - 3Me]^+$, 2539 $[M - 2p\text{-}CH_3C_6H_4CO_2 - 2Me]^+$, 2404 $[M - 3p\text{-}CH_3C_6H_4CO_2 - 2Me]^+$, 1429 $[M - 10p\text{-}CH_3C_6H_4CO_2 - 4Me]^+$, 1444 $[M - 10p\text{-}CH_3C_6H_4CO_2 - 3Me]^+$, 1360 $[M - 11p\text{-}CH_3C_6H_4CO_2]^+$,	1329 $[M - 11p\text{-}CH_3C_6H_4CO_2 - 2Me]^+$, 1294 $[M - 11p\text{-}CH_3C_6H_4CO_2 - 4Me]^+$, 1249 $[M - 11p\text{-}CH_3C_6H_4CO_2 - 7Me]^+$, 1189 $[M - 12p\text{-}CH_3C_6H_4CO_2 - 2Me]^+$, 1129 $[M - 12p\text{-}CH_3C_6H_4CO_2 - 6Me]^+$, 1084 $[M - 13p\text{-}CH_3C_6H_4CO_2]^+$, 1026 $[M - 13p\text{-}CH_3C_6H_4CO_2 - Fe]^+$	$Fe_{11}C_{120}H_{111}O_{42}$[d]	50.64 (50.70)	3.80 (3.91)	– –

[a]Recorded on an Evans Balance at room temperature. [b]Recorded on a Perkin-Elmer Spectrum One FT-IR spectrometer on solid samples. [c]Calculated values are shown in parentheses. [d]Desolvated sample (*cf.* to crystal structure).

Table 22 Spectroscopic and analytical data for the new complexes **35 – 37**

Compound	μ_{eff} (BM)[a]	IR data (cm^{-1})[b]	MALDI Mass spectrum (Da.)	Formula	Microanalysis (%)[c] C	H	N
35	8.96	ν(OH) 3061(w), 3025(w), 1737(w), 1572(s), 1493(m), 1450(w), 1392(s), 1277(w), 1249(w), 1230(w), 1216(w), 1156(w), 1109(w), 1076(w), 1031(w), 1003(w), 985(w), 968(w), 911(w), 883(w), 844(w), 793(w), 741(s), ν(Fe-O) 694(s)	2666 [M – MeOH – $2Ph_2C\{H\}CO_2$]$^+$, 2167 [M – MeOH – $4Ph_2C\{H\}CO_2$ – Ph]$^+$, 2120 [M – MeOH – $4Ph_2C\{H\}CO_2$ – hmp – O]$^+$, 1909 [M – MeOH – $5Ph_2C\{H\}CO_2$ – hmp – O]$^+$, 1709 [M – MeOH – $5Ph_2C\{H\}CO_2$ – 3hmp]$^+$, 1632 [M – MeOH – $5Ph_2C\{H\}CO_2$ – 3hmp – Ph]$^+$, 1498 [M – MeOH – $6Ph_2C\{H\}CO_2$ – 3hmp]$^+$, 1421 [M – MeOH – $6Ph_2C\{H\}CO_2$ – 3hmp – Ph]$^+$, 1313 [M – MeOH – $6Ph_2C\{H\}CO_2$ – 4hmp – Ph]$^+$, 1102 [M – MeOH – $7Ph_2C\{H\}CO_2$ – 4hmp – Ph]$^+$	$Fe_8C_{165}H_{140}O_{31}N_4$[e]	64.15 (63.46)	4.00 (4.49)	1.48 (1.79)
36	12.42	ν(OH) 3639(w), 3380(w), 3060(w), 3025(w), 2845(w), 1953(w), 1574(s), 1492(m), 1451(w), 1393(s), 1337(w), 1250(w), 1174(w), 1156(w), 1108(w), 1075(m), 1047(w), 1031(w), 1003(w), 969(w), 911(w), 882(w), 845(w), 783(w), 742(s), ν(Fe-O) 695(s)	1896 [M – $4Ph_2C\{H\}CO_2$ – O]$^+$, 1608 [M – $5Ph_2C\{H\}CO_2$ – O – Ph]$^+$, 1320 [M – $6Ph_2C\{H\}CO_2$ – O – 2Ph]$^+$, 1502 [M – $5Ph_2C\{H\}CO_2$ – hep – Ph]$^+$, 1490 [M – $6Ph_2C\{H\}CO_2$]$^+$, 1413 [M – $6Ph_2C\{H\}CO_2$ – Ph]$^+$, 1202 [M – $7Ph_2C\{H\}CO_2$ – Ph]$^+$, 1125 [M – $7Ph_2C\{H\}CO_2$ – 2Ph]$^+$	$Fe_6C_{154}H_{128}O_{26}N_2 \cdot 2MeCN \cdot 19H_2O$[e]	59.53 (59.62)	4.77 (5.41)	2.00 (1.76)
37	8.46	ν(OH) 3354(m), 1608(s), 1570(w), 1483(m), 1439(s), 1360(w), 1286(m), 1222(w), 1156(w), 1070(s), 1048(s), 1022(s), 822(w), 757(s), 719(m), ν(Fe-O) 671(s)	871 [M – 4Cl – 4hmp]$^{+d}$	$Fe_6C_{48}H_{48}O_{10}N_8Cl_6 \cdot Et_2O \cdot 6H_2O$	38.00 (38.35)	2.58 (4.30)	6.62 (6.88)

[a]Recorded on an Evans Balance at room temperature. [b]Recorded on a Perkin-Elmer Spectrum One FT-IR spectrometer on solid samples. [c]Calculated values are shown in parentheses. [d]Recorded using FAB mass spectrometry. [e]Desolvated sample (*cf.* to crystal structure).

Table 23 Spectroscopic and analytical data for the new complexes **38a – 38c**

Compound	μ_{eff} (BM)[a]	IR data (cm^{-1})[b]	FAB Mass spectrum (Da.)	Formula	Microanalysis (%)[c] C	H	N
38a	4.08	ν(OH) 3384(w), 3059(w), 3025(w), 1564(s), 1517(m), 1492(m), 1451(w), 1426(m), 1391(s), 1255(w), 1224(w), 1175(w), 1141(w), 1104(w), 1077(w), 1032(w), 1003(w), 966(w), 911(w), 869(m), 846(s), 744(s), 724(s), ν(Fe-O) 696(s)	2036 $[M]^+$, 1883 $[M - 2MeCN - 2Cl]^+$, 1825 $[M - Ph_2CHCO_2]^+$, 1672 $[M - 2MeCN - 2Cl - Ph_2CHCO_2]^+$, 1286 $[M - 2MeCN - Cl - 3Ph_2CHCO_2]^+$	$Fe_4C_{108}H_{82}O_{14}Cl_2N_4 \cdot 2MeCN$	66.40 (66.01)	4.33 (4.32)	3.07 (4.13)
38b	4.65	ν(OH) 3059(w), 3027(w), 1596(s), 1558(s), 1517(s), 1494(m), 1453(w), 1426(s), 1392(s), 1347(m), 1293(w), 1223(w), 1173(w), 1142(w), 1104(w), 1031(w), 1003(w), 961(w), 909(w), 869(w), 842(m), 723(s), ν(Fe-O) 696(s)	1426 $[M - 2Cl]^+$, 1246 $[M - phen - 2Cl]^+$, 1111 $[M - phen - PhCH_2CO_2 - 2Cl]^+$, 976 $[M - phen - 2PhCH_2CO_2 - 2Cl]^+$, 862 $[M - phen - 3PhCH_2CO_2 - Cl - CH_3]^+$, 777 $[M - phen - 4PhCH_2CO_2]^+$	$Fe_4C_{72}H_{58}O_{14}Cl_2N_4$[d]	57.72 (57.72)	3.79 (3.87)	3.64 (3.74)
38c	4.39	ν(OH) 3365(w), 2977(w), 1625(w), 1578(w),1546(s), 1509(s), 1463(s),1423(s), 1370(m), 1336(w), 1294(w), 1241(w), 1224(w), 1206(w), 1140(w), 1102(m), 1075(w), 1043(w), 1001(w), 902(w), 880(w), 867(w), 847(w), 813(w), 786(w), 775(w), 743(w), ν(Fe-O) 723(s), 678(w), 663(w)	1086 $[M - CH_3CH_2]^+$, 1027 $[M - EtCO_2 - CH_3]^+$, 954 $[M - 2EtCO_2 - CH_3]^+$, 877 $[M - phen - 2CH_2CH_3]^+$, 745 $[M - 2EtCO_2 - phen - CH_3 - CH_2CH_3]^+$, 735 $[M - 5EtCO_2 - CH_3]^+$, 624 $[M - 2phen - EtCO_2 - 2CH_2CH_3]^+$, 524 $[M - 2phen - 2Cl - EtCO_2 - 3CH_2CH_3]^+$	$Fe_4C_{42}H_{36}O_{14}Cl_2N_4$	44.53 (45.20)	3.77 (3.23)	4.94 (5.02)

[a]Recorded on an Evans Balance at room temperature. [b]Recorded on a Perkin-Elmer Spectrum One FT-IR spectrometer on solid samples. [c]Calculated values are shown in parentheses. [d]Desolvated sample (*cf.* to crystal structure).

Table 24 Crystallographic and data processing parameters for complexes **33 – 38c**

Complex	33	34	35	36	37	38a	38b	38c
J. Fawcett code	04021	02026	04062	03184	03180	02067	02068	02095
Formula	$C_{132}H_{125}Cl_6Fe_{10}N_{17}Na_2O_{38}$	$C_{150}H_{156}Fe_{11}N_{15}O_{42}$	$C_{340}H_{300}Fe_{16}N_{12}O_{64}$	$C_{89}H_{81}Fe_3N_7O_{13}$	$C_{48}H_{56}Cl_6Fe_6N_8O_{14}$	$C_{112}H_{88}Cl_2Fe_4N_6O_{14}$	$C_{76}H_{64}Cl_2N_6O_{14}Fe_4$	$C_{42}H_{40}Cl_2Fe_4N_4O_{14}$
M	3374.67	3455.25	6467.49	1624.16	1516.80	2036.18	1579.63	1119.08
Crystal size (mm)	0.31 × 0.30 × 0.27	0.28 × 0.18 × 0.16	0.29 × 0.20 × 0.13	0.23 × 0.20 × 0.16	0.23 × 0.19 × 0.16	0.36 × 0.32 × 0.23	0.31 × 0.18 × 0.07	0.36 × 0.34 × 0.28
Temperature (K)	150(2)	150(2)	150(2)	150(2)	150(2)	150(2)	150(2)	150(2)
Crystal system	Monoclinic	Triclinic	Triclinic	Triclinic	Triclinic	Monoclinic	Monoclinic	Rhombohedral
Space group	$P2_1/n$	P-1	P-1	P-1	P-1	$P2_1/c$	$P2_1/c$	R-3
Lattice parameters								
a (Å)	19.7017(17)	17.164(2)	17.1255(12)	14.8683(8)	14.323(4)	15.9131(8)	14.564(4)	33.1366(12)
b (Å)	16.8661(14)	19.126(2)	30.594(2)	16.5792(9)	16.132(4)	16.1030(8)	17.970(5)	33.1366(12)
c (Å)	24.221(2)	25.693(3)	33.717(2)	19.2912(10)	18.861(5)	37.6161(19)	26.881(7)	28.1992(18)
α (°)	90	84.743(2)	115.372(2)	64.8900(10)	73.633(4)	90	90	90
β (°)	106.2050(10)	84.796(2)	90.0110(10)	89.5770(10)	67.687(4)	100.7020	99.146(5)	90
γ (°)	90	74.692(3)	106.2390(10)	69.7170(10)	68.094(4)	90	90	120
U (Å^3)	7728.6(11)	8079.9(18)	15177.8(19)	3983.9(4)	3690.8(16)	9471.4(8)	6946(3)	26815(2)
Z	2	2	2	2	2	4	4	18
D_c (Mg m^{-3})	1.450	1.420	1.419	1.354	1.365	1.428	1.511	1.247
F(000)	3448	3566	6704	1692	1540	4208	3248	10260
μ (Mo-K$_\alpha$) (mm^{-1})	1.096	1.036	0.820	0.608	1.420	0.728	0.968	1.098
Reflections collected	55411	58514	109911	28721	28852	73012	52194	65271
Independent reflections	13598	28203	52943	13878	14296	18555	13637	10458
R_{int}	0.0369	0.0539	0.1293	0.0644	0.0733	0.0498	0.1017	0.1138
Parameters/restraints	931/0	1993/0	3411/0	1075/0	739/0	1243/0	921/0	622/0
Final R indices								
R_1; wR_2 [I>2σ(I)]	0.0449; 0.1483	0.0556; 0.1323	0.0955;0.2126	0.0545; 0.1320	0.1376; 0.3904	0.0612; 0.1528	0.0812; 0.1943	0.0800; 0.1892
R_1; wR_2 (All data)	0.0541; 0.1542	0.0966; 0.1444	0.2033;0.2690	0.0701; 0.1402	0.1950; 0.4220	0.0890; 0.1658	0.1341; 0.2188	0.1458; 0.2145
Goodness of fit on F^2 (all data)	1.068	0.907	0.869	0.995	1.275	1.027	1.005	0.976

Data in common: graphite-monochromated Mo-K$_\alpha$ radiation, λ = 0.71073 Å; $R_1 = \Sigma||F_o| - |F_c||/\Sigma|F_o|$, $wR_2 = [\Sigma w(F_o^2 - F_c^2)^2/\Sigma w(F_o^2)^2]^{1/2}$, $w^{-1} = [\sigma^2(F_o)^2 + (aP)^2]$, $P = [\max(F_o^2,0) + 2(F_c^2)]/3$, where a is a constant adjusted by the program; goodness of fit = $[\Sigma(F_o^2 - F_c^2)2/(n-p)]^{1/2}$ where n is the number of reflections and p the number of parameters.

7.6 Compound in Chapter 6

7.6.1 Synthesis of 39

2,4,6-Trimethylaniline (0.48 cm^3, 3.40 mmol) was treated with *n*-butyllithium (2.13 cm^3, 3.40 mmol, 1.6 M solution in hexane) at – 78 °C with stirring. The solution was allowed to warm to room temperature to give a yellow precipitate of the monolithium salt of 2,4,6-trimethylaniline. The salt was dissolved in THF (10 cm^3) and was added dropwise by cannula to a solution of $FeCl_3$ (0.49 g, 3.02 mmol) in THF (30 cm^3) at – 78 °C. An instantaneous colour change from yellow to turquoise-black was observed. The solution was allowed to warm to room temperature, stirred for a further 2 h and then cooled to – 78 °C. Sodium acetate (0.49 g, 5.98 mmol) was added to the reaction mixture (*via* a solids addition funnel) and the solution then left to stir and warm to room temperature overnight. The volatiles were removed under reduced pressure to give a black solid. The solid was extracted in MeCN (40 cm^3), stirred for 3 h and filtered to remove any salts. The black filtrate was layered with hexane (60 cm^3) and left to stand at ambient temperature. After a few days the hexane layer was removed by cannula and the acetonitrile layer was left to stand at room temperature. After a week, black crystals of $[Fe_2(NMes)\{MeC(O)NMes\}_2Cl_2]$ had formed by slow diffusion (4%, 0.04 g, 0.05 mmol). (Found %: C, 55.54; H, 5.87; N, 9.88. $Fe_2C_{31}H_{39}O_2Cl_2N_3 \cdot 2MeCN$ requires C, 56.02; H, 6.04; N, 9.33). No further analysis was done on the compound due to its air-sensitive nature. The synthetic route was reproduced and resulted in black microcrystalline material the solution part of the decomposing material was a rusty red-brown solid.

Table 25 Crystallographic and data processing parameters for complex **39**

Complex	**39**
J. Fawcett code	02086
Formula	$C_{31}H_{39}Cl_2Fe_2N_3O_2$
M	668.25
Crystal size (mm)	0.38 x 0.22 x 0.20
Temperature (K)	150(2)
Crystal system	Monoclinic
Space group	*C2/c*
Lattice parameters	
a (Å)	18.826(2)
b (Å)	12.4575(15)
c (Å)	14.1868(17)
α (°)	90
β (°)	96.0830(2)
γ (°)	90
U (Å^3)	74.692(3)
Z	4
D_c (Mg m^{-3})	1.344
$F(000)$	1392
μ (Mo-K$_\alpha$) (mm^{-1})	1.070
Reflections collected	9491
Independent reflections	2873
R_{int}	0.0690
Parameters/restraints	188/0
Final R indices	
R_1; wR_2 [I>2σ(I)]	0.0454; 0.1105
R_1; wR_2 (All data)	0.0577; 0.1163
Goodness of fit on F^2 (all data)	0.988

Data in common: graphite-monochromated Mo-K$_\alpha$ radiation, λ = 0.71073 Å; $R_1 = \Sigma||F_o| - |F_c||/\Sigma|F_o|$, $wR_2 = [\Sigma w(F_o^2 - F_c^2)^2/\Sigma w(F_o^2)^2]^{1/2}$, $w^{-1} = [\sigma^2(F_o)^2 + (aP)^2]$, $P = [\max(F_o^2,0) + 2(F_c^2)]/3$, where a is a constant adjusted by the program; goodness of fit = $[\Sigma(F_o^2 - F_c^2)2/(n - p)]^{1/2}$ where n is the number of reflections and p the number of parameters.

7.7 References

1. C.J. O'Connor, *Prog. Inorg. Chem.*, 1982, **29**, 203 and R. C. Weast, *Handbook of Chemistry and Physics*, ed. R. C. Weast, 70th edn., CRC Press, Boca Raton, FL, 1990, p. E134.
2. Data analysis and technical graphics computer program, Microcal™ ORIGIN®, Version 6.0©, Microcal Software Inc., Northampton, USA, 1990 – 1999,
3. D. F. Shriver and M. A. Drezdon, in *The Manipulation of Air Sensitive Compounds*; eds., D. F. Shriver and M. A. Drezdon, Wiley-Interscience, New York, 1986.
4. W. H. Armstrong and S. J. Lippard, *Inorg. Chem*, 1985, **24**, 981.
5. F. Bellezza, A. Cipiciani, G. Gruciani and F. Fringuelli, *J. Chem. Soc, Perkin Trans.* 1, 2000, 4439.
6. G. R. Newkombe, J. Broussard, S. K. Staires and J. D. Sauer, *Synthesis*, 1974, 707.
7. H. Link, A. Decker and D. Fenske, *Z. Anorg. Allg. Chem.*, 2000, **626**, 1567.
8. G. M. Sheldrick, SHELXTL/PC Version 5.0, Siemens Analytical Instruments, Madison, WI, 1996.

Additional Activities

I have attended/participated in the postgraduate activities listed below.

APG - Postgraduate Training Activities, Lectures, Modules and Examinations

APG Training

Demonstration Training

18/9/01 Pre-Session Demonstrator Training

Induction

24/9/01 Departmental Induction

25/9/01 Introduction to Key Techniques and Equipment

26/9/01 Graduate School Induction

27/9/01 Faculty Induction

Information Skills

17/10/01 Information Skills for Chemists Session 1, An Introduction to Chemical Information Databases

24/10/01 Information Skills for Chemists Session 2, Advanced Searching in *Crossfire*

5/12/01 Developing a Personal Skills Portfolio - *Royal Society of Chemistry*

12/6/02 Advanced Scientific Writing for Chemists

12/6/02 Applications of *Endnote*

Module CH501

31/10/01 1D-NMR Spectroscopy

28/11/01 2D-NMR Spectroscopy

30/1/02 The *nOe* Effect

5/6/02 Presentation of NMR data

6/3/02 *Chemdraw*, *Molecular Modelling* and *Powerpoint*

Study, Writing and Presentation Skills

4/3/02, 11/3/02 Study Skills- Effective Management, Reading and Note Making Skills

6/2/02, 13/2/02 Writing Skills

1/5/02 Presentation Skills - Powerful Spoken and Poster Presentations

Career Skills

29/5/02 Developing Skills for a Future Career

Intellectual Property Rights

13/5/02 IPR, Patent Protection and Commercialisation

APG Undergraduate Modules

Semester 1, 2001

Inorganic Rings and Chains CH406	Convenor: Dr. P. W. Dyer, Examined in February 2002 (58 %)
Coursework Comments by Convenor:	Very good and nicely balanced work with reasonable coverage of a good quantity of material. Fairly extensively referenced and well presented work (A+).

Semester 2, 2002

Chemical Crystallography CH404	Convenor: Dr D. R. Russell, Examined in June 2002 (58 %)
Clusters CH415	Convenor: Dr G. A. Solan, Examined in June 2002 (64 %)

Symposia, Conferences and Poster Sessions Attended

23 / 1 / 02 *Royal Society of Chemistry* – Dalton Division
Whole – Day Symposium at the University of Nottingham
'Novel Transition Metal Chemistry: Actions and Reactions'

7 / 3 / 02 *Royal Society of Chemistry* – Dalton Division
Whole – Day symposium at the University of Manchester
'Strategies in Modern Coordination Chemistry'

1 / 7 / 02 – 2 / 7 / 02 Coordination Chemistry Discussion Group (CCDG) *conference, Royal Society of Chemistry; Dalton Division, UK, Loughborough, Loughborough University*
Poster Title: *Paramagnetic Iron Assemblies Featuring Oxo- or Imido-Ligand Scaffolds*

17 / 3 / 03 Nanotechnology Evening Reception, Science, Engineering and Technology (SET) for Britain, House of Commons, UK, London, Westminster
Poster Title: *Paramagnetic Iron Assemblies Featuring Oxo- or Imido-Ligand Scaffolds*

9 / 7 / 03 – 11 / 7 / 03 Coordination Chemistry Discussion Group (CCDG) *conference, Royal Society of Chemistry; Dalton Division, UK, Manchester, Manchester University*
Poster Title: *Blending 2-Pyridine Alcohols with Bifunctional Carboxylates on Paramagnetic Transition Metal Centres* (Awarded First Prize)

23 / 2 / 04 Half-Day Symposium: Catalysis 2004
University of Leicester

27 / 3 / 04 – 30 / 3 / 04 British Council Younger Scientists International Networking of Younger Scientists (INYS) Workshop, Czechoslovakia, Prague / Slany
Selected out of all UK applicants (as one of twelve), included interacting between successful Czech candidates and their research and other issues of research.
Presentation Title: *Paramagnetic Benzilate Clusters; a Time-Honoured Ligand with Novel Aspirations*

12 / 7 / 04 – 14 / 7 / 04 Coordination Chemistry Discussion Group (CCDG) conference, Royal Society of Chemistry; Dalton Division, UK, Leicester, Leicester University
Flash Presentation and Poster 1 Title: *Derivatised Porous Nanoballs Based on Secondary Building Units (SBU)*
Poster 2 Title: *Paramagnetic Chains, Cubes and Open-Cubes Featuring Benzilate Ligands; Syntheses and Magnetic Properties*

18 / 7 / 04 – 23 / 7 / 04 36th International Conference on Coordination Chemistry (ICCC36), Mexico, Yucatán
Theme: *Functional Materials*
Poster Title: *Paramagnetic Chains, Cubes and Open-Cubes Featuring Benzilate Ligands*

PhD Committee Meetings

Committee members: Dr G. A. Solan and D. E. Raven

Meetings: 8 / 10 / 02, 27 / 6 / 03, 4 / 11 / 03 and April 2004

Personal Internal Seminars and Literature Discussion Session Presentations

8 / 11 / 01 PhD first year project outline
Title: *'Paramagnetic Assemblies Based on Imido Ligand Scaffolds'*

18 / 2 / 02 PhD first year project
Title: *'Towards Nano-Scale Assemblies'*

13 / 5 / 02 Literature Discussion Session
Title of Paper: *Carbon – Carbon Bond Activation of R-CN (R = Me, Ar, ^{i}Pr, ^{t}Bu) Using a Cationic Rh(III) Complex.*
Reference: F. L Taw, P. S. White, R. G. Bergman and M. Brookhart, *J. Am. Chem. Soc.*, 2002, **124**, 4192.

14 / 11 / 02 PhD second year project outline
Title: *'Paramagnetic Oxo- and or Imido-Transition Metal Assemblies: SMMs ?'*

25 / 3 / 02 PhD second year project
Title: *'Paramagnetic Oxo- and/or Imido-Transition Metal Assemblies: SMMs ?'*

10 / 2002 Literature Discussion Session
Title of Paper: *'Urea as 'deus ex machina' in Giant Molybdenum Blue Type Cluster Synthesis: an Unusual Hybrid Compound with Perspectives for Related Nano, Supramolecular and Extended Structures'*
Reference: A. Müller, S. Roy, M. Schmidtmann and H. Bögge, *Chem. Commun.*, 2002, 2000.

4 / 12 / 03 PhD third year project
Title: *'Blending 2-Pyridine Alcohols with Bifunctional Carboxylate Ligands on Paramagnetic Transition Metal Centres'*

13 / 11 / 03 Literature Discussion Session
Title of Paper: *'Constructing a Stable Carbene with a Novel Topology and Electronic Framework'*
Reference: P. Bazinet, G. P. A. Yap and D. S. Richeson, *J. Am. Chem. Soc.*, 2003, **125**, 13314.

22 / 6 / 04 Final Year Presentation
Title: *'Controlled Synthesis of Paramagnetic Copper Assemblies'*

Internal Seminars – External Speakers

1 / 10 / 01 *Royal Society of Chemistry Centenary Lecture*

Professor Kyriacos Nicolaou – Scripps Research Institute, California

'Enabling Technologies for Biology and Medicine Arising from Endeavours in Total Synthesis'

4 / 10 / 01 *Royal Society of Chemistry Lecture*

Dr Peter O'Brien – University of York

'Basic Instinct: New Synthetic Adventures with Chiral Bases'

10 / 10 / 01

Dr Didier Bourrissou – Universitié Paul Sabatier, Toulouse

'Stable Carbenes and Diradicals: New Stabilisation and Bonding Modes'

22 / 10 / 02 *Royal Society of Chemistry Student Chemical Society Lecture*

Dr Anthony Hooper – Institute of Arable Crops, Rothamstead

'Sex, Bugs and Rock and Roll: Identification and Synthesis of Semiochemicals and Exploitation of the Ecological Interactions they Regulate as an Approach to Pest Management'

14 / 11 / 01 *Royal Society of Chemistry Joseph Chatt Lecture*

Professor Vernon C. Gibson – Imperial College, London

'Designing Catalysts for Polymer Synthesis'

10 / 12 / 01 Dr Jonathan McMaster – University of Nottingham

'The Electronic Structure of the Active Sites of Molybdenzymes'

14 / 12 / 02 Professor Peter Flecker – Johannes Gutenberg University, Mainz

'Dissecting Intramolecular versus Intermolecular Protein Recognition'

28 / 1 / 02 Professor Judith Howard – University of Durham

'The Application of Very Low Temperature Crystallography to Chemical Problems'

11 / 2 / 02 Dr Robin Bedford – University of Exeter

'High Activity Catalysts for C-C Bond Formation'

25 / 2 / 02 Professor John Nixon – University of Sussex

'The New World of Phospha-Organometallic Chemistry'

4 / 3 / 02 Dr Holger Braunschweig – Imperial College, London

'Compounds with Novel Boron Containing Ligands: Transition Metal Complexes of Boron and [1] Bora – Metallocenophanes'

6 / 3 / 02 Dr Richard Shutt – ExxonMobil, Belgium

'Supercritical Phase Phenomena in Ethylene Polymerisation and Polymer Separation'

8 / 5 / 02 Dr Nick Long – Imperial College, London

'Ferrocene – Ligand Design'

20 / 5 / 02 Dr Martyn Coles – University of Sussex

'Anionic and Neutral Guanidine – based Ligands in Coordination Chemistry and Catalysis'

Internal Seminars and Literature Discussion Sessions – Internal Speakers Project Seminars

11 / 10 / 01 Christopher. J. Davies – PhD second year project outline

1 / 11 / 01 Sukhvinder K. Kandola, Toby Reeve and Samuel Suhard – PhD second year project outlines

29 / 10 / 01 MChem project outlines

8 / 11 / 01 Alice Hickman – PhD first year project outline

22 / 11 / 01 Jérémie D. Pelletier and Omar Duaij – PhD first year project outlines

3 / 12 / 01 Dr. G. A. Solan and Dr P. W. Dyer – Current Projects

6 / 12 / 01 Martin Hanton – PhD third year project outline

4 / 2 / 02 Alice Hickman, Jérémie D. Pelletier and Katie Sharpe – PhD first year projects

18 / 2 / 02 Andrew West and Omar Duaij – PhD first year projects

18 / 3 / 02 Dr. E. Raven and Dr. D. Davies – Current projects

19 / 3 / 02 MChem final presentations

Final Year PhD Presentations attended

27 / 5 / 02 Martin Hanton *(Unattended due to examination)*

17 / 6 / 02 Neesha Patel

24 / 6 / 02 Ben. Croxtall and James Sherrington

Literature Discussion Sessions

29 / 10 / 01 Speakers: M. Hanton and N. Patel, Chair: C. J. Davies

Questioners: B. Croxtall and J. Sherrington

5 / 11 / 02 Speakers: P. Griffith and D. Harding, Chair: M. Dix

Questioners: M. Giardiello and G. Barth

26 / 11 / 01 Speaker: G. Barth, Chair: M. Hanton

Questioners: P. Griffith and D. Harding

11 / 3 / 02 Speakers: T. Reeve, B. Croxtall and S. K. Kandola, Chair: N. Patel

Questioners: C. J. Davies, S. Suhard and M. Hanton

25 / 3 / 02 Speakers: C. J. Davies, S. Suhard and J. Sherrington, Chair: B. Croxtall

Questioners: S. K. Kandola, T. Reeve and N. Patel

24 / 4 / 02 Speakers: A. Hickman, A. West and J. D. Pelletier, Chair: N. Patel

Questioners: R. K. Chaggar, K. Sharp and O. Duaij

13 / 5 / 02 Speakers: O. Duaij, K. Sharp and R. K. Chaggar, Chair: S. K. Kandola

Questioners: A. Hickman and A. West

13 / 11 / 03 Speakers: Y. Champouret, R. K. Chaggar and O. A. Duaij

11 / 12 / 03 Speakers: A. Gregory and E. A. Sabban

PhD Second and Third year Seminars

Internal Seminars – External and Internal Speakers

21 / 10 / 02 Dr Paul Raithby – University of Bath

'Adventures in Organometallic Polymer Chemistry'

28 / 10 / 02 Dr Clive Metcalfe – University of Leicester

'Transition Metal Complexes and their Interaction with DNA'

18 / 11 / 02 Dr Mike Turner – University of Sheffield

'Synthesis of Conjugated Polymers for Polarised Electroluminescence and Polymer Electronics'

9 / 12 / 02 Prof. Todd Marder – University of Durham

'The Role of Transition Metal Boryl Complexes in Catalysed Borylations including Rhodium Catalysed C-H Bond Functionalisation'

17 / 2 / 03 Prof. V. McKee – University of Loughborough

'Manipulating Metal Arrays within Macrocycles'

10 / 3 / 03 Prof. Duncan Bruce – University of Exeter

'Metallomesogens by Design'

28 / 4 / 03 Prof. Kingsley Cavell – University of Cardiff

'Reactions of Heterocyclic Carbene Complexes: Important Ramifications for their Application in Catalysis'

30 / 5 / 03 Dr Carine Aubrey – University of Leicester

'Synthèse, Analyse Stucturale et Activité Biologique d'analogues Rigides d'un Antagoniste de l'octadecaneuropeptide (ODN)'

2 / 6 / 03 Dr Sarah Heath – University of Manchester

'Shedding Light on Biological Systems: the Development of Dinuclear Lanthanide Probes'

Inaugural Lecture

3 / 6 / 03 Prof. Jonathan Percy – Appointed as Professor of Chemistry at the University of Leicester

'Against Nature: Unnatural Products in the Service of Humanity'

9 / 6 / 03 Dr Alan Spivey – Imperial College, London

'Catalytic Asymmetric Acylation – Studies towards the Total Synthesis of Polyol Sesquiterpenes'

29 / 9 / 03 Dr Zoe Pikramenou – University of Birmingham

'Luminescent Supramolecular Architectures: from Shape to Function'

6 / 10 / 03 Dr Chris Richards – Queen Mary, University of London

'Palladium and Platinum Metallacycles for Organic Synthesis'

The Second Tim Norwood Memorial Lecture

8 / 10 / 03 Prof. Ian Campbell – University of Oxford

'NMR and Proteins'

20 / 10 / 03 Dr Sandie Dann – University of Loughborough

'Something Old, Something New Something Borrowed and Something Blue: Complex Oxides and Sulphides'

27 / 10 / 03 Dr Chris Hayes – University of Nottingham

'Natural and non-Natural Products: Total Synthesis and Biological Applications'

3 / 11 / 03 Prof. Helen Fielding – University College London

'Controlling Electrons and Molecules using Light'

17 / 11 / 03 Prof. Chris Binns – Department of Physics University of Leicester

'Building High-Performance Magnetic Materials by Assembling Nanoclusters'

1 / 12 / 03 Prof. Richard Winpenny – University of Manchester

'Synthetic Studies of Metal Wheels and other Cages'

8 / 12 / 03 Prof. Peter Hore – University of Oxford

'Bird Navigation: a Photochemical Magnetic Compass?'

19 / 1 / 04 Prof. Bill Levason – University of Southampton

'Recent Developments in the Chemistry of Antimony Ligands'

9 / 2 / 04 Dr Michael Whittlesey – University of Bath

'Stoichiometric and Catalytic Small Molecule Activation by Ruthenium N-Heterocyclic Carbene Complexes'

8 / 3 / 04 Dr Chris Kay – Free University of Berlin

'Applications of Electron Spin Resonance Spectroscopy to Biological Problems'

Royal Society of Chemistry – East Midlands Local Section sponsored seminar

15 / 3 / 04 Prof. David Schiffrin – University of Liverpool

'Connectivity of Functionalised Nanoparticles and their Arrays'

Royal Society of Chemistry – East Midlands Local Section

26 / 4 / 04 Dr Graham Sandford – University of Durham

'Polyfunctional Heterocycles and Macrocycles'

10 / 5 / 04 Dr Dominic Wright – University of Cambridge

''Cation and Anion Coordination using 'Torocyclic' Ligands''

7 / 6 / 04 Prof. Peter Scott – University of Warwick

'Catalysis with Chiral Metal Complexes'

Internal Seminars and Literature Discussion Sessions – Internal Speakers Project Seminars

24 / 10 / 02 Jérémie Pelletier and Alice Hickman (PhD project update)

31 / 10 / 02 MChem project introductions

7 / 11 / 02 MChem / MSc project introductions

14 / 11 / 02 Rajinder Kaur Chaggar and Omar Al-Duaij (PhD project update)

28 / 11 / 02 Yohan Champouret and Ishaq Dadhiwala (PhD project outlines)

5 / 12 / 02 Samuel Suhard and Sukvinder Kandola (PhD project update)

12 / 12 / 02 Christopher Davies and Toby Reeve (PhD project update)

25 / 3 / 03 Projects seminar

Yohan Champouret (1st year PhD), Jérémie Pelletier (2nd year PhD), Ishaq Dadhiwala (1st year PhD), Carly Anderson (MSc), Omar Al-Duaij (2nd year PhD), Rajinder Kaur Chaggar (2nd year PhD), Alice Hickman (2nd year PhD), Duncan Harding (1st year PhD), Andrew West (2nd year PhD), Nektaria Papadopalou (1st year PhD)

26 / 11 / 03 MChem Introductory Presentations

27 / 11 / 03 Projects Seminar 3rd Year PhD

Jérémie Pelletier and Omar Al-Duaij

4 / 12 / 03 Projects Seminar

Rajinder Kaur Chaggar (3rd year PhD) and Yohan Champouret (2nd year PhD)

11 / 12 / 03 MChem and 1st year PhD Projects Seminar

17 / 3 / 04 MChem Final Presentations

22 / 3 / 04 PhD 1st Year Projects Seminar

E. A. Sabban, R. Griffin, M. Gourlay, J. Bennett, B. Parmar, M. Giardiello and P. Villuendas

20 / 5 / 04 PhD 2nd Year Projects Seminar

Yohan Champouret, Nektaria Papadopalou and Duncan Harding

22 / 6 / 04 Final Year PhD Presentations

Rajinder Kaur Chaggar, Andrew West, Omar Al-Duaij, Jérémie Pelletier and Katie Sharp